



HAL
open science

Cooperative effects with group 10 metals : Multi-cooperative catalysis and non-innocent ligands

Arnaud Clerc

► **To cite this version:**

Arnaud Clerc. Cooperative effects with group 10 metals : Multi-cooperative catalysis and non-innocent ligands. Coordination chemistry. Université Paul Sabatier - Toulouse III, 2022. English. NNT : 2022TOU30033 . tel-03714203

HAL Id: tel-03714203

<https://theses.hal.science/tel-03714203v1>

Submitted on 5 Jul 2022

HAL is a multi-disciplinary open access archive for the deposit and dissemination of scientific research documents, whether they are published or not. The documents may come from teaching and research institutions in France or abroad, or from public or private research centers.

L'archive ouverte pluridisciplinaire **HAL**, est destinée au dépôt et à la diffusion de documents scientifiques de niveau recherche, publiés ou non, émanant des établissements d'enseignement et de recherche français ou étrangers, des laboratoires publics ou privés.



THÈSE

En vue de l'obtention du
DOCTORAT DE L'UNIVERSITÉ DE TOULOUSE
Délivré par l'Université Toulouse 3 - Paul Sabatier

Présentée et soutenue par
Arnaud CLERC

Le 25 février 2022

Effets coopératifs avec les métaux du groupe 10 : catalyse multi-cooperative et ligands non-innocents

Ecole doctorale : **SDM - SCIENCES DE LA MATIERE - Toulouse**

Spécialité : **Chimie Organométallique et de Coordination**

Unité de recherche :

LHFA - Laboratoire Hétérochimie Fondamentale et Appliquée

Thèse dirigée par

Blanca MARTIN-VACA et Julien MONOT

Jury

Mme Ana ALBÉNIZ, Rapporteur

M. Régis GAUVIN, Rapporteur

Mme Katerina SOULANTICA, Examinatrice

Mme Blanca MARTIN-VACA, Directrice de thèse

Acknowledgments / Remerciements

I would like to begin by expressing my gratitude to the members of the committee that agreed to review and report on this Ph.D. work, Ana C. Albéniz and Régis Gauvin. Also, I would like to thank Katerina Soulantica for presiding over this jury. Thank you all for your interest in this work, and I thoroughly enjoyed the scientific discussion during the defense.

Je voudrais ensuite remercier mes directeurs de thèse en commençant par ma directrice, Blanca. Cette histoire, dont une page se tourne ici, a commencé au tout début de mes études de chimie, lorsque que je t'ai eu comme enseignante. En tant qu'étudiant, on ressent tout de suite ta passion et ton engagement pour la chimie organométallique et c'est génial ! C'est ce qui nous donne envie de continuer à creuser dans ce domaine et il est clair que c'est grâce à toi, et à tout ça, que je suis arrivé aussi loin aujourd'hui. Au cours de ma thèse, tu as toujours eu ta porte grande ouverte pour discuter, me guider et me prodiguer des conseils. Ta bienveillance et ton dynamisme qui te caractérisent font que l'ambiance générale est très agréable, merci pour tout.

Julien, ça a été une sacrée aventure ! Quel chemin parcouru ! Tout a commencé par la semaine de TP où le lundi, on finit à pas d'heure (mais en musique !). Quelques années plus tard, nous voilà ensemble pour enseigner ces TP. Au début de ma thèse, on était même voisins de paillasse ! Tes qualités scientifiques et humaines font que tu es toujours prêt à nous donner des petites techniques ou des petits « tips » pour lancer les manip (pas trop loin surtout !), comme le coup le pipette pasteur pour activer le magnésium (qu'un exemple parmi tant d'autres !). J'en garde pleins en tête et cela me servira toute ma carrière. Tu es très proche des étudiants et c'est un énorme atout pour nous. Tu as toujours su trouver les mots pour me calmer et me rassurer lors des coups de stress, ça va beaucoup me manquer... Même si nous n'avons pas la même passion pour Star Wars, on partage la Formule 1 ! Rendez-vous au premier virage au grand prix de Montréal ?

Didier, merci de m'avoir accueilli au laboratoire et au sein de l'équipe. Ta capacité à avoir une vision d'ensemble et de poser toujours les bonnes questions est impressionnante. Tu pilotes toujours le bateau dans la bonne direction avec ta méthodologie et ta rigueur scientifique qui te distingue, en nous faisant lever la tête et voir plus loin lorsque on force un peu tête baissée. Merci.

Ghenwa, tu es une personne géniale avec un niveau et une rigueur scientifique extraordinaire. Avec toi aussi, l'aventure a commencé lorsque j'étais étudiant sur les bancs de la fac. Merci pour ton coaching lors des répétes (l'hyperconjugaison !!!) et pour toutes les discussions que l'on a pu avoir pendant ces quelques années.

Merci aussi à Gyorgy, notamment pour nos discussions et ton aide, notamment lors des expériences de voltammétrie cyclique et les réductions !

Un énorme merci aussi à toute la plateforme scientifique, technique, et administrative du laboratoire ! Merci à Maryse, Sérah, Florence et Miguel qui nous rendent vraiment la vie facile. Merci aussi à Olivier Volpato pour tout ce que tu as fait pour nous au quotidien. Lorsqu'on vient chercher des fournitures ou te demander quelque chose à ton bureau, on ne pouvait jamais sortir de ton bureau sans une blague !

Je voudrais aussi remercier les « anciens » du labo, Paul, Charlie, Saam : ça a été un vrai plaisir d'arriver au sein de la famille LBPB avec vous.

Enrico, Grande ragazzo !!! Tu as initié le projet Conia-ène, ce qui m'a permis de commencer ma thèse dans de très bonnes conditions. Je suis très content qu'on ait réussi à faire cette publication ensemble. Je garde beaucoup d'amitié pour toi et ça m'a fait très plaisir d'échanger avec toi à Milan, je te souhaite énormément de bonheur à Copenhague !

Un énorme merci à Max, avec qui j'ai pu partager la première moitié de ma thèse. Merci pour toutes les discussions qu'on a pu avoir, de chimie (ou non !), les différents malaises, les grosses rigolades, et pour les différents verres au Black (et à l'Ice). C'était vraiment top de t'avoir comme collègue et je suis sûr que ton avenir sera brillant ! On se verra à Chicago ou à Montréal c'est sûr !

Aaaaah Cylileuuh ! Toujours, en train de courir et à 1000 à l'heure ! C'était top de partager le labo avec toi, tu es super curieux et dynamique (ça se voit très bien au group meetings !) et j'ai beaucoup aimé t'avoir comme collègue. On a beaucoup échangé pendant ces quelques années partagées au labo, que ce soit au journal club, à la pause-café, au bar ou au labo ! Tu es un chimiste extraordinaire et je te souhaite le meilleur.

Maryne, tu étais toujours prête à nous ramener des gâteaux ou des crêpes pour les petit-déj et la pause-café ! Merci pour tout !

Omar, notre canado/égyptien préféré ! Merci pour toutes les discussions que nous avons pu avoir, que ce soit d'un point de vue chimie, ou avenir et recherche de job. Tu es un excellent chimiste et une belle personne. Je te souhaite le meilleur pour la suite. On reste en contact !!

Merci aussi aux golden boys/girls de l'équipe : Alexis, le fan de Nadal !!! Nos chemins se sont croisés au LHFA pendant relativement peu de temps mais j'ai énormément apprécié te rencontrer, entre discussions Koh-lanta, foot, et F1, il y avait aussi un peu de chimie ! J'espère que tu te régales dans ton nouveau job à Dijon et qu'on se recroisera.

Tusen takk Marte, notre coca-cola/pepsi girl ! Je sais que ton français est maintenant parfait alors j'écris dans la langue de Molière. Tu es toujours de bonne humeur et prête à discuter, c'est vraiment très agréable (merci aussi de m'avoir fait découvrir les bonbons norvégiens à la réglisse) !

Thanks a lot also to Nereida, David, and Felix for the good times, all the best to the three of you.

Mathildosaurus !!! C'était top de partager ces années avec toi. Lors de mon arrivée au labo, tu as toujours pris le temps de m'aider (souvent à trouver ce qui était sous mon nez !). On a eu de sacrés délires lors des tournages LBPB et on a aussi eu des échanges scientifiques super intéressants. Tu as aussi su être là lors des coups de stress ou de blues, alors merci ! Je te souhaite plein de réussite à toi ainsi qu'à Adri !

Après les anciens, les nouveaux !!! Merci à Arnaud et bon courage pour les BP, mais je suis sûr que tu vas très bien t'en sortir, tu as la personnalité pour. J'espère que tu auras regardé drive to survive avant de soutenir tout de même.

Marceline, tu as rejoint le labo et la pincer team un tout petit peu avant le début de ma rédaction, pas forcément la période où j'étais le plus disponible pour te filer un coup de main. Ton arrivée a tout de suite apporté de la cohésion au sein de l'équipe et ça c'est vraiment génial. Entre les loisirs créatifs et les sorties rando, tu as une personnalité très attachante et je suis sûr que tu vas réussir, accroche-toi !

Merci aussi à tout le reste du LHFA, notamment à Ugo et Aymeric de l'équipe ECOIH, à Soukaina et à Julien de l'équipe SHEN, sans oublier l'équipe SYMAC, COP et KISS.

Je voudrais aussi remercier les ingénieurs, Julien, Olivier, Mathieu, Christian et Isabelle. Vous êtes toujours prêts à nous aider et à nous prodiguer des conseils, merci. Je n'oublie pas non

plus Louis, le TAZ du labo ! On a été brièvement voisins de paillasse et il est clair que tu es un excellent chimiste, très créatif ! Un peu désordonné aussi mais tellement gentil que tout passe.

Un énorme merci à Sonia et Nathalie, ce n'était pas si simple de cristalliser ces complexes et vous vous êtes accrochées et démenées pour que l'on puisse sortir un maximum de structures avec des échantillons pas toujours terribles et tout ça avec le sourire ! C'était génial de travailler avec vous.

Je voudrais aussi remercier la plateforme RMN, Caro, Stéphane, Marc et Pierre pour leur accueil au MHT ou au service commun qui ont été cruciaux pour la réussite de ces travaux.

Merci à mes amis chimistes Yoyo et Simon ! On a fait une bonne partie du parcours ensemble, que ce soit sur les bancs de la fac ou à l'extérieur. Merci pour tous les bons moments !

Un grand merci à mes amis non-chimistes : Gab, Manon, Quentin, pour tout ce que vous avez fait pendant toutes ces années, les rigolades, les week-ends, les baby-foots et j'en passe...

Je voudrais maintenant remercier ma mère, à qui je dois énormément. Tu es un véritable puit sans fond de générosité et tu m'as accompagné depuis le début, en faisant toujours tout pour que je sois heureux ! Je ne te remercierai jamais assez pour tout ce que tu as fait et ce que tu continues à faire. Merci aussi à Pascal, pour toutes les valeurs que tu m'as transmises, pour les coups de boost dans les moments difficiles et aussi quand tout va bien !

Papa, merci pour tout ce que tu m'as transmis et pour tout ce que tu as fait pour moi depuis des années, sans toi rien de tout ça n'aurait été possible. Un gros merci aussi à Géralde et à Paul pour leur accompagnement et leur soutien (dans quelques années, ça sera ton tour !).

Un immense merci aussi à ma sœur Mélanie, tu es un vrai rayon de soleil et une personne incroyable ! Très facile à vivre et toujours souriante, j'ai énormément de chance de t'avoir. Tu m'as beaucoup aidé pendant toutes ces années et je sais que je peux toujours compter sur toi, alors merci. Merci aussi à Paul et Vincent, mes « brotha from another mothaaa » !!! pour tous les bons moments.

Un énorme merci aussi mes grands-parents Papi Mic et Papi Guy (sans oublier Jaqueline, et Christine !). Merci à mon tonton Vincent, pour tous les bons moments que l'on a partagés, entre skate-park et bobsleigh maison ! Merci aussi au reste de ma famille, je ne peux pas tous vous citer ici mais sans votre soutien au quotidien, cela n'aurait pas été possible.

Un gros merci aussi à Mario, Cristina et Mathieu pour tout leur soutien et leur aide pendant cette aventure.

Pour finir, un énorme merci à celle qui partage ma vie, Mélanie. Tu as fait le pari de venir me rejoindre à Toulouse, pendant ces 3 années. C'était un gros risque professionnel, mais tu as fait un parcours sans faille, on peut dire pari réussi maintenant ?! Merci pour ton soutien dans les moments difficiles comme dans les bons moments, pour ta patience pendant la rédaction, et pour tout ce que tu fais pour moi au quotidien.

Table of contents

General introduction	11
General remarks on the experimental work	14
Abbreviation list	15
List of complexes	16
I) Bibliographic study: metal-ligand cooperativity and group 10 metals	17
I.1) MLC between a group 10 transition metal and an electron-rich site	18
a) Pincer carbene complexes and related	18
b) M-X type pincer complexes for cooperative bond activation	44
c) Aromatization/dearomatization strategy	57
I.2) MLC between a group 10 transition metal and a Lewis acid	80
a) Functional group reservoir	80
d) Oxidative addition assistance	88
I.3) Miscellaneous examples	97
a) Si center as acceptor and donor of organic fragments	98
e) π -groups as hydrogen acceptors	104
I.4) Conclusion and PhD project	106
I.5) References	108
II) Metal–ligand–Lewis acid multi-cooperative catalysis: a step forward in the Conia-ene reaction	113
II.1) Introduction	113
II.2) Results and discussion	115
II.3) Conclusions	129
II.4) Experimental Section	131
II.5) References	156
III) Synthesis of a new non-innocent platform and generation of a dearomatized active species 159	
III.1) Context and introduction	159
III.2) Synthesis of a new non-innocent platform	162
III.3) Aromatization/dearomatization cooperativity	165

a)	Generation and characterization of the deprotonated complex.....	165
b)	Stoichiometric activation of polar E-X bonds.....	168
c)	C-H activation of alkynes:	170
d)	Dehydrogenation of alcohols	174
e)	DMAB Dehydrogenation and H ₂ activation.....	176
III.4)	Conclusion and perspectives:.....	181
III.5)	Experimental Section.....	183
III.6)	References.....	197
IV)	An additional mode of cooperativity: Pd-S.....	199
IV.1)	Context and introduction:.....	199
IV.2)	Generation of the active species, characterization, and stoichiometric bond activation reactions:.....	208
IV.3)	Stoichiometric hydroelementation reactions:.....	214
IV.4)	Initial catalytic results and mechanistic implications	215
IV.5)	Substrate scope of the catalytic hydrosilylation reaction	219
IV.6)	Extension to other E-H bonds	224
IV.7)	Conclusion and perspectives.....	226
IV.8)	Experimental section.....	228
IV.9)	References.....	237
	General conclusion and perspectives.....	239
	Résumé des travaux en Français	245

General introduction

In the world we live in, it is estimated that around 85% of all manufactured products involve catalysis at some point in the production chain. Involved in petroleum refining, transport, food, pharmaceuticals, plastics (and much more !), catalytic processes are estimated to contribute up to 40% of the global GDP. The research for new catalytic approaches is therefore of considerable interest to the chemist, and in a broader sense to humanity. In nature and biological systems, catalysis occurs mostly through enzymes. Millions of years of natural selection and evolution have tailored these highly efficient 3D catalytic architectures capable of impressive selective transformations under mild conditions. In enzymatic systems, multiple sites within the active pocket work in concert toward the same catalytic transformation (Figure 1).

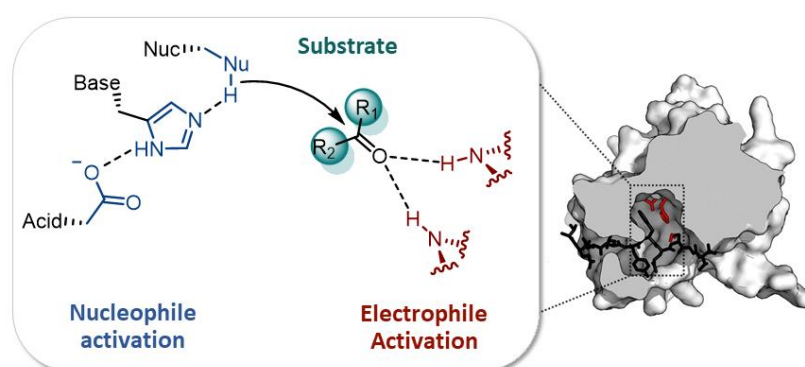


Figure 1: General mode of action of an enzyme with multiple sites working cooperatively. Right enzyme image extracted from Wikipedia - catalytic triad - under Creative Commons License

In transition metal (TM) chemistry at the bench, traditional homogeneous catalysis mostly relies on designing and using the right set of ligands, to fine-tune the stereo-electronic properties of the metal and achieve a good catalytic efficiency (in terms of activity and selectivity). This approach has been receiving a lot of interest and has led to ground-breaking discoveries since the second half of the XXth century. Most representative is the emergence of Pd-catalyzed cross-coupling reactions, the impact of which was recognized by the Nobel committee in 2010.

Taking inspiration from nature, the concept of cooperative effects in catalysis was only recently introduced and formalized by chemists. In this field, much like in enzymes, multiple chemical functions work together towards the catalytic transformation. In transition metal

catalysis, the cooperative entity can be an external co-catalyst or can even be embedded within the ligand architecture, called Metal-Ligand cooperativity (or MLC). In this area, approaches where the ligand does not only modulate the stereo-electronic properties of the metal but is chemically involved in the bond-breaking/bond-forming steps led to exciting discoveries (Figure 2).

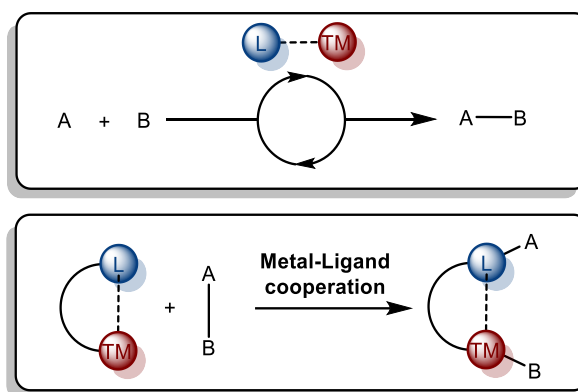


Figure 2: General view of “classical” TM-catalysis and chemical non-innocence in Metal-Ligand cooperativity

This Ph.D. project and manuscript are focused on ligand design for metal-ligand cooperation and more specifically, pincer ligands and group 10 metals.

In the first chapter of this manuscript, an extensive bibliographic survey of the pincer/bidentate group 10 metal complexes exhibiting MLC will be presented. The objective was first to have an overview of MLC with group 10 metals, an approach less developed than for other TM and thereby to lay the groundwork for a review to be published in 2022. Three main categories depending on the reactivity exhibited by the non-innocent ligand were identified (electron-rich, Lewis acid, and other), and the main features related to stoichiometric or catalytic cooperative transformations will be discussed.

The second chapter will present the development of a new multi-cooperative catalytic system combining MLC at the (SCS)-Pd complex previously developed in the group, with an external Lewis acid. The electron-rich backbone at the ligand was found compatible with hard oxophilic Lewis acids. With this new system, the efficient formation of C-C bonds was achieved through catalytic Conia-ene cycloisomerization reaction (Figure 2). An unusually wide scope of substrates was cyclized with this system and the ring size could be varied up to challenging 7-membered rings. Internal alkynes were also efficiently cyclized. More importantly, our system exhibited a complementary selectivity compared to that reported in the literature by

promoting the formation of the more sterically demanding *Z* alkene. With these results, the relevance of developing the cooperative approach with group 10 metals was further demonstrated and prompted us to develop a new ligand architecture.

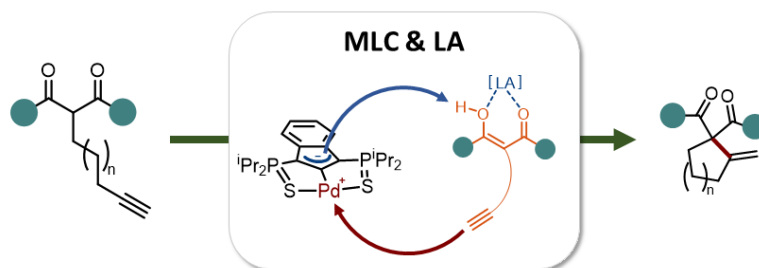


Figure 2: Combination of MLC and LA synergy for C-C bond formation

In the third chapter of this thesis, the design and synthesis of a new non-innocent pincer ligand based on a quinoline scaffold will be presented (Figure 3). The coordination of the PNS ligand to palladium and the generation of a dearomatized complex was successfully achieved. Evidence for the cooperative bond activation was also substantiated by E-H bond activation reactions.



Figure 3: PNS ligand design for MLC with palladium and the two associated modes of non-innocence

Thanks to our ligand design, an additional mode of cooperativity based on the direct interaction of the palladium with a chemically non-innocent sulfur was possible and will be explored in the fourth chapter of this manuscript. To explore this new mode of cooperativity, much like in the previous case, our methodology was to prove the cooperative bond activation through stoichiometric reactions, then apply this to catalytic transformations. In our case, the stoichiometric Si-H bond activation was successfully achieved, and the resulting complex was found catalytically relevant in the hydroelementation of unsaturated compound

General remarks on the experimental work

All reactions and manipulations were carried out under argon atmosphere using standard Schlenk techniques unless otherwise stated. Dry, oxygen-free solvents were employed. All organic reagents were obtained from commercial sources and used as received or prepared from known literature procedures. % of complexes for catalyst loadings are always given relative to the effective [Pd] concentration.

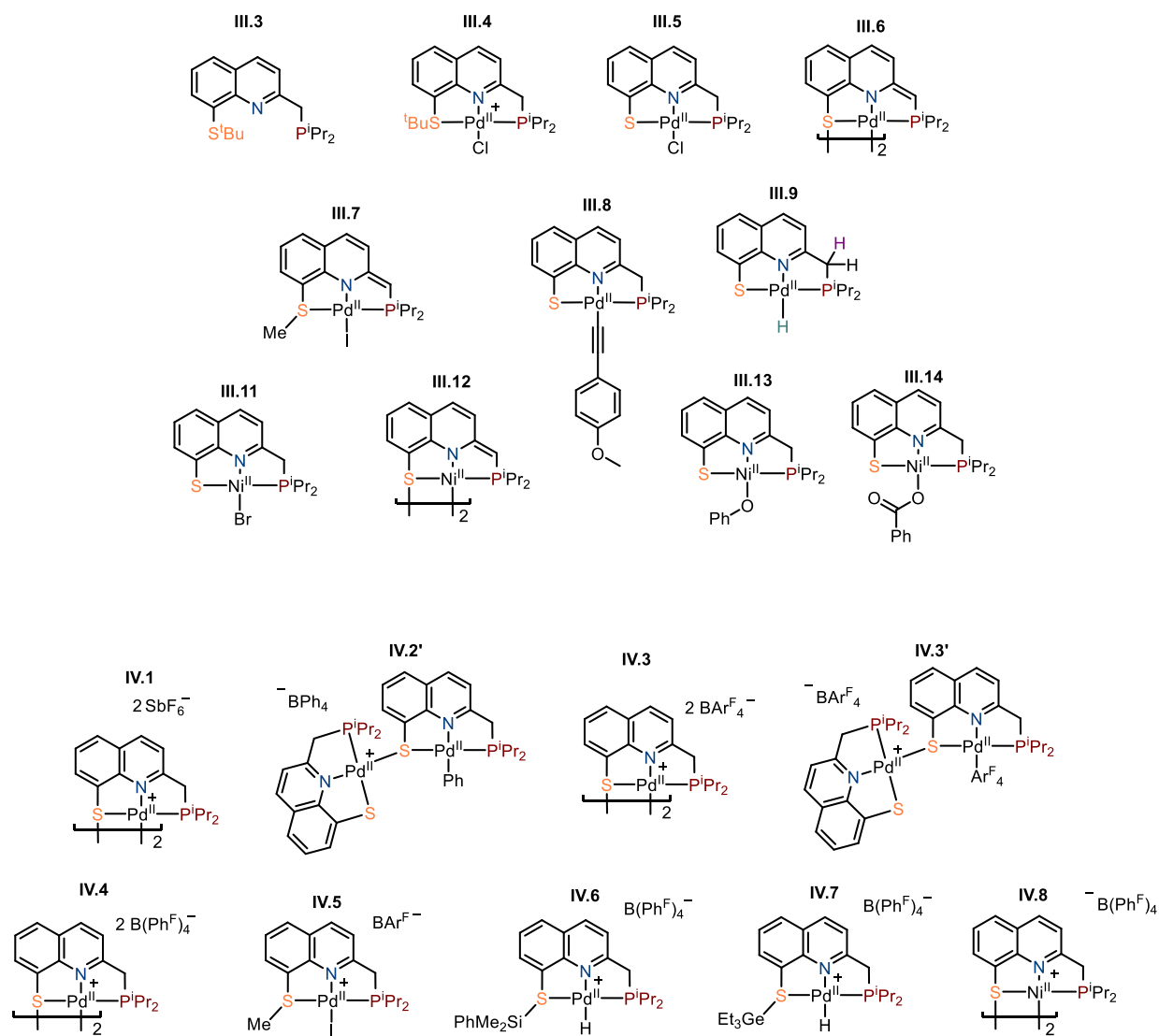
^1H , ^{11}B , ^{13}C , ^{19}F , ^{31}P , and ^{29}Si spectra were obtained on Bruker Avance 300, 400, or 500 MHz spectrometers. Chemical shifts are given in ppm relative to residual solvent as an internal standard (for example CDCl_3 : $\delta = 7.26$ ppm for ^1H and $\delta = 77.16$ ppm for ^{13}C).^[1] Unless otherwise stated, NMR spectra were recorded at 293 K. When necessary, ADEQUATE, NOESY, NOESY ZQF selective analyses were used to determine the regio- and stereochemistry of the obtained products. ^{15}N NMR was recorded using ^1H - ^{15}N HSQC experiments using NH_3 as a reference.

- [1] G. R. Fulmer, A. J. M. Miller, N. H. Sherden, H. E. Gottlieb, A. Nudelman, B. M. Stoltz, J. E. Bercaw, K. I. Goldberg, *Organometallics* **2010**, *29*, 2176–2179.

Abbreviation list

Alk: alkyl
Ar: aryl
Atm: atmosphere
BAr^F: tetrakis(3,5-bis(trifluoromethyl)phenyl)-borate
B(Ph^F)₄: tetrakis(perfluorophenyl)-borate
Bn: benzyl
cod: 1,5-cyclooctadiene
conv : conversion
Cp: cyclopentadienyl
Cp*: pentamethylcyclopentadienyl
Cy: cyclohexyl
d: doublet
DBU: 1,8-diazabicyclo[5.4.0]Undec-7-ene
DCE: 1,2-dichloroethane
DCM: dichloromethane
DFT: Density Functional Theory
DIPEA: di-iso-propylethylamine
DMSO: dimethylsulfoxide
equiv: equivalent
Et: ethyl
FLP: frustrated Lewis Pair
HMDS: hexamethyldisilazane
HOMO: highest occupied molecular orbital
HSAB: hard soft acid and base
Int: intermediate
ⁱPr: isopropyl
L: L-type ligand
LUMO: lowest unoccupied molecular orbital
Me: methyl
ⁿBu: n-butyl
NHC: N-heterocyclic carbene
NMR: nuclear magnetic resonance
OAc: acetate
OTf: triflate
Ph: phenyl
ppm: parts per million
Py: pyridine
R: alkyl fragment
rt: room temperature
s: singlet
t: triplet
tBu: tert-Butyl
TFA: trifluoroacetic acid
THF: tetrahydrofuran
TM: transition metal
TON: turn Over Number
Ts: tosyl
TS: transition State
X: X-type ligand

List of complexes



I) Bibliographic study: metal-ligand cooperativity and group 10 metals

In this chapter, models from the literature of pincer and chelate group 10 metal complexes exhibiting chemical non-innocence will be presented. In this area, contributions can be sorted into 3 main categories depending on the reactivity exhibited by the ligand backbone.

The most developed approach, where the ligand acts as an electron-rich site will be treated first. Then the “opposite” strategy with examples of Lewis-acid incorporated in the ligand will be presented. Finally, other miscellaneous examples where chemical non-innocence is observed at the ligand will be described.

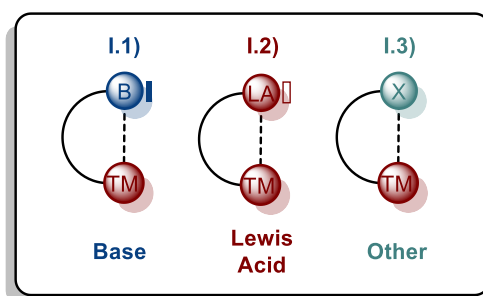


Figure I.1: Overview of the categories of MLC with group 10 metal complexes treated in this chapter

I.1) MLC between a group 10 transition metal and an electron-rich site

Most of the studies performed on metal-ligand cooperativity deal with the combination of a basic Brønsted site at the ligand and a Lewis acidic metal center. The main challenge resides in the mutual quenching of both partners. Combination of two antagonists has been proven possible and even synergistic upon careful design. Substantial improvements, not only in catalytic efficiency but also in the number and complexity of achievable transformations has been achieved through this cooperative approach.^[1] The contributions in this field can be organized into three major categories: (Figure I.2) pincer carbene-“like” complexes with an active site (C, Si, or Ge) either directly bonded to the metal or in a remote position (a). M-heteroatom pincer/chelate complexes with a reactive lone pair at the heteroatom (b). Finally, aromatization/dearomatization based complexes including examples with remote C=X (X: C, H, O) bonds engaged in π -delocalization with a pyridine or Cp-type ligands c).

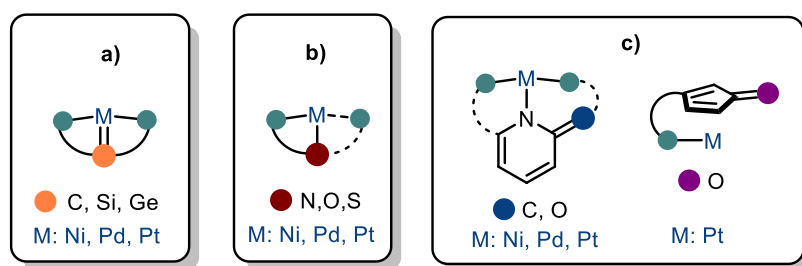


Figure I.2: Overview of the complexes and ligand designs exhibiting cooperativity between a basic-site and a group 10 transition metal.

In this chapter, examples of such cooperative systems will be detailed by first presenting their stoichiometric reactivity, evidencing the chemical non-innocence at the ligand and then, when relevant, their catalytic applications.

a) Pincer carbene complexes and related

Widely used in organometallic chemistry, carbene complexes can be divided into two types:

- Fischer carbenes with an electrophilic carbene center
- Schrock carbenes with a nucleophilic carbene center

The nucleophilic or electrophilic properties make carbene complexes available as group transfer reagents.^[2] However, after the exclusion of NHCs, examples of group 10 carbene complexes are rare. Indeed, the first case of an isolable carbene of Pd^{II} was reported by

Broning in 2003.^[3] Unfortunately, no selective reactivity with nucleophiles or electrophiles was described precluding classification as a Fischer or Schrock carbene. Following this, new group 10 carbene complexes were developed by several research groups with the intention to exploit the reactivity of the metal and the carbene moiety synergistically. This area can be best treated by first studying the key contributions of Cavell and Le Floch with a methanediide ligand design flanked by 2 coordinating groups (Figure I.3). This field of research was then deepened by Iluc and Piers with two *o*-phenylenephosphine coordinating groups. A ligand design merging the approach of Iluc and Le Floch was introduced by Gessner for nickel and palladium. A chemically non-innocent NHC was also reported by Roesler with nickel. Finally, a new family of complexes based on the in-plane coordination of indene at palladium and platinum was reported by our group.

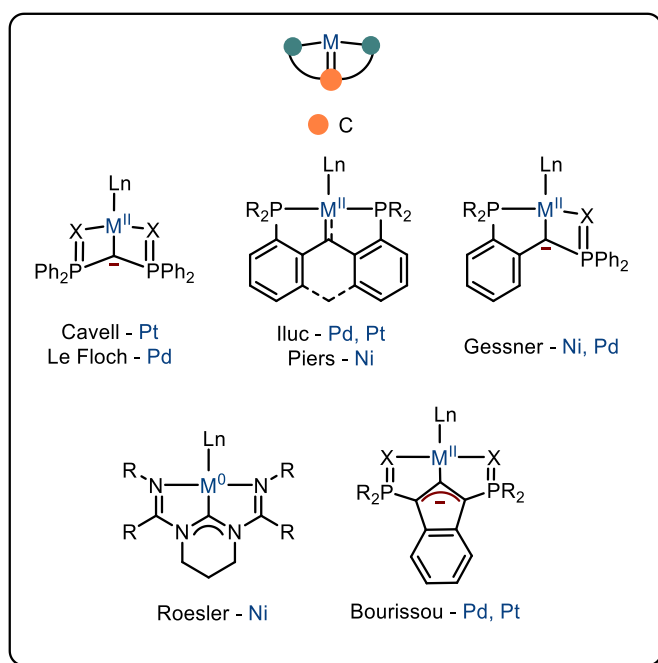
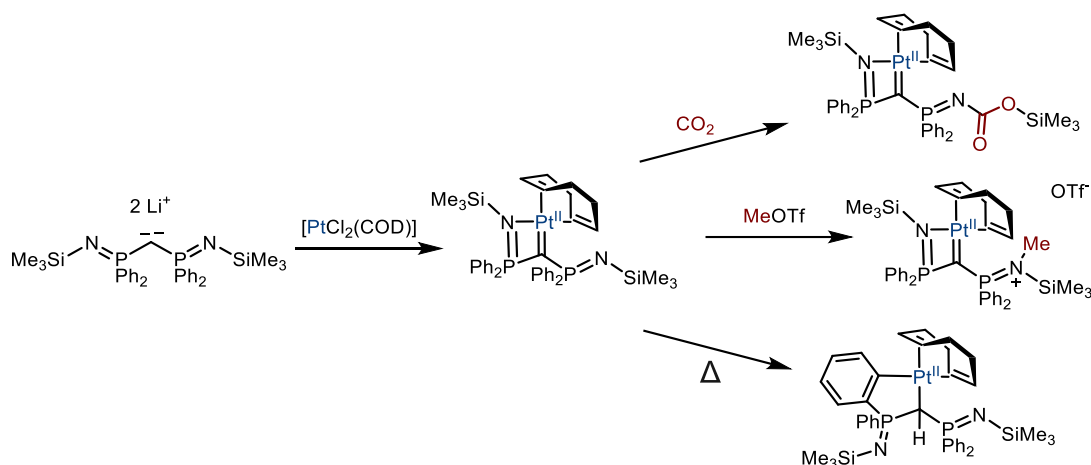


Figure I.3: Group 10 carbene complexes and analogs exhibiting MLC behavior

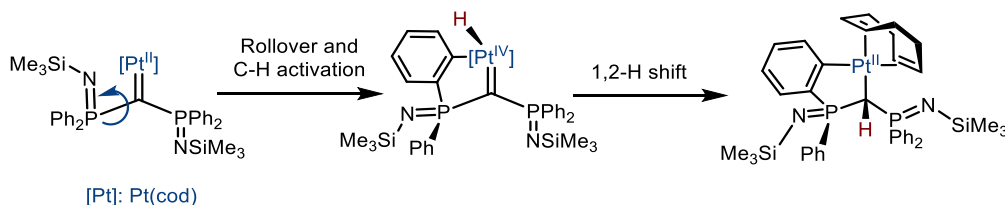
In 2003, the group of Cavell reported the first example of a chemically non-innocent carbene at platinum (Scheme I.1).^[4] In this work, the carbene was generated by reaction of a carbon-centered dianion stabilized by two phosphazene groups with a Pt^{II} fragment. Geminal dianions are inherently challenging due to their extremely high sensitivity and reactivity the critical impact of the substituents at carbon on the reactivity was underlined by multiple contributions in this field.^[5] In this example, the carbene was only coordinated in a bidentate fashion with a remaining pendant phosphazene group. The charge bared by the carbon is

delocalized over the phosphazene groups. Electrophiles (CO_2 , MeOTf) react at the pendant nitrogen with no involvement of the $\text{Pt}=\text{C}$ moiety.



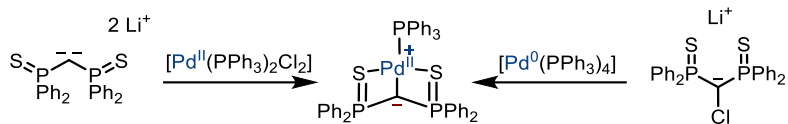
Scheme I.1: Synthesis and reactivity of Cavell's Pt^{II} carbene complex

Thermolysis of the carbene in benzene at 100°C for 20h induced *ortho*-metalation of one of the phenyl rings (Scheme I.21). Remarkably, in this case, the reactive site was not the pendant nitrogen, but the $\text{C}_{\text{carbene}}$ directly bonded to Pt^{II} . The following mechanism was proposed for this transformation (Scheme I.2): First decoordination and rotation of the $\text{P}=\text{N}$ arm occurs, then *ortho*- $\text{C}-\text{H}$ metalation follows with formation of the corresponding $\text{Pt}^{\text{IV}}-\text{H}$. Finally, a 1,2- H shift forms the final complex as a mixture of two enantiomers.



Scheme I.2: Proposed mechanism for the thermolysis of the Pt^{II} carbene complex – The other enantiomer was also formed but not drawn here

The “dianion to carbene” approach was extended by Le Floch in 2004 with the reaction of bis(thiophosphinoyl)methanediide dianion with Pd^{II} (Scheme I.3).^[6] In this case, PPh_3 as coligand and $\text{P}=\text{S}$ as chelating arms were used resulting in a different coordination mode compared to the example of Cavell. Remarkably, the synthesis of the complex could also be achieved by treatment of a Pd^0 source with the corresponding carbenoid. The origin of the electrons (dianion and Pd^{II} or carbenoid and Pd^0) was thereby shown to have no impact on the structure of the formed complex.



Scheme 1.3: Synthesis of Le Floch's carbene complex via dianion or carbenoid to carbene

The bonding between the carbene and the Pd^{II} center was then studied by the authors and an unusual bonding situation was described. In the classical interaction between a neutral Fischer carbene and a transition metal, the bonding situation consists of a Metal-Carbon double bond: (Figure I.4 - A)

- A σ -bond resulting from the overlap of the Highest Occupied Molecular Orbital (HOMO) of the carbene and the Lowest Unoccupied Molecular Orbital (LUMO) of the metallic center
- A π -bond resulting from backdonation, from the HOMO of the metallic center to the LUMO of the carbene.

In this case, both the π -bonding and π^* -antibonding combination are occupied, thanks to the dianionic nature of the ligand (Figure I.4 - B). Accordingly, the carbene-metal interaction would be best described as zwitterionic with a negatively charged carbene and a cationic transition metal.

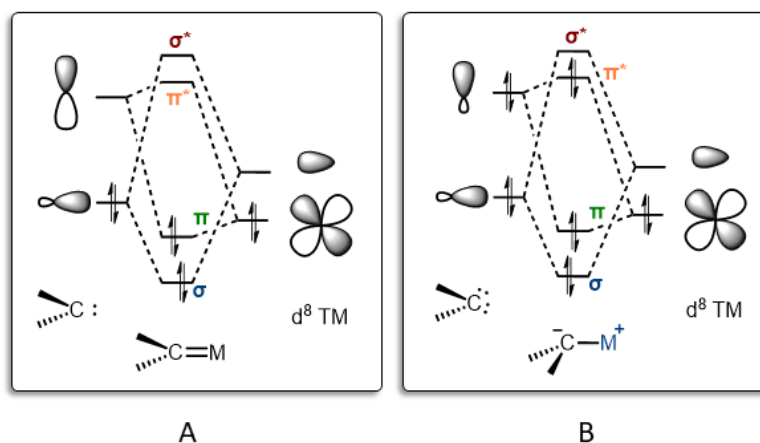


Figure I.4: A – Usual bonding situation in carbene complexes; B – Bonding situation in the case of Cavell's and Le Floch's complexes

This bonding description was further confirmed by DFT calculations, showing the π^* orbital as HOMO of the complex. In the X-ray structure, a pyramidalized C_{carbene} with an important sp³ character was reported (Figure I.5). Remarkably, in the earlier example of Cavell no

pyramidalization of the carbon center was found, in line with a more pronounced π -delocalization in the P=N complex than in the P=S of Le Floch.

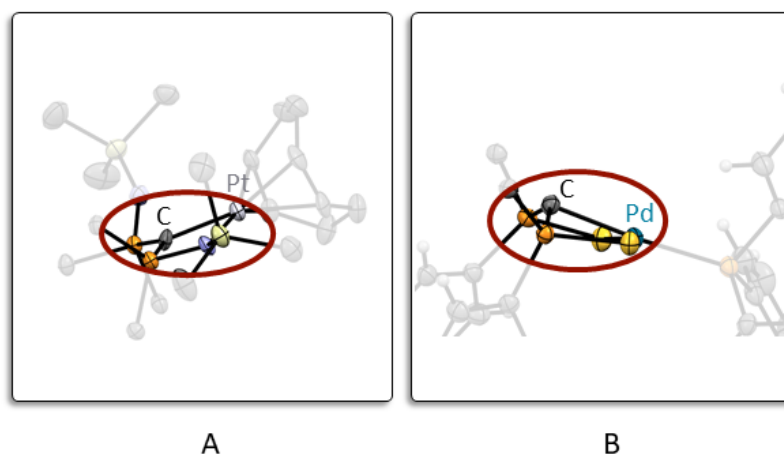
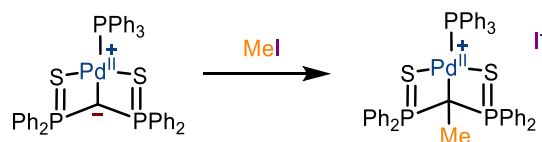


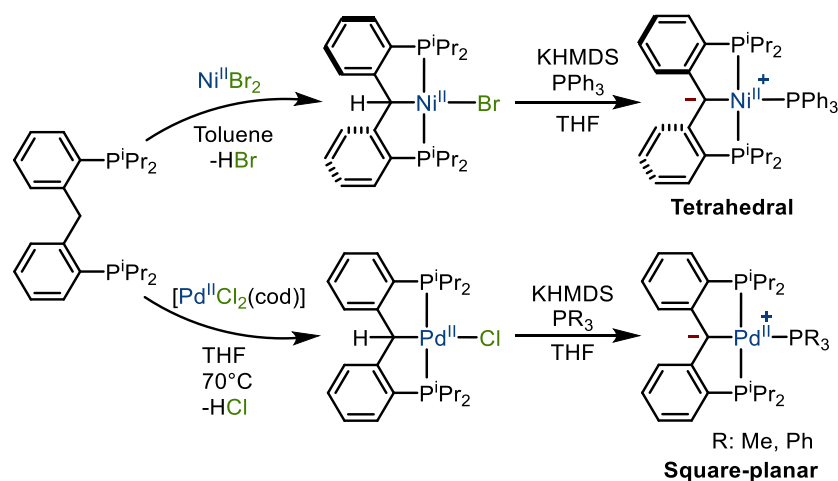
Figure I.5: A – XRD structure of Cavell's planar carbene complex; B – XRD structure of Le Floch's carbene complex (Ph substituents at phosphorus omitted for clarity)

Accordingly, a high electron density at the carbon was found by NBO analysis (-1.39 carbon, +0.37 palladium) and the nucleophilic character of the carbene was evidenced by reaction with iodomethane (Scheme I.4). Only a slight variation in the Pd^{II}-C bond length from the carbene complex to the methylated analog (2.113 Å, to 2.146 Å respectively) was reported, supporting the high single-bond character of this interaction in the carbene complex.



Scheme I.4: Nucleophilic character of Le Floch's Pd^{II} carbene illustrated by reaction with MeI

Following these reports, another framework based on a diphenyl carbene complex was introduced by the group of Iluc with palladium, and by the group of Piers with nickel (Scheme I.5).^[7,8] In both cases, the synthetic strategy was not the previously described dianion to carbene approach but the treatment of the corresponding CH₂-diphosphine pro-ligand with a metal-halide salt. The first H⁺ was removed during the C-H activation step with concomitant loss of H-Halide, forming the PHCP-M^{II}-X complex. Subsequent deprotonation with KHMDS in the presence of a phosphine coligand led to the corresponding carbene complex. While on paper very similar, distinctly different structural features were observed by XRD analysis for both complexes.



Scheme I.5: Synthesis of PCP Pincer carbene Pd^{II} and Ni^{II} complexes by C-H activation and subsequent deprotonation

In the case of nickel, upon deprotonation, the C_{carbene}-Ni^{II} bond length was reported to decrease from 1.973 Å in the parent CH-Ni^{II} to 1.908 Å in the carbene complex. This change was accompanied with an important distortion from the ideal square-planar environment at Ni^{II} with a τ_4 parameter of 0.55 (where 0.0 = ideal square plane and 1.0 = ideal tetrahedron). This distortion was attributed to steric congestion between the PⁱPr₂ side-arms and PPh₃ coligand (Figure I.6).

For palladium, the metallic center adapts a quasi-ideal square planar environment in both PMe₃ and PPh₃ complexes ($\tau_4 = 0.13$). The Pd^{II}-C distance was reported to vary only slightly from the parent C(sp³)-H complex (2.0738 Å) to the carbene complexes (2.0755 Å; Carbene-Pd-PPh₃ and 2.086 Å; Carbene-Pd-PMe₃). DFT calculations were conducted and an antibonding interaction between palladium and the central carbon was found as HOMO, reminiscent of the previous example of Le Floch and in accordance with the single-bond character of the Pd-C bond. This observation was further supported by NBO analysis with a Pd-C bond order of 0.89 and charges of -0.38 at carbon vs +0.23 at palladium. Overall, these data suggested that the bonding situation could be best described as a zwitterionic complex with a negative charge on the carbon and a positive charge on the metal. However, unlike the case of Le Floch, the pyramidal character of the carbene center was reduced, probably because of the π -delocalization offered by the phenyl spacers (Figure I.6). Unfortunately, no DFT calculations were reported on the nickel analog. In this chapter, it was represented in its zwitterionic form, in accordance with the reported reactivity.

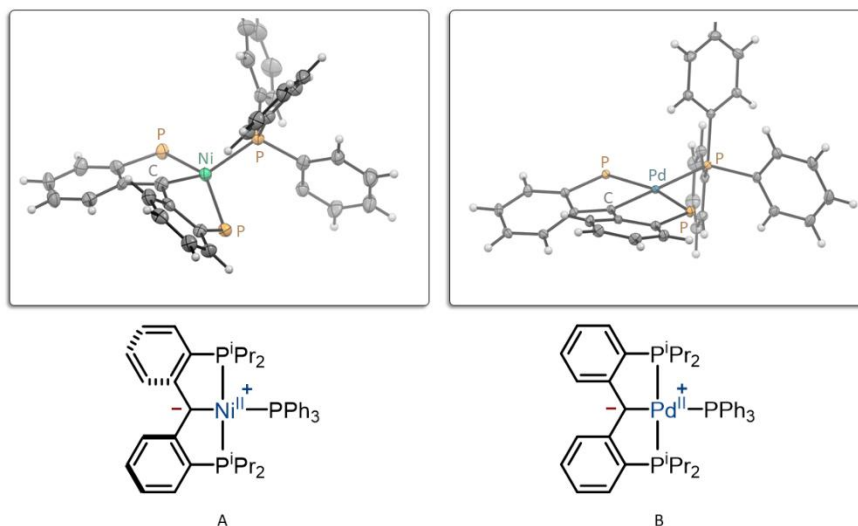


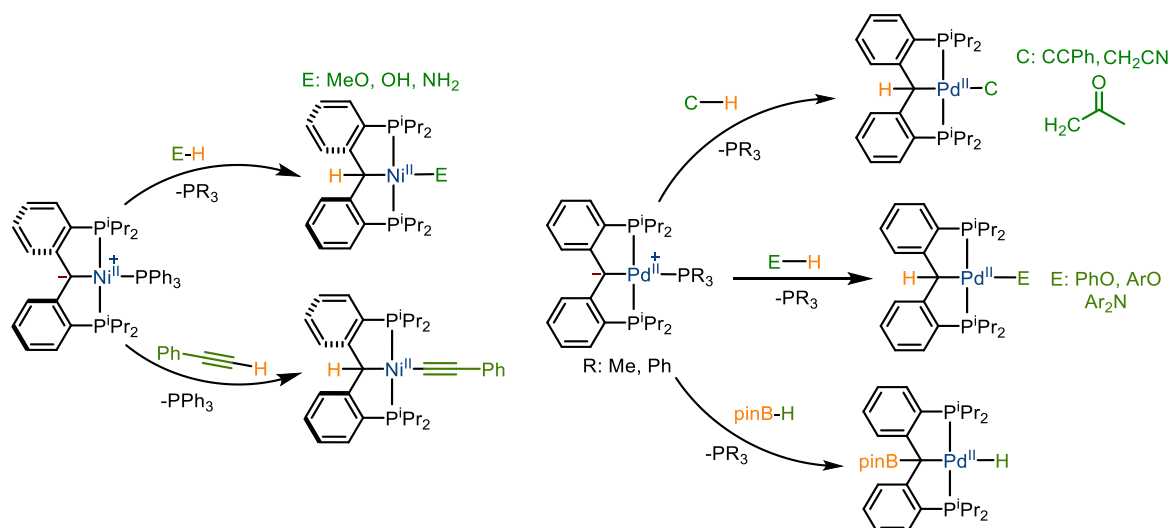
Figure I.6: A - XRD structure of Piers' Ni^{II} complex; B -XRD structure of Iluc's Pd^{II} complex; ⁱPr substituents at phosphorus were omitted for clarity

The bifunctional character of both complexes was illustrated by the authors through the activation of various E-H bonds (Scheme I.6).

In both cases, when the hydrogen has an acidic character (E = O, N, C), coordination of the E fragment to the metal was reported with addition of the proton to the carbene, in line with the charge distribution. In this area, O-H bonds such as in methanol were both activated by nickel and palladium.^[7-9]

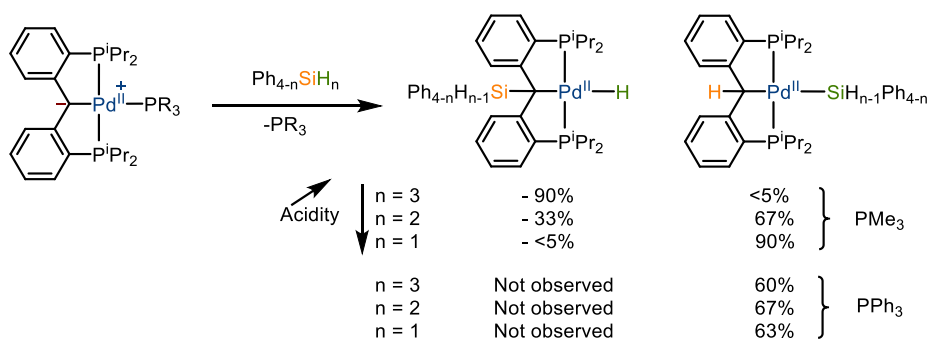
A divergence in reactivity of the two metals was reported with N-H and C-H bonds. While nickel was shown reactive towards ammonia, palladium was only reactive with the more acidic N-H bond of toluidine. With C-H bonds, phenylacetylene was activated by both complexes but this stoichiometric reactivity was extended to other bonds with pK_a < 29 (such as acetone or acetonitrile) with palladium only.^[10]

The "reversed" addition reaction (i.e incorporation of E at C_{carbene} and H at the metal) was reported by Iluc with pinacolborane. Formation of the palladium-hydride complex with addition of the boron onto the central carbon was described upon B-H activation. The high Lewis acidity of boron and the hydridic character of the hydrogen explains this reactivity.^[11]



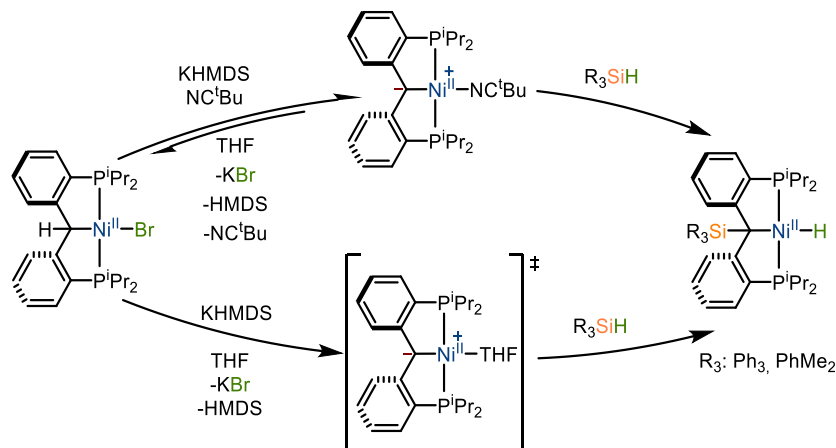
Scheme I.6: Reactivity of Piers' and Iluc's carbene complexes towards E-H bonds

At palladium, a breaking point in this reactivity inversion between E-H bonds was reached with E = Si (Scheme I.7). When treated with various silanes ($R_{4-n}SiH_n$), a critical impact of the substituents at silicon was reported. While the formation of the metal-silyl complex was favored with triphenylsilane ($n = 1$), the palladium-hydride was preferentially formed with phenylsilane ($n = 3$), and a mixture of both products were formed with diphenylsilane.^[11] This behavior was suggested by the authors to result from the different acidity of the silanes. Triphenylsilane, more acidic, would favor the protonation of the carbene compared to phenylsilane that would favor hydride formation. Furthermore, this reactivity inversion was only displayed by the Pd-PMe₃ carbene and not by the Pd-PPh₃ carbene. The higher nucleophilicity of the Pd-PPh₃ over the Pd-PMe₃ carbene (determined by the partial charges calculated by DFT $C_{(\text{Carbene-PPh}_3)} = 0.20$ $C_{(\text{Carbene-PMe}_3)} = 0.18$) was suggested to overcome the silane acidity difference with the exclusive formation of the metal-hydride complex.



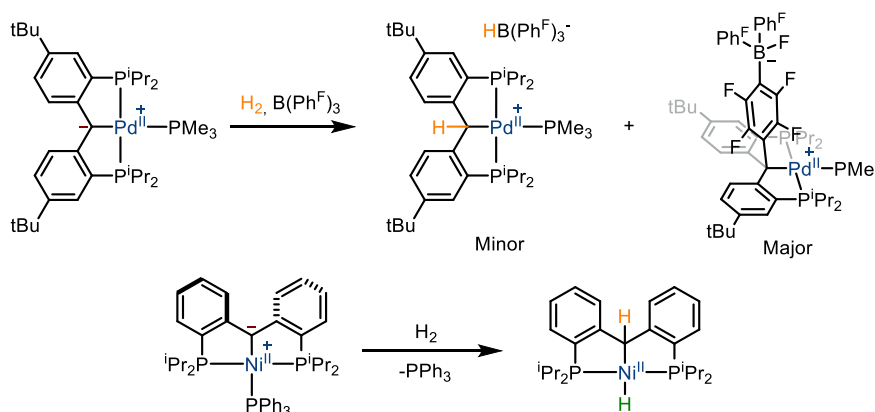
Scheme I.7: Product distribution for Si-H activation depending on the substituents at Si and P

In the case of nickel, Si-H activation with the PPh_3 coordinated carbene complex has not been reported, precluding the direct comparison between the two. Si-H activation was described however with nitrile or THF (from *in-situ* generated carbene) as coligand and in all cases, only the nickel hydride was reported even with Ph_3SiH (Scheme I.8).^[12]



Scheme I.8: Silane activation by Piers' $\text{Ni}^{\text{II}}\text{-THF}/\text{Ni}^{\text{II}}\text{-Nitrile}$ carbene complex

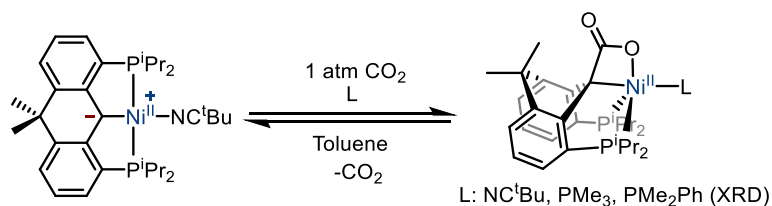
Remarkably, when treated with H_2 , divergent reactivities were observed for the two complexes (Scheme I.9). With palladium, an external Lewis acid (BCF) was required but was shown incompatible with the nucleophilic character of the carbene.^[13] In the case of nickel, H_2 activation across the C-Ni bond was proven possible and reversible. Indeed, D incorporation at the benzylic position was reported upon treatment of the $\text{CH-Ni}^{\text{II}}\text{-H}$ complex (from H_2 activation) with D_2 . To this day however, this system has not been applied in catalysis.^[8]



Scheme I.9: Top - H_2 activation by the association of Pd-carbene and BCF; Bottom - direct H_2 activation by the Ni-carbene complex

Interestingly, a more rigid ligand architecture was later reported by the group of Piers (Scheme I.10). This new scaffold was shown to react at the nucleophilic carbene center with

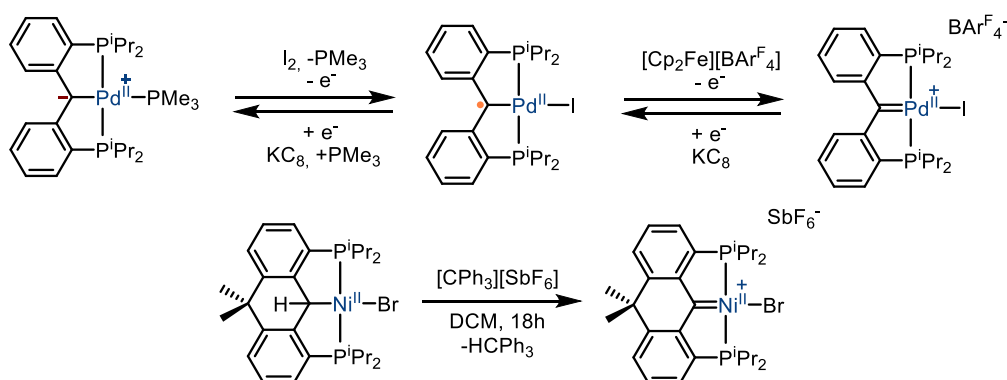
CO₂ forming the 4-membered metallactone. The binding of CO₂ was proven reversible (with ¹³CO₂ experiments and by submitting the metallactone to vacuum) but no catalytic activity was reported so far.^[14]



Scheme I.10: CO₂ activation and formation of metallactone with the Ni-Carbene of Piers.

In the previous examples, the cooperativity between a nucleophilic Schrock-type carbene and a group 10 transition metal was illustrated with stoichiometric reactions. The oxidation of such carbene complexes (for cooperative bond activation) was first studied by the group of Iluc with Pd^{II}. The successive one-electron oxidation of the carbene to the radical and cationic species was then reported (Scheme I.11).^[15] The reversibility of the reaction was also studied by Iluc in the reduction of the cationic species to the radical and the zwitterionic complexes.

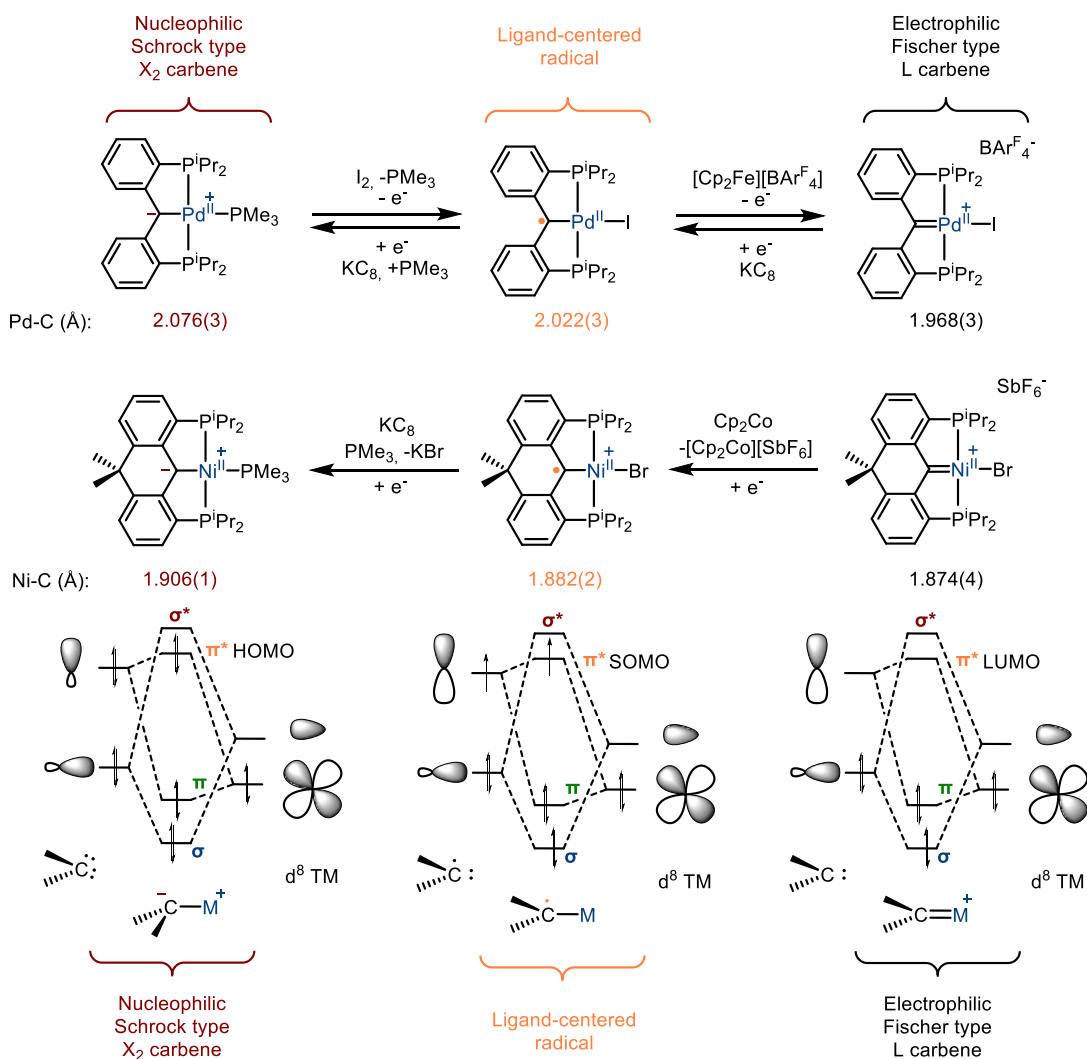
The Ni^{II} analog however was prepared by the group of Piers from hydride abstraction of the parent CH_{sp3}-Ni^{II}-Br and also studied towards one-electron reduction (Scheme I.11).^[16]



Scheme I.11: Two synthetic strategies for the generation of the Fischer carbene: By successive one-electron oxidation (Pd - Iluc) or by Hydride abstraction (Ni - Piers)

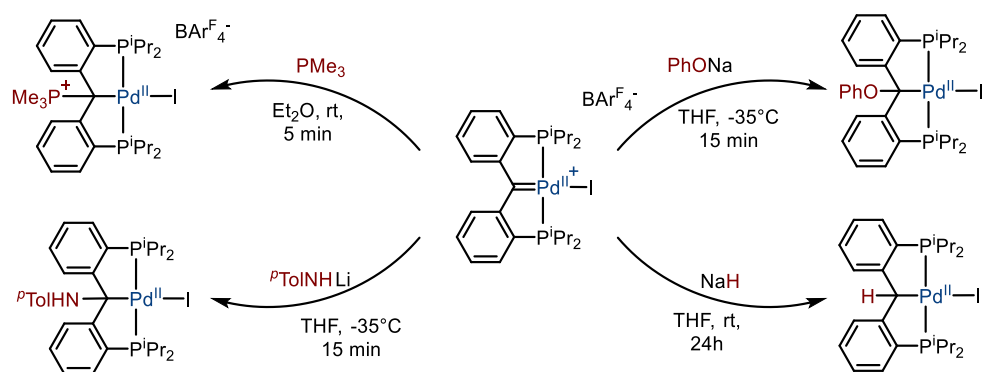
Reduction of the cationic Ni^{II}-carbene was reported to form successively the corresponding radical and the zwitterionic complex (Scheme I.12). Remarkably, the reduced, radical, and oxidized species were unambiguously characterized by X-ray diffraction studies in all cases for Pd^{II} and Ni^{II}. The bonding situation was analyzed by DFT calculations (and structures). Contraction of the Pd-C bond from 2.076(3) Å to 2.022(3) Å, and 1.968(3) Å was reported upon successive one-electron oxidations of the Pd complex (Scheme I.12).^[15] In the

case of nickel, the bond length was shortened from 1.906(1) Å in the reduced zwitterionic complex, to 1.882(2) Å in the radical species, to 1.874(4) Å in the cationic carbene complex.^[16] These reports were in accordance with the previous discussion on the bonding situation in these types of complexes (Figure I.4 and Scheme I.11). Contraction of the M-C bond would be the result of electron removal from the $\pi^*(M=C)$ orbital. These experimental observations were further supported by DFT calculations, revealing this antibonding π -interaction to be the Single-Occupied Molecular Orbital (SOMO) for the radical complex, and the LUMO for the cationic complex.



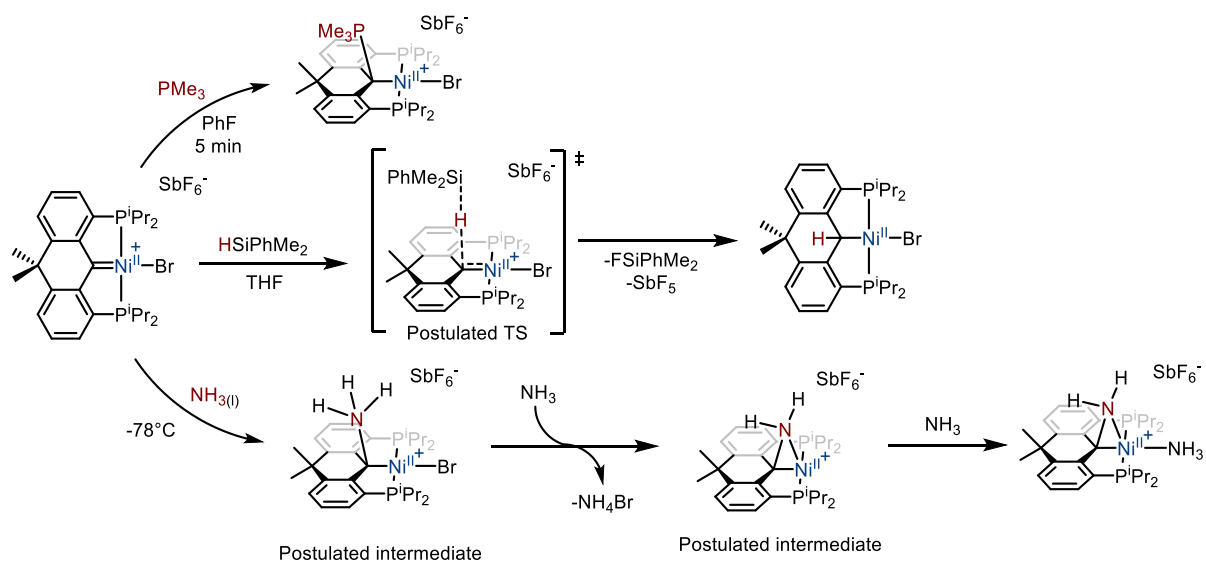
Scheme I.12: Bonding situations in the successive one electron oxidation/reduction of group 10 metal carbenes

According to this bonding scheme, an Umpolung reactivity was anticipated for the carbene center upon oxidation/reduction. While in the case of the zwitterionic complex, the carbene was shown to exhibit nucleophilic character, in the case of the cationic complex resulting from oxidation or hydride abstraction, an electrophilic behavior should be displayed by the carbene. This was experimentally confirmed in both cases by facile and rapid addition of PMe_3 to the carbene center (Scheme I.13 and Scheme I.14). While the electrophilic character of both complexes was highlighted through this experiment, their reactivity was shown divergent in several ways. In addition to PMe_3 , the palladium complex was shown only reactive towards strong nucleophiles such as sodium phenoxide/hydride or lithium *p*-toluidine (Scheme I.13).^[15]



Scheme I.13: Electrophilic character of the $2e^-$ oxidized Pd-carbene complex developed by Iluc

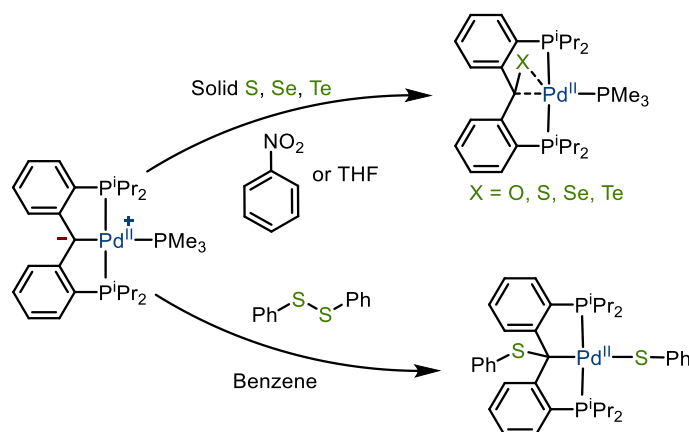
In contrast, the nickel complex was reported to react with milder hydride sources such as PhMe_2SiH as well as with NH_3 (Scheme I.14).^[16]



Scheme I.14: Electrophilic character of the $2e^-$ oxidized Ni-carbene complex developed by Piers

Recently, a similar successive one-electron removal process has been reported for the platinum analog but no reactivity has been reported yet.^[17]

Later, the behavior of the reduced Pd^{II} carbene towards various chalcogens was studied (O, S, Se, Te). Formation of the corresponding chalcogenoketones upon oxidation was reported (Scheme I.15).^[18] While direct oxidation of the carbene with O₂ was unsuccessful, the corresponding ketone was quantitatively formed with nitrobenzene. With the heavier congeners (S, Se and Te), the formation of the chalcogenoketone was reported upon reaction with the elemental chalcogen in THF. The bonding situation of the products is interesting. Here, the C-Chalcogen has a partial double bond character, and the Pd-C bond was partially broken, resulting in a bonding situation somewhere in between the side-on η²-chalcogenoketone bonded to palladium and the metallacycle. The direct oxidation of the carbene complex with 1 equivalent of diphenyldisulfide, in the absence of nitrobenzene was also reported leading to the carbene oxidation and formation of a Pd^{II}-S bond.



Scheme I.15: Oxidation of Iluc's Pd^{II}-carbene to chalcogenoketones with nitrobenzene and group 16 elements, and oxidation with diphenyldisulfide

In 2019, the group of Gessner reported the synthesis a PC_{carbene}S Pincer ligand combining on one side the thiophosphoryl arm, similar to Le Floch and on the other side the phenylphosphine arm, analogous to Iluc (Figure I.7).^[19]

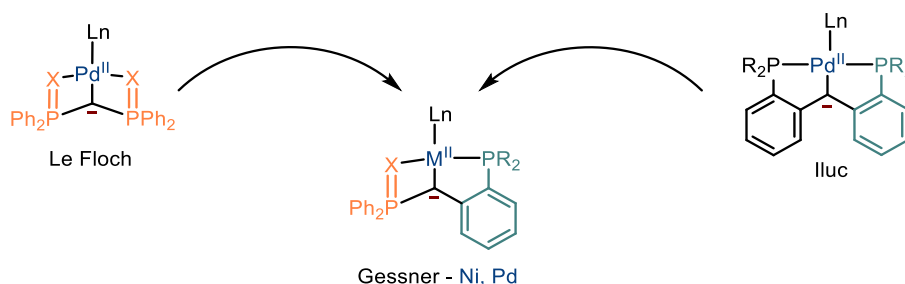
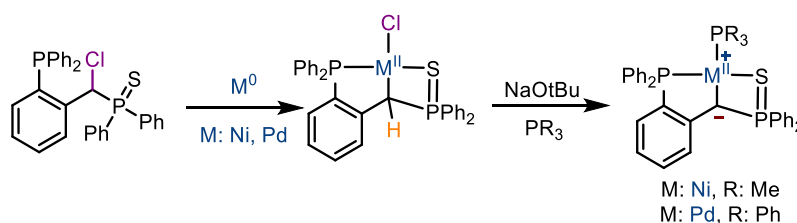


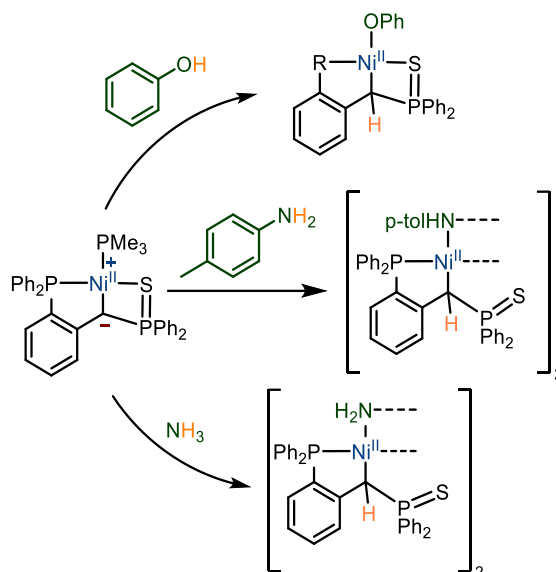
Figure I.7: Gessner's approach merging Le Floch and Iluc's ligand design

The Pd^{II} and Ni^{II} complexes were prepared by treatment of the corresponding M⁰ with the halogenated proligand (Scheme I.16). Finally, the carbene complex was formed by deprotonation with sodium tert-butoxide in presence of a phosphine ligand. Notably, compared to the example of Le Floch, the pyramidalization of the carbon was diminished by the increased π -delocalization offered by the presence of conjugated phenyl substituents.



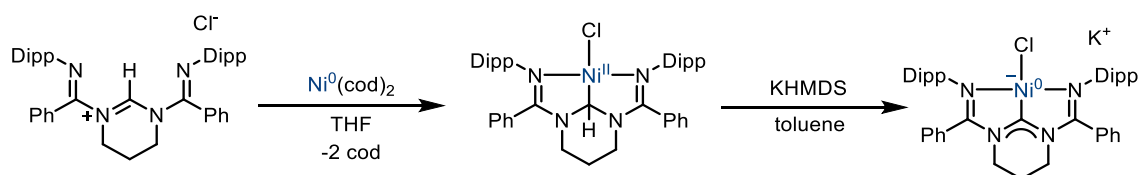
Scheme I.16: Synthesis of the PCS-Pd carbene complex by the group of Gessner

Interestingly, no clear reactivity on the activation of E-H and H-H bond was demonstrated with the palladium complex whereas incorporation of the proton on the C_{carbene} and formation of the corresponding Ni-E bond was reported for the Ni-analog (Scheme I.17). Remarkably, similarly to the NCN-Pt complex of Cavell with the pendant phosphazene (see (a) §2), the thiophosphinoyl arms was reported to be only weakly coordinated to nickel, favoring S-decoordination and N-bridging dimerization upon treatment with N-H pro-nucleophiles. One explanation for this observation could result from the HSAB theory with a hard Ni^{II} center favoring N-Ni^{II} interaction rather than soft S-Ni^{II}.



Scheme I.17: E-H bond activation with the PCS-Ni^{II} complex of Gessner with dimerization in the case of N-nucleophiles

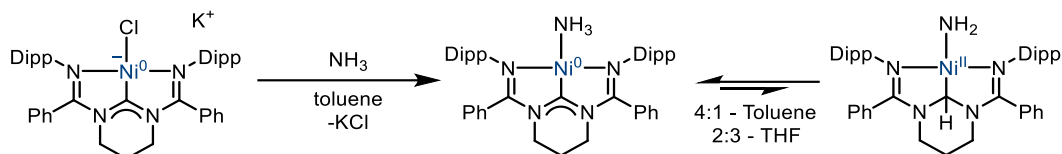
In all the previous examples, the electron density at the carbene was stabilized by the presence in α -position of a phosphazene/thiophosphoryl groups and/or aryl substituents. Another class of stabilized carbenes, NHCs, well-known and widely used in transition metal chemistry as ligands have been scarcely found to engage into cooperative bond activation. In this area, a rare and first contribution with nickel was reported in 2015 by Roesler (Scheme I.18).^[20] The synthesis of the Ni^{II} complex was achieved by treatment of the corresponding pyrimidinium salt with Ni⁰(cod). The resulting complex was then deprotonated and reduced with KHMDS to yield the anionic NHC-Ni⁰-Cl.



Scheme I.18: Synthesis of an anionic Ni⁰-NHC complex by deprotonation and reduction of the CH-Ni^{II}-Cl

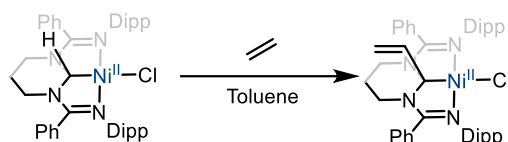
When submitted to NH₃ gas at atmospheric pressure in toluene or THF, two products formed (Scheme I.19): the Ni⁰-NH₃ complex resulting from the substitution of halide by ammonia and the product of ligand-assisted NH₃ activation. The two products were characterized spectroscopically in solution, but their X-ray structure was not reported. Notably, the two forms were found to be in equilibrium, the position of which depended on

the solvent. A four to one ratio of Ni⁰ to Ni^{II} product was reported in the less polar toluene, while a two to three ratio was found in THF.



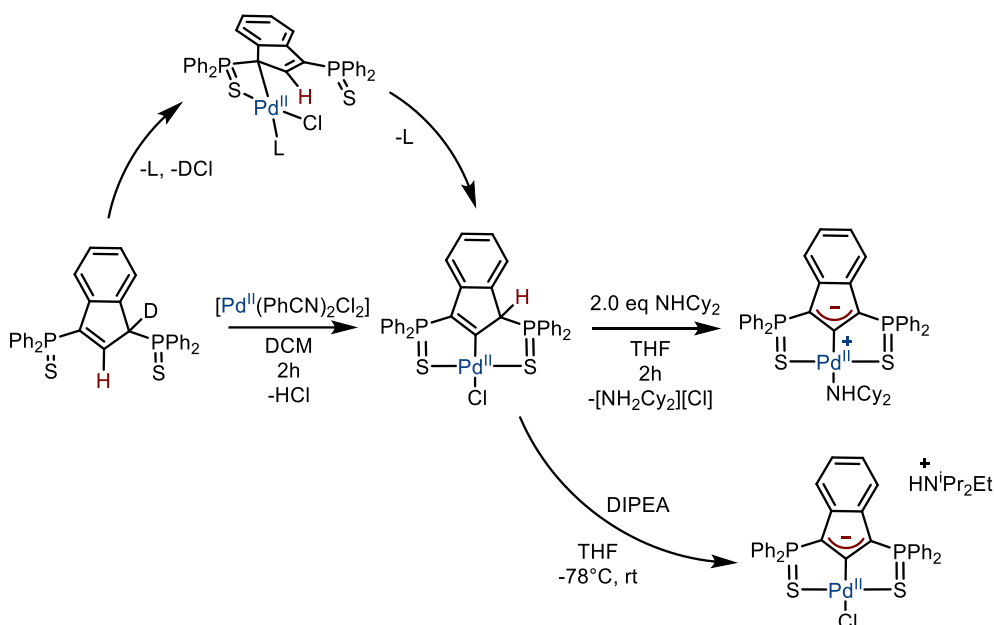
Scheme I.19: NHC-assisted N-H bond activation and solvent dependent equilibrium

This first example of N-H activation at NHC with nickel complexes has not been further developed to this day. But another interesting reactivity was reported two years later in 2017 (Scheme I.20).^[21] In this example, the previously described NHC-Ni^{II}-Cl complex, prior to deprotonation, was reported to undergo ethylene insertion at the C_{sp3}. Unfortunately, the mechanism of this interesting transformation has not been elucidated yet.

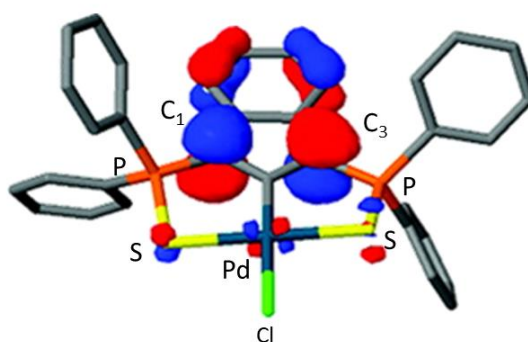


Scheme I.20: Ethylene insertion at the NHC moiety of an NCN-Ni^{II} pincer complex

In 2009, an original system based on the in-plane coordination of an indenyl scaffold was reported by our group (Scheme I.21).^[22] In this case, the synthesis was achieved by coordination of the thiophosfinoyl indene derivative to a Pd^{II} source forming the in-plane coordinated 2-indenyl complex. Deprotonation and generation of a chloropalladate complex was achieved with diisopropylethylamine.^[23] In addition, deprotonation and substitution of the chloride could be performed with 2 equivalents of N,N-dicyclohexylamine. This example of original coordination mode of an indene moiety to palladium, was even more noteworthy from a mechanistic point of view (Scheme I.21). Indeed, a direct C-H activation occurring at the C₂ of indene would be intuitively expected (reminiscent of the previous strategies by C-H activation to prepare aryl based pincer complexes). However, D labeling experiment revealed that C-H activation at the most acidic C₁ position occurred first followed by palladium migration to yield the net product of C-H activation at the C₂ position with no D at C₁.^[23]

Scheme I.21: Synthesis and coordination mechanism of the SCS-Pd^{II} complex

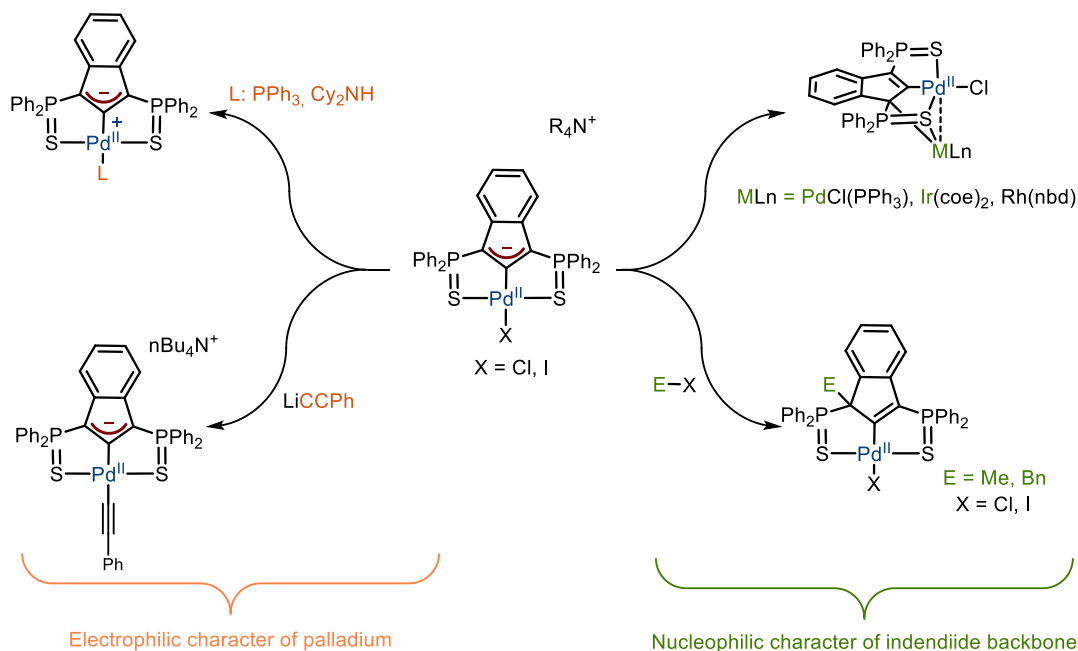
A strong covalent σ -bond between C₂ and palladium, with little to no π -bond was indicated by experimental spectroscopic data reinforced by DFT calculations. The experimental Pd-C distance of 1.984 Å, closely matched the calculated distance of 1.97 Å indicative of single-bond character. Overall, this complex was best described with a negative charge delocalized on the carbons of C₁ and C₃ and a C₂-Pd single bond (See HOMO - Scheme I.22).



Scheme I.22: Representation of the HOMO showing the delocalized charge at the C1 and C3 positions

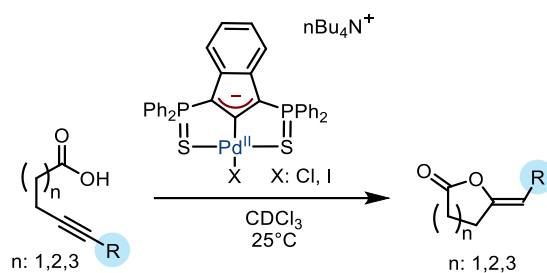
Experimentally, the bifunctional character of the complex was first evidenced by treatment with organic electrophiles such as MeI or BnCl, forming the products of backbone alkylation in accordance with the nucleophilic character of C₁ and C₃ (Scheme I.23).^[24] Interestingly, inorganic electrophiles (Pd, Ir, Rh) were also compatible partners and formed the corresponding (hetero)-bimetallic complexes.^[25] On the other hand, the electrophilic

character of the palladium center was retained allowing for the preparation of a rare example of an alkynyl palladate complex.



Scheme I.23: Evidencing the bifunctional character of the Indenediide-Pd complex

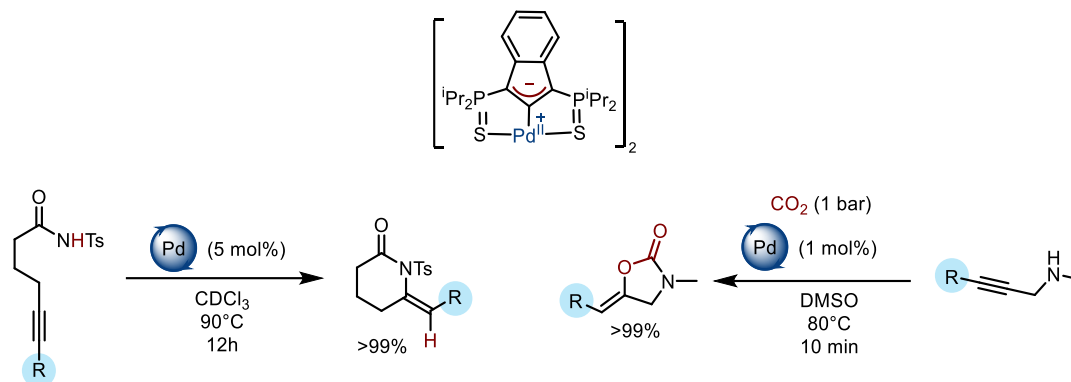
The catalytic relevance of this system was first established by our group in 2014, with the cycloisomerization of alkynoic acids (Scheme I.24).^[26] A broad substrate scope and a high-selectivity was displayed with ring sizes variation from 5 to 7 with terminal and internal alkynes in the absence of external base.



Scheme I.24: Cycloisomerization of alkynoic acids with the non-innocent SCS-Pd^{II} complex

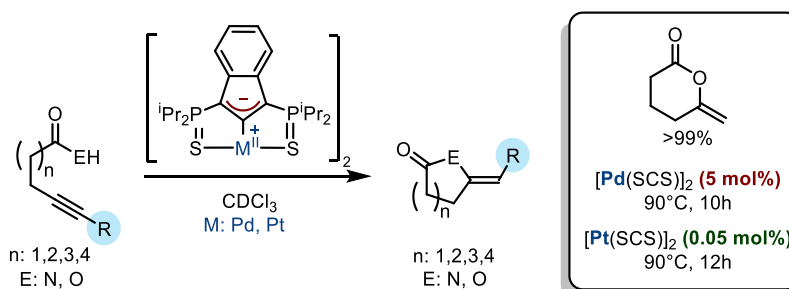
Unfortunately, the use of harsher reaction conditions was not possible as thermolysis of an intermediate was reported upon prolonged heating. The development of a second generation of catalysts was then achieved by substitution of the phenyl substituents at phosphorus for ⁱPr. Furthermore, upon deprotonation with ^tBuOK, the formation of a head-to-tail dimeric structure was observed. With this complex, cycloisomerization reactions were

extended to previously inaccessible lactones, N-H bonds with lactams, and even a cascade combining CO₂ capture and cyclization (Scheme I.25).^{[27],[28]}



Scheme I.25: IInd generation of SCS-catalyst, unlocking more challenging transformations

Interestingly,^a a drastic increase in reactivity was reported upon variation of the metal center from Pd^{II} to Pt^{II} (Scheme I.26).^[29] While a broad substrate scope was exhibited by both systems, the ring size could be increased to the notoriously challenging 6,7-membered rings with the Pt^{II} complex. As a representative example, the 6-membered lactone was formed in >99% yield by both complexes but a catalytic loading a hundred-fold less was required for the platinum version (0.05 mol%) compared to the palladium complex (5 mol%).

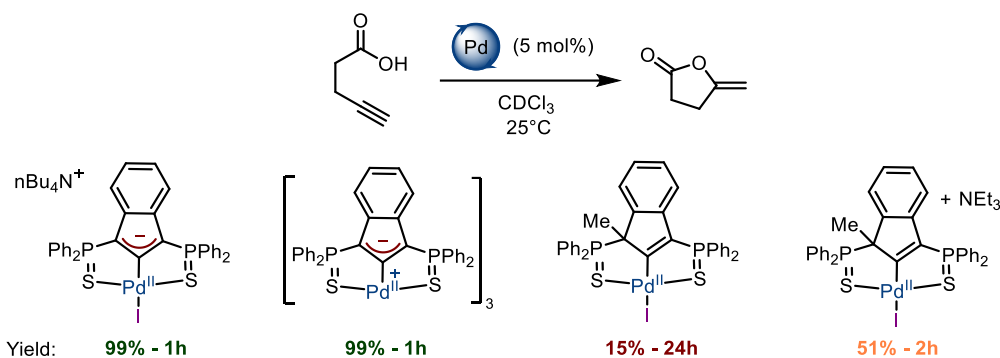


Scheme I.26: Cycloisomerization reactions catalyzed by the SCS-Pt^{II} complex and reactivity comparison

The non-innocent character of the backbone in these transformations was supported by the comparison with methylated versions of the complex (Scheme I.27). In this case, drastically decreased catalytic activities were observed even after addition of an external

^a No reactivity in the cascade CO₂ capture and cyclisation was observed with the Pt^{II} complexes due to strong interaction between DMSO and the complex.

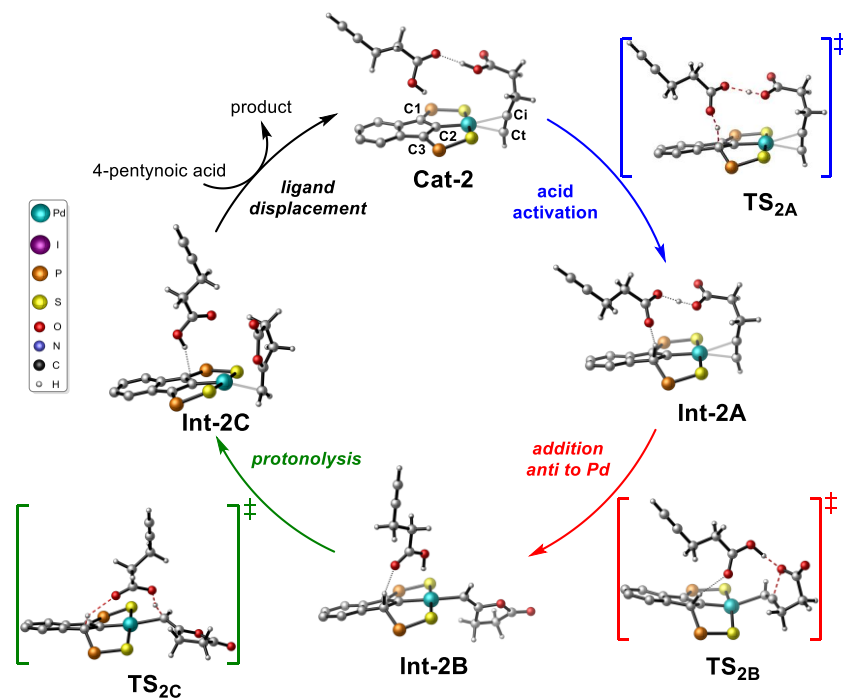
base, suggesting a synergistic effect of the basic site and the electrophilic Pd^{II} within the same structure.



Scheme I.27: Comparison of the catalytic activities for the cycloisomerization of pentynoic acid

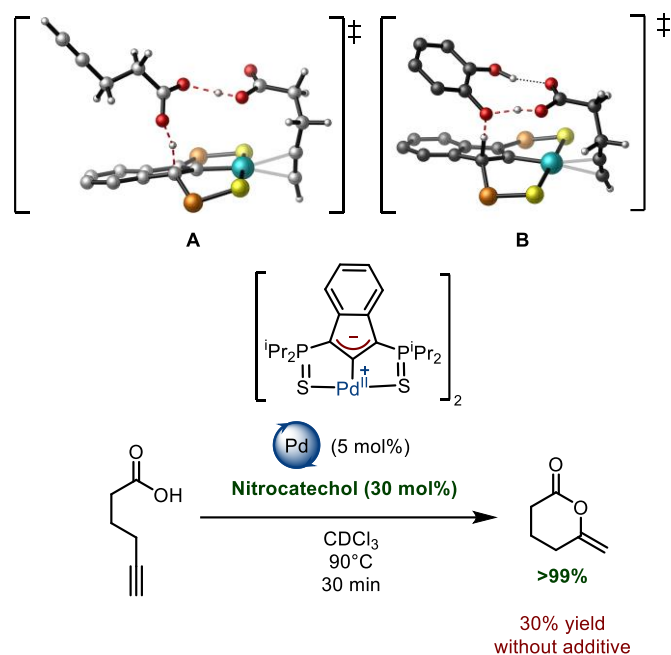
Thorough mechanistic studies were then conducted by our group and the involvement of two substrate molecules within the catalytic cycle was revealed by kinetic studies.^[30] The role of this second molecule was proposed as a proton-shuttle in the deprotonation and protodepalladation step (Scheme I.28). This was further supported by DFT calculations performed in collaboration with L. Maron.

Indeed, the catalytic cycle is proposed to start with π -coordination of the alkyne to yield **Cat-2** (Scheme I.28). Then, a substrate-assisted acid activation by the ligand backbone occurs through **TS_{2A}** to yield **Int-2A**. The addition of the carboxylate *anti* to palladium then takes place forming **Int-2B**. Finally, an acid-assisted protodepalladation generates the corresponding lactone and after ligand displacement by an alkynoic acid, the cycle repeats.



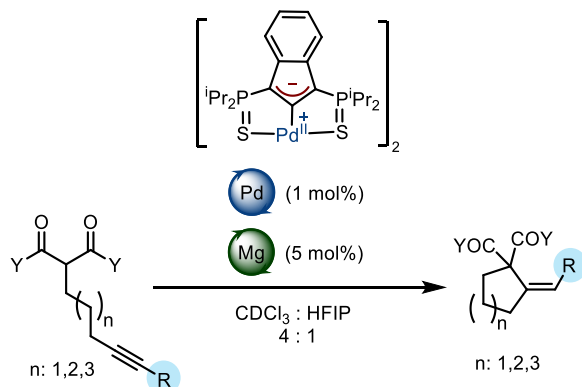
Scheme 1.28: Catalytic cycle of the cycloisomerization of alkynoic acids catalyzed by the chemically non-innocent SCS-Pd complex; Reproduced from Ref ^[30] with permission from the Royal Society of Chemistry.

Based on these results, the use of adapted proton shuttling additives such as catechols boosted the catalytic potential of this non-innocent system (Scheme 1.29). Indeed, after 30 minutes at 90°C, 30% of hexynoic acid was converted to the corresponding lactone, while in the presence of 30% of catechol, 99% yield was observed.



Scheme I.29: A - Calculated transition state of the substrate-assisted deprotonation event; B - Calculated transition state for the catechol-assisted deprotonation; Reactivity comparison with and without proton-shuttling additive

Recently, this approach was extended further with the combined use of MLC, H-bonding additives and an external Lewis Acid as a multi-cooperative catalytic system in the Conia-ene reaction (Scheme I.30).^[31] This work was performed during my PhD and will be developed further in Chapter II. The relevance of this tool was highlighted by an unusually broad substrate scope and the complementary selectivity towards internal alkynes compared to previous reports. In this case, the mode of action of the complex with π -activation by Pd^{II} was suggested to play a crucial role in the selective formation of the more sterically demanding Z-alkenes.



Scheme I.30: Multi-cooperative catalytic system for Conia-ene type cycloisomerization

In previous examples, the bond/substrate activation involve the group 10 metal and a non-innocent carbene moiety. Heavier analogs, silylenes and germynes, are also relevant and competent in MLC they will be presented hereafter starting from the contribution of Driess with two flanking silylenes coordinated to a Ni^0 center. Then, the example with a central germylene coordinated to Pd^0 of Cabeza will be discussed.

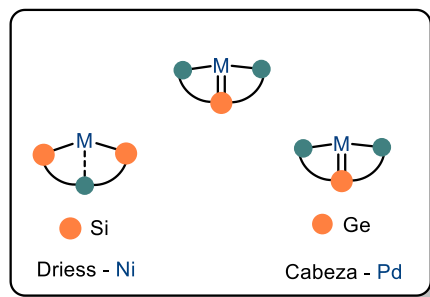
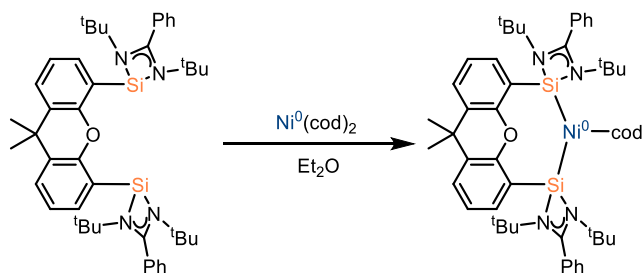


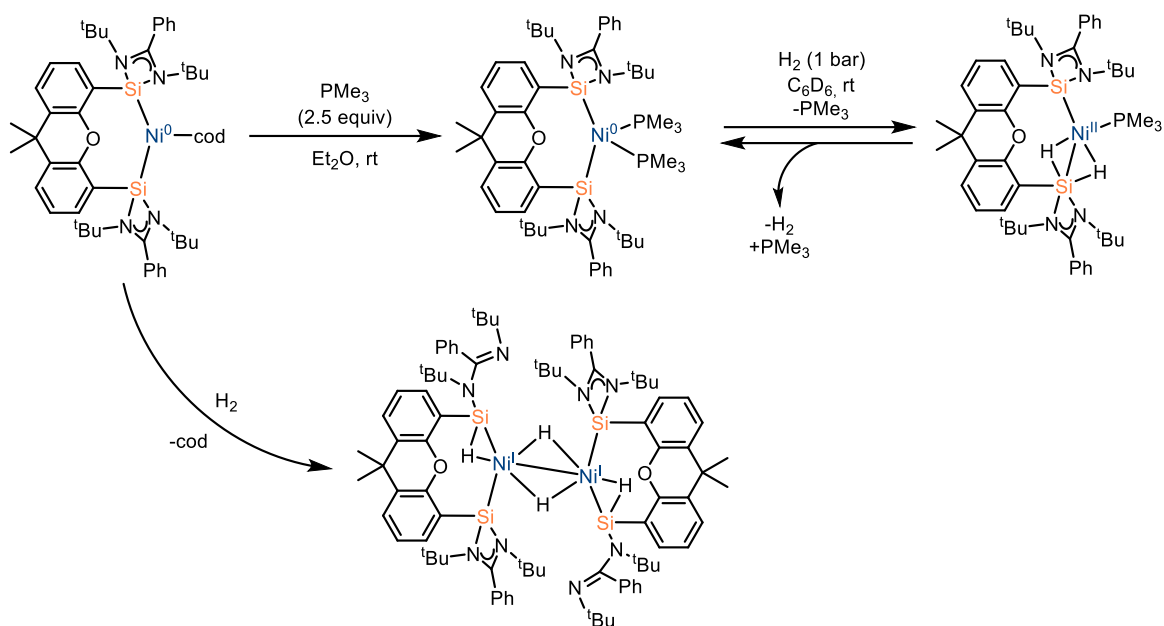
Figure I.8: Overview of the carbene analogs for MLC

The ligand design of Driess features two chelating silylene centers with a xantheno spacer.^[32] The complex was synthesized by reaction of the corresponding proligand and a Ni^0 source (Scheme I.31).



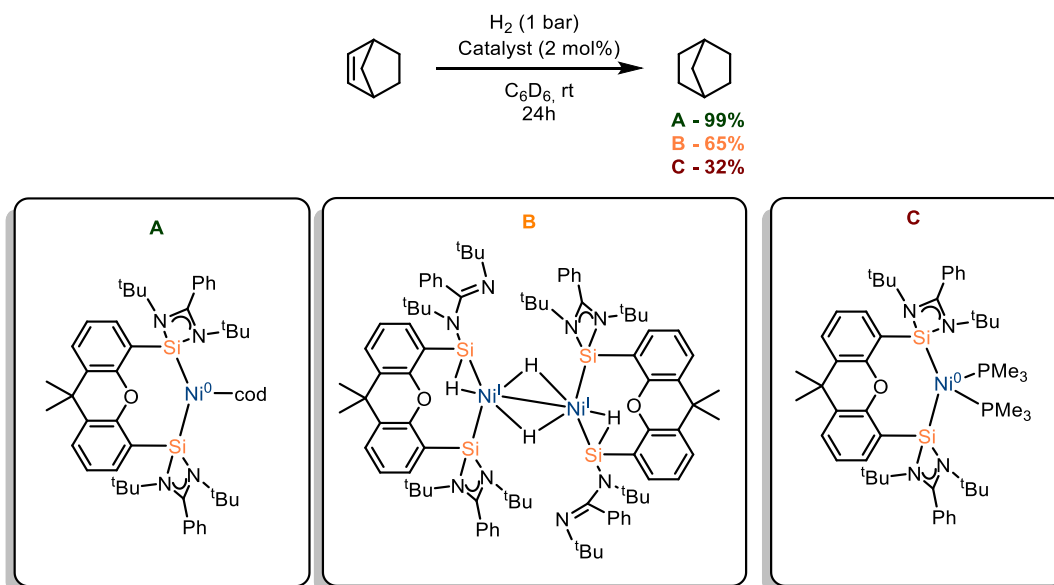
Scheme I.31: Synthesis of the Bis-silylene Ni^0 complex of Driess

Cod substitution by PMe_3 was reported upon treatment with 2.5 equivalents of the phosphine (Scheme I.32). Interestingly, when submitted to H_2 , oxidative addition was reported with the formation of a rare Ni^{II} -dihydrido complex. Significant Si-H bonding and a rapid exchange between the Si centers was suggested by NMR analysis highlighting the role of both Si-centers in stabilization of this complex. Interestingly, upon H_2 removal and degassing, the Ni^0 - $(\text{PMe}_3)_2$ complex was regenerated albeit with a low yield (29%) suggesting a reversible H_2 activation process. Remarkably, when the Ni^0 -cod complex was treated with H_2 the formation of cyclooctene and further evolution to cyclooctane was observed. The formation of a dimeric Ni^{I} species was described after cod hydrogenation.



Scheme I.32: Reactivity of Silylene-Ni⁰ complexes with H₂ and chemical non-innocence of the silylene fragment

The activity of these complexes in hydrogenation of alkenes was already suggested by the rapid formation of the Ni-dimer and cyclooctane. Norbornene was then chosen by the authors. The highest activity was reported for the Ni⁰-(cod) complex, and 29 alkenes were hydrogenated with this system while a decreased activity was shown by the two other complexes (Scheme I.33).



Scheme I.33: Catalytic activities of the various complexes towards hydrogenation of alkenes

Mechanistic studies were then conducted by DFT calculations supporting the non-innocence of the silylene ligands (Figure I.9). The starting point was chosen with a Ni⁰-ethylene

complex. A first exergonic step of H₂ coordination occurs (Figure I.9; B and C) followed by H₂ activation with stabilization by Si (Figure I.9; D). Then, migratory insertion of ethylene into the Ni-H bond (Figure I.9; E) takes place, followed by isomerization into F. Further isomerization prior to ethylene coordination occurs (Figure I.9; G and H) and the complex undergoes reductive elimination with concomitant formation of ethane and regeneration of the starting Ni⁰-ethylene complex. In this case, the role of the silylene ligand in stabilization of the Ni^{II} hydride was clearly depicted through intermediate C, D and E.

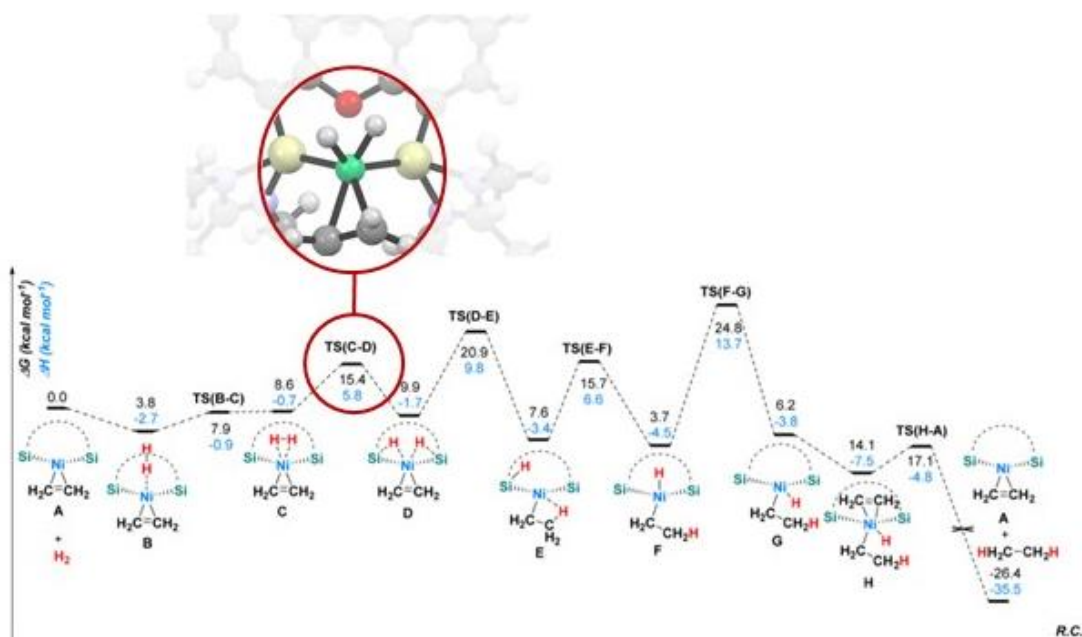
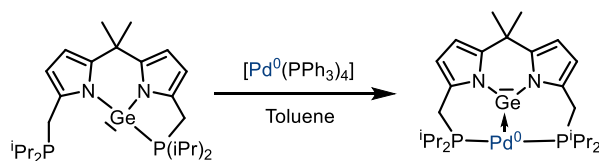


Figure I.9: Mechanistic pathway calculated by DFT for the hydrogenation of ethylene by the silylene Ni⁰ complex - Adapted with permission from J. Am. Chem. Soc. 2017, 139, 13499–13506. Copyright 2017 American Chemical Society.

While the previous example was focused on nickel, with a ligand design bearing lateral silylene ligands, a relevant example with palladium and a central germylene was reported by Cabeza.^[33] In this case, a P-Ge-P proligand was subjected to Pd⁰ precursor and formation a T-shaped complex was reported based on NMR spectroscopy and DFT calculations (Scheme I.34).



Scheme I.34: T-shaped Pd⁰ complex synthesis by Cabeza

A remarkable bonding situation was delineated by DFT calculations and NBO analysis. In this case, the Pd^0 was shown to donate electron density to the empty p orbital at germanium, while the lone pair of the germylene was involved in an antibonding π^* -orbital (Figure I.10), resulting overall in a reversed situation compared to classical carbene complexes.

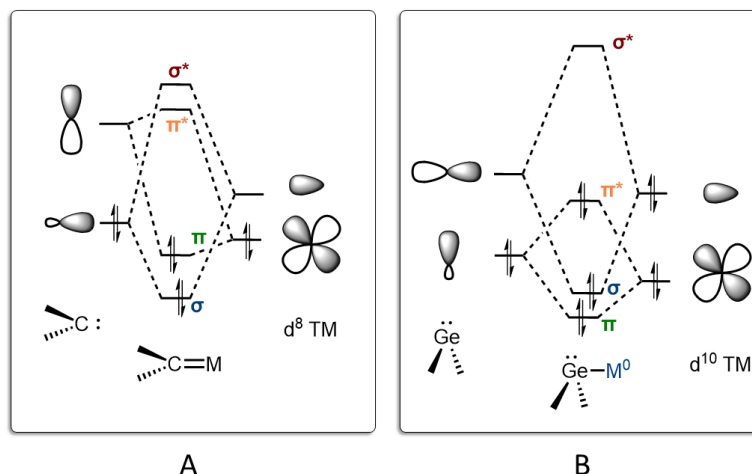
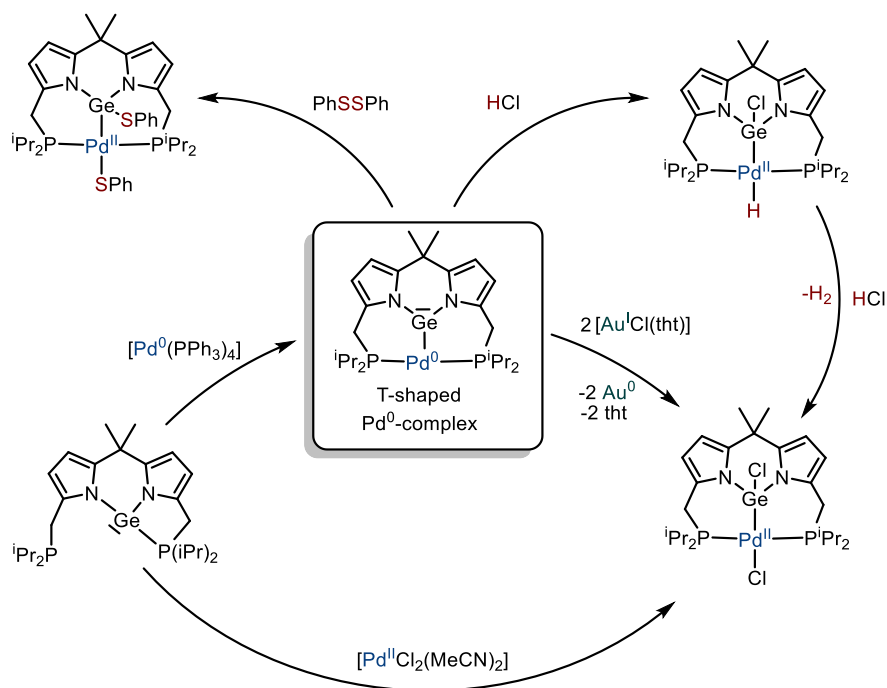


Figure I.10: A - Bonding situation in carbene complexes with d^8 metals - B bonding situation with a bent-germylene and d^{10} metal

When treated with the Au^{I} source $[\text{Au}^{\text{I}}\text{Cl}(\text{tht})]$, formation of Au^0 with oxidation of both the germylene and palladium was observed (Scheme I.35). Interestingly, when the Pd^0 complex was reacted with HCl , formation of a $\text{Pd}^{\text{II}}\text{-H}$ and Ge-Cl was reported. Overall, an “Umpolung” character of this complex was suggested by these results, with a Lewis-acidic center at Germanium but in accordance with the electronic situation depicted in **B** (Figure I.10).

When further treated with HCl , dihydrogen evolution occurs, and formation of the $\text{GeCl-Pd}^{\text{II}}\text{-Cl}$ complex was reported. It is interesting to note that this complex was also obtained by direct treatment of the germylene ligand with $\text{Pd}^{\text{II}}\text{-Cl}_2$ source. Other oxidants like diphenyl disulfide were probed and incorporation of both fragments at Ge and Pd were observed, reminiscent of the reactivity described by Iluc (Scheme I.15).^[18]

Scheme I.35: Synthesis of Germylene-Pd⁰ complex by Cabeza and reactivity

b) M-X type pincer complexes for cooperative bond activation

In the previous examples, the chemically non-innocent character of a remote or directly bonded carbene-type center was exploited. In the following section, examples involving a group 15-16 heteroatom directly bonded to the metal will be presented by first studying the historical example of Sellman with sulfur and the updated version of Liu with oxygen. Afterwards, non-innocent nitrogen-containing pincer complexes will be discussed with the major contributions of Schneider, Caulton and Ozerov.

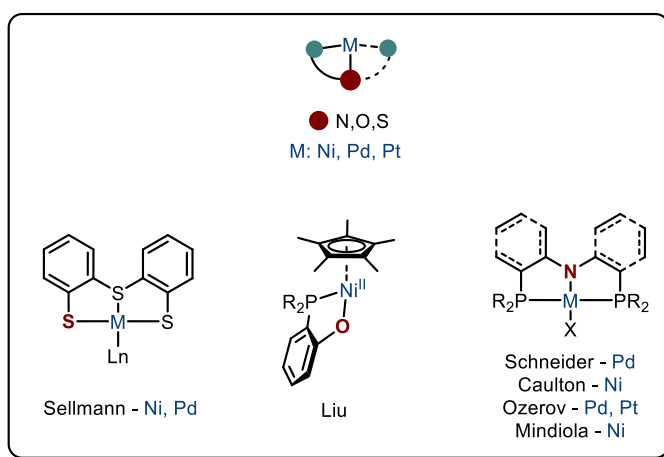
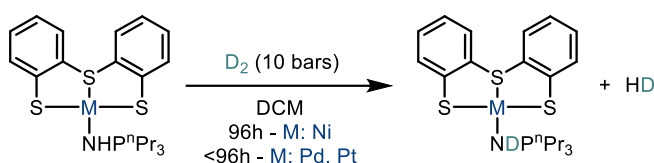


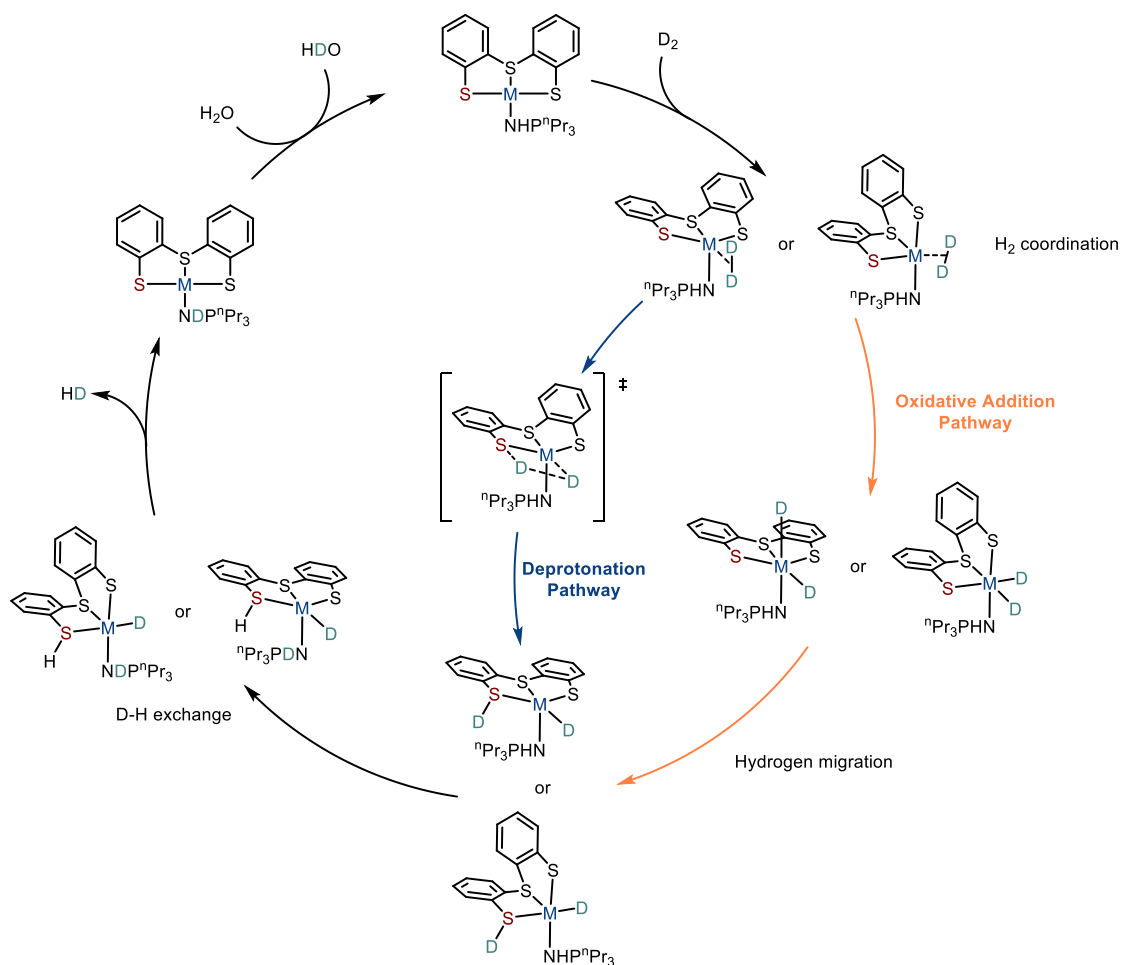
Figure I.11: Group 15-16 heteroatom tethered non-innocent complexes of group 10 metals

The cooperativity between a heteroatom and a group-10 metal pincer complex was first unveiled by Sellmann in 2000 in an attempt to model the notorious [NiFe] hydrogenase.^[34] In the biological system, the Ni-S cluster was proposed to play a redox non-innocent role. In the well-defined organometallic complex however, the role of the sulfur center was indicated as chemically non-innocent in H₂ and D₂ activation. To probe this behavior, the complex was treated with ten bars of D₂, and incorporation of deuterium at the phosphazene and formation of HD was slowly (96h with nickel!) detected by ¹H NMR analysis (Scheme I.36). While the palladium and platinum complexes were reported more active, no definitive number was disclosed in the original report.



Scheme I.36: D₂ activation by M-S cooperativity

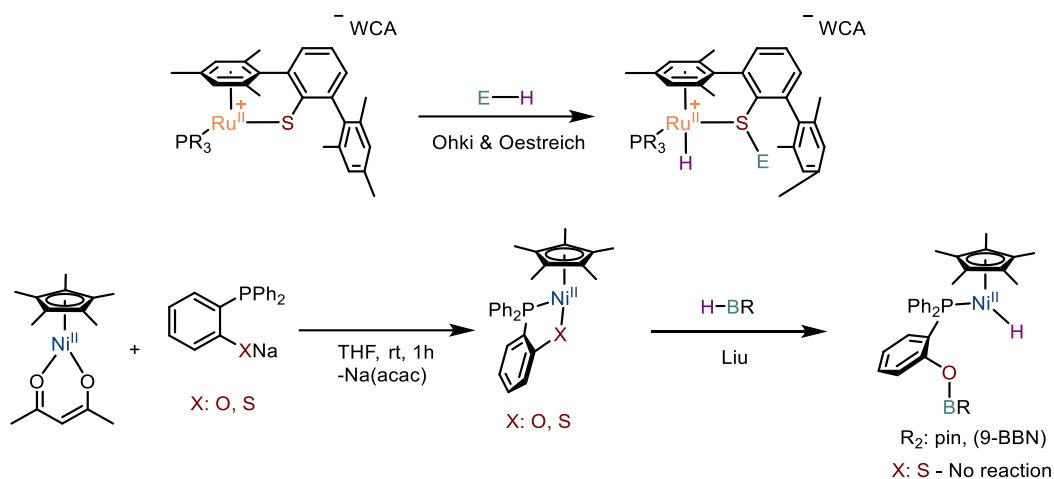
The mode of action of the complexes was proposed in 2005 by De Gioia through DFT calculations. Slightly different behaviors were reported for palladium and nickel (Scheme I.37).^[35] In the first step of H₂ coordination, a strong accommodation and reorganization of the ligand was necessary and in both cases, this initial step was shown endergonic. The strength of the H₂ bonding in organometallic complexes depends on two factors: The strength of the interaction between the σ -bond of H₂ and the transition metal, and the amount of π -backdonation from to metal into the σ^* -bond of H₂. In the case of palladium, the first interaction was found stronger with less backdonation compared to nickel. In terms of mechanism, this was translated with nickel, by a preferred oxidative addition pathway due to stronger Ni^{II}->H₂ backdonation. On the contrary, with palladium, the stronger H₂->Pd^{II} donation resulted in an exacerbated H₂ acidity and a more facile deprotonation by the thiolate, resulting in both pathways being accessible *in silico*.



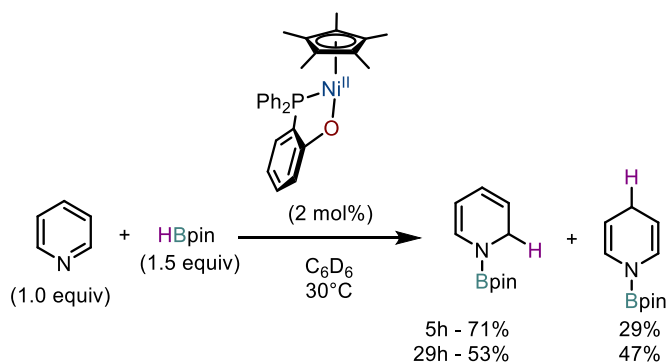
Scheme I.37: Calculated mechanism of H₂ activation by S₃-Ni/Pd complexes – Orange oxidative addition pathway preferred for Ni^{II} - Blue deprotonation and oxidative addition pathways were found reasonable for Pd^{II}

It is interesting to note that while the “FLP-like” cooperativity between a thiophenolate and a Lewis-acidic transition-metal was extensively studied with Ru by Oestreich, this remains, to date, the only example of Pd^{II}-S cooperativity (examples of M-S cooperativity will be further presented in Chapter 4; Scheme I.38).^[36,37]

Remarkably, thiophenolate and phenolate complexes were recently reported by Liu with Ni^{II}.^[38] The synthesis of the complexes was readily achieved by treatment of Cp*Ni(acac) with the corresponding sodium salt of the *o*-phenyl-phosphine-chalcogen (Scheme I.38). While both complexes were probed for heterolytic B-H bond activation (with HBpin and (9-BBN)₂) only the Ni-O complex was shown effective with incorporation of the hydride on nickel and formation of an oxygen-stabilized borane.

Scheme I.38: Ohki Ru-S complex and Liu's approach with Ni^{II}

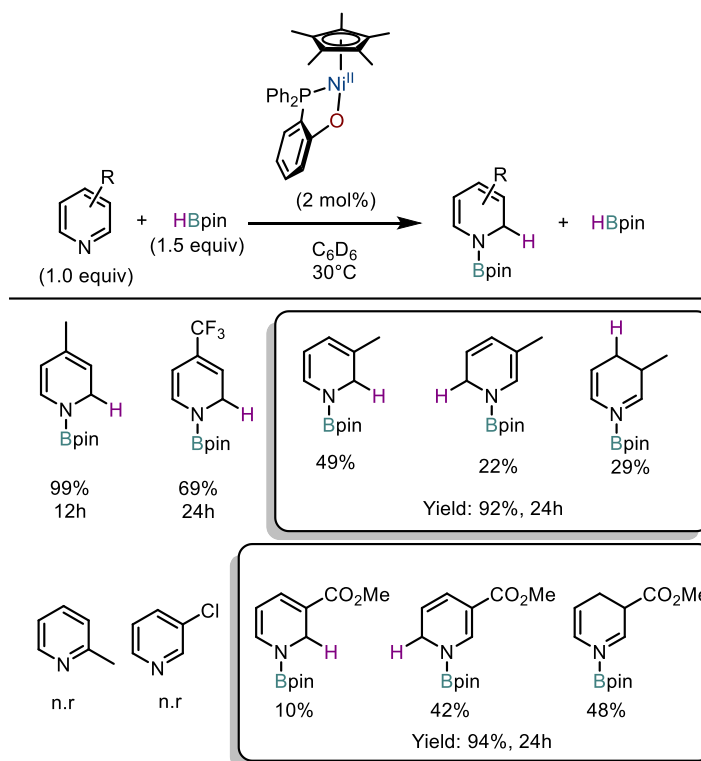
This result was explained by the authors through the higher polarity of the Ni-O bond (and the thermodynamic advantage of the B-O bond) and was further confirmed by DFT calculations. In the case of Ni-S, the heterolytic B-H bond splitting was found endergonic (25.3 kcal.mol⁻¹ for HBpin and 13.3 kcal.mol⁻¹ for (9-BBN)₂) while in the case of Ni-O, this activation was found exergonic (-2.2 kcal.mol⁻¹ for HBpin and -9.5 kcal.mol⁻¹ for (9-BBN)₂). Interestingly, this cooperative system was even amenable to catalysis, in the hydroboration of pyridine (Scheme I.39). After 5h, all the pyridine was converted into a mixture of N-borylated 1,2 and 1,4-dihydropyridines. While the 1,2- product was reported largely majoritary after 5h, an approximately one to one ratio of 1,2 and 1,4- products was found after 29h.



Scheme I.39: Catalytic hydroboration of pyridines with the non-innocent Ni-O complex

The substrate scope of this transformation was then studied with various substituted pyridines and selected examples are represented below (Scheme I.40). The electronics at the aromatic ring were varied from electron-rich to electron-poor pyridines with sensible loss of yield (69% for p-CF₃-pyridine). The substitution pattern was also changed with 3-

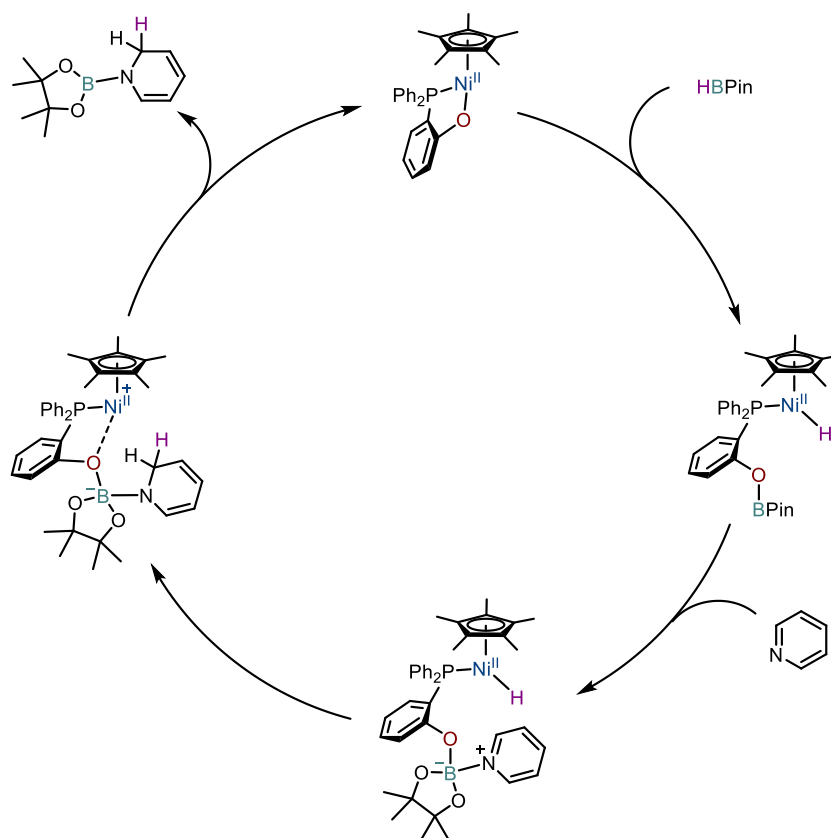
methylpyridine, and a mixture of 1,2- and 1,4- products was reported. Functional groups such as esters were tolerated by this system, but 2-substituted pyridines were found unreactive.



Scheme I.40: Catalytic hydroboration reaction catalyzed by Liu's Ni^{II} complex

A tentative mechanism for this transformation, supported by DFT calculations, is depicted in Scheme I.41: First, heterolytic B-H bond activation by the Ni^{II}-O complex occurs with the formation of the corresponding Ni^{II}-hydrido borane complex. The pendant, Lewis-acidic borane then reacts with pyridine to generate the pyridinium-borate adduct. The hydride is then transferred from the Ni^{II}-H complex to the pyridinium. B-O bond cleavage finally generates the product and closes the catalytic cycle. Remarkably, generation of the 1,4-product with this pathway was found prohibitively high in energy (33 kcal.mol⁻¹)^b.

^b In the original publication, a mechanism involving radicals was proposed to account for the formation of the product of 1,4-hydroboration. However, this mechanism did not explain the isomerization of the 1,2-product into the 1,4-product.



Scheme I.41: Mechanism of the 1,2-hydroboration of pyridines by the Ni-O complex of Liu

In the previous contributions, the lone pairs of an oxygen or sulfur atom, directly bonded to the metal were exploited in cooperative bond activation. In a similar fashion with a nitrogen atom, a historical breakthrough in Metal-Ligand Cooperativity was achieved by Noyori in 1987. A Ru-BINAP-diamine system was developed for asymmetric hydrogenation. In this pioneering work, whose impact was recognized by the Nobel committee in 2001, the lone pair of an amino group was acting in cooperation with the transition metal. The cooperative combination of a nitrogen center and a group 10 metal was first applied in 2009 by Schneider with an aliphatic diphosphine amido ligand (Figure I.12).^[39] However, due to the high-flexibility and the tendency to undergo β -H elimination reaction, the initial ligand design was scarcely used. To circumvent this issue, substituted or more rigid ligand architectures were employed by Caulton and Ozerov.

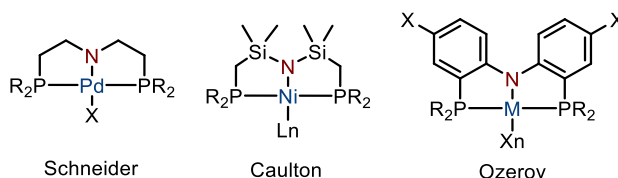
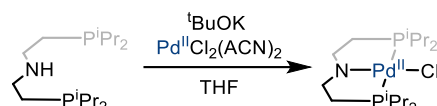


Figure I.12: Evolution of the PNP-scaffold from the initial design of Schneider to the dimethylsilyl-substituted version of Caulton and the diaryl version of Ozerov

Schneider's complex was prepared by treatment of the diphosphine proligand with a Pd^{II} source in presence of potassium tert-butoxide (Scheme I.42).



Scheme I.42: Synthesis of Schneider's complex

Remarkably, the lone pair at the nitrogen did not contribute to any significant π -bonding with d⁸ group 10 metals, resulting in a similar situation to that met by Cavell and Le Floch in carbene complexes (Figure I.13; see: § a)).

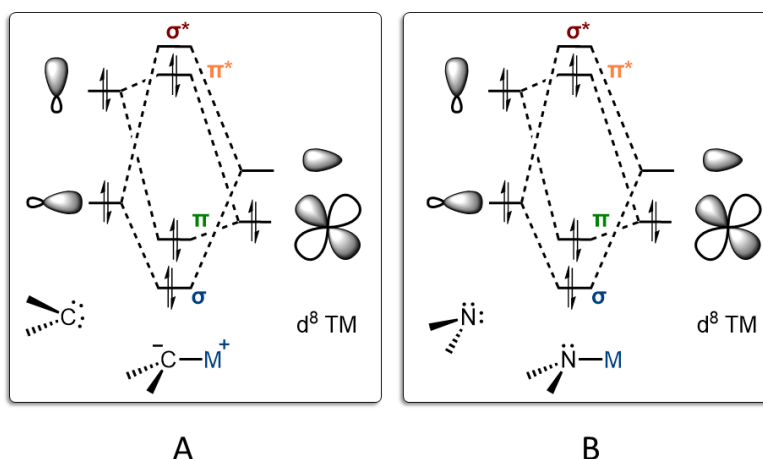
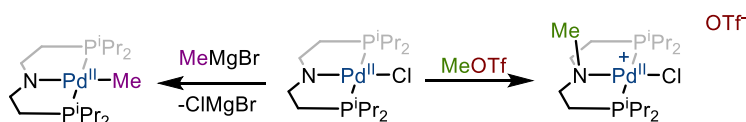


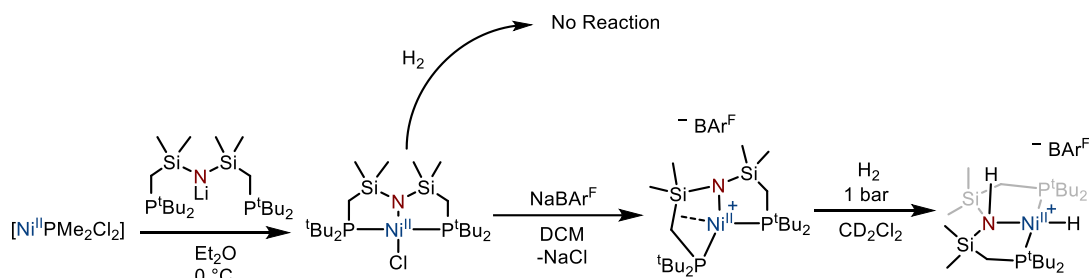
Figure I.13: A - Bonding situation in d⁸-dianion complexes; B - bonding situation in d⁸-amido complexes

The reactivity of the coordinated amido group was first explored experimentally by treatment with methyl triflate as strong electrophile resulting in the formation of the quaternary ammonium (Scheme I.43). Interestingly, the electrophilic character of the metal center was also demonstrated through the addition of methyl-Grignard.



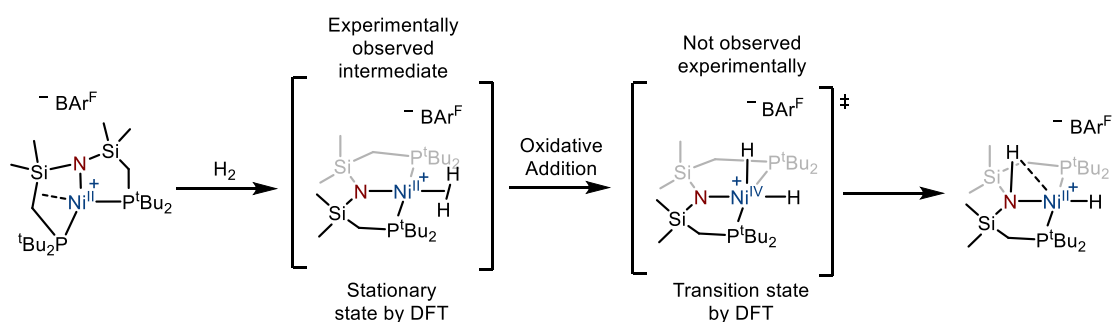
Scheme I.43: Reaction of PNP-Pd^{II} complex with a strong electrophile showing the nucleophilic character of the amine

A similar complex with dimethylsilyl groups at the backbone was reported by Caulton (Scheme I.44). It activates H_2 .^[40] A high-flexibility, without the possibility of β -H elimination was allowed through this ligand design. The flexible character of the ligand was shown particularly important through halogen abstraction by $NaBAR^F$. The resulting Ni^{II} species was stabilized by an interaction between the Si-C σ -bond and the cationic Ni^{II} .



Scheme I.44: Synthesis of PNP- Ni^{II} complex and heterolytic H_2 splitting

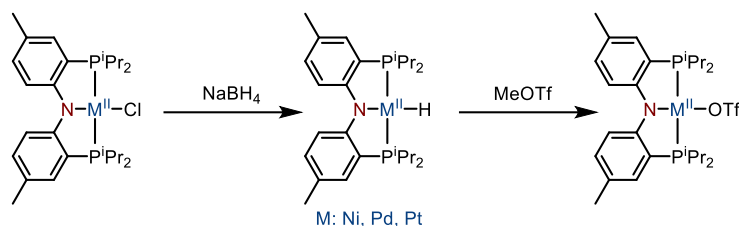
While the chloride precursor was found unreactive towards H_2 , the cationic species was reported to heterolytically split H_2 into the corresponding N-H, nickel-hydride complex. A mechanism of H_2 activation involving the nitrogen was proposed based on DFT calculations (Scheme I.45). An H_2 approach along the Ni^{II} -N axis was reported to directly minimize to the final product of heterolytic splitting. A stationary state containing a σ -interaction was found with an H_2 approach nearly along the P- Ni^{II} -P axis. From this, a transition state containing the Ni^{IV} dihydride was then reported with the two hydrides perpendicular to the P-Ni-P axis (Scheme I.45). The formation of the product was complemented with a Ni^{II} -H(N) distance of 2.40 \AA , interpreted by the authors as a weak H-bonding with the filled d_{z^2} orbital of nickel. Experimentally, under five bars of dihydrogen at $-60\text{ }^\circ C$, the σ - H_2 complex was observed and characterized spectroscopically.



Scheme I.45: Mechanistic pathway for H_2 activation through σ -bonded H_2 intermediate

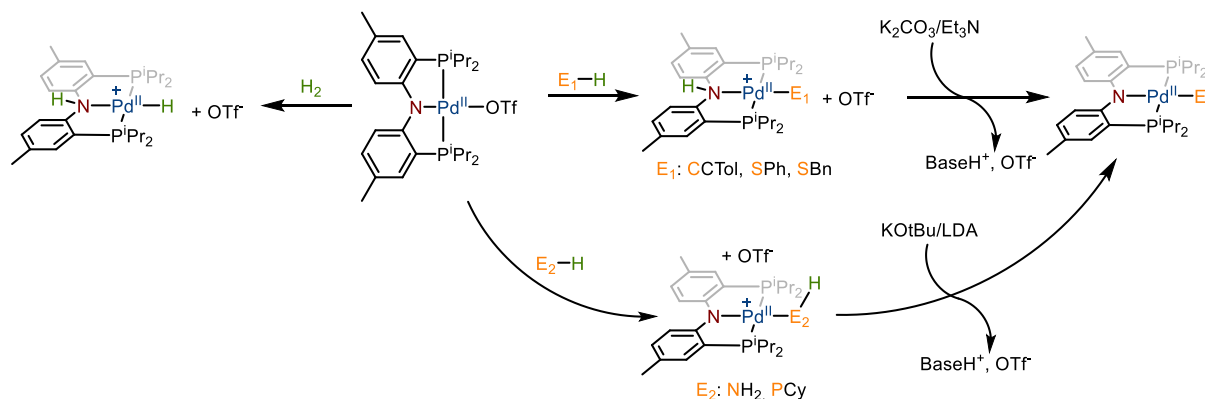
This approach was then incremented by the contribution of Ozerov with a more rigid PNP Pd^{II} complex with ortho-phenylene spacers. Remarkably, the synthesis of the metal-triflate

complex (also achieved for Ni^{II} and Pt^{II}) was not achieved by cationization with the classically used Ag(OTf) but through formation of a metal-hydride and hydride abstraction with methyl triflate (Scheme I.46).^[41]



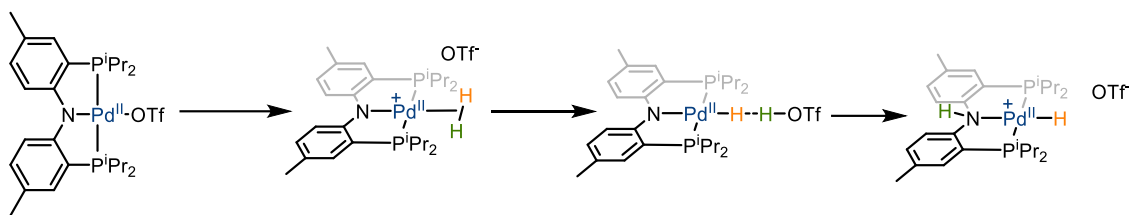
Scheme I.46: Synthesis of the PNP-M^{II}-OTf complexes reported by Ozerov

While ortho-phenylene skeletons bring increased stability, the reactivity of the nitrogen center was reduced by the π -delocalization over the aromatic rings. Nevertheless, this complex was probed for the activation of non-polar σ -bonds such as in H₂ and more polar E-H bonds such as S-H, N-H, P-H and C-H bonds (Scheme I.47).^[42]



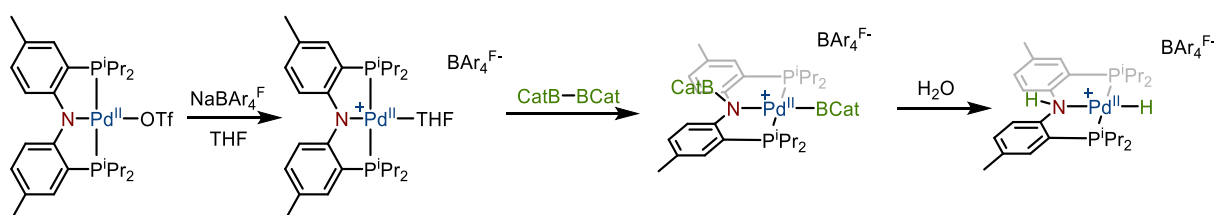
Scheme I.47: Polar and non-polar bond activation by the PNP-Pd complex of Ozerov

In the case of alkynes or thiols, the cationic complexes resulting from E-H bond activation were easily deprotonated by a base (Et₃N or K₂CO₃). With secondary phosphines and ammonia however, initial formation of the P/N-coordinated cationic complex was reported and E-H activation proved too high in energy for the complex alone. Nevertheless, stronger bases such as KO^tBu or LDA were able to perform the deprotonation. A mechanism of E-H bond activation across the Pd^{II}-N bond was proposed, based on DFT calculations (Scheme I.48).^[42] An exogeneous base, whose nature depends on the type of E-H bond involved, assists proton transfer from the coordinated E-H fragment to the nitrogen of the ligand.

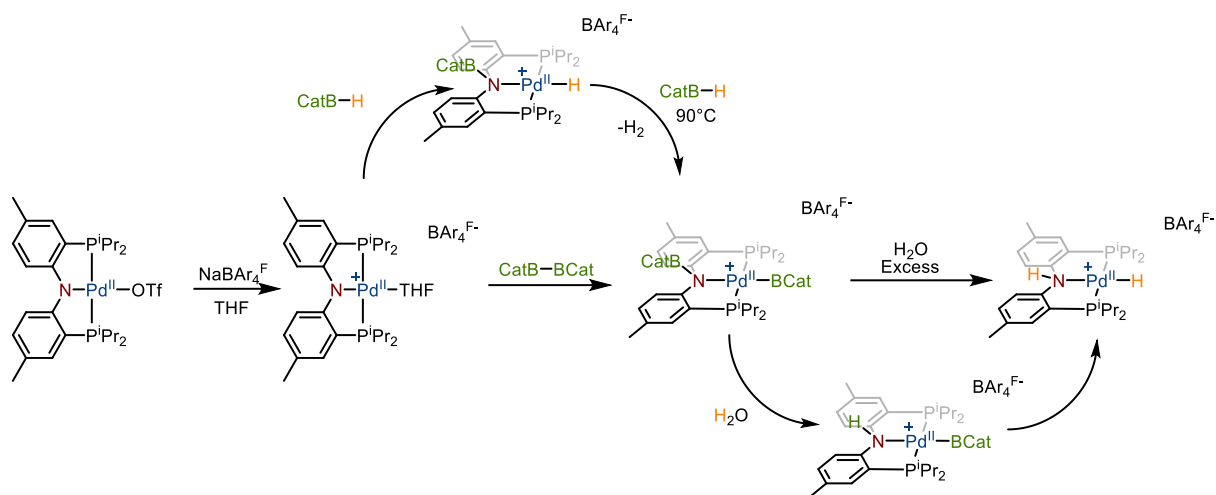
Scheme I.48: Mechanism of heterolytic H₂ activation with proton transfer assisted by an exogenous base

In the previous work, the Pd^{II}-OTf complex was used as a convenient precursor for the [(PNP)Pd⁺] synthon. When tested for B-H or B-B bond activation however, only complex mixtures were produced.

Less coordinating (and lacking a potentially reactive oxygen center) counter-ions were then explored by the authors. Upon cationization with NaBAR₄^F in THF, B-B bond activation was reported to yield an amido-borane palladium-boryl complex (Scheme I.49).^[43] The resulting complex was then hydrolyzed with excess H₂O and the net product of H₂ activation was generated (direct treatment of the cationic complex with H₂ was also reported as a viable pathway).

Scheme I.49: B-B bond activation and hydrolysis of Pd^{II}-Boryl complex

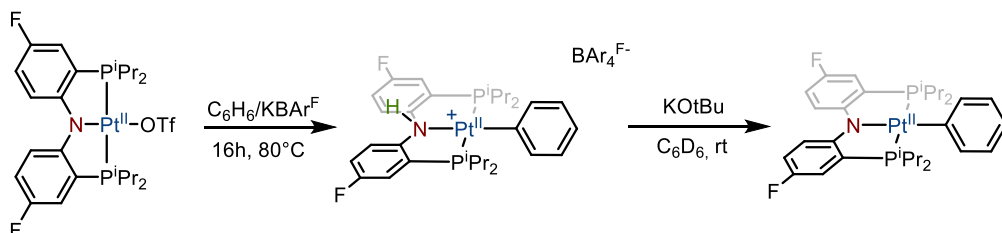
Interestingly, the Pd^{II}-H was formed upon treatment of the cationic complex with catecholborane and the addition of the electrophilic boron on the nitrogen was reported (Scheme I.50). Further reaction of the Pd^{II}-H with another equivalent of borane at 90°C was also observed, resulting in the formation of the net product of B-B bond activation. Remarkably, the B-N bond could then be selectively hydrolyzed with 1 equivalent of H₂O, to yield the net product of umpolung B-H bond activation. An impressive ability to navigate between the various activation and selective hydrolysis products was illustrated by this work. However, no catalytic applications have been reported yet.



Scheme I.50: Pathway and navigation between the activation and hydrolysis products

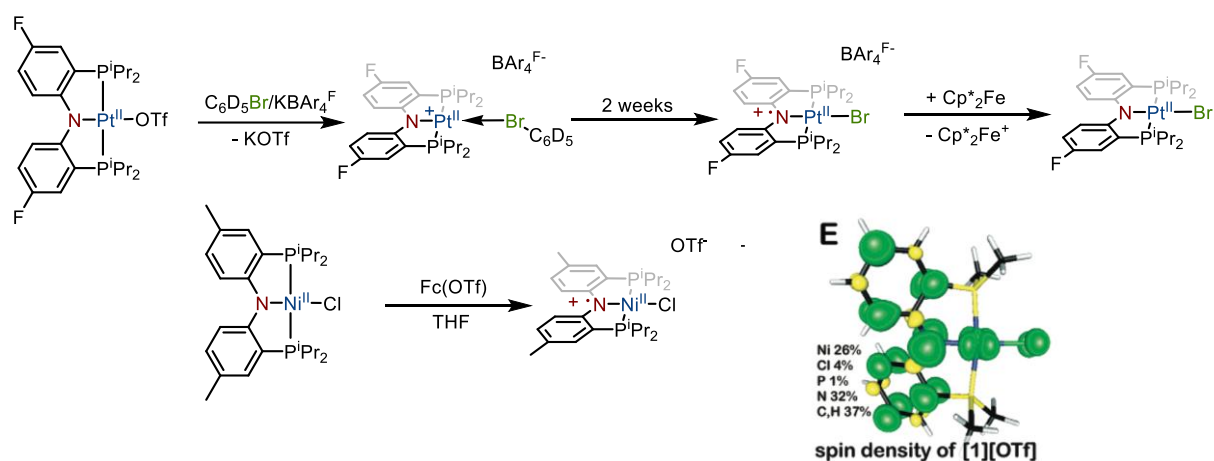
The research on this type of ligand was extended to other group 10 metals in 2013 by the group of Ozerov. With Pt^{II} , the synthesis of a fluorinated analog of the previously described methylated complex was reported (Scheme I.51).^[44] Benzene C-H activation was then observed upon cationization with KBAR_4^{F} in benzene with formation of a $\text{Pt}^{\text{II}}\text{-Ar}$ complex and incorporation of the proton onto the nitrogen. It is interesting to note here that no triflate could play the role of exogenous base or proton shuttle (see Scheme I.48) and this role could not be endorsed by the BAR_4^{F} anion. Unfortunately, no DFT calculations were conducted to shed light into the mechanism (oxidative addition?, adventitious water?).

Analogous to the Pd^{II} counterpart, deprotonation of the addition product was achieved with KO^tBu . It should be noted that the palladium analog was also probed for this reactivity, but the desired activation product was not observed. Reversibility experiments were also attempted on this complex, but no exchange was detected indicating an irreversible addition and thus a catalytic version would not be straightforward. However, this rare example of such non-activated aryl C-H activation emphasizes the relevance and interest of the cooperative strategy.



Scheme I.51: C-H activation by MLC trough Pt-N bond by the cationic Pt complex

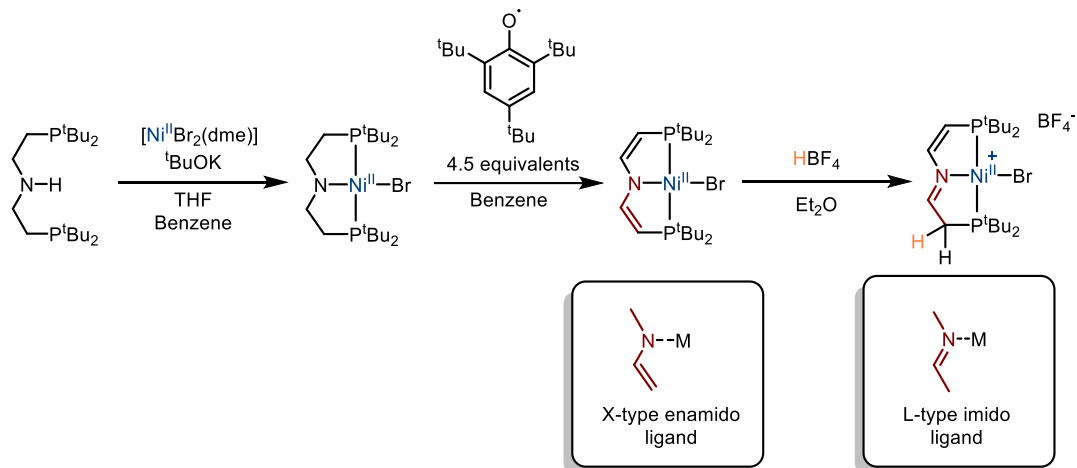
Interestingly, upon treatment (for two weeks!) of the cationic Pt^{II} complex with deuterated bromoaryls, halogen abstraction was reported, resulting in formal one electron oxidation of the complex (Scheme I.52). One electron reduction of the resulting oxidized complex to its neutral Pt^{II} form was then achieved with Cp₂*Fe. Actually, redox-active behavior of such a ligand had been already reported by Szilagyi and Mindiola with Ni^{II}.^[45] In their study, oxidation of a similar nickel complex was performed with Fc(OTf) to yield a cationic Ni^{II} radical complex. A ligand-centered radical was supported by a thorough study using XRD, DFT and ESR. The unpaired electron was mostly located at nitrogen and at the aryl carbons in ortho and para positions (*vide infra*). While a similar behavior with platinum was suggested by Ozerov based on XRD and NMR spectroscopy, no ESR study was performed for the unambiguous determination of the nature of the radical.



Scheme I.52: Halogen abstraction and radical formation by Ozerov and Mindiola – Spin density of Ni^{II}-Cl complex adapted with permission from J. AM. CHEM. SOC. 2008, 130, 3676-3682. Copyright 2008 American Chemical Society.

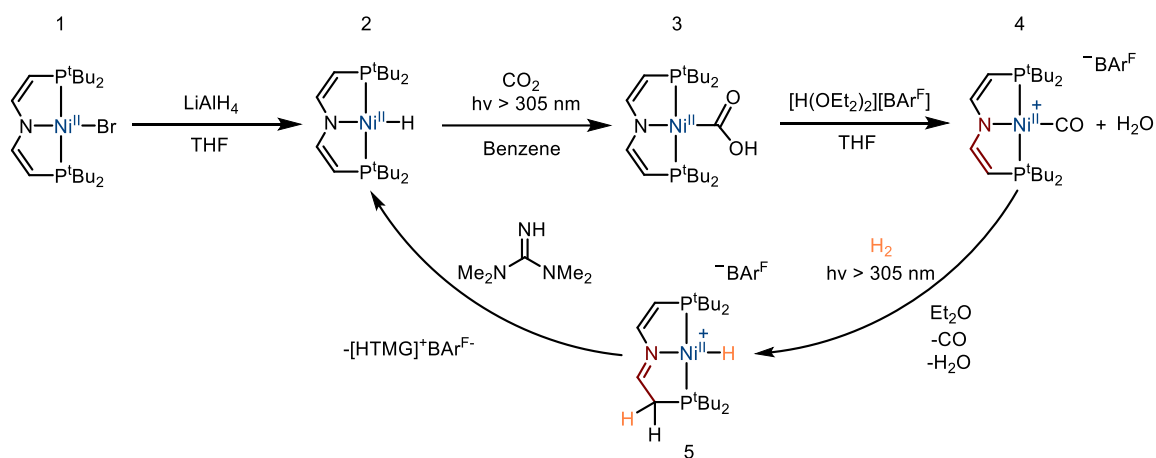
The behavior of radical species deriving from aliphatic PNP-pincer complexes was studied in 2017 by Schneider.^[46] The synthesis of the PNP-Ni^{II}-Br complex was reported by treatment of PNHP pro-ligand with NiBr₂(dme) in THF, followed by deprotonation with ^tBuOK in benzene (Scheme I.53). The initial formation of the aliphatic PNP-Ni^{II}-Br complex was followed by 4 hydrogen atom transfer (HAT) with 2,4,5-tri(tertbutyl)phenoxy radical to form vinyl bonds at the spacers. Interestingly, upon treatment with an acid such as HBF₄, this complex was converted to the cationic species with incorporation of the H⁺ at the carbon backbone. While in the previous examples, the non-innocent site (O, S, N) was directly bonded to the metal, in

this case, the reactive site is a remote carbon center, involved in N=C=C conjugation. Remarkably, the non-innocent character of the backbone was accompanied by a coordination switch from an X-type enamido ligand (in the basic form) to an L-type imido ligand (in the protonated form).



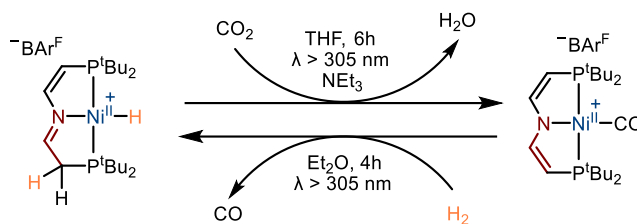
Scheme I.53: PNP-Ni complex of Schneider and reactivity towards acid

Conversion of the Ni^{II}-halide into the corresponding hydride was reported by treatment with LiAlH₄ (complex 2 - Scheme I.54). Interestingly, under irradiation, abnormal CO₂ insertion was observed to form the corresponding Ni^{II}-COOH (complex 3 - Scheme I.54).^[47] When treated with acids, formation of the Ni^{II}-carbonyl complex was reported along with H₂O (complex 4 - Scheme I.54). Remarkably, the cationic Ni^{II} carbonyl complex activates H₂ under irradiation, with participation of the PNP ligand (complex 5 - Scheme I.54). Further deprotonation and regeneration of the enamido motif at the backbone was achieved with tetramethylguanidine (complex 5 to complex 2 - Scheme I.54).



Scheme I.54: Reversed water gas shift reaction with MLC by Schneider

While a catalytic version was not yet achieved, a simple two-step process was established for the reversed water gas shift reaction (i.e., formation of H₂O and CO from CO₂ and H₂) using the combination of photochemical activation and MLC (Scheme I.55).



Scheme I.55: Two step reversed water-gas shift reaction

c) Aromatization/dearomatization strategy

The previous example, based on the enamido-imido coordination switch is reminiscent of the notorious aromatization/dearomatization of pyridines introduced by Milstein. This strategy was shown to have a tremendous activation/transfer impact in the chemical community, especially with d⁶ metals and in reactions involving H₂. Even if this approach was much less studied with d⁸ group 10 metals, two main types of ligand design can be identified, based on the basic site at the ligand.

In the first one, an exocyclic CH₂ spacer would generate the dearomatized pyridine upon deprotonation and re-aromatization would then occur upon H-X bond activation (Figure I.14 – c) i.). For the second one, an exocyclic carbonyl basic site bound either to pyridine or to cyclopentadiene (Figure I.14 – c) ii.) could play the role of a basic site at a ligand, involving a rearrangement of the π -system upon deprotonation.

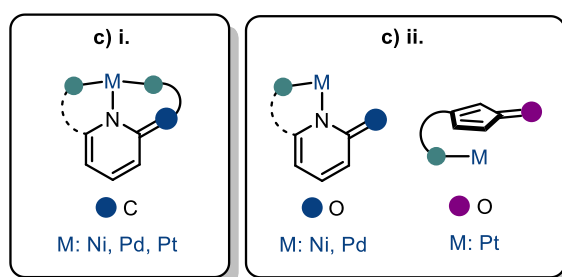


Figure I.14: Two-types of basic site in the aromatization/dearomatization approach

i. Carbon-based basic site

Contributions in this area would be best presented by starting with the initial study of Milstein with a ligand design featuring a central pyridine flanked by two phosphine groups. This approach was then further extended by Auffrant keeping the central pyridine with a

lateral phosphine and phosphazene. A bidentate approach was then introduced by Van der vlugt, and Vigalok further extended this concept with a PNF backbone taking advantage of the hemilabile character of the fluorine.

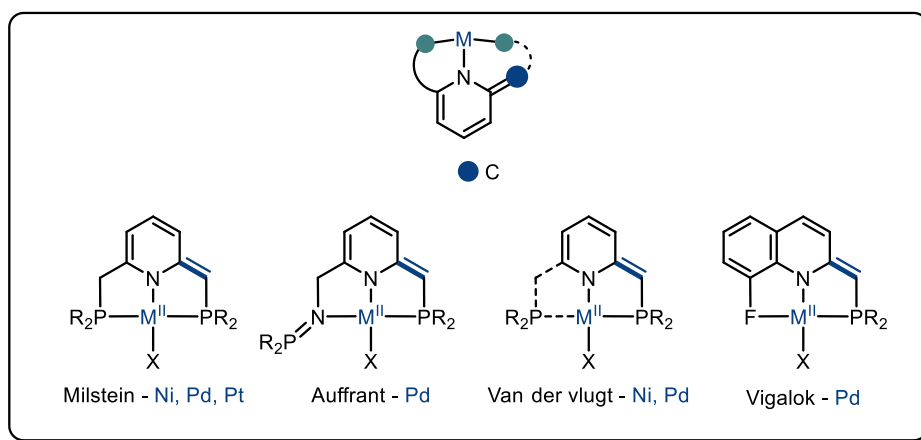
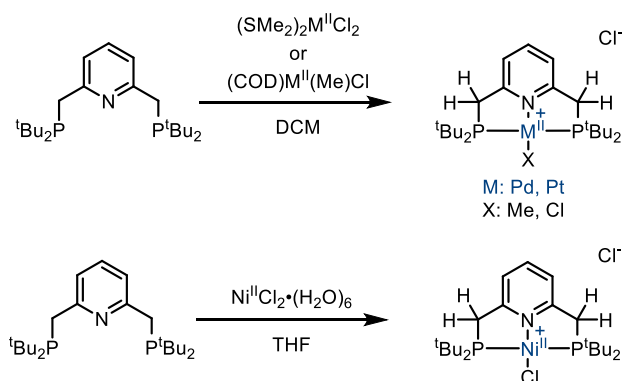


Figure I.15: Main contributions in the aromatization/dearomatization approach with group 10 metal complexes

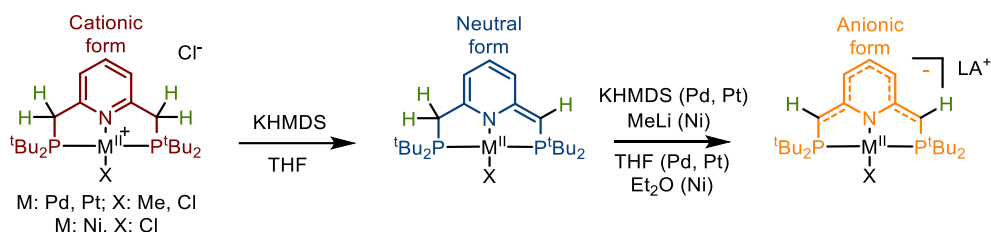
The synthesis and characterization of diphosphine pyridine (PNP) Pd^{II} and Pt^{II} complexes in their cationic, neutral and anionic forms was initially reported in 2010 and extended to nickel in 2013 (Scheme I.56).^[48,49] The cationic form was first accessed by treatment of the proligand with the corresponding metal salt resulting in the formation of a cationic [PNP-M^{II}-X]⁺ with an outer-sphere chloride. The aromatic nature of the pyridine backbone was established by XRD experiments with variation of the bond lengths within the pyridine system from 1.37-1.40 Å.



Scheme I.56: Synthesis of the cationic PNP-M^{II}-X complexes

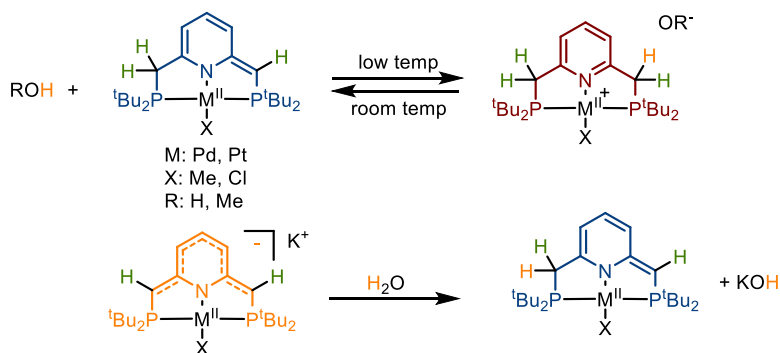
The neutral form was accessed by deprotonation of the methylene spacer with KHMDS (Scheme I.57). An alternating motif of single and double bonds was found by single-crystal X-ray crystallography, resulting in a bonding situation best described as an enamido motif with a de-aromatized pyridine backbone. The anionic form was then accessed through further

deprotonation with KHMDS in the case of palladium and platinum and with MeLi for nickel. For Pd^{II} and Pt^{II}, the complex was proven too unstable for XRD experiments. For Ni^{II} however, the structure was elucidated showing a π -system containing the carbon ring and the exocyclic double bonds with intermediate single/double-bond character, as deduced from XRD, NMR data and DFT calculations.



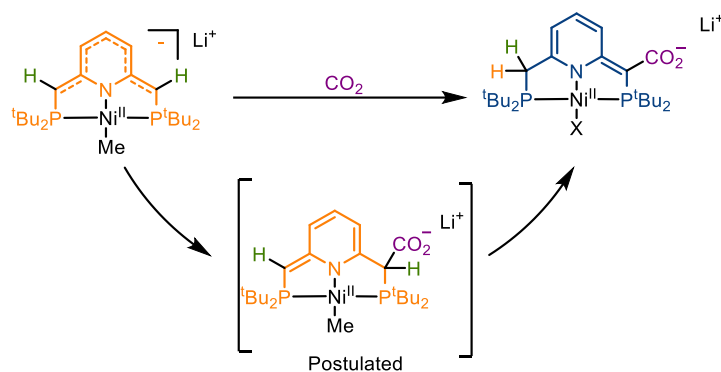
Scheme I.57: Group-10 pincer complexes reported by Milstein in their cationic, neutral, and anionic forms

Interestingly, in the case of Pd^{II} and Pt^{II}, the neutral species were probed for the activation of E-H bonds (more specifically O-H bonds) and reversible protonation was reported upon treatment with MeOH or H₂O (Scheme I.58). The equilibrium between the neutral and cationic species could be adjusted by varying the temperature. At low temperatures, the cationic product resulting from O-H activation is favored whereas the neutral form prevails at room temperature.

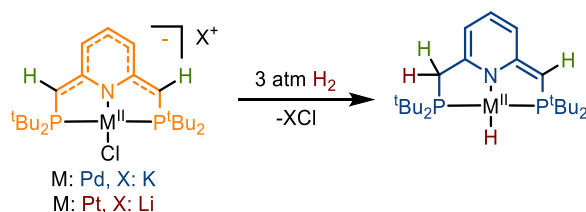


Scheme I.58: E-H bond activation and hydrolysis of PNP-M complexes

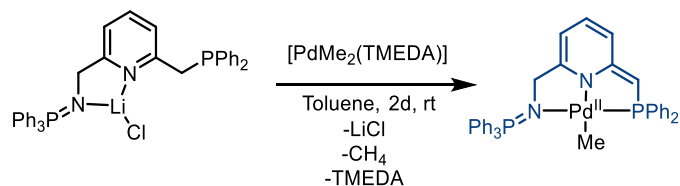
On the other hand, the anionic complex showed irreversible protonation of the anionic site when exposed to H₂O. Interestingly, no reactivity was reported for the neutral Ni^{II} complex, but the anionic version however was shown to react with CO₂ (Scheme I.59). Incorporation of the carboxylate at the vinylic position and formation of a methylene spacer was reported. This result was explained by the authors by an initial step of nucleophilic attack of the backbone with formation of the CH-carboxylate and subsequent tautomerization to yield the final complex.

Scheme I.59: CO₂ fixation at the backbone of the anionic Ni^{II} complex

Further reactivity of the anionic complexes was developed 4 years later with Pd^{II} and Pt^{II} by the group of Goldberg.^[50] Treatment of the anionic Pd^{II} or Pt^{II} complexes with H₂ (3 atm) resulted in the incorporation of a proton onto the methylene backbone and formation of the corresponding metal hydride (Scheme I.60).

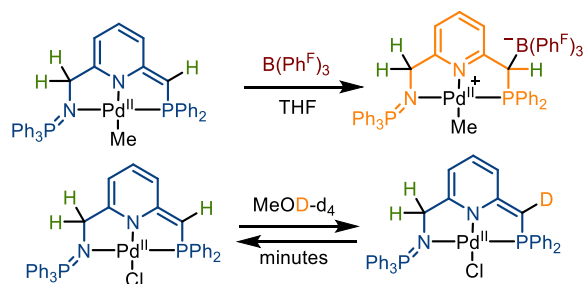
Scheme I.60: H₂ activation by the anion Pd and Pt PNP complexes

Variation of the ligand scaffold from the PNP version to the PNN was achieved by Auffrant with a phosphine-iminophosphorane Pd^{II} complex.^[51] The synthesis was achieved by treatment of the LiCl adduct of the ligand with [PdMe₂(TMEDA)] and interestingly, after two days at room temperature in toluene, the deprotonated form was directly generated with concomitant elimination of methane (Scheme I.61).

Scheme I.61: *in situ* generation of the dearomatized PNN-Pd complex of Auffrant

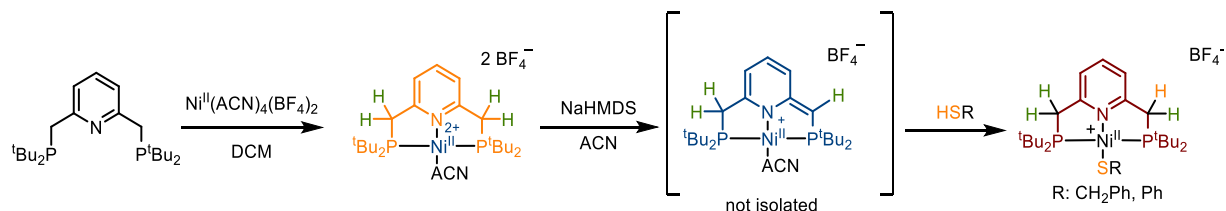
In this case, the nucleophilic character of the backbone was supported experimentally by addition of BCF as electrophile leading to its incorporation at the vinylic position. Furthermore, treatment of the deprotonated complex with CD₃OD lead to deuterium incorporation in the vinylic position. This result is in accordance with the previous observations of Milstein

(Scheme I.58). Notably, D-incorporation only occurs at the PPh₂ site as the other position appears unreactive.



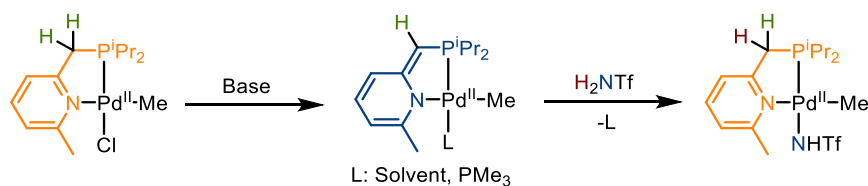
Scheme I.62: Nucleophilic character and reversible O-D bond activation by the dearomatized PNN-Pd complex

In the previous cases, the complete occupation of the coordination sites of d⁸ group 10 metals could be responsible for the difficulty to access the standard MLC product with incorporation of the proton at the backbone and substitution at the metal center. This issue was addressed in 2009 by Van der vlugt, with the synthesis of a cationic PNP-Ni^{II} complex bearing a labile acetonitrile ligand (Scheme I.63). Generation of the dicationic PNP-Ni^{II}-ACN was achieved by treatment of the PNP ligand with Ni^{II}(ACN)₄(BF₄)₂. The active species was then generated *in situ* by deprotonation with NaHMDS. This cationic complex was then reported to further react with thiols to yield the expected product of S-H activation by MLC. The thiobenzyl or thiophenyl group was coordinated to the metal and aromatization of the pyridine ring was observed with the protonation of the exocyclic C=C backbone.



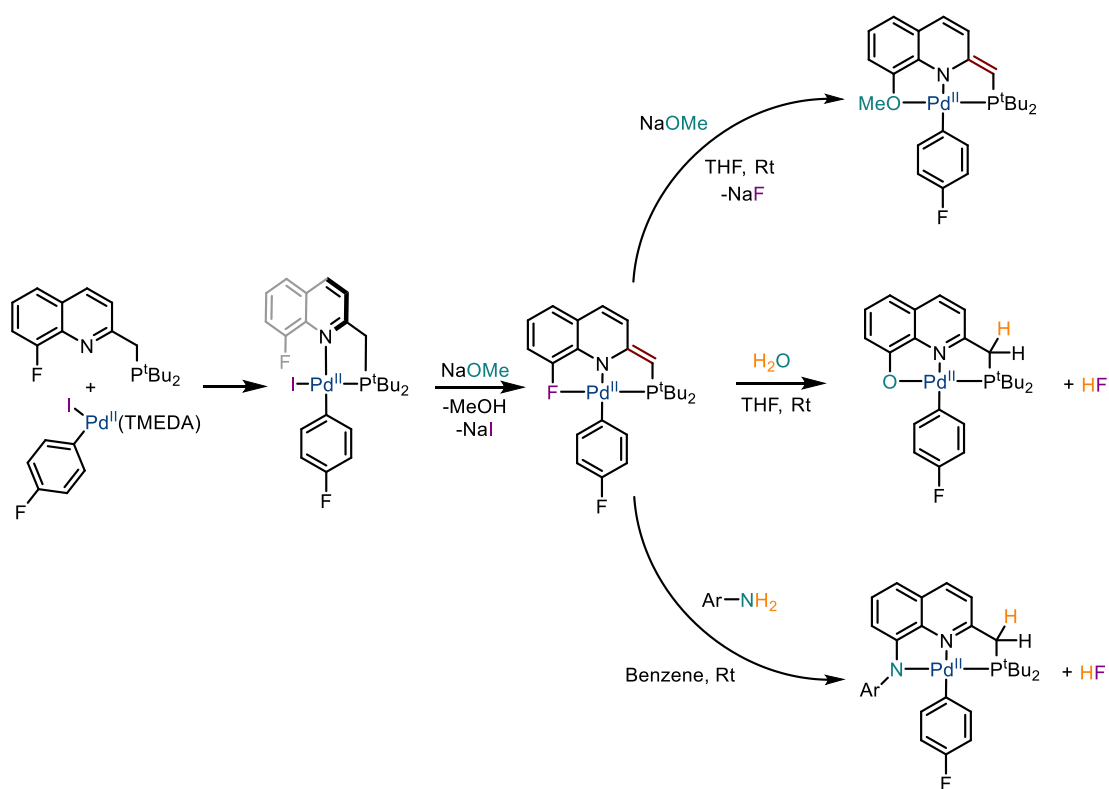
Scheme I.63: S-H bond activation by the dearomatized Ni complex of Van der Vlugt

Another interesting strategy was also reported by Van der vlugt with a bidentate version of the neutral Pd^{II} complex (Scheme I.64). Interestingly enough, while examples of neutral dearomatized palladium complexes were previously studied several times, only this complex showed the desired reactivity and was able to activate the N-H bond of triflamide.^[52]



Scheme I.64: N-H activation by the bidentate dearomatized Pd complex

In this context, the group of Vigalok developed a new type of “pincer” complexes based on a quinoline scaffold (Scheme I.65).^[53] This complex was readily synthesized by reaction of the PNF ligand and the corresponding [(Iodoaryl)Pd^{II}(TMEDA)] complex. Dearomatization was achieved by further treatment of the resulting PNF-Pd^{II} complex with NaOMe. Remarkably, when another equivalent of NaOMe was added, nucleophilic substitution of the fluorine by a methoxy group occurred (top reaction - Scheme I.65). Other pro-nucleophiles such as H₂O or anilines were employed to study the reactivity of the dearomatized system (middle and bottom reactions - Scheme I.65).^[54] The aromatized products of substitution in the 8-position of the quinoline were formed rapidly (within seconds for aniline) with very high yields.



Scheme I.65: Synthesis of the dearomatized PNF-Pd^{II} complex of Vigalok and stoichiometric E-H bond activation and SnAr

A mechanism for the aniline substitution was then proposed based on DFT calculations, using N-methylaniline (NMA) as model substrate (Figure I.16).^[55] First, the direct intermolecular substitution reaction was explored but quickly discarded as the Gibbs activation energy proved to be prohibitively high (>40 kcal.mol⁻¹). A second pathway of first coordination of NMA to palladium followed by NH deprotonation to yield the rearomatized

complex was proven accessible upon addition of a proton-shuttle. This complex then undergoes Pd-assisted intramolecular nucleophilic substitution, followed by deprotonation of the methylene backbone (once again proton-shuttle assisted) to yield the resulting dearomatized complex and HF as concomitant product. Three compounds were probed for their proton-shuttling ability in this mechanism: NMA, residual H₂O and HF. DFT calculations and experimental observations showed that HF was the most likely partner as this pathway involves activation energies accessible at room temperature.

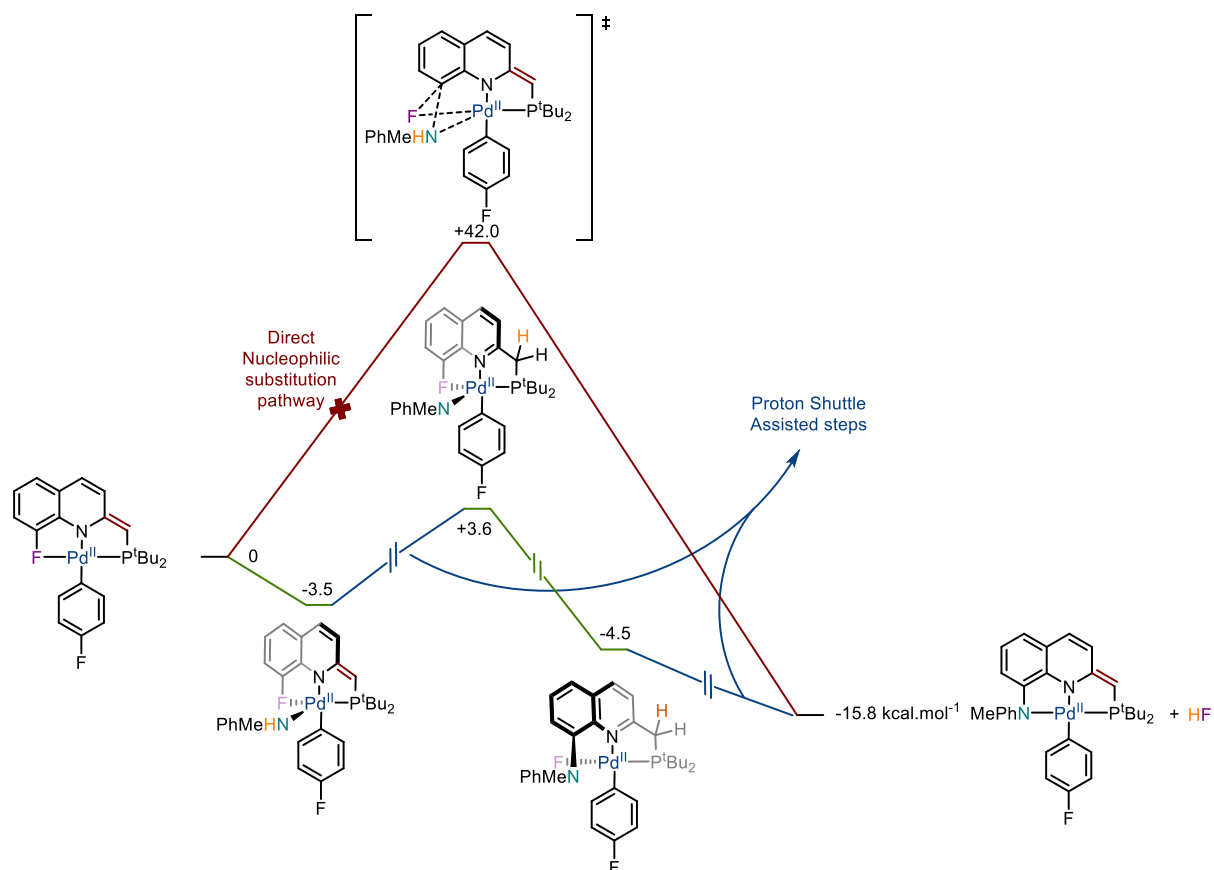
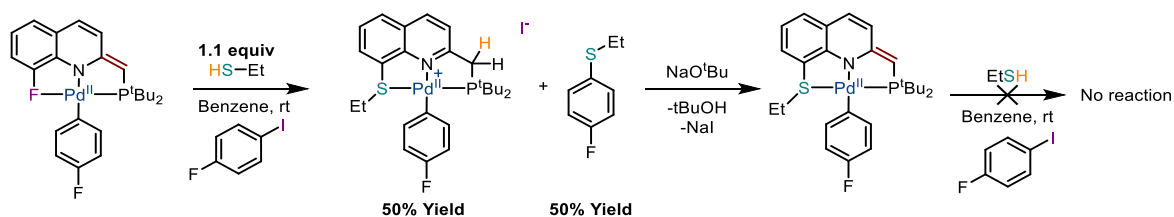


Figure I.16: Mechanistic pathways computed for the nucleophilic aromatic substitution by NMA

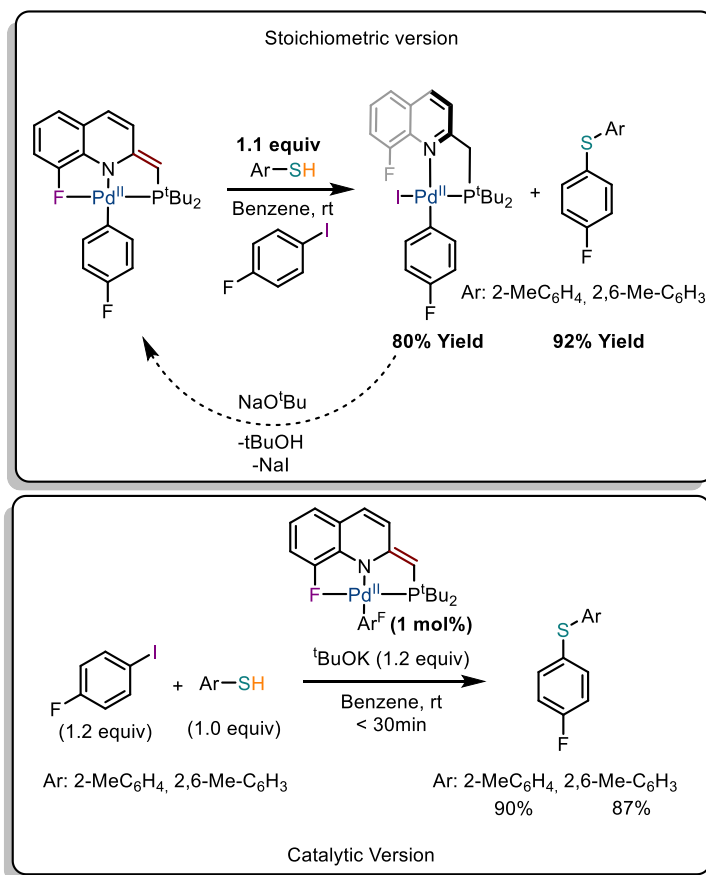
Interestingly, when S pro-nucleophiles such as EtSH were probed in the presence of p-IC₆H₄F, cleavage of the palladium-carbon bond and formation of EtS-C₆H₄F occurred in competition to the substitution reaction (Scheme I.66). The competition between the two reactions was further supported by a one-to-one ratio between the product of reductive elimination (the aryl thioether) and the product of substitution. Notably, the deprotonated form of the substitution product was also prepared and was found unreactive towards an excess of thiol in presence of p-IC₆H₄F suggesting that reductive elimination occurs before

nucleophilic substitution. While mechanisms for the substitution and for the reductive elimination were proposed based on DFT calculations, no explanation for this difference in reactivity between N-nucleophiles and S-nucleophiles was provided.



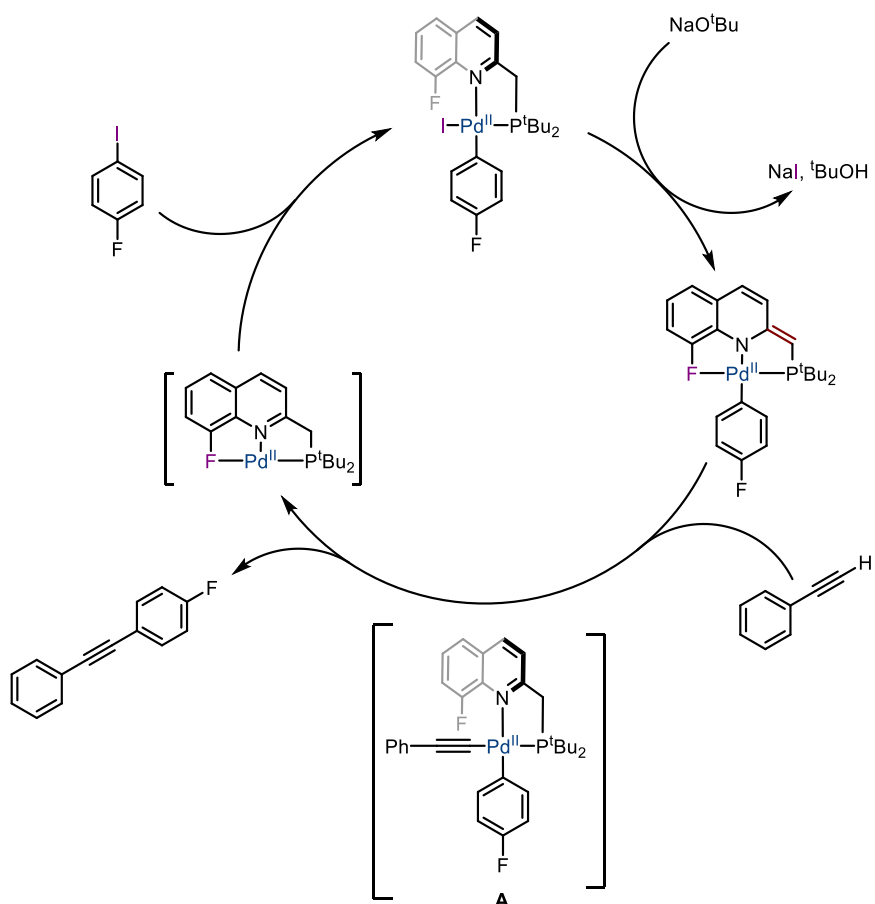
Scheme I.66: Substitution and reductive elimination with alkyl-substituted thiols

Remarkably, when the less nucleophilic and more sterically encumbered *m*-thiocresol and 2,6-dimethylbenzenethiol were used in presence of p-IC₆H₄F, exclusive formation of the C-S coupling product was observed (Stoichiometric version - Scheme I.67). Remarkably, this was accompanied by the formation of the product of oxidative addition of p-IC₆H₄F (and precursor to the dearomatized PNF-Pd^{II} complex). The catalytic version of this transformation was then explored in presence of a base, and the cross-coupling between thioaryls and iodoaryls was achieved with only 1% of dearomatized PNF complex (Catalytic version - Scheme I.67).



Scheme I.67: Catalytic activity towards S-C cross-coupling of Vigalok's PNF-Pd complex

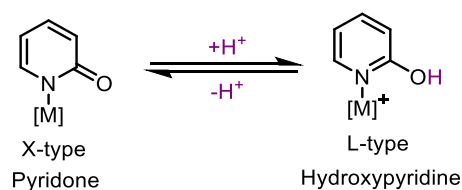
Going even further, the dearomatized PNF-Pd^{II} complex was proven catalytically active in a copper-free Sonogashira-type cross-coupling reaction (Scheme I.68).^[56] The hemilabile behavior of the fluorine fragment, in addition to the non-innocent character of the backbone (contributing to alkyne activation as supported by D-labeling experiments), were reported by the authors as crucial factors in this rare reactivity. Unfortunately, the exact mechanism of C-C coupling has not been elucidated yet, but it is reasonable to envision it involves **A** (Scheme I.68). While metal-ligand cooperativity can be seen as a thriving research area, examples of MLC for carbon-carbon bond formation are rare and it remains to date, one of the rare examples with group 10 metals.



Scheme I.68: Proposed catalytic cycle by Vigalok for the catalytic copper-free Sonogashira-type cross-coupling

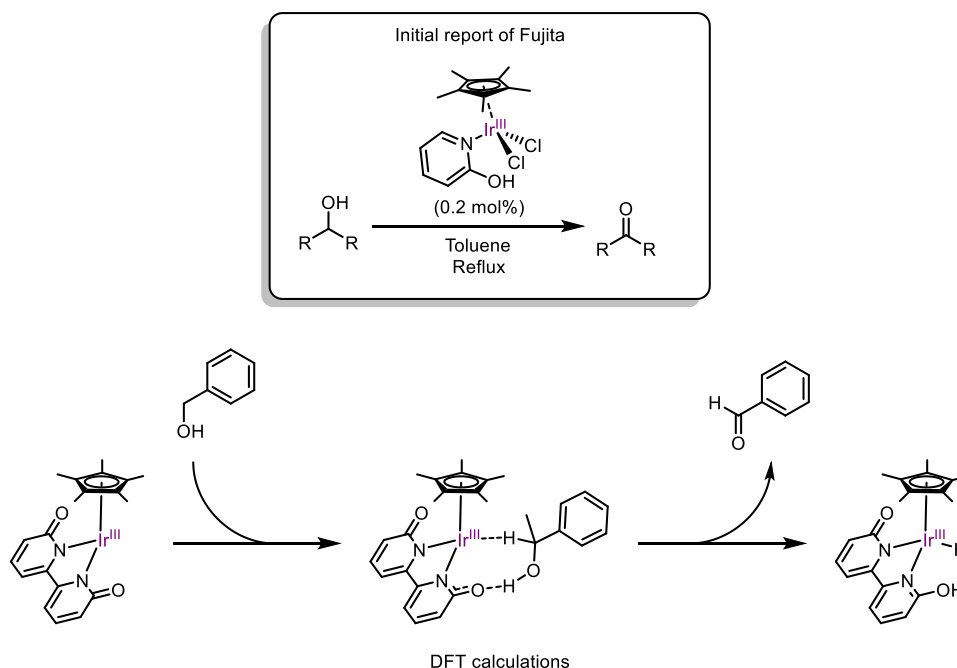
ii. Carbonyl-based basic site

In the previous examples, the nitrogen-based ligand was able to navigate between L- and X-type coordination, upon deprotonation/protonation of the exocyclic methylene spacer. Another approach on the same type of mechanism was developed with oxygen as a remote basic site prone to pyridone/hydroxypyridine switch (Scheme I.69).



Scheme I.69: General reaction scheme of pyridine/hydroxypyridine protonation

This ligand design was first introduced by Fujita and Yamaguchi in 2007 in the catalytic dehydrogenation of alcohols with Iridium (Scheme I.70).^[57] The working hypothesis involving MLC was supported by DFT calculations on the bidentate version of this ligand.^[58]



Scheme I.70: Initial report of Fujita with the cooperative dehydrogenation of alcohols.

A few contributions involving group 10 metals have been reported over the years with such ligand scaffolds. The quinoline Ni^{II} complexes developed by Jones will be presented first followed by the work of Yu with Pd^{II} (Figure I.17). Next, a bidentate N-N version of the ligand with a flanking pyridine reported by Albéniz will be discussed, followed by a N-S version, with a lateral sulfoxide of Jiao.

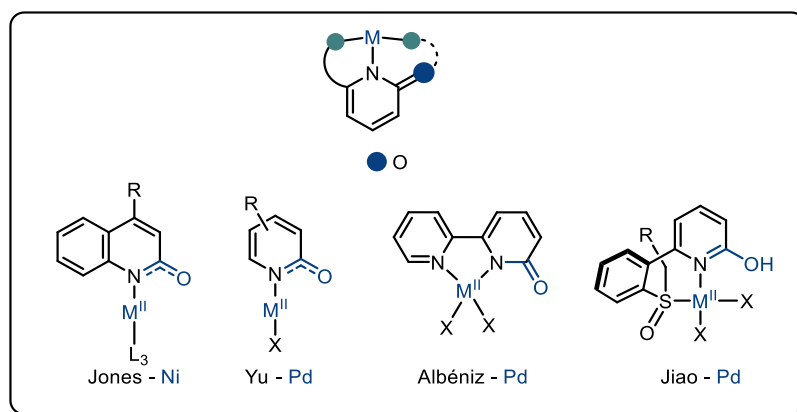
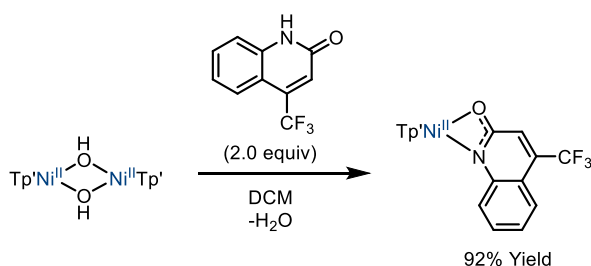
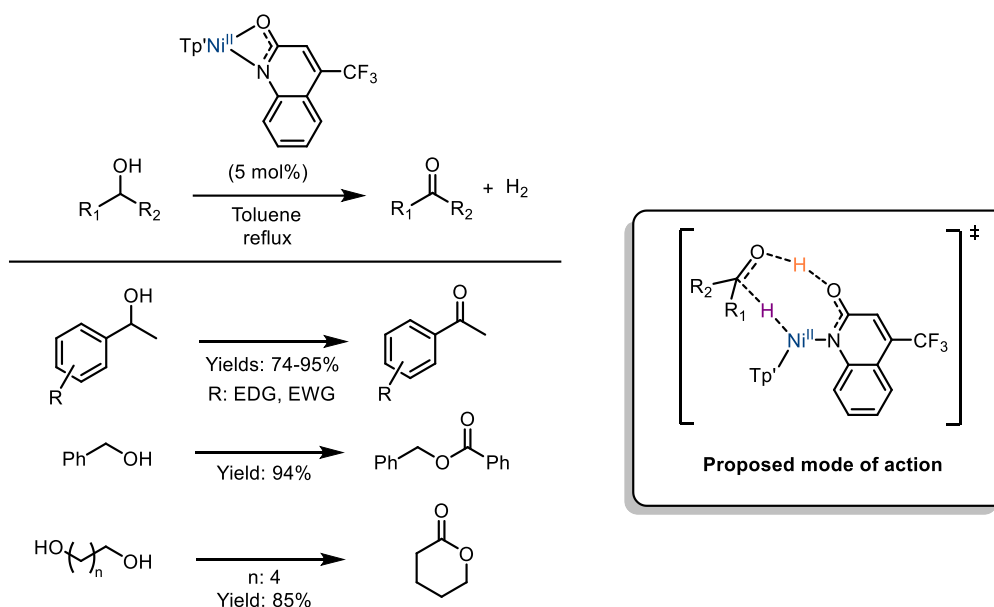


Figure I.17: Major contributions in the field of pyridone/hydroxypyridine cooperativity with group 10 metals

In 2015, the synthesis of a quinolinone-Ni^{II} complex was reported by Jones (Scheme I.71).^[59] The complex was formed by treatment of tris(3,5-dimethylpyrazolyl)borate (abbreviated Tp') Ni^{II} hydroxide dimer with the corresponding proligand in DCM.

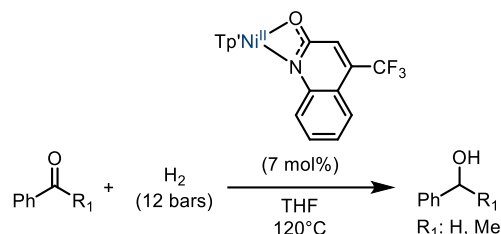
Scheme I.71: Synthetic pathway for the (Tp')-Ni^{II}-quinolone complex reported by Jones

The catalytic ability of this complex was then explored towards the acceptorless dehydrogenation of alcohols (Scheme I.72). Ketones were efficiently formed from secondary alcohols, while esters were formed with activated primary alcohols such as benzyl alcohol. Remarkably, 1,5-pentandiol was cyclized into δ -valerolactone upon dehydrogenation. The proposed mode of action (Scheme I.72) was supported by the comparison with Simple Tp'Ni complexes such as Tp'Ni(OAc) or [Tp'Ni(μ -OH)]₂. In this case, the activity was completely shut down with yields ranging from 4% to 7%.

Scheme I.72: Selected examples of the scope of the non-innocent nickel^{II}-catalyzed acceptorless alcohol dehydrogenation

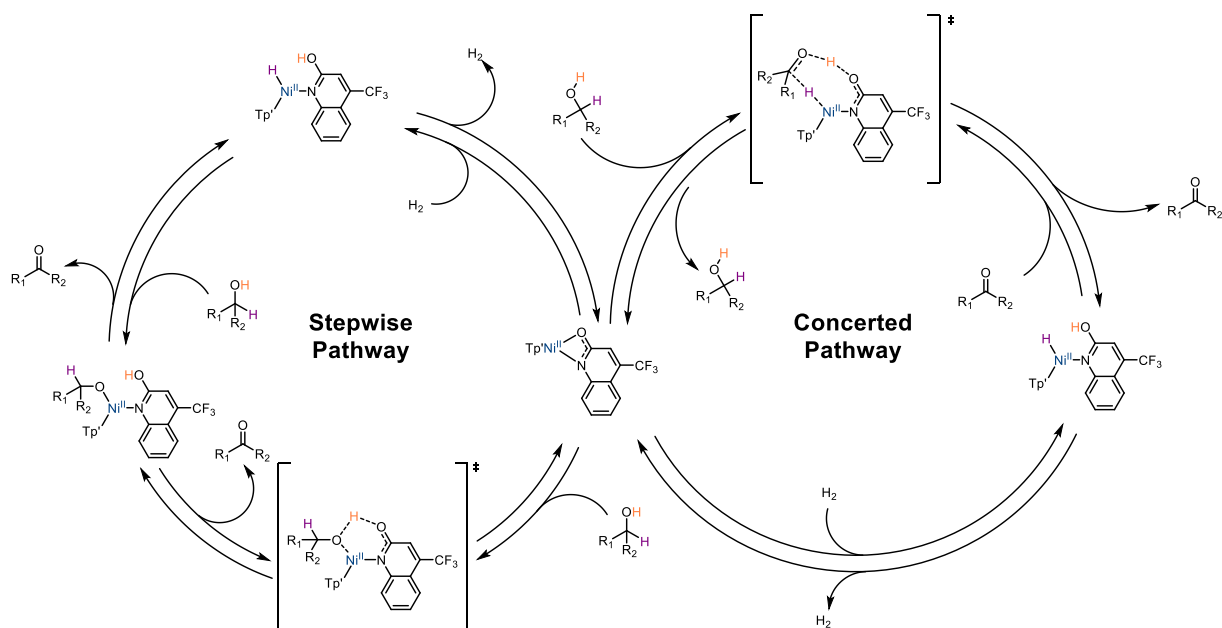
Going further, the reverse transformation (i.e. the hydrogenation of carbonylated compounds) was also studied with this system. Under 12 bars of H₂ at 120°C in THF, acetophenone and benzaldehyde were quantitatively hydrogenated into the corresponding 1-phenylethan-1-ol and benzylalcohol respectively (Scheme I.73). Under lower pressure of H₂ (5 bars), no hydrogenation occurred. Remarkably, even if strongly dependent on the H₂

pressure, this catalytic system was found active in both hydrogenation and dehydrogenation, an uncommon feature for homogeneous systems. It must be noted however that the fate of the catalyst throughout both reactions (hydrogenation and dehydrogenation) was not discussed.



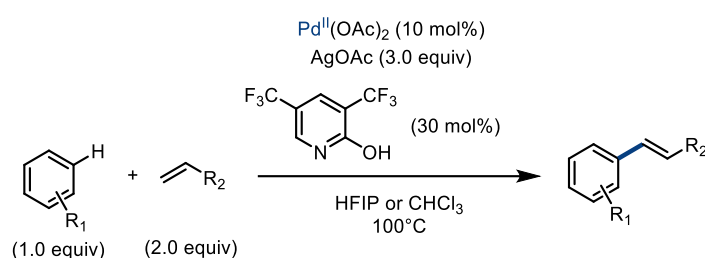
Scheme I.73: Hydrogenation of carbonyls by the Ni^{II}-quinolone complex of Jones

Mechanistically, stepwise and concerted pathways, both involving MLC, were proposed by the authors (Scheme I.74). In the first one, alcohol deprotonation and metal-hydride formation was suggested to occur in two successive steps, while in the second one, this was proposed as a single step. DFT calculations were previously performed on the iridium system and pointed towards a concerted mechanism.^[58] To support a similar mechanism in the case of nickel, the authors independently prepared the Tp'-nickel-alkoxide complex (a supposed intermediate in the stepwise pathway). No formation of nickel hydride and benzaldehyde by β -H elimination was reported upon heating, supporting that the nickel system was more likely to follow the concerted mechanism.



Scheme I.74: Two suggested mechanisms for the hydrogenation/dehydrogenation of alcohols

A related design was explored by Yu with Pd^{II} in 2017 for the non-directed C-H functionalization of arenes (with formation of C-C bonds!) (Scheme I.75).^[60] Remarkably, in this type of reactivity, the arene can usually be found as solvent or in a large excess. In this case, taking advantage of the pyridone/hydroxypyridine ligand tautomerism in MLC, simple arenes (as limiting reagents !) were functionalized in a Heck-type coupling. The complex was generated *in situ* from a Pd^{II} precursor, treated in presence of silver acetate in HFIP or chloroform with the hydroxypyridine ligand. The impressive scope of this system, containing more than 76 examples will not be presented here. However, it is worth noting that very simple arenes such as benzene as well as complex bioactive molecules were found reactive.



Scheme I.75: Heck-type coupling of arenes with Yu's non-innocent Pd^{II} complex

Compared to the previously discussed examples where stoichiometric reactivities were used to support the non-innocent character of the ligand, this time the involvement of MLC was only supported by DFT calculations and kinetic experiments. A complete catalytic cycle was not presented, but a rate-limiting C-H activation step was reported based on kinetic isotope effect experiments with deuterated arenes. In this area, the role of the ligand was proposed to facilitate the limiting C-H activation through a ligand assisted concerted metallation-deprotonation mechanism (Figure I.18). This was further supported through DFT calculations that showed a relative increase in energy of the transition state of the CMD step. The transition state involving two pyridone ligands with one assisting in the CMD was set as reference to 0.0 kcal.mol⁻¹ and an increase from 4.4 to 9.6 kcal.mol⁻¹ without the combined use of pyridones or with acetates as bases was then observed in the other cases.

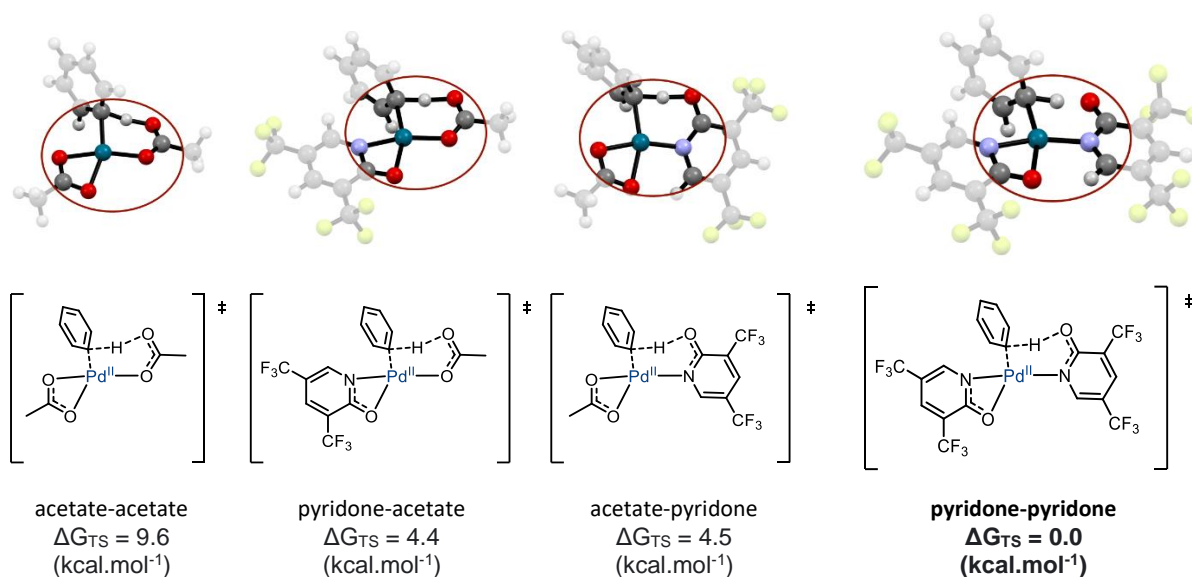
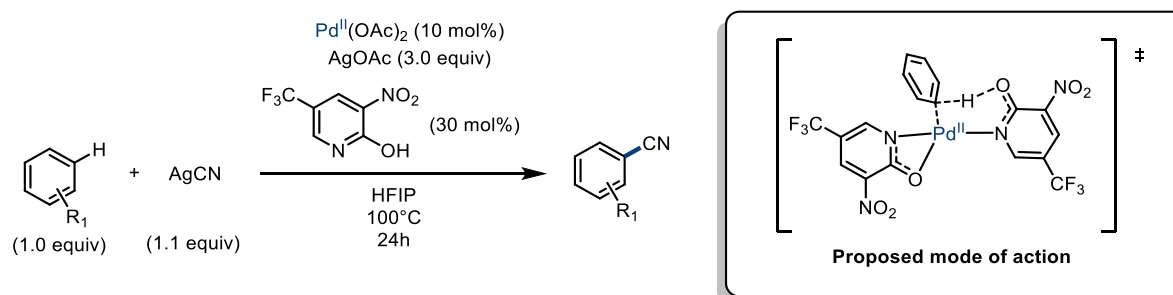


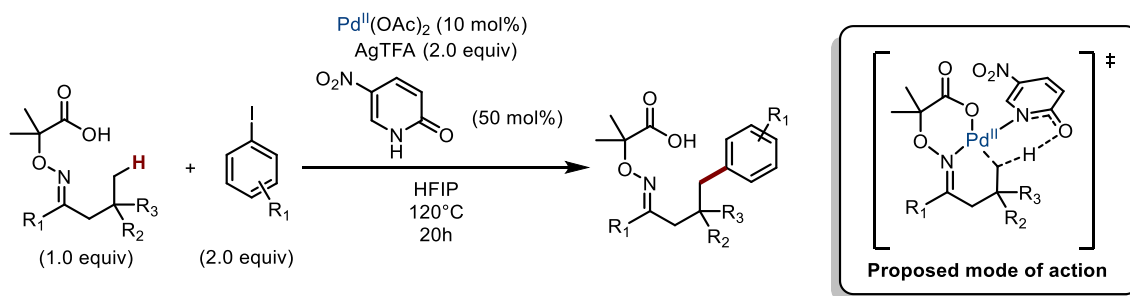
Figure I.18: Calculated DFT transition state and associated energy for the ligand assisted CMD

This approach was then extended to the catalytic cyanation of arenes and a similar mode of action of the complex was proposed (Scheme I.76).^[61]



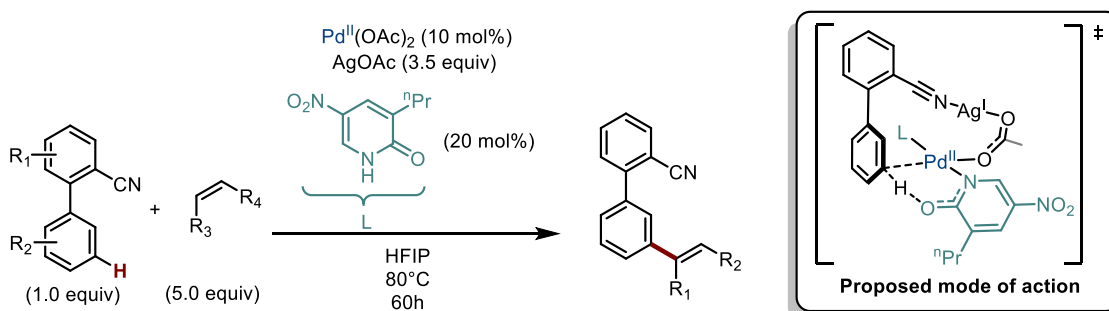
Scheme I.76: Catalytic non-directed cyanation of arenes by ligand assisted CMD

In the previous examples from Yu, undirected C_{sp2}-H activation was achieved by MLC. However, for C_{sp3}-H activation, a directing group (in this case a masked ketone) was required at the substrate (Scheme I.77).^[62] The cross coupling between aryl iodides and γ -C_{sp3}-H was achieved, and once-again MLC was proposed to assist the C-H activation step.



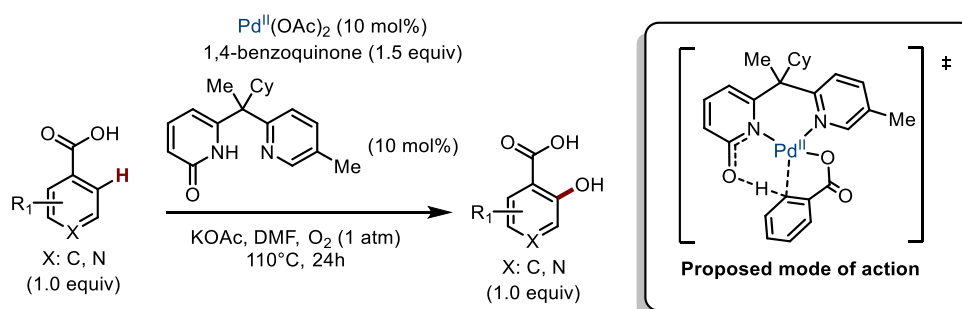
Scheme I.77: Cross-coupling between aryl iodides and $\gamma\text{-C}_{\text{sp}^3}\text{-H}$, with proposed involvement of MLC in the C-H activation step

The use of directing groups for remote C-H activation assisted by MLC was further established in 2020 by the same group in a Heck-type coupling of biphenyls (Scheme I.77)^[63], the formation of a transient, heterobimetallic non-innocent complex was proposed (on the basis of DFT calculations) as key step for the remote, meta-selective CMD.



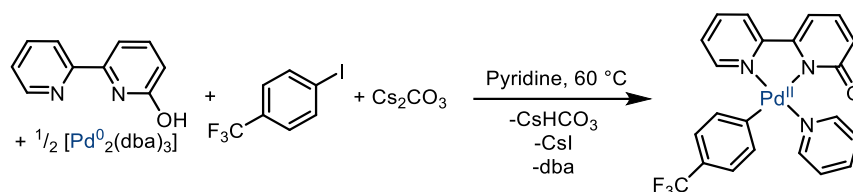
Scheme I.78: Remote meta-selective Heck-type coupling assisted by the transient formation of a non-innocent heterobimetallic complex

Recently, the C-H hydroxylation of arenes with molecular oxygen was reported using a bidentate ligand design (Scheme I.79). In this case, a carboxylic acid was used as directing group for the ortho-selective, ligand-assisted C-H activation step.



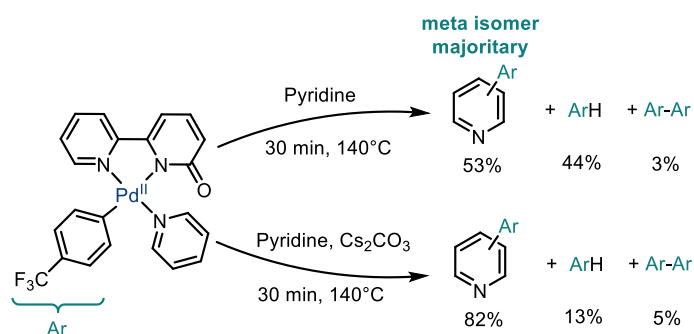
Scheme I.79: Hydroxylation of arenes with a non-innocent bidentate ligand assisting in the C-H activation step

It is interesting to note that the first bidentate version of this ligand design with palladium was reported by Albéniz in 2018 (Scheme I.80).^[64] The complex was synthesized via oxidative addition of an aryl iodide to a Pd⁰ precursor in presence of the bipy ligand.



Scheme I.80: Synthesis of the pyridone-Pd complex by Albéniz

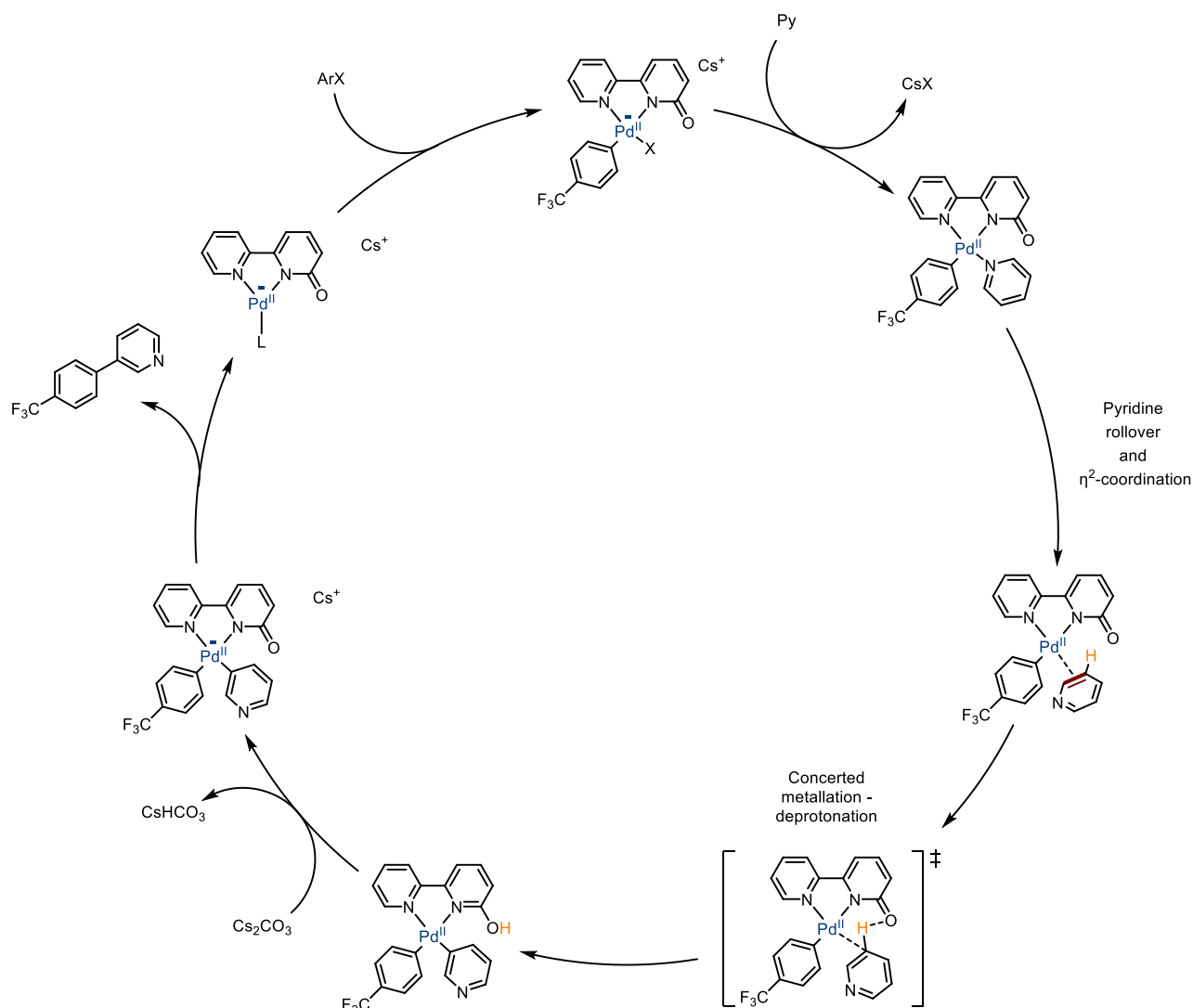
This ligand framework results in a close proximity between the basic C=O site and the pyridine. C-H activation of pyridine was reported upon heating at 140 °C (Scheme I.81). Remarkably, while ortho C-H activation could be expected from its proximity with the basic site, the formation of meta-coupling product as well as 44% of product of reduction ArH was reported. The origin of the reduction product was attributed to the formation of acid. When Cs₂CO₃ was added, the side product formation was drastically reduced to 13%.



Scheme I.81: C-H activation and reductive elimination of pyridone-Pd complex

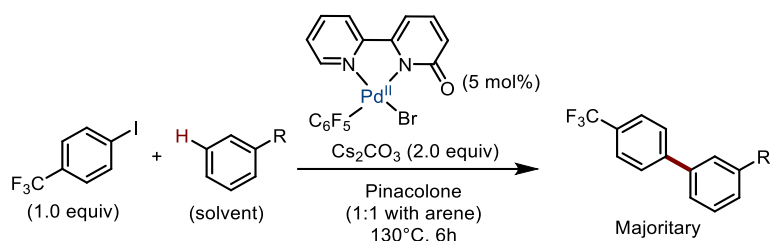
DFT calculations were performed to shed light into the mechanism and the non-innocent character of the ligand (Scheme I.82). Accordingly, the reaction was presumed to proceed as follows:

- A first step of decooordination and rolover of the pyridine ring is described, resulting in a proximity of the meta proton and the basic site. C-H activation is then proposed as a next step by concerted metalation-deprotonation. The resulting pyridine-OH is then further deprotonated by Cs₂CO₃ and the coupling product is formed after reductive elimination. Oxidative addition of halogenoaryl on the palladate is then suggested, followed by substitution of the halogen by the pyridine and the catalytic cycle is closed by formation of CsX.



Scheme I.82: Catalytic cycle of the Ar-Py cross coupling reaction described by Albéniz

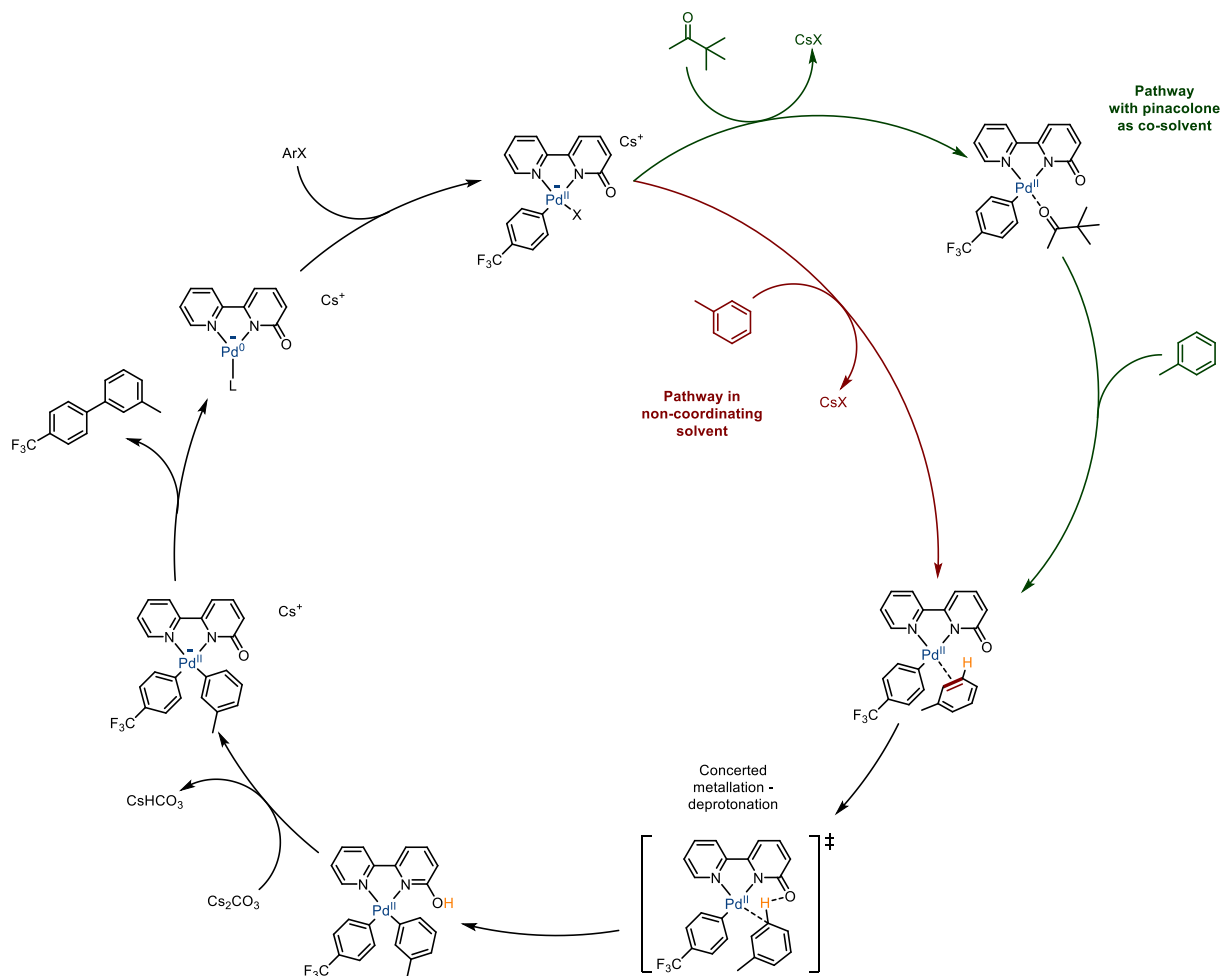
Further work from the Albéniz group recently extended this methodology to arenes (Scheme I.83).^[65]



Scheme I.83: Solvent effects in the ligand assisted C-C cross coupling of arenes

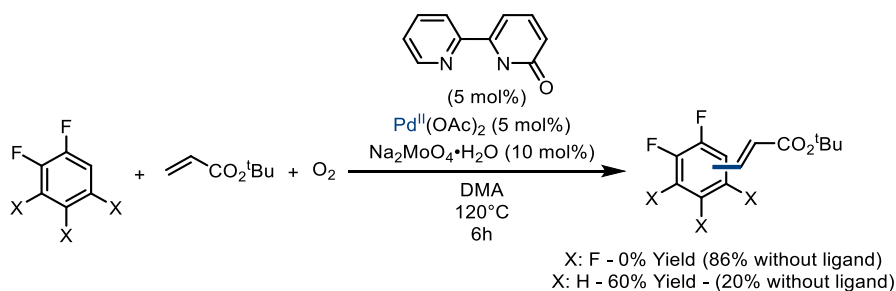
A surprising accelerating effect was found using moderately coordinating solvents such as pinacolone. This effect was explained by the authors by the formation of a new resting state of the catalyst, decreasing the energy barrier of the ligand substitution before C-H activation

and facilitating the overall reaction (Scheme I.84). The presence of non-productive C-H activation of the solvent was also reported. However, the C_{sp^3} - C_{sp^2} reductive elimination barrier was found higher in energy and thus not detrimental to the desired reactivity. In absence of an easier reductive elimination (i.e. in absence of toluene) the coupling product between the pinacolone solvent and Ar-I was reported with a low yield (15%).



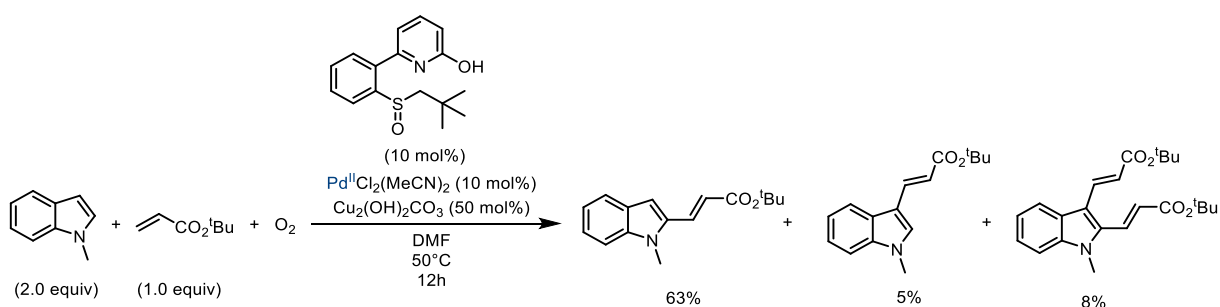
Scheme I.84: Catalytic cycle of the C-C cross-coupling reaction developed by Albéniz with and without pinacolone as co-solvent

The ligand-assistance in concerted metallation-deprotonation was further studied by Albéniz in the aerobic Heck-type coupling of arenes (Scheme I.85).^[66] Interestingly, in this case, a high-activity with perfluorinated activated arenes was reported in absence of cooperative ligand, with even a deleterious effect of the presence of the ligand. This was explained by the authors with the ligand hampering the other steps of the catalytic cycle in the case of a facile C-H activation. However, when the acidity of the arene is lowered, the C-H activation and the overall reaction clearly benefits from the presence of the cooperative ligand.



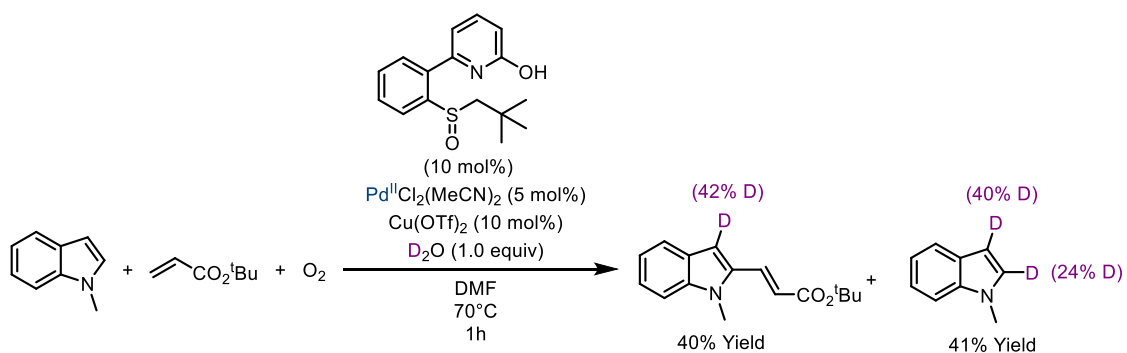
Scheme I.85: Comparison between activated and unactivated arenes in Albéniz's catalytic system with and without ligand

An alternative ligand design, with a flanking sulfoxide instead of a pyridine was described by the group of Jiao for the palladium catalyzed C-H alkenylation of indoles (Scheme I.86).^[67]



Scheme I.86: Catalytic activity and synthesis of Jiao's complex for the catalytic alkenylation of indoles

The crucial role of the ligand in an unusual regiodetermining step was demonstrated by strong experimental data, further supported by DFT calculations. Classically in Heck alkenylation of indoles, the product outcome is determined by the C-H activation step in C₃ or C₂ position. In this case however, a reversible deprotonation step was reported based on D-labeling experiments (Scheme I.87).



Scheme I.87: D-labeling experiments with D₂O showing D incorporation at the C₂ and C₃ position: Reaction was performed in presence of D₂O and stopped at half conversion

DFT calculations were then used to clarify the mechanism (Figure I.19). A quasi-reversible ligand assisted C₂ and C₃ deprotonation was reported, in accordance with the D-labeling

experimental results. The full mechanism was proposed as follows: The Pd^{II} bis-halide precursor is suggested to first undergo halide abstraction and formation of HOTf with a Cu^{II} salt. Indole coordination on the corresponding complex then occurs, followed by C-H activation (reversible at C3 or C2). Insertion of the alkene into the Pd-C bond is then proposed as the rate and regio-determining step.

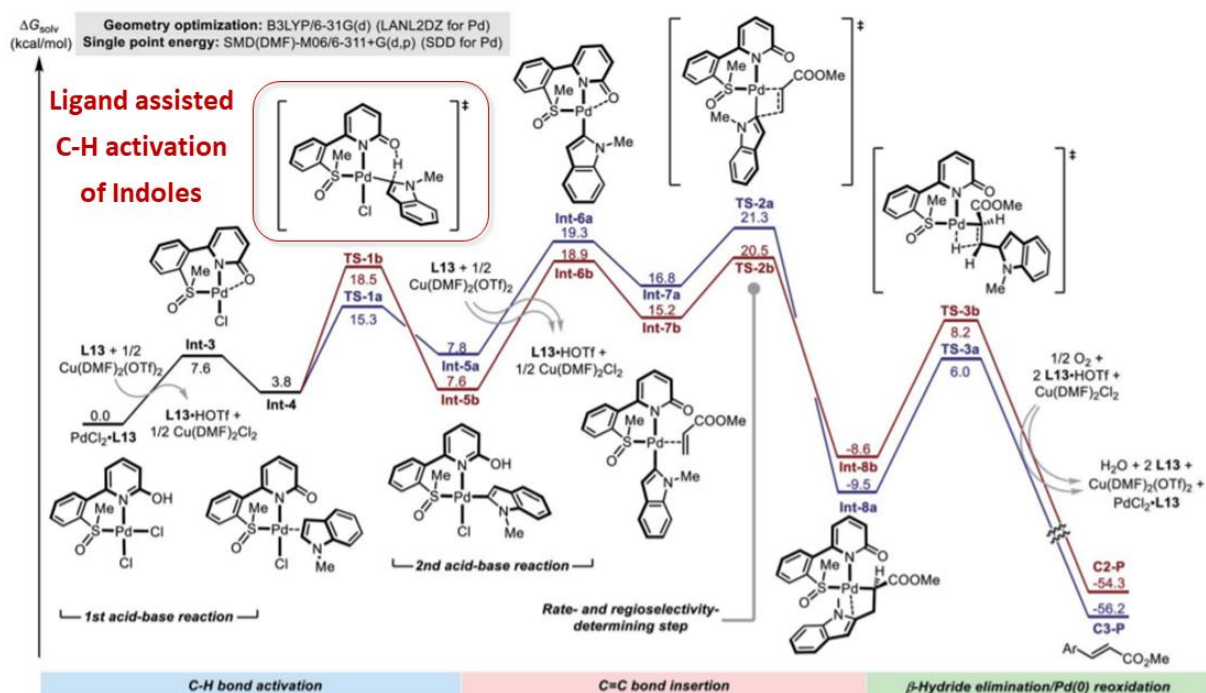


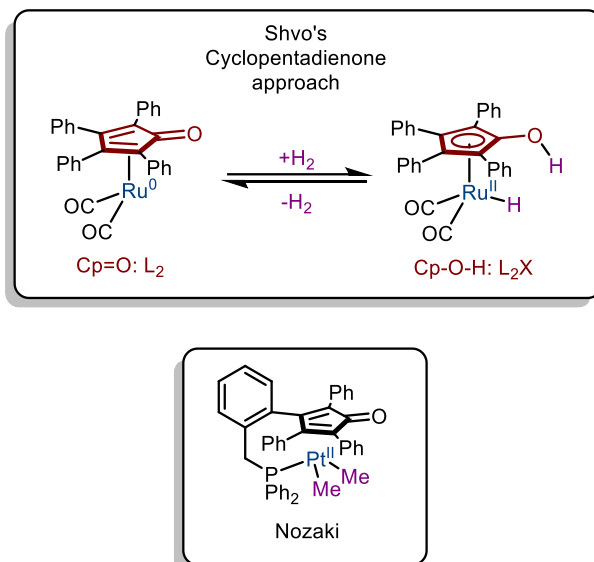
Figure I.19: Adapted with permission from Chem. Sci., 2020, 11, 11042–11054 under creative commons license.

Energy of the transition states and intermediates involved in the C2 (depicted in red, b.) and C3 (blue, a.) alkenylations of indoles.

In the previous examples, the non-innocent character of a carbonyl fragment, delocalized within the π -system of a pyridone ring was established through stoichiometric and catalytic transformations. High catalytic activities and unusual selectivities were achieved through this ligand design.

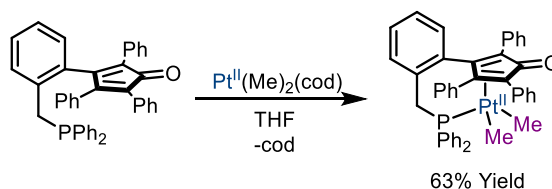
Another approach not based on a pyridone ring but on cyclopentadienone was introduced by Shvo with ruthenium and is considered as the first example of metal-ligand cooperativity (Scheme I.87).^[68] In this case, heterolytic H₂ activation leads to the protonation of the oxygen center and the formation of a Ru^{II}-Hydride. A coordination switch from the initially L₂ cyclopentadienone to L₂X was reported upon protonation and formation of the Ru^{II}-H. While

many applications of this catalyst can be found in the literature, only one example with group 10 metals was reported by Nozaki. ^[69,70] In this case, the non-innocent character of the cyclopentadienone backbone was illustrated in the assistance of a stoichiometric elementary step.



Scheme I.88: Comparison of Shvo's cyclopentadienone complex and Nozaki's approach

The complex was synthesized by treatment of the corresponding proligand with Pt^{II}(Me)₂(cod) in THF (Scheme I.89).



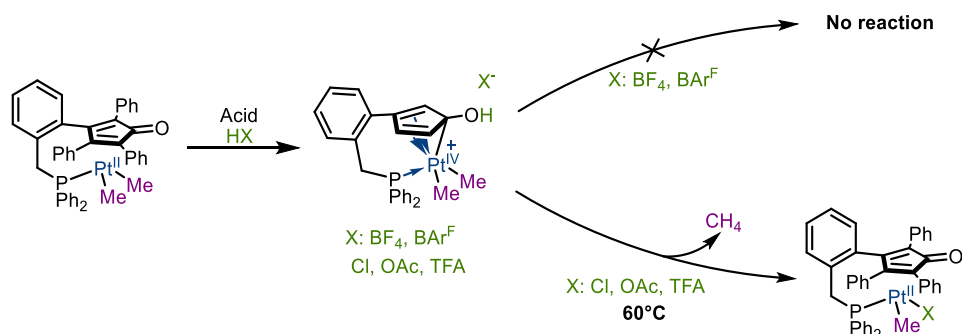
Scheme I.89: Synthesis of the π -arene Pt^{II} complex of Nozaki

The resulting complex was then reacted with acids and protonation of the cyclopentadienone ligand was observed (Scheme I.90). A rearrangement of the π -system was triggered by protonation, resulting in a formal Pt^{II} to Pt^{IV} oxidation of the metal center. Single crystal X-ray analyses of the cyclopentadienone Pt^{II} and protonated cationic Pt^{IV} complexes were performed. An elongation of the C=O bond from 1.221 to 1.312 Å was observed confirming the double and single bond character in the respective complexes. The Pt-C distance of the C₃-Cp ring was significantly shortened from 2.516 to 2.374 Å upon protonation.

Remarkably, protonolysis of the C_{sp3}-Pt^{IV} was observed upon heating, and this phenomenon was found strongly dependent on the acid used. While the strength of the acid

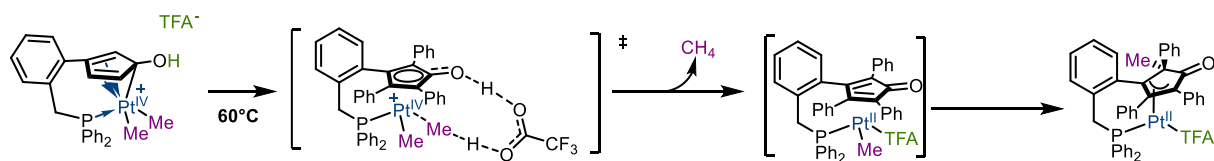
was already reported to play a role in the protonolysis of Pt^{II} complexes (with the strongest acid reacting faster),^[71] an opposite reactivity trend was observed in this case.

No reaction was reported with HBF₄ and HBAR^F₄, 30% of conversion was achieved with HCl, while the weaker TFA and acetic acid were the best partners with 36% and 62% conversion, respectively, after 24h (Scheme I.90).



Scheme I.90: Nozaki Pt-C_{sp3} protonation and protonolysis of C_{sp3}-Pt bonds with cyclopentadienone Pt^{II} complex

Based on these results, (alternative to the direct protonolysis), an outer-sphere mechanism compared of the Pt-C_{sp3} bond was proposed and supported by DFT calculations. The counter-ion was found to have a crucial proton-shuttling role from the O-H of the backbone to the backside of the Pt^{IV}-C_{sp3} bond (Scheme I.91). Remarkably, the relevance of proton shuttling in MLC with group 10 metals was already highlighted by our group in 2016.^{[30],c} Interestingly, in the case of TFA, further evolution of the complex after the protonation/reductive elimination sequence was observed with insertion of one of the C=C bonds into the remaining Pt-C_{sp3} bond.



Scheme I.91: Proton-shuttling role of the conjugated base and further reaction of the Pt complex with TFA

All along section I.1, examples of an appended basic site at the backbone of a ligand with a group 10 transition metal have been presented through their bonding situation, their stoichiometric bond activation reactions, and their catalytic behavior. In most cases, many

^c The roles of proton-shuttles in H₂ activation *via* MLC was also highlighted by Hazari - *J. Am. Chem. Soc.* 2019, 141, 43, 17350–17360

experimental and *in silico* evidence was reported in support of a cooperative activity of the transition metal and the basic site. In the next section, the cooperativity between a tethered Lewis-acid at the backbone and a transition metal will be presented. While a lot of efforts were made, experimental evidence of the cooperativity between the two centers remains much more limited.

I.2) MLC between a group 10 transition metal and a Lewis acid

The synergy between transition metal complexes and Lewis acids was recognized by the Nobel committee in 1963 as the prestigious prize was awarded to Karl Ziegler and Giulio Natta for their work on alkene polymerization. In this example, the Lewis acid (AlEt_3 or MAO) was used as an external co-catalyst (for the activation of the Ti catalyst). Tethering the Lewis-acid within the ligand architecture was also reported to have a beneficial influence on silane dehydrogenative catalysis by Zargarian in 2004.^[72] Since then, other approaches were developed. This section is focused on examples with group 10 metals involving a temporary rupture of the M-LA interaction. Contributions in this area can be divided in two, according to the role of the Lewis-acid: as functional group reservoir (Figure I.20; a) or as an “assistant” towards oxidative addition (Figure I.20; b).

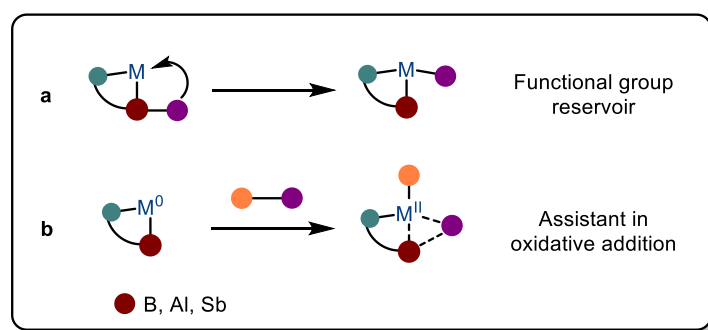


Figure I.20: Overview of the two main roles of a chemically non-innocent Lewis acid at the ligand

a) Functional group reservoir

i. *Ligand exchange at the transition metal*

In the following examples, the Lewis acid (typically a boron center) was reported to transfer one (or more) functional groups to the transition metal. The widespread use of boron reagents in cross-coupling reactions makes the study of functional group transfer between boron and transition metal highly relevant. Representative examples of this reactivity will be

presented first by discussing the contribution of Vedernikov with Pt^{IV}, followed by the example of Emslie with Pt^{II} and by Tauchert with Pd⁰ (Figure I.21).

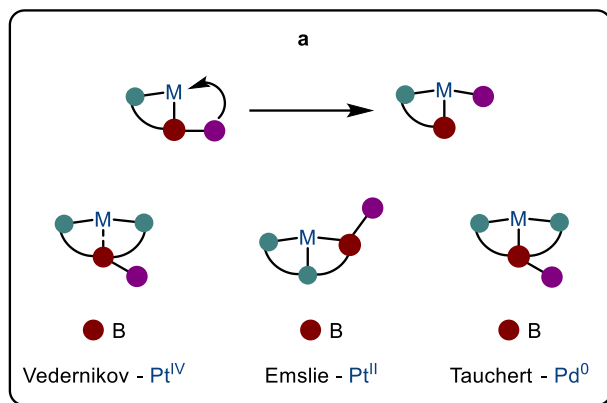
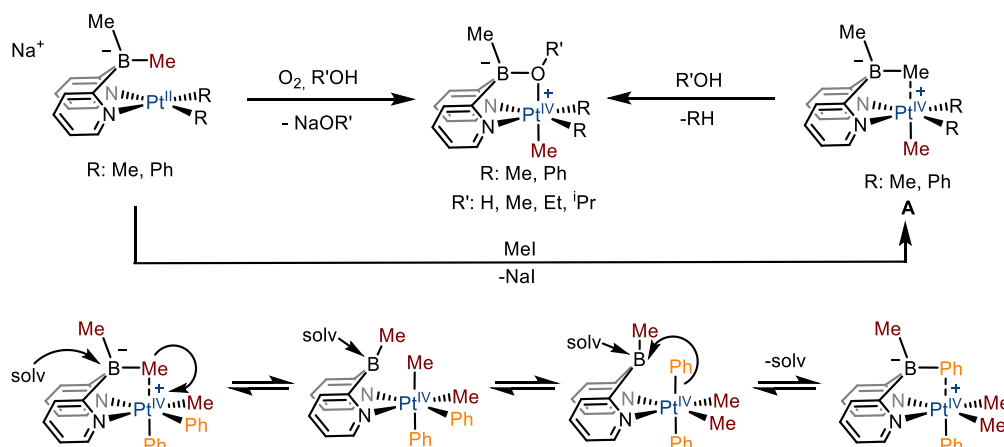


Figure I.21: Main contributions in the B-mediated ligand exchange strategy

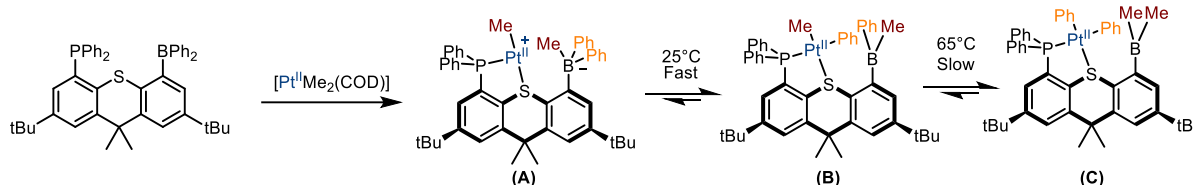
In the initial example of Vedernikov, back in 2007, the irreversible boron-mediated migration of a methyl group at Pt^{IV} was reported (Scheme I.92). The functional group transfer was triggered either by oxidation or by treatment with a protic solvent. Notably, a rare agostic CH-Pt^{IV} interaction was encountered in complex **A** (Scheme I.92). A reversible variant of this transformation was discovered as a solvent-mediated exchange of methyl and phenyl between boron and Pt^{IV} (Scheme I.92, bottom).^[73,74] In this case, the formation of the nucleophilic borate was reported in presence of the Lewis-basic solvent DMSO. Transfer of the methyl group from boron to Pt^{IV} was then described followed by back-transfer of a phenyl group from Pt^{IV} to boron to give a new zwitterionic borate-Pt^{IV} complex.



Scheme I.92: First example of group exchange mediated by boron reported by Vedernikov

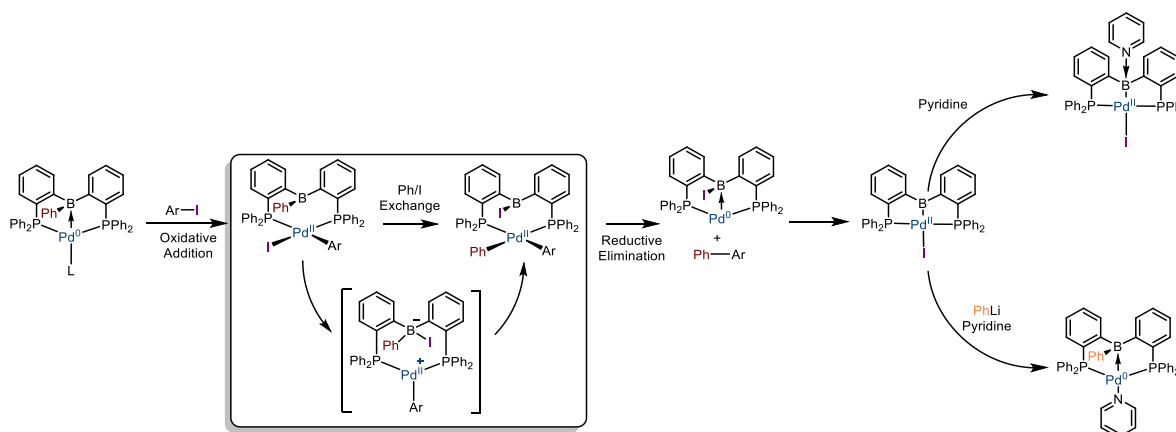
A similar conversion was reported in 2015 by the group of Emslie with Pt^{II} using a phosphine/borane ligand with a thioxanthene spacer (also called TXPB).^[75] A zwitterionic

complex was initially formed upon treatment of TXPB ligand with $[\text{Pt}^{\text{II}}\text{Me}_2(\text{COD})]$ (Scheme I.93; **A**). Interestingly, while in the case of Vedernikov, the methyl group at boron was transferred to Pt with back transfer of a phenyl group, in this case, the reactivity was turned the other way around. Abstraction of a methyl group from the metal by the boron was proposed and was described in an equilibrium at 25°C between the zwitterionic (Scheme I.93; **A**) and neutral (Scheme I.93; **B**) forms. A second phenyl transfer was also reported at 65°C in a slow equilibrium between **B** and **C** (Scheme I.93).



Scheme I.93: Group exchange between Pt^{II} and boron in the TXPB- Pt^{II} complex of Emslie

This field was then extended to Pd^0 by the contribution of Tauchert with the DPB (diphosphine borane) ligand architecture (Scheme I.94).^[76] In this case, the DPB- Pd^0 was reacted with an aryl-iodide to yield the corresponding Pd^{II} complex *via* oxidative addition. This complex then underwent boron-mediated halogen abstraction and phenyl transfer to Pd^{II} . Formation of the product of reductive elimination was then reported to yield a Pd^0 -iodoborane complex. Intramolecular oxidative addition of the B-I bond was then observed with the formation of the iodo- Pd^{II} -boryl complex. The Lewis-acidic character of the boron center was retained as suggested by formation of the pyridine adduct (Scheme I.94). Back transfer of a phenyl group to boron was also reported upon reaction with PhLi and pyridine.



Scheme I.94: Boron-mediated halide abstraction and group transfer in DPB- Pd^{II} complex as reported by Tauchert

ii. *Temporary acceptor of functional group*

In the previous strategies, the ability of the boron center to abstract/transfer a functional group from/to a transition metal was presented. In the following section, the role of the Lewis acid can be described as a temporary acceptor of a functional group, with transient breaking of the M-B interaction allowing for further reactivity (Figure I.22).

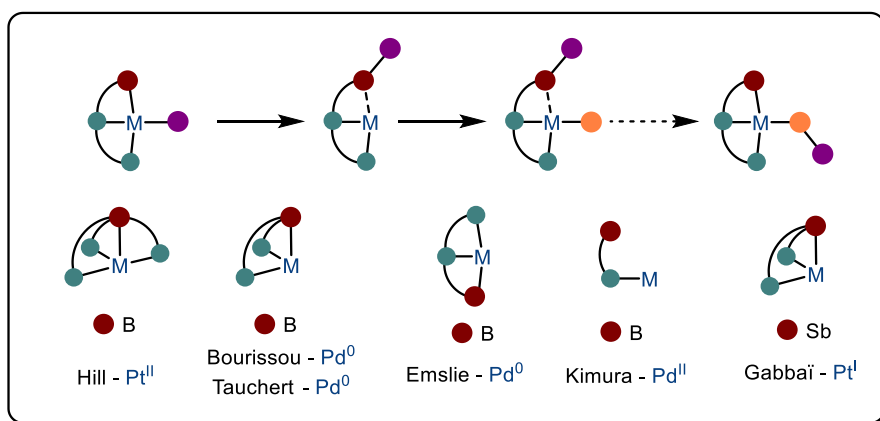
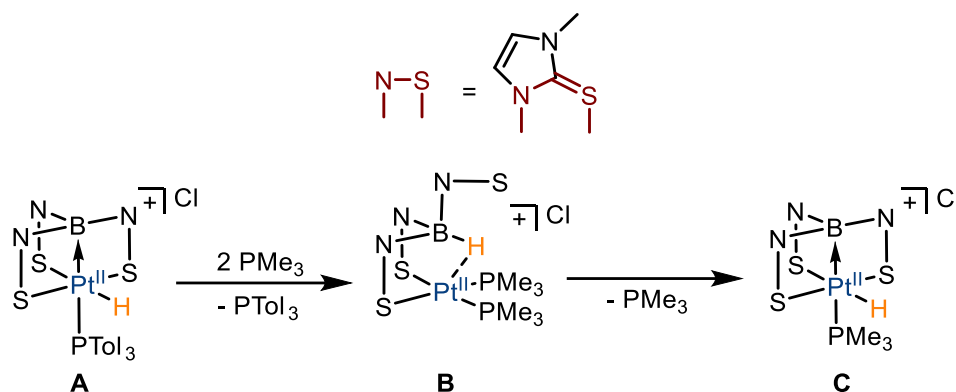


Figure I.22: Overview of the contributions where the Lewis acid acts as a temporary acceptor of functional groups

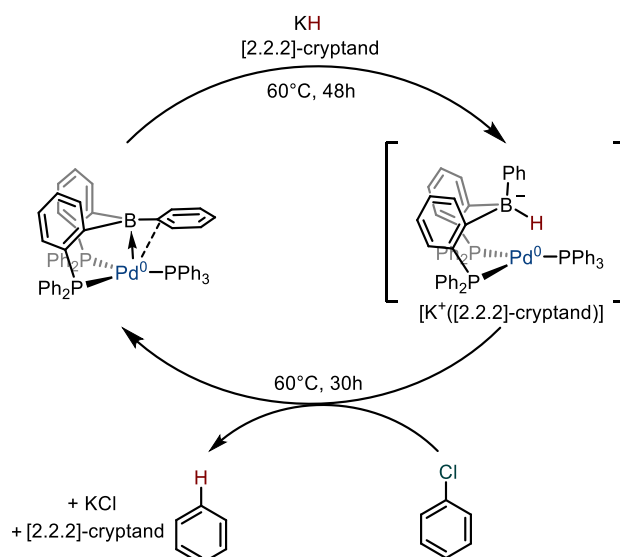
The first relevant example was reported by Hill in 2007 with an original mechanism of phosphine substitution at a metallaboratrane (Scheme I.95).^[77]

In this case, upon treatment of the platinaboratrane complex **A** with 2 equivalents of PMe_3 , formal substitution of PTol_3 was reported. The involvement of a borohydride complex was suggested by IR and ^{11}B NMR spectroscopy. The following mechanism was proposed: First, decoordination of one of the chelating arms, in tandem to a displacement of the hydride onto the boron and substitution by the two phosphine ligands to yield the square-planar Pt^{II} complex (Scheme I.95; **B**). The formal insertion of the metallic center into the B-H bond was then induced by the rigidity of the ligand architecture and the proximity of the resulting borohydride. The net product of phosphine substitution would finally form upon coordination of the metallaboratrane arm (Scheme I.95; **C**).



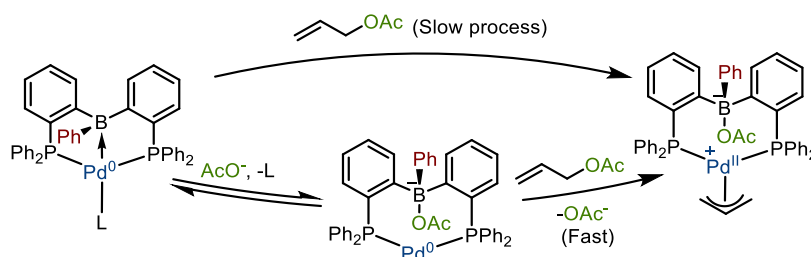
Scheme I.95: Boron as temporary acceptor of hydride for phosphine substitution at metallaboratrane

In the previous example, the boron center was able to act as a temporary reservoir of a hydride for an original phosphine substitution mechanism. In 2019, a similar strategy was reported by Kameo and Bourissou with a Pd^0 complex bearing a diphosphine-borane ligand (Scheme I.96).^[78] In this case, the DPB-Pd^0 complex was treated with KH in the presence of a cryptand, forming an anionic borohydride complex. The strong Z-type interaction between boron and palladium was thereby broken and the oxidative addition of aryl-halides was allowed thanks to the increased electron density at the metal center. The catalytic hydro/deutero-dechlorination was then reported with this system with a reverse order of steps compared to usual $\text{Pd}^0/\text{Pd}^{\text{II}}$ catalytic cycles. While oxidative addition at Pd^0 is usually considered the first step, a viable alternative pathway involving first functional group transfer, followed by oxidative addition was highlighted by this work through the mediation of a Lewis acid.



Scheme I.96: Hydro/deutero-dechlorination by the DPB-Pd⁰ complex with transient breaking of the M->B interaction allowing for oxidative addition

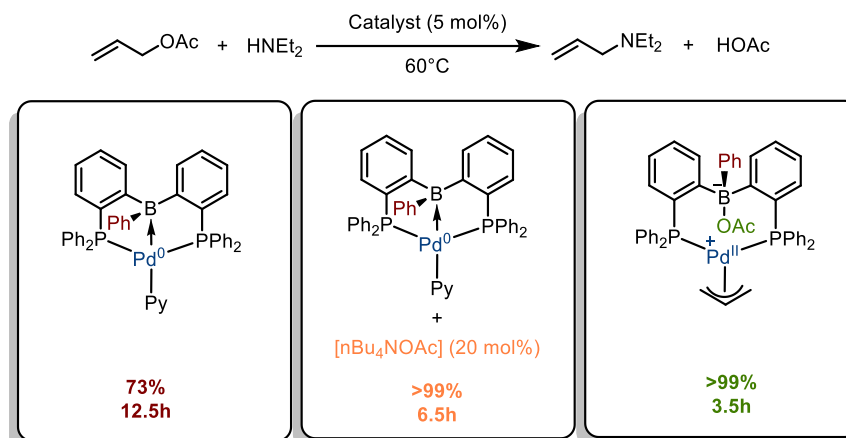
In 2015, the oxidative addition of allyl acetates to the DPB-Pd⁰ complex was studied by Tauchert (Scheme I.97).^[79] In this case, the strong Z-type interaction was shown to be detrimental to the oxidative addition, favoring low-oxidation states. The presence of a catalytic amount of acetate, however, was suggested to facilitate oxidative addition by the transient breaking of the Pd->B interaction (and thus the recovery of high electron density at the metal). It is interesting to note that while a more challenging oxidative addition could translate in an easier reductive elimination (further facilitated by product stabilization through M->Z interaction), a recent survey by Tauchert showed little to no impact of the Pd^{II}->B bond on the inner-sphere reductive elimination rate.^[80]



Scheme I.97: Impact of the B-M bond on the oxidative addition of allyl acetates

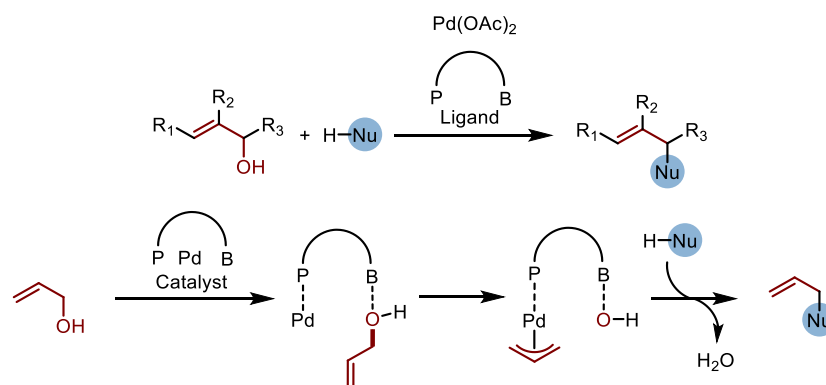
The inhibiting effect of the M->B interaction was further illustrated through the catalytic allylation of diethylamine (Scheme I.98). In this case, when the standard complex with a strong Pd⁰->B interaction was used, 73% yield was achieved after 12.5 hours. Upon addition of a catalytic amount of acetate, complete conversion was reached after 6.5 hours and when the

performed complex (i.e with the Pd⁰->B bond already broken) was employed, complete conversion was achieved even faster, within 3.5 hours.



Scheme I.98: Catalytic allylation of diethylamine with DPB-Pd⁰ complexes with and without B-M interaction

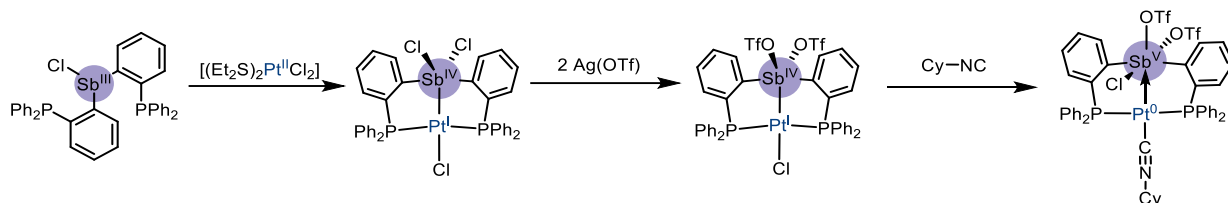
Interestingly, boron-assisted allylation reactions were studied by the group of Kimura. In their case, the direct allylation (and benzylation) of amines and the allylation of malonates was reported with Pd^{II} precursors and phosphine-borane ligands (Scheme I.99).^[81-83] While little experimental or theoretical data were reported in order to shed light into the mechanism, the mode of action of this system was proposed as follows. The P-B ligand first forms a complex with the Pd^{II} and acts as a template for coordination of the allyl alcohol, directing the formation of the π -allyl. The resulting borate moiety was then proposed to act as an internal base for the nucleophile, forming the C-Nu bond and regenerating the catalyst.



Scheme I.99: Proposed mode of activation of Boron-appended phosphine ligands in Kimura's templated reactions

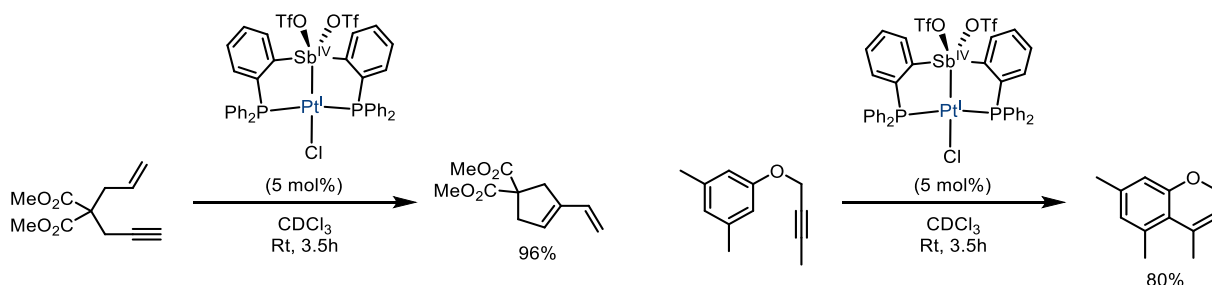
While in the previous examples, the Lewis acid was always a boron atom, an alternative system was introduced by Gabbaï with antimony (Scheme I.100).^[84] A PSbCl₂P platform was prepared by reaction of the diphosphinechlorostilbine ligand with [(Et₂S)₂PtCl₂].^[85] Upon

treatment with two equivalents of $\text{Ag}(\text{OTf})$, the chlorides at antimony were selectively exchanged for triflate groups. Remarkably, the resulting Lewis-acidic antimony center was described to act as intramolecular, self-activating, halogen abstractor upon treatment with a L-type ligand.



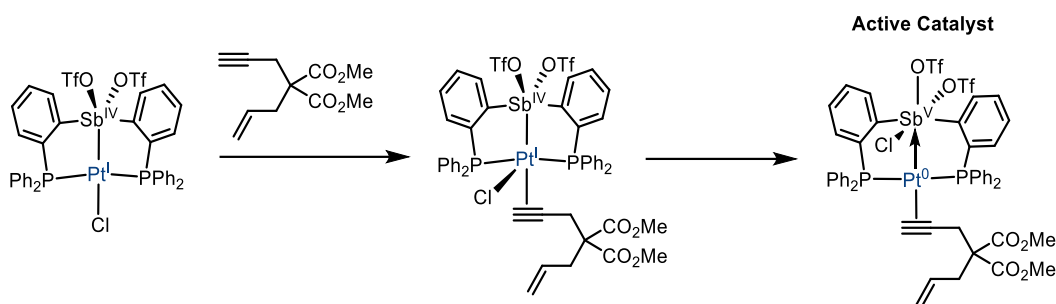
Scheme I.100: Synthesis and reactivity of Sb appended self-activating Pt complex reported by Gabbaï

Such a behavior was leveraged to catalysis, first in the cycloisomerization of enynes, and later in intramolecular hydroarylation (Scheme I.101).^[84]



Scheme I.101: Catalytic activity of PSbP-Pt complex in enyne cyclization and intramolecular hydroarylation reactions

The mechanism of these transformations, and more importantly the mode of action of the complex, was supported by computational studies performed in 2019 by Li Dang (Scheme I.102).^[86] The working hypothesis of a self-activating complex was supported by these calculations with the formation of a transient 5-coordinate Pt^{I} complex upon coordination of the alkyne. Intramolecular chloride abstraction by the Sb^{IV} changes the overall electronic configuration of the complex in favor of a π -coordinated $\text{Pt}^{\text{0}} \rightarrow \text{Sb}^{\text{V}}$ pincer, depicted as the active species.

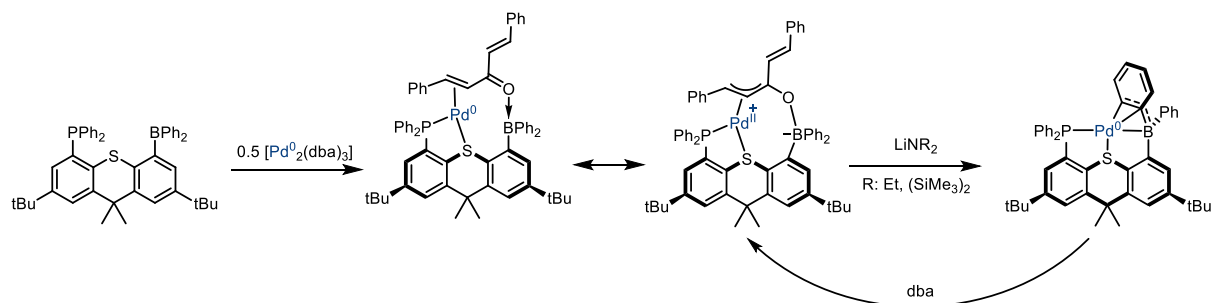
Scheme I.102: Proposed pathway for the self-activation of Figeroa's Pt^I complex

In the previous examples, the ability of the Lewis-acid to act as a reservoir or an acceptor of functional groups was demonstrated. New mechanistic pathways and transformations were achieved thanks to this Metal / Lewis acid cooperativity.

Most importantly, oxidative addition was found sensitive to the M- \rightarrow LA interaction, and the associated electron-density decrease at the transition metal. Transient breaking of this interaction was then shown to facilitate this elementary step.

d) Oxidative addition assistance

In the historical example reported by Emslie in 2006, a zwitterionic Pd^{II} complex was formed by coordination of the TXPB ligand to [Pd⁰₂(dba)₃] (Scheme I.103).^[87] The Lewis-acidic character of boron and the thermodynamically advantageous B-O bond was reported to strongly polarize the organic fragment. Oxidation of the palladium center was then reported with formation of the corresponding zwitterionic π -allyl complex. Interestingly, upon treatment with lithium amides, the metal center was reduced to Pd⁰ and the BPh₂ group was engaged in a 3-center BCC coordination (the fate of the organic fragment could not be established). Remarkably, the zwitterionic complex was regenerated by addition of dba to the reduced complex.^[88]

Scheme I.103: Boron-assisted oxidation of Pd⁰ to Pd^{II} upon coordination of TXPB to Pd⁰(dba)³

Another strategy was also developed based on boron assistance in true oxidative additions (Figure I.23). The first contribution in this area was reported by Peters in 2012 with Ni⁰. This

approach was then extended to palladium and platinum by Emslie and Bourissou with ligands featuring a lateral and central borane moiety, respectively. Finally, another approach with a lateral Lewis-acid was developed by Figueroa and Bourissou based on strained 4-membered metallacycles.

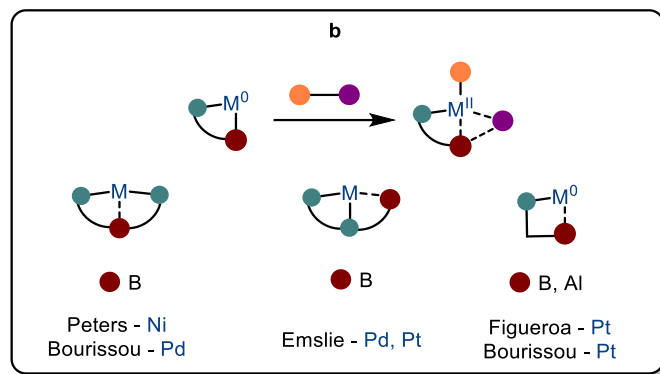
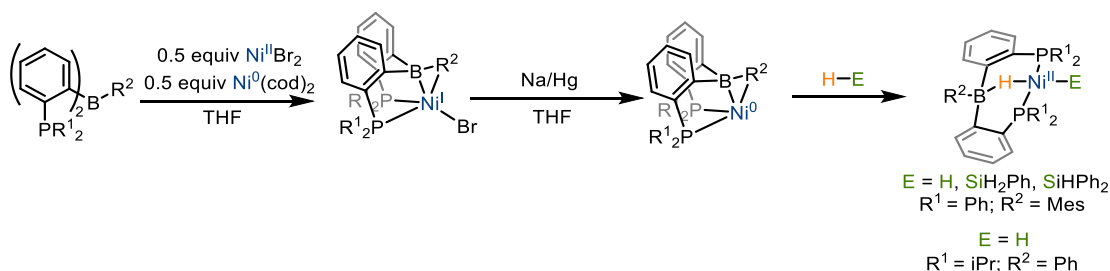


Figure I.23: Overview of the contributions in Lewis-acid assisted oxidative addition reactions

i. DPB Ligand design with central boron

In the initial report of Peters in 2012, a DPB Ni^I complex was first prepared by comproportionation of Ni^{II} and Ni⁰ (Scheme I.104).^[89] Further reduction to Ni⁰ was achieved with Na/Hg in THF. The resulting strong Ni⁰->B interaction was believed to inhibit oxidative addition, and more specifically H₂ activation. While no reaction with H₂ was reported with Ph²DPB^{Ph}, modification of the phenyl substituent at boron for a mesityl or the substituents at phosphorus for isopropyls allowed for H₂ activation.^[90,91]

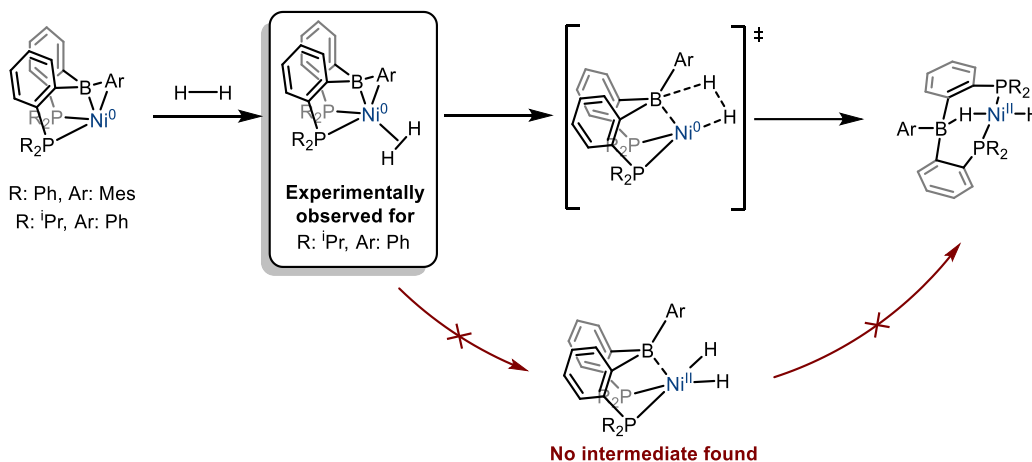


Scheme I.104: Boron-assisted E-H bond activation in DPB-Ni⁰ complexes

The chemical involvement of boron in the H₂ cleavage step was supported in both complexes by means of DFT calculations.^[91,92] The reaction was proposed to proceed as follows: First, a σ-H₂ complex forms upon side-on coordination of H₂ (Scheme I.105).

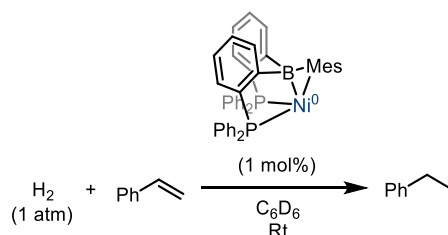
Remarkably, the σ-H₂ complex could be isolated and characterized spectroscopically in the case of ⁱPrDPB^{Ph} (a rare example of a d¹⁰-H₂ adduct). Then, a boron-assisted H-H bond cleavage follows with the formation of a square-planar borohydrido-Ni^{II}-hydrido complex. It must also

be noted that in both complexes, no Ni^{II}-dihydride intermediates were identified, stressing the important role of boron in the H₂ activation step.



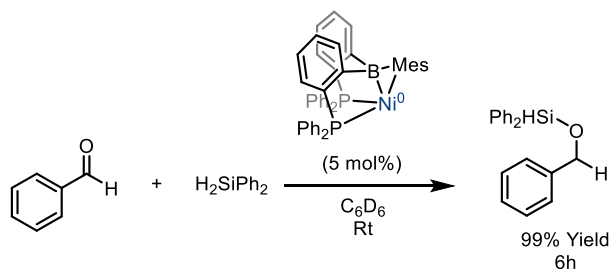
Scheme I.105: Mechanism of boron-assisted H₂ activation in DPB-Ni⁰ complexes

Interestingly, when the Ni⁰ complex was submitted to H₂ in the presence of an unsaturated substrate such as styrene, hydrogenation was observed. The reaction is catalytic and works well with a loading as low as 1% molar (Scheme I.107).



Scheme I.106: Catalytic hydrogenation of styrene by the DPB-Ni⁰ complex of Peters

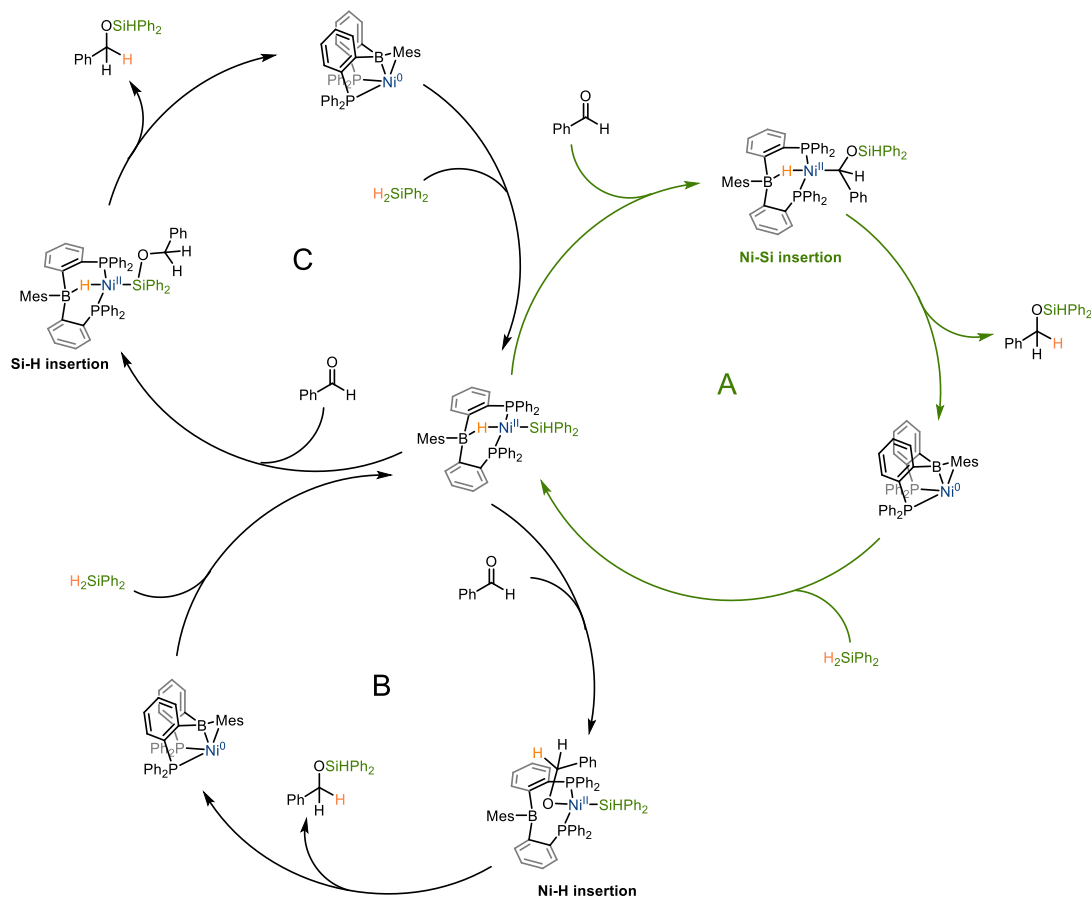
Remarkably, this complex was later shown active in the hydrosilylation of carbonyl compounds such as benzaldehyde (Scheme I.107).^[90] In this case, complete conversion was reported after 6h in deuterated benzene at room temperature.



Scheme I.107: Catalytic hydrosilylation of carbonyls by the DPB-Ni⁰ complex of Peters

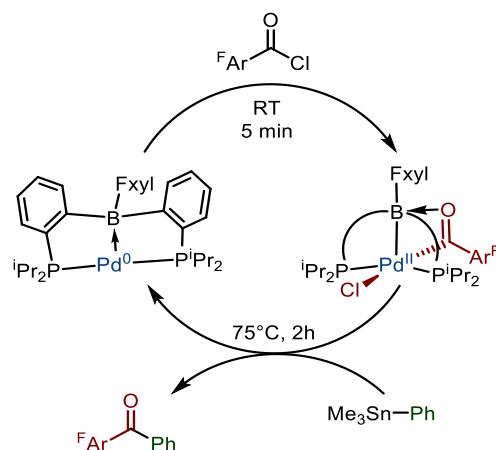
Three mechanisms were considered to explain this reactivity, all of them involving oxidative addition of the silane to Ni⁰ and then carbonyl insertion but with 3 different

outcomes: Insertion into the Ni^{II}-Si bond (Pathway A; Scheme I.108), into the Ni^{II}-H bond (Pathway B; Scheme I.108) or within the Si-H bond (Pathway C; Scheme I.108). NMR data of the insertion product ruled out the latter two paths. Pathway A was thus considered as the most probable with insertion into the Ni^{II}-Si bond and a last step of reductive elimination to yield the corresponding product of hydrosilylation.



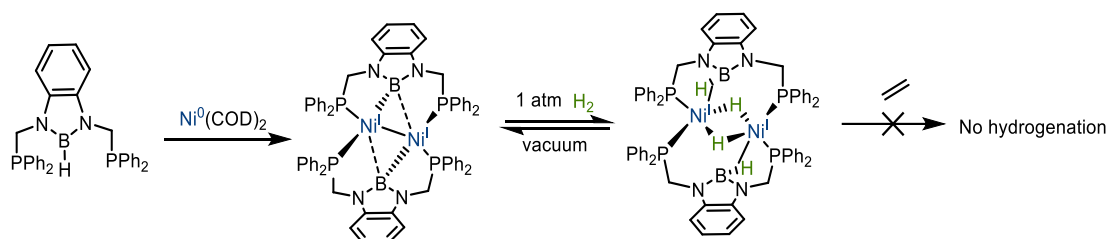
Scheme I.108: Postulated mechanisms of carbonyl hydrosilylation by the DPB-Ni⁰ complex of Peters

Further non-innocent behavior of the DPB ligand design was reported by our group with palladium in 2021 (Scheme I.109).^[93] While in the previous example, the boron center was found in interaction with a nickel hydride, in this case, boron-directed oxidative addition of acyl chlorides was reported. The secondary interaction between the oxygen center and the Lewis acid within the ligand architecture was exploited to achieve the chemoselective catalytic version of Stille coupling. Multiple other electrophiles were found compatible with this system such as aryl-halides and triflates, allowing for further functionalization.



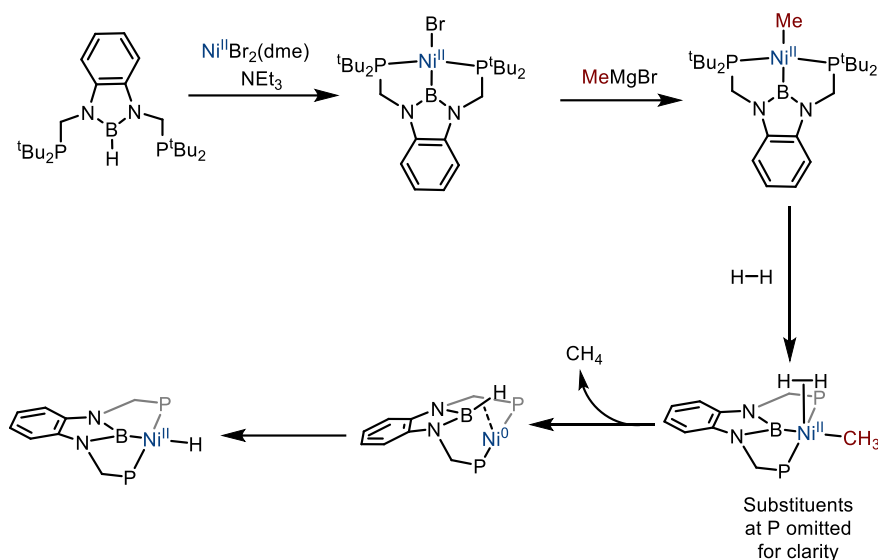
Scheme I.109: Chemo selective Stille-coupling with a beneficial effect of the DPB ligand

In 2014, another approach based on an original Ni^I-boryl bimetallic complex was reported by Peters (Scheme I.110). A bimetallic complex was formed by reaction of the B-H proligand with Ni⁰ in THF. Incorporation of two H₂ molecules within the structure was then achieved by treatment with one atmosphere of H₂. The structure of the ensuing complex was best depicted as Ni^I-(μ-H)₂-Ni^I bridged dimer with two η²-hydridoborane ligands. The H₂ activation phenomenon proved reversible as the Ni^I species was regenerated upon vacuum application. While the participation of the boron atom and the reversibility of the process was clearly described, no catalytic hydrogenation reaction was reported.^[94]

Scheme I.110: Boron assistance in reversible H₂ activation with DPBoryl-Ni complex

Interestingly, a boryl-assisted pathway for the synthesis of monomeric Ni^{II}-H was reported soon after by Rodríguez with the same ligand framework, but with ^tBu substituents at phosphorus (Scheme I.111).^[95] In this case, the methyl-Ni^{II}-boryl complex was prepared by transmetalation of the corresponding halogeno-nickel precursor with MeMgBr. Hydrogenolysis of the Ni^{II}-alkyl bond was then achieved under two atmospheres of H₂, and a mechanism involving cooperation of the boryl moiety was proposed based on DFT calculations. In the first step, H₂ approaches to nickel parallel to the Ni-B bond. Hydrogenolysis

of the CH₃ fragment then occurs with formation of η^2 -(B-H) Ni⁰ complex. Intramolecular oxidative addition finally affords the Ni^{II}-H species.

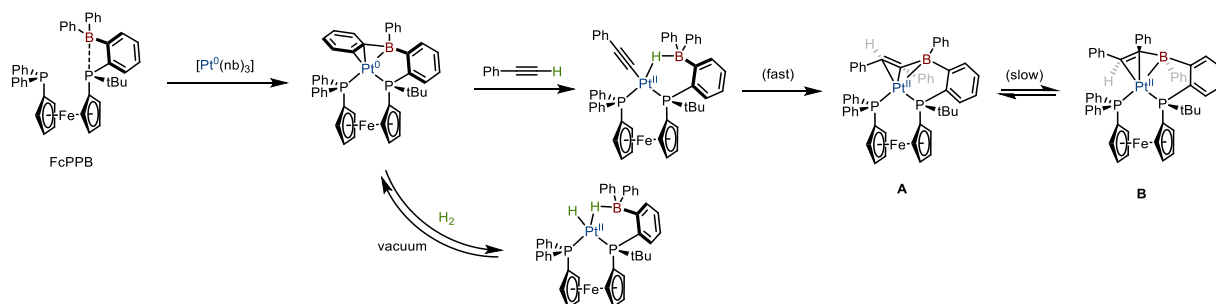


Scheme I.111: Boryl-assisted hydrogenolysis of C(sp³) bond and formation of a Ni^{II}-H complex

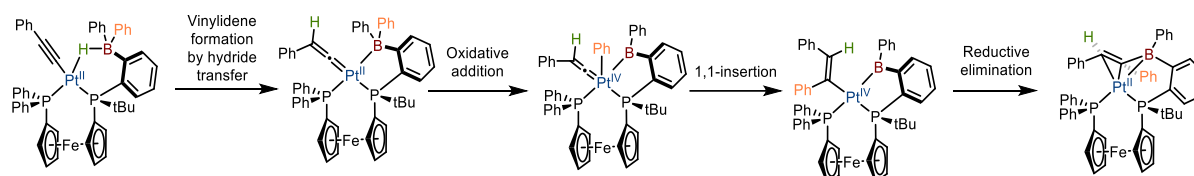
In this example, the non-innocent role of the boryl substituent in the H₂ cleavage process was clearly demonstrated through the formation of the η^2 -B-H Ni⁰ complex. It must also be noted that the boryl-Ni^{II}-H complex was reported active in catalytic hydrogenation of alkenes but the non-innocent role of the boryl fragment remains to be demonstrated.^[89,94]**4**

ii. DPB ligand design with lateral borane

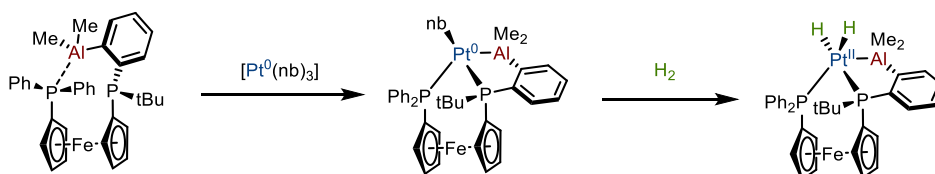
A ligand design with two strongly coordinating phosphines and a lateral borane was then reported by Emslie (Scheme I.112).^[96] The corresponding Pt⁰ complex was formed by reaction of the FcPPB ligand with [Pt⁰(nb)₃]. It adopts an η^3 -BCC coordination mode. The non-innocent character of the boron center was established by reaction of this complex with H₂. Oxidative addition was observed, and a stabilizing, bridging Pt^{II}-H-B interaction was detected by NMR spectroscopy, reinforced by DFT calculations. A slow H₂ release upon removal of the H₂ atmosphere (fast under vacuum) was also described with regeneration of the FcPPB-Pt⁰ complex. Reaction of the Pt⁰ complex with phenylacetylene formed the product of net Pt⁰ insertion into the C-H bond, stabilized by Pt^{II}-H-B bridging coordination. Rapid isomerization (within minutes) into complex **A** (Scheme I.112) and slow conversion into **B** was also reported.

Scheme I.112: H₂ and C-H activation at a FcPPB-Pt⁰ complex and Pt^{II}-alkynyl isomerization

A mechanism was proposed for the formation of **A** (Scheme I.113). Migration of the hydride was suggested as a first step to form Pt^{II}-vinylidene, followed by B-Ph oxidative addition to Pt^{II}, 1,1-insertion and finally reductive elimination.

Scheme I.113: Proposed mechanism for the isomerization of the FcPPB-Pt^{II} complex

It should be noted that the heavier analog FcPPAI-Pt⁰ complex was also synthesized, and a two center Pt⁰->Al interaction was found in this case (Scheme I.114). Oxidative addition of Pt⁰ to H₂ was demonstrated, but the Pt^{II}->Al interaction was retained, and no reactivity involving the aluminum center was reported.^[97]

Scheme I.114: PPAI-Pt⁰ complex and activation of H₂

iii. Strained 4-membered metallacycle

In contrast to earlier examples where the assistance of the Lewis acid was illustrated through strong B-O bond formation and/or stabilization of the product of oxidative addition, an alternative strategy based on ring-strain release as a driving-force was developed by Figueroa in 2014 and by Bourissou in 2016 (Figure I.24).^[98,99]

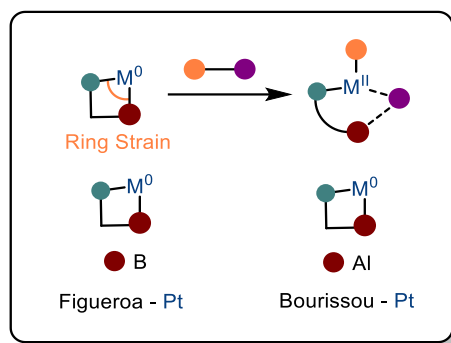


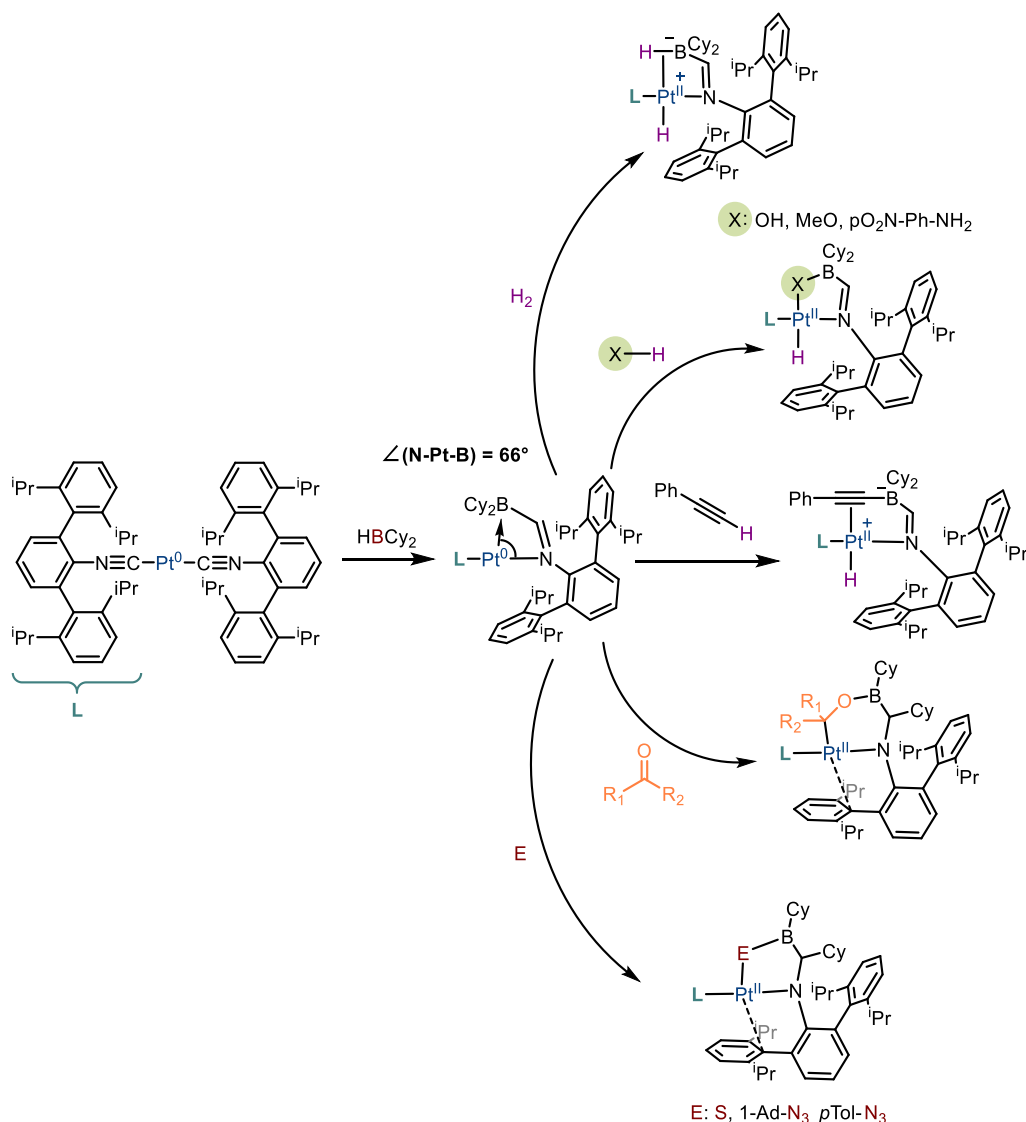
Figure I.24: Overview of the ring-strain release strategy for bond activation at the M-LA bond

In the first example of Figueroa, a $N\text{-Pt}^0\text{->B}$ metallacycle was synthesized by *in situ* hydroboration of a bis (isonitrile) complex (Scheme I.115). A constrained angle of 66° for the $N\text{-Pt}^0\text{->B}$ was reported in the crystal structure of this complex. Remarkably, a versatile MLC reactivity towards polar and apolar bonds was allowed through the breaking the $M^0\text{->LA}$ bond and release of this ring strain.

Notably, in contrast to the case of Emslie (Scheme I.112), where the borane-stabilized dihydride was formed upon H_2 activation, here, complete hydride abstraction by the Lewis acid was observed (top - Scheme I.115). The corresponding complex would then be best described as cationic platinum-hydride with an η^2 -coordinated borohydride. With the more polar X-H bonds (such as N-H and O-H), formation of the corresponding Pt^{II} -hydride and fixation of the X-group to boron was reported as the result of bond activation.

Remarkably, oxidative addition of phenylacetylene was described with once again a sharp reactivity contrast compared to the previous report of Emslie (Scheme I.112). In this case, a cationic Pt^{II} -hydride was formed and instead of a B-H- Pt^{II} interaction, complete abstraction of the alkynyl fragment by boron was observed, accompanied by its π -coordination to Pt.

Formation of a metallacycle by formal insertion of the C=O bond into the $Pt^0\text{-B}$ bond was observed upon reaction with carbonyls. In line with the Lewis basic/acid character of Pt^0 /boron, the carbon atom of the carbonyl derivative binds to Pt^{II} and the oxygen atom to boron. Interestingly, a 1,2-cyclohexyl shift from boron to the imine was also observed in this transformation. This result was explained by the increased nucleophilic character of the borate resulting from the addition of the carbonyl, in supplement to the vicinal position of the electrophilic imine. With azides and with elemental sulfur, oxidative insertion into the $Pt^0\text{->B}$ bond was reported.^[100]



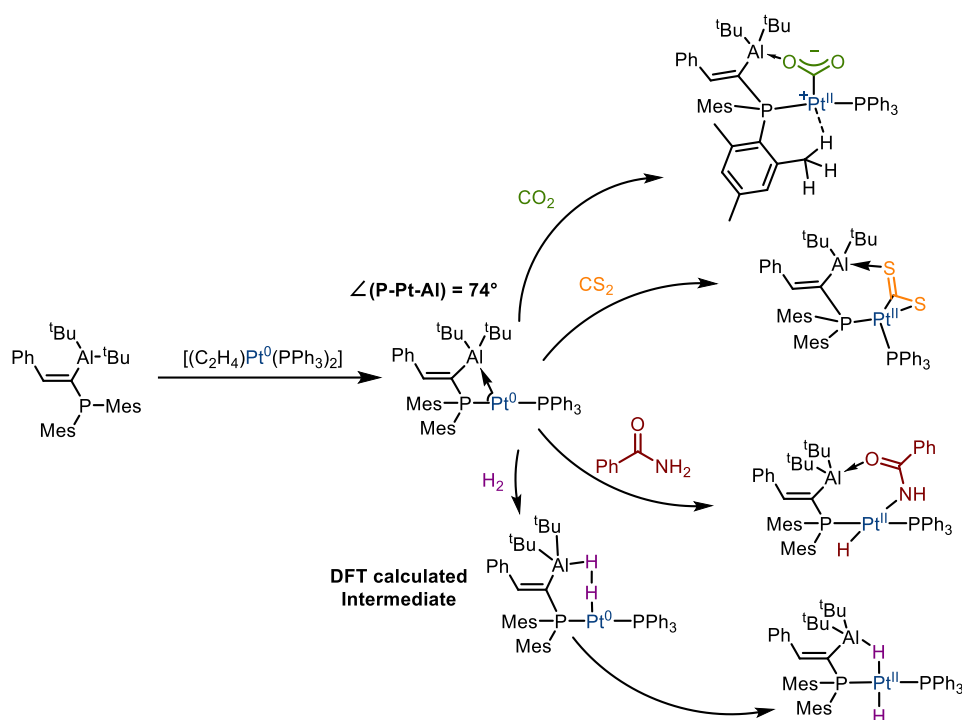
Scheme I.115: Versatile MLC reactivity by ring-strain release of Figueroa's Pt-B complex

An additional example of a ring-strain release upon bond activation was reported by our group in 2016 (Scheme I.116).^[99] A T-shaped platinum complex featuring a constrained $\text{Pt}^0 \rightarrow \text{Al}$ interaction ($\angle(\text{P-Pt-Al}) = 74^\circ$) was initially reacted with 1 bar of CO_2 . An original $\eta^1\text{-CO}_2$ coordinated complex was formed, as formal product of nucleophilic addition of Pt^0 to CO_2 with extra-charge stabilisation at aluminum. Single-crystal X-ray crystallography showed that CO_2 formally undergoes insertion into the $\text{Pt}^0 \rightarrow \text{Al}$ bond resulting in a zwitterionic Pt^{II} complex. Notably, a σ -agostic interaction was observed between the cationic Pt^{II} complex and a C-H bond of mesityl substituent at phosphorus. Unfortunately, coordination of CO_2 was reported irreversible, precluding any catalytic application at this stage.

A different behaviour was exhibited by the heavier homolog CS_2 . While insertion into the $\text{Pt}^0 \rightarrow \text{Al}$ bond and formation of a $\text{Pt}^{\text{II}}-\text{C}$ bond was also reported, the accumulated electronic charge was found not only stabilized by aluminum but by Pt^{II} also (probably due to its strong affinity with sulfur) resulting in a distorted 3-membered ring.

With polar N-H bonds such as in benzamide, N-H splitting was reported with formation of a $\text{Pt}^{\text{II}}-\text{hydride}$ and coordination of the nitrogen. The oxygen of the benzamide moiety was found to interact with the Lewis-acidic aluminum.

H_2 was also activated by this complex with the formation of a $\text{Pt}^{\text{II}}-\text{dihydride}$ stabilized by a $\text{Pt}^{\text{II}}-\text{H}-\text{Al}$ bridging interaction. The assistance of the aluminum in the H_2 activation step was suggested by DFT calculations. Dihydrogen was first reported to insert into the $\text{Pt}^0 \rightarrow \text{Al}$ bond with a side-on coordination to aluminum and end-on coordination to Pt^0 . The corresponding dihydride was then formed after oxidative addition.



Scheme I.116: Polar and apolar bond activation through a constrained Pt-Al 3-membered ring

I.3) Miscellaneous examples

In the previous sections, the cooperativity between a Lewis base/acid incorporated within the ligand backbone and a group 10 transition metal has been presented and illustrated through stoichiometric, and when relevant, catalytic reactions. In the following section, miscellaneous examples where the cooperative site cannot be described as a Lewis acid nor

as a Lewis base will be discussed. These examples can be best treated by studying first the silicon-mediated functional group migrations described by Iwasawa and Lee (a; Figure I.25). Then the example of Moret with an imine for Si-H bond activation will be presented (b; Figure I.25).

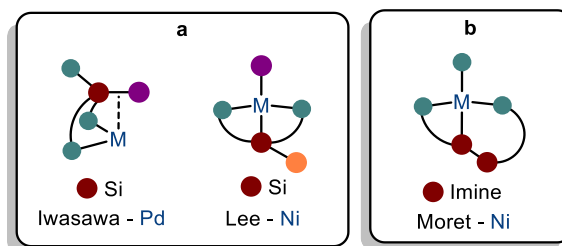
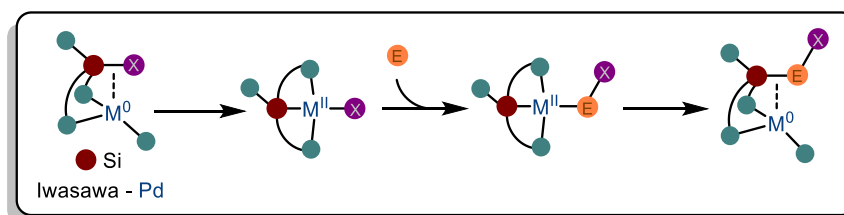


Figure I.25: Overview of the other examples of MLC with group 10 metals

a) Si center as acceptor and donor of organic fragments

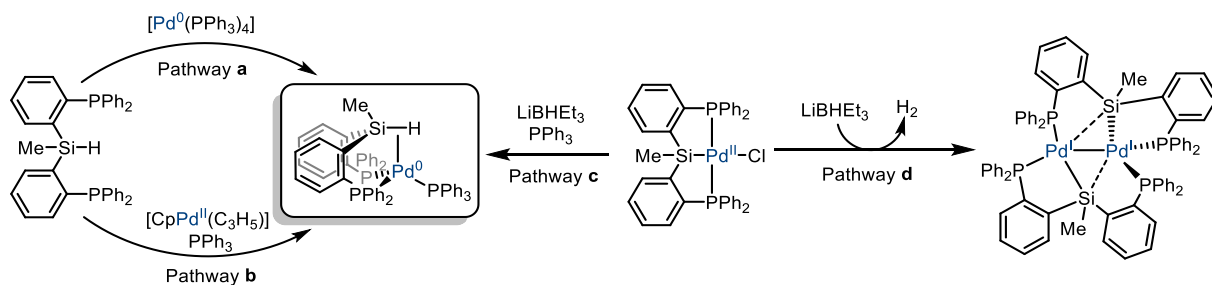
In this first example, a Si-X Pd⁰ σ -complex was proposed to act as a masked form of Si-Pd^{II}-X upon intramolecular oxidative addition (Scheme I.117). The square planar Pd^{II}-X would then undergo further reactivity (with E) and undergo Si-E reductive elimination to generate the net product of E insertion into the Si-X bond.



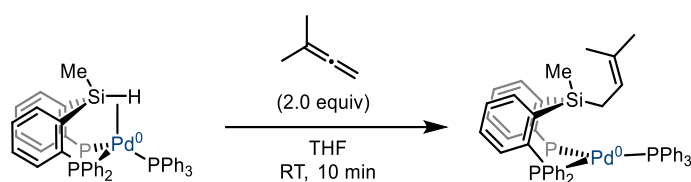
Scheme I.117: Schematic view of the non-innocent behavior of the Si-center in Iwasawa's complex

This reactivity was first displayed with X = H, and the synthesis of a Si-H η^2 -Pd⁰ was reported by Iwasawa via different synthetic strategies:

Direct treatment of the PSiHP pro-ligand with Pd⁰ tetrakis triphenylphosphine (Scheme I.118; Pathway **a**) or with Pd⁰ generated *in situ*: Either from [CpPd^{II}(C₃H₅)] (Scheme I.118; Pathway **b**) in presence of PPh₃ or by reduction of the Pd^{II}-Cl complex with LiBHET₃ in presence of PPh₃ (Scheme I.118; Pathway **b**).^[101,102] The presence of PPh₃ was found critical for the stability the σ -complex. Indeed, in the absence of such ligand, the Pd^{II}-H formed with LiBHET₃ was reported to evolve to the Pd^I-Pd^I dimer with concomitant loss of H₂ (Scheme I.118; Pathway **d**).

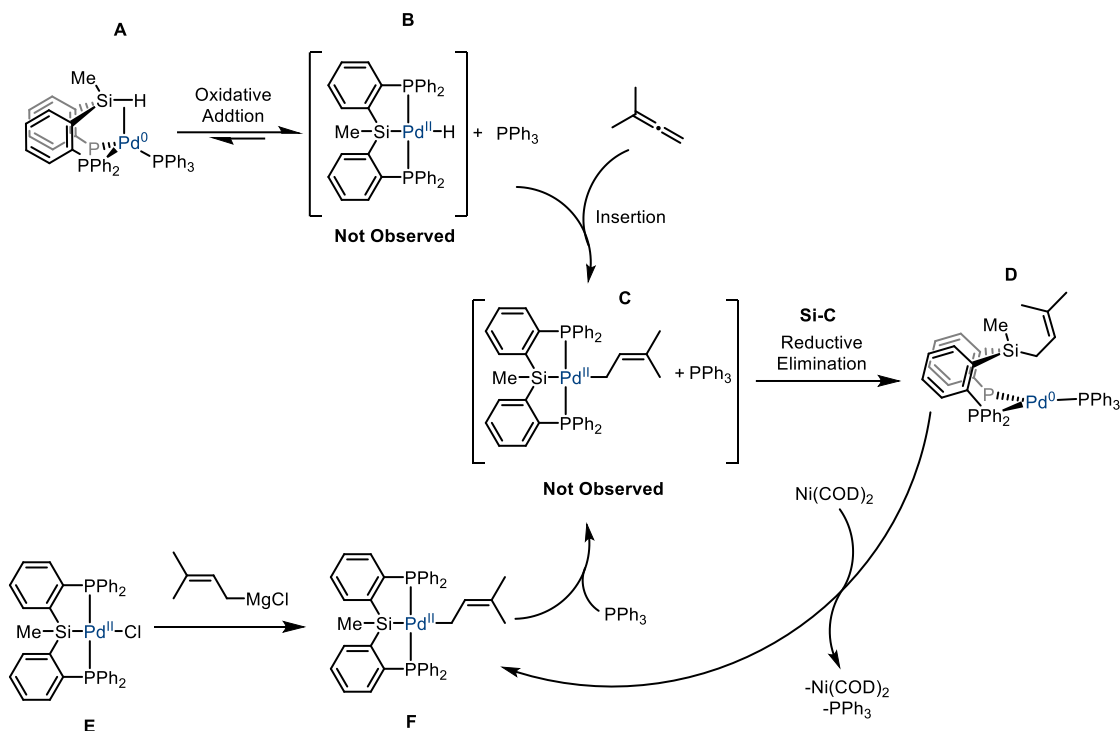
Scheme I.118: Synthetic strategies for the synthesis of the η^2 -Pd⁰ σ -complex of Iwasawa

Remarkably, when the Pd⁰ σ -complex was subjected to 3-methylbuta-1,2-diene, formal insertion of the allene into the Si-H bond was reported with the formation of a trigonal planar Pd⁰ complex (Scheme I.119).

Scheme I.119: Allene insertion into the Si-H bond on the Pd⁰ pincer complex of Iwasawa

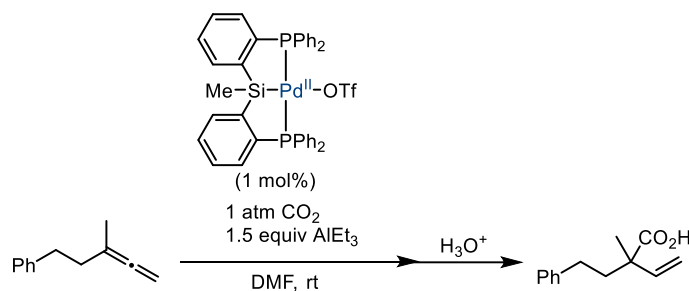
As the direct insertion of allene into the Si-H bond is unlikely, an alternative pathway was explored by the authors (Scheme I.120). The SiH-Pd⁰-PPh₃ system was proposed to act as a precursor of Pd^{II}-H upon PPh₃ decoordination and oxidative addition of the η^2 -SiH bond to Pd⁰ (**A** to **B** - Scheme I.120). Then, the allene inserts into the Pd^{II}-H to form the transient η^1 -prennyl-Pd^{II} complex then could occur (**C** - Scheme I.120) and the corresponding Si-prennyl-Pd⁰-PPh₃ complex of formal insertion into the Si-H bond is then formed by reductive elimination (**D** - Scheme I.120). To support this chemical pathway, the Si-Pd^{II}-prennyl complex was independently prepared by transmetalation of P^{Ph}SiP-Pd^{II}-Cl with prennyl-Mg-Cl (**F** - Scheme I.120) and the Si-prennyl-Pd⁰ complex was formed upon addition of PPh₃ (**E** - Scheme I.120). In addition, the reverse reaction was proven accessible by the reaction of Si-prennyl-Pd⁰-PPh₃ (**D** - Scheme I.120) with Ni⁰(COD)₂ as phosphine abstractor, resulting in formation of the Pd^{II}-prennyl (**F** - Scheme I.120) complex in a 10:1 ratio.

In this example, the non-innocent silicon center in the starting complex (**A** - Scheme I.120) acts as a reservoir of hydride and a masked, stable form of Pd^{II}-H. After further reactivity at the metal-hydride bond, the silicon group can take back the organic fragment after reductive elimination from the Pd^{II} complex.

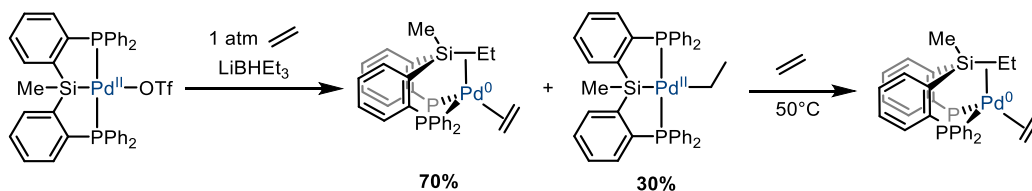


Scheme I.120: PSiP as hydride donor and organic functional group acceptor as described by Iwasawa

It is interesting to note that the Pd^{II}-H complex (proposed in Scheme I.120; complex **B**) was found as key intermediate in the hydrocarboxylation of allenes with CO₂ catalyzed by P^{Ph}SiP-Pd^{II}-OTf (Scheme I.121).^[103] A detailed mechanistic study conducted by Hazari showed that the main factor in the unusually high activity of this complex was not due to chemical non-innocence but was rather the result of the high trans effect of the silyl ligand.^[104]

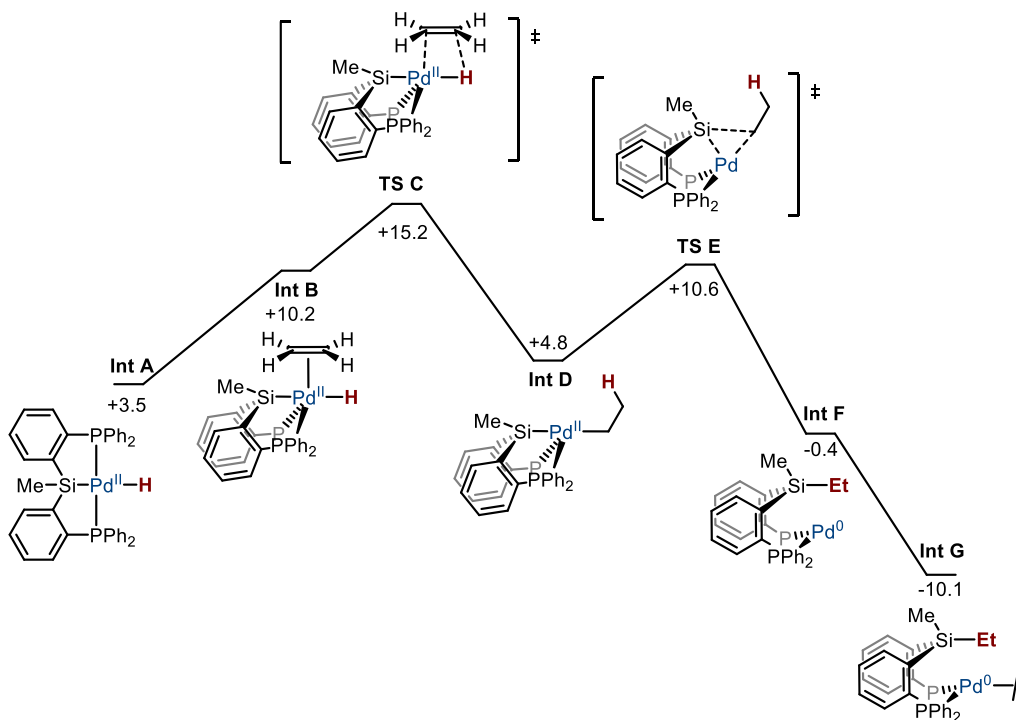
Scheme I.121: Catalytic hydrocarboxylation of allenes using the PSiP-Pd^{II}-OTf complex

Nevertheless, the ability of silicon to act as a donor/acceptor of functional groups was demonstrated with ethylene by the same group in 2014 (Scheme I.122).^[105] In this example, the palladium hydride was generated by treatment of the triflate complex PSiP-Pd^{II}-OTf with LiBHET₃ in the presence of ethylene. A mixture of η²-coordinated Si-Ethyl-Pd⁰ and Si-Pd^{II}-Ethyl was obtained, which evolved to the exclusive formation of Si-Ethyl-Pd⁰ upon heating to 50°C.



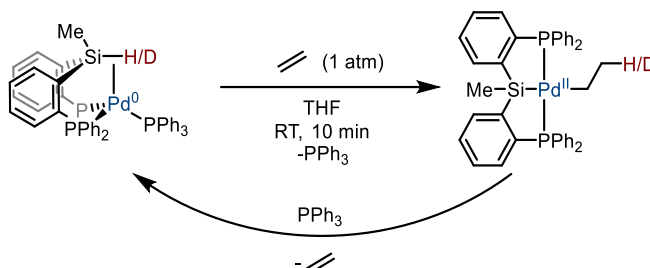
Scheme I.122: Generation of Pd-H and insertion of ethylene with subsequent Si-assisted reductive elimination

A plausible mechanism for this transformation was proposed based on DFT calculations. The formation of the Pd^{II}-H species (**Int A**; Scheme I.123) is followed by coordination of ethylene (**Int B**; Scheme I.123). Insertion into the Pd^{II}-H bond (through **TS C**; Scheme I.123)) then leads to the formation of the Pd^{II}-ethyl complex (**Int D**; Scheme I.123). The Si-center would then act as an acceptor for the ethyl fragment upon reductive elimination (**TS E**; Scheme I.123) to generate the Si-Ethyl-Pd⁰ complex (**Int F**; Scheme I.123) and a final step of ethylene coordination drives the C-Si reductive elimination to the final product (**Int G**; Scheme I.123).

Scheme I.123: Proposed mechanism based on DFT calculations of the Si-mediated reductive elimination of Si-Pd^{II}-Ethyl. (Energies are in kcal.mol⁻¹)

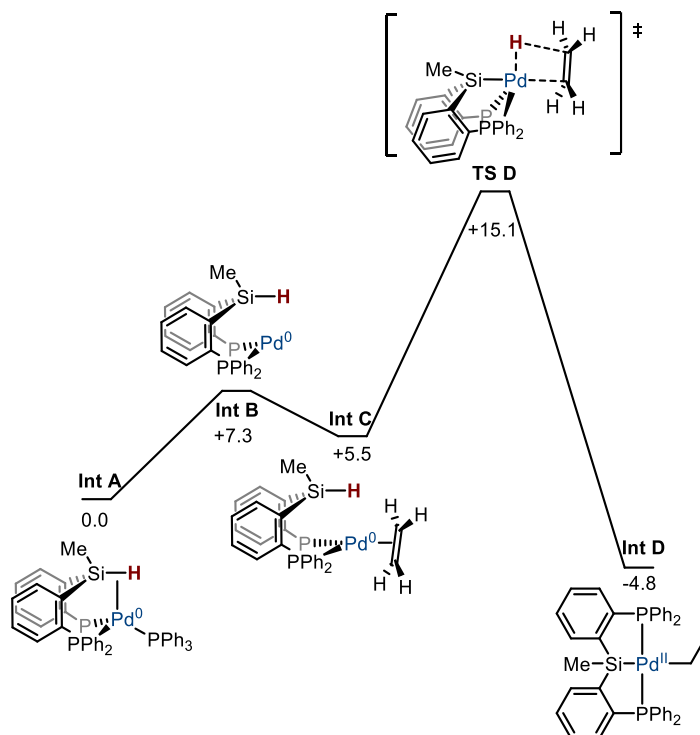
Interestingly, when SiH-Pd⁰-PPh₃ complex (previously proposed as a stable form of Pd^{II}-H) was subjected to ethylene, formation of the Pd^{II}-Ethyl was obtained. Incorporation of the H initially at Si was supported by D-labeling experiments (Scheme I.124). Of note, addition of PPh₃ to the Pd^{II}-Ethyl complex does not induce migration of the organic fragment to Si but β-

H elimination with ethylene evolution and regeneration of the SiH-Pd⁰-PPh₃. This result is in direct contrast with the previous report on the Pd^{II}-prenyl complex, presented in Scheme I.120.



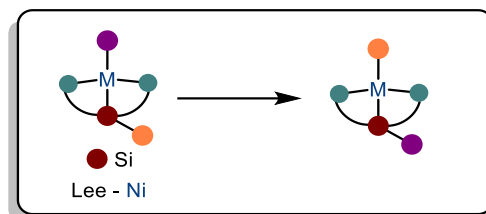
Scheme I.124: SiH-Pd⁰-PPh₃ as a masked form of Pd^{II}-H for ethylene insertion

The active role of the silicon center on the interconversion between the Pd⁰ σ -complex and the Pd^{II}-ethyl was proposed based on DFT calculations. A different pathway compared to Scheme I.123 was suggested. First, decooordination of the phosphine occurs (**Int B**; Scheme I.125) followed by coordination of ethylene (**Int C**; Scheme I.125). Finally, a concerted step of hydride transfer and Pd-CH₂ bond formation (through **TS D**; Scheme I.125) yields the Pd^{II}-Ethyl complex (**Int D**; Scheme I.125).



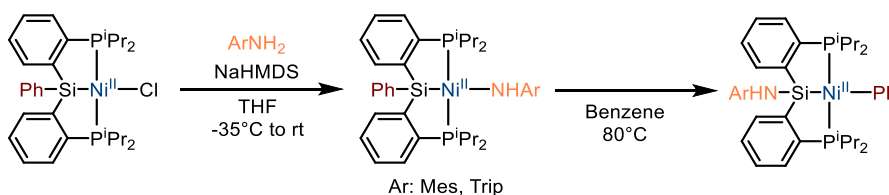
Scheme I.125: Proposed mechanism based on DFT calculations for the silyl-mediated insertion/ β -H elimination of ethylene. (Energies are in kcal.mol⁻¹)

While the mechanism in these transformations was shown slightly different, the silicon center acts in all cases as an acceptor or a donor of functional groups. In 2019, the use of silicon for the exchange of organic fragments with nickel was introduced by Lee (Scheme I.126).^[106]



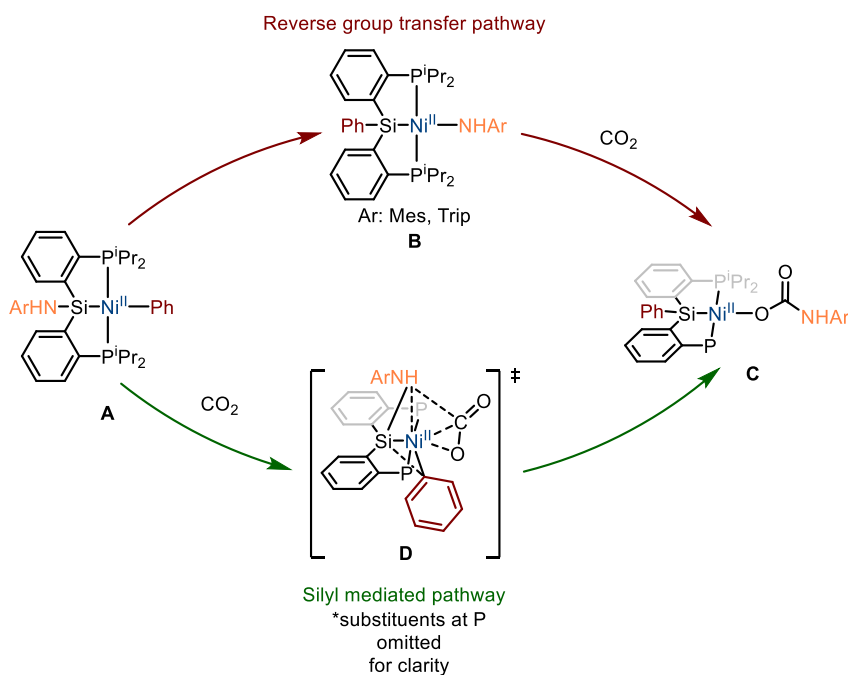
Scheme I.126: Schematic view of the silicon-mediated group exchange at the transition metal by the Ni-complex of Lee

The synthesis of a Ni^{II}-amido complex was achieved by treatment of the Ni^{II}-X precursor with the corresponding arylamine in the presence of a base (Scheme I.127). When heated to 80°C in benzene, functional group exchange between the silicon and nickel was reported.



Scheme I.127: Synthesis of PSiP-Ni^{II}-X complex and ligand exchange with silicon

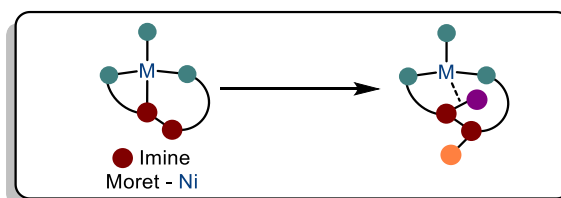
Surprisingly, when this Ni^{II}-Aryl complex was subjected to CO₂, formation of the Ni^{II}-carbamate was observed and no CO₂ insertion into the Ni^{II}-C_{aryl} bond was reported (Scheme I.128 - C). Two pathways were proposed for this transformation. A reverse group transfer reaction would yield the Ni^{II}-NHAr complex (Scheme I.128 - B) and CO₂ insertion into the Ni^{II}-NH bond would then occur. This pathway was considered unlikely as the conversion from **A** to **B** (Scheme I.128) was found strongly affected by the presence of π-acidic ligands such as ^tBuNC but the CO₂ insertion reaction rate was unchanged in the presence or absence of ^tBuNC. An alternative mechanism was then proposed with the silyl ligand mediating the transfer of the amido fragment to CO₂ and concomitantly accepting the phenyl moiety from nickel (Scheme I.128 C).

Scheme I.128: Synthesis of PSiP-Ni^{II}-X complex and mechanism of silyl-mediated CO₂ insertion

Overall, in the previous examples of Iwasawa and Lee, a silyl fragment at the ligand was proposed mediates the exchange of functionals groups with the transition metal.

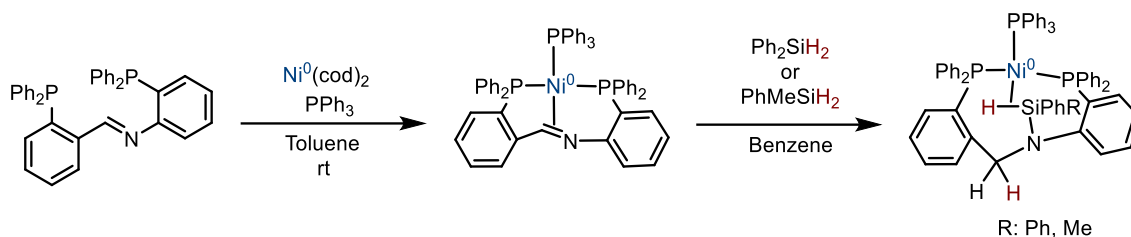
e) π -groups as hydrogen acceptors

Another approach, based on the accepting properties of imines was introduced by Moret with nickel (Scheme I.129).^[107]

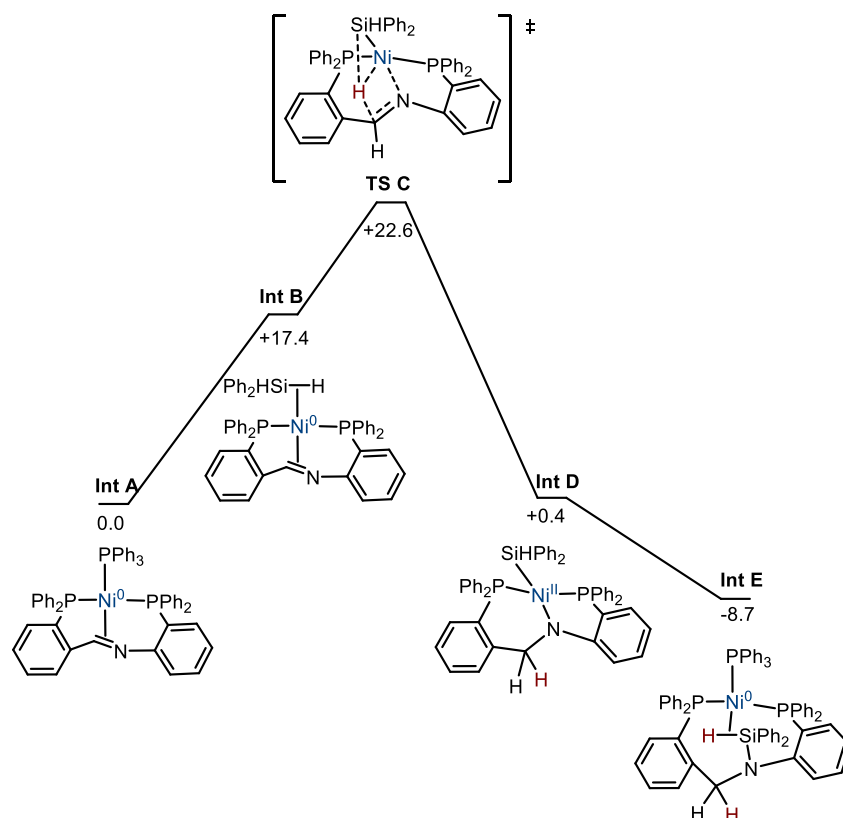


Scheme I.129: Illustration of the chemical non-innocence in the example of Moret

In this case, the synthesis of the Ni⁰ complex was achieved by treatment of the corresponding ligand with a Ni⁰ source in the presence of triphenylphosphine (Scheme I.130). The obtained Ni⁰ complex was then reacted with a silane (R₂SiH₂). Remarkably, formation of a η^2 -SiH-Ni⁰ complex was reported and the non-innocent character of the η^2 -imino fragment was demonstrated. A hydride from the silane is transferred to the electrophilic C=N carbon, and an N-Si bond is formed.

Scheme I.130: Synthesis of the Ni⁰ complex and non-innocent character of the imine backbone

DFT calculations were performed to get insight into the role of the imine in this transformation (Scheme I.131). First, PPh₃ decoordination occurs along with silane coordination to the Ni⁰ center (**Int B**; Scheme I.131). Then, a hydride transfer from the Ni⁰-coordinated silane to the carbon of the imine follows, inducing a coordination switch of the ligand from L-type (imino) to X-type (amido) (**TS C**; Scheme I.131). The resulting Si-Ni^{II}-N complex (**Int D**; Scheme I.131) finally undergoes reductive elimination and coordination of PPh₃ to yield the experimentally observed η²-SiH-Ni⁰ complex (**Int E**; Scheme I.131). Remarkably, this Si-H bond activation pathway was shown to be reversible via silane scrambling experiments but no catalytic hydrosilylation reaction were reported to this day.

Scheme I.131: Proposed mechanism of the chemically non-innocent Si-H bond activation by the Ni⁰-imine complex based on DFT calculations

I.4) Conclusion and PhD project

In this chapter, a general overview of chemically non-innocent ligands (in pincer and chelate group 10 metal complexes) has been presented and were divided in three main categories.

The first one involves the bifunctional combination of a Lewis acidic metal and a basic site at the ligand. To date, this approach remains the most studied and, in many cases, substantial experimental and *in silico* evidence was reported to support the cooperativity between the ligand and the metal.

The second approach stems from the combination of a Lewis acidic center at the ligand and a transition metal. This approach has been less developed and not as much evidence is available to support the cooperativity. Nevertheless, efforts were made towards this objective.

Finally, miscellaneous examples were presented taking advantage of the ability of silicon and imines to accept/donate functional groups, acting as chemical reservoirs.

In all three cases, Metal-Ligand cooperation imparts interesting reactivity and often involves new mechanistic paths. However, catalytic examples of MLC with group 10 metals are not numerous and the potential is clearly underexploited.

As we have also seen in this chapter, the LBPB team of the LHFA introduced and developed a family non-innocent $[(SCS)-M^II]_2$ complexes, highly efficient in cycloisomerization reactions (Scheme I.24). The objectives of this PhD project were to first extend the reactivity of the $[(SCS)-Pd]_2$ complex to C-C bond formation and the synthesis of carbocycles. To this end, a multi-cooperative system with the combined use of MLC, H-bonding and Lewis acid additives was developed and will be presented in the following chapter.

Given the potential and catalytic relevance of MLC with group 10 metals, we then aimed to design and study a new pincer scaffold for MLC. Compared to more “traditional” designs, our PNS ligand framework may exhibit, within the same complex, two different modes of chemical non-innocence. In the third chapter of this thesis, the first mode of cooperativity, based on the aromatization/dearomatization of a pyridine-type backbone will be presented. Stoichiometric and catalytic reactions involving the activation of polar E-H bond will be studied with the dearomatized complex.

The second mode, based on the polar nature of the M-S fragment will be presented in the final chapter of this thesis. Stoichiometric reactions of this complex will be discussed along with catalytic hydroelementation reactions.

I.5) References

- [1] J. R. Khusnutdinova, D. Milstein, *Angew. Chem. Int. Ed.* **2015**, *54*, 12236–12273.
- [2] N. D. Harrold, R. Waterman, G. L. Hillhouse, T. R. Cundari, *J. Am. Chem. Soc.* **2009**, *131*, 12872–12873.
- [3] M. Bröring, C. D. Brandt, S. Stellwag, *Chem. Commun.* **2003**, 2344–2345.
- [4] N. D. Jones, G. Lin, R. A. Gossage, R. McDonald, R. G. Cavell, *Organometallics* **2003**, *22*, 5378–5378.
- [5] T. Cantat, N. Mézailles, A. Auffrant, P. L. Floch, *Dalton Trans.* **2008**, 1957–1972.
- [6] T. Cantat, N. Mézailles, L. Ricard, Y. Jean, P. L. Floch, *Angew. Chem. Int. Ed.* **2004**, *43*, 6382–6385.
- [7] C. C. Comanescu, V. M. Iluc, *Organometallics* **2014**, *33*, 6059–6064.
- [8] D. V. Gutsulyak, W. E. Piers, J. Borau-Garcia, M. Parvez, *J. Am. Chem. Soc.* **2013**, *135*, 11776–11779.
- [9] C. C. Comanescu, V. M. Iluc, *Polyhedron* **2018**, *143*, 176–183.
- [10] C. C. Comanescu, V. M. Iluc, *Organometallics* **2015**, *34*, 4684–4692.
- [11] C. C. Comanescu, V. M. Iluc, *Chem. Commun.* **2016**, *52*, 9048–9051.
- [12] E. A. LaPierre, W. E. Piers, D. M. Spasyuk, D. W. Bi, *Chem. Commun.* **2016**, *52*, 1361–1364.
- [13] P. Cui, C. C. Comanescu, V. M. Iluc, *Chem. Commun.* **2015**, *51*, 6206–6209.
- [14] E. A. LaPierre, W. E. Piers, C. Gendy, *Organometallics* **2018**, *37*, 3394–3398.
- [15] P. Cui, V. M. Iluc, *Chem. Sci.* **2015**, *6*, 7343–7354.
- [16] E. A. LaPierre, W. E. Piers, C. Gendy, *Dalton Trans.* **2018**, *47*, 16789–16797.
- [17] A. P. Deziel, M. R. Hoffbauer, V. M. Iluc, *Organometallics* **2019**, *38*, 879–887.
- [18] P. E. Rothstein, C. C. Comanescu, V. M. Iluc, *Chem. – Eur. J.* **2017**, *23*, 16948–16952.
- [19] L. T. Scharf, A. Kowsari, T. Scherpf, K.-S. Feichtner, V. H. Gessner, *Organometallics* **2019**, *38*, 4093–4104.
- [20] R. M. Brown, J. Borau Garcia, J. Valjus, C. J. Roberts, H. M. Tuononen, M. Parvez, R. Roesler, *Angew. Chem. Int. Ed.* **2015**, *54*, 6274–6277.
- [21] X. Ren, C. Gourlaouen, M. Wesolek, P. Braunstein, *Angew. Chem. Int. Ed.* **2017**, *56*, 12557–12560.
- [22] P. Oulié, N. Nebra, N. Saffon, L. Maron, B. Martin-Vaca, D. Bourissou, *J. Am. Chem. Soc.* **2009**, *131*, 3493–3498.
- [23] N. Nebra, J. Lisena, N. Saffon, L. Maron, B. Martin-Vaca, D. Bourissou, *Dalton Trans.* **2011**, *40*, 8912–8921.
- [24] P. Oulié, N. Nebra, S. Ladeira, B. Martin-Vaca, D. Bourissou, *Organometallics* **2011**, *30*, 6416–6422.
- [25] N. Nebra, S. Ladeira, L. Maron, B. Martin-Vaca, D. Bourissou, *Chem. – Eur. J.* **2012**, *18*, 8474–8481.
- [26] N. Nebra, J. Monot, R. Shaw, B. Martin-Vaca, D. Bourissou, *ACS Catal.* **2013**, *3*, 2930–2934.
- [27] N. Á. Espinosa-Jalapa, D. Ke, N. Nebra, L. Le Goanvic, S. Mallet-Ladeira, J. Monot, B. Martin-Vaca, D. Bourissou, *ACS Catal.* **2014**, *4*, 3605–3611.
- [28] P. Brunel, J. Monot, C. E. Kefalidis, L. Maron, B. Martin-Vaca, D. Bourissou, *ACS Catal.* **2017**, *7*, 2652–2660.

- [29] D. Ke, N. Á. Espinosa, S. Mallet-Ladeira, J. Monot, B. Martin-Vaca, D. Bourissou, *Adv. Synth. Catal.* **2016**, *358*, 2324–2331.
- [30] J. Monot, P. Brunel, C. E. Kefalidis, N. Á. Espinosa-Jalapa, L. Maron, B. Martin-Vaca, D. Bourissou, *Chem. Sci.* **2016**, *7*, 2179–2187.
- [31] A. Clerc, E. Marelli, N. Adet, J. Monot, B. Martín-Vaca, D. Bourissou, *Chem. Sci.* **2021**, *12*, 435–441.
- [32] Y. Wang, A. Kostenko, S. Yao, M. Driess, *J. Am. Chem. Soc.* **2017**, *139*, 13499–13506.
- [33] J. A. Cabeza, P. García-Álvarez, C. J. Laglera-Gándara, E. Pérez-Carreño, *Chem. Commun.* **2020**, *56*, 14095–14097.
- [34] D. Sellmann, F. Geipel, M. Moll, *Angew. Chem. Int. Ed.* **2000**, *39*, 561–563.
- [35] G. Zampella, M. Bruschi, P. Fantucci, L. De Gioia, *J. Am. Chem. Soc.* **2005**, *127*, 13180–13189.
- [36] Y. Ohki, Y. Takikawa, H. Sadohara, C. Kesenheimer, B. Engendahl, E. Kapatina, K. Tatsumi, *Chem. – Asian J.* **2008**, *3*, 1625–1635.
- [37] L. Omann, C. D. F. Königs, H. F. T. Klare, M. Oestreich, *Acc. Chem. Res.* **2017**, *50*, 1258–1269.
- [38] J. Liu, J.-Y. Chen, M. Jia, B. Ming, J. Jia, R.-Z. Liao, C.-H. Tung, W. Wang, *ACS Catal.* **2019**, *9*, 3849–3857.
- [39] A. N. Marziale, E. Herdtweck, J. Eppinger, S. Schneider, *Inorg. Chem.* **2009**, *48*, 3699–3709.
- [40] T. He, N. P. Tsvetkov, J. G. Andino, X. Gao, B. C. Fullmer, K. G. Caulton, *J. Am. Chem. Soc.* **2010**, *132*, 910–911.
- [41] L. Fan, O. V. Ozerov, *Chem. Commun.* **2005**, 4450–4452.
- [42] L. C. Gregor, C.-H. Chen, C. M. Fafard, L. Fan, C. Guo, B. M. Foxman, D. G. Gusev, O. V. Ozerov, *Dalton Trans.* **2010**, *39*, 3195–3202.
- [43] Y. Zhu, C.-H. Chen, C. M. Fafard, B. M. Foxman, O. V. Ozerov, *Inorg. Chem.* **2011**, *50*, 7980–7987.
- [44] J. C. DeMott, N. Bhuvanesh, O. V. Ozerov, *Chem. Sci.* **2013**, *4*, 642–649.
- [45] D. Adhikari, S. Mossin, F. Basuli, J. C. Huffman, R. K. Szilagyi, K. Meyer, D. J. Mindiola, *J. Am. Chem. Soc.* **2008**, *130*, 3676–3682.
- [46] F. Schneck, M. Finger, M. Tromp, S. Schneider, *Chem. – Eur. J.* **2017**, *23*, 33–37.
- [47] F. Schneck, J. Ahrens, M. Finger, A. C. Stückl, C. Würtele, D. Schwarzer, S. Schneider, *Nat. Commun.* **2018**, *9*, 1161.
- [48] M. Feller, E. Ben-Ari, M. A. Iron, Y. Diskin-Posner, G. Leituss, L. J. W. Shimon, L. Konstantinovski, D. Milstein, *Inorg. Chem.* **2010**, *49*, 1615–1625.
- [49] M. Vogt, O. Rivada-Wheeler, M. A. Iron, G. Leituss, Y. Diskin-Posner, L. J. W. Shimon, Y. Ben-David, D. Milstein, *Organometallics* **2013**, *32*, 300–308.
- [50] W. D. Bailey, W. Kaminsky, R. A. Kemp, K. I. Goldberg, *Organometallics* **2014**, *33*, 2503–2509.
- [51] T. Cheisson, A. Auffrant, *Dalton Trans.* **2016**, *45*, 2069–2078.
- [52] S. Y. de Boer, Y. Gloaguen, J. N. H. Reek, M. Lutz, J. I. van der Vlugt, *Dalton Trans.* **2012**, *41*, 11276–11283.
- [53] A. Scharf, I. Goldberg, A. Vigalok, *Organometallics* **2012**, *31*, 1275–1277.
- [54] A. Scharf, I. Goldberg, A. Vigalok, *Inorg. Chem.* **2014**, *53*, 12–14.

- [55] A. Scharf, I. Goldberg, A. Vigalok, A. N. Vedernikov, *Eur. J. Inorg. Chem.* **2015**, 2015, 4761–4768.
- [56] A. Scharf, I. Goldberg, A. Vigalok, *J. Am. Chem. Soc.* **2013**, 135, 967–970.
- [57] K. Fujita, N. Tanino, R. Yamaguchi, *Org. Lett.* **2007**, 9, 109–111.
- [58] G. Zeng, S. Sakaki, K. Fujita, H. Sano, R. Yamaguchi, *ACS Catal.* **2014**, 4, 1010–1020.
- [59] S. Chakraborty, P. E. Pizsel, W. W. Brennessel, W. D. Jones, *Organometallics* **2015**, 34, 5203–5206.
- [60] P. Wang, P. Verma, G. Xia, J. Shi, J. X. Qiao, S. Tao, P. T. W. Cheng, M. A. Poss, M. E. Farmer, K.-S. Yeung, J.-Q. Yu, *Nature* **2017**, 551, 489–493.
- [61] L.-Y. Liu, K.-S. Yeung, J.-Q. Yu, *Chem. – Eur. J.* **2019**, 25, 2199–2202.
- [62] R.-Y. Zhu, Z.-Q. Li, H. S. Park, C. H. Senanayake, J.-Q. Yu, *J. Am. Chem. Soc.* **2018**, 140, 3564–3568.
- [63] Z. Fan, K. L. Bay, X. Chen, Z. Zhuang, H. S. Park, K.-S. Yeung, K. N. Houk, J.-Q. Yu, *Angew. Chem. Int. Ed.* **2020**, 59, 4770–4777.
- [64] V. Salamanca, A. Toledo, A. C. Albéniz, *J. Am. Chem. Soc.* **2018**, 140, 17851–17856.
- [65] V. Salamanca, A. C. Albéniz, *Org. Chem. Front.* **2021**, 8, 1941–1951.
- [66] F. Villalba, A. C. Albéniz, *Adv. Synth. Catal.* **2021**, 363, 4795–4804.
- [67] Y.-J. Wang, C.-H. Yuan, D.-Z. Chu, L. Jiao, *Chem. Sci.* **2020**, 11, 11042–11054.
- [68] Y. Blum, D. Czarkie, Y. Rahamim, Y. Shvo, *Organometallics* **1985**, 4, 1459–1461.
- [69] B. L. Conley, M. K. Pennington-Boggio, E. Boz, T. J. Williams, *Chem. Rev.* **2010**, 110, 2294–2312.
- [70] T. Higashi, H. Ando, S. Kusumoto, K. Nozaki, *J. Am. Chem. Soc.* **2019**, 141, 2247–2250.
- [71] J. E. Bercaw, G. S. Chen, J. A. Labinger, B.-L. Lin, *Organometallics* **2010**, 29, 4354–4359.
- [72] F.-G. Fontaine, D. Zargarian, *J. Am. Chem. Soc.* **2004**, 126, 8786–8794.
- [73] E. Khaskin, P. Y. Zavalij, A. N. Vedernikov, *Angew. Chem. Int. Ed.* **2007**, 46, 6309–6312.
- [74] E. Khaskin, P. Y. Zavalij, A. N. Vedernikov, *J. Am. Chem. Soc.* **2008**, 130, 10088–10089.
- [75] B. E. Cowie, D. J. H. Emslie, *Organometallics* **2015**, 34, 2737–2746.
- [76] D. Schuhknecht, F. Ritter, M. E. Tauchert, *Chem. Commun.* **2016**, 52, 11823–11826.
- [77] I. R. Crossley, A. F. Hill, *Dalton Trans.* **2007**, 201–203.
- [78] H. Kameo, J. Yamamoto, A. Asada, H. Nakazawa, H. Matsuzaka, D. Bourissou, *Angew. Chem. Int. Ed.* **2019**, 58, 18783–18787.
- [79] T. Schindler, M. Lux, M. Peters, L. T. Scharf, H. Osseili, L. Maron, M. E. Tauchert, *Organometallics* **2015**, 34, 1978–1984.
- [80] F. Ritter, L. John, T. Schindler, J. P. Schroers, S. Teeuwen, M. E. Tauchert, *Chem. – Eur. J.* **2020**, 26, 13436–13444.
- [81] G. Hirata, H. Satomura, H. Kumagae, A. Shimizu, G. Onodera, M. Kimura, *Org. Lett.* **2017**, 19, 6148–6151.
- [82] A. Shimizu, G. Hirata, G. Onodera, M. Kimura, *Adv. Synth. Catal.* **2018**, 360, 1954–1960.
- [83] G. Onodera, H. Kumagae, D. Nakamura, T. Hayasaki, T. Fukuda, M. Kimura, *Tetrahedron Lett.* **2020**, 61, 152537.
- [84] D. You, F. P. Gabbai, *J. Am. Chem. Soc.* **2017**, 139, 6843–6846.
- [85] H. Yang, F. P. Gabbai, *J. Am. Chem. Soc.* **2014**, 136, 10866–10869.
- [86] M.-M. Zhou, B.-L. Jiang, S.-F. Ni, L. Dang, *J. Org. Chem.* **2019**, 84, 9454–9459.
- [87] D. J. H. Emslie, James. M. Blackwell, J. F. Britten, L. E. Harrington, *Organometallics* **2006**, 25, 2412–2414.

- [88] D. J. H. Emslie, L. E. Harrington, H. A. Jenkins, C. M. Robertson, J. F. Britten, *Organometallics* **2008**, *27*, 5317–5325.
- [89] W. H. Harman, J. C. Peters, *J. Am. Chem. Soc.* **2012**, *134*, 5080–5082.
- [90] S. N. MacMillan, W. H. Harman, J. C. Peters, *Chem. Sci.* **2013**, *5*, 590–597.
- [91] W. H. Harman, T.-P. Lin, J. C. Peters, *Angew. Chem. Int. Ed.* **2014**, *53*, 1081–1086.
- [92] G. Zeng, S. Sakaki, *Inorg. Chem.* **2013**, *52*, 2844–2853.
- [93] M. Boudjelel, O. Sadek, S. Mallet-Ladeira, Y. García-Rodeja, E. D. Sosa Carrizo, K. Miqueu, G. Bouhadir, D. Bourissou, *ACS Catal.* **2021**, *11*, 3822–3829.
- [94] T.-P. Lin, J. C. Peters, *J. Am. Chem. Soc.* **2014**, *136*, 13672–13683.
- [95] N. Curado, C. Maya, J. López-Serrano, A. Rodríguez, *Chem. Commun.* **2014**, *50*, 15718–15721.
- [96] B. E. Cowie, D. J. H. Emslie, *Chem. – Eur. J.* **2014**, *20*, 16899–16912.
- [97] B. E. Cowie, F. A. Tsao, D. J. H. Emslie, *Angew. Chem. Int. Ed.* **2015**, *54*, 2165–2169.
- [98] B. R. Barnett, C. E. Moore, A. L. Rheingold, J. S. Figueroa, *J. Am. Chem. Soc.* **2014**, *136*, 10262–10265.
- [99] M. Devillard, R. Declercq, E. Nicolas, A. W. Ehlers, J. Backs, N. Saffon-Merceron, G. Bouhadir, J. C. Sloatweg, W. Uhl, D. Bourissou, *J. Am. Chem. Soc.* **2016**, *138*, 4917–4926.
- [100] B. R. Barnett, M. L. Neville, C. E. Moore, A. L. Rheingold, J. S. Figueroa, *Angew. Chem. Int. Ed.* **2017**, *56*, 7195–7199.
- [101] A. Nova, H.-W. Suh, T. J. Schmeier, L. M. Guard, O. Eisenstein, N. Hazari, F. Maseras, *Angew. Chem. Int. Ed.* **2014**, *53*, 1103–1108.
- [102] J. Takaya, N. Iwasawa, *Organometallics* **2009**, *28*, 6636–6638.
- [103] J. Takaya, N. Iwasawa, *J. Am. Chem. Soc.* **2008**, *130*, 15254–15255.
- [104] H.-W. Suh, L. M. Guard, N. Hazari, *Chem. Sci.* **2014**, *5*, 3859–3872.
- [105] J. Takaya, N. Iwasawa, *Chem. – Eur. J.* **2014**, *20*, 11812–11819.
- [106] J. Kim, Y.-E. Kim, K. Park, Y. Lee, *Inorg. Chem.* **2019**, *58*, 11534–11545.
- [107] D. G. A. Verhoeven, A. F. Orsino, R. L. M. Bienenmann, M. Lutz, M.-E. Moret, *Organometallics* **2020**, *39*, 623–629.

II) Metal–ligand–Lewis acid multi-cooperative catalysis: a step forward in the Conia-ene reaction

This chapter relates to the corresponding publication. A. Clerc, E. Marelli, N. Adet, J. Monot, B. Martin-Vaca, D. Bourissou. *Chem. Sci.*, **2021**, *12*, 435–441.

II.1) Introduction

Major breakthroughs have been made in homogeneous catalysis thanks to cooperative approaches.^[1–6] Concomitant and synergistic participation of several active sites, as in enzymes, is very attractive to achieve chemical transformations under milder conditions and reduce wastes. Thanks to cooperativity, not only the efficiency and selectivity of catalysts can be improved, but the diversity and complexity of the obtainable chemical compounds can also be expanded. In this context, metal–ligand cooperativity (MLC) is clearly prominent.^[7,8]

Here, a ligand participates directly in substrate activation, in addition to modulating the stereoelectronic properties of the metal center. Complexes of the group 7–9 metals featuring non-innocent pincer ligands, in particular amido and pyridine-based scaffolds, occupy a forefront position in this area.^[9] Tremendous achievements in hydrogenation and dehydrogenation reactions have been reported with these catalysts.^[10–13] Extending the scope of transformations and developing the MLC catalytic approach further are currently a major endeavor, along with the diversification of complexes displaying MLC.^[14–19] Our group introduced a few years ago an SCS pincer framework featuring an electron-rich indenediide backbone.^[20] The paucity of MLC behavior reported^[21–26] for Pd and Pt complexes, despite the prominent role of these metals in homogeneous catalysis, led us to study complexes of type I (Figure II.1).

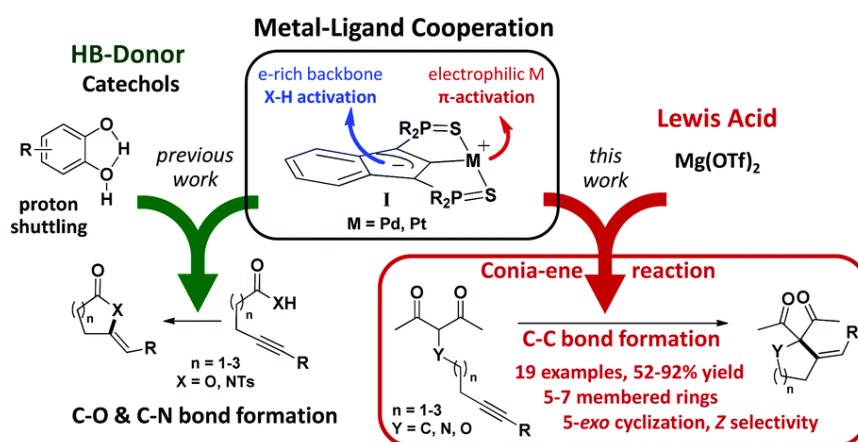


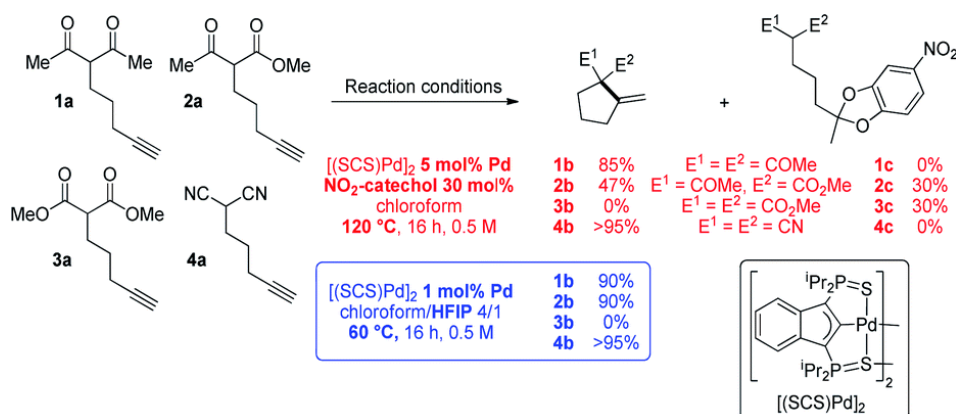
Figure II.1: Multi-cooperative catalysis combining metal–ligand cooperation (MLC, indenediide-based (SCS)M pincer complexes) with hydrogen-bond donors (HBD, previous work) or Lewis acid activation (LA, this work) to promote cycloisomerization reactions (C–O, C–N and C–C bond formation).

The electron-rich indenediide motif was shown to be non-innocent and to open an MLC pathway for Pd and Pt-catalyzed C–O and C–N bond formation. The (SCS)-Pd,Pt complexes proved to very efficiently promote the cycloisomerization of alkyne acids and N-tosyl alkynylamides, giving access in high yield and selectivity to a wide variety of alkylidene lactones and lactams, including seven-membered rings.^[27–29] Of note, in-depth mechanistic studies substantiated the participation of proton shuttling in addition to MLC.^[30] This drove us to use catechols as hydrogen bond donor (HBD) additives. The activity and selectivity of the (SCS)-Pd,Pt complexes were thereby spectacularly improved.^[30] The synergy between MLC and proton shuttling is a very appealing approach to boost catalytic performance. It has been proposed for many hydrogenation/dehydrogenation reactions involving MLC^[31–35] and recently unequivocally demonstrated by Hazari et al.^[36] Its impact in intermolecular hydroamination reactions has also been substantiated.^[26] Encouraged by these results, we wondered about the possibility of developing new multi-cooperative catalytic approaches based on MLC. Another aim was to expand the scope of (SCS)-Pd,Pt catalysts to more challenging transformations. In this work, we focused on Conia-ene cyclizations, i.e. the formation of carbo- and heterocycles by C–C coupling between an enolizable group, typically a β-dicarbonyl moiety, and an alkyne. As pointed out by Enders et al. in their recent review,^[37] this is a very powerful transformation and much progress has been achieved recently from

both methodological and synthetic viewpoints, but several limitations still need to be addressed. While investigating the ability of the MLC Pd indenediide complex to catalyze Conia-ene cyclizations, we discovered that it is extremely efficient and versatile when associated with a Lewis acid (LA). The combined use of TM catalysts and Lewis acids (often referred to as dual activation) has attracted increasing interest and led to impressive developments over the last decade,^[38–41] including in the Conia-ene reaction.^[37,42–47] Yet, synergistic effects between MLC and LA activation have not been realized so far. As reported hereafter, the association of $[(SCS)\text{-Pd}]_2$ and $\text{Mg}(\text{OTf})_2$ provides a first example of such a dual and multi-cooperative catalytic system. It is a very efficient and useful catalyst for Conia-ene cyclizations, displaying broad substrate scope and high regio as well as stereo-selectivity.

II.2) Results and discussion

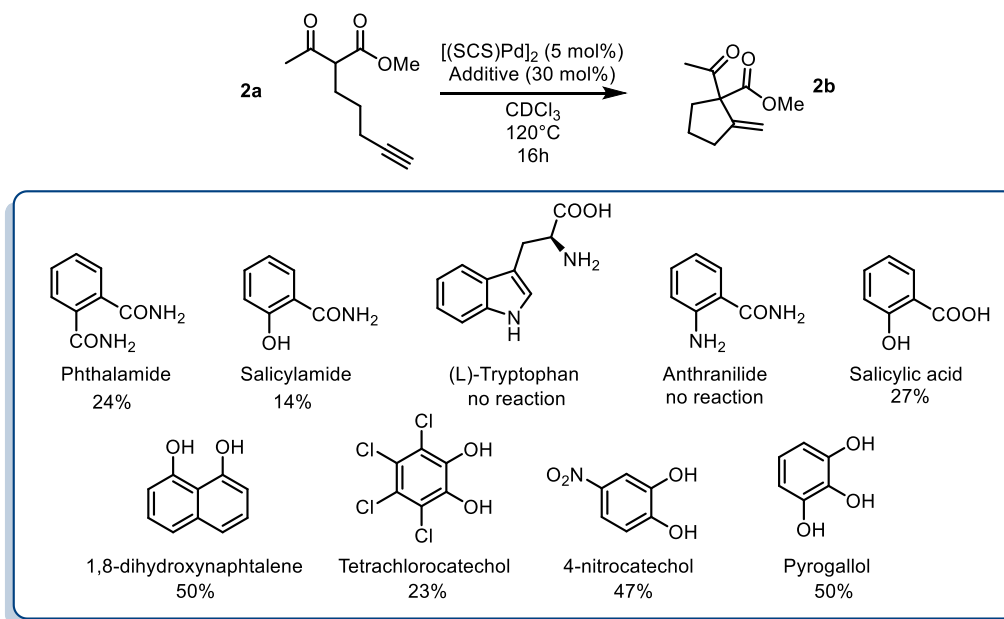
To start with, the carbo-cyclization of the β -dicarbonyl compounds **1a–3a** and β -dinitrile **4a** bearing an alkyne moiety was studied applying the reaction conditions previously optimized for the cycloisomerization of alkynoic acids (Scheme II.1).^[30]



Scheme II.1: Conia-ene cyclization of the β -dicarbonyl and β -dinitrile substrates **1a–4a** catalyzed by the $[(SCS)\text{Pd}]_2$ complex in the presence of 4-nitrocatechol or HFIP. Throughout this chapter, the a/b letters in the compound numbers refer to the substrate/cyclized Conia-ene product, respectively

A series of hydrogen-bond donors (catechols and other HB-donor derivatives - Scheme II.2; More details in Experimental Section II.4); Table 2) were probed as proton shuttling additives to the indenediide-derived Pd complex $[(SCS)\text{Pd}]_2$ (5 mol% Pd). The best results were obtained with 4-nitrocatechol. Heating at 120°C for 16 h, full conversion could be achieved in

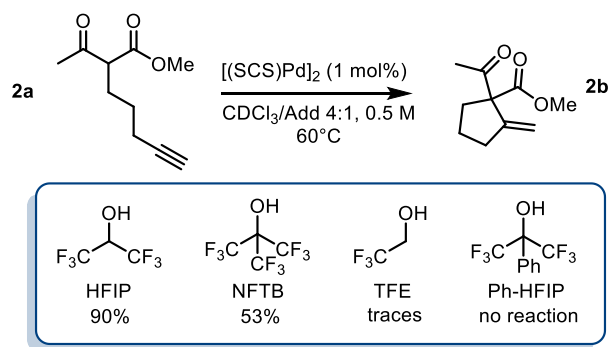
all cases but **3a** (only 30% in this case). The expected cyclized products **1b** and **4b** were selectively obtained from the β -diketone and β -dinitrile substrates **1a** and **4a**, whereas **2a** led to the formation of a secondary product **2c** (30% yield) resulting from double addition of the catechol to the $C\equiv C$ triple bond,^[48,49] besides the targeted carbocycle **2b** (47% yield). As for the β -diester **3a**, no cyclized product **3b** was formed, only the secondary product **3c** was obtained.



Scheme II.2: Overview of the HB-bonding additives screening for the cycloisomerization of **2a**

The known ability of hexafluoroisopropanol (HFIP) and other fluorinated alcohols to form hydrogen-bond networks and participate in proton shuttling prompted us to screen them as additives.^[50–52] This resulted in noticeable improvement of activity and selectivity (Scheme II.3; More details in Experimental Section II.4); Table 3). Using a 4/1 chloroform/HFIP solvent mixture, high conversions of the β -diketone **1a** and β -dinitrile **4a** were achieved in this case at $60^\circ C$ with only 1 mol% of Pd (Experimental Section II.4); Table 3: entry 16). The fact that **4a** was readily cyclized is particularly noteworthy since β -dinitriles are usually significantly less reactive than β -dicarbonyl substrates in the Conia-ene reaction. It is because the linear geometry of the cyano group is not suited for intramolecular hydrogen-bonding and thus tautomerization is more demanding. Under these milder conditions, the β -keto,ester **2a** could also be efficiently cyclized and **2b** was formed in high yield without side reaction. In turn, the

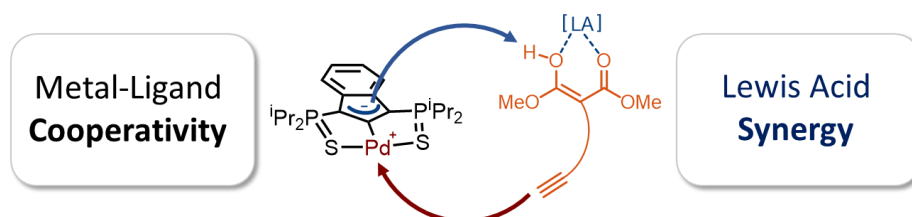
β -diester **3a** was unreactive. Due to their weaker acidity, β -diester substrates are notoriously less reactive and more challenging in the Conia-ene reaction. The contribution of proton shuttling to the carbocyclization of **1a**, **2a** and **4a** in the presence of HFIP is supported by a strong solvent dependence. While toluene and dichloromethane gave results close to those obtained in chloroform, hydrogen-bond accepting solvents such as THF or DMSO completely inhibited the reaction.



Scheme II.3: Overview of the fluorinated alcohols screening for the cycloisomerization of **2a** into **2b**

Thus, the indenediide pincer Pd complex $[(SCS)Pd]_2$ is a competent catalyst for the Conia-ene reaction of β -diketo, β -keto, ester and β -dinitrile substrates, when combined with HFIP as a co-solvent. However, it fails to cyclize the corresponding β -diester under the same conditions. Although the $[(SCS)Pt]_2$ complex proved to be superior for the cyclization of challenging alkyne acids and amides,^[29] no improvement was observed in the Conia-ene reaction upon changing Pd for Pt. The Pt complex proved to be in fact less active, with only 40% (vs. 90%) conversion of **2a** after 16 h (Experimental Section II.4); Table 3: entry 9). Looking for another way to boost the catalytic activity, we envisioned to use di or trivalent Lewis acids, which are known to activate β -dicarbonyl compounds and facilitate the formation of the corresponding enols. Combinations of hard and soft Lewis acids have been occasionally used in Conia-ene reactions. Such dual activation proved in particular successful to promote enantioselective cyclization of β -diketo and β -keto, ester derivatives.^[42–44,47] With MLC, Milstein reported very recently a tandem catalytic approach for the oxidation of alkenes by water.^[53] Given these precedents, we wondered about the possibility of implementing a new type of multi-cooperative catalytic approach by merging metal–ligand cooperation, as

achieved by the (SCS)-Pd complex, with the activation of the β -dicarbonyl moiety by a LA (Scheme II.4).



Scheme II.4: Combination of MLC and LA activation of β -dicarbonyl compounds

Multi-cooperative catalytic systems are very attractive but challenging to achieve. They inherently raise compatibility issues, and the different components must be carefully adjusted to act synergistically. In the case of the (SCS)-Pd complex, the Lewis acid additive may interact with the electron-rich indenediide motif as well as the sulfur atoms and thereby interfere with the Pd–ligand cooperativity.^[54–56] A series of triflate salts were evaluated as LA additives to $[(\text{SCS})\text{Pd}]_2$ in the cyclization of the β -keto,ester **2a** in 4/1 chloroform/HFIP as solvent. Initial screenings were performed at 60°C with 1 mol% Pd and 20 mol% LA (Figure II.2; More details in Experimental Section II.4); Table 4).

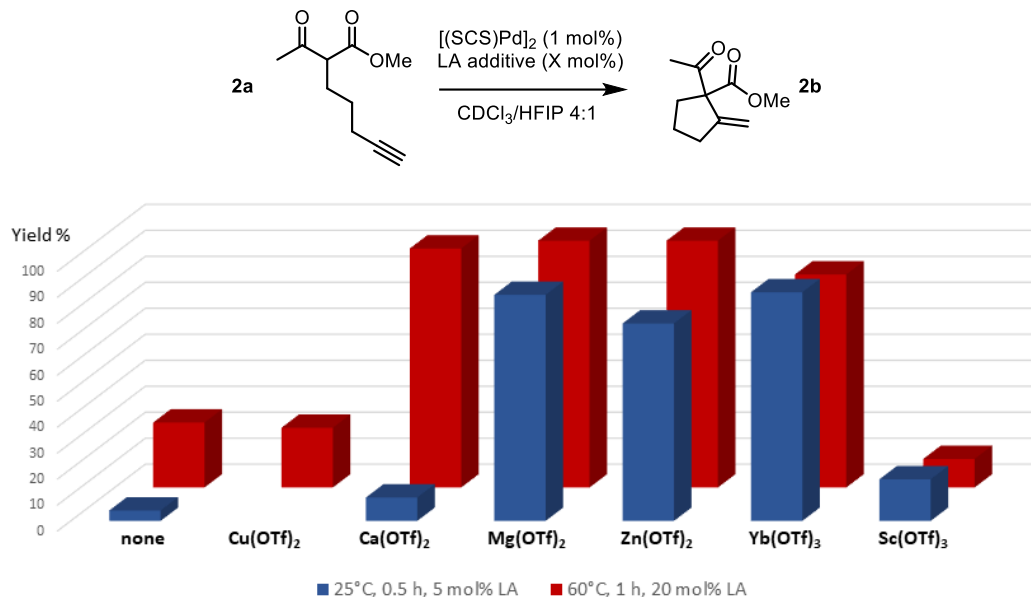
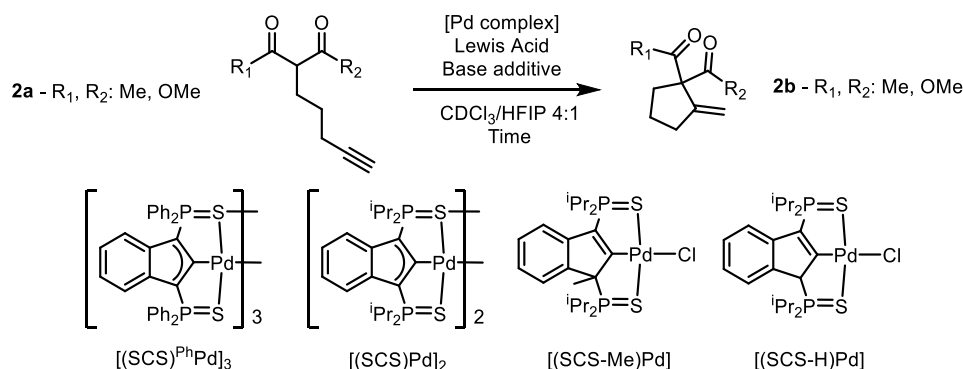


Figure II.2: Evaluation of the catalytic activity of the Pd complex $[(\text{SCS})\text{Pd}]_2$ in the presence of LA additives

While $\text{Cu}(\text{OTf})_2$ and $\text{Sc}(\text{OTf})_3$ had no or negative impact on catalysis, significant improvement of activity was observed with $\text{Ca}(\text{II})$, $\text{Mg}(\text{II})$, $\text{Zn}(\text{II})$ and $\text{Yb}(\text{III})$ salts (Figure II.2; Red - Back). Indeed, in the case of $\text{Cu}(\text{OTf})_2$, $^{31}\text{P}\{^1\text{H}\}$ NMR monitoring showed a rapid reaction between $[(\text{SCS})\text{Pd}]_2$ and $\text{Cu}(\text{OTf})_2$, while no change was observed for the other salts. High conversions were achieved in only 1 h (>82% vs. only 25% without a LA), demonstrating the compatibility and synergy between MLC with the $[(\text{SCS})\text{Pd}]_2$ complex and electrophilic activation of the β -dicarbonyl moiety with a LA. Taking advantage of the catalytic boost triggered by the LA additive, milder reaction conditions were then used. The temperature was decreased to 25 °C and the LA loading was reduced to 5 mol% (Figure II.2; Blue - Front). Under these mild conditions, $\text{Mg}(\text{OTf})_2$ and $\text{Yb}(\text{OTf})_3$ led to the best results with 90% conversion to **2b** within only 30 min, and >95% after 1.5 h. The β -diketo substrate **1a** was also readily cyclized under these conditions (>95% after 8 h). In contrast, similar results were obtained with and without Lewis acids in the case of the β -dinitrile **4a** (85% conv. is achieved in 16 h at 25°C; Experimental Section II.4); Table 4: Entry 19). Chelating coordination of the two cyano groups is not possible geometrically, and thus the LA cannot facilitate deprotonation, as in the case of the β -dicarbonyl substrates. Most remarkably, the combination of $[(\text{SCS})\text{Pd}]_2$ with the LA allowed for the cyclization of the challenging β -diester **3a** as well. Here, $\text{Mg}(\text{OTf})_2$ significantly outperformed $\text{Yb}(\text{OTf})_3$ (83 vs. 13% conversion of **3a** within 30 min Experimental Section II.4); Table 4: Entries 17,18). Given the superior efficiency, abundance and biological tolerance of Mg over Yb, catalytic studies were continued with $\text{Mg}(\text{OTf})_2$ as the LA. Furthermore, direct NMR monitoring was prohibited by the paramagnetic $\text{Yb}(\text{OTf})_3$, giving a practical advantage to $\text{Mg}(\text{OTf})_2$ over the ytterbium salt.

To ascertain the need and synergy of all the catalytic components, a series of control reactions were carried out for the cyclization of the β -keto,ester substrate **2a**. The results obtained under conditions deviating from the optimal ones [1 mol% Pd, 5 mol% $\text{Mg}(\text{OTf})_2$, chloroform/HFIP 4:1, 25°C] are disclosed in Table 1.

Table 1: Impact of the different components of the catalytic system (Pd complex, Lewis acid, proton shuttle additive) on the carbocyclization of the keto,ester 2a.



Entry	Reaction conditions, deviations from the optimal	Conv./reaction time
1	Optimal: [(SCS)Pd] ₂ 1 mol% Pd, 5 mol% Mg(OTf) ₂ CDCl ₃ :HFIP 4:1, 25°C	>95%/1.5 h
2	[(SCS)Pd] ₂ 5 mol% Pd, 20 mol% Mg(OTf) ₂ No HFIP	46%/60 h
3	No Mg salt, 60°C	>95%/22 h
4	No Pd complex, No Mg salt, 60°C	Traces/16 h
5	No Pd complex, 20 mol% Mg(OTf) ₂	0%/2 h
6	Indenyl [(SCS-Me)Pd] complex	>95%/8.5 h
7	Indenyl [(SCS-Me)Pd] complex, 5 mol% Pd, no Mg salt, 60°C	89%/15 days
8	Indenyl [(SCS-H)Pd] complex	>95%/8.5 h
9	Indenyl [(SCS-H)Pd] complex, 5 mol% Pd, no Mg salt, 60°C	95%/12 days
10	[PdCl(allyl)] ₂ 1 mol% Pd	6%/24 h
11	[PdCl ₂ (PhCN) ₂] 1 mol% Pd	7%/24 h
12	[PdCl ₂ (PhCN) ₂] 1 mol% Pd, dppe 1 mol%	35%/24 h
13	[PdCl ₂ (PhCN) ₂] 1 mol% Pd, dppe 1 mol% ⁱ Pr ₂ EtN 1 mol%	78%/24 h
14	[(SCS) ^{Ph} Pd] ₃ 5 mol% Pd, 20 mol% Mg(OTf) ₂	>95%/20 min

As previously pointed out, the presence of HFIP and Mg(OTf)₂ is crucial to boost the catalytic activity and makes the Conia-ene reaction work at 25°C with low Pd loadings (Table 1; Entries 1,2,3). Conversely, in the absence of the Pd complex, no cyclized product (or only a very small amount) was formed with HFIP alone or with a mixture of Mg(OTf)₂ and HFIP (Table 1; Entries 4,5). The electron-rich indenediide moiety of the SCS ligand also plays a major role, as substantiated by the noticeable decrease in activity observed when shifting to the corresponding 1-Me-2-indenyl Pd complex (Table 1; Entries 6,7) or the 1-H-2-indenyl Pd complex (Table 1; Entries 8,9).

In addition, much lower conversions were observed with $[\text{PdCl}(\text{allyl})]_2$ and $[\text{PdCl}_2(\text{PhCN})_2]$ (6–7% after 24 h), as well as $[\text{PdCl}_2(\text{dppe})]$ (35%) (Table 1; Entries 10,11,12). Even the combination of $[\text{PdCl}_2(\text{dppe})]$ with a base ($i\text{Pr}_2\text{EtN}$, 1 mol%) performed poorly (78% conversion after 24 h) compared to the $[(\text{SCS})\text{Pd}]_2$ system (>95% in 1.5 h) (Table 1; Entries 13,1).

Seeking to evidence the non-innocent character of the ligand via the formation of indenyl $[(\text{SCS-H})\text{PdX}]$ species, several catalytic reactions were *in situ* analyzed by $^{31}\text{P}\{^1\text{H}\}$ NMR spectroscopy (*vide infra* Figure II.3; More details in Experimental Section II.4); Figure II.9; Figure II.10). These monitorings were complicated by the fact that HFIP has an impact on the structure/association degree of the catalyst, and only broad signals could be observed (the dimer $[(\text{SCS})\text{Pd}]_2$ was recovered intact after evaporation of the solvent at the end of the catalytic reaction). When the reaction was carried out in the absence of HFIP, only the dimer $[(\text{SCS})\text{Pd}]_2$ was observed along the reaction, indicating that it is the resting state. This behavior is reminiscent of that observed in the cycloisomerization of alkynoic acids and is consistent with the tight association of the two (SCS)Pd fragments.^[30] We decided then to evaluate the behavior of a pre-catalyst bearing Ph instead of $i\text{Pr}$ groups on the P atoms. The less electron-donating $\text{Ph}_2\text{P}=\text{S}$ sidearms led to weaker association of the two $(\text{SCS})^{\text{Ph}}\text{-Pd}$ fragments.^[27] Only broad signals were again observed in the presence of HFIP (Experimental Section II.4); Figure II.10), but when the reaction was carried out in the absence of HFIP, minor signals corresponding to indenyl species were clearly detected by $^{31}\text{P}\{^1\text{H}\}$ NMR spectroscopy (Figure II.3). Although $[(\text{SCS})^{\text{Ph}}\text{Pd}]_3$ remains the major species, the observation of indenyl species during the catalytic transformation is consistent with the indenediide ligand backbone acting as a base.

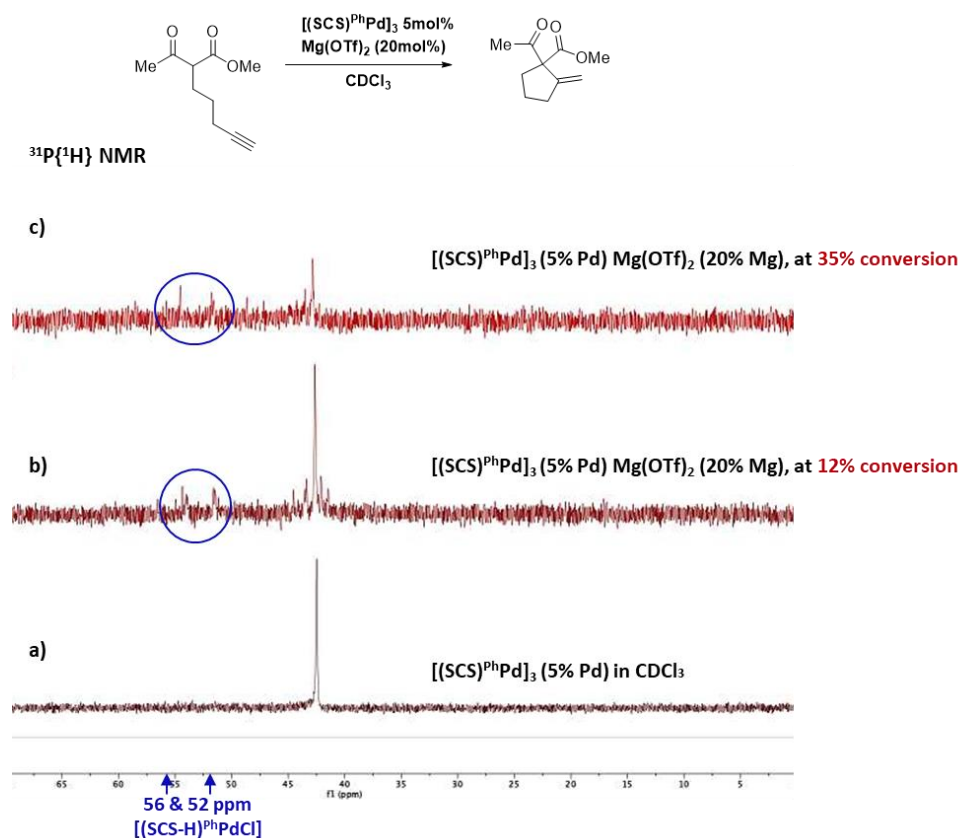
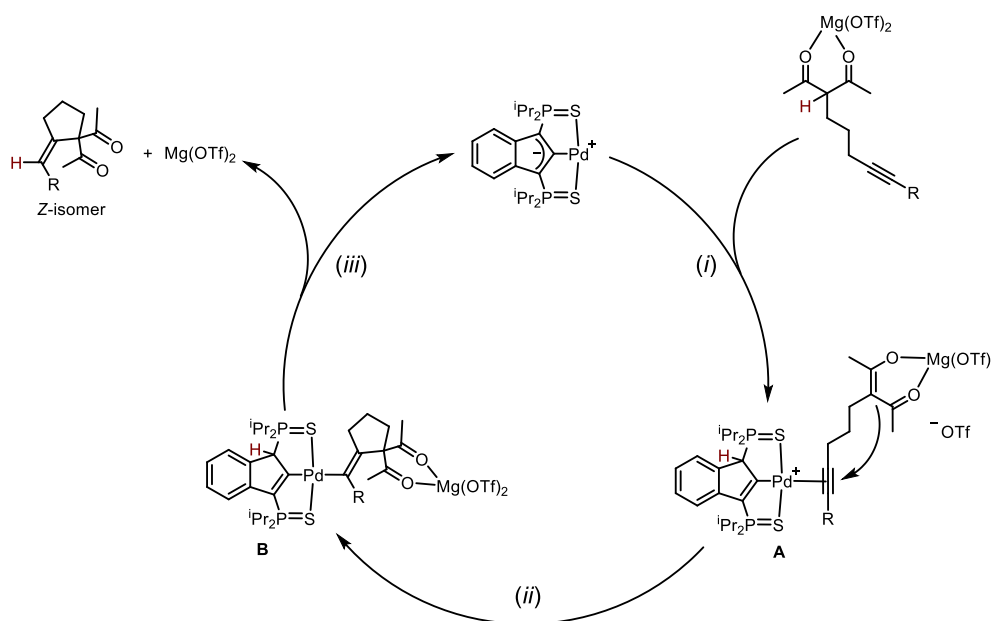


Figure II.3: $^{31}\text{P}\{^1\text{H}\}$ NMR Monitoring of $[(\text{SCS})^{\text{Ph}}\text{Pd}]_3$ under catalytic reaction conditions without HFIP

A simplified 3-step mechanism for the Conia-ene reaction catalyzed by the association of $[(\text{SCS})\text{Pd}]_2$ and $\text{Mg}(\text{OTf})_2$ is depicted in Scheme II.5: *(i)* double activation of the substrate: the LA chelates the β -dicarbonyl moiety, the acidic proton is transferred to the electron-rich indenediide backbone of the SCS ligand while the alkyne coordinates to palladium (intermediate **A**); *(ii)* cyclization: the ensuing enolate adds to the π -activated $\text{C}\equiv\text{C}$ triple bond to give the alkenyl Pd complex **B**; *(iii)* product release: back-transfer of the proton from the ligand backbone to the C_{sp^2} atom bonded to Pd results in proto-depalladation and regenerates the indenediide Pd catalyst. HFIP is presumed to help dissociate the dimeric pre-catalyst,^[52] and to promote proton shuttling from the substrate to the indenediide moiety in step *(i)* and from the ligand backbone to the C_{sp^2} carbon at Pd in step *(iii)*.



Scheme II.5: Catalytic cycle proposed to account for the Conia-ene reaction catalyzed by the (SCS)Pd complex and Mg(OTf)₂

The scope and functional group tolerance of the reaction were then explored (Figure II.4). Our aim was not only to probe the generality of the new MLC–LA dual catalytic approach, but also to improve the efficiency of the Conia-ene transformation and expand its synthetic interest. Substrates with a terminal alkyne and prone to 5-*exo* cyclization were investigated first. The (SCS)Pd–Mg association proved to be particularly efficient to cyclize β -diesters **5a**–**7a** featuring an adjacent heteroatom (N or O). The amide-tethered substrate **5a** was quantitatively cyclized in only 5 min at 25 °C. Shifting the amide moiety at the *exo* position (**6a**) slowed down the transformation somewhat, but it still proceeded rapidly and efficiently at 25°C (>95% in 50 min). Cyclization of the ether-tethered substrate **7a** was more challenging, but heating to 75°C enabled to achieve high conversion (90%) in only 4.25 h.

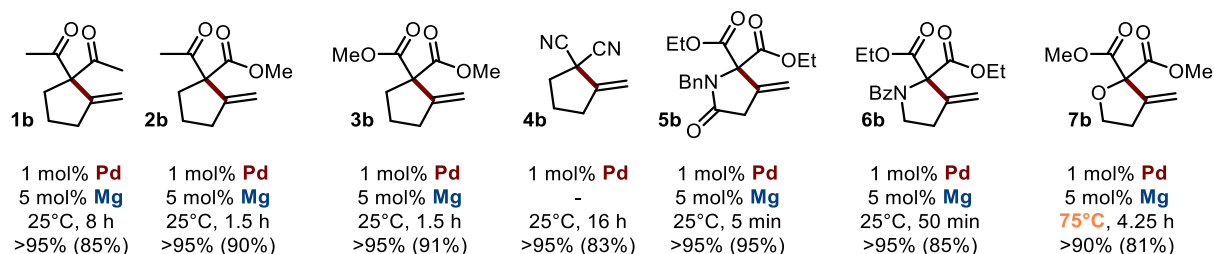
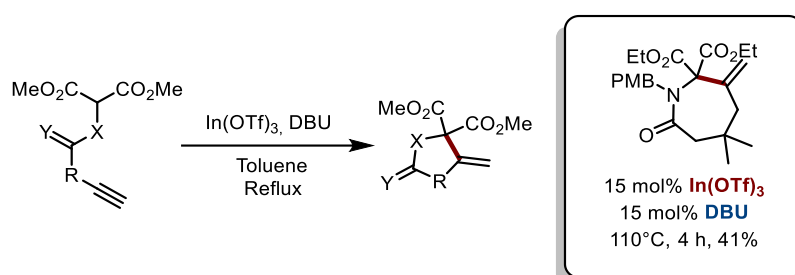


Figure II.4: 5-*exo* cyclization of terminal alkynes; isolated yields are indicated in brackets

The length of the linker between the β -dicarbonyl moiety and the terminal alkyne was then modified with the aim to access larger rings (Figure II.5; **8a**–**12a**). 6-*exo* cyclization of β -

keto,esters such as **8a** featuring a flexible butylene tether is tricky. It has only been scarcely achieved, using a Au(I) complex featuring a tris-alkynyl phosphine with bulky end caps (1 mol%, 25 °C, 1.5 h) or In(NTf₂)₃ (1 mol%, 80 °C, 4 h).^[57,58] Pleasingly, the methylenecyclohexane product **8b** could also be obtained efficiently using the [(SCS)Pd]₂ complex (5 mol% Pd) and Mg(OTf)₂ (20 mol%) within 20 h at 75 °C (90%). The dual catalytic system proved to be particularly efficient when the enol position bears an oxygen or nitrogen atom. Such substrates have been shown by Hatakeyama *et al.* to provide straightforward entry to valuable heterocycles and very good results in terms of activity and selectivity were obtained using In(OTf)₃ with DBU (5-15 mol% each) in refluxing toluene (Scheme II.6).^[59]



Scheme II.6: Synthesis of heterocycles *via* Conia-ene cyclization catalyzed by the In(OTf)₃/DBU system developed by Hatakeyama

In our hands, the β -diester substrates **9a-11a** reacted smoothly and high yields (>85%) were achieved with low catalytic loadings (1 mol% Pd, 5 mol% Mg) (Figure II.5). Particularly noteworthy is the formation of the δ -valerolactame **10b** which was accomplished in only 2.5 h at 25 °C. Even 7-*exo* cyclization was possible and highly yielding. Using the same conditions as for **8a**, the 3-caprolactame **12b** was obtained in 90% yield within 40 h, and the reaction time could be reduced to 7 h using microwave irradiation.^[60,61] The preparation of such seven-membered rings was previously described using In(OTf)₃/DBU as the catalyst, but in modest yield (41%) and with high catalytic loading (15 mol%) (*vide supra* Scheme II.6).^[59]

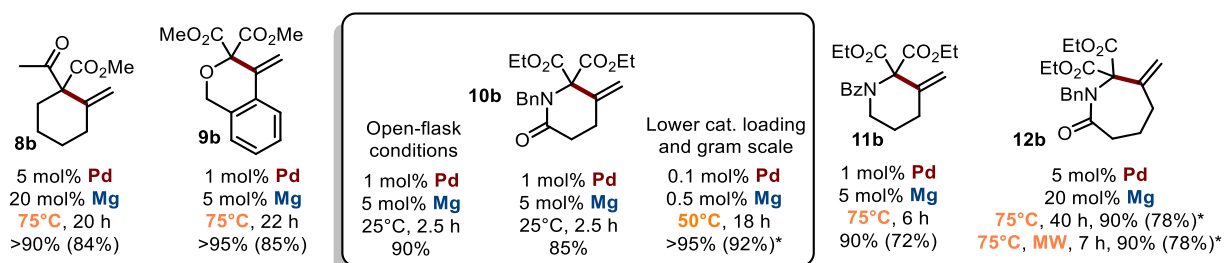
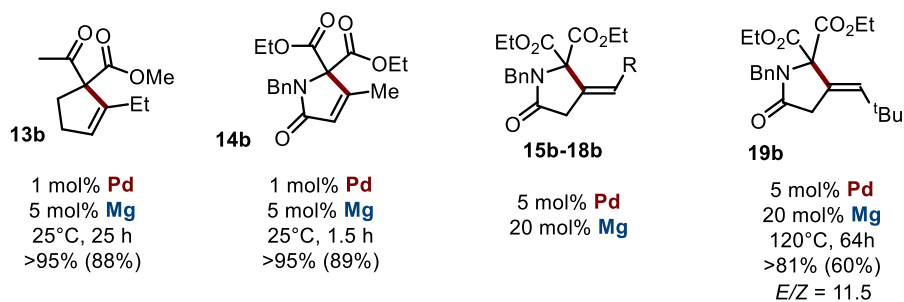


Figure II.5: >5-*exo* cyclization of terminal alkynes; isolated yields are indicated in brackets; *stands for 0.1 M substrate concentration instead of 0.5 M.

To assess the robustness of the Pd–Mg dual catalytic system, the cyclization of the amide-tethered substrate **10a** was carried out under the optimized conditions (25°C, 1 mol% Pd, 5 mol% Mg, chloroform/HFIP 4/1) but under open-flask conditions and with technical grade solvents. The δ -valerolactame **10b** was obtained in similar yield compared to under inert conditions, demonstrating that the reaction does not require stringent precautions. Furthermore, when the catalytic loading was reduced by a factor of ten (0.1 mol% Pd and 0.5 mol% Mg), the product was still obtained in very high yield (>95% in 18 h at 50°C). These reaction conditions were successfully applied to larger scale: 920 mg of pure product **10b** were prepared using only 1.4 mg of [(SCS)Pd]₂ and 4.5 mg of Mg(OTf)₂. Merging metal–ligand cooperation and Lewis acid activation, as realized with the [(SCS)Pd]₂ complex and Mg(OTf)₂, thus appears general, practical and of synthetic value. It promotes 5, 6 and 7-*exo* cyclization of β -dicarbonyl substrates featuring terminal alkynes under mild conditions and gives access to a variety of carbo- and hetero-cycles.

The good performance of the dual Pd–Mg catalytic system prompted us to explore then the cyclization of substrates bearing internal alkynes, which are significantly more challenging than terminal alkynes (Figure II.6). Being way less reactive, these substrates require harsher conditions, which often results in regio-selectivity issues with the formation of mixtures of *exo* and *endo* cyclization products.^[62,63]

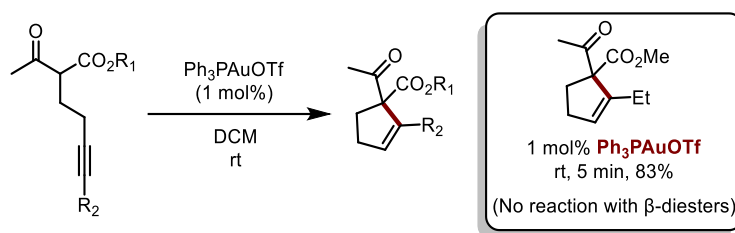


R	T °C	Time	Yield	Z/E
Me (15b)	25	3	85%	>50
Et (16b)	25	24	85%	>50
Cy (17b)	120	32	76% (52% Z)	7
Ph (18b)	75	16	79% (65% Z)	10

Figure II.6: 5-*endo* and 5-*exo* cyclisation of internal alkynes

Given the preference of 5-*endo* against 4-*exo*-dig cyclization, the β -keto,ester **13a** and β -diester **14a** were tested first. A longer reaction time was needed for **13a** than for **14a** (25 vs.

1.5 h) but in both cases, the reaction proceeded readily at 25°C and afforded high yield (95%) of the 5-*endo* product. No trace of the less favored 4-*exo* product was detected by ^1H NMR spectroscopy. Our dual catalytic system does not compete with $(\text{Ph}_3\text{P})\text{AuOTf}$ for the formation of cyclopentene **13b** (83% yield was achieved in only 5 min at room temperature using 1 mol% Au),^[64] but on the other hand, the gold catalyst works only with β -keto,esters and failed to cyclize β -diesters (Scheme II.7).^[58] As far as the cyclization of **14a** is concerned, it had only been efficiently accomplished with Zn halides (10 mol%) but required high temperature and long reaction times (100°C, 15 h).^[65]



Scheme II.7: Gold catalyzed 5-*endo* Conia-ene cyclizations of internal alkynes reported by Toste

We then investigated 5-*exo* Conia-ene cyclization with internal alkynes (β -diester substrates **15a-19a**). The terminal substituent was varied ($\text{R} = \text{Me}, \text{Et}, \text{Cy}, \text{Ph}, \text{tBu}$) to assess the impact of sterics and electronics. It should be noted that precedents of Conia-ene cyclization with internal alkynes mostly involve aryl and primary alkyl substituents, while examples with secondary alkyl groups are much rarer and tertiary ones are unprecedented.^[37,59,64,65] Due to the lower reactivity of these substrates, the catalytic loadings were fixed to 5 mol% Pd and 20 mol% Mg. For the less hindered substrates, with Me (**15a**) and Et (**16a**) substituents, cyclization occurred at 25°C within 3 and 24 h, respectively, while those bearing Cy (**17a**), Ph (**18a**) and tBu (**19a**) groups required heating at 75–120°C to achieve high conversions. For all substrates, including the tBu -substituted **19a**, the reaction was highly selective. The structures of the obtained products were unambiguously determined thanks to thorough ^1H and ^{13}C NMR spectroscopic analyses including ADEQUATE, NOESY and dsel-HSQC-IPAP experiments.

As a representative example, the ADEQUATE spectrum obtained for the cyclohexyl-substituted **17a** is represented below (Figure II.7). This experiment allows for the unambiguous determination of the ^1J connectivity between carbon centers, discriminating between 5-*exo* and 6-*endo* structures.

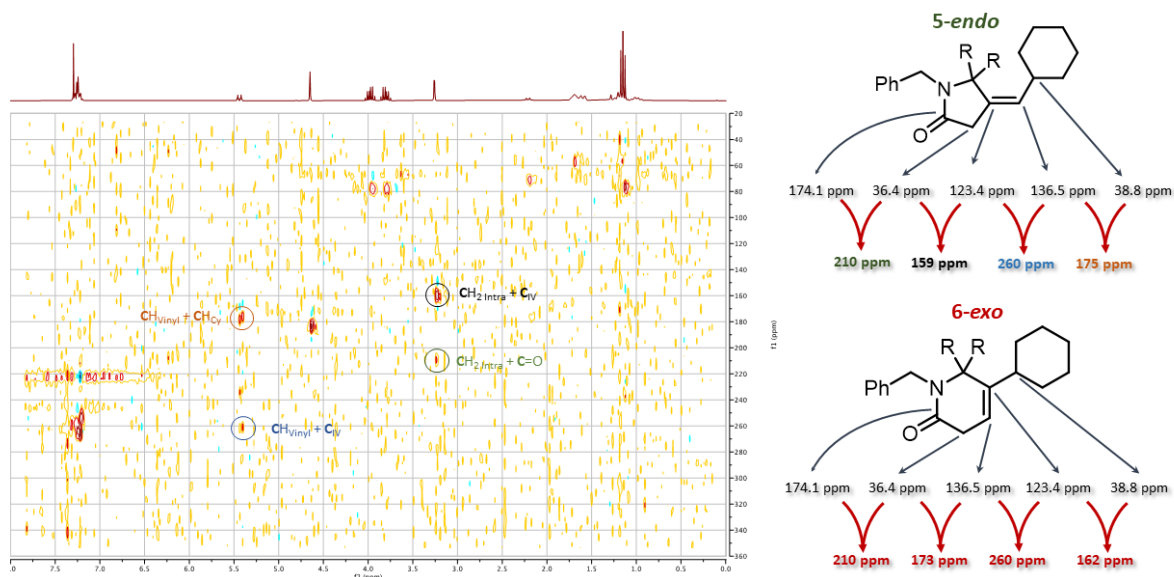


Figure II.7: ADEQUATE NMR experiment to unambiguously determine the connectivity between the carbons

To interpret the spectrum and determine the connectivity, a prior assignment of the ^{13}C chemical shifts of each carbon involved is necessary. Then, the 2D spectrum shows correlation between the proton-bearing carbon and the sum of the chemical shifts of each carbon it is bonded to. For example, the endocyclic CH_2 signal (at 3.22 ppm in ^1H ; 36.4 ppm in ^{13}C) shows two correlations spots (green and black at 210 ppm and 159 ppm; Right side - Figure II.7), arising from the two carbons it is connected to. Subtracting 36 to each correlation spot then gives 174 and 123 ppm, corresponding to the $\text{C}=\text{O}$ and the vinylic C_{IV} in accordance with a 5-*exo* structure. In the case of the 6-*endo*, these two correlations spots would have been found at 210 and 173 ppm. The same principle applies for all spots shown here, allowing the unambiguous determination of the ring-size.

Complete selectivity in favor of 5-*exo* vs 6-*endo* cyclization was observed, whatever the substituent at the alkyne (alkyl or phenyl). For **15a** and **16a**, a single 5-*exo* product was obtained, authenticated as the *Z* isomer by comparison with the literature data. For the substrates **17a** and **18a** bearing bulkier groups, which required higher reaction temperature, two 5-*exo* products were formed. NOESY NMR experiments were employed on each isolated compounds to determine the *Z/E* nature of the isomer. Illustrated below with the cyclohexyl substituted *Z*-alkene **17a**, the discrimination was done thanks to the clear correlation between the endocyclic CH_2 and the vinylic CH proton (Figure II.8). In all cases, the *Z* isomer was very major (*Z/E* ratio from 7 to 10).

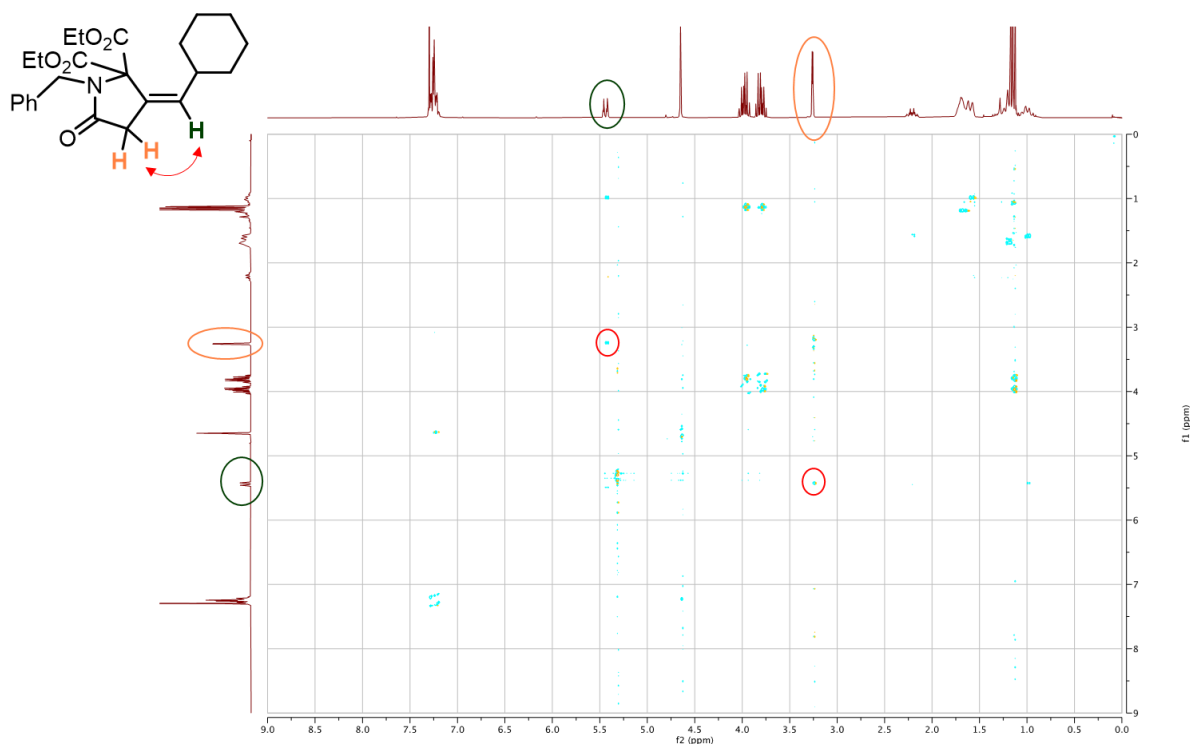
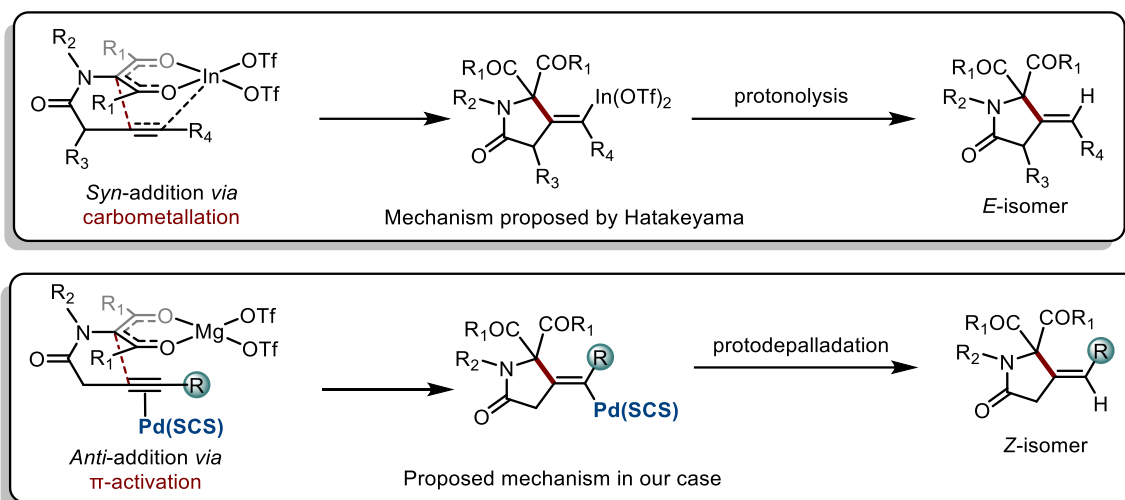


Figure II.8: NOESY NMR of an isolated isomer of **17a** with correlation spots between the endocyclic CH₂ and the vinyl CH, authenticated at the *Z*-isomer

In the case of the ^tBu group however, residual COSY signal on the NOESY analysis precluded the unambiguous discrimination between the *Z* and *E* stereochemistry. This was finally stated thanks to NOESY ZQF Selective analyses and to the determination of the ³J_{CH} values by double selective-HSQMBC-IPAP. Attribution of the stereochemistry was done taking into account that ³J_{CH} (*trans*) > ³J_{CH} (*cis*). The opposite stereo-selectivity was observed.^[66]

Steric congestion favored here the *E* product (*E/Z* of 11.5). Reaction monitoring indicated that it is not due to isomerization of **19b** over prolonged heating, the same *E/Z* ratio being observed from the beginning of the cyclization. From a mechanistic viewpoint, the *Z*-selectivity observed with **15a-18a** is consistent with the outer-sphere approach outlined in Scheme II.5. The enolate adds to the π-activated alkyne *trans* to Pd, resulting in the *Z* product after proto-depalladation (Scheme II.8).^[67] This *Z*-selectivity markedly contrasts with the *E*-selectivity induced by the In(OTf)₃/DBU catalyst (with R₄ = Me, ⁿBu; Scheme II.8).^[59] In the latter case, the reaction was proposed to proceed by *syn* carbometalation, with the In(III) center simultaneously activating the β-dicarbonyl and alkyne moieties.^[68] Formation of the *E*

product **19b** most likely results from isomerization of the vinyl-Pd intermediate prior to protodepalladation, due to steric congestion.^[69–71]



Scheme II.8: Proposed mechanisms proposed to account for the formation of the *E*-isomer in the case of Hatakeyama and the *Z*-isomer in our case

II.3) Conclusions

When combined with $\text{Mg}(\text{OTf})_2$ and HFIP, the indenediide-based SCS Pd pincer complex was found to be a very powerful catalyst for Conia-ene cyclizations. It works with a variety of substrates, β -keto, esters as well as β -dinitriles and β -diesters, and gives access with complete regio-selectivity to 5, 6 and 7-membered carbo- as well as heterocycles. It is robust and operates at low catalytic loadings (down to 0.1 mol% Pd and 0.5 mol% Mg). Most remarkably, it is also active and selective with substrates featuring internal alkynes. Whatever the substituent at the terminal position is (1°/2°/3° alkyl, aryl), 5-*exo* fully prevails over 6-*endo* cyclization. Moreover, except for the highly congested ^tBu product, the reaction occurs with high *Z*-selectivity. This behavior is in contrast with the *E*-selectivity observed with In-based catalysts, the other known catalysts for internal alkynes. This is due to the way the C–C bond formation and cyclization proceeds with the dual Pd/Mg catalyst; the Mg-chelated enolate attacks the π -coordinated $\text{C}\equiv\text{C}$ triple bond trans to Pd.

These results expand the scope of MLC catalysis in terms of metal (the potential of Pd complexes in MLC catalysis is clearly under-exploited) and catalytic transformations (while hydrogenation/dehydrogenation processes have been extensively developed, examples of C–C bond forming reactions are very rare). Moreover, this work introduces a new multi-

cooperative catalytic approach combining MLC and Lewis acid activation. The MLC/LA synergy parallels and complements that involving MLC and proton shuttling. It also represents a new type of dual activation, in which the TM catalyst displays MLC behavior (towards the enolizable C–H bond in this case) while the LA activates another reactive site of the substrate (the β -dicarbonyl motif).

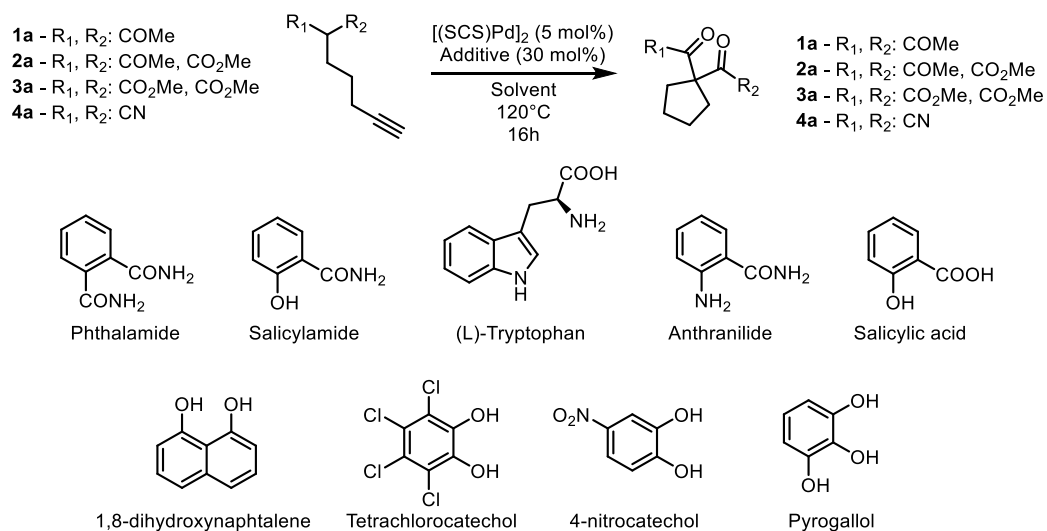
II.4) Experimental Section

General Remarks:

Preparative HPLC were performed using an Xbridge C18 150x19 mm column with a flowrate of 20 mL.min⁻¹. H₂O (0.1% HCOOH) and acetonitrile (0.1% HCOOH) were used as solvents. The complexes ([SCS]^{Ph}Pd)₃, [(SCS-H)Pd], [(SCS)Pd]₂, [(SCS)Pt]₂ were synthesized using methods previously reported by our group.^{[27],[28],[72]} Complex [(SCS-Me)Pd] was prepared using the same method reported for the corresponding phenyl derivative.^[73]

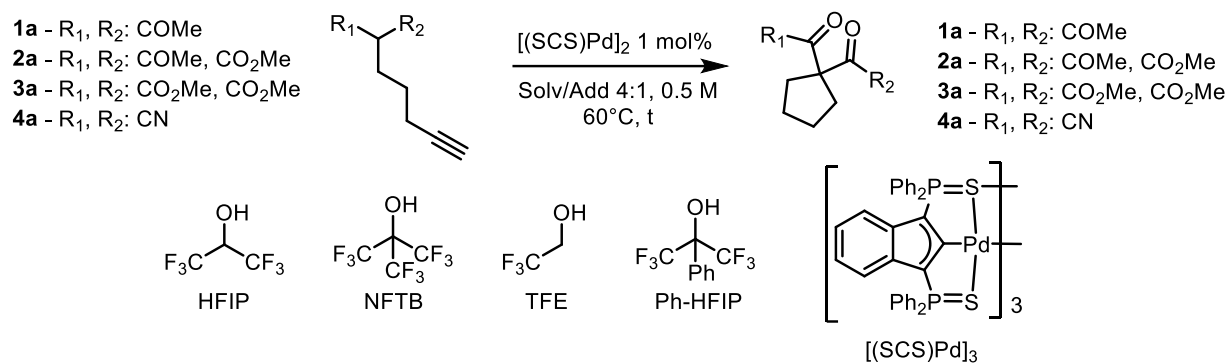
Conditions screening, optimization, and general procedure:

The model substrate (0.25 mmol), the additive and catalyst were dissolved in 0.5 mL of solvent in an NMR tube. The reaction was then heated at the indicated temperature for the corresponding time. Yields were determined by ¹H NMR analysis with 1,2,4,5-tetramethylbenzene as internal standard.



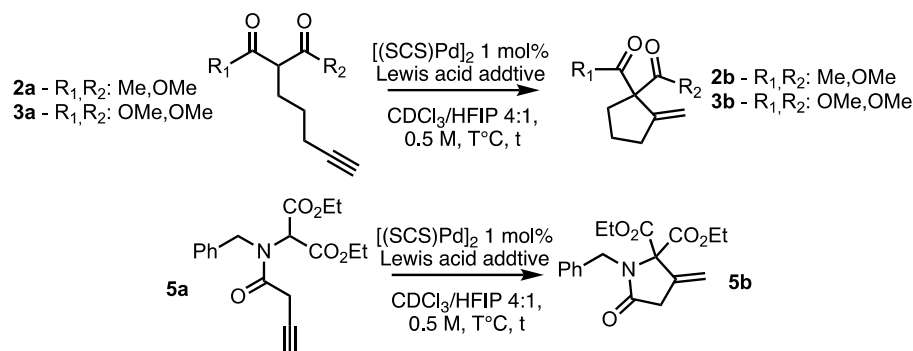
Entry	Substrate	Solvent	Additive	Yield
1	2a	CDCl ₃	none	No
2	2a	CDCl ₃	Phthalamide	24
3	2a	CDCl ₃	Salicylamide	14
4	2a	CDCl ₃	(L)-Tryptophan	No
5	2a	CDCl ₃	Anthranilide	No
6	2a	CDCl ₃	Salicylic acid	27
7	2a	CDCl ₃	1,8-	50
8	2a	CDCl ₃	Tetrachlorocatechol	23
9	2a	CDCl ₃	Nitrocatechol	47 ^[a]
10	2a	CDCl ₃	Pyrogallol	50
11	2a	Toluene-	Nitrocatechol	63 ^[a]
12	2a	DMSO-d ₆	Nitrocatechol	12
13	2a	Toluene-	Pyrogallol	61
14	1a	CDCl ₃	Nitrocatechol	85
15	3a	CDCl ₃	Nitrocatechol	0 ^[a]
16	4a	CDCl ₃	Nitrocatechol	>95

Table 2: Screening of catechols and other H-bonding additives; [a] ca. 30 mol% of product of addition of 4-nitrocatechol on the triple bond was detected by ¹H NMR



Entry	Substrate	Solvent	Catalyst	Additive	Time (h)	Yield
1	2a	CDCl ₃	[(SCS)Pd] ₂	NFTB	16	53 ^[a]
2	2a	CDCl ₃	[(SCS)Pd] ₂	HFIP	16	90 ^[a]
3	2a	CDCl ₃	[(SCS)Pd] ₂	HFIP	4	58 ^[b]
4	2a	CDCl ₃	[(SCS)Pd] ₂	TFE	4	Traces
5	2a	CDCl ₃	[(SCS)Pd] ₂	Isopropanol	16	n.r.
6	2a	CDCl ₃	[(SCS)Pd] ₂	Ph-HFIP	16	n.r.
7	2a	CDCl ₃	-	HFIP	16	Traces ^[c]
8	2a	CDCl ₃	[(SCS) ^{Ph} Pd] ₃	HFIP	16	8
9	2a	CDCl ₃	[(SCS)Pt] ₂	HFIP	16	40
10	2a	THF-d ₈	[(SCS)Pd] ₂	HFIP	16	n.r.
11	2a	DMSO-d ₆	[(SCS)Pd] ₂	HFIP	16	n.r.
12	2a	Toluene-d ₈	[(SCS)Pd] ₂	HFIP	16	90
13	2a	CD ₂ Cl ₂	[(SCS)Pd] ₂	HFIP	16	88
14	1a	CDCl ₃	[(SCS)Pd] ₂	HFIP	16	90
15	3a	CDCl ₃	[(SCS)Pd] ₂	HFIP	16	n.r.
16	4a	CDCl ₃	[(SCS)Pd] ₂	HFIP	16	>95

Table 3: Fluorinated additive and catalyst screening; [a] T = 90°C; [b] 90% after 16h; [c] full conversion and ca. 80% yield at 120°C

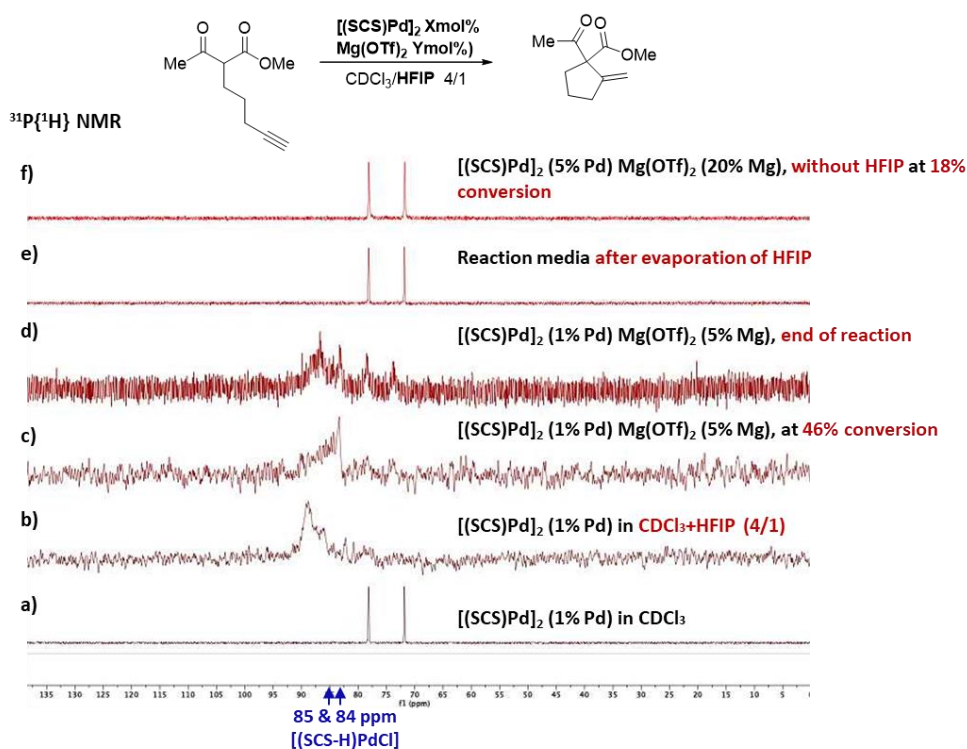
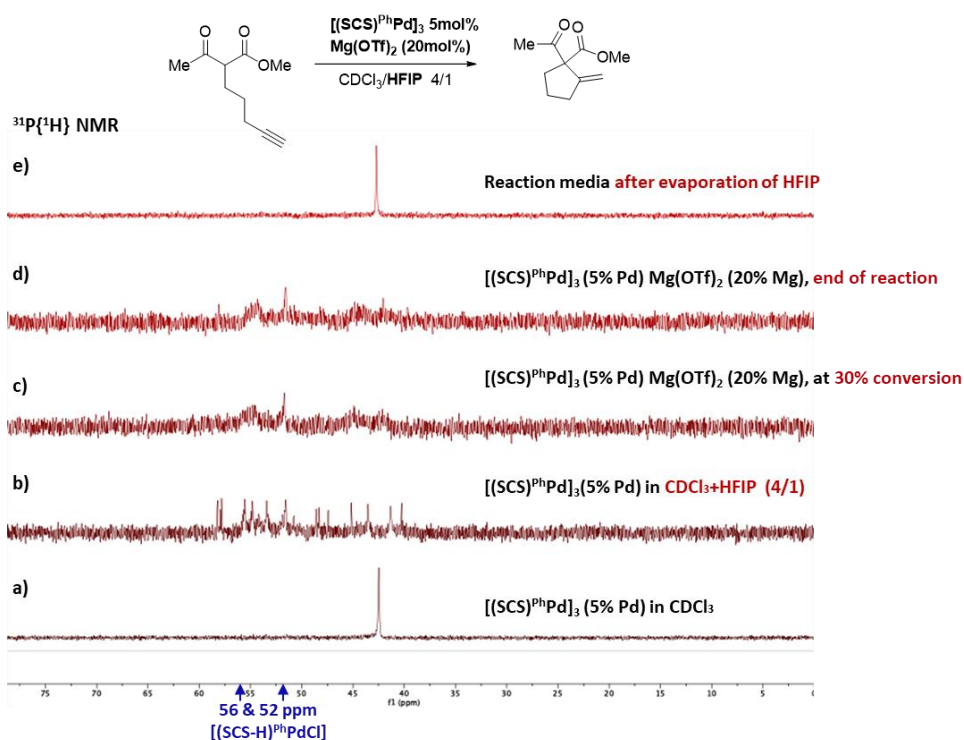


Entry	Substrate	LA (mol %)	$T^\circ C$	Time (h)	Yield
1	2a	none	60	1	25
2	2a	Sc(OTf) ₃ (20)	60	1	11
3	2a	Cu(OTf) ₂ (20)	60	1	23
4	2a	Ca(OTf) ₂ (20)	60	1	92
5	2a	Mg(OTf) ₂ (20)	60	1	>95
6	2a	Zn(OTf) ₂ (20)	60	1	>95 ^[a]
7	2a	Yb(OTf) ₃ (20)	60	1	82 ^[b]
8	2a	Ca(OTf) ₂ (20)	40	1	24
9	2a	Mg(OTf) ₂ (20)	40	1	>95
10	2a	none	25	0.5	4
11	2a	Zn(OTf) ₂ (5), No	25	0.5	27
12	2a	Zn(OTf) ₂ (5)	25	0.5	76
13	2a	Ca(OTf) ₂ (5)	25	0.5	9
14	2a	Mg(OTf) ₂ (5)	25	0.5	87
15	2a	Yb(OTf) ₃ (5)	25	0.5	88 ^[b]
16	2a	Sc(OTf) ₃ (5)	25	0.5	16
17	3a	Mg(OTf) ₂ (5)	25	0.5	83
18	3a	Yb(OTf) ₃ (5)	25	0.5	13 ^[b]
19	4a	none	25	16h	>95
20	4a	Mg(OTf) ₂ (5)	25	16h	>95
21	5a	Mg(OTf) ₂ (5)	25	0.5	87
22	5a	Yb(OTf) ₃ (5)	25	0.5	No reaction ^[b]

Table 4: Lewis acid screening; [a] The reaction was accomplished in 1h even in absence of Pd complex; [b] Direct NMR analysis was hampered due to distortion caused by the Yb salt, the yield reported is the isolated yield after work up.

$^{31}\text{P}\{^1\text{H}\}$ monitoring of catalytic reactions:

Seeking to evidence the contribution of the indenediide ligand via the formation of indenyl species, several catalytic reactions under optimized conditions were monitored by ^{31}P NMR spectroscopy (Figure II.3; Figure II.9; Figure II.10). Upon addition of HFIP to a CDCl_3 solution of $[(\text{SCS})\text{Pd}]_2$, the two singlet signals corresponding to the inequivalent P atoms of the dimeric complex (Figure II.9, a) disappear to give rise to a broad signal at ca 85 ppm, in the typical region for indenyl-Pd species (b).^[28] Upon addition of the substrate and Mg Lewis acid, the Conia-Ene reaction occurs, during which no significant change was observed in the ^{31}P spectrum (c). At the end of the reaction, two additional small broad signals appeared in the indenediide region (d). Evaporation of the HFIP/ CDCl_3 mixture and addition of pure CDCl_3 resulted in the clean reformation of the dimeric $[(\text{SCS})\text{Pd}]_2$, as evidenced by the two singlet signals depicted by the ^{31}P spectrum (e). This observation supports the robustness of the catalyst that is fully regenerated at the end of the reaction. When the reaction was carried out in the absence of HFIP, the sole species detected during the reaction was the pre-catalyst $[(\text{SCS})\text{Pd}]_2$, it is the resting-state of the process. This behavior is reminiscent of that observed in the cycloisomerization of alkynoic acids,^[30] and is consistent with the tight association of the two (SCS)Pd fragments. We decided then to evaluate the behavior of a pre-catalyst bearing Ph instead of ^iPr groups on the P atoms. The less electron-donating Ph_2P groups lead to weaker association of the $(\text{SCS})^{\text{Ph}}\text{Pd}$ fragments,^[27,28] supported by the observation of only one signal on the ^{31}P spectrum, despite its trimeric structure in the solid state.^[27] Again, addition of HFIP to a CDCl_3 solution of $[(\text{SCS})^{\text{Ph}}\text{Pd}]_3$ results in the disappearance of the initial signal in the ^{31}P spectrum (Figure II.10, a), while a series of signals appears in the indenyl and indenediide regions (b). Addition of the substrate leads to the broadening of the signals (c,d) and at the end of the reaction, and $[(\text{SCS})^{\text{Ph}}\text{Pd}]_3$ is fully regenerated after removal of HFIP (e). However, when the reaction was carried out in the absence of HFIP (Figure II.3, a), minor indenyl Pd complexes could be clearly observed, although $[(\text{SCS})^{\text{Ph}}\text{Pd}]_3$ remains the major species (a). Even if they are minor, the observation of these indenyl species during the catalytic transformation is consistent with the indenediide ligand backbone acting as a base.

Figure II.9: NMR Monitoring of [(SCS)Pd]₂ under catalytic reaction conditionsFigure II.10: NMR Monitoring of [(SCS)PhPd]₃ under catalytic reaction conditions

Synthesis of precursors:**i) General procedure A for the synthesis of the precursors:**

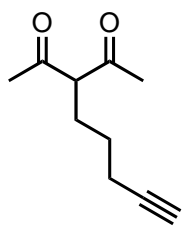
The pro-nucleophile (1.2 equiv) was added dropwise to a suspension of NaH (60% dispersed in mineral oil - 1.3 equiv) in THF:DMF (1:1) (0.33 M) at 5°C. The reaction was then allowed to warm at to room temperature and stirred for 15 min. The electrophile was then added dropwise (1.0 eq) and the reaction media was heated at 85°C for 24 h. The volatiles were removed, and the reaction was quenched with a saturated solution of $\text{NH}_4\text{Cl}_{(\text{aq})}$ and EtOAc was added. The organic layer was washed with H_2O , dried over Na_2SO_4 and the solvent was removed *in vacuo* to yield the corresponding precursor that was either directly used or further purified by column chromatography.

ii) General procedure A for the synthesis of the precursors:

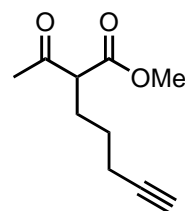
A couple of drops of DMF were added to a stirred solution of the corresponding carboxylic acid (1.2 equiv) in DCM (1 M). Then oxalyl chloride (1.1 equiv) was dropwise added and the reaction media was allowed to stir for 1 h (Caution: bubbling of CO_2 and CO occurs). The crude acyl chloride solution was then added to a strongly stirred mixture of the corresponding amine (1.0 equiv) in DCM (0.67 M) and $\text{NaHCO}_3(\text{sat})$ (1.0 mL.mmol⁻¹). After 1h, the solution was filtered through a silica pad using Et_2O as eluent to yield the crude amide. Further purification was achieved by column chromatography.

iii) General procedure A for the synthesis of the precursors:

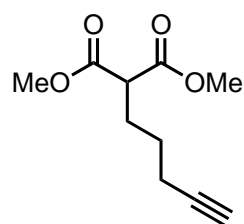
The method is a modified version of Sammakia's procedure.^[74] To a solution of the corresponding *t*Bu ester (1.0 equiv) in SOCl_2 (10.0 equiv), H_2O (1.0 equiv) was added and the resulting mixture was allowed to stir overnight at room temperature. Then, the thionyl chloride was removed *in vacuo* or by distillation. The residual amount of SOCl_2 was removed by azeotropic distillation with toluene (repeated three times). After complete removal of solvent, the crude acyl chloride was dissolved in DCM (1 M) and added to a solution of the corresponding amine (1.0 equiv) in DCM (0.67 M) and $\text{NaHCO}_3(\text{sat})$ (1.0 mL.mmol⁻¹). After 1h, the solution was filtered through a silica pad using Et_2O as eluent to yield the crude amide. Further purification was achieved by column chromatography.

3-(pent-4-yn-1-yl)pentane-2,4-dione - 1a - CAS [88459-71-6]:

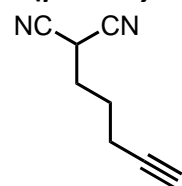
Using general procedure **A**, with acetylacetone (1.2 g - 12 mmol) and 5-chloropent-1-yne (1.16 g - 10 mmol) pure 3-(pent-4-yn-1-yl)pentane-2,4-dione (549 mg - 48% yield) was obtained as a clear oil after purification via column chromatography (95:5 Pentane:EtOAc). Mixture of keto-enol tautomers. $^1\text{H NMR}$ (300 MHz, CDCl_3): δ = 3.64 (t, J = 7.2 Hz, 1H, $-\text{CH}-(\text{COMe})_2$), 2.39 - 2.32 (m, 1H, $\text{CH}_a-\text{CH}-(\text{COMe})_2$), 2.29 - 2.20 (m, 2H, $-\text{CH}_2-\text{C}\equiv$), 2.19 (s, 3H, CH_3), 2.16 (s, 3H, CH_3), 2.03 - 1.90 (m, 2H, $\text{CH}_b-\text{CH}-(\text{COMe})_2$, $\text{C}\equiv\text{CH}$), 1.68 - 1.40 (m, 2H, $\text{CH}_2-\text{CH}_2-\text{CH}_2$). Spectroscopic data in accordance with literature.^[75]

Methyl 2-acetylhept-6-ynoate - 2a - CAS [131190-10-8]:

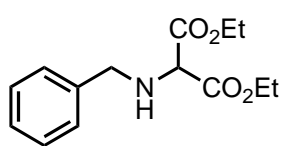
Using General procedure **A**, with methyl 3-oxobutanoate (1.17 g - 10 mmol) and 5-chloropentyne (975 mg - 8.4 mmol) pure Methyl 2-acetylhept-6-ynoate (1.01 g - 66% yield) was obtained as a clear oil after purification via column chromatography (95:5 Pentane:EtOAc). Mixture of keto-enol tautomers. $^1\text{H NMR}$ (300 MHz, CDCl_3): δ = 3.74 (s, 3H, CH_3-O), 3.46 (t, J = 7.4 Hz, 1H, $\text{CO}_2\text{Me}-\text{CH}-\text{COMe}$), 2.23 (s, 3H, $\text{CH}_3-\text{C}=\text{O}$), 2.26 - 2.17 (m, 2H, $-\text{CH}_2-\text{C}\equiv$), 2.06 - 1.90 (m, 3H, $-\text{CH}-\text{CH}_2-\text{CH}_2$; $\text{C}\equiv\text{CH}$), 1.62 - 1.42 (m, 2H, $\text{CH}_2-\text{CH}_2-\text{CH}_2$). Spectroscopic data in accordance with literature.^[76]

Dimethyl 2-(pent-4-yn-1-yl)malonate - 3a - CAS [130905-55-4]:

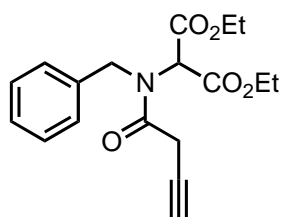
Using General procedure **A**, with dimethyl malonate (653 mg - 5 mmol) and 5-chloropentyne (480 mg - 4.1 mmol) pure dimethyl 2-(pent-4-yn-1-yl)malonate (609 mg - 72% yield) was obtained as a clear oil after purification via column chromatography (90:10 Cyclohexane:EtOAc). $^1\text{H NMR}$ (300 MHz, CDCl_3): δ = 3.74 (s, 6H, $(\text{OCH}_3)_2$), 3.39 (t, J = 7.5 Hz, 1H, $\text{CH}-\text{CO}_2\text{Me}$), 2.23 (td, J = 7.0, 2.6 Hz, 2H, $-\text{CH}_2-\text{C}\equiv\text{CH}$), 2.08 - 1.98 (m, 2H, $-\text{CH}-\text{CH}_2-\text{CH}_2$), 1.96 (t, J = 2.6 Hz, 1H, $\text{C}\equiv\text{CH}$), 1.62 - 1.50 (m, 2H, CH_2-CH_2). Spectroscopic data in accordance with literature.^[77]

2-(pent-4-yn-1-yl)malonitrile - 4a - CAS [106814-30-6]:

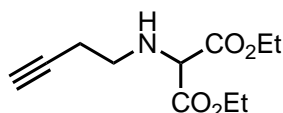
Using general procedure **A**, with malonitrile (680 mg - 10.3 mmol) and 5-chloropent-1-yne (1 g - 8.6 mmol) pure 2-(pent-4-yn-1-yl)malonitrile (549 mg - 48% yield) was obtained as a clear oil after purification via column chromatography (70:30 Pentane:DCM). $^1\text{H NMR}$ (300 MHz, CDCl_3): δ = 3.83 (t, J = 7.0 Hz, 1H, $\text{CH}-(\text{CN})_2$), 2.36 (td, J = 6.6, 2.7 Hz, 2H, $-\text{CH}_2-\text{C}\equiv$), 2.22 - 2.10 (m, 2H, $-\text{CH}-\text{CH}_2-\text{CH}_2$), 2.05 (t, J = 2.7 Hz, 1H, $\text{C}\equiv\text{CH}$), 1.87 - 1.72 (m, 2H, $\text{CH}_2-\text{CH}_2-\text{CH}_2$). Spectroscopic data in accordance with literature.^[77]

Diethyl 2-(benzylamino)malonate - CAS [56599-00-9] :

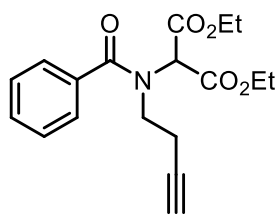
Freshly ground K_2CO_3 (10.36 g - 75 mmol - 1.0 eq) was added to a solution of benzylamine (8.2 mL - 75 mmol - 1.0 eq) and diethylbromomalonate (12.81 mL - 75 mmol - 1.0 eq) in acetonitrile (500 mL). The resulting suspension was heated at reflux overnight. The next day the volatiles were removed. DCM (100 mL) and H_2O (200 mL) were then added and the organic layer was separated. The aqueous layer was then extracted with DCM (2x100 mL). The combined organic layers were dried over Na_2SO_4 and the solvent was removed in vacuo. Pure diethyl 2-(benzylamino)malonate (5.97 g - 30% yield) was obtained as a clear oil after purification by column chromatography (using a gradient from 100:0 to 70:30 of Pentane:EtOAc). 1H NMR (300 MHz, $CDCl_3$): δ = 7.41 – 7.22 (m, 5H, H_{arom}), 4.23 (qd, J = 7.1, 0.9 Hz, 4H, $2xCH_2-CH_3$), 4.05 (s, 1H, $CH-CO_2Et$), 3.81 (s, 2H, $Ph-CH_2-NH$), 2.08 (bs, 1H, NH), 1.28 (t, J = 7.1 Hz, 6H, $2xCH_3-CH_2$). Spectroscopic data in accordance with literature.^[78]

Diethyl 2-(N-benzylbut-3-ynamido)malonate - 5a - CAS [1383445-11-1] :

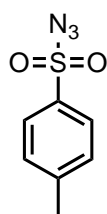
Using the general procedure **B**, with but-3-ynoic acid (250 mg - 2.97 mmol) and diethyl 2-(benzylamino)malonate (657 mg - 2.47 mmol). The corresponding diethyl 2-(N-benzylbut-3-ynamido)malonate (439 mg - 53% Yield) was obtained as an orange oil together with cyclized side product (20%). Mixture of 2 rotamers at room temperature (89%:11%), only the major rotamer is assigned. 1H NMR (300 MHz, $CDCl_3$): δ = 7.43 – 7.13 (m, 5H, H_{arom}), 5.44 (s, 1H, $CH-CO_2Et$), 4.79 (s, 2H, $Ph-CH_2-N$), 4.26 – 4.01 (m, 4H, $2xCH_2-CH_3$), 3.32 (d, J = 2.7 Hz, 2H, $-CH_2-C\equiv CH$), 2.23 (t, J = 2.7 Hz, 1H, $-C\equiv CH$), 1.21 (t, J = 7.1 Hz, 6H, $2xCH_2-CH_3$). Spectroscopic data in accordance with literature.^[79]

Diethyl 2-(but-3-yn-1-ylamino)malonate - CAS [1258538-10-1]:

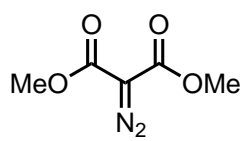
Diethyl bromomalonate (1.16 mL - 6.81 mmol - 1.0 eq) was added to a solution of 1-amino-3-butyne (471 mg - 6.81 mmol - 1.0 eq), NEt_3 (1.1 mL - 8.17 mmol - 1.2 eq) in $CHCl_3$ (12 mL). The resulting solution was heated to 55°C for 48 h. It was then allowed to cool down to room temperature and quenched by addition of 1M NaOH (40 mL). The layers were then separated and the aqueous layer extracted 3 times with EtOAc. The combined organic layers were dried over Na_2SO_4 and the solvent removed in vacuo. Pure diethyl 2-(but-3-yn-1-ylamino)malonate (330 mg - 21% Yield) was obtained after purification via column chromatography (80:20 Pentane:EtOAc). 1H NMR (300 MHz, $CDCl_3$): δ = 4.24 (q, J = 7.1, 1.1 Hz, 4H, $2xCH_2-CH_3$), 4.08 (s, 1H, $CH-CO_2Et$), 2.79 (t, J = 6.8 Hz, 2H, CH_2-NH), 2.41 (td, J = 6.8, 2.7 Hz, 2H, $CH_2-C\equiv$), 2.36 (bs, 1H, NH), 2.01 (t, J = 2.7 Hz, 1H, $C\equiv CH$), 1.29 (t, J = 7.1 Hz, 6H, $2xCH_3-CH_2$). Spectroscopic data in accordance with literature.^[80]

Diethyl 2-(N-(but-3-yn-1-yl)benzamido)malonate - 6a:

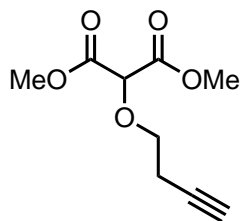
Using the general procedure B, with benzoic acid (258 mg - 2.11 mmol) and diethyl 2-(but-3-yn-1-ylamino)malonate (400 mg - 1.76 mmol). The corresponding diethyl 2-(N-(but-3-yn-1-yl)benzamido)malonate (264 mg - Yield 45%) was obtained as a clear oil (Mixture of two rotamers (55:45 in CDCl₃; 74:26 in CD₃OD), after purification by column chromatography (80:20 to 70:30 Pentane:EtOAc). (Only the major isomer is assigned) ¹H NMR (300 MHz, CDCl₃): δ = 7.51 – 7.33 (bs, 5H, H_{arom}), 5.41 – 5.02 (bs, 1H, CH-CO₂Et), 4.42 – 4.14 (bs, 4H, 2xCH₂-CH₃), 3.79 – 3.47 (bs, 2H, N-CH₂-), 2.82 – 2.25 (bs, 2H, -CH₂-C≡), 2.01 – 1.90 (bs, 1H, -C≡CH), 1.43 – 1.19 (bs, 6H, 2xCH₃-CH₂). NMR signals are all broad and not well defined in CDCl₃. Characterization was done in CD₃OD in an attempt to get a better spectrum (Only the major isomer is assigned). ¹H NMR (500 MHz, CD₃OD): δ = 7.61 – 7.32 (m, 5H, H_{arom}), 4.36 – 4.29 (q, J = 7.1 Hz, 4H, 2xCH₂-CH₃), 3.53 (bs, 2H, N-CH₂-), 2.44 (bs, 2H, -CH₂-C≡), 2.33 (bs, 1H, -C≡CH), 1.33 (t, J = 6.8 Hz, 6H, 2xCH₃-CH₂), CH-(CO₂Et) not observed. ¹³C NMR (126 MHz, CD₃OD): δ = 174.4 (Ph-C=O), 167.0 (-O-C=O), 136.3 (C_{arom}), 131.3 (CH_{arom} para), 129.9 (2xCH_{arom}), 127.6 (2xCH_{arom}), 81.2 (-C≡CH), 72.1 (-C≡CH), 63.8 (N-CH-(CO₂Et)₂), 63.2 (CH₂-CH₃), 50.7 (-CH₂-N), 19.7 (CH₂-CH₂-C), 14.4 (CH₂-CH₃). HRMS (DCI-CH₄) m/z (%): Calculated: 332.1498 (C₁₈H₂₂NO₅); Found: 332.1503

4-methylbenzenesulfonyl azide - CAS [941-55-9]:

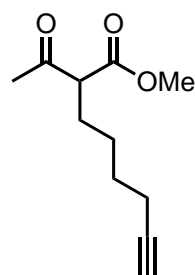
A solution of p-toluenesulfonyl chloride (3.85 g - 20 mmol - 1.0 eq) in acetone (20 mL) was added dropwise to a solution of NaN₃ (2 g - 30 mmol - 1.5 eq) in water (10 mL) at 5°C. The reaction was then allowed to warm at room temperature and stirred overnight. The volatiles were then removed, the aqueous layer was extracted 3 times with EtOAc. The organic combined layers were dried using Na₂SO₄ and the solvent was removed in vacuo to yield Tosyl azide (3.7 g - 94% Yield) used in the next step without further purification. ¹H NMR (300 MHz, CDCl₃): δ = 7.85 (d, J = 8.7 Hz, 2H, H_{arom}), 7.41 (d, J = 8.7 Hz, 2H, H_{arom}), 2.4 (s, 3H, CH₃). Spectroscopic data in accordance with literature.^[81]

Dimethyl 2-diazomalonate - CAS [6773-29-1]:

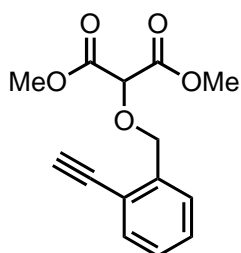
DBU (1.7 mL - 11.35 mmol - 1.5 eq) was added dropwise to a stirred solution of malonate (1g - 7.57 mmol - 1.0 eq) and Tosylazide (1.38 mL - 9.08 mmol - 1.2 eq) in acetonitrile (20 mL) at 5°C. Upon addition of DBU the reaction turns brown. It was then allowed to warm at room temperature and stirred overnight. The volatiles were removed, and the residue dissolved in DCM (20 mL). The organic layer was then washed 3 times with H₂O, dried over Na₂SO₄. The DCM was removed in vacuo. Pure Dimethyl 2-diazomalonate (1 g - 84% Yield) was obtained after purification by column chromatography (80:20 to 60:40 Pentane:Et₂O). ¹H NMR (300 MHz, CDCl₃): δ = 3.84 (s, 6H, 2xCH₃). Spectroscopic data in accordance with literature.^[82]

Dimethyl 2-(but-3-yn-1-yloxy)malonate - 7a - CAS [214914-77-9]:

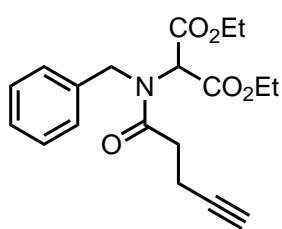
Rhodium acetate dimer (4.5 mg – 0.01 mmol – 0.5 mol%) was added to a solution of dimethyl 2-diazomalonate (332 mg – 2.1 mmol – 1.05 eq) and but-3-yn-1-ol (140 mg – 2.0 mmol – 1.0 eq) in benzene (7 mL). The resulting solution was heated at 60°C for 2 h. The volatiles were then removed and the residue was purified by column chromatography (80:20 Pentane:EtOAc) to yield pure dimethyl 2-(but-3-yn-1-yloxy)malonate (125 mg – 31% yield) as a clear oil. $^1\text{H NMR}$ (300 MHz, CDCl_3): δ = 4.61 (s, 1H, $(\text{CO}_2\text{Me})_2\text{-CH-O-}$), 3.82 (s, 6H, $2\times(\text{CH}_3\text{-O})$), 3.75 (t, J = 7.2 Hz, 2H, $\text{O-CH}_2\text{-CH}_2\text{-}$), 2.58 (td, J = 7.2, 2.7 Hz, 2H, $\text{-CH}_2\text{-C}\equiv\text{CH}$), 1.99 (t, J = 2.7 Hz, 1H, $\text{-C}\equiv\text{CH}$). Spectroscopic data in accordance with literature.^[83]

Methyl 2-acetyloct-7-ynoate - 8a - CAS [134149-22-7]:

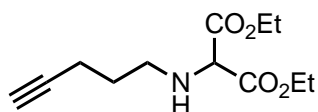
Using general procedure A, with methyl 3-oxobutanoate (1.16 g - 10 mmol) and 6-chlorohex-1-yne (979 mg - 8.4 mmol) pure methyl 2-acetyloct-7-ynoate (511 mg - 31% Yield) was obtained as a colorless oil via column chromatography (90:10 to 60:40 Pentane:Et₂O). Mixture of keto-enol tautomers. $^1\text{H NMR}$ (300 MHz, CDCl_3): δ = 3.74 (s, 3H, $\text{CH}_3\text{-O}$), 3.43 (t, J = 7.4 Hz, 1H, $\text{COMe-CH-CO}_2\text{Me}$), 2.23 (s, 3H, $\text{CH}_3\text{-C}$), 2.19 (td, J = 6.8, 2.5 Hz, 2H, $\text{-CH}_2\text{-C}\equiv\text{CH}$), 1.93 (t, J = 2.5 Hz, 1H, $\text{-C}\equiv\text{CH}$), 1.91 – 1.81 (m, 2H, $\text{CH-CH}_2\text{-CH}_2\text{-}$), 1.55 (m, 2H, $\text{CH}_2\text{-CH}_2\text{-C}\equiv\text{CH}$), 1.45 – 1.31 (m, 2H, $\text{CH-CH}_2\text{-CH}_2\text{-CH}_2\text{-}$). Spectroscopic data in accordance with literature.^[76]

Dimethyl 2-((2-ethynylbenzyl)oxy)malonate - 9a:

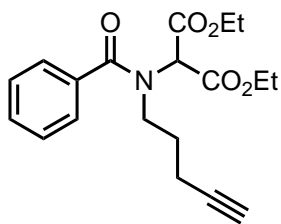
Rhodium acetate dimer (4.5 mg - 0.01 mmol - 0.5 mol%) was added to a solution of dimethyl 2-diazomalonate (350 mg - 2.2 mmol - 1.0 eq) and 2-ethynylbenzyl alcohol (307 mg - 2.3 mmol - 1.05 eq), in benzene (6 mL). The resulting solution was then heated at 60°C for 2 h. The volatiles were removed and the residue was purified by column chromatography (80:20 Pentane:EtOAc) to yield pure dimethyl 2-((2-ethynylbenzyl)oxy)malonate as an orange oil (156 mg - 27% Yield). $^1\text{H NMR}$ (300 MHz, CDCl_3): δ = 7.58 – 7.53 (m, 1H, H_{arom}), 7.49 (pseudo-dd, J = 7.6, 1.4 Hz, 1H, H_{arom}), 7.37 (pseudo-td, J = 7.6, 1.5 Hz, 1H, H_{arom}), 7.30 – 7.21 (m, 1H, H_{arom}), 4.89 (s, 2H, CH_2), 4.64 (s, 1H, $\text{-CO}_2\text{Me-CH-O-}$), 3.80 (s, 6H, $\text{CH}_3\text{-O}$), 3.29 (s, 1H, $\text{-C}\equiv\text{CH}$). $^{13}\text{C NMR}$ (75 MHz, CDCl_3): δ = 166.9 (-O-C=O), 138.7 ($\text{CH}_2\text{-C}_{\text{arom}}$), 132.8 (CH_{arom}), 129.3 (CH_{arom}), 128.3 (CH_{arom}), 128.0 (CH_{arom}), 121.1 ($\equiv\text{C-C}_{\text{arom}}$), 82.2 ($\text{-C}\equiv\text{CH}$), 81.1 ($\text{-C}\equiv\text{CH}$), 78.3 ($\text{O-CH-(CO}_2\text{Me)}_2$), 70.9 ($\text{-CH}_2\text{-}$), 53.0 (-CH_3). HRMS (DCI-CH₄) m/z : Calculated: 263.0919 (C₁₄H₁₅O₅); Found: 263.0921.

Diethyl 2-(N-benzylpent-4-ynamido)malonate - 10a - CAS [1351364-67-4]:

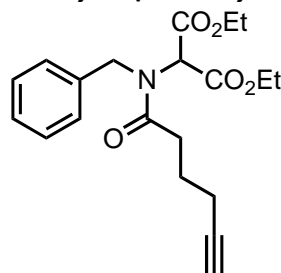
Using the general procedure **A**, with pent-4-ynoic acid (208 mg - 2.14 mmol) and diethyl 2-(benzylamino)malonate (469 mg - 1.77 mmol). The corresponding diethyl 2-(N-benzylpent-4-ynamido)malonate (486 mg - 80% Yield) was obtained as a clear oil after purification by column chromatography (50:50 Pentane:Et₂O). Mixture of 2 rotamers at room temperature (91%:9%), only the major rotamer is assigned. ¹H NMR (300 MHz, CDCl₃): δ = 7.39 – 7.18 (m, 5H, H_{arom}), 5.54 (s, 1H, CH-CO₂Et), 4.74 (s, 2H, Ph-CH₂-N), 4.22 – 3.88 (m, 4H, 2xCH₂-CH₃), 2.71 – 2.47 (m, 4H, -CH₂-CH₂;-CH₂-CH₂), 1.94 (t, J = 2.5 Hz, 1H, -C≡CH), 1.19 (t, J = 7.1 Hz, 6H, 2x(CH₃-CH₂-)). Spectroscopic data in accordance with literature.^[79]

Diethyl 2-(pent-4-yn-1-ylamino)malonate:

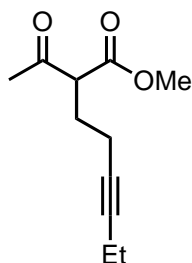
To a solution of pent-4-yn-1-amine (270 mg, 3.25 mmol, 1.0 eq), diethyl bromomalonate (555 μL, 3.25 mmol, 1.0 eq) in 6 mL of CHCl₃ was added triethylamine (520 μL, 3.9 mmol, 1.2 eq). The solution was heated to 75°C for 16 h. The resulting black mixture was then poured into a separatory funnel containing 15 mL of 2M NaOH, and the aqueous layer was extracted 3 times with 15 mL of EtOAc. The organic layers were combined, dried over Na₂SO₄ and the volatiles were removed in vacuo. Diethyl 2-(pent-4-yn-1-ylamino)malonate (329 mg - 42% Yield) was then obtained as a black oil after column chromatography (80:20; Pentane:EtOAc; 1% of NEt₃). ¹H NMR (300 MHz, CDCl₃) δ = 4.24 (qd, J = 7.2, 0.8 Hz, 4H, CH₂-CH₃), 4.05 (s, 1H, CO₂Et-CH-CO₂Et), 2.73 (t, J = 7.0 Hz, 2H, CH₂-CH₂-NH), 2.30 (td, J = 7.0, 2.7 Hz, 2H, ≡C-CH₂-CH₂), 2.08 (s, 1H, NH), 1.96 (t, J = 2.7 Hz, 1H, C≡CH), 1.74 (pseudo-quint, J = 7.0 Hz, 2H, CH₂-CH₂-CH₂), 1.31 (t, J = 7.2 Hz, 6H, CH₂-CH₃). ¹³C NMR (75 MHz, CDCl₃) δ = 168.7 (C=O), 83.9 (≡CH), 68.8 (-C≡), 65.2 (NH-CH-(C=O)₂), 61.7 (CH₂-CH₃), 46.7 (-CH₂-NH), 28.8 (CH₂-CH₂-CH₂), 16.2 (CH₂-CH₂-C≡), 14.2 (CH₃). HRMS (DCI-CH₄) m/z (%): Calculated: 242.1392 (C₁₂H₂₀NO₄); Found: 242.1387.

Diethyl 2-(N-(pent-4-yn-1-yl)benzamido)malonate - 11a:

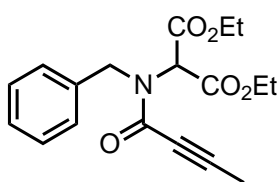
Using the general procedure **B**, with benzoic acid (146 mg - 1.2 mmol) and diethyl 2-(pent-4-yn-1-ylamino)malonate (241 mg - 1.0 mmol). The corresponding diethyl 2-(N-(pent-4-yn-1-yl)benzamido)malonate (206 mg - Yield 60%) was obtained as yellow crystals after purification by column chromatography (100:0 to 80:20 Pentane:EtOAc). $^1\text{H NMR}$ (300 MHz, CD_3OD , 25°C): δ = 7.57 – 7.27 (m, 5H, H_{arom}), 4.29 (q, J = 7.1 Hz, 4H, $2\times\text{CH}_2\text{-CH}_3$), 3.48 (t, J = 7.6 Hz, 2H, $\text{CH}_2\text{-N}$), 2.33 - 1.99 (m, 3H, $\text{C}\equiv\text{CH}$; $\text{CH}_2\text{-C}\equiv$), 1.82 - 1.65 (m, 2H, $-\text{CH}_2\text{-CH}_2\text{-CH}_2-$), 1.33 (t, J = 7.1 Hz, 6H, $2\times\text{CH}_3\text{-CH}_2$), $\text{CH}(\text{CO}_2\text{Et})$ not observed. It should be stressed that at room temperature NMR Signals are broad and not well resolved. Data acquired at -60°C gave a better signal. $^1\text{H NMR}$ (400 MHz, CD_3OD , -60°C): δ = 7.60 – 7.33 (m, 5H, H_{arom}), 4.27 (q, J = 7.1 Hz, 4H, $2\times\text{CH}_2\text{-CH}_3$), 3.47 (t_{app} , J = 7.3 Hz, 2H, $\text{CH}_2\text{-N}$), 2.25 (bs, 1H, $\text{C}\equiv\text{CH}$), 2.10 (td, J = 7.0, 2.6 Hz, 2H, $-\text{CH}_2\text{-C}\equiv$), 1.82 – 1.73 (m, 2H, $-\text{CH}_2\text{-CH}_2\text{-CH}_2-$), 1.33 (t, J = 7.1 Hz, 6H, $2\times\text{CH}_3\text{-CH}_2$), $\text{CH}(\text{CO}_2\text{Et})$ not observed. $^{13}\text{C NMR}$ (75 MHz, CDCl_3 , 25°C): 167.1 ($-\text{O}-\text{C}=\text{O}$), 136.5 (C_{arom}), 131.2 ($\text{CH}_{\text{arom para}}$), 129.8 ($2\times\text{CH}_{\text{arom}}$), 127.6 ($2\times\text{CH}_{\text{arom}}$), 83.3 ($-\text{C}\equiv\text{CH}$), 70.4 ($\text{C}\equiv\text{CH}$), 63.2 ($2\times\text{CH}_2\text{-CH}_3$), 50.9 ($\text{CH}_2\text{-N}$), 28.7 ($\text{CH}_2\text{-CH}_2\text{-CH}_2-$), 16.1 ($-\text{CH}_2\text{-C}\equiv$), 14.4 ($2\times\text{CH}_3$). **MS** (HR-ESI) m/z (%): Calculated: 346.1654 ($\text{C}_{19}\text{H}_{24}\text{NO}_5$); Found: 346.1660.

Diethyl 2-(N-benzylhex-5-ynamido)malonate - 12a:

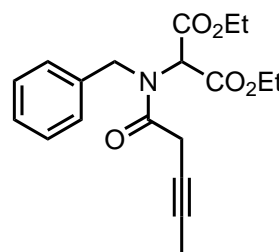
Using the general procedure **A**, with 5-hexynoic acid (507 mg - 4.52 mmol) and diethyl 2-(benzylamino)malonate (1 g - 3.77 mmol). The corresponding diethyl 2-(N-benzylhex-5-ynamido)malonate (1.23 g - Yield 91%) was obtained as a clear oil after purification by column chromatography (60:40 Pentane:Et₂O). Mixture of 2 rotamers at room temperature (94%:06%), only the major rotamer is assigned. $^1\text{H NMR}$ (300 MHz, CDCl_3): δ = 7.39 – 7.20 (m, 5H, H_{arom}), 5.45 (s, 1H, $\text{CH-CO}_2\text{Et}$), 4.74 (s, 2H, $\text{C-CH}_2\text{-N}$), 4.23 – 3.94 (m, 4H, $\text{CH}_2\text{-CH}_3$), 2.53 (t, J = 7.1 Hz, 2H, $\text{CH}_2\text{-C}=\text{O}$), 2.25 (td, J = 6.8, 2.7 Hz, 2H, $\text{CH}_2\text{-C}\equiv\text{C}$), 1.98 – 1.78 (m, 3H, $\text{C}\equiv\text{CH}$, $\text{CH}_2\text{-CH}_2\text{-CH}_2$), 1.20 (t, J = 7.1 Hz, 6H, $\text{CH}_3\text{-CH}_2$). $^{13}\text{C NMR}$ (75 MHz, CDCl_3): δ = 173.9 ($\text{N-C}=\text{O}$), 166.3 (CO_2Et), 136.5 (C_{arom}), 128.7 (CH_{arom}), 127.6 ($\text{CH}_{\text{arom para}}$), 126.5 (CH_{arom}), 83.6 ($-\text{C}\equiv\text{CH}$), 69.2 ($-\text{C}\equiv\text{CH}$), 62.1 ($2\times\text{CH}_2\text{-CH}_3$), 61.2 ($\text{CH}(\text{CO}_2\text{Et})_2$), 50.9 ($\text{N-CH}_2\text{-Ph}$), 31.6 ($\text{O}=\text{C-CH}_2-$), 23.8 ($-\text{CH}_2\text{-CH}_2\text{-CH}_2-$), 17.7 ($-\text{CH}_2\text{-C}\equiv$), 13.9 ($-\text{CH}_3$). **HRMS** (ESI) m/z (%): Calculated: 360.1811 ($\text{C}_{20}\text{H}_{26}\text{NO}_5$); Found: 360.1805

Methyl 2-acetyloct-5-ynoate - CAS [811784-45-9] - 13a:

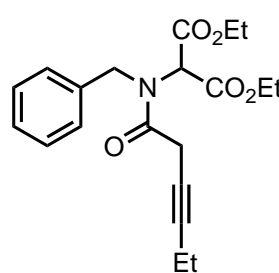
Using general procedure **A**, with methyl 3-oxobutanoate (392 mg - 3.38 mmol) and 1-bromohex-3-yne (500 mg - 2.8 mmol) pure methyl 2-acetyloct-5-ynoate (112 mg - 20% Yield) was obtained as a clear oil via column chromatography (95:05 Pentane:EtOAc). Mixture of keto-enol tautomers. $^1\text{H NMR}$ (300 MHz, CDCl_3): δ = 3.74 (s, 3H, $\text{CH}_3\text{-O}$), 3.72 (t, J = 7.2 Hz, 1H, $\text{COMe-CH-CO}_2\text{Me}$), 2.27 (s, 3H, $\text{CH}_3\text{-C}$), 2.24 – 1.99 (m, 6H, $3\times\text{CH}_2-$), 1.11 (t, J = 7.5 Hz, 3H, $\text{CH}_2\text{-CH}_3$).

Diethyl 2-(N-benzylbut-2-ynamido)malonate - 14a:

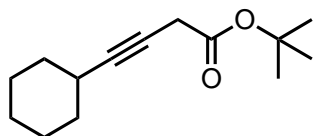
Using the general procedure **A**, with but-2-ynoic acid (250 mg - 2.97 mmol) and diethyl 2-(benzylamino)malonate (656 mg - 2.47 mmol). The corresponding diethyl 2-(N-benzylbut-2-ynamido)malonate (800 mg - 97% Yield) was obtained as a white solid after purification by column chromatography (using a gradient from 80:20 to 60:40 of Pentane:EtOAc). Mixture of 2 rotamers at room temperature (77%:23%), only the major rotamer is assigned. mp = 50 °C. $^1\text{H NMR}$ (300 MHz, CDCl_3): δ = 7.37-7.17 (m, 5H, H_{arom}), 5.30 (s, 1H, $\text{CH-CO}_2\text{Et}$), 4.97 (s, 2H, $\text{Ph-CH}_2\text{-N}$), 4.13-4.02 (m, 2H, $\text{CH}_2\text{-CH}_3$), 3.97-3.84 (m, 2H, $\text{CH}_2\text{-CH}_3$), 1.97 (s, 3H, $\text{CH}_3\text{-C}\equiv\text{C}$), 1.15 (t, 3H, $2\times\text{CH}_3\text{-CH}_2$). $^{13}\text{C NMR}$ (75 MHz, CDCl_3): δ = 165.6 (CO_2Et), 155.8 (N-C=O), 136.2 (C_{arom}), 128.5 (CH_{arom}), 127.8 (CH_{arom}), 127.7 (CH_{arom}), 91.3 ($\text{-C}\equiv\text{C-CH}_3$), 72.9 ($\text{O=C-C}\equiv\text{C-}$), 62.2 ($\text{-CH}_2\text{-CH}_3$), 59.8 ($\text{-CH-(CO}_2\text{Et)}$), 52.3 ($\text{-CH}_2\text{-Ph}$), 13.9 ($\text{-CH}_2\text{-CH}_3$), 4.3 ($\equiv\text{C-CH}_3$). HRMS (DCI- CH_4) m/z (%): Calculated: 332.1498 ($\text{C}_{18}\text{H}_{22}\text{NO}_5$); Found: 332.1501.

Diethyl 2-(N-benzylpent-3-ynamido)malonate - 15a - CAS [1351364-62-9]:

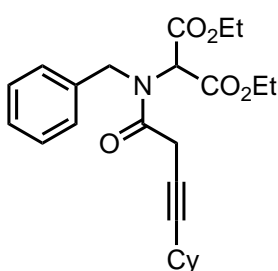
Using the general procedure **B**, with pent-3-ynoic acid (250 mg - 2.55 mmol) and diethyl 2-(benzylamino)malonate (563 mg - 2.12 mmol). The corresponding diethyl 2-(N-benzylpent-3-ynamido)malonate (423 mg - 53% Yield) was obtained as a clear oil after purification by column chromatography (75:25 Pentane:EtOAc). Mixture of 2 rotamers at room temperature (87%:23%), only the major rotamer is assigned. $^1\text{H NMR}$ (300 MHz, CDCl_3): δ = 7.40 – 7.17 (m, 5H, H_{arom}), 5.38 (s, 1H, $\text{CH-CO}_2\text{Et}$), 4.79 (s, 2H, $\text{Ph-CH}_2\text{-N}$), 4.22 – 3.97 (m, 4H, $2\times\text{CH}_2\text{-CH}_3$), 3.27 (q, J = 2.6 Hz, 2H, $\text{-CH}_2\text{-C}\equiv\text{C}$), 1.77 (t, J = 2.6 Hz, 3H, $\text{-C}\equiv\text{C-CH}_3$), 1.21 (t, J = 7.1 Hz, 6H, $2\times\text{CH}_2\text{-CH}_3$). Spectroscopic data in accordance with literature.^[79]

Diethyl 2-(N-benzylhex-3-ynamido)malonate - 16a - CAS [1351364-36-0]:

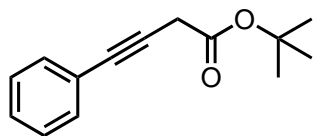
Using the general procedure **B**, with hex-3-ynoic acid (284 mg - 2.53 mmol) and diethyl 2-(benzylamino)malonate (560 mg - 2.11 mmol). The corresponding diethyl 2-(N-benzylhex-3-ynamido)malonate (279 mg - 38% Yield) was obtained as a clear oil (mixture of two rotamers 85%:15%) after purification by column chromatography (75:25 Pentane:EtOAc). Mixture of 2 rotamers at room temperature (85%:15%), only the major rotamer is assigned. $^1\text{H NMR}$ (300 MHz, CDCl_3): δ = 7.39 – 7.17 (m, 5H, H_{arom}), 5.37 (s, 1H, $\text{CH-CO}_2\text{Et}$), 4.80 (s, 2H, $\text{Ph-CH}_2\text{-N}$), 4.22 – 3.98 (m, 4H, $2\times\text{CH}_2\text{-CH}_3$), 3.29 (t, J = 2.4 Hz, 2H, $\text{-CH}_2\text{-C}\equiv\text{C}$), 2.23 – 2.06 (m, 2H, $\text{-C}\equiv\text{C-CH}_2$), 1.21 (t, J = 7.2 Hz, 6H, $2\times(\text{CH}_3\text{-CH}_2\text{-CO}_2\text{-})$), 1.08 (t, J = 7.5 Hz, 3H, $\text{C-CH}_2\text{-CH}_3$). Spectroscopic data in accordance with literature.^[79]

Tert-butyl 4-cyclohexylbut-3-ynoate :

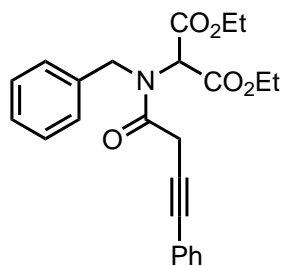
Using the procedure described by Fu et al. tBu-diazoacetate (640 mg - 4.5 mmol) was added dropwise to a solution of ethynylcyclohexane (458 mg - 4.5 mmol), CuI (43 mg - 5% mol) in acetonitrile (7 mL).^[84] The corresponding tert-butyl 4-cyclohexylbut-3-ynoate (902 mg - 90% yield) was obtained as a clear oil after filtration through a short silica plug (80:20 Pentane:DCM). ¹H NMR (300 MHz, CDCl₃): δ = 3.17 (d, J = 2.2 Hz, 2H, C-CH₂-CO), 2.45 – 2.27 (m, 1H, CH₂-CH-CH₂), 1.85 – 1.59 (m, 4H, 2x(CH₂)-CH-), 1.44 (s, 9H, 3xCH₃), 1.54 – 1.19 (m, 6H, 3x(-CH₂-). ¹³C NMR (75 MHz, CDCl₃): δ = 168.3 (C=O), 87.8 (C≡C-), 81.5 (C≡C-CH₂-), 72.1 (-C(CH₃)₃), 32.8 (2xCH₂), 29.2 (-CH-), 28.0 (3xCH₃-), 27.4 (2xCH₂), 26.0 (-CH₂-), 24.9 (-CH₂-). HRMS (DCI-CH₄) m/z (%): Calculated: 221.1542 (C₁₄H₂₁O₂); Found: 221.1534

Diethyl 2-(N-benzyl-4-cyclohexylbut-3-ynamido)malonate - 17a:

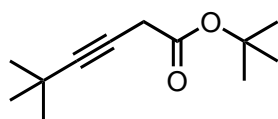
Using the general procedure C, with tert-butyl 4-cyclohexylbut-3-ynoate (372 mg - 2.04 mmol) and diethyl 2-(benzylamino)malonate hydrochloride (491 mg - 1.62 mmol - 0.75 eq) the corresponding diethyl 2-(N-benzyl-5,5-dimethylhex-3-ynamido)malonate (141 mg - 18% Yield) was obtained as a pale yellow oil after HPLC purification. Mixture of 2 rotamers at room temperature (87%:13%), only the major rotamer is assigned. ¹H NMR (300 MHz, CDCl₃): δ = 7.42 – 7.11 (m, 5H, H_{arom}), 5.35 (s, 1H, CH-CO₂Et), 4.82 (s, 2H, Ph-CH₂-N), 4.28 – 3.92 (m, 4H, 2xCH₂-CH₃), 3.30 (d, J = 2.2 Hz, 2H, -CH₂-C≡C), 2.32 (br, 1H, C≡C-CH-), 1.98 – 1.23 (m, 10H, 5xCH₂-Cy), 1.20 (t, J = 7.1 Hz, 6H, 2x(CH₃-CH₂-). ¹³C NMR (75 MHz, CDCl₃): δ = 169.5 (C=O), 166.1 (O-C=O), 136.2 (C_{arom}^{IV}), 128.8 (2xCH_{arom} - meta), 127.8 (CH_{arom} - para), 126.8 (2xCH_{arom} - ortho), 89.2 (C≡C-Cy; Not visible in ¹³C-zgpg but in HMBC), 70.2 (C≡C-Cy), 62.2 (CH₂-CH₃), 61.4 (O=C-CH-C=O), 51.5 (Ph-CH₂-), 32.7 (C_{Cy}), 29.8 (C_{Cy}), 29.3 (CH-Cy), 26.8 (C_{Cy}), 26.0 (C_{Cy}), 25.0 (C_{Cy}), 14.0 (CH₃-CH₂). HRMS (DCI-CH₄) m/z (%): Calculated: 414.2280 (C₂₄H₃₂NO₅); Found: 414.2300

Tert-butyl 4-phenylbut-3-ynoate - CAS [945488-48-2]:

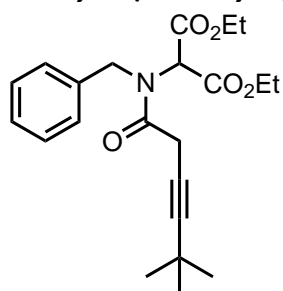
Using the procedure described by Fu et al. tert-Butyl diazoacetate (355 mg - 2.5 mmol) was added dropwise to a solution of phenylacetylene (255 mg - 2.5 mmol), CuI (24 mg - 5 mol%) in acetonitrile (3 mL).^[84] The resulting solution was stirred at room temperature for 16h. The volatiles were removed in vacuo and the residue was filtered through a silica pad with Et₂O as eluent. The amount of allenic ester was then quantified using ¹H NMR spectroscopy with an internal standard. PyHBr₃ (1.0 equivalent - towards the amount of allenic ester) was added in CHCl₃ to the residue and the reaction was stirred for 20h. The volatiles were removed in vacuo and the residue was purified by column chromatography (using a gradient from 100:0 to 80:20 Heptane:DCM) to yield the corresponding tert-butyl 4-phenylbut-3-ynoate (157 mg - 28% Yield) as a pale-yellow oil. ¹H NMR (300 MHz, CDCl₃): δ = 7.48 – 7.27 (m, 5H, H_{arom}), 3.42 (s, 2H, -CH₂-), 1.50 (s, 9H, 3xCH₃). Spectroscopic data in accordance with literature.^[85]

Diethyl 2-(N-benzyl-4-phenylbut-3-ynamido)malonate - 18a - CAS [1351364-66-3]:

Using the general procedure C, with tert-butyl 4-phenylbut-3-ynoate (100 mg - 0.46 mmol) and diethyl 2-(benzylamino)malonate hydrochloride (139 mg - 0.46 mmol) the corresponding diethyl 2-(N-benzyl-4-phenylbut-3-ynamido)malonate (132 mg - 70% Yield) was obtained as a yellow oil after HPLC purification. Mixture of 2 rotamers at room temperature (86%:14%), only the major rotamer is assigned. $^1\text{H NMR}$ (300 MHz, CDCl_3): δ = 7.39 – 7.21 (m, 10H, H_{arom}), 5.39 (s, 1H, $\text{CH-CO}_2\text{Et}$), 4.88 (s, 2H, $\text{Ph-CH}_2\text{-N}$), 4.25 – 4.00 (m, 4H, $2\times\text{CH}_2\text{-CH}_3$), 3.56 (s, 2H, $-\text{CH}_2\text{-C}\equiv\text{C}$), 1.21 (t, J = 7.2 Hz, 6H, $2\times(\text{CH}_3\text{-CH}_2\text{-})$). Spectroscopic data in accordance with literature.^[79]

Tert-butyl 5,5-dimethylhex-3-ynoate:

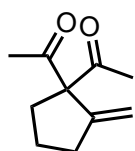
Using the procedure described by Fu et al. tert-Butyl diazoacetate (854 mg - 6 mmol) was added dropwise to a solution of 3,3-dimethylbut-1-yne (1.14 g - 6 mmol), CuI (56 mg - 5% mol) in acetonitrile (8 mL).^[84] The corresponding tert-butyl 5,5-dimethylhex-3-ynoate (888 mg - 81% Yield) was obtained as a pale-yellow oil after purification via column chromatography (80:20 Pentane:DCM). $^1\text{H NMR}$ (300 MHz, CDCl_3): δ = 3.14 (s, 2H, CH_2), 1.46 (s, 9H, tBu-O), 1.22 (s, 9H, $\text{tBu-C}\equiv$). $^{13}\text{C NMR}$ (75 MHz, CDCl_3): δ = 168.2 (O-C=O), 91.9 ($\text{tBu-C}\equiv$), 81.4 ($\text{C}\equiv\text{C-CH}_2$), 70.7 ($\text{O-C(CH}_3)_3$), 31.1 ($(\text{CH}_3)_3\text{-C-C}\equiv$), 28.0 ($(\text{CH}_3)_3\text{-C-O}$), 27.4 ($(\text{CH}_3)_3\text{-C-C}\equiv$), 27.3 ($\text{C-CH}_2\text{-C}$). HRMS (DCI- CH_4) m/z (%): Calculated: 197.1542 ($\text{C}_{12}\text{H}_{21}\text{O}_2$); Found: 197.1533.

Diethyl 2-(N-benzyl-5,5-dimethylhex-3-ynamido)malonate - 19a:

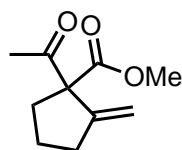
Using the general procedure C and heptane to remove the SOCl_2 by azeotropic distillation, with tert-butyl 5,5-dimethylhex-3-ynoate (372 mg - 2.04 mmol) and diethyl 2-(benzylamino)malonate hydrochloride (491 mg - 1.62 mmol - 0.75 eq) the corresponding diethyl 2-(N-benzyl-5,5-dimethylhex-3-ynamido)malonate (141 mg - 18% Yield) was obtained as a slightly yellow oil after HPLC purification. Mixture of 2 rotamers at room temperature (86%:14%), only the major rotamer is assigned. $^1\text{H NMR}$ (300 MHz, CDCl_3): δ = 7.40 – 7.15 (m, 5H, H_{arom}), 5.32 (s, 1H, $\text{CH-CO}_2\text{Et}$), 4.82 (s, 2H, $\text{Ph-CH}_2\text{-N}$), 4.22 – 3.87 (m, 4H, $2\times\text{CH}_2\text{-CH}_3$), 3.29 (s, 2H, $-\text{CH}_2\text{-C}\equiv\text{C}$), 1.21 (t, J = 7.2 Hz, 6H, $2\times(\text{CH}_3\text{-CH}_2\text{-})$), 1.17 (s, 9H, tBu). $^{13}\text{C NMR}$ (75 MHz, CDCl_3): δ = 169.5 (C=O), 166.1 (O-C=O), 136.2 (C_{arom}), 128.9 ($2\times\text{CH}_{\text{arom}}$ - meta), 127.9 (CH_{arom} - para), 126.9 ($2\times\text{CH}_{\text{arom}}$ - ortho), 93.0 ($\text{tBu-C}\equiv\text{C}$; Not visible in ^{13}C -zgpg but in HMBC), 70.5 ($\text{CH}_2\text{-C}\equiv\text{C}$; Not visible in ^{13}C -zgpg but in HMBC) 62.2 ($\text{CH}_2\text{-CH}_3$), 61.4 (O=C-CH-C=O), 51.5 ($\text{N-CH}_2\text{-Ph}$), 31.0 ($(\text{CH}_3)_3\text{-C}$), 27.6 ($(\text{CH}_3)_3\text{-C-C}$), 26.8 ($\text{C-CH}_2\text{-C=O}$), 14.0 ($\text{CH}_2\text{-CH}_3$). HRMS (DCI- CH_4) m/z (%): Calculated: 388.2124 ($\text{C}_{22}\text{H}_{30}\text{NO}_5$); Found: 388.2143

General procedure for the Conia-ene cyclisation:

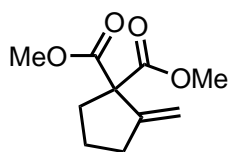
The substrate, $\text{Mg}(\text{OTf})_2$, HFIP (100 μL), the internal standard and complex were added in CDCl_3 (400 μL) in an NMR tube and the resulting solution was heated at the indicated temperature for the indicated time.

Cyclized products:***1,1'-(2-methylenecyclopentane-1,1-diyl)bis(ethan-1-one) - 1b - CAS [88459-74-9]:***

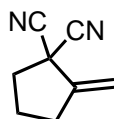
Using the general procedure, with 3-(pent-4-yn-1-yl)pentane-2,4-dione (0.25 mmol - [0.5M]), $\text{Pd}_2(\text{SCS})_2$ (1 mol% Pd), $\text{Mg}(\text{OTf})_2$ (5 mol%) and 1,3,5-trimethoxybenzene as internal standard, 1,1'-(2-methylenecyclopentane-1,1-diyl)bis(ethan-1-one) was formed with >95% yield after 2 h at 25°C as estimated by ^1H NMR analysis. Isolated by filtering on a silica pad with DCM as eluant (35 mg - 85% Yield). ^1H NMR (300 MHz, Chloroform- d): δ = 5.34 (t, J = 2.2 Hz, 1H, H_{vinyl}), 5.14 (t, J = 2.2 Hz, 1H, H_{vinyl}), 2.45 (tt, J = 7.3, 2.2 Hz, 2H, $\text{CH}_2\text{-CH}_2\text{-C=}$), 2.28 (t, J = 6.9 Hz, 2H, $(\text{MeOC})_2\text{-C-CH}_2\text{-CH}_2\text{-}$), 2.20 (s, 6H, $2\times\text{CH}_3$), 1.73 (quint, J = 7.3 Hz, 2H, $\text{CH}_2\text{-CH}_2\text{-CH}_2$). Spectroscopic data in accordance with literature.^[86]

Methyl 1-acetyl-2-methylenecyclopentane-1-carboxylate - 2b - CAS [146445-28-5]:

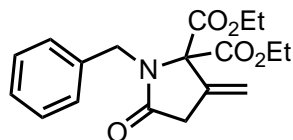
Using the general procedure, with methyl 2-acetylhept-6-ynoate (0.25 mmol - [0.5M]), $\text{Pd}_2(\text{SCS})_2$ (1 mol% Pd), $\text{Mg}(\text{OTf})_2$ (5 mol%) and 1,3,5-trimethoxybenzene as internal standard methyl 1-acetyl-2-methylenecyclopentane-1-carboxylate was formed with >95% yield after 1 h 30 min at 25°C as estimated by ^1H NMR analysis. Isolated by filtering on a silica pad with DCM as eluant (41 mg - 90% Yield). ^1H NMR (300 MHz, CDCl_3): δ = 5.30 (t, J = 2.2 Hz, 1H, H_{vinyl}), 5.23 (t, J = 2.3 Hz, 1H, H_{vinyl}), 3.75 (s, 3H, $\text{CH}_3\text{-O}$), 2.51 – 2.33 (m, 3H, $\text{CH}_2\text{-CH}_2\text{-C}(\text{CO}_2\text{Me})\text{-}$; $\text{-CH}_2\text{-CH}_2\text{-C}_{\text{vinyl}}$), 2.23-2.14 (m, 1H, $\text{CH}_2\text{-CH}_b\text{-C}$), 2.22 (s, 3H, $\text{CH}_3\text{-C}$), 1.85 – 1.59 (m, 2H, $\text{-CH}_2\text{-CH}_2\text{-CH}_2\text{-}$). Spectroscopic data in accordance with literature.^[87]

Dimethyl 2-methylenecyclopentane-1,1-dicarboxylate - 3b - CAS [134149-18-1]:

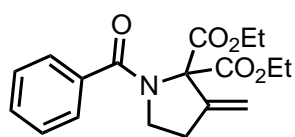
Using the general procedure, with methyl 2-acetylhept-6-ynoate (0.25 mmol - [0.5M]), Pd₂(SCS)₂ (1 mol% Pd), Mg(OTf)₂ (5 mol%) and 1,2,4,5-tetramethylbenzene as internal standard Dimethyl 2-methylenecyclopentane-1,1-dicarboxylate was formed with >95% yield after 1 h 30 min at 25°C as estimated by ¹H NMR analysis. Isolated by filtering on a silica pad with DCM as eluant (45 mg - 91% Yield). ¹H NMR (300 MHz, CDCl₃): δ = 5.30 (t, *J* = 2.3 Hz, 1H, H_{vinyl}), 5.27 (t, *J* = 2.1 Hz, 1H, H_{vinyl}), 3.74 (s, 6H, 2xCH₃-O), 2.46 (tt, *J* = 7.3, 2.2 Hz, 2H, -CH₂-C_{vinyl}), 2.35 (t, *J* = 6.9 Hz, 2H, -CH₂-CH₂-C(CO₂Me)₂), 1.74 (quint, *J* = 7.1 Hz, 2H, -CH₂-CH₂-CH₂-). Spectroscopic data in accordance with literature.^[88]

2-methylenecyclopentane-1,1-dicarbonitrile - 4b - CAS [201146-05-6]:

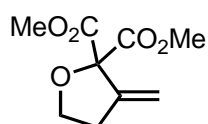
Using the general procedure, with 2-(pent-4-yn-1-yl)malononitrile (0.25 mmol - [0.5M]), Pd₂(SCS)₂ (1 mol% Pd), without Mg(OTf)₂ and anisole as internal standard 2-methylenecyclopentane-1,1-dicarbonitrile was formed with >95% yield after 16 h at 25°C as estimated by ¹H NMR analysis. Isolated by filtering on a silica pad with DCM as eluant (27.5 mg - 83% Yield). ¹H NMR (300 MHz, CDCl₃): δ = 5.68 (pseudo-q, *J* = 2.1 Hz, 1H, H_{vinyl}), 5.45 (q, *J* = 2.1 Hz, 1H, H_{vinyl}), 2.61 (tt, *J* = 7.5, 2.4 Hz, 2H, -CH₂-C_{vinyl}), 2.48 (t, *J* = 6.9 Hz, 2H, -CH₂-C(CN)₂), 2.06 (quint, *J* = 7.1 Hz, 2H, -CH₂-CH₂-CH₂-). Spectroscopic data in accordance with literature.^[89]

Diethyl 1-benzyl-3-methylene-5-oxopyrrolidine-2,2-dicarboxylate - 5b - CAS [1383445-13-3]:

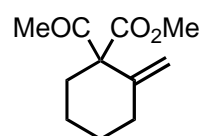
Using the general procedure, with diethyl 2-(*N*-benzylbut-3-ynamido)malonate (0.25 mmol - [0.5M]), Pd₂(SCS)₂ (1 mol% Pd), Mg(OTf)₂ (5 mol%) and 1,2,4,5-tetramethylbenzene as internal standard diethyl 1-benzyl-3-methylene-5-oxopyrrolidine-2,2-dicarboxylate was formed with >95% yield after less than 5 minutes at 25°C as estimated by ¹H NMR analysis. Isolated by column chromatography (80:20 Pentane:EtOAc - 79 mg - 95% Yield). ¹H NMR (300 MHz, CDCl₃): δ = 7.31 – 7.13 (m, 5H, H_{arom}), 5.56 (td, *J* = 2.7, 0.8 Hz, 1H, H_{vinyl}), 5.41 (td, *J* = 2.4, 0.8 Hz, 1H, H_{vinyl}), 4.73 (s, 2H, Ph-CH₂-N) 4.03 – 3.80 (m, 4H, 2xCH₂-CH₃), 3.31 (t, *J* = 2.6 Hz, 2H, -C-CH₂-C), 1.10 (t, *J* = 7.1 Hz, 6H, CH₃-CH₂). Spectroscopic data in accordance with literature.^[79]

Diethyl 1-benzoyl-3-methylenepyrrolidine-2,2-dicarboxylate - 6b:

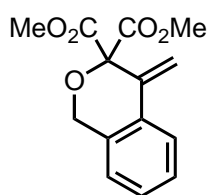
Using the general procedure with diethyl 2-(*N*-(but-3-yn-1-yl)benzamido)malonate (0.25 mmol - [0.5M]), Pd₂(SCS)₂ (1 mol% Pd), Mg(OTf)₂ (5 mol%) and (methoxymethyl)benzene as internal standard, diethyl 1-benzoyl-3-methylenepyrrolidine-2,2-dicarboxylate was formed with >95% yield after 50 minutes at 25°C as estimated by ¹H NMR analysis. Isolated as a white solid by column chromatography (80:20 Pentane:EtOAc - 70 mg - 85% Yield). ¹H NMR (300 MHz, CDCl₃) δ = 7.58 – 7.35 (m, 5H, H_{arom}), 5.62 (t, *J* = 2.1 Hz, 1H, C=CH_aH_b), 5.23 (t, *J* = 2.1 Hz, 1H, C=CH_aH_b), 4.43 – 4.09 (m, 4H, CH₂-CH₃), 3.71 (t, *J* = 7.2 Hz, 2H, CH₂-N), 2.76 (tt, *J* = 7.2, 2.1 Hz, 2H, CH₂-CH₂-C), 1.30 (t, *J* = 7.1 Hz, 6H, CH₂-CH₃). ¹³C NMR (75 MHz, CDCl₃): δ = 166.4 (C=O₂Et), 136.0 (C_{arom}), 130.3 (CH_{arom}), 128.5 2x(CH_{arom}), 127.0 2x(CH_{arom}), 111.8 (CH₂vinyl), 62.2 (2xCH₂-CH₃), 48.9 (N-CH₂-CH₂), 32.6 (CH₂-CH₂-C_{vinyl}), 14.1 (2xCH₃-CH₂). C=O_{benzoyl} and C_{quat} vinyl not observed. HRMS (DCI-CH₄) *m/z* (%): Calculated: 332.1498 (C₁₈H₂₂NO₅); Found: 332.1502

Dimethyl 3-methylenedihydrofuran-2,2(3H)-dicarboxylate - 7b - CAS [1067676-30-5]:

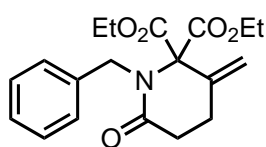
Using the general procedure, with dimethyl 2-(but-3-yn-1-yloxy)malonate (0.25 mmol - [0.5M]), Pd₂(SCS)₂ (1 mol% Pd), Mg(OTf)₂ (5 mol%) and 1,3,5-trimethoxybenzene as internal standard dimethyl 3-methylenedihydrofuran-2,2(3H)-dicarboxylate was formed with 90% yield after 4 h 15 min at 75°C as estimated by ¹H NMR analysis. Isolated by column chromatography (80:20 Pentane:EtOAc - 40.5 mg - 81% Yield). ¹H NMR (300 MHz, CDCl₃): δ = 5.53 (t, *J* = 2.3 Hz, 1H, H_{vinyl}), 5.40 (t, *J* = 2.2 Hz, 1H, H_{vinyl}), 4.13 (t, *J* = 7.0 Hz, 2H, -O-CH₂-CH₂-), 3.80 (s, 6H 2xCH₃-O), 2.72 (tt, *J* = 7.0, 2.2 Hz, 2H, CH₂-CH₂-C). Spectroscopic data in accordance with literature.^[83]

Methyl 1-acetyl-2-methylenecyclohexane-1-carboxylate - 8b - CAS [134149-23-8]:

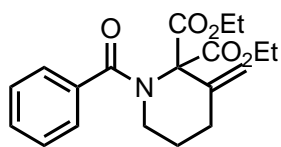
Using the general procedure with methyl 2-acetyloct-7-ynoate (0.25 mmol - [0.5M]), Pd₂(SCS)₂ (5 mol% Pd), Mg(OTf)₂ (20 mol%) and (methoxymethyl)benzene as internal standard methyl 1-acetyl-2-methylenecyclohexane-1-carboxylate was formed with 90% yield after 20 h at 75°C as estimated by ¹H NMR analysis. Isolated by column chromatography (90:10 Pentane:EtOAc - 41 mg - 84% Yield). ¹H NMR (300 MHz, CDCl₃): δ = 5.05 (s, 1H, H_{vinyl}), 4.62 (s, 1H, H_{vinyl}), 3.77 (s, 3H, CH₃-O), 2.42 – 2.30 (m, 1H, (CO₂Me)C-CH_a-CH₂-), 2.24 (s, 3H, CH₃-C), 2.29 – 2.00 (m, 3H, (CO₂Me)C-CH_b-CH₂-; -CH₂-), 1.72 – 1.16 (m, 4H, -CH₂-; -CH₂-). Spectroscopic data in accordance with literature.^[88]

Dimethyl 4-methyleneisochromane-3,3-dicarboxylate - 9b:

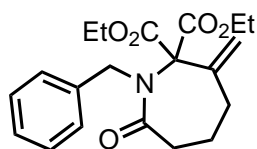
Using the general procedure with dimethyl 2-(but-3-yn-1-yloxy)malonate (0.05 mmol - [0.1M]), Pd₂(SCS)₂ (1 mol% Pd), Mg(OTf)₂ (5 mol%) and 1,3,5-trimethoxybenzene as internal standard dimethyl 3-methylenedihydrofuran-2,2(3H)-dicarboxylate was formed with >95% yield after 22 h at 75°C as estimated by ¹H NMR analysis. Isolated by column chromatography (80:20 Pentane:EtOAc - 12.0mg - 85% Yield). ¹H NMR (500 MHz, CDCl₃): δ = 7.68 – 7.63 (m, 1H, H_{Arom}), 7.32 – 7.27 (m, 2H, 2xH_{Arom}), 7.06 – 7.00 (m, 1H, H_{Arom}), 5.96 (s, 1H, H_{aVinyl}), 5.37 (s, 1H, H_{bVinyl}), 4.91 (s, 2H, CH₂-O), 3.84 (s, 6H, 2xCH₃-O). ¹³C NMR (126 MHz, CDCl₃): δ = 168.1 (C=O), 135.3 (C_{Arom}), 132.6 (C_{Arom}), 128.5 (C_{Arom}), 127.8 (CH_{Arom}), 124.4 (CH_{Arom}), 124.4 (CH_{Arom}), 113.5 (CH₂vinyl), 84.6 (C_{quat}), 65.7 (C-CH₂-O), 53.5 (CH₃-O). HRMS (DCI-CH₄) m/z (%): Calculated: 263.0919 (C₁₄H₁₅O₅); Found: 263.0912.

Diethyl 1-benzyl-3-methylene-6-oxopiperidine-2,2-dicarboxylate - 10b - CAS [1351364-86-7]:

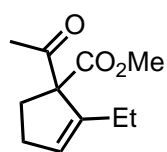
In a 250 mL Schlenk round bottom flask was placed diethyl 2-(N-benzylpent-4-ynamido)malonate (1g - 2.89 mmol) along with Mg(OTf)₂ (4.6 mg - 0.014 mmol - 0.5 mol%), 5.8 mL of HFIP, 23 mL of CHCl₃ finally the Pd₂(SCS)₂ (1.4 mg - 0.0029 mmol - 0.1 mol%) was added and the reaction was stirred at 50°C for 16 h. The volatiles were then removed *in vacuo* and the residue was purified by column chromatography (70:30 Pentane:EtOAc) to yield pure diethyl 1-benzyl-3-methylene-6-oxopiperidine-2,2-dicarboxylate (920 mg - 92% Yield). ¹H NMR (300 MHz, CDCl₃): δ = 7.26 – 7.12 (m, 5H, H_{Arom}), 5.25 (s, 1H, H_{vinyl}), 5.24 (s, 1H, H_{vinyl}), 4.61 (s, 2H, Ph-CH₂-N), 4.09-3.98 (m, 2H, 2x-CH_aH_b-CH₃), 3.91-3.80 (m, 2H, 2x-CH_aH_b-CH₃), 2.71-2.55 (m, 4H O=C-CH₂-CH₂-C_{vinyl}; O=C-CH₂-CH₂-C_{vinyl}), 1.11 (t, J = 7.1 Hz, 6H, 2xCH₃-CH₂). Spectroscopic data in accordance with literature.^[79]

Diethyl 1-benzoyl-3-methylenepiperidine-2,2-dicarboxylate - 11b:

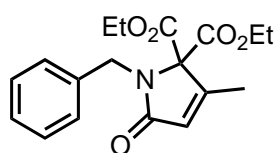
Using the general procedure with diethyl 2-(*N*-(pent-4-yn-1-yl)benzamido)malonate (0.05 mmol - [0.1M]), Pd₂(SCS)₂ (1 mol% Pd), Mg(OTf)₂ (5 mol%) and 1,3,5-trimethoxybenzene as internal standard, diethyl 1-benzoyl-3-methylenepiperidine-2,2-dicarboxylate was formed with 90% yield after 16 h at 75°C as estimated by ¹H NMR analysis. Isolated as by column chromatography (80:20 Pentane:EtOAc - 12.5 mg - 72% Yield). ¹H NMR (300 MHz, CDCl₃): δ = 7.52 – 7.35 (m, 5H, H_{arom}), 5.23 (s, 1H, C=CH₂), 5.20 (s, 1H, C=CH₂), 4.29 (q, *J* = 7.1 Hz, 4H, CH₂-CH₃), 3.50 – 3.44 (m, 2H, CH₂-N), 2.42 – 2.34 (t, *J* = 6.5 Hz, 2H, CH₂-CH₂-C), 1.85 – 1.72 (quint, *J* = 6.5 Hz, 2H, -CH₂-CH₂-CH₂-), 1.30 (t, *J* = 7.1 Hz, 6H, CH₃). ¹³C NMR (75 MHz, CDCl₃): δ = 173.15 (C=O), 166.66 (CO₂Et), 139.7 (C_{quat}), 136.1 (C_{quat}), 130.2 (CH_{arom} para), 128.6 (CH_{arom}), 127.1 (CH_{arom}), 116.2 (=CH₂), 73.3 (-C-(C=O)₂), 62.3 (-CH₂-CH₃), 46.3 (-CH₂-N), 30.8 (-CH₂-CH₂-C), 23.8 (-CH₂-CH₂-CH₂-), 14.2 (CH₃). HRMS (DCI-CH₄) m/z (%): Calculated: 346.1654 (C₁₉H₂₄NO₅); Found: 346.1648

Diethyl 1-benzyl-3-methylene-7-oxoazepane-2,2-dicarboxylate - 12b:

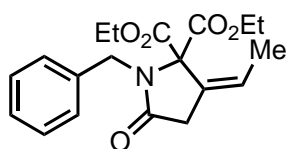
Using general procedure with diethyl 2-(*N*-benzylhex-5-ynamido)malonate (0.05 mmol - [0.1M]), Pd₂(SCS)₂ (5 mol% Pd), Mg(OTf)₂ (20 mol%) and 1,3,5-trimethoxybenzene as internal standard, diethyl 1-benzyl-3-methylene-7-oxoazepane-2,2-dicarboxylate was formed in 90% yield after 40 h at 75°C as estimated by ¹H NMR analysis. Isolated by column chromatography (80:20 Pentane:EtOAc - 70 mg - 78% Yield). ¹H NMR (300 MHz, CDCl₃): δ = 7.40 – 7.07 (m, 5H, H_{arom}), 5.63 (s, 1H, H_{vinyl}), 5.26 (s, 1H, H_{vinyl}), 4.60 (s, 2H, Ph-CH₂-N), 4.17-4.06 (m, 2H, 2x-CH_aH_b-CH₃), 3.95-3.84 (m, 2H, 2x-CH_aH_b-CH₃), 2.68 (t, *J* = 7.2 Hz, 2H, O=C-CH₂-CH₂-), 2.47 (t, *J* = 7.0 Hz, 2H, -CH₂-CH₂-C_{vinyl}), 1.96 – 1.81 (q, 2H, -CH₂-CH₂-CH₂-), 1.06 (t, *J* = 7.1 Hz, 6H, 2xCH₃-CH₂). ¹³C NMR (75 MHz, CDCl₃): δ = 175.6 (O=C-N), 167.3 (2xCO₂Et), 142.6 (C_{vinyl}), 138.8 (C_{arom}), 128.1 (2xCH_{arom}), 126.8 (CH_{arom} para), 126.6 (2xCH_{arom}), 117.3 (CH₂vinyl), 77.2 (C_{vinyl}-C-N), 62.7 (2xCH₂-CH₃), 52.0 (Ph-CH₂-N), 33.4 (O=C-CH₂-CH₂-), 31.9 (-CH₂-CH₂-C_{vinyl}), 23.1 (CH₂-CH₂-CH₂), 13.6 (CH₃-CH₂-). HRMS (HR-ESI) m/z (%): Calculated: 360.1811 (C₂₀H₂₆NO₅); Found: 360.1810

Methyl 1-acetyl-2-ethylcyclopent-2-ene-1-carboxylate - 13b - CAS [811784-57-3]:

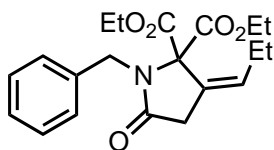
Using the general procedure, with Methyl 2-acetyloct-5-ynoate (0.25 mmol - [0.5M]), Pd₂(SCS)₂ (1 mol% Pd), Mg(OTf)₂ (5 mol%) and 1,3,5-trimethoxybenzene as internal standard methyl 1-acetyl-2-ethylcyclopent-2-ene-1-carboxylate was formed with 95% yield after 25 h at 25°C as estimated by ¹H NMR analysis. Isolated by column chromatography (95:05 Pentane:EtOAc - 43 mg - 88% Yield). ¹H NMR (300 MHz, CDCl₃): δ = 5.73 (quint, *J* = 2.1 Hz, 1H, H_{Vinyl}), 3.75 (s, 3H, O-CH₃), 2.68 – 2.56 (m, 1H, -C-CH_bH_a-CH₂), 2.47 – 2.35 (m, 2H, CH₂-CH₂-CH_{Vinyl}), 2.29 – 2.05 (m, 3H, -CH₂-CH₃; -C-CH_bH_a-CH₂), 2.16 (s, 3H, CH₃-C=O) 1.10 (t, *J* = 7.3 Hz, 3H, CH₃-CH₂). Spectroscopic data in accordance with literature.^[90]

Diethyl 1-benzyl-3-methyl-5-oxo-1,5-dihydro-2H-pyrrole-2,2-dicarboxylate - 14b:

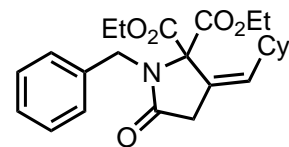
Using the general procedure with diethyl 2-(*N*-benzylbut-2-ynamido)malonate (0.25 mmol - [0.5M]), Pd₂(SCS)₂ (1 mol% Pd), Mg(OTf)₂ (5 mol%) (methoxymethyl)benzene as internal standard diethyl 1-benzyl-3-methyl-5-oxo-1,5-dihydro-2H-pyrrole-2,2-dicarboxylate was formed with >95% yield after 1 h 30 min at 25°C as estimated by ¹H NMR analysis. Isolated by column chromatography (70:30 Pentane:EtOAc - 74 mg - 89% Yield). ¹H NMR (300 MHz, CDCl₃): δ = 7.28 – 7.09 (m, 5H, H_{arom}), 6.09 (q, *J* = 1.6 Hz, 1H, CH_{Vinyl}), 4.77 (s, 2H, CH₂-Ph), 4.04 – 3.79 (m, 4H, 2xCH₂-CH₃), 2.12 (d, *J* = 1.6 Hz, 3H, CH₃-C), 1.10 (t, *J* = 7.2 Hz, 6H, 2xCH₃-CH₂-). ¹³C NMR (75 MHz, CDCl₃): δ = 171.8 (O=C-N), 165.2 (CO₂Et), 154.0 (CH₃-C_{quat}-CH), 137.7 (C_{arom}), 128.4 (2xCH_{arom}), 127.2 (2xCH_{arom}), 127.1 (CH_{arom} para), 125.7 (O=C-CH=C_{quat}), 77.9 (N-C-(CO₂Et)₂), 62.8 (CH₂-CH₃), 45.1 (CH₂-Ph), 14.5 (CH₃-C_{quat}), 13.8 (CH₃-CH₂-). HRMS (DCI-CH₄) *m/z* (%): Calculated: 332.1498 (C₁₈H₂₂NO₅); Found: 332.1511

Diethyl (Z)-1-benzyl-3-ethylidene-5-oxopyrrolidine-2,2-dicarboxylate - 15b - CAS [1383445-15-5]:

Using the general procedure, with diethyl 2-(*N*-benzylpent-3-ynamido)malonate (0.25 mmol - [0.5M]), Pd₂(SCS)₂ (1 mol% Pd), Mg(OTf)₂ (5 mol%) and 1,2,4,5-tetramethylbenzene as internal standard diethyl (Z)-1-benzyl-3-ethylidene-5-oxopyrrolidine-2,2-dicarboxylate was formed with 85% yield after 3 h at 25°C as estimated by ¹H NMR analysis. Isolated by column chromatography (80:20 Pentane:EtOAc - 72 mg - 83% Yield). ¹H NMR (300 MHz, CDCl₃): δ = 7.30 – 7.14 (m, 5H, H_{arom}), 5.75 (qt, *J* = 7.3, 2.3 Hz, 1H, H_{Vinyl}), 4.64 (s, 2H, Ph-CH₂-N), 4.00-3.90 (m, 2H, 2x-CH_aH_b-CH₃), 3.86-3.75 (m, 2H, 2x-CH_aH_b-CH₃), 3.24 (quint, *J* = 2.2 Hz, 2H, -C-CH₂-C), 1.67 (dt, *J* = 7.3, 2.2 Hz, 3H -CH-CH₃), 1.12 (t, *J* = 7.1 Hz, 6H, 2xCH₃-CH₂). Spectroscopic data in accordance with literature.^[79]

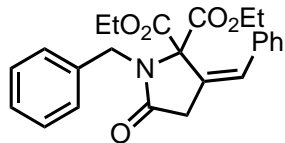
Diethyl (Z)-1-benzyl-5-oxo-3-propylidenepyrrolidine-2,2-dicarboxylate - 16b - CAS [1383445-16-6]:

Using the general procedure, with diethyl 2-(*N*-benzylhex-3-ynamido)malonate (0.25 mmol - [0.5M]), Pd₂(SCS)₂ (1 mol% Pd), Mg(OTf)₂ (5 mol%) and (methoxymethyl)benzene as internal standard diethyl (Z)-1-benzyl-3-ethylidene-5-oxopyrrolidine-2,2-dicarboxylate was formed with 84% yield after 24 h at 25°C as estimated by ¹H NMR analysis. Isolated by column chromatography (80:20 Pentane:EtOAc - 75 mg - 83% Yield). ¹H NMR (300 MHz, CDCl₃): δ = 7.30 – 7.11 (m, 5H, H_{arom}), 5.59 (tt, *J* = 7.8, 2.2 Hz, 1H, H_{vinyl}), 4.64 (s, 2H, Ph-CH₂-N), 4.00-3.89 (m, 2H, 2x-CH_aH_b-CH₃), 3.84-3.73 (m, 2H, 2x-CH_aH_b-CH₃), 3.24 (pseudo-q, *J* = 2.0 Hz, 2H, C-CH₂-C), 2.15-2.00 (m, 2H -C_{vinyl}-CH₂-CH₃), 1.11 (t, *J* = 7.2 Hz, 6H, 2xOOC-CH₃-CH₂), 0.93 (t, *J* = 7.4 Hz, 3H, -C_{vinyl}-CH₂-CH₃). Spectroscopic data in accordance with literature.^[79]

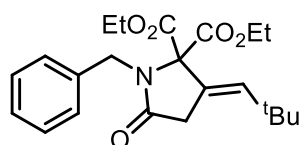
Diethyl (Z)-1-benzyl-3-(cyclohexylmethylene)-5-oxopyrrolidine-2,2-dicarboxylate - 17b:

Using the general procedure, with diethyl 2-(*N*-benzyl-4-cyclohexylbut-3-ynamido)malonate (0.25 mmol - [0.5M]), Pd₂(SCS)₂ (5 mol% Pd), Mg(OTf)₂ (20 mol%) and 1,2,4,5-tetramethylbenzene as internal standard diethyl (Z)-1-benzyl-3-(cyclohexylmethylene)-5-oxopyrrolidine-2,2-dicarboxylate was obtained with 76% yield after 32 h at 120 °C (Isolated yield 52%). During this experiment, 17% of (*E*) isomer was also formed (Isolated yield 10%). **Z-isomer:** ¹H NMR (300 MHz, CDCl₃): δ = 7.30-7.12 (m, 5H, H_{arom}), 5.40 (dt, *J* = 11.2, 2.2 Hz, 1H, H_{vinyl}), 4.61 (s, 2H, Ph-CH₂-N), 4.01-3.88 (m, 2H, 2x-CH_aH_b-CH₃), 3.83-3.69 (m, 2H, 2x-CH_aH_b-CH₃), 3.22 (d, *J* = 2.2 Hz, 2H, O=C-CH₂-C), 2.18 (qt, *J* = 11.2, 3.4 Hz, 1H, CH_{Cy}), 1.74-1.51 (m, 6H, 3xCH₂Cy), 1.11 (t, *J* = 7.1 Hz, 6H, 2xCH₃-CH₂), 1.31-0.88 (m, 4H, 2xCH₂Cy). ¹³C NMR (75 MHz, CDCl₃): δ = 174.1 (O=C-N), 167.3 (CO₂Et), 136.7 (C_{arom}), 136.5 (CH_{vinyl}), 128.2 (2xCH_{arom}), 128.0 (2xCH_{arom}), 127.3 (CH_{arom para}), 123.4 (-C=CH_{vinyl}), 75.0 (C_{quat}, Not visible in ¹³C-jmod but in HMBC), 62.6 (2xCH₂-CH₃), 45.7 (Ph-CH₂-N), 38.8 (CH_{Cy}), 36.4 (C-CH₂-C=), 31.7 (2xCH₂Cy), 26.0 (CH₂Cy), 25.6 (2xCH₂Cy), 13.8 (2xCH₃-CH₂-). **HRMS (DCI-CH₄) m/z (%):** Calculated: 414.2280 (C₂₄H₃₂NO₅); Found: 414.2285. **E-isomer:** ¹H NMR (300 MHz, CDCl₃): δ = 7.30 – 7.13 (m, 5H, H_{arom}), 5.72 (dt, *J* = 9.6, 2.8 Hz, 1H, H_{vinyl}), 4.70 (s, 2H, Ph-CH₂-N), 3.95-3.84 (m, *J* = 7.1, 1.4 Hz, 4H, 2xCH₂-CH₃), 3.21 (d, *J* = 2.8 Hz, 2H, O=C-CH₂-C), 2.17 – 1.99 (m, 1H, CH_{Cy}), 1.80 - 1.15 (m, 10H, 5xCH₂Cy), 1.08 (t, *J* = 7.1 Hz, 6H, 2xCH₃-CH₂). ¹³C NMR (126 MHz, CDCl₃): δ = 174.1 (O=C-N), 167.4 (CO₂Et), 136.9 (C_{arom}), 136.0 (CH_{vinyl}), 128.3 (2xCH_{arom}), 127.5 (2xCH_{arom}), 127.2 (CH_{arom para}), 124.9 (-C=CH_{vinyl}), 75.7 (C_{quat}), 62.3 (2xCH₂-CH₃), 46.0 (Ph-CH₂-N), 39.1 (CH_{Cy}), 32.9 (C-CH₂-C=), 32.0 (2xCH₂Cy), 26.0 (2xCH₂Cy), 25.7 (2xCH₂Cy), 13.8 (2xCH₃-CH₂-). **HRMS (DCI-CH₄) m/z (%):** Calculated: 414.2280 (C₂₄H₃₂NO₅); Found: 414.2280.

The structures of **17b-(Z)** and **17b-(E)** have been determined based on ¹³C-¹³C ADEQUATE and NOESY NMR analysis.

Diethyl (Z)-1-benzyl-3-benzylidene-5-oxopyrrolidine-2,2-dicarboxylate - 18b - CAS [1383445-19-9]:

Using the general procedure, with diethyl 2-(*N*-benzyl-4-phenylbut-3-ynamido)malonate (0.25 mmol - [0.5M]), Pd₂(SCS)₂ (5 mol% Pd), Mg(OTf)₂ (20 mol%) and 1,2,4,5-tetramethylbenzene as internal standard diethyl (Z)-1-benzyl-3-benzylidene-5-oxopyrrolidine-2,2-dicarboxylate was formed with 79% yield after 16 h at 75°C as estimated by ¹H NMR analysis. Isolated by column chromatography (using a gradient from 80:20 to 70:30 Pentane:EtOAc - 66 mg - 65% Yield). During this experiment 8% of (*E*) isomer was also formed (Confirmed by NOESY experiment - Isolated yield - 5 mg - 5%). **Z-isomer:** ¹H NMR (500 MHz, CDCl₃): δ = 7.47 – 7.42 (m, 2H, H_{arom}), 7.30 – 7.25 (m, 2H, H_{arom}), 7.24 – 7.13 (m, 6H, H_{arom}), 6.69 (t, *J* = 2.2 Hz, 1H, H_{vinyl}), 4.61 (s, 2H, Ph-CH₂-N), 3.72-3.66 (m, 2H, 2x-CH_aH_b-CH₃), 3.60-3.54 (m, 2H, 2x-CH_aH_b-CH₃), 3.39 (d, *J* = 2.2 Hz, 2H, C-CH₂-C), 0.87 (t, *J* = 7.2 Hz, 6H, 2xOOC-CH₂-CH₃). ¹³C NMR (126 MHz, CDCl₃): δ = 173.2 (N-C=O), 166.2 (O-C=O), 136.6 (CH₂-C_{arom}), 135.1 (CH-C_{arom}), 129.8 (CH_{vinyl}), 128.8 (2xCH_{arom}), 128.4 (2xCH_{arom}), 128.2 (4xCH_{arom}), 128.0 (CH_{arom}), 127.8 (C_{quat}=CH_{vinyl}), 127.4 (CH_{arom}), 75.4 (N-C-(CO₂Et)₂), 62.5 (2xCH₂-CH₃), 45.9 (CH₂-Ph), 38.9 (O=C-CH₂-), 13.5 (2xCH₃). **E-isomer:** ¹H NMR (500 MHz, CDCl₃): δ = 7.42 – 7.37 (m, 2H, H_{arom}), 7.35 – 7.27 (m, 4H, H_{arom}), 7.26 – 7.16 (m, 4H, H_{arom}), 6.83 (t, *J* = 2.8 Hz, 1H, H_{vinyl}), 4.76 (s, 2H, Ph-CH₂-N), 4.01 – 3.85 (m, 4H, 2xCH₂-CH₃), 3.56 (d, *J* = 2.8 Hz, 2H, C-CH₂-C), 1.12 (t, *J* = 7.1 Hz, 6H, 2xCH₃-CH₂). ¹³C NMR (126 MHz, CDCl₃): δ = 173.8 (N-C=O), 167.2 (O-C=O), 136.8 (CH₂-C_{arom}), 135.8 (CH-C_{arom}), 129.3 (CH_{vinyl}), 128.9 (2xCH_{arom}), 128.8 (2xCH_{arom}), 128.4 (2xCH_{arom}), 128.3 (CH_{arom}), 127.5 (2xCH_{arom} + C_{quat}=CH_{vinyl}), 127.3 (CH_{arom}), 77.4 (N-C-(CO₂Et)₂), 62.7 (2xCH₂-CH₃), 46.1 (CH₂-Ph), 35.2 (O=C-CH₂-), 13.9 (2xCH₃). The structures of **18b-(Z)** and **18b-(E)** have been determined based on ¹³C and NOESY NMR analyses.

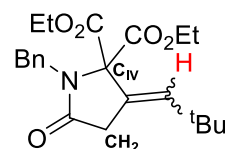
Diethyl (Z)-1-benzyl-3-(2,2-dimethylpropylidene)-5-oxopyrrolidine-2,2-dicarboxylate - 19b:

Using the general procedure, with diethyl 2-(*N*-benzyl-5,5-dimethylhex-3-ynamido)malonate (0.25 mmol - [0.5M]), Pd₂(SCS)₂ (5 mol% Pd), Mg(OTf)₂ (20 mol%) and 1,2,4,5-tetramethylbenzene as internal standard. diethyl (*E*)-1 benzyl-3-(2,2-dimethylpropylidene)-5-oxopyrrolidine-2,2-dicarboxylate was formed with 81% yield after 64 h at 120°C as estimated by ¹H NMR analysis. Isolated by column chromatography (using a gradient from 80:20 to 70:30 Pentane:EtOAc - 58 mg - 60% Yield). During this experiment 7% of (*Z*) isomer was also formed (Isolated yield - 6 mg - 6%). **E-isomer:** ¹H NMR (300 MHz, CDCl₃): δ = 7.32 – 7.09 (m, 5H, H_{arom}), 5.81 (t, *J* = 2.8 Hz, 1H, C-CH-C), 4.70 (s, 2H, CH₂-Ph), 3.90 (q, *J* = 7.1 Hz, 4H, 2xCH₂-CH₃), 3.38 (d, *J* = 2.8 Hz, 2H, O=C-CH₂-C), 1.11 (s, 9H, (CH₃)₃-C), 1.09 (t, *J* = 7.1 Hz, 5H, CH₃-CH₂). ¹³C NMR (75 MHz, CDCl₃): δ = 174.5 (N-C=O), 167.5 (O-C=O), 140.5 (C-CH-C), 136.8 (C_{arom}), 128.3 (2xCH_{arom}), 127.6 (2xCH_{arom}), 127.2 (CH_{arom} para), 123.6 (CH₂-C-CH), 77.4 (C-

(CO₂Et)₂, 62.2 (C₂H₂-CH₃), 45.9 (C₂H₂-Ph), 34.0 ((CH₃)₃-C-CH), 33.6 (C-C₂H₂-C=O), 29.8 (CH₃)₃-C), 13.8 (CH₃-CH₂). HRMS (DCI-CH₄) m/z (%): Calculated: 388.2126 (C₂₂H₃₀NO₅); Found: 388.2124. **Z-isomer:** ¹H NMR (300 MHz, CDCl₃): δ = 7.30-7.17 (m, 5H, H_{arom}), 5.52 (t, J = 2.2 Hz, 1H, C-CH-C), 4.52 (s, 2H, CH₂-Ph), 4.09-3.84 (m, 2H, 2xCH_aH_b-CH₃), 3.79-3.62 (m, 2H, 2xCH_aH_b-CH₃), 3.32 (d, J = 2.2 Hz, 2H, O=C-CH₂-C), 1.11 (t, J = 7.2 Hz, 6H, CH₃-CH₂), 1.04 (s, 9H, (CH₃)₃-C). ¹³C NMR (126 MHz, CDCl₃): δ = 173.8 (N-C=O), 166.9 (O-C=O), 140.1 (C-CH-C), 136.4 (C_{arom}), 128.4 (2xCH_{arom}), 128.3 (2xCH_{arom}), 127.4 (CH_{arom para}), 122.1 (CH₂-C-CH), 74.1 (C-(CO₂Et)₂), 62.4 (CH₂-CH₃), 45.7 (CH₂-Ph), 39.3 (C-C₂H₂-C=O), 34.7 ((CH₃)₃-C-CH), 29.6 (CH₃)₃-C), 13.8 (CH₃-CH₂). HRMS (DCI-CH₄) m/z (%): Calculated: 388.2126 (C₂₂H₃₀NO₅); Found: 388.2125.

The structures of **19b-(E)** and **19b-(Z)** have been determined based on ¹³C-¹³C ADEQUATE, NOESY, NOESY ZQF Selective and Double selective-HSQMBC-IPAP NMR analyses. Attribution of the stereochemistry was done taking into account that ³J_{CH} (*trans*) > ³J_{CH} (*cis*).^[66]

	Major product E-isomer	Minor product Z-isomer
³ J _{C_{IV}-H}	6.5 Hz	11.4 Hz
³ J _{CH₂-H}	8.9 Hz	7.6 Hz



II.5) References

- [1] Y. J. Park, J.-W. Park, C.-H. Jun, *Acc. Chem. Res.* **2008**, *41*, 222–234.
- [2] A. E. Allen, D. W. C. MacMillan, *Chem. Sci.* **2012**, *3*, 633–658.
- [3] Z. Du, Z. Shao, *Chem. Soc. Rev.* **2013**, *42*, 1337–1378.
- [4] R. Peters, *Cooperative Catalysis: Designing Efficient Catalysts for Synthesis*, Wiley, **2015**.
- [5] S. Afewerki, A. Córdova, *Chem. Rev.* **2016**, *116*, 13512–13570.
- [6] D.-S. Kim, W.-J. Park, C.-H. Jun, *Chem. Rev.* **2017**, *117*, 8977–9015.
- [7] J. R. Khusnutdinova, D. Milstein, *Angew. Chem. Int. Ed.* **2015**, *54*, 12236–12273.
- [8] T. Higashi, S. Kusumoto, K. Nozaki, *Chem. Rev.* **2019**, *119*, 10393–10402.
- [9] D. Morales-Morales, *Pincer Compounds Chemistry and Applications*, Elsevier, **2018**.
- [10] C. Gunanathan, D. Milstein, *Science* **2013**, *341*, DOI 10.1126/science.1229712.
- [11] C. Gunanathan, D. Milstein, *Chem. Rev.* **2014**, *114*, 12024–12087.
- [12] R. H. Crabtree, *Chem. Rev.* **2017**, *117*, 9228–9246.
- [13] L. Alig, M. Fritz, S. Schneider, *Chem. Rev.* **2019**, *119*, 2681–2751.
- [14] S. Kuwata, T. Ikariya, *Chem. – Eur. J.* **2011**, *17*, 3542–3556.
- [15] S. Tobisch, *Chem. – Eur. J.* **2012**, *18*, 7248–7262.
- [16] A. Nerush, M. Vogt, U. Gellrich, G. Leitus, Y. Ben-David, D. Milstein, *J. Am. Chem. Soc.* **2016**, *138*, 6985–6997.
- [17] U. K. Das, S. Chakraborty, Y. Diskin-Posner, D. Milstein, *Angew. Chem. Int. Ed.* **2018**, *57*, 13444–13448.
- [18] S. Chakraborty, P. Daw, Y. Ben David, D. Milstein, *ACS Catal.* **2018**, *8*, 10300–10305.
- [19] J. Bruffaerts, N. von Wolff, Y. Diskin-Posner, Y. Ben-David, D. Milstein, *J. Am. Chem. Soc.* **2019**, *141*, 16486–16493.
- [20] P. Oulié, N. Nebra, N. Saffon, L. Maron, B. Martin-Vaca, D. Bourissou, *J. Am. Chem. Soc.* **2009**, *131*, 3493–3498.
- [21] A. Scharf, I. Goldberg, A. Vigalok, *J. Am. Chem. Soc.* **2013**, *135*, 967–970.
- [22] J. Takaya, N. Iwasawa, *Chem. – Eur. J.* **2014**, *20*, 11812–11819.
- [23] A. Scharf, I. Goldberg, A. Vigalok, A. N. Vedernikov, *Eur. J. Inorg. Chem.* **2015**, *2015*, 4761–4768.
- [24] V. Salamanca, A. Toledo, A. C. Albéniz, *J. Am. Chem. Soc.* **2018**, *140*, 17851–17856.
- [25] H. Kameo, J. Yamamoto, A. Asada, H. Nakazawa, H. Matsuzaka, D. Bourissou, *Angew. Chem. Int. Ed.* **2019**, *58*, 18783–18787.
- [26] M. Virant, M. Mihelač, M. Gazvoda, A. E. Cotman, A. Frantar, B. Pinter, J. Košmrlj, *Org. Lett.* **2020**, *22*, 2157–2161.
- [27] N. Nebra, J. Monot, R. Shaw, B. Martin-Vaca, D. Bourissou, *ACS Catal.* **2013**, *3*, 2930–2934.
- [28] N. Á. Espinosa-Jalapa, D. Ke, N. Nebra, L. Le Goanvic, S. Mallet-Ladeira, J. Monot, B. Martin-Vaca, D. Bourissou, *ACS Catal.* **2014**, *4*, 3605–3611.
- [29] D. Ke, N. Á. Espinosa, S. Mallet-Ladeira, J. Monot, B. Martin-Vaca, D. Bourissou, *Adv. Synth. Catal.* **2016**, *358*, 2324–2331.
- [30] J. Monot, P. Brunel, C. E. Kefalidis, N. Á. Espinosa-Jalapa, L. Maron, B. Martin-Vaca, D. Bourissou, *Chem. Sci.* **2016**, *7*, 2179–2187.
- [31] J. Li, Y. Shiota, K. Yoshizawa, *J. Am. Chem. Soc.* **2009**, *131*, 13584–13585.
- [32] S. Qu, Y. Dang, C. Song, M. Wen, K.-W. Huang, Z.-X. Wang, *J. Am. Chem. Soc.* **2014**, *136*, 4974–4991.

- [33] X. Yang, *ACS Catal.* **2014**, *4*, 1129–1133.
- [34] S. Chakraborty, P. O. Lagaditis, M. Förster, E. A. Bielinski, N. Hazari, M. C. Holthausen, W. D. Jones, S. Schneider, *ACS Catal.* **2014**, *4*, 3994–4003.
- [35] U. Gellrich, J. R. Khusnutdinova, G. M. Leitus, D. Milstein, *J. Am. Chem. Soc.* **2015**, *137*, 4851–4859.
- [36] N. E. Smith, W. H. Bernskoetter, N. Hazari, *J. Am. Chem. Soc.* **2019**, *141*, 17350–17360.
- [37] D. Hack, M. Blümel, P. Chauhan, A. R. Philipps, D. Enders, *Chem. Soc. Rev.* **2015**, *44*, 6059–6093.
- [38] G. Bouhadir, D. Bourissou, *Chem. Soc. Rev.* **2016**, *45*, 1065–1079.
- [39] W. Guan, G. Zeng, H. Kameo, Y. Nakao, S. Sakaki, *Chem. Rec.* **2016**, *16*, 2405–2425.
- [40] D. You, F. P. Gabbaï, *Trends Chem.* **2019**, *1*, 485–496.
- [41] J. Becica, G. E. Dobereiner, *Org. Biomol. Chem.* **2019**, *17*, 2055–2069.
- [42] B. K. Corkey, F. D. Toste, *J. Am. Chem. Soc.* **2005**, *127*, 17168–17169.
- [43] A. Matsuzawa, T. Mashiko, N. Kumagai, M. Shibasaki, *Angew. Chem. Int. Ed.* **2011**, *50*, 7616–7619.
- [44] S. Suzuki, E. Tokunaga, D. S. Reddy, T. Matsumoto, M. Shiro, N. Shibata, *Angew. Chem. Int. Ed.* **2012**, *51*, 4131–4135.
- [45] P. Barrio, M. Kumar, Z. Lu, J. Han, B. Xu, G. B. Hammond, *Chem. – Eur. J.* **2016**, *22*, 16410–16414.
- [46] M. Cao, A. Yesilcimen, M. Wasa, *J. Am. Chem. Soc.* **2019**, *141*, 4199–4203.
- [47] T. Horibe, M. Sakakibara, R. Hiramatsu, K. Takeda, K. Ishihara, *Angew. Chem. Int. Ed.* **2020**, *59*, 16470–16474.
- [48] M. Li, R. Hua, *J. Org. Chem.* **2008**, *73*, 8658–8660.
- [49] Y. Oonishi, A. Gómez-Suárez, A. R. Martin, S. P. Nolan, *Angew. Chem. Int. Ed.* **2013**, *52*, 9767–9771.
- [50] I. Colomer, A. E. R. Chamberlain, M. B. Haughey, T. J. Donohoe, *Nat. Rev. Chem.* **2017**, *1*, 1–12.
- [51] C. Yu, J. Sanjosé-Orduna, F. W. Patureau, M. H. Pérez-Temprano, *Chem. Soc. Rev.* **2020**, *49*, 1643–1652.
- [52] V. Pozhydaiev, M. Power, V. Gandon, J. Moran, D. Lebœuf, *Chem. Commun.* **2020**, *56*, 11548–11564.
- [53] S. Tang, Y. Ben-David, D. Milstein, *J. Am. Chem. Soc.* **2020**, *142*, 5980–5984.
- [54] P. Oulié, N. Nebra, S. Ladeira, B. Martin-Vaca, D. Bourissou, *Organometallics* **2011**, *30*, 6416–6422.
- [55] N. Nebra, N. Saffon, L. Maron, B. Martin-Vaca, D. Bourissou, *Inorg. Chem.* **2011**, *50*, 6378–6383.
- [56] N. Nebra, S. Ladeira, L. Maron, B. Martin-Vaca, D. Bourissou, *Chem. – Eur. J.* **2012**, *18*, 8474–8481.
- [57] A. Ochida, H. Ito, M. Sawamura, *J. Am. Chem. Soc.* **2006**, *128*, 16486–16487.
- [58] J. J. Kennedy-Smith, S. T. Staben, F. D. Toste, *J. Am. Chem. Soc.* **2004**, *126*, 4526–4527.
- [59] K. Takahashi, M. Midori, K. Kawano, J. Ishihara, S. Hatakeyama, *Angew. Chem. Int. Ed.* **2008**, *47*, 6244–6246.
- [60] H. Tsuji, K. Yamagata, Y. Itoh, K. Endo, M. Nakamura, E. Nakamura, *Angew. Chem. Int. Ed.* **2007**, *46*, 8060–8062.

- [61] Y. Itoh, H. Tsuji, K. Yamagata, K. Endo, I. Tanaka, M. Nakamura, E. Nakamura, *J. Am. Chem. Soc.* **2008**, *130*, 17161–17167.
- [62] H. Ito, Y. Makida, A. Ochida, H. Ohmiya, M. Sawamura, *Org. Lett.* **2008**, *10*, 5051–5054.
- [63] W. Chaładaj, A. Kołodziejczyk, S. Domański, *ChemCatChem* **2017**, *9*, 4334–4339.
- [64] S. T. Staben, J. J. Kennedy-Smith, F. D. Toste, *Angew. Chem. Int. Ed.* **2004**, *43*, 5350–5352.
- [65] W. Hess, J. W. Burton, *Adv. Synth. Catal.* **2011**, *353*, 2966–2970.
- [66] U. R. Couto, A. Navarro-Vázquez, C. F. Tormena, *Magn. Reson. Chem.* **2019**, *57*, 939–945.
- [67] M. L. O’Duill, K. M. Engle, *Synthesis* **2018**, *50*, 4699–4714.
- [68] S. Montel, D. Bouyssi, G. Balme, *Adv. Synth. Catal.* **2010**, *352*, 2315–2320.
- [69] C. Amatore, S. Bensalem, S. Ghalem, A. Jutand, *J. Organomet. Chem.* **2004**, *689*, 4642–4646.
- [70] N. Panda, R. Mothkuri, *J. Org. Chem.* **2012**, *77*, 9407–9412.
- [71] J. Aziz, G. Frison, P. Le Menez, J.-D. Brion, A. Hamze, M. Alami, *Adv. Synth. Catal.* **2013**, *355*, 3425–3436.
- [72] D. Ke, N. Á. Espinosa, S. Mallet-Ladeira, J. Monot, B. Martin-Vaca, D. Bourissou, *Adv. Synth. Catal.* **2016**, *358*, 2324–2331.
- [73] N. Nebra, J. Lisena, N. Saffon, L. Maron, B. Martin-Vaca, D. Bourissou, *Dalton Trans.* **2011**, *40*, 8912–8921.
- [74] J. A. Greenberg, T. Sammakia, *J. Org. Chem.* **2017**, *82*, 3245–3251.
- [75] N. Monteiro, J. Gore, G. Balme, *Tetrahedron* **1992**, *48*, 10103–10114.
- [76] P. Cruciani, R. Stammer, C. Aubert, M. Malacria, *J. Org. Chem.* **1996**, *61*, 2699–2708.
- [77] E. C. Taylor, J. E. Macor, L. G. French, *J. Org. Chem.* **1991**, *56*, 1807–1812.
- [78] I. Ugarriza, U. Uria, L. Carrillo, J. L. Vicario, E. Reyes, *Chem. - Eur. J.* **2014**, *20*, 11650–11654.
- [79] H. A. Keane, W. Hess, J. W. Burton, *Chem. Commun.* **2012**, *48*, 6496–6498.
- [80] W. Hess, J. W. Burton, *Chem. – Eur. J.* **2010**, *16*, 12303–12306.
- [81] J. Waser, B. Gaspar, H. Nambu, E. M. Carreira, *J. Am. Chem. Soc.* **2006**, *128*, 11693–11712.
- [82] X. Wang, K. Nozaki, *J. Am. Chem. Soc.* **2018**, *140*, 15635–15640.
- [83] K. Takahashi, M. Midori, K. Kawano, J. Ishihara, S. Hatakeyama, *Angew. Chem. Int. Ed.* **2008**, *47*, 6244–6246.
- [84] A. Suárez, G. C. Fu, *Angew. Chem. Int. Ed.* **2004**, *43*, 3580–3582.
- [85] H. Liu, D. Leow, K.-W. Huang, C.-H. Tan, *J. Am. Chem. Soc.* **2009**, *131*, 7212–7213.
- [86] M. Blümel, D. Hack, L. Ronkartz, C. Vermeeren, D. Enders, *Chem. Commun.* **2017**, *53*, 3956–3959.
- [87] C.-L. Deng, T. Zou, Z.-Q. Wang, R.-J. Song, J.-H. Li, *J. Org. Chem.* **2009**, *74*, 412–414.
- [88] C.-L. Deng, R.-J. Song, Y.-L. Liu, J.-H. Li, *Adv. Synth. Catal.* **2009**, *351*, 3096–3100.
- [89] N. Tsukada, Y. Yamamoto, *Angew. Chem. Int. Ed. Engl.* **1997**, *36*, 2477–2480.
- [90] S. T. Staben, J. J. Kennedy-Smith, F. D. Toste, *Angew. Chem. Int. Ed.* **2004**, *43*, 5350–5352.

III) Synthesis of a new non-innocent platform and generation of a dearomatized active species

III.1) Context and introduction

In the first chapter of this manuscript, we have seen that interesting reactivities and selectivities were accessible through metal-ligand cooperation. In this approach the cooperation between an electron-rich site at the ligand and a Lewis acidic transition metal (TM) is clearly the leading strategy.

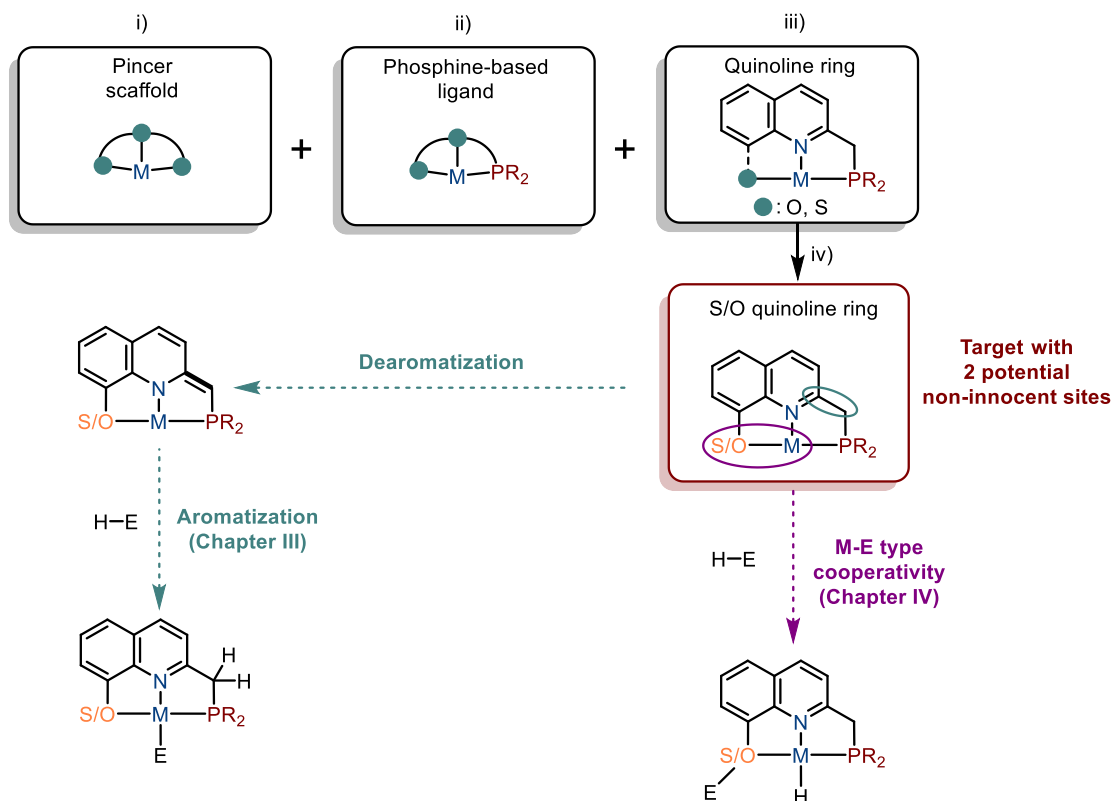
In the second chapter, the combination of MLC with an external Lewis acid was found possible and even synergistic. The efficient synthesis of carbocycles and heterocycles was then achieved thanks to our multi-cooperative system combining H-bonding additives, Lewis acid synergy and MLC to promote C-C bond formation.

To continue our study in MLC, we became interested in designing a new chemically non-innocent ligand with two main objectives. First, generalize the cooperative methodology and introduce a new ligand framework relevant to MLC. Second, extend MLC to new Pd-catalyzed transformations and beyond (other group 10 metals and potentially other TM!). To this end, the following features were selected for the design of the ligand (Scheme III.1):

- i) A pincer scaffold was identified as a first requirement. The robustness and modularity provided by these ligands make them particularly good candidates for MLC applications.^[1]
- ii) Then, a phosphine-based ligand was selected, at least for one of the coordinating sites. Indeed, phosphorus-metal interactions are usually robust, in particular for late TM, and the practical advantage of an NMR probe directly bonded to the metal is very significant in our methodology.
- iii) Next, a rigid quinoline ring with an exocyclic CH₂ spacer to the phosphine was targeted to enter aromatization/dearomatization processes. Of note, a dearomatized PNF-quinoline Pd^{II} complex was first introduced by Vigalok as rare example of MLC for C-C bond formation (already presented in the first chapter of this thesis; section I.1)c).^[2] However, this scaffold was only scarcely developed and no significant improvement has been reported since.

- iv) In our approach, we sought to enforce the pincer coordination by replacing the fluorine atom by a stronger coordinating site. We chose to tailor the third chelation site available at the quinoline depending on the metal by targeting a PNO/PNS quinoline scaffold. This model has the additional advantage of a potential mode of cooperativity based on the direct M-O/S interaction.

This chapter will be focused on the aromatization/dearomatization type of cooperativity. The M-X type cooperativity will be presented in the following chapter.



Scheme III.1: Criteria for the ligand design and potential modes of non-innocence

A related PNO-Rh complex was already reported by Kakiuchi but the potential for ligand non-innocence by aromatization/dearomatization was not exploited neither mentioned (Figure III.1).

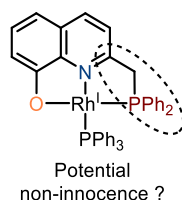
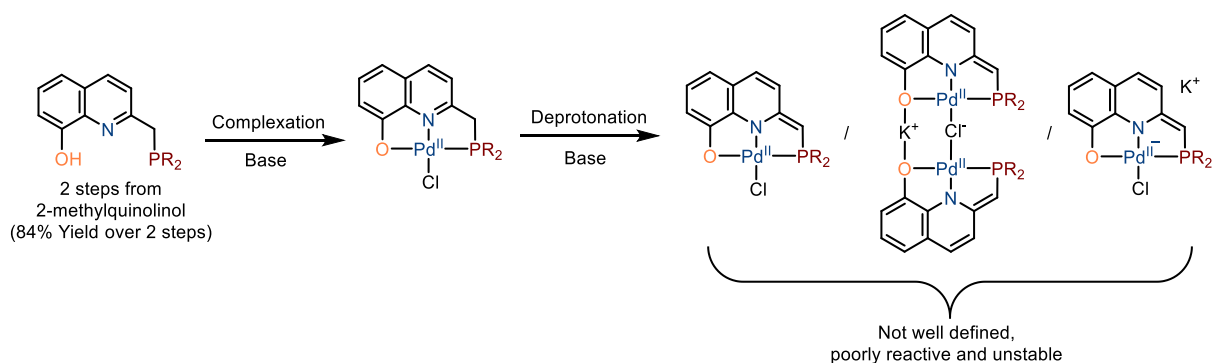


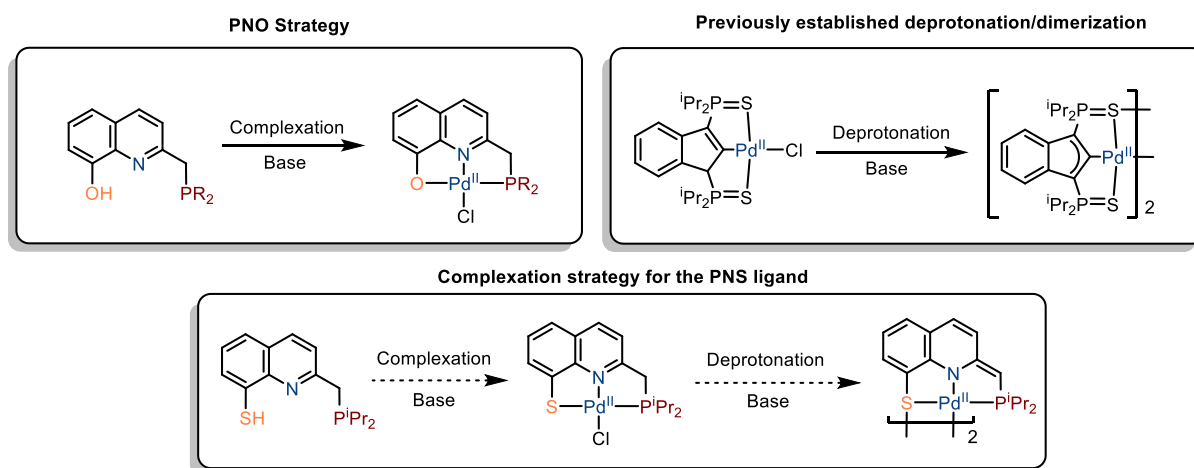
Figure III.1: PNO-Rh^I complex of Kakiuchi and potential site for chemical non-innocence

As the synthesis of the quinolinol proligand was quite straightforward, this pathway was first explored with palladium.^[3] Preliminary results obtained by a Master student in the group (Laurens Vedder) showed an easy synthesis of the PNO-Pd^{II}-Cl complex in three steps (Scheme III.2). The generation of a dearomatized complex was achieved upon deprotonation of the exocyclic CH₂. However, the precise structure of the formed compound (mono-/ di-nuclear) could not be confirmed. Indeed, the low tendency of oxygen to form bridged compounds most likely precluded the formation of a well-defined dimeric species. In fact, most of the crystallized Pd-O bridged dimers are formed with electron-rich phenols or with hydroxides (CCDC database search). Anyway, the reactivity of this dearomatized species was probed and the complex showed low stability, as free ligand being observed in most cases.



Scheme III.2: Synthesis of a PNO-Pd^{II} complex and initial results towards the generation of dearomatized species

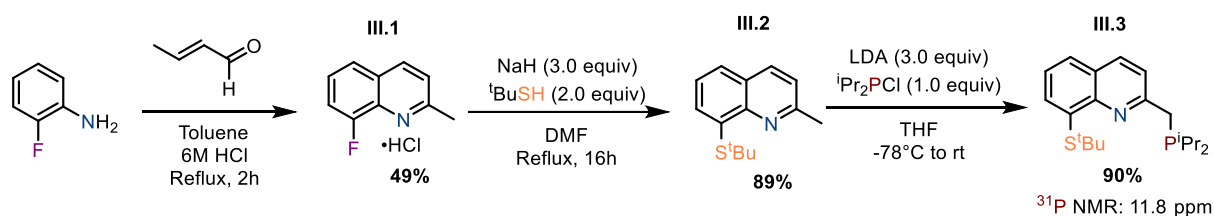
The low Pd^{II}-O affinity and the lability of such bond was proposed to play an important role in the observed instability. We then surmized that a switch to the sulfur analog could provide a solution to both issues at hand (i.e the instability of the complex and the formation of ill-defined species). Indeed, Pd^{II}-S bonds are stronger than Pd^{II}-O and should form a more robust complex. Furthermore, the increased availability of the lone pairs at sulfur could favor the formation of a well-defined dimeric species upon deprotonation. Indeed, upon searching for Pd-S dimeric structures, more than 200 hits were found in the CCDC database (compared to around 70 for Pd-O). However, the dissociation of the dimer should be possible for further reaction. In fact, this strategy was already well established in the group and was previously used in the [(SCS)-Pd] complexes forming a head-to-tail dimeric complex upon deprotonation (Scheme III.3). With this in mind, the synthesis of the PNS^H ligand was first targeted.



Scheme III.3: New PNS-Pd target complex and potential benefits of switching from oxygen to sulfur

III.2) Synthesis of a new non-innocent platform

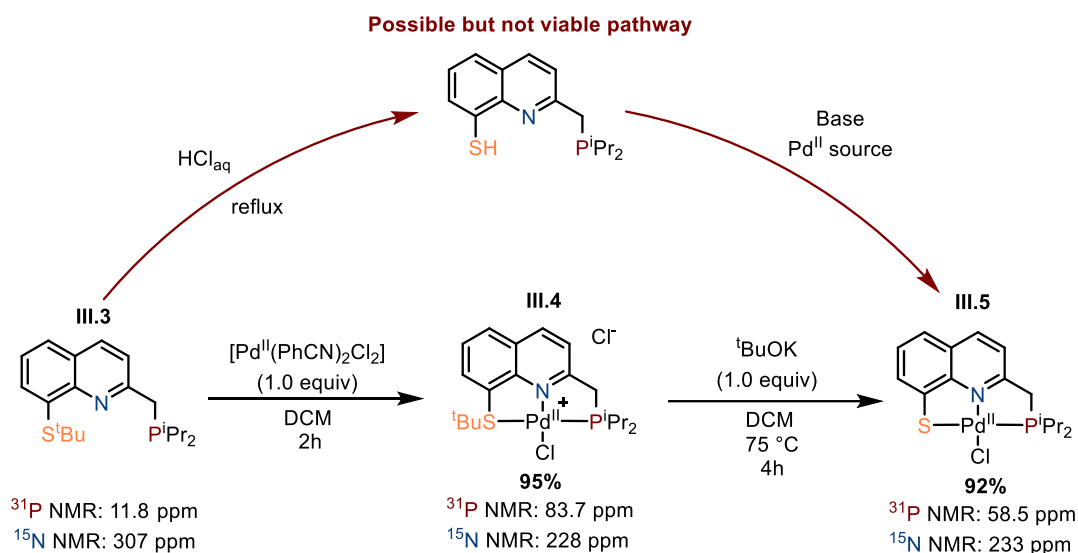
Unfortunately, compared to the PNO analog, the ligand synthesis was not as straightforward and had to be started from the synthesis of the quinoline scaffold. Based on procedures from the literature, an optimized synthesis of the PNS^{tBu} pro-ligand was achieved with the help of András Kotschy, a Master student in the group.^[4] Starting from the commercial *o*-fluoroaniline, the quinoline is formed upon reaction with crotonaldehyde. The resulting fluoroquinoline is then isolated as a chlorhydrate salt **III.1** and purified by recrystallization, allowing for a convenient large-scale synthesis without column chromatography (up to 13 g of pure product). Nucleophilic aromatic substitution with ^tBuSNa is then performed and after workup, the compound **III.2** could be engaged in the next step without further purification. The phosphine arm was finally built by deprotonation with LDA and addition of chlorophosphine to yield the corresponding PNS^{tBu} proligand **III.3** with a global yield from the chlorhydrate **III.1** of 80%.

Scheme III.4: Synthetic pathway for the PNS^{tBu} proligand in 3 steps starting from *o*-fluoroaniline

As the synthesis of the PNO-Pd^{II}-Cl complex was previously achieved with the free alcohol, generation of the PNS^H ligand by acidic ^tBuS deprotection of **III.3** was initially attempted (top

- Scheme III.5). This pathway, involving harsh conditions afforded us a small quantity of the desired PNS^{H} proligand that could in the presence of a base lead to the PNS-Pd-Cl complex **III.5**. Even if this synthesis shows the accessibility of the complex **III.5**, the formation of the PNS^{H} proligand was not straightforward (a large amount of concentrated HCl was required), nor reproducible and scalable.

We then designed a simpler route, directly using palladium instead of a Brønsted acid for the deprotection (bottom - Scheme III.5). Even if uncommon, formation of a metal-thiolate bond from a ^tBuS -thioether was already reported in 2012 by Milstein in the case of a pyridine based PNS-Ru complex.^[5] In our case, the corresponding cationic square planar complex **III.4** was easily obtained in high yields by treatment of the $\text{PNS}^{t\text{Bu}}$ proligand with a palladium^{II} source in DCM.



Scheme III.5: Initial synthetic pathway with acidic ^tBuS deprotection and Pd-assisted synthesis of the $\text{PNS-Pd}^{\text{II}}\text{-Cl}$ complex

Complexation of the phosphine arm was supported by an upfield shift in ^{31}P NMR from 11.8 ppm in the free ligand **III.3** to 83.7 ppm in the cationic complex **III.4**. Coordination of the aromatic nitrogen center was apparent from the shielding of the ^{15}N NMR signal from 307 ppm in the free ligand to 228 ppm in the cationic **III.4** complex. This upfield shift of 79 ppm falls within the range of the usually reported shifts upon coordination to Pd^{II} .^[6] Single-crystal XRD analysis of the complex **III.4** was then conducted and a cationic Pd^{II} complex bonded to P,N,Cl and S with an outer-sphere chloride structure was unambiguously determined (Figure III.2 - Left). Only a slight deviation from the ideal square planar geometry was observed in the

complex **III.4** with a four-coordinate geometry index of $\tau_4 = 0.11$ (where 0.0 means square planar and 1.0 means tetrahedral).^[7] A Pd^{II}-N bond distance of 2.024(2) Å was observed along with a Pd^{II}-S bond of 2.4074(7) Å and a Pd^{II}-P bond of 2.2229(7) Å. These data are in line with the bond lengths reported by Vigalok in the case of the cationic PNS^{Et}-Pd^{II}-Ar complex (Pd^{II}-N: 2.072(4); Pd^{II}-S: 2.3414(13); Pd^{II}-P: 2.2741(13)).^[8]

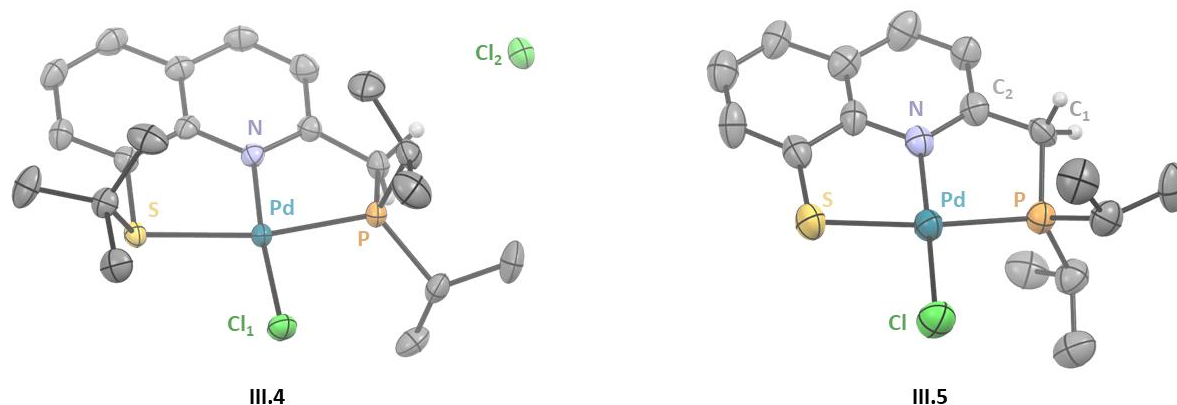


Figure III.2: XRD structure of the cationic PNS^{tBu}-Pd-Cl complex **III.4** and the neutral PNS-Pd-Cl **III.5** with an outer-sphere chloride; H and DCM molecules were omitted for clarity

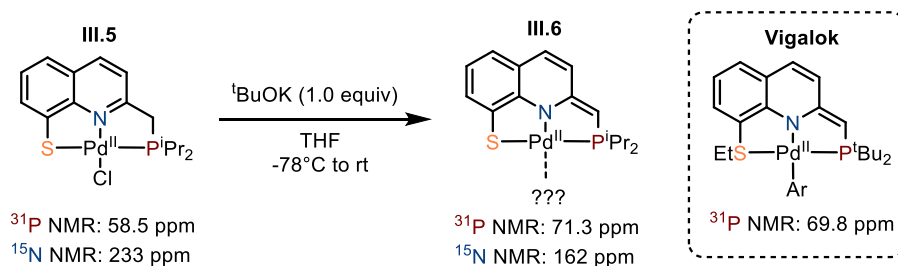
Removal of the ^tBu group in **III.4** to yield the target complex **III.5** was achieved by treatment with ^tBuOK in DCM at 75°C in a sealed ace tube. This new complex displays a ³¹P NMR signal at 58.5 ppm while only a slight variation was observed in ¹⁵N NMR (from 228 ppm in **III.4** to 233 in **III.5**). In ¹H NMR, a global downfield shift of signals was observed from the cationic **III.4** to the neutral **III.5**. Indeed, the quinoline signals located in the 8.9-7.7 ppm region in **III.4** were shifted to the 8.3-7.4 region in **III.5**. In addition, the CH₂ signal found at 5.07 ppm in **III.4** was observed at 3.77 ppm in **III.5**. Single crystals of **III.5** were obtained and analyzed by XRD. Structurally, the geometry around the palladium center is less distorted in **III.5** ($\tau_4 = 0.07$). A contraction of the Pd-S bond was observed by XRD (2.4074(7) Å in **III.4** compared to 2.3055(3) Å in **III.5**) while the Pd-N distance was only slightly reduced (2.024(2) Å in **III.4** and 2.017(9) Å in **III.5**) and the Pd-P was slightly elongated (2.250(3) Å in **III.5** and 2.2229(7) Å in **III.4**).

Thus, the PNS complex **III.5** was conveniently and efficiently prepared by simple coordination of **III.3** to Pd and S^tBu deprotection under basic conditions. With the synthetic target in hand, we were first interested in the generation of the dearomatized species.

III.3) Aromatization/dearomatization cooperativity

a) Generation and characterization of the deprotonated complex

The deprotonation of the CH₂ linker on **III.5** could be simply carried out by addition of 1.0 equivalent of ^tBuOK in a suspension of the complex in cold THF (Scheme III.6). Upon addition, an immediate color change from yellow to dark red was observed, transitioning to dark green upon warming up to room temperature. After removal of the volatiles, the deprotonated complex could be isolated as a dark solid by addition of DCM, filtration, and evaporation.



Scheme III.6: Synthesis of the dearomatized complex **III.6** by deprotonation

Only one product at 71.3 ppm was observed in ³¹P NMR, in accordance with the observation of Vigalok in the related PNS^{Et}-Pd-Ar complex.^[8] Dearomatization of the quinoline ring was clearly indicated by ¹H NMR (Figure III.3). Indeed, a diagnostic shift of the signals from the aromatic region (8.28-7.38 ppm) in the PNS-Pd^{II}-Cl complex **III.5** to the vinyl region (7.28-6.51 ppm) in **III.6** was found. Furthermore, the integral of the CH₂ doublet in **III.5** was changed to one in **III.6** and is slightly shielded, once again in line with the report of Vigalok.^[8] ¹⁵N NMR was also found diagnostic of a hybridization switch from aromatic sp²-N (233 ppm) in **III.5** to amido sp³-N (162 ppm) in **III.6**. Interestingly, the ⁱPr signals were found completely split with two CH signals (circled in Figure III.3) and 4 CH₃ signals, some of them particularly shielded. This fact could suggest a different chemical environment and an aggregated species.

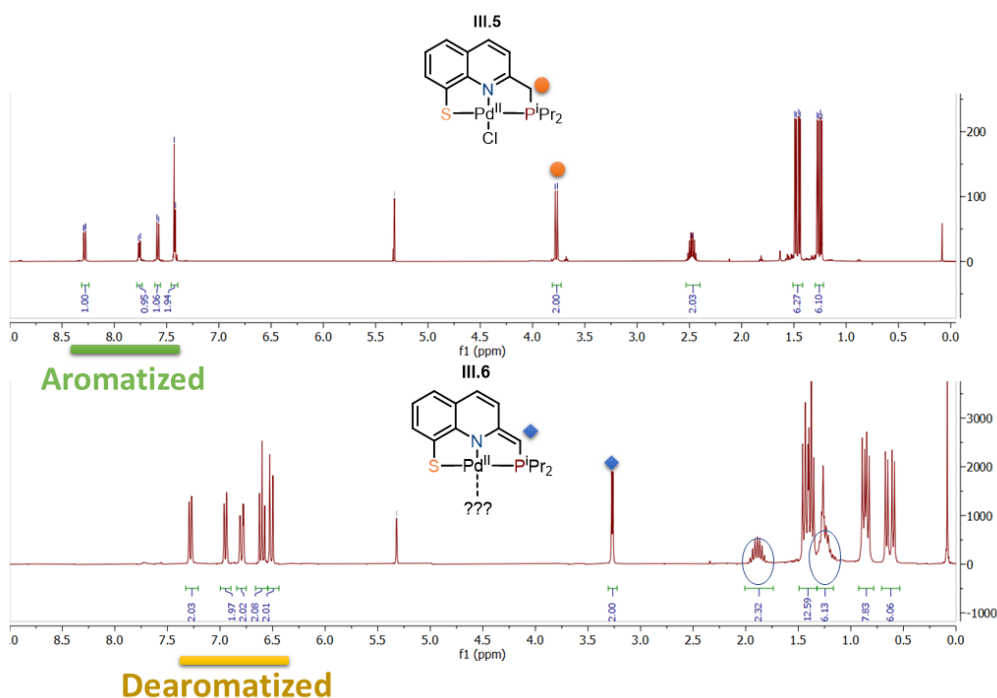


Figure III.3: ^1H NMR spectra comparison of PNS-Pd-Cl complex **III.5** and the dearomatized $[\text{PNS-Pd}]_2$ **III.6**

Single crystals of **III.6** suitable for XRD analysis could be obtained by slow evaporation of a concentrated pentane solution (Figure III.4). Gratifyingly, the expected head-to-tail dimeric structure with bridging sulfur atoms was found in the solid state. Notably, an isopropyl fragment was located straight above the π -electron system of the other quinoline moiety (blue dashed arrow - Figure III.4). It is now understood that the non-equivalent and shielded ^iPr signals observed in ^1H NMR (circled in Figure III.3) are due to the magnetic anisotropic effect and are diagnostic of a dimeric structure also in solution. Furthermore, in NOESY NMR, a clear “intermolecular” correlation between the less shielded isopropyl CH_3 at 1.4 ppm (thus, the one located not straight above the quinoline π -system) and the *ortho*-CH of the S containing ring of was found (red arrow - Figure III.4).

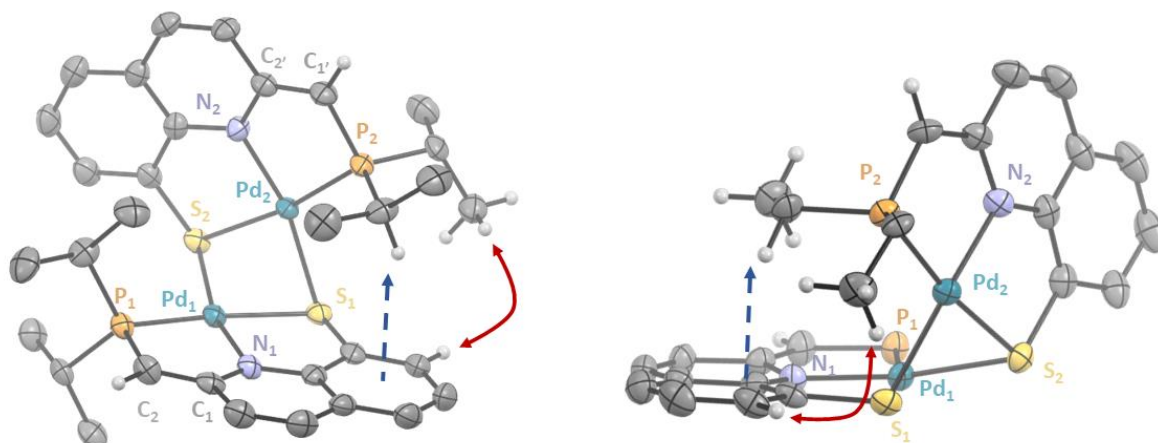
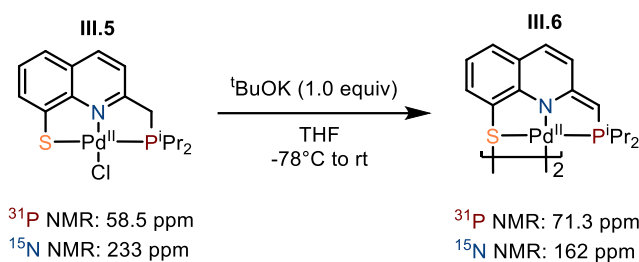


Figure III.4: XRD Structure of the dimeric complex **III.6** with side view; The shielding of the ⁱPr signals by magnetic anisotropic effect is indicated by the dashed blue arrow; The NOESY interaction observed by ¹H NMR is indicated by the double red arrow. Hydrogens and ⁱPr substituents at P are omitted for clarity except when relevant

The two metallic centers are slightly distorted from the ideal square planar geometry with a parameter $\tau_4 = 0.17$. This distortion is probably due to the rigid ligand architecture and the pyramidal geometry of the sulfur atom. Indeed, as each sulfur completes the coordination sphere of the other metallic center, a butterfly-shaped dimer is observed.^[9]

A contraction of the C₂-C₁ (and C_{2'}-C_{1'}) bond from 1.48(1) Å in PNS-Pd-Cl **III.5** to 1.355(6) Å and 1.366(6) Å in the dearomatized dimeric complex [PNS-Pd]₂ **III.6** is observed, in accordance with a single and double bond character in the respective complexes (Figure III.4). The Pd-S distances are found somewhat shorter in the “intermolecular” interactions rather than the “intramolecular” bonds probably due to the rigid nature of the ligand (i.e: **inter**-Pd₂-S₁: 2.343(1) Å / **inter**-Pd₁-S₂: 2.341(1) Å compared to **intra**-Pd₁-S₁: 2.365(1) Å and **intra**-Pd₂-S₂: 2.371(1) Å). The Pd-N distances are not significantly affected by the coordination switch from L-type in the aromatized **III.5** compared to the X-type in **III.6** (2.017(9) Å in **III.5** compared to 2.027(3) Å Pd₂-N₂; 2.016(4) Å Pd₁-N₁ in **III.6**). Similarly, the Pd-P distances are almost identical (2.247(1) Å and 2.245(1) Å in **III.6** compared to 2.250(3) Å **III.5**).

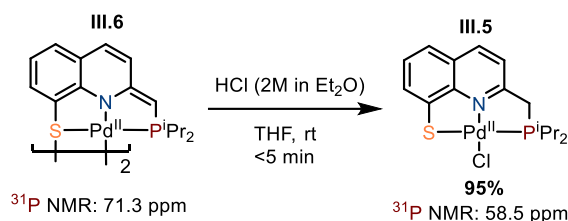
Overall, the efficient synthesis of the well-defined dearomatized Pd^{II} complex **III.6** was achieved by simple deprotonation contrary to the ill-defined, dearomatized PNO analog (Scheme III.2). Furthermore, the dearomatized complex was found stable in DCM, in contrast to the PNO analog which was unstable in chlorinated solvents.

Scheme III.7: Deprotonation of **III.5** with *t*BuOK to yield the well-defined dearomatized dimeric complex **III.6**

Next, our first objective was to illustrate the cooperativity between the transition metal and the backbone, first under stoichiometric conditions and if possible, to switch to catalytic transformations. For this purpose, the activation of polar E-X bonds was studied first.

b) Stoichiometric activation of polar E-X bonds

As a first model reaction, we were interested in the regeneration of the aromatized PNS-Pd-Cl **III.5** complex upon reaction of **III.6** with HCl. A THF solution of dearomatized complex was then treated with 1.0 equivalent of HCl (2M in Et₂O). Immediately upon addition, a clear red solution was formed. Only one species at 58.5 ppm was observed in ³¹P NMR and after precipitation in pentane, complex **III.5** was recovered in 95% yield.

Scheme III.8: Regeneration of **III.5** by protonation of the dearomatized dimer **III.6** with HCl

Even if HCl is a strongly polarized and very reactive compound, the proof of concept was demonstrated here. The dearomatized [PNS-Pd]₂ dimer **III.6** contains an available basic site at the vinylic C-H and can dissociate back to give a mononuclear complex.

Interestingly, when **III.6** was subjected to electrophiles such as iodomethane, another site at the ligand was found reactive (Scheme III.9). Indeed, a new signal was observed at 82.3 ppm in ³¹P NMR after 1 h at 50 °C. A dearomatized backbone was suggested by ¹H NMR analysis with the quinoline signals located in the 6.75-6.35 ppm region (Figure III.5).

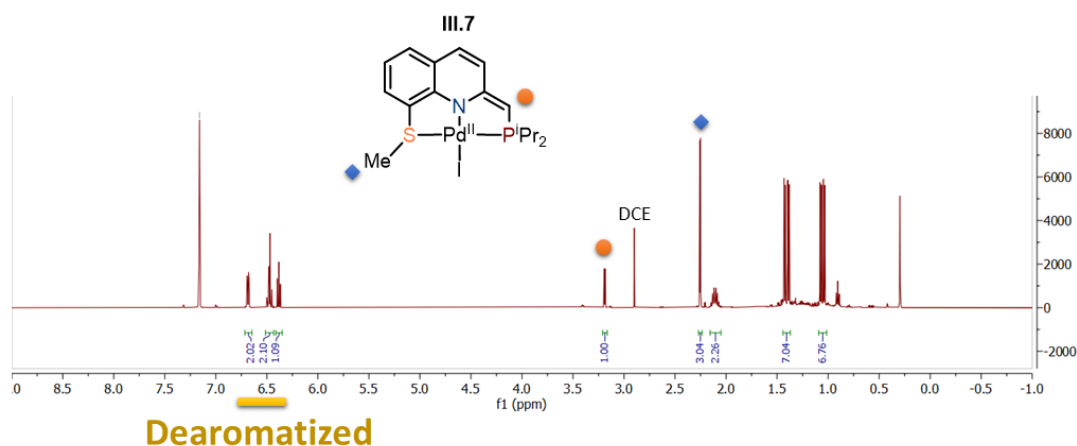
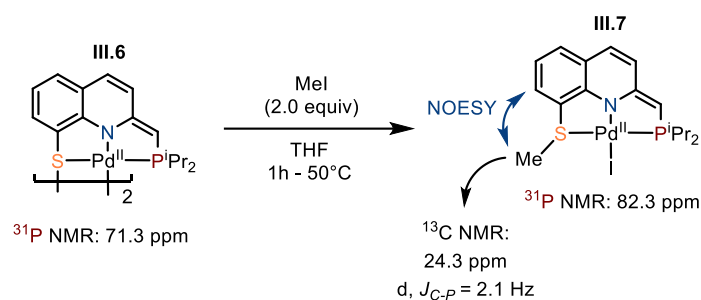


Figure III.5: ^1H NMR spectrum of the complex **III.7** resulting from the reaction with MeI; DCE was present in the complex from the precipitation attempt

The vinyl CH was almost untouched compared to **III.6** (3.19 ppm in **III.7** and 3.26 ppm for **III.6**) and a new doublet at 2.25 ppm accounting for three protons was found. A dearomatized backbone with incorporation of the methyl at the sulfur of was envisioned and later confirmed by ^{13}C and NOESY NMR (Scheme III.9).



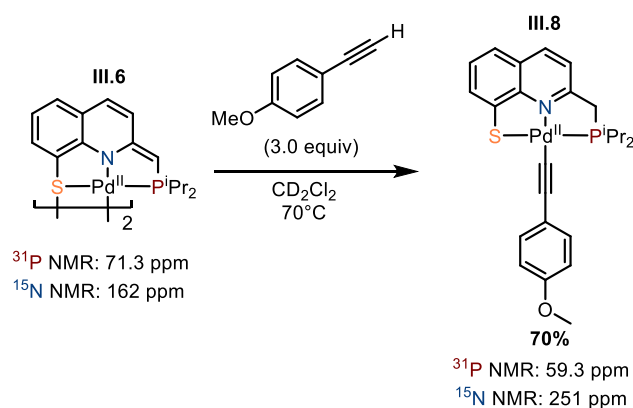
Scheme III.9: Reaction of the dearomatized complex at S with electrophiles

This behavior, with two non-innocent sites at the ligand is a remarkable feature of this architecture with a basic (Brønsted) site at the dearomatized C-H and a nucleophilic site at the sulfur. It is to note that, in the reaction of **III.6** with HCl, it is possible that protonation occurs first at sulfur, and H^+ migration then gives **III.5**.

The cooperativity between the ligand and transition metal has been illustrated with very reactive partners first. We then turned to more challenging substrates.

c) C-H activation of alkynes:

First, the C-H activation of alkynes such as *para*-methoxyphenylacetylene was attempted. In the presence of 3.0 equivalents, a transition from a dark green solution to a deep red was noticed over 10 h at 70 °C. In ^{31}P NMR (spectra acquired at room temperature), the disappearance of the signal at 71.3 ppm of **III.6** and the formation of new signal at 59.3 ppm was observed with no intermediates. The rearomatization of the quinoline backbone and the formation of a Pd^{II} -alkynyl complex **III.8** was observed clearly apparent from ^1H and ^{13}C NMR (Scheme III.10).



Scheme III.10: C-H activation of alkynes by the dearomatized Pd^{II} dimeric complex **III.6**

Indeed, the previously shielded signals of the quinoline in **III.6** were now shifted in the aromatic region (from 8.28 to 6.75 ppm) and a doublet at 3.83 ppm corresponding to the exocyclic CH_2 was formed (Figure III.6). The rearomatization of the quinoline backbone was further supported by ^{15}N NMR and a signal at 251 ppm was observed. A coupling between the alkynyl carbons and phosphorus was also observed by ^{13}C NMR (86.9 ppm $^2J_{\text{C-P}} = 19.7$ Hz; 112.1 ppm $^3J_{\text{C-P}} = 4.6$ Hz), strongly supporting coordination of the alkynyl moiety to Pd.

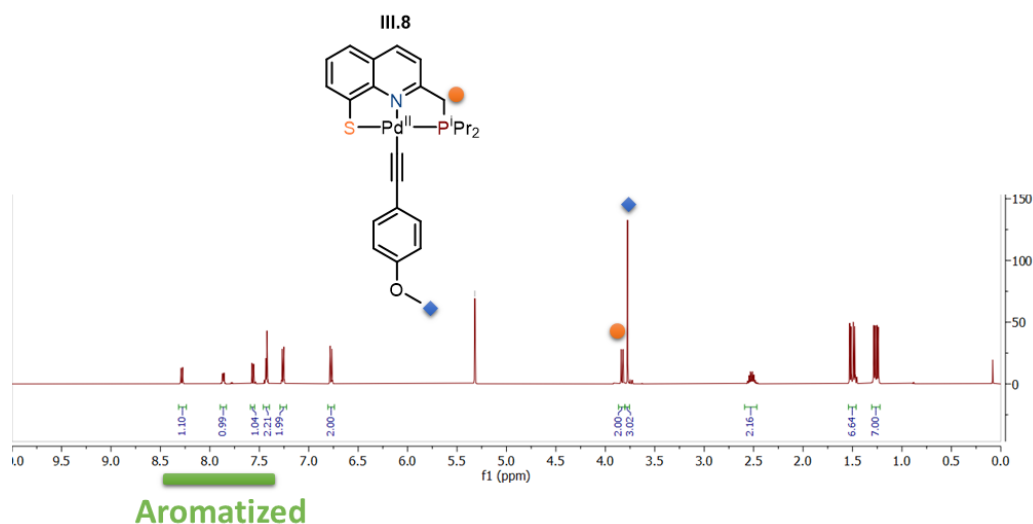


Figure III.6: ^1H NMR of the aromatized complex **III.8** resulting of the C-H activation of *p*-MeO-phenylacetylene

Single crystals of this complex could be grown by vapor diffusion of pentane into a concentrated DCM solution and were analyzed by XRD. The formation of a mononuclear Pd-C \equiv C alkynyl complex was confirmed and a short C₃-C₄ distance of 1.141(3) Å (typical of a C \equiv C triple bond) was found. Less distortion was observed in the complex as the palladium center sits closer to the ideal square planar geometry with a parameter $\tau_4 = 0.09$. The rearomatization of the quinoline backbone and the regeneration of the methylene spacer was confirmed and a C₁-C₂ distance in accordance with a single bond was found (Figure III.7; 1.355(6)/1.366(6) Å in **III.6** to 1.499(2) Å in **III.8**). The Pd-N, Pd-S and Pd-P distances were mostly unaffected (as is usually observed with this rigid ligand; Pd-N = 2.041(1) Å; Pd-S = 2.3159(6) and Pd-P: 2.2527(5) Å in **III.8**).

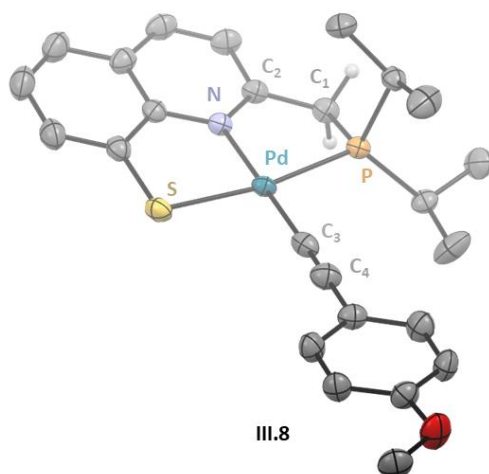
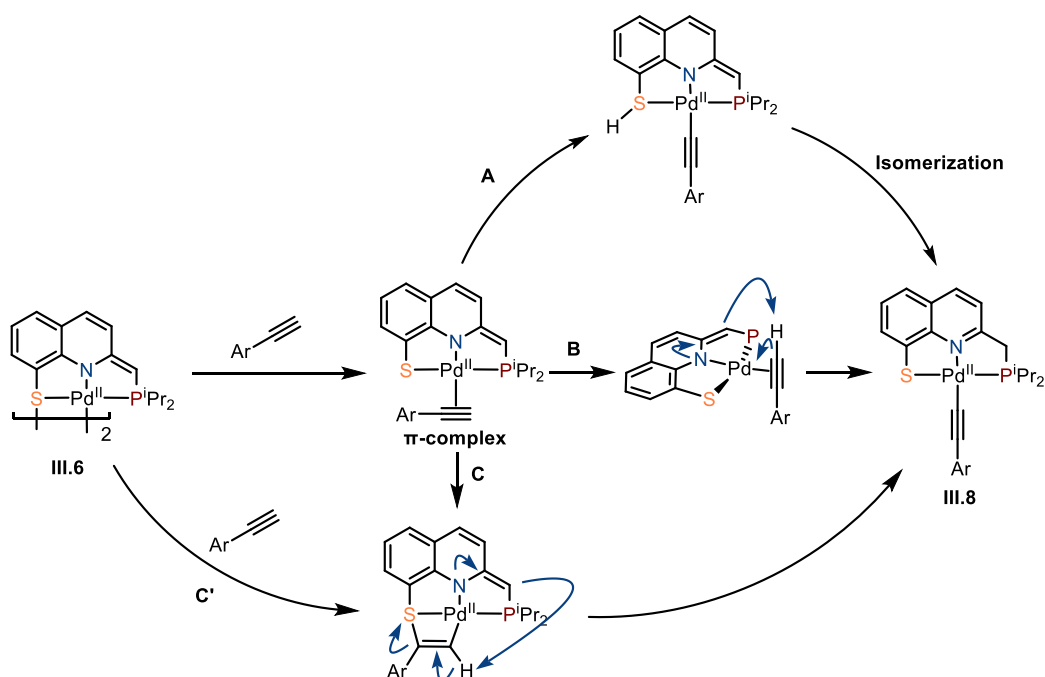


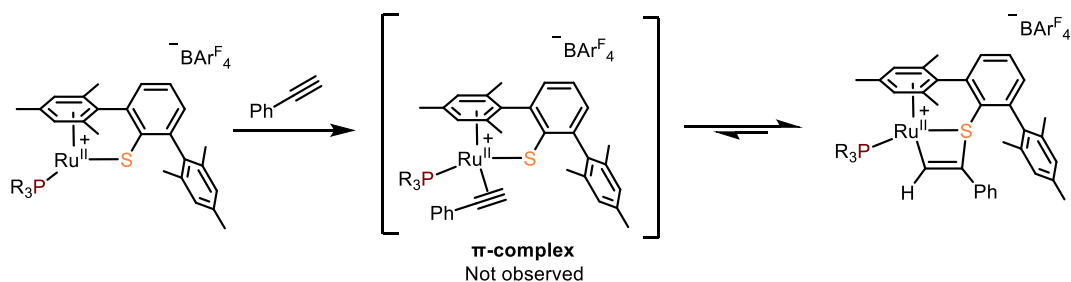
Figure III.7: Crystalline structure of the PNS-Pd-alkynyl complex **III.8**; H are omitted for clarity except when relevant

Mechanistically, three main pathways can be proposed for this C-H activation (Scheme III.11). For **A**, **B**, and **C**, the first step would be the dimer dissociation and formation of a π -complex. Then in pathway in **A**, the C-H activation might occur across the palladium-sulfide motif to yield the corresponding dearomatized thioquinolinol-Pd^{II}-alkynyl. This complex would then undergo proton migration to yield complex **III.8**. Even though the direct S to C proton transfer is probably not possible geometrically, this process could be bimolecular, or assisted by a proton-shuttle. In fact, proton-shuttling additives such as adventitious water were found critical in the rearomatization of the related PNF-Pd^{II} complex of Vigalok.^[10] Alternatively in pathway **B**, the C-H activation could occur directly at the vinyl CH of the backbone after the formation of the π -complex with assistance (or not) of a proton-shuttle.



Scheme III.11: Proposed mechanisms for the C-H activation of alkynes by the dearomatized Pd complex **III.6**

Finally, a third pathway **C** can be proposed. In this case a vinyl palladacycle could be formed upon reaction with phenylacetylene. Then, like in **A** or **B** isomerization (or an intermolecular process) would yield the aromatized complex **III.8**. This process could occur via a π-complex (**C**) or a shortcut can be envisioned (**C'**) where the palladacycle would be formed by direct reaction of **III.6** on the alkyne. In line with this mechanism, a previous publication by Ohki reported the formation of a vinyl-sulfide complex upon treatment of the DmpS-Ru complex with phenylacetylene (Scheme III.12).^[11]



Scheme III.12: Ru-vinyl complex of Ohki upon reaction of phenylacetylene with the cationic Ruthenium-thiolate complex

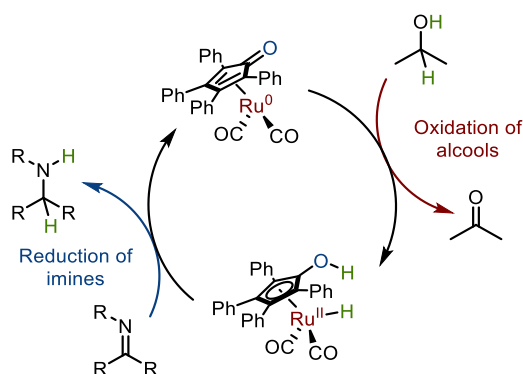
In our case, no intermediate was detected during the monitoring of the reaction. Nonetheless, the dearomatized dimer **III.6** was submitted to 5.0 equivalents of Ph-CC-Me to see if the corresponding internal alkyne could promote the dissociation of the catalyst and the

formation of a π -complex, but no reaction was observed (spectra acquired at room temperature in both cases).

Overall, with the previous stoichiometric reactions, the cooperativity between the dearomatized backbone and the metallic center was demonstrated. At this point, a catalytic application would not be straightforward, we then decided to focus on other reactivities.

d) Dehydrogenation of alcohols

Historically, the first example of a reaction involving MLC was the catalytic dehydrogenation of alcohols into esters, reported by Shvo in 1985 (the non-innocent character of the ligand in this transformation was only discovered the following year).^[12,13] Since then, this finding has had a tremendous fallout in the chemical community and multiple transformations have been reported with this catalyst (mostly involving H-transfer processes). As an example, a simplified mechanism of alcohol oxidation and imine reduction involving Shvo's catalyst is presented below (Scheme III.13).^[14,15]

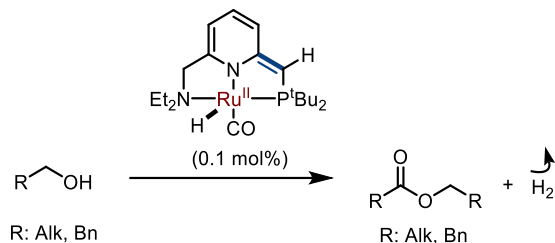


Scheme III.13: Simplified mechanism of the tandem oxidation of alcohol and reduction of imine using Shvo's catalyst

Remarkably, in the cycle, a two-electron redox process at the metal occurs with a change of the oxidation state from Ru^0 to Ru^{II} . It is also interesting to notice that the reduced Ru^0 species is responsible for the oxidation of alcohols and the oxidized Ru^{II} species is the reducing agent for the imine.

A breakthrough was achieved in 2005 with the aromatization/dearomatization of pyridines as a key ligand design introduced by Milstein.^[16] Interestingly, just like the previous example of Shvo, the first catalytic reaction reported was the dehydrogenation of alcohols into esters. The catalytic cycle of this transformation sparked a lot of interest, and a revised

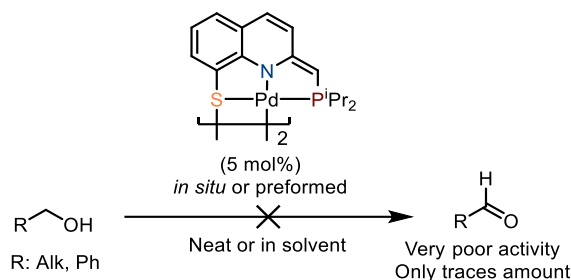
mechanism was recently published by Gusev.^[17] It is interesting to note however, that a key feature of this ligand design resides in the ability to act cooperatively in E-H bond activation without any change in the oxidation state of the metal (already presented in the first chapter of this thesis with group 10 metals; section I.1)c).



Scheme III.14: Dehydrogenation of alcohols into esters catalyzed by the non-innocent PNN complex of Milstein

As this transformation can be seen as a “benchmark” for MLC systems, we wondered if our dimeric dearomatized complex was catalytically relevant. Furthermore, Pd catalysts are classically used in reduction reactions but not so much in oxidations such as the dehydrogenation of alcohols. Our usual way to operate consists in NMR monitoring of closed systems. This time, to maximize our chances at observing any reactivity, the experimental setup had to be different to allow generated gas to escape. Reactions were thus run in Schlenk tubes equipped with reflux condensers and a bubbler. Conversion of the alcohol and reaction monitoring was done by GC.

The dearomatized complex was added to the corresponding alcohol and the mixture was heated at reflux. Multiple conditions, classically used in this type of reaction were employed (in pure alcohol, in high-boiling point solvents, with pre-formed or with *in situ* generated catalyst, in presence of amine and 4 Å MS...) but no reactivity was observed and at best, only 5% of aldehydes were detected by GC (barely one turnover!). ³¹P NMR at the end of the reactions revealed multiple unidentified species but the dearomatized complex was still the major one. In this case, it may be that the properties of the ligand and the metal are not best suited for this reactivity. The basicity of the non-innocent backbone could be too low due to the increased delocalization offered by the quinoline skeleton for O-H activation. Furthermore, in these transformations, Ni could be a better candidate, thanks to its affinity for O.



Scheme III.15: Absence of reactivity in the catalytic dehydrogenation of alcohols the dearomatized dimeric complex.

e) DMAB Dehydrogenation and H₂ activation

Still, the extent of H-transfer reactions in MLC prompted us to probe the behavior of our complex towards H₂ and surrogates. Initially, dimethylamine-borane (DMAB) a simple and polar source of H₂ was used. In DMAB, the hydrogen at the amine exhibits an acidic character and the hydrogen at the borane is hydridic.^[18] In this case, the incorporation of the proton at the backbone and the formation of a metal hydride should be favored and occur upon cooperative DMAB activation.

Upon treatment with 5.0 equivalent of DMAB at 70°C, the formation of a new species at 62.3 ppm in ³¹P{¹H} NMR was observed. In addition, complete conversion of the DMAB into the dehydrogenated dimer was evidenced by the disappearance of a signal at -12.9 ppm (DMAB) in ¹¹B{¹H} NMR and the formation of a new signal at 5.4 ppm (dehydrogenated dimer).^[19] In ¹H NMR, the formation of H₂ was observed as a singlet at 4.5 ppm. As for the Pd complex, the quinoline signals were found “rearomatized”, with chemical shifts ranging from 8.23 to 7.12 ppm while the “aromatized” CH₂ was located at 3.82 ppm (Figure III.8). Furthermore, and most importantly, a hydride signal was found as a doublet at -12.57 ppm (²J_{H-P} = 6.0 Hz).

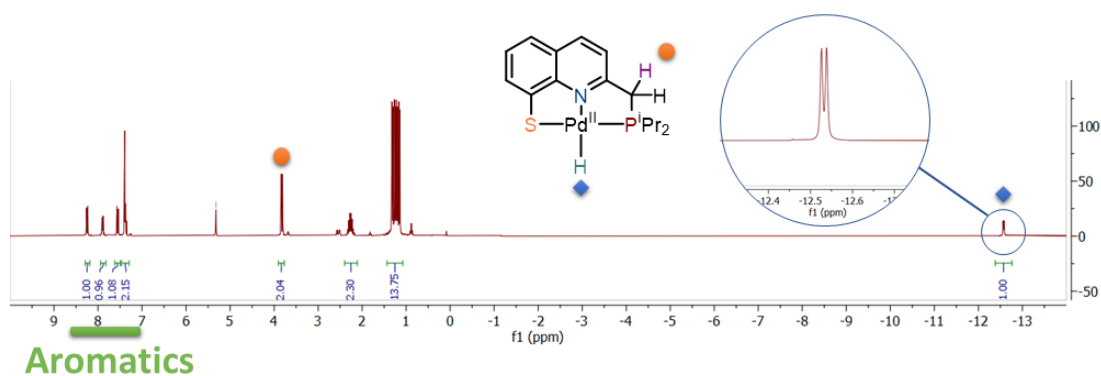


Figure III.8: ^1H NMR in CD_2Cl_2 of isolated **III.10** bearing a hydride signal and an aromatized quinoline backbone

Single crystals of this complex could be grown by layering pentane over a DCM solution of **III.9**. Analysis of the crystalline structure confirmed a $\text{PNS-Pd}^{\text{II}}\text{-H}$ structure as the hydride was located (not added!) trans to nitrogen (Figure III.9). Like in the previous cases less distortion was observed compared to **III.6** with a parameter $\tau_4 = 0.09$ (0.17 in **III.6**). The single bond character of the $\text{C}_1\text{-C}_2$ interaction was clearly indicated by a distance of 1.496(9) Å, much like in the aromatized **III.8** (1.499(2) Å). Once again, the Pd-N, Pd-S and Pd-P distances were mostly unaffected (Pd-N = 2.077(5) Å; Pd-S = 2.322(2) and Pd-P = 2.220(2) in **III.9**).

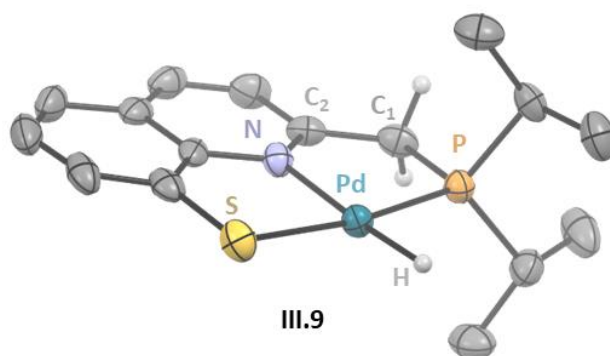
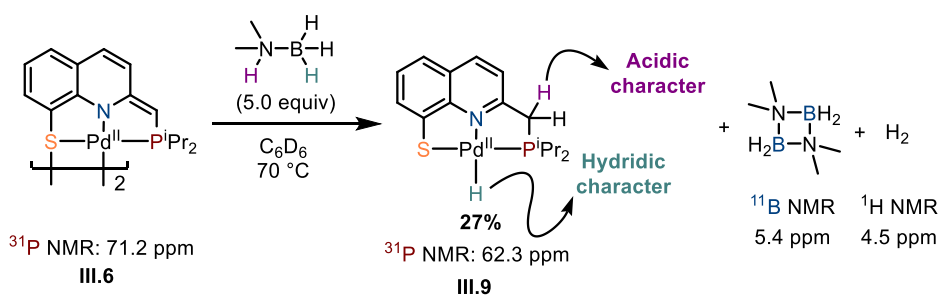


Figure III.9: XRD structure of the aromatized Pd-H complex **III.9**

Overall, the formation an “aromatized” $\text{PNS-Pd}^{\text{II}}\text{-H}$ **III.9** was observed upon reaction of the dearomatized dimer **III.6** with DMAB (Scheme III.16). In this complex, two antagonistic hydrogen centers are captured, one with acidic character at the non-innocent backbone, and one with hydridic character at the transition metal. This is a rather rare occurrence in the literature, and even more so with palladium.



Scheme III.16: Stoichiometric reaction of the dearomatized complex III.6 with DMAB

Indeed, in the first chapter of this thesis, examples of pincer group 10 metal-hydrides complexes bearing an acidic proton at a non-innocent backbone were also presented.^[20–24] Out of 4 examples (only!), 3 of them were with nickel and only one of them with palladium. It is also interesting to note that none of them were synthesized using a polar source of H_2 but rather using H_2 directly, or by hydrolysis/hydrogenolysis of B-M/B-N bonds. It should also be pointed out that no cooperative catalytic hydrogenation or dehydrogenation were reported with any of these complexes.

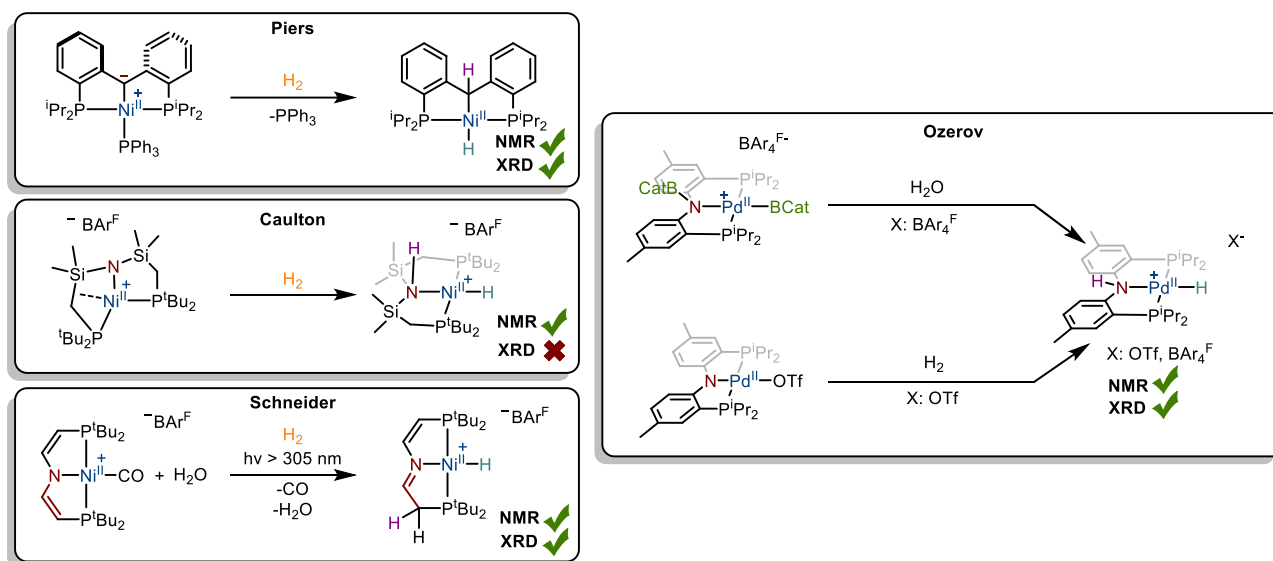
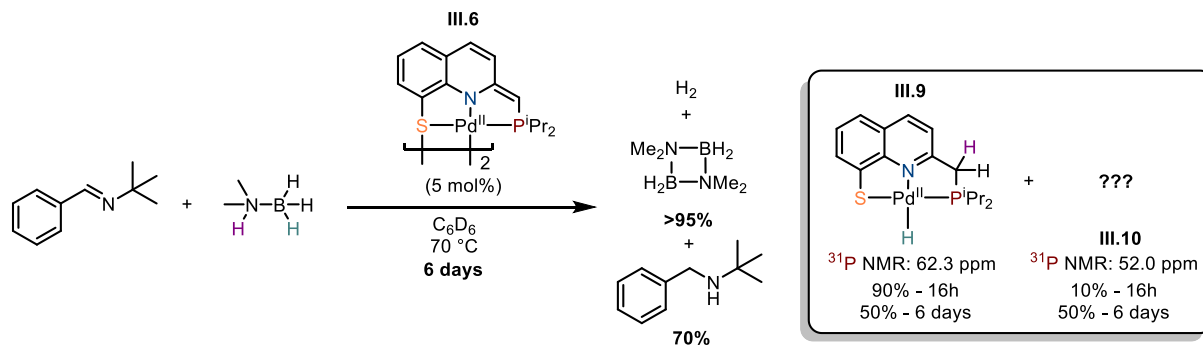


Figure III.10: Examples from the literature of pincer group 10 metal hydrides bearing an acidic proton at the ligand backbone

In our case, and with this well-behaved cooperative DMAB activation, the catalytic dehydrogenation was attempted at 5 mol% catalytic loading. After 16 h at 70 °C, H_2 was observed by ^1H NMR but only 16% of conversion into the dehydrogenated dimer was reached. ^{31}P NMR analysis showed the formation of two species: the “aromatized” Pd-H complex III.9 (90%) and an unidentified complex III.10 (10%). To promote the reaction, it was started again

in the presence of an imine as H₂ scavenger acceptor (Scheme III.17). The dehydrogenation was somewhat accelerated (reaching 40% conversion after 16 h at 70 °C) but still very sluggish and full conversion was only achieved after 6 days at 70 °C with 70% of incorporation of hydrogen at the imine acceptor.

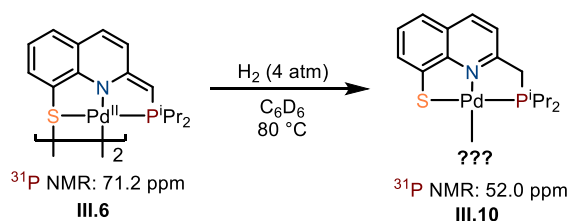


Scheme III.17: Catalytic dehydrogenation of DMAB by the dearomatized complex III.6 in presence of a H₂ acceptor

Compared to the literature, our system is extremely slow. Highly efficient and simple palladium complexes (such as [Pd(MeCN)₄][BF₄]₂) were reported to completely dehydrogenate DMAB in seconds at 25 °C with 3 mol% catalyst loading.^[25] Even if it would have been obviously nice to find an efficient catalyst for DMAB dehydrogenation, our approach was rather focused on a better understanding of the behavior of our system towards cooperative H₂ release.

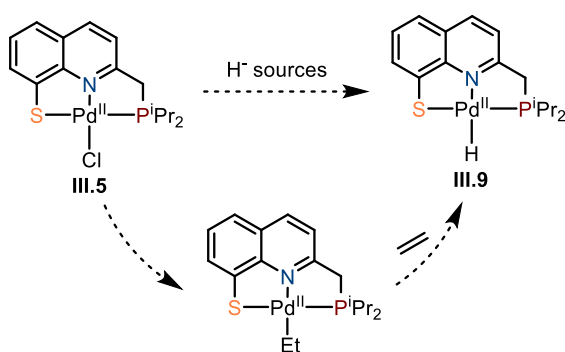
To this end, our idea was first to develop a preparative synthesis of the “aromatized” Pd^{II}-H III.9. Then, to test its ability to release H₂ and regenerate the “dearomatized” complex III.6 with, if needed, the help of additives such as H₂ acceptors, H-shuttling additives, *etc.*...

However, the stoichiometric reaction with DMAB (Scheme III.16) to generate III.9 was not very reproducible, and the yield was poor. The direct reaction of III.6 with H₂ was also attempted but directly evolved to III.10 with only traces of a hydride signal being formed after heating.



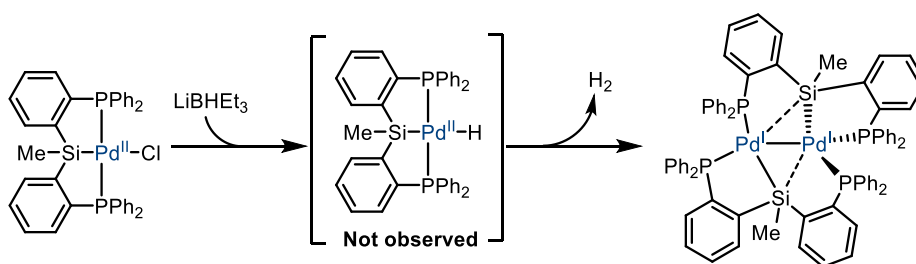
Scheme III.18: Direct reaction of the dearomatized complex III.6 with H₂

Treatment of the PNS-Pd-Cl **III.5** precursor with hydride sources was then considered as the synthesis would be more direct and proceed under milder conditions, maybe preventing the formation of **III.10**. The main challenge in this approach stems from the presence of an acidic proton at the CH₂ backbone. Indeed, basic hydride source such as LiBHEt₃ or LiAlH₄ were found incompatible, as deprotonation occurred. Promising results were obtained with NaBH₄ but evolution to **III.10** and isolation of solely **III.9** proved once again difficult. At this point, a preparative synthesis has not been achieved. Alternatively, the use of AlEt₃ could also be considered, with Cl to Et substitution at Pd in **III.5** followed by β-H elimination which may give **III.9**.



Scheme III.19: Planned synthesis of the Pd-H **III.9** with hydride sources

An explanation for the instability of the complex **III.9** and its evolution to **III.10** could be proposed based on the work of Hazari.^[26] Indeed, in the first chapter of this thesis, the formation of P^{Ph}SiP-Pd^{II}-H through transmetalation with LiBHEt₃ was reported to directly evolve to a Pd^I-Pd^I dimer with concomitant loss of H₂.



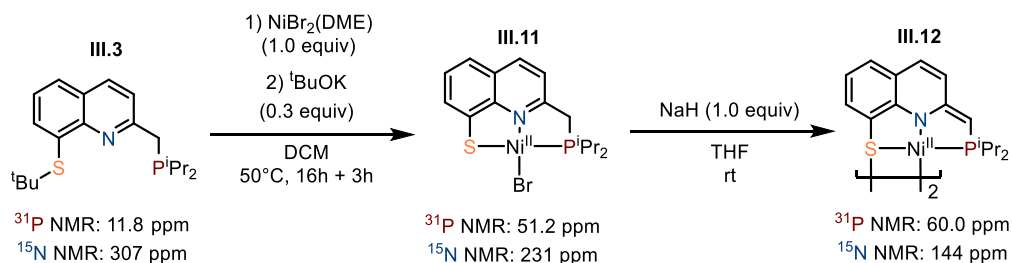
Scheme III.20: Formation of a dinuclear Pd^I dimer from transient (PSiP)-Pd^{II}-H complex as proposed by Hazari

This could also be the case in our complex, and further work is currently underway to authenticate complex **III.10** but unfortunately, as these lines are written the structure remains elusive.

III.4) Conclusion and perspectives:

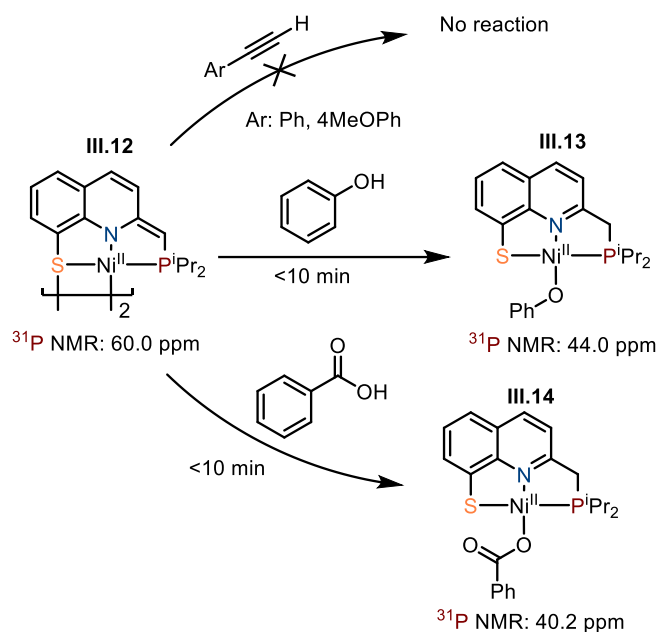
In this chapter, the efficient synthesis of a new non-innocent platform was achieved and a “dearomatized” complex could be simply generated by deprotonation. The cooperativity between the dearomatized backbone and the transition metal was unambiguously established by stoichiometric reactions. In this area, an interesting Pd^{II}-H complex was also formed upon reaction with DMAB. Unfortunately, due to the time constraints, the identification of evolution product **III.10** was not achieved and a preparative synthesis of the Pd^{II}-H complex **III.9** remains a bottleneck. Understanding the mechanisms of H₂ release from the Pd^{II}-H **III.9** to regenerate **III.6** is crucial to open the door for H-transfer reaction to be achieved efficiently with the dearomatized complex **III.6**. This is still a work in progress.

Another objective of our strategy with this ligand design was to extend the use of cooperative ligands to other metals. Thanks to Andras, a Master’s student in the group, the PNS-nickel-analog was synthesized (a first example of a nickel complex in the team! Scheme III.21). Overall, the synthesis follows a similar scheme with first, treatment of the ligand with a Ni^{II}-source followed by deprotection under basic conditions. Finally, the dearomatized complex was conveniently generated with NaH in THF.



Scheme III.21: Synthesis of the PNS-Ni-Br complex **III.11** and deprotonation to generate the dearomatized nickel dimer **III.12**

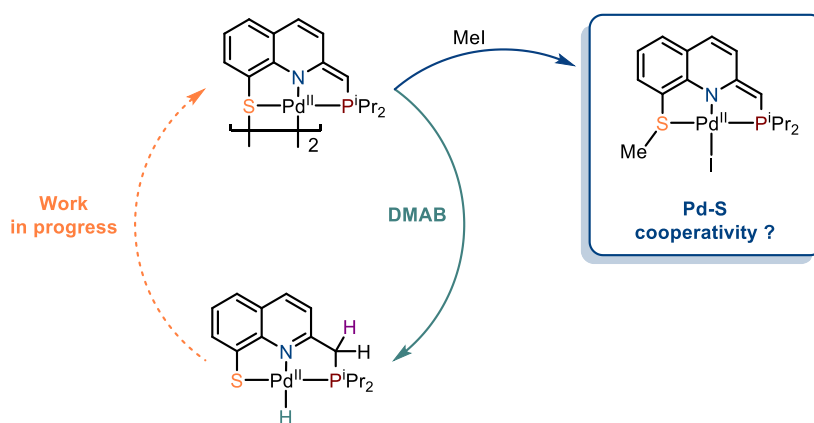
Contrary to the Pd^{II} analog, the deprotonated complex **III.12** was not active in the C-H activation of arylalkynes. However, the desired MLC reactivity was achieved with oxygen containing nucleophiles such as phenol and benzoic acid (Scheme III.22).



Scheme III.22: C-H activation with the dearomatized Nickel complex III.12

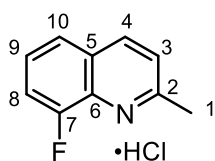
These results highlight the importance of tuning the metal to the desired reactivity. The comparison between the Pd and Ni system will be explored further.

A key feature of our ligand design was also highlighted upon reaction of the dearomatized complex III.6 with electrophiles. The nucleophilicity of the appended sulfur atom and its ability to act cooperatively with the metallic center will be discussed in the following chapter.



Scheme III.23: Challenges in closing the aromatization/dearomatization cycle and entry point to of Pd-S type cooperativity

III.5) Experimental Section

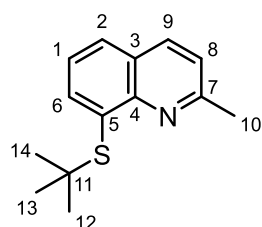
Synthesis of organic compounds and complexes:**8-fluoro-2-methyl-quinolin-1-ium chloride:**

Under air and without specific precautions, to stirred solution of 2-fluoroaniline (13.0 mL, 135 mmol, 1 eq) in toluene (180 mL) and 6M HCl (600 mL) was added crotonaldehyde (22.6 mL, 270 mmol, 2 eq). The reaction was equipped with a condenser and heated at reflux for two hours. After full conversion was observed by TLC, the reaction was allowed to cool down to room temperature. 6M NaOH was then added carefully until a pH of ~10 was reached. The aqueous phase was then extracted with DCM and the organic phases were combined and dried over Na₂SO₄. The solvent was removed *in vacuo* and the resulting crude mixture was retaken in Et₂O. HCl gas was then bubbled through the stirred Et₂O solution until the precipitate stops forming. The solid was filtered, washed with Et₂O and recrystallized from chloroform to yield pure 8-fluoro-2-methyl-quinolin-1-ium chloride (13.0 g, 49%).

¹H NMR (500 MHz, CD₂Cl₂): δ = 8.73 (dd, *J* = 8.6, 1.7 Hz, 1H, H₄), 7.92-7.89 (m, 1H, H₁₀), 7.82-7.75 (m, 2H, H_{8,9}), 7.77 (d, *J* = 8.6 Hz, 1H, H₃), 3.44 (s, 3H, H₁).

¹³C{¹H} NMR (126 MHz, CD₂Cl₂): δ = 160.9 (C₂), 153.3 (d, *J* = 263.0 Hz, C₇), 145.0 (d, *J* = 2.4 Hz) (C₄), 129.9 (d, *J* = 6.5 Hz, C₉), 129.0 (d, *J* = 1.9 Hz, C₅), 128.5 (d, *J* = 14.5 Hz, C₆), 125.4 (C₃), 124.6 (d, *J* = 4.8 Hz, C₁₀), 119.2 (d, *J* = 16.7 Hz, C₈), 21.3 (C₁).

HRMS (ESI) *m/z*: calculated: 162.0719 (C₁₀H₉NF), measured: 162.0721 (M-Cl⁻)

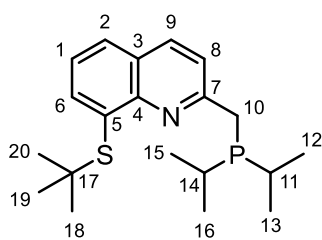
8-tert-butylsulfanyl-2-methyl-quinoline - CAS [653570-21-9]:

To a suspension of NaH (4.74 g, 197 mmol, 3.0 equiv) in DMF (500 mL) was dropwise added 2-methylpropane thiol (14.8 mL, 131.6 mmol, 2.0 equiv). Then quinoline hydrochloride (13.0 g, 65.78 mmol, 1.0 equiv) was slowly added and the mixture was heated to reflux overnight. The conversion was monitored via ¹⁹F NMR and after full conversion was reached, the DMF was removed *via* trap-to-trap distillation. The resulting crude was retaken in EtOAc (150 mL) and washed 3 times with water (30 mL). The organic phase was then dried with Na₂SO₄ and the solvent was removed *in vacuo* to give the pure product as a brown solid (13.5 g, 89%).

¹H NMR (500 MHz, CDCl₃): δ = 7.97–8.06 (m, 2H, H_{9,6}), 7.73 (d, *J* = 8.0 Hz, 1H, H₂), 7.41 (dd, *J* = 7.7, 7.8, 1H, H₈), 7.29 (d, *J* = 8.0, 1H, H₁), 2.79 (s, 3H, H₁₀), 1.38 (s, 9H, H₁₂₋₁₄).

¹³C{¹H} NMR (126 MHz, CDCl₃): δ = 158.7 (C₇), 148.3 (C₄), 137.6 (C₆), 136.0 (C₉), 132.7 (C₅), 128.0 (C₂), 126.5 (C₃), 124.5 (C₈), 121.6 (C₁), 46.4 (C₁₁), 30.9 (C₁₂₋₁₄), 25.1 (C₁₀).

Spectroscopic data in accordance with literature.^[27]

(8-tert-butylsulfanyl-2-quinolyl)methyl-diisopropyl-phosphane - III.3:

To a stirring solution at $-78\text{ }^{\circ}\text{C}$ of dry and distilled diisopropylamine (9.14 mL, 64.8 mmol, 3.0 equiv) in THF (250 mL) was dropwise added 2.5 M *n*-BuLi solution (25.9 mL, 64.8 mmol, 3.0 equiv) and the reaction was stirred for about 15 minutes. A solution of 8-tert-butylsulfanyl-2-methyl-quinoline (5.0 g, 21.6 mmol, 1.0 equiv) in THF (50 mL) was then dropwise added to the clear stirring solution of LDA and the mixture immediately turns deep red. After 1 hour of stirring, diisopropyl phosphine chloride (3.4 mL, 21.6 mmol, 1.0 equiv) was added and the mixture was allowed to warm up to room temperature. Complete conversion was monitored by ^{31}P NMR, and the solvent was removed *in vacuo*. The residue was then retaken in Et₂O (50 mL) and washed 3 times with 10% w/w KH₂PO₄ solution (30 mL). The organic phase was dried over Na₂SO₄, filtered and the solvent was removed *in vacuo* to give the pure product **III.3** as a viscous oil (6.66 g, 90 %).

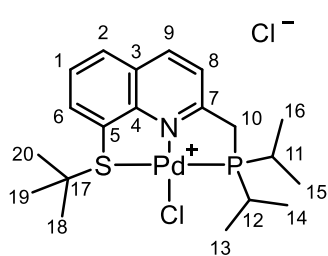
^1H NMR (500 MHz, CDCl₃): δ = 8.04 (d, J = 8.4 Hz, 1H, H₉), 7.99 (dd, J = 7.2, 1.5 Hz, 1H, H₆), 7.75 (dd, J = 8.1, 1.5 Hz, 1H, H₂), 7.55 (d, J = 8.4 Hz, 1H, H₈), 7.42 (pt, 1H, H₁), 3.27 (d, $J_{\text{H-P}}$ = 2.8 Hz, 1H, H₁₀), 1.90 (heptd, $J_{\text{H-H}}$ = 7.1, $J_{\text{H-P}}$ = 2.0 Hz, 2H, H_{11,14}), 1.39 (s, 9H, H₁₈₋₂₀), 1.15 – 1.03 (m, 12H, H_{12,13,15,16}).

$^{13}\text{C}\{^1\text{H}\}$ NMR (126 MHz, CDCl₃): δ = 161.5 (d, $J_{\text{C-P}}$ = 9.7 Hz, C₇), 149.0 (C₄), 138.4 (C₆), 136.3 (C₉), 133.2 (C₅), 128.7 (C₂), 127.2 (C₃), 125.0 (C₁), 122.2 (d, $J_{\text{C-P}}$ = 8.1 Hz, C₈), 46.8 (C₁₇), 34.3 (d, $J_{\text{C-P}}$ = 21.7 Hz, C₁₀), 31.5 (C₁₈₋₂₁), 23.7 (d, $J_{\text{C-P}}$ = 13.6 Hz, C_{11,14}), 19.8 (d, $J_{\text{C-P}}$ = 14.7 Hz, C₁₂₋₁₆), 19.2 (d, $J_{\text{C-P}}$ = 10.3 Hz, C₁₂₋₁₆)

$^{31}\text{P}\{^1\text{H}\}$ NMR (202 MHz, CDCl₃): δ = 11.8 (s).

^{15}N NMR (51 MHz, CDCl₃): δ = 307 (s).

HRMS (DCI-CH₄) m/z : calculated: 347.1843 (C₂₀H₃₀NPS), measured: 347.1840.

PNS^tBu-Pd-Cl - III.4:

Notes: Commercial [PdCl₂(PhCN)₂] was washed with Et₂O prior to use; The exclusive formation of **III.4** (³¹P NMR: 83.7 ppm) was usually observed but in some cases (especially on hot days) some amount of **III.5** (³¹P NMR: 59.2 ppm) was detected. Removal of **III.5** from **III.4** could be achieved by washing with acetone but is not a requirement for the next step.

To a stirred suspension of [PdCl₂(PhCN)₂] (1.623 g, 4.231 mmol, 1.0 equiv) in DCM (200 mL) was dropwise added over 30 minutes a solution of **III.3** (1.5 g, 4.316 mmol, 1.02 equiv) in DCM (20 mL). After 30 minutes, the resulting clear solution was analysed by ³¹P NMR. After complete conversion was observed, the solution was concentrated to about 30 mL and dropwise added to a vigorously stirred solution of pentane (400 mL). The resulting yellow solid was then washed 2 times with pentane (20 mL) and dried *in vacuo* to yield pure **III.4** (2.11 g, 95%).

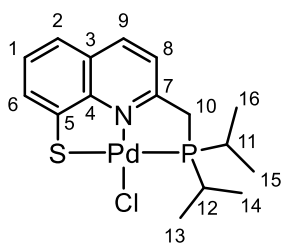
¹H NMR (500 MHz, CDCl₃): δ = 8.81 (d, *J* = 8.3 Hz, 1H, H₈), 8.67 (d, *J* = 8.3 Hz, 1H, H₉), 8.23 (dd, *J* = 8.1, 0.9 Hz, 1H, H₂), 8.05 (dd, *J* = 7.4, 0.9 Hz, 1H, H₆), 7.79 (pt, 1H, H₁), 5.07 (d, *J*_{H-P} = 11.3 Hz, 2H, H₁₀), 2.83-2.71 (m, 2H, H_{11,12}), 1.60 (s, 9H, H₁₈₋₂₀), 1.54 (dd, *J*_{H-P} = 19.3, *J*_{H-H} = 7.0 Hz, 6H, H₁₃₋₁₆), 1.40 (dd, *J*_{H-P} = 17.8, *J*_{H-H} = 6.8 Hz, 6H, H₁₃₋₁₆).

¹³C{¹H} NMR (126 MHz, CDCl₃): δ = 168.9 (d, *J*_{C-P} = 2.6 Hz, C₇), 150.4 (C₄), 141.4 (C₉), 140.4 (d, *J*_{C-P} = 2.6 Hz, C₆), 132.3 (C₂), 129.8 (C₅), 127.9 (C₁), 127.6 (d, *J*_{C-P} = 2.3 Hz, C₄), 124.9 (d, *J*_{C-P} = 12.9 Hz, C₈), 60.3 (C₁₇), 39.1 (d, *J*_{C-P} = 27.0 Hz, C₁₀), 31.1 (C₁₈₋₂₀), 26.07 (d, *J*_{C-P} = 26.6 Hz, C_{11,12}), 18.3 (C₁₃₋₁₆), 17.9 (C₁₃₋₁₆).

³¹P{¹H} NMR (202 MHz, CDCl₃): δ = 83.7 (s).

¹⁵N NMR (51 MHz, CDCl₃): δ = 227 (s).

HRMS (ESI+) *m/z*: calculated: 490.0557 (C₂₀H₃₀ClNPPdS), found: 490.0556.

PNS-Pd-Cl - III.5:

In a sealed ace-tube in the glovebox were added **III.5** (1g, 1.905 mmol, 1.0 equiv), tBuOK (214 mg, 1.905 mg, 1.0 equiv) and DCM (80 mL). The resulting suspension was taken out of the glovebox, stirred, and heated at 75°C for 7h. After complete conversion was indicated by ^{31}P NMR, the reaction was allowed to cool down to room temperature. The solution was filtered, concentrated to around 10 mL and dropwise added to a stirred solution of pentane (60 mL). The

resulting solid was then washed two times with pentane (10 mL) and dried *in vacuo* to yield **III.5** as a yellow solid (752 mg, 92%).

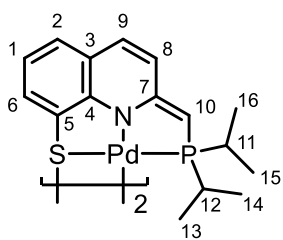
^1H NMR (500 MHz, CD_2Cl_2): δ = 8.28 (dd, J = 8.5, 1.1 Hz, 1H, H₉), 7.76 (dd, J = 5.3, 3.3 Hz, 1H, H₆), 7.58 (d, J = 8.5 Hz, 1H, H₈), 7.45-7.38 (m, 2H, H_{1,2}), 3.77 (d, $J_{\text{H-P}}$ = 10.5 Hz, 2H, H₁₀), 2.52 (dhept, $J_{\text{H-P}}$ = 10.8, $J_{\text{H-H}}$ = 7.1 Hz, 2H, H_{11,12}), 1.47 (dd, $J_{\text{H-P}}$ = 18.2, $J_{\text{H-H}}$ = 7.1 Hz, 6H, H_{13,14}), 1.26 (dd, $J_{\text{H-P}}$ = 15.8, $J_{\text{H-H}}$ = 7.0 Hz, 6H, H_{15,16}).

$^{13}\text{C}\{^1\text{H}\}$ NMR (126 MHz, CDCl_3): δ = 162.6 (d, $J_{\text{C-P}}$ = 6.9 Hz, C₇), 151.6 (d, $J_{\text{C-P}}$ = 4.0 Hz, C₅), 150.6 (d, $J_{\text{C-P}}$ = 3.4 Hz, C₄), 140.7 (C₉), 132.5 (d, $J_{\text{C-P}}$ = 6.4 Hz, C₆), 129.5 (C₃), 128.3 (d, $J_{\text{C-P}}$ = 1.3 Hz, C₁), 120.8 (C₂), 120.1 (d, $J_{\text{C-P}}$ = 12.4 Hz, C₈), 36.9 (d, $J_{\text{C-P}}$ = 22.5 Hz, C₁₀), 24.7 (d, $J_{\text{C-P}}$ = 22.6 Hz, C_{11,12}), 18.3 (d, $J_{\text{C-P}}$ = 3.5 Hz, C₁₃₋₁₆), 17.7 (d, $J_{\text{C-P}}$ = 1.4 Hz, C₁₃₋₁₆).

$^{31}\text{P}\{^1\text{H}\}$ NMR (202 MHz, CDCl_3): δ = 58.5 (s).

^{15}N NMR (51 MHz, CDCl_3): δ = 233 (s).

HRMS (ESI+) m/z : calculated: 433.9930 (C₁₆H₂₁ClNPPdS), found: 433.9933.

[PNS-Pd]₂ - III.6:

To a stirred suspension of **III.5** (400 mg, 0.92 mmol, 1.0 equiv) at -78 °C in THF (40 mL) was dropwise added ^tBuOK (104 mg, 0.92 mmol, 1.0 equiv) as solution in THF (10 mL). Upon addition the mixture immediately turns deep red, and the reaction was allowed to warm-up to room temperature. Upon warming up, a transition to a deep green was observed and complete conversion was monitored by ³¹P NMR. The solution was then concentrated to a few mL and DCM was added. The resulting suspension was filtered, and the volatiles were removed *in vacuo* to yield pure **III.6** as a very dark solid (309 mg, 85%)

Note: If the reaction was not worked-up quickly enough, another signal at 68.2 ppm can be observed.

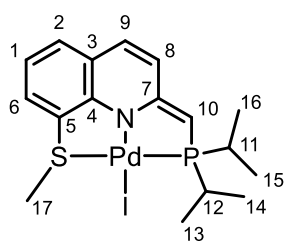
¹H NMR (500 MHz, CD₂Cl₂): δ = 7.28 (dd, *J* = 7.6, 1.3 Hz, 2H, H₆), 6.95 (dd, *J* = 7.5, 1.3 Hz, 2H, H₂), 6.79 (dd, *J* = 9.2, 2.2 Hz, 2H, H₉), 6.60 (pt, 2H, H₁), 6.51 (d, *J* = 9.2 Hz, 2H, H₈), 3.27 (d, *J*_{H-P} = 3.9 Hz, 2H, H₁₀), 1.88 (dhept, *J*_{H-P} = 20.9, *J*_{H-H} 6.9 Hz, 2H, H₁₁), 1.42 (dd, *J*_{H-P} = 11.8, *J*_{H-H} = 6.3 Hz, 6H, H₁₅), 1.39 (dd, *J*_{H-P} = 10.9, *J*_{H-H} = 6.3 Hz, 6H, H₁₆), 1.30-1.21 (m, 2H, H₁₂), 0.86 (dd, *J*_{H-P} = 12.9, *J*_{H-H} = 7.0 Hz, 6H, H₁₃), 0.63 (dd, *J*_{H-P} = 19.2, *J*_{H-H} 7.0 Hz, 6H, H₁₄).

¹³C{¹H} NMR (126 MHz, CDCl₃): δ = 168.3 (d, *J*_{C-P} = 16.2 Hz, C₇), 158.2 (C₄), 136.2-136.1 (m, C₆), 131.2 (C₉), 126.3 (C₂), 123.3 (C₃), 121.3 (C₅), 120.8-120.4 (m, C₈), 118.0 (C₁), 67.6 (d, *J*_{C-P} = 57.5 Hz, C₁₀), 27.6-27.1 (m, C₁₁), 22.9-22.4 (m, C₁₂), 19.6-19.4 (m, C₁₅), 19.0-18.9 (m, C₁₆), 18.2-18.1 (m, C₁₃), 16.1-16.0 (m, C₁₄)

³¹P{¹H} NMR (202 MHz, CDCl₃): δ = 71.3 (s).

¹⁵N NMR (51 MHz, CDCl₃): δ = 162 (s).

HRMS (ESI+) *m/z*: calculated: 793.0272 (C₃₂H₄₁N₂P₂S₂Pd₂), found: 793.0288

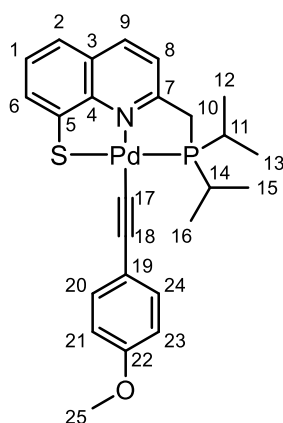
PNS^{Me}-Pd-I - III.7:

To a stirred solution of **III.6** (94mg, 0.231 mmol, 1.0 equiv) in THF at -78°C was added MeI (66 mg, 0.462 mmol, 2.0 equiv) as solution in THF (150 μL). The reaction was allowed to warm up to room temperature and then heated to 50°C for 1h. Complete conversion was observed by ^{31}P NMR, and the volatiles were removed *in vacuo* to yield the corresponding complex **III.7** as a red solid.

^1H NMR (500 MHz, C_6D_6): δ = 6.70-6.66 (m, 2H, H_{6,2}), 6.52-6.42 (m, 2H, H_{8,9}), 6.38 (pt, 1H, H₁), 3.19 (d, $J_{\text{H-P}}$ = 4.5 Hz, 1H, H₁₀), 2.25 (d, $J_{\text{H-P}}$ = 3.3 Hz, 1H, H₁₇), 2.16-2.05 (m, 2H, H_{11,12}), 1.41 (dd, $J_{\text{H-P}}$ = 18.1, $J_{\text{H-H}}$ = 7.0 Hz, 6H, H₁₃₋₁₆), 1.06 (dd, $J_{\text{H-P}}$ = 16.1, $J_{\text{H-H}}$ = 7.0 Hz, 6H, H₁₃₋₁₆).

$^{13}\text{C}\{^1\text{H}\}$ NMR (126 MHz, C_6D_6): δ = 167.4 (d, $J_{\text{C-P}}$ = 15.3 Hz, C₇), 153.6 (C₄), 134.2 (d, $J_{\text{C-P}}$ = 2.7 Hz, C₆), 130.7 (C₉), 123.0 (d, $J_{\text{C-P}}$ = 2.7 Hz, C₅), 122.9 (C₃), 120.8 (d, $J_{\text{C-P}}$ = 21.3 Hz, C₈), 118.8 (C₁), 68.7 (d, $J_{\text{C-P}}$ = 55.5 Hz, C₁₀), 27.6 (d, $J_{\text{C-P}}$ = 32.8 Hz, C_{12,11}), 24.3 (d, $J_{\text{C-P}}$ = 2.1 Hz, C₁₇), 19.26 (d, $J_{\text{C-P}}$ = 2.3 Hz, C₁₃₋₁₆), 17.50 (d, $J_{\text{C-P}}$ = 1.5 Hz, C₁₃₋₁₆).

$^{31}\text{P}\{^1\text{H}\}$ NMR (121 MHz, CD_2Cl_2): δ = 83.4 (s).

Palladium alkynyl complex - III.8:

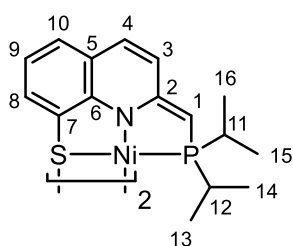
A J-young NMR tube was charged with **III.6** (14 mg, 0.035 mmol, 1.0 equiv) and *p*MeO-PhCCH (14 mg, 0.106 mmol, 3.0 equiv) in 0.6 mL of CD_2Cl_2 . The resulting dark green solution was heated to 70°C and the reaction was monitored by ^{31}P and ^1H NMR. Full conversion was achieved after 10h and a clear, deep red solution was obtained. The solution was then dropwise added to a stirred solution of pentane (5 mL) and a red precipitate was formed. The solid was then washed with pentane (2x3 mL) and dried *in vacuo*, to yield the pure complex as a red solid (13 mg, 70% Yield). Single crystals were grown by pentane layering over a concentrated DCM solution.

^1H NMR (500 MHz, CD_2Cl_2): δ = 8.28 (dd, J = 8.5, 1.1 Hz, 1H, H₉), 7.89-7.84 (dd, J = 5.8, 2.8 Hz, 1H, H₆), 7.57 (d, J = 8.5 Hz, 1H, H₈), 7.44-7.40 (m, 2H, H_{1,2}), 7.28-7.22 (m, 2H, H_{24,20}), 6.81-6.75 (m, 2H, H_{21,23}), 3.83 (d, $J_{\text{H-P}}$ = 9.9 Hz, 2H, H₁₀), 3.77 (s, 3H, H₂₅), 2.52 (dhept, $J_{\text{H-P}}$ = 9.9, $J_{\text{H-H}}$ = 7.0 Hz, 2H, H_{14,11}), 1.50 (dd, $J_{\text{H-P}}$ = 18.2, $J_{\text{H-H}}$ = 7.1 Hz, 6H, H_{12,13,15,16}), 1.26 (dd, $J_{\text{H-P}}$ = 15.9, $J_{\text{H-H}}$ = 7.0 Hz, 6H, H_{12,13,15,16}).

$^{13}\text{C}\{^1\text{H}\}$ NMR (126 MHz, CD_2Cl_2): δ = 161.1 (d, $J_{\text{C-P}}$ = 6.5 Hz, C₇), 158.1 (C₁₉), 153.8 (d, $J_{\text{C-P}}$ = 3.5 Hz, C₅), 149.2 (d, $J_{\text{C-P}}$ = 3.7 Hz, C₄), 140.3 (C₉), 133.1 (d, $J_{\text{C-P}}$ = 6.5 Hz, C₆), 132.5 (C_{20,24}), 129.2 (C₃), 128.1 (d, $J_{\text{C-P}}$ = 1.2 Hz, C₁), 120.9 (C₁₉), 120.3 (C₂), 119.7 (d, J = 11.9 Hz, C₈), 113.8 (C_{22,23}), 112.1 (d, $J_{\text{C-P}}$ = 4.6 Hz, C₁₈), 86.9 (d, $J_{\text{C-P}}$ = 19.7 Hz, C₁₇), 55.6 (C₂₅), 37.9 (d, $J_{\text{C-P}}$ = 20.8 Hz, C₁₀), 25.1 (d, $J_{\text{C-P}}$ = 25.2 Hz, C_{11,14}), 18.7 (d, $J_{\text{C-P}}$ = 3.7 Hz, C_{12,13,15,16}), 18.0-17.9 (m, C_{12,13,15,16}).

$^{31}\text{P}\{^1\text{H}\}$ NMR (202 MHz, CD_2Cl_2): δ = 59.2 (s).

^{15}N NMR (51 MHz, CD_2Cl_2): δ = 251.6 (s).

[PNS-Ni]₂ - III.12:

To a stirring suspension of NaH (18.4 mg, 0.768 mmol, 1 equiv) in THF (10 mL) was dropwise added a solution of the complex **III.11** (330 mg, 0.768 mmol, 1 equiv) in THF (10 mL). The mixture was then stirred for one hour and the conversion was monitored by ³¹P NMR. After reaching full conversion, the solvent was removed *in vacuo* and the residue was dissolved in pentane. The salts were removed by filtration and the solvent was evaporated to yield the pure product

III.12 (262 mg, 98 %).

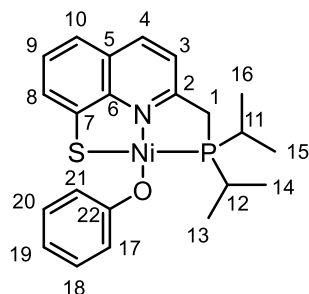
¹H NMR (500 MHz, CD₂Cl₂): δ = 7.20 (dd, *J* = 7.6, 1.3 Hz, 2H, H₈), 6.92 (dd, *J* = 7.4, 1.3 Hz, 2H, H₁₀), 6.74 (dd, *J* = 9.2, 2.1 Hz, 2H, H₄), 6.53 (pt, 2H, H₉), 6.42 (d, *J* = 9.2 Hz, 2H, H₃), 3.41 (d, *J*_{H-P} = 2.0 Hz, 2H, H₁), 1.87 (dhept, *J*_{H-P} = 13.8, *J*_{H-H} = 7.0 Hz, 2H, H₁₂), 1.65 (dd, *J*_{H-P} = 16.5, *J*_{H-H} = 7.0 Hz, 6H, H₁₃), 1.54 (dd, *J*_{H-P} = 16.6, *J*_{H-H} = 7.0 Hz, 6H, H₁₄), 1.11 – 1.05 (m, 2H, H₁₁), 1.03 (dd, *J*_{H-P} = 18.6, *J*_{H-H} = 6.2 Hz, 6H, H₁₅), 0.91 (dd, *J*_{H-P} = 12.0, *J*_{H-H} = 6.6 Hz, 6H, H₁₆).

¹³C{¹H} NMR (126 MHz, CD₂Cl₂): δ = 168.13 – 167.74 (m, C₂), 158.64 – 158.31 (m, C₆), 133.6 (C₈), 130.4 (C₄), 125.5 (C₁₀), 122.6 (C₅), 120.5–120.1 (m, C₃), 119.1 (C₇), 117.0 (C₉), 68.7 (d, C₁), 27 – 26.6 (m, C_{11,12}), 21.7 – 21.3 (m, C_{11,12}), 19.6–19.4 (m, C₁₃₋₁₆), 18.6–18.5 (m, C₁₃₋₁₆), 18.2–18.1 (m, C₁₃₋₁₆), 16.1–15.9 (m, C₁₃₋₁₆).

³¹P{¹H} NMR (202 MHz, CD₂Cl₂) δ = 60.0 (s).

¹⁵N NMR (51 MHz, CD₂Cl₂): 144.6 (s).

HRMS (DCI-CH₄) *m/z*: 694.1130 (C₃₂H₄₀N₂Ni₂P₂S₂), measured: 694.1128

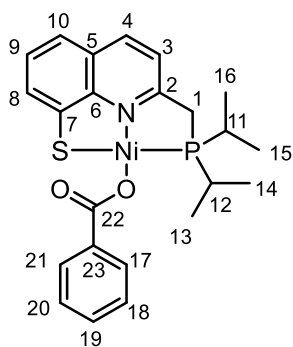
[PNS-Ni-OPh] - III.13:

In a pressure NMR tube **III.12** (20 mg, 0.0287 mmol, 1 eq) and phenol (5.4 mg, 0.0575 mmol, 2.0 eq) were dissolved in 0.7 mL CDCl₃. No isolated yield.

¹H NMR (500 MHz, CD₂Cl₂): δ = 8.13 (d, *J* = 8.4 Hz, 1H, H₄), 7.68 (d, *J* = 7.4, 1H, H₈), 7.37 (pt, 1H, H₉), 7.31 (d, *J* = 7.3 Hz, 1H, H₁₀), 7.28 (d, *J* = 8.4 Hz, 1H, H₃), 7.24 – 7.19 (m, 2H, H_{17,21}), 7.00 – 6.93 (m, 2H, H_{18,20}), 6.47 – 6.40 (m, 1H, H₁₉), 3.39 (d, *J*_{H-P} = 9.8 Hz, 2H, H₁), 2.27 – 2.15 (m, 2H, H_{11,12}), 1.52 – 1.41 (m, 12H, H₁₃₋₁₆).

¹³C{¹H} NMR (126 MHz, CD₂Cl₂): δ = 166.1 (C₂₂), 163.5 (d, *J*_{C-P} = 9.3 Hz, C₂), 150.3 (d, *J*_{C-P} = 6.6 Hz, C₆), 149.7 (d, *J*_{C-P} = 2.4 Hz, C₇), 139.6 (C₄), 129.6 (d, *J*_{C-P} = 4.3 Hz, C₈), 128.5 (C_{20,18}), 128.4 (C₅), 128.2 (C₉), 121.7 (C_{17,21}), 120.3 (d, *J*_{C-P} = 10.1 Hz, C₃), 120.2 (C₁₀), 114.3 (C₁₉), 32.9 (d, *J*_{C-P} = 21.0 Hz, C₁), 23.3 (d, *J*_{C-P} = 20.5 Hz, C_{11,12}), 18.02 (d, *J*_{C-P} = 3.6 Hz, C₁₃₋₁₆), 17.63 (d, *J*_{C-P} = 1.3 Hz, C₁₃₋₁₆).

³¹P{¹H} NMR (202 MHz, CD₂Cl₂) δ = 44.0 (s).

[PNS-Ni-OOCPh] - III.14:

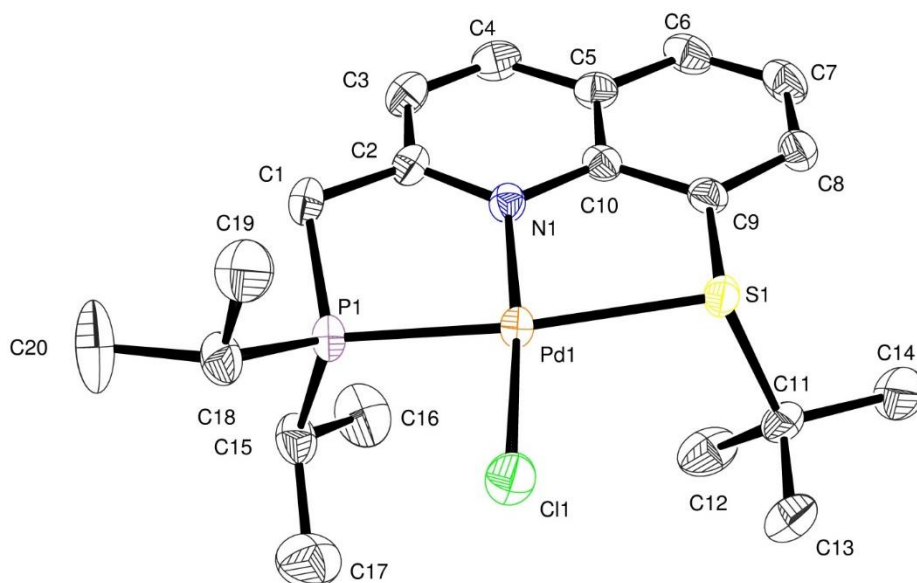
In a pressure NMR tube **III.12** (20 mg, 0.0287 mmol, 1 eq) and benzoic acid (7 mg, 0.0575 mmol, 2.0 eq) were dissolved in 0.7 mL CDCl₃. No isolated yield.

¹H NMR (500 MHz, CD₂Cl₂): δ = 8.18 (d, *J* = 8.3 Hz, 1H, H₄), 7.95-7.80 (br m, 2H, H_{17,21}), 7.80 – 7.65 (m, 1H, H₈), 7.53 – 7.25 (m, 6H, H_{3,9,10,18-20}), 3.49 (d, *J*_{H-P} = 9.9 Hz, 2H, H₁), 2.39 (m, 2H, H_{11,12}), 1.55 (dd, *J*_{H-P} = 17.4, *J*_{H-H} = 7.1 Hz, 6H, H_{13,14}), 1.49 (dd, *J*_{H-P} = 15.0, *J*_{H-H} = 6.9 Hz, 6H, H_{15,16}).

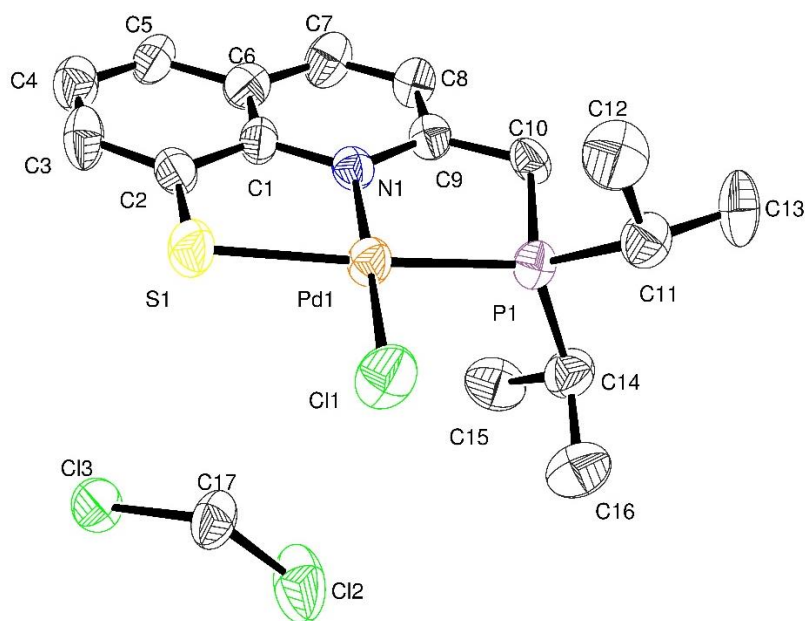
¹³C{¹H} NMR (126 MHz, CD₂Cl₂): δ = 171.6 (C₂₂), 163.7 (d, *J* = 9.1 Hz, C₂), 150.6 (d, *J* = 6.2 Hz, C₆) 149.1 (C₇), 139.9 (C₄), 134.9 (bs, C₂₃), 130.1

(bs, C₁₉), 129.2 (bs, C_{17,21}), 129.1 (d, *J*_{C-P} = 3.9 Hz, C₈), 128.0 (C₅), 127.9 (C₉), 127.5 (bs, C_{18,20}), 119.9 (C₁₀), 119.8 (d, *J* = 10.2 Hz, C₃), 32.6 (d, *J* = 21.6 Hz, C₁) 23.7 (d, *J* = 20.5 Hz, C_{11,12}), 18.01 (d, *J* = 3.4 Hz, C₁₃₋₁₆) 17.3 (C₁₃₋₁₆)

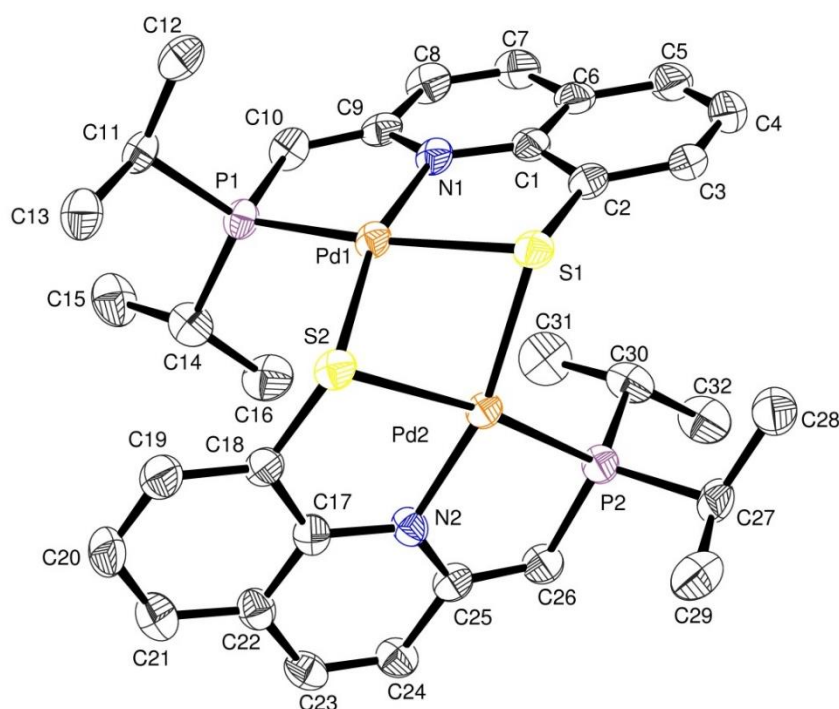
³¹P{¹H} NMR (202 MHz, CD₂Cl₂) δ = 40.2 (s).

Crystallographic Data***PNS^{tBu}-Pd-Cl - III.4***

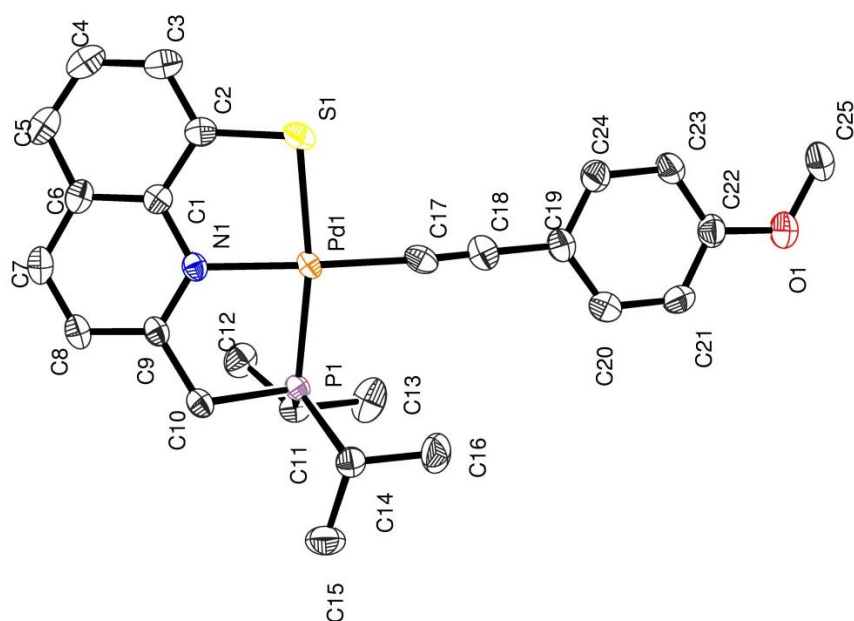
Identification code	AC190620
Empirical formula	C ₂₀ H ₃₀ Cl N P Pd S, C H ₂ Cl ₂ , Cl
Formula weight	609.71
Temperature	193(2) K
Wavelength	0.71073 Å
Crystal system, space group	Monoclinic, P 2 ₁ /c
Unit cell dimensions	a = 13.3230(10) Å alpha = 90 deg. b = 12.3014(9) Å beta = 91.613(2) deg. c = 16.0219(12) Å gamma = 90 deg.
Volume	2624.8(3) Å ³
Z, Calculated density	4, 1.543 Mg/m ³
Absorption coefficient	1.264 mm ⁻¹
F (000)	1240
Crystal size	0.18 x 0.04 x 0.02 mm
Theta range for data collection	5.139 to 27.103 deg.
Limiting indices	-17 ≤ h ≤ 17, -15 ≤ k ≤ 15, -20 ≤ l ≤ 20
Reflections collected / unique	79710 / 5751 [R(int) = 0.0678]
Completeness to theta = 25.242	99.1 %
Refinement method	Full-matrix least-squares on F ²
Data / restraints / parameters	5751 / 0 / 269
Goodness-of-fit on F ²	1.034
Final R indices [I > 2σ(I)]	R1 = 0.0305, wR2 = 0.0639
R indices (all data)	R1 = 0.0442, wR2 = 0.0711
Largest diff. peak and hole	1.570 and -1.082 e.Å ⁻³

PNS-Pd-Cl - III.5

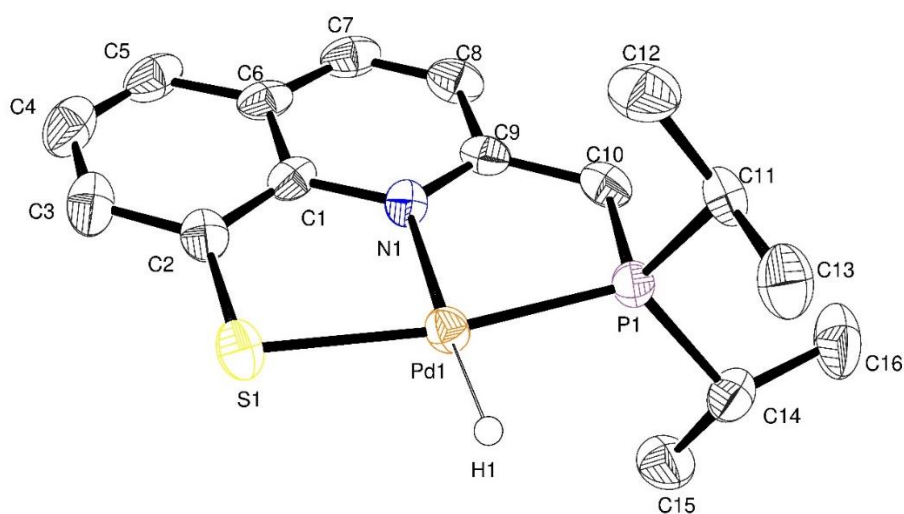
Identification code	AC250920
Empirical formula	C ₁₆ H ₂₁ Cl ₂ N ₁ P ₁ Pd ₁ S ₁ , 0.5(C ₂ H ₂ Cl ₂)
Formula weight	474.68
Temperature	193(2) K
Wavelength	1.54178 Å
Crystal system, space group	Monoclinic, P 2 ₁ /n
Unit cell dimensions	a = 8.0265(3) Å alpha = 90 deg. b = 22.9092(9) Å beta = 90.036(2) deg. c = 11.1739(4) Å gamma = 90 deg.
Volume	2054.66(13) Å ³
Z, Calculated density	4, 1.535 Mg/m ³
Absorption coefficient	11.330 mm ⁻¹
F(000)	956
Crystal size	0.100 x 0.080 x 0.060 mm
Theta range for data collection	1.928 to 68.332 deg.
Limiting indices	-9 ≤ h ≤ 9, -26 ≤ k ≤ 27, -13 ≤ l ≤ 12
Reflections collected / unique	19185 / 3777 [R(int) = 0.0619]
Completeness to theta = 67.679	99.9 %
Refinement method	Full-matrix least-squares on F ²
Data / restraints / parameters	3777 / 15 / 223
Goodness-of-fit on F ²	1.117
Final R indices [I > 2σ(I)]	R1 = 0.0741, wR2 = 0.2108
R indices (all data)	R1 = 0.0819, wR2 = 0.2163
Largest diff. peak and hole	3.775 and -0.836 e.Å ⁻³

[PNS-Pd]₂ - III.6

Identification code	AC040321
Empirical formula	C ₃₂ H ₄₀ N ₂ P ₂ Pd ₂ S ₂
Formula weight	791.52
Temperature	193(2) K
Wavelength	0.71073 Å
Crystal system, space group	Monoclinic, P 2 ₁ /n
Unit cell dimensions	a = 8.6930(10) Å alpha = 90 deg. b = 16.625(2) Å beta = 92.641(4) deg. c = 22.513(3) Å gamma = 90 deg.
Volume	3250.2(7) Å ³
Z, Calculated density	4, 1.618 Mg/m ³
Absorption coefficient	1.358 mm ⁻¹
F (000)	1600
Crystal size	0.100 x 0.080 x 0.040 mm
Theta range for data collection	3.146 to 23.857 deg.
Limiting indices	-9<=h<=9, -18<=k<=18, -25<=l<=25
Reflections collected / unique	88232 / 4759 [R(int) = 0.0939]
Completeness to theta = 23.857	95.1 %
Refinement method	Full-matrix least-squares on F ²
Data / restraints / parameters	4759 / 0 / 369
Goodness-of-fit on F ²	1.023
Final R indices [I>2sigma(I)]	R1 = 0.0360, wR2 = 0.0847
R indices (all data)	R1 = 0.0499, wR2 = 0.0903
Largest diff. peak and hole	0.622 and -1.027 e.Å ⁻³

[PNS-Pd-Alkynyl] - III.8

Identification code	Pd-Alkyne
Empirical formula	C ₂₅ H ₂₈ N O P Pd S
Formula weight	527.91
Temperature	193(2) K
Wavelength	0.71073 Å
Crystal system, space group	Orthorhombic, P b c a
Unit cell dimensions	a = 13.1513(6) Å alpha = 90 deg. b = 13.4615(5) Å beta = 90 deg. c = 25.6301(12) Å gamma = 90 deg.
Volume	4537.5(3) Å ³
Z, Calculated density	8, 1.546 Mg/m ³
Absorption coefficient	0.998 mm ⁻¹
F (000)	2160
Crystal size	0.160 x 0.120 x 0.010 mm
Theta range for data collection	2.686 to 33.155 deg.
Limiting indices	-20 ≤ h ≤ 20, -18 ≤ k ≤ 20, -39 ≤ l ≤ 39
Reflections collected / unique	176233 / 8528 [R(int) = 0.0385]
Completeness to theta = 25.242	98.4 %
Refinement method	Full-matrix least-squares on F ²
Data / restraints / parameters	8528 / 0 / 276
Goodness-of-fit on F ²	1.080
Final R indices [I > 2σ(I)]	R1 = 0.0316, wR2 = 0.0790
R indices (all data)	R1 = 0.0370, wR2 = 0.0818
Largest diff. peak and hole	0.875 and -0.429 e.Å ⁻³

[PNS-Pd-H] - III.9

Identification code	AC200521
Empirical formula	C ₁₆ H ₂₂ N P Pd S
Formula weight	397.78
Temperature	193(2) K
Wavelength	0.71073 Å
Crystal system, space group	Orthorhombic, P 2 ₁ 2 ₁ 2 ₁
Unit cell dimensions	a = 7.0543(12) Å alpha = 90 deg. b = 14.528(3) Å beta = 90 deg. c = 16.228(3) Å gamma = 90 deg.
Volume	1663.1(5) Å ³
Z, Calculated density	4, 1.589 Mg/m ³
Absorption coefficient	1.327 mm ⁻¹
F (000)	808
Crystal size	0.060 x 0.040 x 0.040 mm
Theta range for data collection	4.747 to 27.115 deg.
Limiting indices	-9 ≤ h ≤ 9, -18 ≤ k ≤ 18, -20 ≤ l ≤ 20
Reflections collected / unique	43766 / 3642 [R(int) = 0.0948]
Completeness to theta = 25.242	99.1 %
Refinement method	Full-matrix least-squares on F ²
Data / restraints / parameters	3642 / 0 / 189
Goodness-of-fit on F ²	1.084
Final R indices [I > 2σ(I)]	R1 = 0.0353, wR2 = 0.0560
R indices (all data)	R1 = 0.0626, wR2 = 0.0637
Absolute structure parameter	-0.02(2)
Largest diff. peak and hole	0.405 and -0.463 e.Å ⁻³

III.6) References

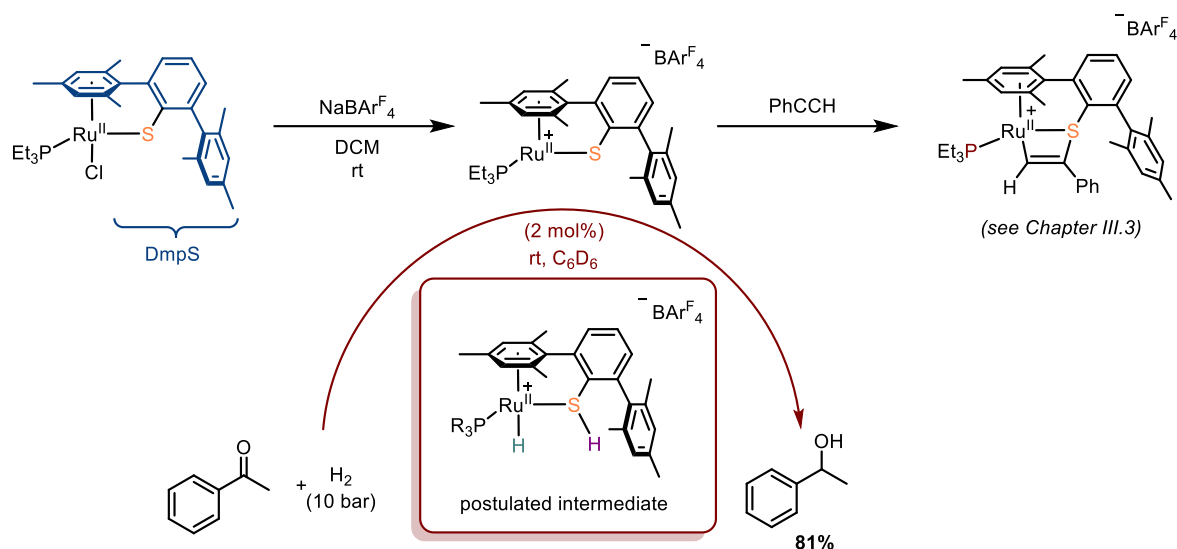
- [1] D. Morales-Morales, *Pincer Compounds Chemistry and Applications*, Elsevier, **2018**.
- [2] A. Scharf, I. Goldberg, A. Vigalok, *J. Am. Chem. Soc.* **2013**, *135*, 967–970.
- [3] S. Takano, T. Kochi, F. Kakiuchi, *Chem. Lett.* **2017**, *46*, 1620–1623.
- [4] S. Clavier, Ø. Rist, S. Hansen, L.-O. Gerlach, T. Högberg, J. Bergman, *Org. Biomol. Chem.* **2003**, *1*, 4248–4253.
- [5] M. Gargir, Y. Ben-David, G. Leituss, Y. Diskin-Posner, L. J. W. Shimon, D. Milstein, *Organometallics* **2012**, *31*, 6207–6214.
- [6] H. Andersson, A.-C. C. Carlsson, B. Nekoueishahraki, U. Brath, M. Erdélyi, in *Annu. Rep. NMR Spectrosc.* (Ed.: G.A. Webb), Academic Press, **2015**, pp. 73–210.
- [7] L. Yang, D. R. Powell, R. P. Houser, *Dalton Trans.* **2007**, *0*, 955–964.
- [8] A. Scharf, I. Goldberg, A. Vigalok, *Inorg. Chem.* **2014**, *53*, 12–14.
- [9] A. Clerc, N. Saffon-Merceron, J. Monot, B. Martin Vaca, D. Bourissou, *Acta Crystallogr. Sect. E Crystallogr. Commun.* **2022**, *78*, 18–22.
- [10] A. Scharf, I. Goldberg, A. Vigalok, A. N. Vedernikov, *Eur. J. Inorg. Chem.* **2015**, *2015*, 4761–4768.
- [11] Y. Ohki, Y. Takikawa, H. Sadohara, C. Kesenheimer, B. Engendahl, E. Kapatina, K. Tatsumi, *Chem. – Asian J.* **2008**, *3*, 1625–1635.
- [12] Y. Blum, Y. Shvo, *J. Organomet. Chem.* **1985**, *282*, C7–C10.
- [13] Youval. Shvo, Dorothea. Czarkie, Yocheved. Rahamim, D. F. Chodosh, *J. Am. Chem. Soc.* **1986**, *108*, 7400–7402.
- [14] B. L. Conley, M. K. Pennington-Boggio, E. Boz, T. J. Williams, *Chem. Rev.* **2010**, *110*, 2294–2312.
- [15] D. G. Gusev, D. M. Spasyuk, *ACS Catal.* **2018**, *8*, 6851–6861.
- [16] J. Zhang, G. Leituss, Y. Ben-David, D. Milstein, *J. Am. Chem. Soc.* **2005**, *127*, 10840–10841.
- [17] D. G. Gusev, *Organometallics* **2020**, *39*, 258–270.
- [18] A. Rossin, M. Peruzzini, *Chem. Rev.* **2016**, *116*, 8848–8872.
- [19] M. Boudjelel, E. D. Sosa Carrizo, S. Mallet-Ladeira, S. Massou, K. Miqueu, G. Bouhadir, D. Bourissou, *ACS Catal.* **2018**, *8*, 4459–4464.
- [20] F. Schneck, F. Schendzielorz, N. Hatami, M. Finger, C. Würtele, S. Schneider, *Angew. Chem. Int. Ed.* **2018**, *57*, 14482–14487.
- [21] L. C. Gregor, C.-H. Chen, C. M. Fafard, L. Fan, C. Guo, B. M. Foxman, D. G. Gusev, O. V. Ozerov, *Dalton Trans.* **2010**, *39*, 3195–3202.
- [22] Y. Zhu, C.-H. Chen, C. M. Fafard, B. M. Foxman, O. V. Ozerov, *Inorg. Chem.* **2011**, *50*, 7980–7987.
- [23] T. He, N. P. Tsvetkov, J. G. Andino, X. Gao, B. C. Fullmer, K. G. Caulton, *J. Am. Chem. Soc.* **2010**, *132*, 910–911.
- [24] D. V. Gutsulyak, W. E. Piers, J. Borau-Garcia, M. Parvez, *J. Am. Chem. Soc.* **2013**, *135*, 11776–11779.
- [25] S.-K. Kim, W.-S. Han, T.-J. Kim, T.-Y. Kim, S. W. Nam, M. Mitoraj, Ł. Piekoś, A. Michalak, S.-J. Hwang, S. O. Kang, *J. Am. Chem. Soc.* **2010**, *132*, 9954–9955.
- [26] A. Nova, H.-W. Suh, T. J. Schmeier, L. M. Guard, O. Eisenstein, N. Hazari, F. Maseras, *Angew. Chem. Int. Ed.* **2014**, *53*, 1103–1108.
- [27] L. Canovese, F. Visentin, C. Santo, V. Bertolasi, *J. Organomet. Chem.* **2014**, *749*, 379–386.

IV) An additional mode of cooperativity: Pd-S

IV.1) Context and introduction:

The activation of E-H bonds by addition across M-S bonds has already been studied with other metals than palladium and remains a vibrant area of research.^[1] For the sake of conciseness, only selected examples based on aromatic thiols will be presented hereafter, starting first by the Ru^{II} complex featuring a dimesitylphenyl thiolate (DmpS) ligand as initially reported by Ohki and Tatsumi. Then, a more recent example by Wang with a 2-(diphenylphosphine)thiophenol (and the phenol analog) ligand applied to nickel and molybdenum reported will be discussed.

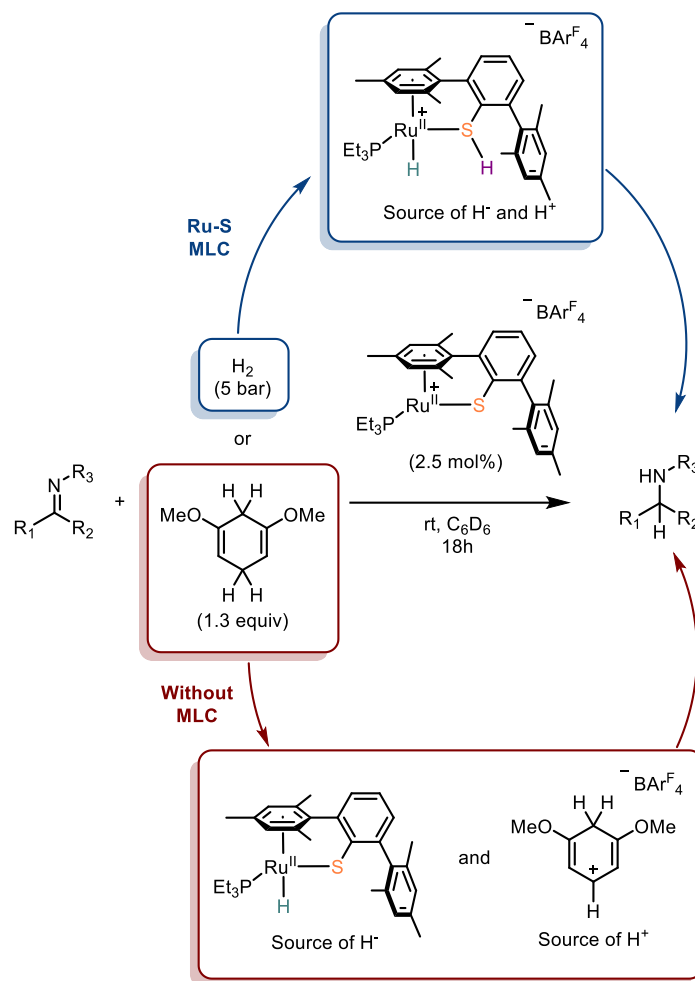
In their original report of 2008, a stable Ru^{II} π -arene complex bearing a DmpS ligand was described by Ohki and Tatsumi. After halide abstraction with NaBAR^F, the formation of a cationic Ru^{II} complex was observed and characterized by XRD. The bulky mesityl substituents at the aromatic thiolate were specifically chosen to prevent the formation of a sulfur-bridged dimer upon cationization (Scheme IV.1).^[2] An interesting property of this complex resides in the bifunctional character of the Ru-S motif. Indeed, a cationic (and Lewis acidic) ruthenium center is coordinated to a thiolate ligand with Lewis basic lone pairs. The cooperativity between those two sites was first evidenced through the stoichiometric reaction with phenylacetylene but no catalytic transformation involving alkynes was reported (already presented in Chapter III; Section III.3).^[2] Remarkably, this cooperative behavior was proposed to play an important role in the catalytic hydrogenation of acetophenone under 10 bar of H₂. Indeed, Ohki and Tatsumi proposed the heterolytic splitting of dihydrogen across the Ru-S bond to form the corresponding DmpS^H-Ru^{II}-H as key intermediate, although it could not be detected by NMR (postulated intermediate; Scheme IV.1).



Scheme IV.1: Generation of the cationic [DmpS-Ru^{II}-PEt₃] complex of Ohki and catalytic activity in hydrogenation of acetophenone

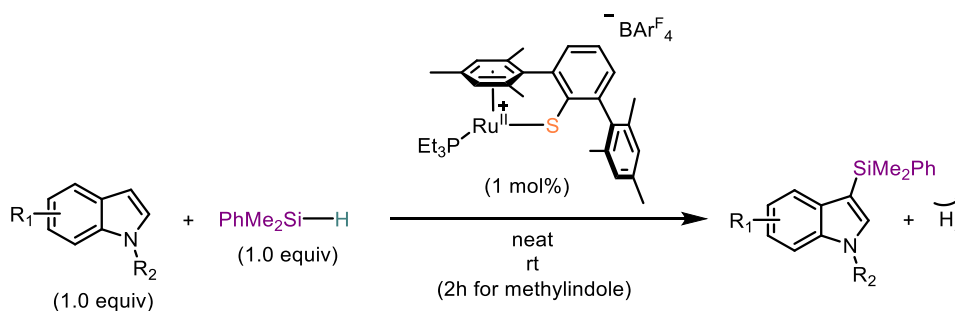
8 years later, the catalytic activity of the DmpS-Ru^{II} complex in hydrogenation and transfer hydrogenation of imines was reported by Oestreich. When the hydrogenation is carried out at 5 bar of H₂, a mechanism involving the cooperative H₂ splitting across the Ru^{II}-S bond after η²-coordination of H₂ was proposed and supported by DFT calculations (top; Scheme IV.2).^[3]

It is interesting to note however that with H₂ surrogates such as cyclohexa-1,4-diene derivatives, another mechanism without Ru^{II}-S cooperativity was found operative. In this case, the cationic Ru^{II} center was proposed to react as a Lewis acid with 1,5-dimethoxycyclohexa-1,4-diene to form the corresponding neutral Ru^{II}-H and the Wheland intermediate (bottom; Scheme IV.2).^[3] The latter then acts as a Brønsted acid towards the imine, which after protonation reacts with the Ru^{II}-H to form the hydrogenated amine.



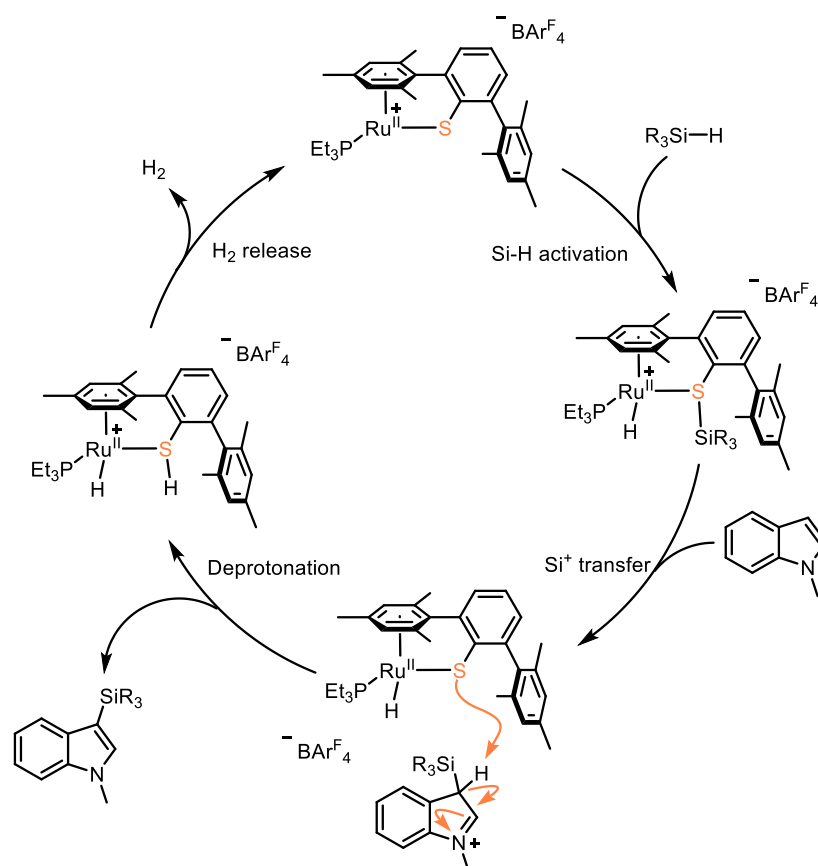
Scheme IV.2: Different mechanisms for the hydrogenation of imines, based on H₂ activation by MLC (top) or with the DmpS-Ru^{II} complex as a Lewis acid (bottom)

The bifunctional Ru^{II}-S motif was also found to be highly active in the activation of Si-H bonds and transfer of R₃Si groups.^[4] Indeed, the catalytic dehydrogenative silylation of indoles was reported in 2011 by Ohki in collaboration with the group of Oestreich (Scheme IV.3). In this case, only 1 mol% of complex was required to perform the C3-selective dehydrogenative silylation of indoles.



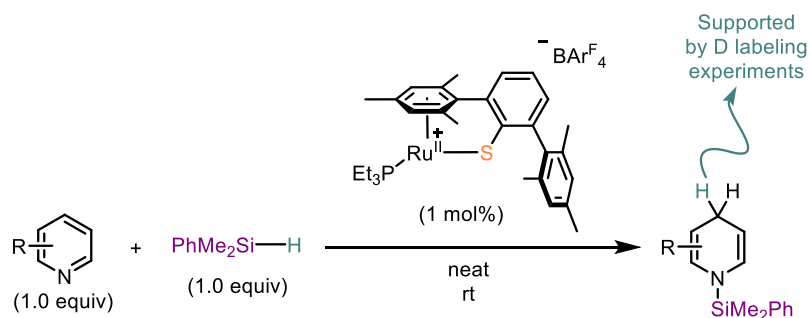
Scheme IV.3: Dehydrogenative silylation of indoles by the cationic DmpS-Ru^{II} complex

This reaction was proposed to start by the heterolytic splitting of the Si-H bond to form the corresponding cationic $\text{Ru}^{\text{II}}\text{-H}$ with a silicon center bonded to the sulfur. This first step was already studied independently by Oestreich through stoichiometric experiments, and the resulting complex of Si-H bond activation was even characterized by XRD.^[5] Then, a silyl cation transfer to indole takes place to yield the indolinium intermediate. The basic thiolate center of the ligand finally deprotonates the indolinium to generate the product of dehydrogenative silylation and the $\text{DmpS}^{\text{H}}\text{-Ru}^{\text{II}}\text{-H}$ complex which then loses H_2 (in line with the harsh reaction conditions needed to activate H_2 , 5 or 10 bar) and the cycle repeats.



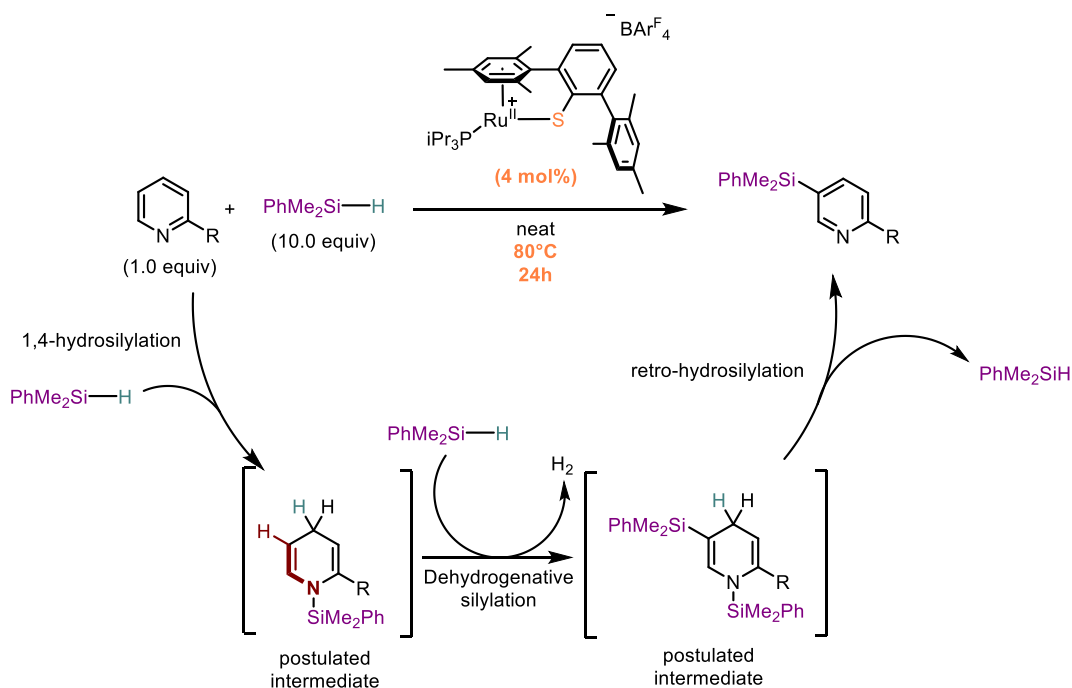
Scheme IV.4: Proposed mechanism for the dehydrogenative silylation of indoles by the cationic DmpS-Ru complex

In the absence of an acidic proton to perform dehydrogenative coupling, the hydrosilylation reaction can be promoted.^[6] This was demonstrated through the 1,4-hydrosilylation of pyridines (Scheme IV.5). In this case, a wide variety of pyridines were found reactive at room temperature, except the *ortho*-substituted ones. This was attributed to steric hinderance, hampering the transfer of the R_3Si^+ group to nitrogen.



Scheme IV.5: Hydrosilylation of pyridines catalyzed by the DmpS-Ru^{II} complex; incorporation of the hydrogen bared by the Si at the *para*-position was supported by D labeling experiments

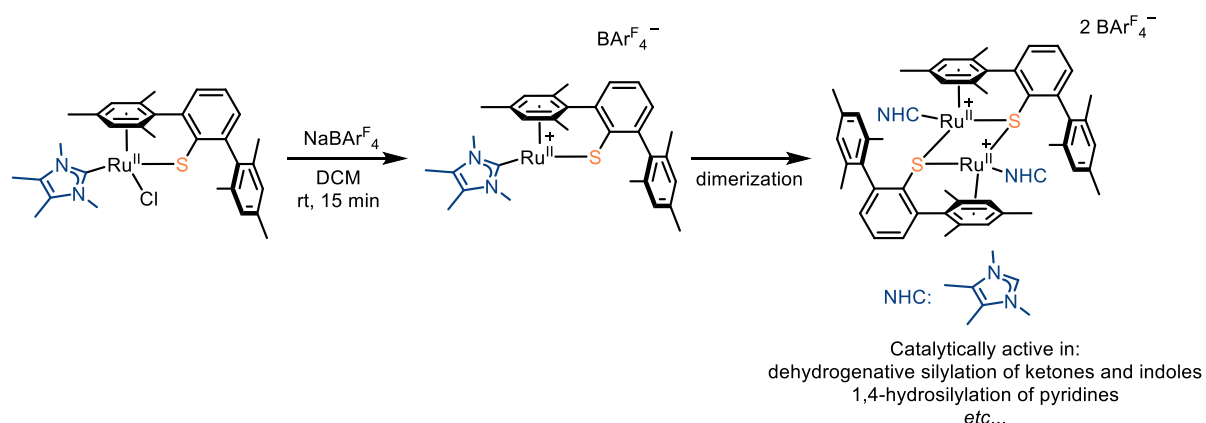
Interestingly, upon using harsher conditions (excess of SiH and 80 °C), a dehydrogenative coupling pathway was found operative and the *meta*-selective dehydrogenative silylation of pyridines was reported (Scheme IV.6).^[7] In this case, the reaction was proposed to form first the dearomatized product of 1,4-hydrosilylation (note: *ortho*-substituted pyridines, unreactive previously worked in this case at 80 °C). This 1,4-hydrosilylation product would then undergo dehydrogenative silylation at the *meta* position through a mechanism similar to the one reported with indoles. The retro-hydrosilylation of the disilylated compound at high temperature finally yields the *meta*-silylated pyridine.



Scheme IV.6: *meta*-selective dehydrogenative silylation of pyridines reported by Oestreich using the cationic DmpS-Ru^{II} complex

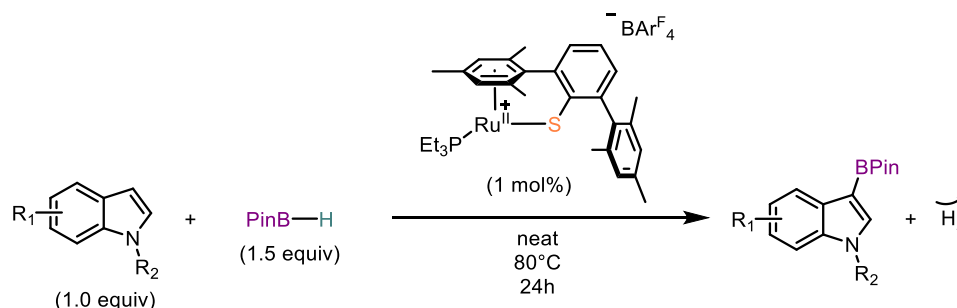
Other studies were also conducted on the dehydrogenative coupling of Si-H with imines or ketones but these examples will not be detailed here.^[1,8,9]

Note that all the initial work of Ohki and Oestreich was performed with PR₃ as co-ligand for the DmpS-Ru^{II} complex to avoid dimerization. However, in 2016, a binuclear dicationic Ru^{II}-S complex with an NHC ancillary ligand was reported as an air-stable precatalyst in the previously mentioned couplings (i.e. dehydrogenative silylation of indoles and ketones, 1,4-hydrosilylation of pyridines, *etc*; Scheme IV.7).^[10] Remarkably, and importantly for us and our S-bridged design, a similar activity compared to the phosphine analog was observed meaning that the dimeric structure does not hamper the catalytic activity. It is also interesting to note that in the initial publication of Ohki, the formation of a sulfur-bridged dimer (with acetophenone as coligand) was identified as an out-of-cycle product, inactive in the hydrogenation reaction (H₂ activation).^[2]



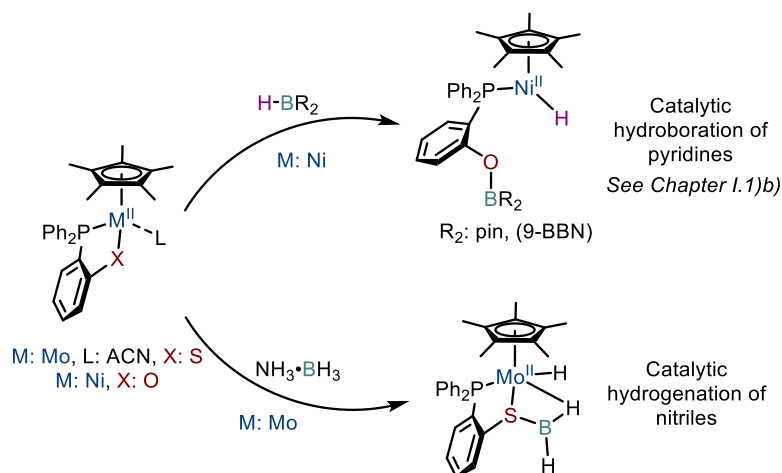
Scheme IV.7: Formation of binuclear Ru-S bridged dimer with an NHC ancillary ligand

The cooperative bond activation by the DmpS-Ru^{II} complex was also extended by Ohki and Oestreich to B-H bonds and the catalytic dehydrogenative borylation of indoles (Scheme IV.8).^[11]



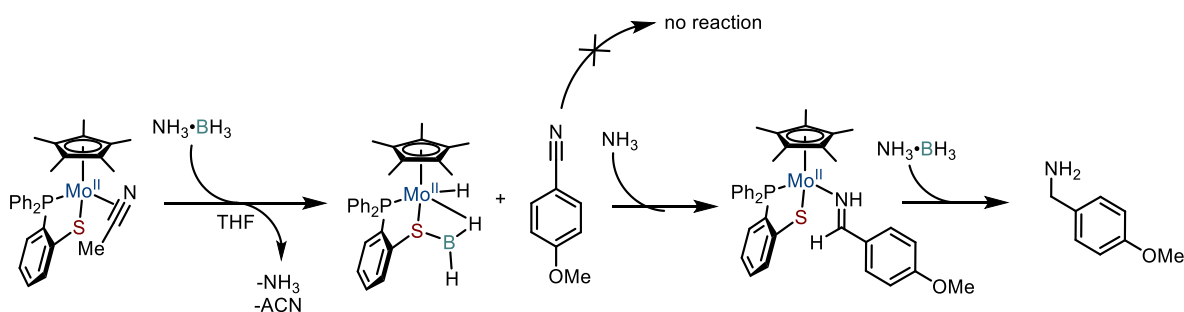
Scheme IV.8: General reaction scheme of the catalytic dehydrogenative borylation reported by Ohki and Oestreich with the cationic DmpS-Ru^{II} complex

Recently, the cooperative B-H bond activation was reported with a P-X (X: S,O) ligand with an *ortho*-phenylene spacer and the O version was used with Ni^{II} (as already presented in chapter I; Section I.1)b) and the S version with Mo^{II}.^{[12][13]}



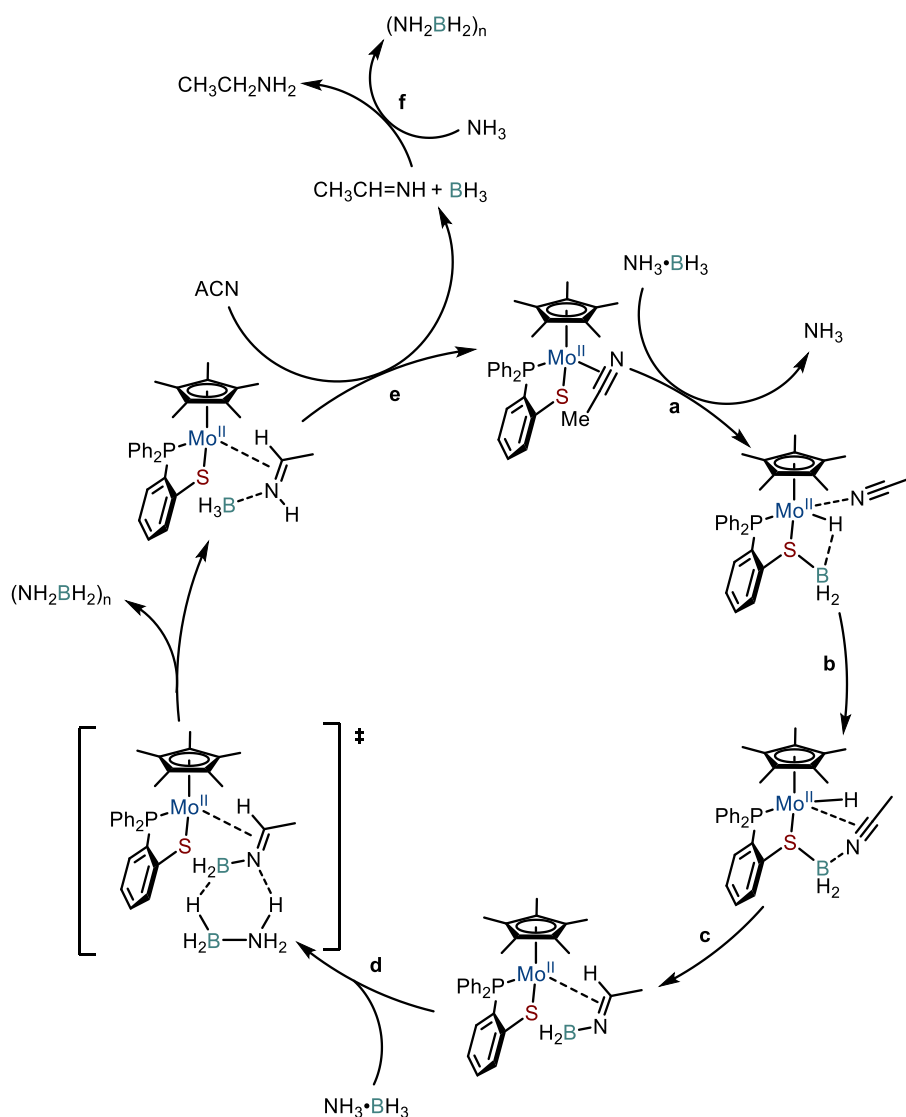
Scheme IV.9: Piano-stool complexes of Wang for cooperative M-X bond activation and catalytic reactions

The cooperativity between the TM and the sulfur was demonstrated through stoichiometric experiments further supported by DFT calculations. Indeed, upon stoichiometric reaction of the piano-stool Mo^{II} complex with amine borane (AB), the formation of a Mo^{II}-H with incorporation of BH₂ at sulfur was observed after removal of the volatiles, evidencing BH bond activation (Scheme IV.10). When this complex was subjected to nitriles such as *para*-methoxybenzoxonitrile, no reaction was observed even after heating. However, when NH₃ was added, the formation of the Mo^{II} complex with a coordinated arylmethanimine was observed (no comment was made on the fate of the dehydrogenated amine borane). Further treatment of this complex with AB afforded the hydrogenated *para*-methoxyphenylmethanamine (this final step does not necessitate the presence of a transition metal).



Scheme IV.10: Stoichiometric reaction of the Mo^{II} complex with amine borane and subsequent partial hydrogenation of paramethoxybenzoxonitrile

This system was found amenable to catalysis and the following mechanism was proposed based on the previous stoichiometric experiments and supported by DFT calculations. First, and thanks to Mo^{II}-S cooperativity, formation of the Mo^{II}-H occurs with a S-bonded borane (Scheme IV.11; **a**). The Lewis acidic borane then interacts with the η^1 -coordinated nitrile to favor $\eta^1 \rightarrow \eta^2$ coordination (Scheme IV.11; **b**), and transfer of the hydride from the Mo^{II}-H to the electrophilic carbon of the nitrile occurs (Scheme IV.11; **c**). Outer-sphere concomitant protonation of the borylimine and H- transfer to BH₂ then takes place with a new molecule of AB which results in the loss of (NH₂BH₂)_n (Scheme IV.11; **d**). The resulting imine-BH₃ adduct is replaced by an entering molecule of nitrile and the catalytic cycle repeats (Scheme IV.11; **e**). The imine is then reduced by the combination of BH₃·NH₃ out of the catalytic cycle (Scheme IV.11; **f**).



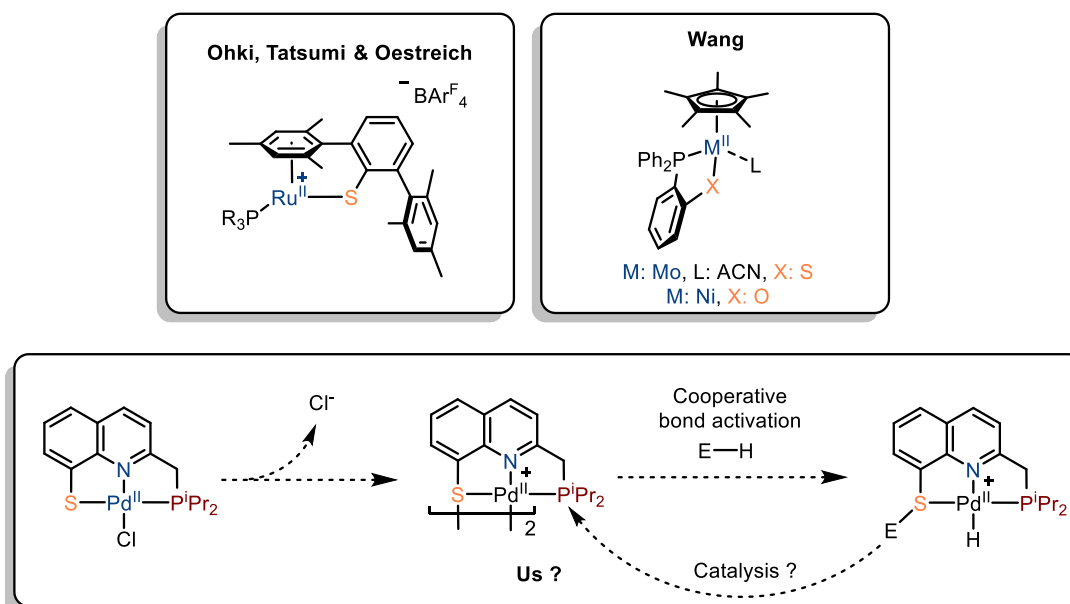
Scheme IV.11: Proposed catalytic cycle for the hydrogenation of nitrile with amine borane catalyzed by the Mo^{II}-S complex of Wang

The previous examples substantiate the interest of M-S cooperativity in terms of E-H bond activation and the associated catalytic transformations.^[1] In particular, the DmpS ligand was successfully applied to Si-H and B-H bond activation, and a spectacular activity in dehydrogenative couplings was reported with this system. Recently, Wang applied P-X ligands to B-H bond activations with O-Ni on the one hand, and with S-Mo on the other hand. A good match between the ligand and the desired mode of action is always essential.

Extending the diversity of cooperative M-S complexes is highly attractive and remains a challenge. This could enable the approach to other transformations and impact the selectivity of the corresponding reactions.

A key feature of our PNS ligand was the potential addition of substrates across the Pd-S bond. Besides the rareness of Pd-S cooperativity, M-S cooperativity with a quinoline backbone is unprecedented. It is also likely that the Pd-S complex will display a reactivity profile complementary to the Ru-S systems previously mentioned.

In the previous chapter, the affinity between Pd^{II} and sulfides was supported by the formation of a sulfur-bridged dimer upon dearomatization. The availability of the lone pairs at sulfur in this dimeric form was also suggested by the reaction with iodomethane. Here, our goal was to generate an active species without dearomatization, through abstraction of the halogen at the PNS-Pd^{II}-Cl complex **III.5** so that a coordination site at Pd^{II} is liberated. Then, we aimed to illustrate the cooperativity through stoichiometric reactions, and finally demonstrate the catalytic relevance and interest of the Pd-S complex.

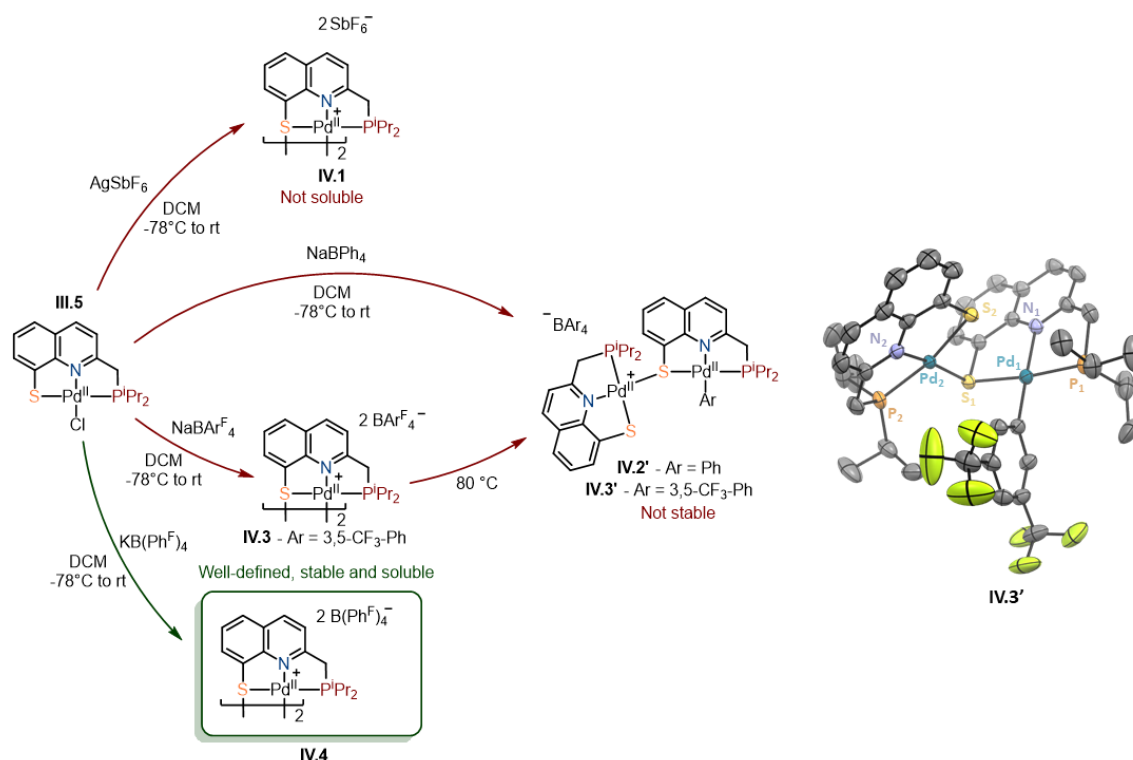


Scheme IV.12: Overview of the presented systems and ligand designs exhibiting M-X cooperativity and potential applications of our quinoline PNS ligand design for Pd-S cooperativity

IV.2) Generation of the active species, characterization, and stoichiometric bond activation reactions:

To open a coordination site at palladium in **III.5**, various halide abstractors were explored (Scheme IV.13). First, AgSbF₆ was used, but the resulting dicationic complex was only marginally soluble in organic solvents and thus not practical. To overcome this issue, borate salts such as NaBPh₄ and NaBAr^F₄ (Ar^F = 3,5-bis(trifluoromethyl)phenyl) were tested, but

transfer of one of the Ph/Ar^F group to the electrophilic palladium center was observed. Indeed, transmetalation occurred at room temperature for BPh₄, or upon heating to 80°C for the BAr^F₄ resulting in the partially cationic bimetallic complexes **IV.2** and **IV.3'**, respectively (characterized by XRD). We then switched to the less nucleophilic perfluorinated [BPh^F₄]⁻ anion (Ph^F = perfluorophenyl) and obtained a soluble, well-defined, and thermally stable species (no transmetalation was observed by ³¹P NMR after days in solution at 120°C).



Scheme IV.13: Halide abstraction at **III.5** and formation of the various PNS-Pd cationic complexes; XRD structure of **IV.3'**, H and BAr^F₄ anion are omitted for clarity

Unfortunately, single crystals of **IV.4** could not be grown so far. Attempts resulted in the complex oiling-out of solution. However, crystals of the less soluble and more crystalline **IV.1** could be grown and were analyzed by XRD.^[14] The expected head-to-tail dimeric structure was obtained and structural parameters similar to those of the dimeric dearomatized complex **III.6** were observed.

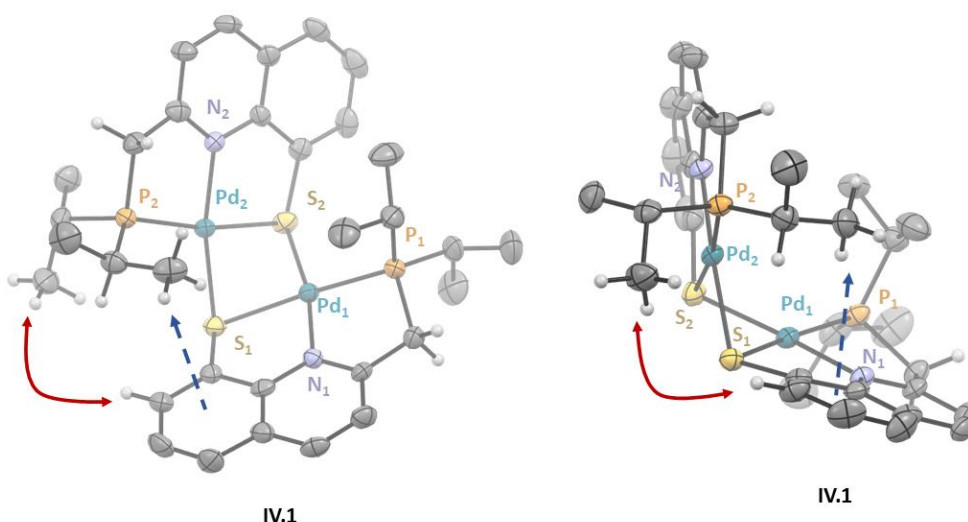


Figure IV.1: XRD structure of the dicationic complex **IV.1** with two different view angles; The shielding of the ⁱPr signals by magnetic anisotropic effect observed by ¹H NMR is indicated by the dashed blue arrow; The NOESY interaction observed by ¹H NMR is indicated by the double red arrow; Other H atoms and two SbF₆ anions are omitted for clarity except when relevant

Accordingly, the two metallic centers were slightly distorted from the ideal square planar geometry with $\tau_4 = 0.15$ ($\tau_4 = 0.17$ in **III.6**). The “intermolecular” Pd-S distances are shorter than the intramolecular ones (i.e. **inter-Pd₂-S₁**: 2.319(2) Å / **inter-Pd₁-S₂**: 2.315(2) Å in **IV.1** compared to **inter-Pd₂-S₁**: 2.343(1) Å / **inter-Pd₁-S₂**: 2.341(1) Å in **III.6**) probably due to the increased electrophilicity of the cationic palladium center and the reduced trans-effect of a sp^2 -N_{1,2} (in **IV.1**) compared to sp^3 -N_{1,2} in **III.6**.

Even if no single crystals of **IV.4** could be obtained, spectroscopic data of **IV.1** and **IV.4** are closely related, supporting a dimeric structure in solution for both complexes. Indeed, in ¹H NMR, the CH₂ signal of the spacer is splitted, due to the diastereotopic character of these two protons in the dimeric form (in the dearomatized **III.6**, this was not observed as it is a vinylic CH). Furthermore, the diagnostic separation of the ⁱPr signals is also present and supported by a NOESY correlation (red and blue arrows; Figure IV.1 and Figure IV.2).

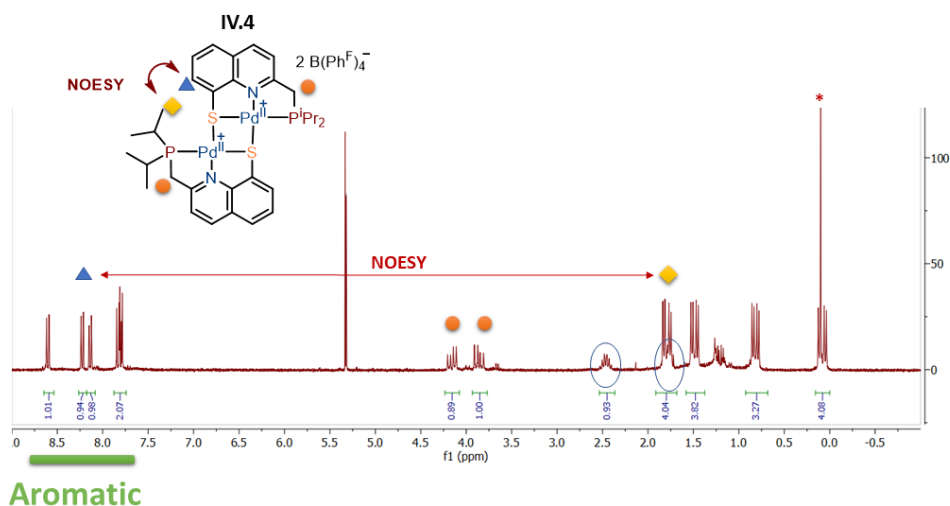
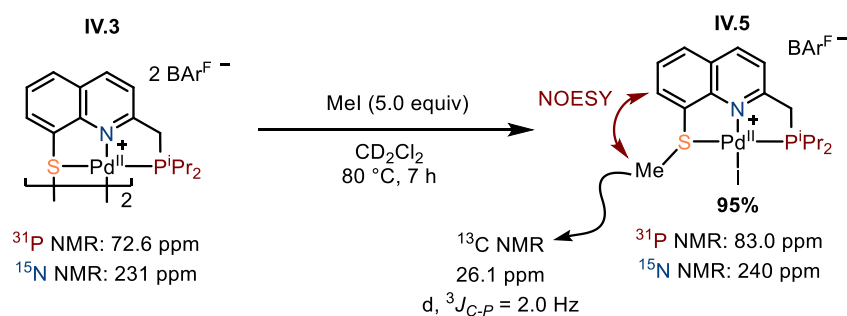


Figure IV.2: ^1H NMR spectrum of dimeric complex **IV.4** with diagnostic signals of a dimeric structure; * residual grease

With the dicationic compound in hands, our first objective was to illustrate the bifunctional character and the availability of the $\text{Pd}^{\text{II}}\text{-S}$ motif through stoichiometric bond activations.

To this end, the cationic dimer **IV.3** was reacted with MeI and the formation of a new compound was indicated by a ^{31}P NMR signal at 83.0 ppm (reminiscent of **III.4**; ^{31}P NMR: 83.7 ppm). In ^1H NMR, a mononuclear species was suggested by the symmetric CH_2 and $i\text{Pr}$ signals. A new signal attributed to the methyl was located at 3.08 ppm, and this CH_3 was positioned at sulfur thanks to its NOESY NMR interaction with the *ortho*-CH. This was further supported by a $^3J_{\text{C-P}}$ coupling constant of 2.0 Hz with phosphorus (Scheme IV.14 and Figure IV.3).



Scheme IV.14: Reaction of the cationic complex **IV.3** with MeI and generation of the new **IV.5** complex - This reaction was performed prior to the observation of the transmetallation in **IV.3**

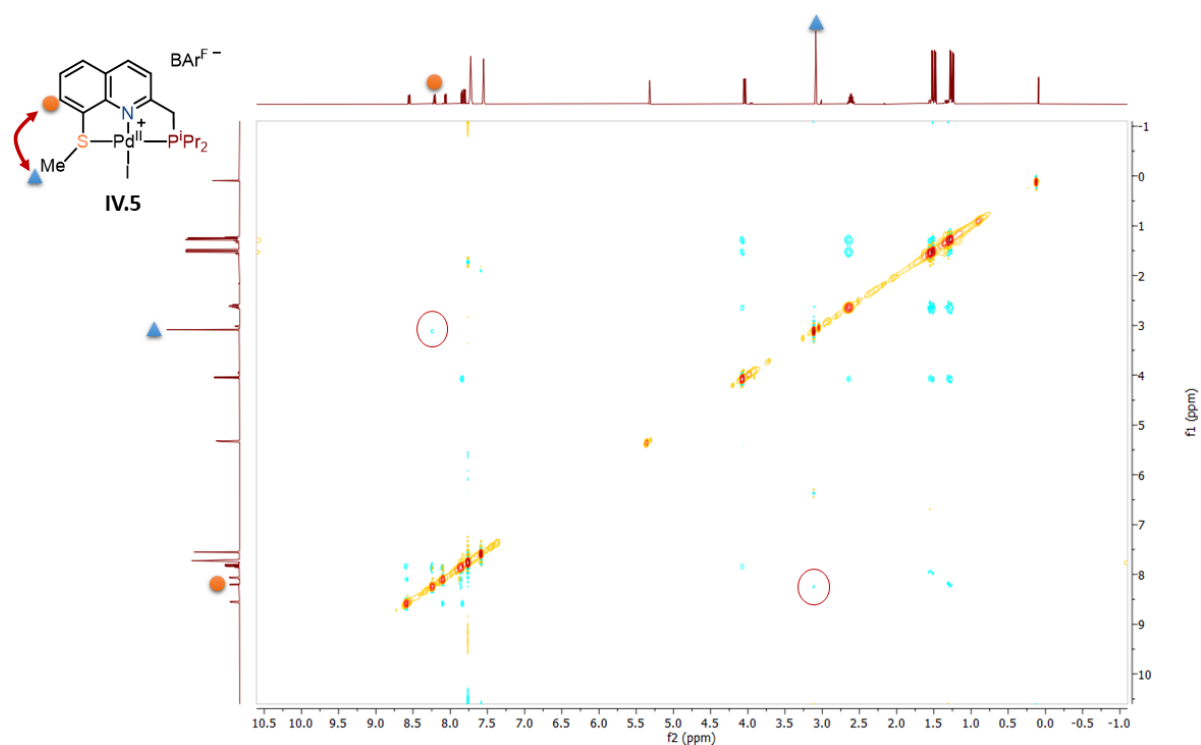


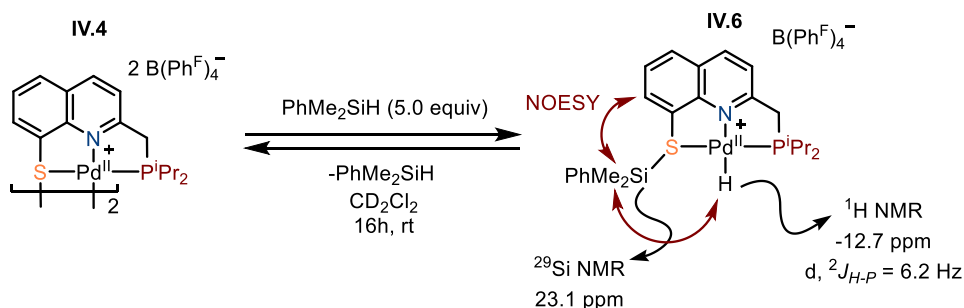
Figure IV.3: NOESY NMR of complex **IV.5** interactions between the S-CH₃ and the *ortho*-CH are circled in red

With this initial result providing the proof-of-concept for Pd-S non-innocence, we wanted to move on to more challenging bond activation reactions.

Silane activation was then attempted by treating the dicationic complex **IV.4** with 5 equivalents of PhMe₂SiH in CD₂Cl₂. The reaction was monitored by ¹H, ³¹P and ²⁹Si NMR. After 16 h at room temperature, the disappearance of the signal of **IV.4** and the appearance of a new signal at 76.4 ppm was observed by ³¹P NMR. In ¹H NMR, a monomeric structure was indicated by the symmetric CH₂ and ⁱPr signals and most importantly, a hydride signal was observed at -12.74 ppm (d, ²J_{H-P} = 6.2 Hz) integrating for 1H (Figure IV.4). As for the PhMe₂Si group, in addition to the signal at -17.0 ppm of PhMe₂SiH, a new signal (major) at 23.1 ppm was observed. This is in line with the observations of Oestreich in the DmpS-Ru system (²⁹Si NMR: δ = 28.4 ppm) for the complex of Si-H activation.^{[5],d} Furthermore, a correlation between

^d - When the experiment was performed with the BArF₄⁻ anion, a similar spectroscopic signature was collected (¹H, ³¹P, ²⁹Si and NOESY) but a small J_{P-Si} coupling constant of 1.5 Hz was observed in the ²⁹Si spectrum. Supporting the proposed structure and in line with the results obtained with MeI in ¹³C NMR. This complex was not used further due to its thermal instability.

the methyls of PhMe₂Si and both the *ortho*-C-H of the thiophenolate ring and the hydride was observed in NOESY NMR (no exchange with the excess silane was detected). Overall, the spectroscopic data gathered supports the addition of the Si-H bond across the Pd-S motif with formation of a cationic PNS-Pd^{II}-H complex **IV.6** and incorporation of the R₃Si⁺ at sulfur.



Scheme IV.15: Reversible Si-H activation by the dicationic dimer **IV.4** and spectroscopic features

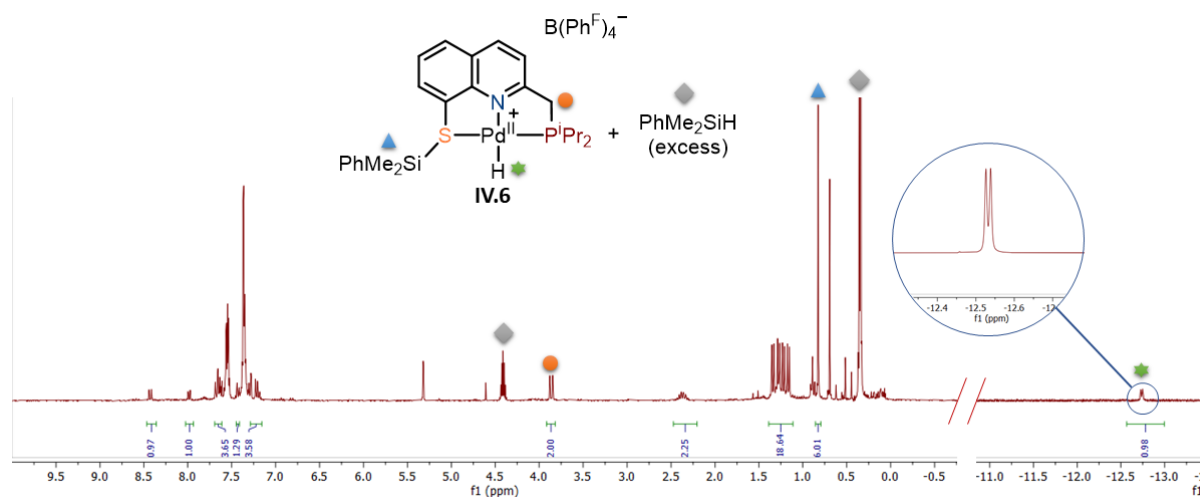


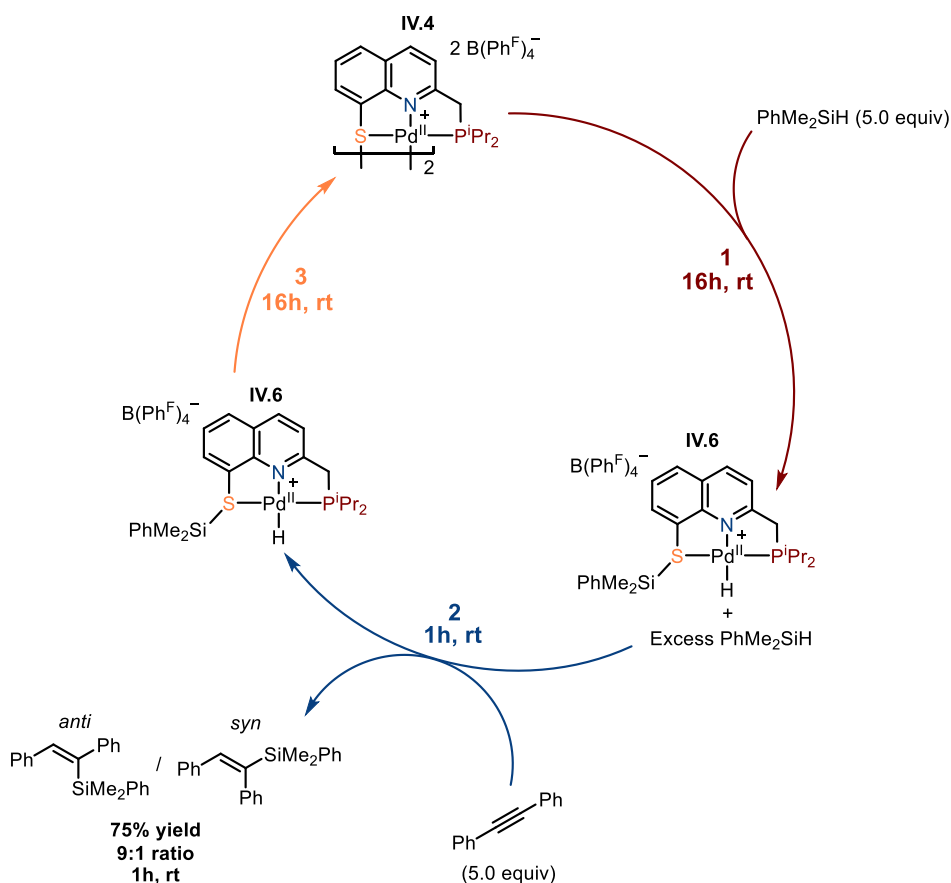
Figure IV.4: ¹H NMR of **IV.6** after treatment of **IV.4** with 5.0 equivalents of PhMe₂SiH in CD₂Cl₂

The complex was found to be stable only in the presence of an excess of PhMe₂SiH as precipitation of **IV.6** in pentane regenerated the cationic dimer **IV.4** (similarly to the observations of Oestreich).^[5] Unfortunately, no single crystal of this complex was obtained so far but this is still a work in progress.

With strong spectroscopic evidence demonstrating the ability of the Pd^{II}-S motif to heterolytically cleave Si-H bonds, the catalytic hydrosilylation of pyridines and the dehydrogenative silylation of indoles was attempted with **IV.4** without success. In absence of activity, we turned our attention to the ability of this new complex to transfer the Si-H motif to unsaturated substrates.

IV.3) Stoichiometric hydroelementation reactions:

To this end, the complex **IV.6** of Si-H activation was generated using the previously established method (step 1; Scheme IV.16). In this case, the amount of product of Si-H activation and excess PhMe_2SiH was quantified by ^1H NMR using an internal standard (1,2,4,5-tetramethylbenzene). Then, a solution of 5.0 equivalents of Ph-CC-Ph with a different internal standard (diphenylmethane) was added and the reaction was monitored by NMR (step 2; Scheme IV.16). After 1 h at rt, complete silane conversion and 75% yield of alkyne hydrosilylation was determined by ^1H NMR. The complex **IV.6** of Si-H activation was still present in solution as the major organometallic species. It slowly disappeared overnight to regenerate the dicationic dimeric **IV.4** (step 3; Scheme IV.16).



Scheme IV.16: Stoichiometric transfer of silane to Ph-CC-Ph by the complex **IV.6** and regeneration of **IV.4**

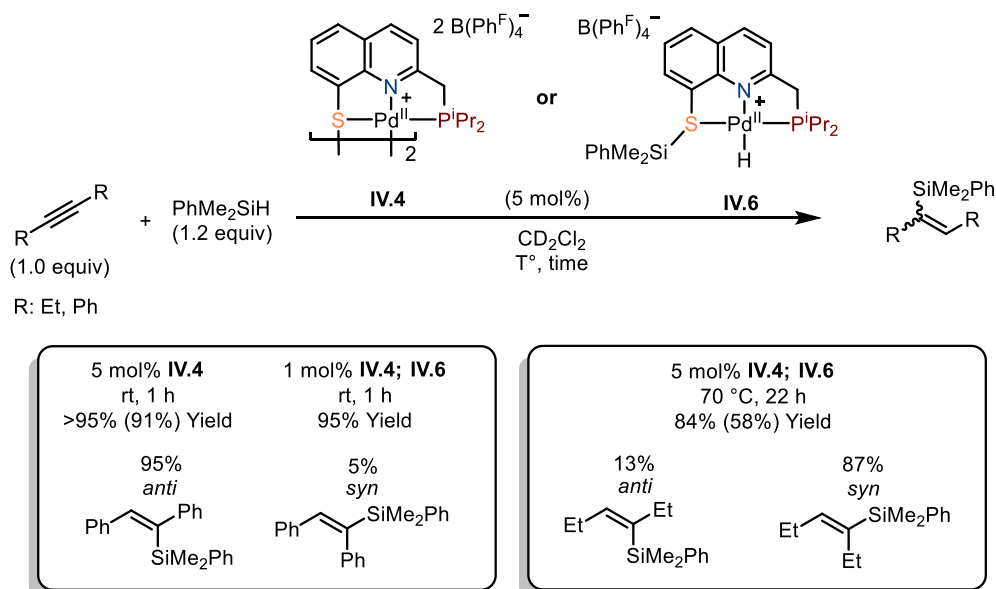
Overall, the ability of the complex **IV.6** to transfer a *supra*-stoichiometric amount of silane to an alkyne was demonstrated and thus, its catalytic potential (here at 20 mol% catalytic loading). Furthermore, the potential use of **IV.4** as a pre-catalyst for the hydrosilylation of alkynes was suggested by its regeneration at the end of the reaction. Last but not least, the

formation of the *Z* isomer as a major product (9:1) indicates a rare and interesting example of *anti* hydrosilylation.

IV.4) Initial catalytic results and mechanistic implications

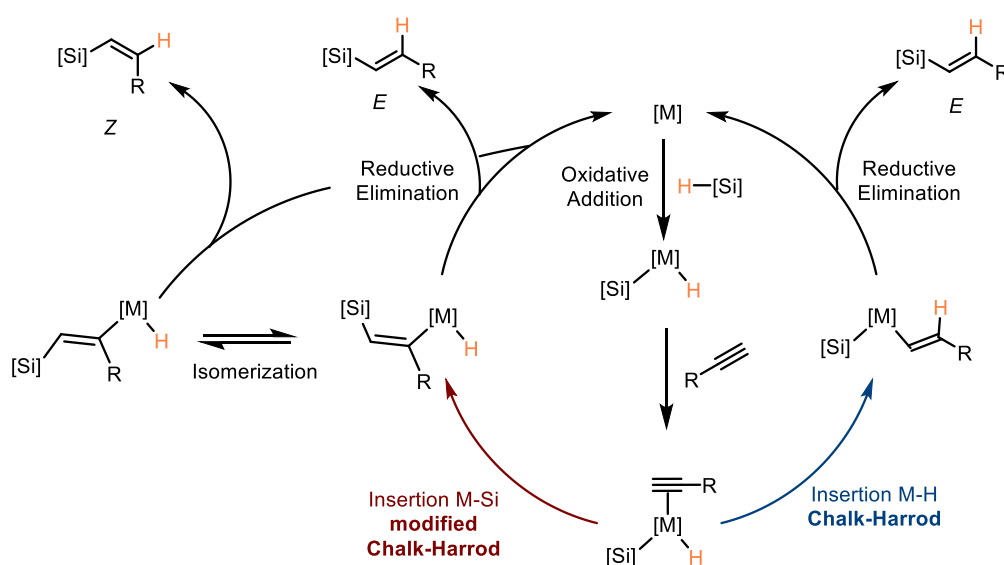
In the direct continuity of the “stoichiometric” experiments, the catalytic hydrosilylation of tolane and hex-3-yne as symmetric (aryl and alkyl-substituted) internal alkynes was next attempted at 5 mol% catalytic loading of **IV.4** (Scheme IV.17). Under these conditions, quantitative hydrosilylation of tolane (Ph-CC-Ph) was observed in less than 1 h (97% *anti*/3% *syn*). The catalytic loading was then reduced to 1 mol% and the reaction reached 95% yield in 1 h with 95% of *anti*-addition product and 5% of *syn*-addition. When 1 mol% of the preformed complex of Si-H activation **IV.6** was employed as a catalyst instead of **IV.4**, the same yields were observed with a boost in reactivity (86% yield after <10 min with **IV.6** compared to 16% with **IV.4**).

Interestingly, with hex-3-yne, the reaction required harsher conditions and the product distribution was reversed, reaching 84% yield after 22 h at 70°C with 87% *syn* and 13% *anti* products. When the preformed complex **IV.6** was used, the reactivity and product distribution were comparable with a very slight boost in reaction time in particular in the first stage of the reaction (46% yield after 6 h compared to 31% after 6 h).



Scheme IV.17: Catalytic hydrosilylation of symmetric internal alkynes using **IV.4** or **IV.6**; Isolated yields are given in brackets.

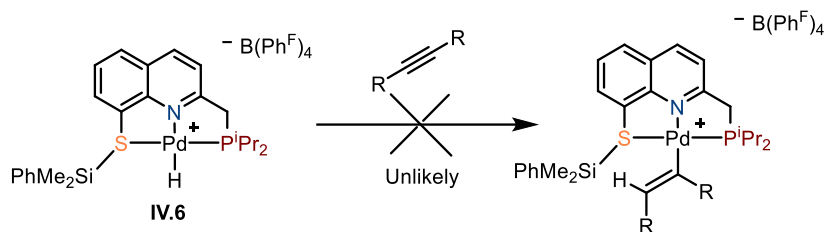
The formation of the *anti*-hydrosilylation as a major product for tolane is a quite remarkable feature as the synthesis of *trans*-hydrosilylation products is unusual. In transition-metal catalyzed hydrosilylation reaction, two usually accepted mechanisms can be found: the Chalk-Harrod and modified Chalk-Harrod (Scheme IV.18).^[15] Both start with the oxidative addition of Si-H to the metal. In the Chalk-Harrod mechanism, insertion into the M-H occurs and in the modified Chalk-Harrod insertion into the M-Si bond occurs, followed in both cases by reductive elimination. When insertion into the M-Si bond occurs, isomerization of the *Z/E* vinyl-silyl intermediate might be favored (typically with Co and Rh complexes) leading to the *Z* isomer.^[16]



Scheme IV.18: Catalytic cycles of TM catalyzed hydrosilylation: Chalk-Harrod and modified Chalk-Harrod mechanisms.

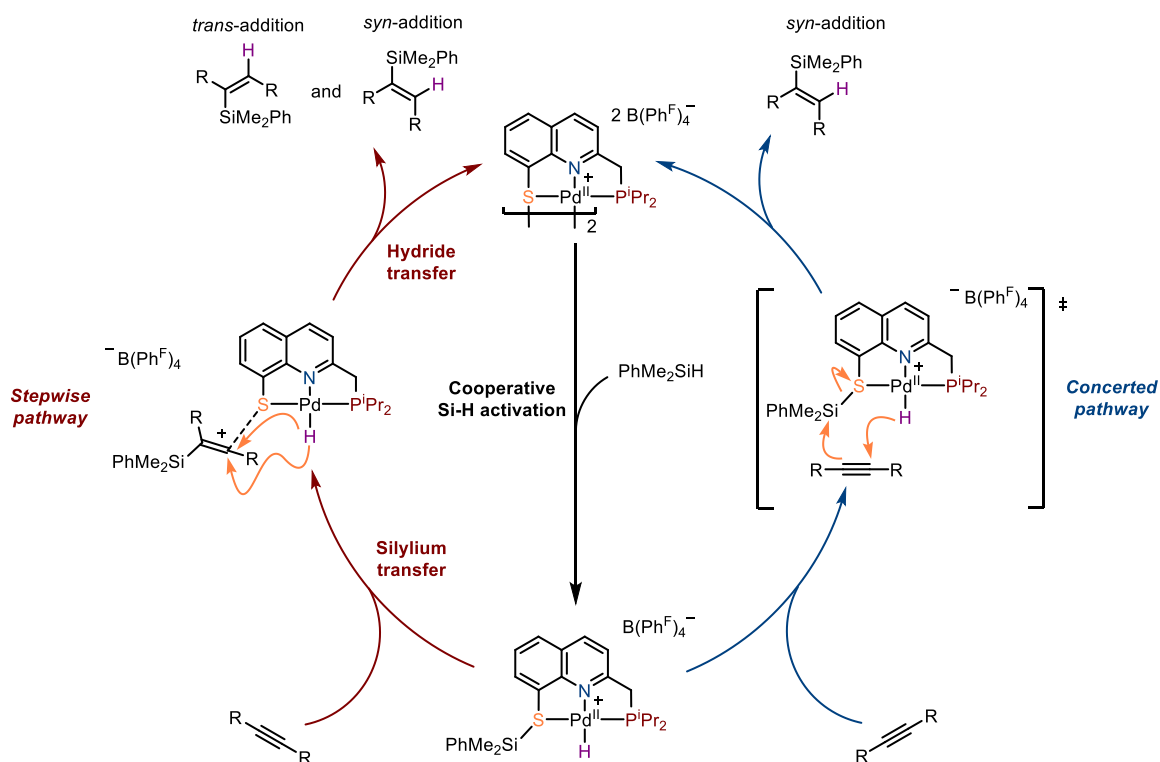
However, none of these two mechanisms is probably in play in our case. Indeed, redox processes are unlikely to be operative with our rigid PNS-Pd^{II} pincer architecture and a Pd^{II}/Pd^{IV} process would require strongly oxidizing conditions.

Alternatively, insertion into the Pd^{II}-H bond of the Si-H activation complex **IV.6** can be envisioned (Scheme IV.19). Once again, this mechanism can be considered unlikely due to the challenging nature of insertion reaction in related PNP-Pd^{II}-H pincer complexes.^[17,18] Indeed, insertion reaction in tetracoordinate square-planar Pd^{II} complexes requires ligand dissociation, a difficult task in rigid pincer complexes. Furthermore, even if the insertion reaction was occurring, it is *syn* selective and could not explain the formation of the *anti*-product in the case of tolane.

Scheme IV.19: Insertion of alkyne in the Pd^{II}-H bond of the product of Si-H activation **IV.6**

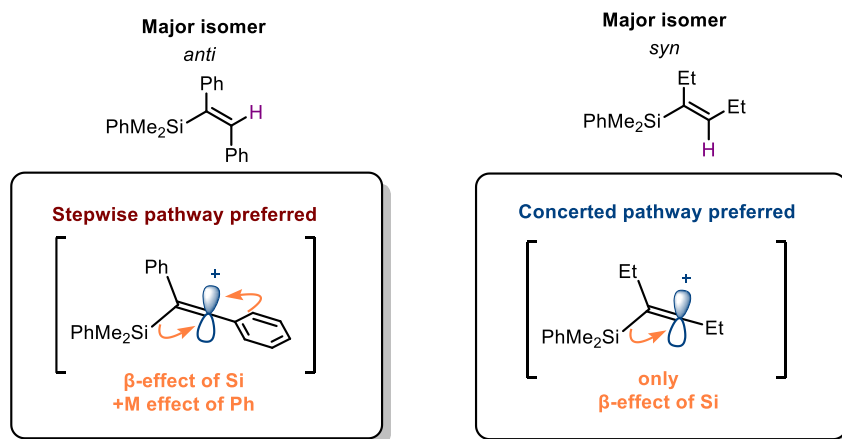
Alternatively, a pathway involving the transfer of a silylium cation to the alkyne from **IV.6**, analogous to the previous mechanisms in play with the DmpS-Ru^{II} complex of Ohki and Tatsumi (*vide infra* Scheme IV.4) with R₃Si⁺ transfer to indoles or pyridines can be envisioned. In fact, this type of hydrosilylation mechanism would be comparable to the ones already reported with strong Lewis-acids such as aluminum salts and phosphoniums.^[19–22]

In our case, to explain the formation of both the *anti* and the *syn*-addition product, two mechanisms with **IV.6** as a common intermediate can be proposed (Scheme IV.20). First, and in both cases, the cooperative Si-H bond activation occurs to yield the product of heterolytic Si-H bond splitting **IV.6**. Then, in the *stepwise pathway*, transfer of the silylium to the alkyne takes place to generate a reactive vinyl-silyl cation, which finally abstracts the hydride from Pd^{II}. In this case, the hydride abstraction can occur *syn* or *anti* to the Si group depending on the interplay of the steric and electronic factors to yield the respecting vinylsilanes products and the catalytic cycle can repeat. Alternatively, in the *concerted pathway*, the silyl and hydride transfers occur in a concerted manner which results in the exclusive formation of *syn*-addition product. Depending on the alkyne, the two mechanisms could be operational, or one could be preponderant.



Scheme IV.20: Plausible simplified mechanisms for the hydrosilylation of alkynes by Pd-S cooperativity

For tolane, the formation of the *anti* product as the major isomer is in line with a preferred stepwise pathway which involves a vinyl carbocation. In this case, it would be stabilized by both the β -effect of the R_3Si and the mesomeric effect of the Ph (Scheme IV.21). However, in the case of hex-3-yne, only the β -effect of the silicon would be in play. This may favor the concerted pathway in this case and explain the formation of the *syn* isomer as major product.

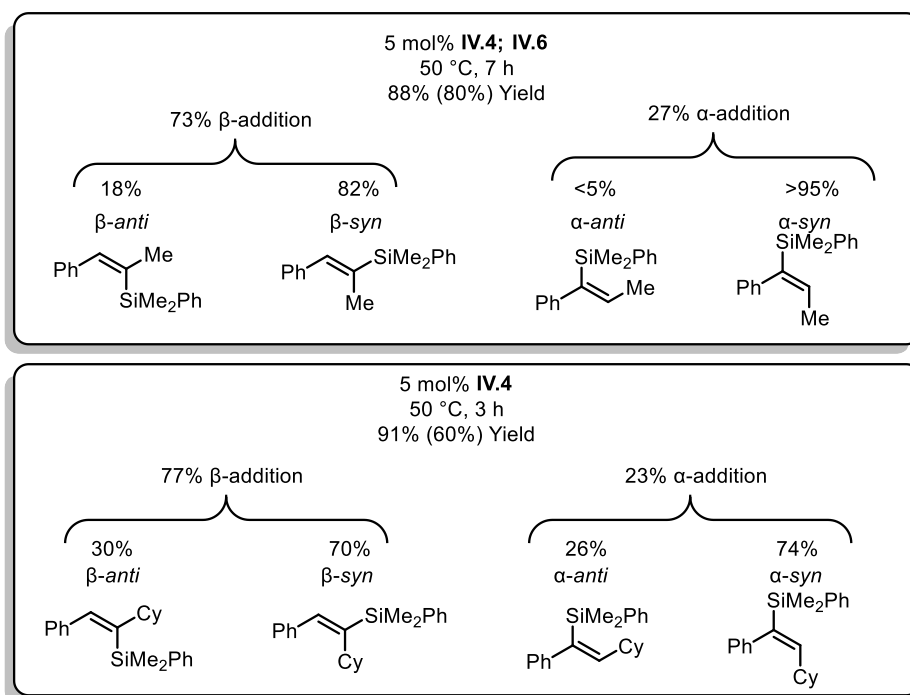


Scheme IV.21: Formation of a carbocation and resulting stabilizing effects in the case of tolane and in the case of hex-3-yne.

With these elements in mind, selected substrates were used in this catalytic hydrosilylation to get more insight into the catalytic cycle and into the scope of the transformation.

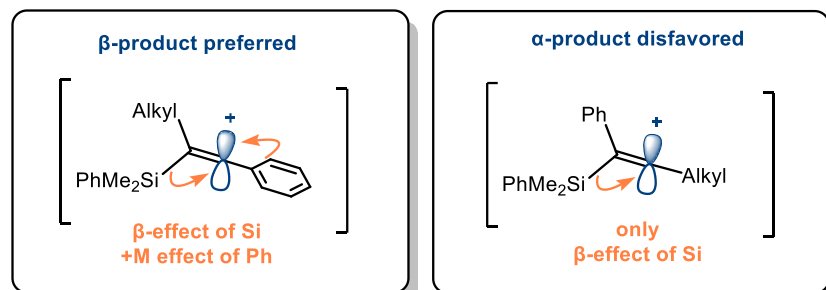
IV.5) Substrate scope of the catalytic hydrosilylation reaction

Dissymmetric aryl-alkyl internal alkynes were first tested with Ph-CC-Me. An intermediate reactivity compared to hex-3-yne and toluene was observed with 88% of hydrosilylation after 7 h at 50 °C. In terms of product distribution, 73% of Si addition β to Ph (82% *syn* and 18% *anti*) was found, with 27% of addition α to Ph (>95% *syn* and <5% *anti*) (Figure IV.5). The steric environment at the alkyl group was then varied from a methyl to a bulkier cyclohexyl to monitor the impact of the steric parameters on the product distribution (Figure IV.5). A similar reactivity was observed in this case with 91% yield after 3 h at 50°C. The observed stereo and regioselectivities are also relatively close with 77% of Si addition β to Ph (70% *syn* and 30% *anti*) and 23% of α addition to Ph was found (74% *syn* and 26% *anti*) (Figure IV.5). It must be noted that the ratio of all compounds was constant throughout the reaction and no significant isomerization was noticed after full conversion.

Figure IV.5: Hydrosilylation of dissymmetric internal alkynes with **IV.4** or **IV.6**

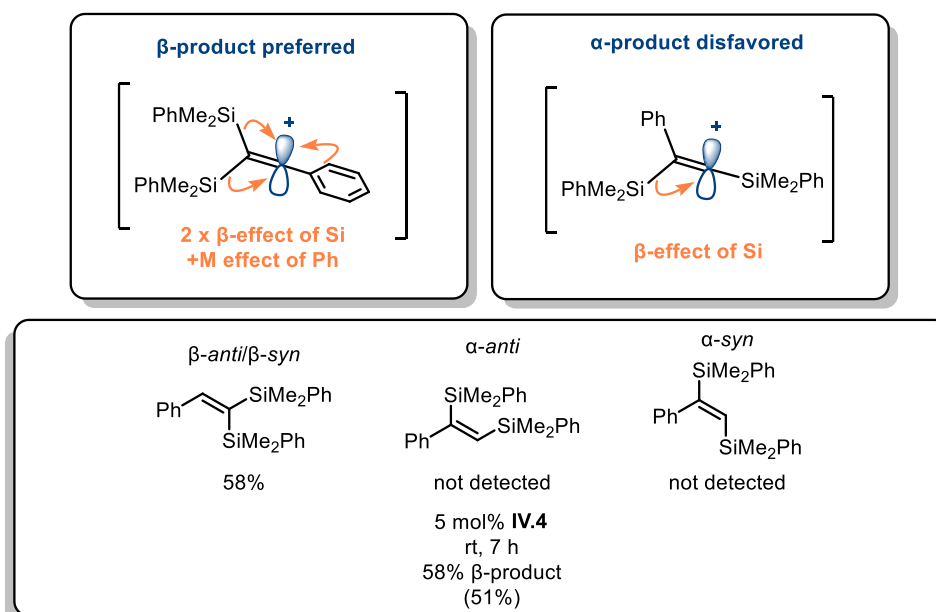
The observation of the β -addition as a major product in both cases is in accordance with our proposed mechanisms. Indeed, the electronic vacancy induced by a Si^+ transfer would be compensated in the case of a β -addition by both the β -effect of the silicon and the +M effect of the Ph, whatever the synchronicity of the Si^+/H^- transfer (Scheme IV.22). The vinyl cation

resulting from α -addition would only be stabilized by the β -silyl group, which may explain a minor α -addition (<30% in the two cases of Ph-CC-Me and Ph-CC-Cy). It also appears that the steric parameters do not have a huge impact here with both substrates exhibiting similar reactivity and product distribution.

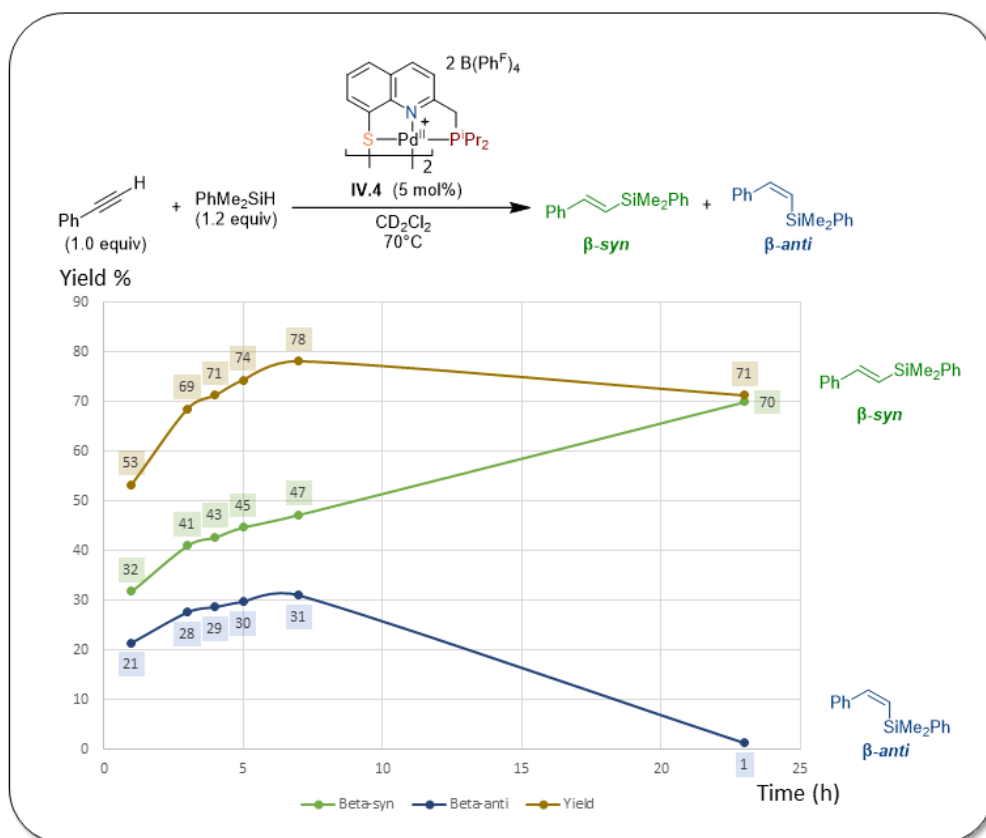


Scheme IV.22: Stabilization in the case of a dissymmetric aryl-alkyl internal alkyne and proposed explanation for the β -preference.

As the steric parameters seem to have low impact on the product distribution, we turned to Ph-CC-SiMe₂Ph as an electronically biased internal alkyne to further corroborate (or disprove) the proposed mechanism (Figure IV.6). Only the product of β -addition to the phenyl was observed with 58% yield after 7 h at room temperature (compared to Ph-CC-Me and Ph-CC-Cy that proceeded at 50 °C). However, the reaction reaches a plateau and does not evolve further, even with silane still present. The exclusive formation of the β -hydrosilylation product in this case, further corroborates a Si⁺/H⁻ transfer mechanism with this time all electronic effects converging towards a β -addition (Figure IV.6). However, the origin of the reactivity plateau still needs to be elucidated.

Figure IV.6: Hydrosilylation of the electronically biased internal alkyne Ph-CC-SiMe₂Ph with **IV.4**

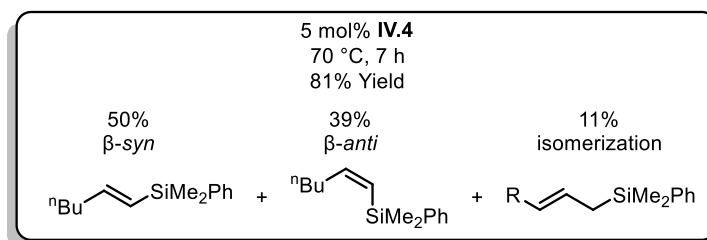
The hydrosilylation of terminal alkynes was attempted next. In the case of phenylacetylene, complete conversion and fully selective β -addition was observed after 7h at 70°C. Concerning the stereoselectivity, a mixture of *syn/anti* product was observed from the beginning, and after full conversion, isomerization of the *anti* isomer into the more stable *syn* product occurred (Scheme IV.23).



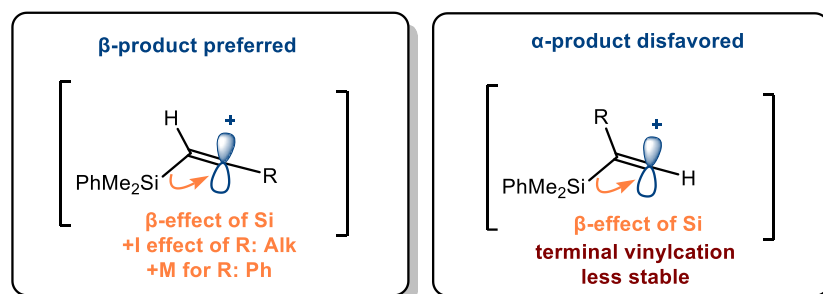
Scheme IV.23: Monitoring over time of the hydrosilylation of phenylacetylene using IV.4

At this stage, it is difficult to conclude whether the *syn* isomer is formed as the result of the hydrosilylation mechanism or is simply the result of isomerization of the *anti* isomer and this remains to be checked by independent experiments.

With alkyl substituted terminal alkynes such as hex-1-yne, 81% of hydrosilylation product was observed after 7 h at 70 °C with once again, complete selectivity towards β-hydrosilylation (50% *syn* and 39% *anti*). However, 11% of isomerization of the alkene to the allyl silane was observed. Allowing the reaction to proceed for an additional 48 h showed a stable amount of *syn* product but important isomerization of the *anti* into the allyl (*syn/anti/allyl* - 48%/13.5%/38.5%)

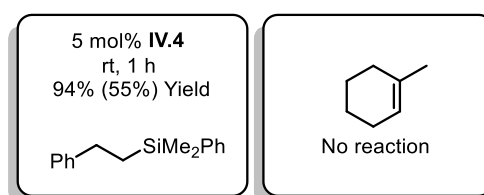
Figure IV.7: Hydrosilylation of hex-1-yne at 70 °C with **IV.4**

Overall, it appears that the major formation of the β -addition product is occurring in all cases (Scheme IV.24). These results are for the time being, in line with our proposed mechanisms but other phenomenon are in play with terminal alkynes as isomerization of the resulting vinyl silanes are observed. Further investigations are necessary to assess the origin of this isomerization and obtain a full mechanistic picture.



Scheme IV.24: Stabilization of electronic vacancy in the case of the hydrosilylation of aryl and alkyl substituted terminal alkynes

We were then interested in the hydrosilylation of alkenes such as styrene (Figure IV.8). In this case, 94% yield was achieved after 1h at room temperature with the exclusive formation of the β -hydrosilylation product. With the sterically congested 1-methylcyclohexene however, no reaction was observed.

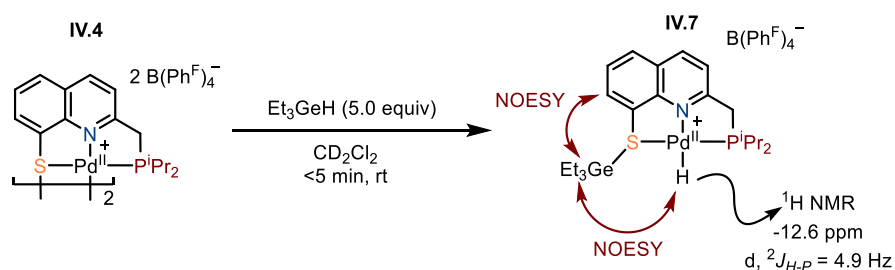
Figure IV.8: Hydrosilylation of alkenes with the cationic Pd complex **IV.4**

Overall, the ability of the cationic complex **IV.4** and in some cases, the preformed complex of Si-H activation **IV.6**, to catalyze the hydrosilylation of alkynes and alkenes was clearly established through these examples. Even if there is still work to do to fully understand the

behavior of these complexes (especially towards terminal alkynes), the obtained results are in accordance with the proposed mechanism involving the transfer of a formal Si^+ cation. We were then interested in the generalization of this activation to other type of E-H bonds.

IV.6) Extension to other E-H bonds

The stoichiometric activation of R_3GeH was then attempted with Ph_3GeH and no reaction was observed at rt. With Et_3GeH however, after only 5 minutes, the disappearance of the signal of **IV.4** in ^{31}P NMR and the formation a new signal at 74.8 ppm was observed. In ^1H NMR, a hydride signal at -12.6 ppm with a 1H integration was found along with a spectroscopic signature similar to that of **IV.6**. Unfortunately, all attempts to analyze the resulting complex by ^{73}Ge NMR failed, precluding the observation of ^{73}Ge - ^{31}P coupling. Despite an overlap with the excess Et_3GeH , a NOESY correlation between the Et_3Ge fragment and both the hydride and the *ortho*-CH was observed.



Scheme IV.25: GeH activation through Pd-S cooperativity with the cationic complex **IV.4**

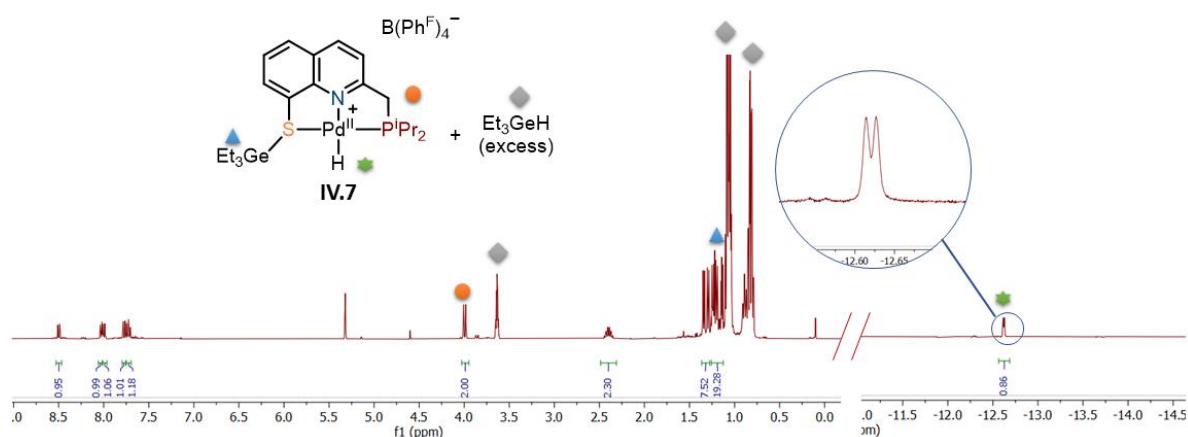
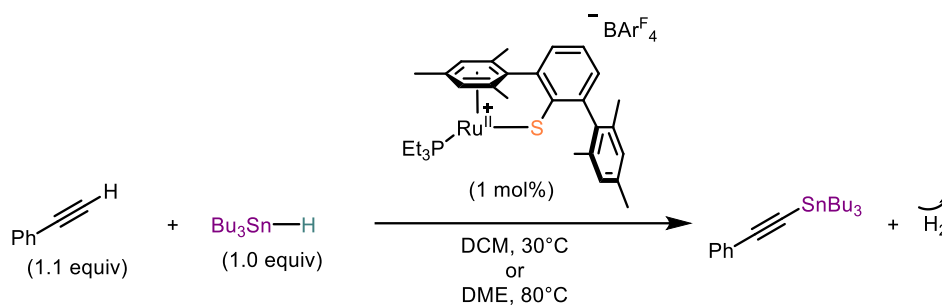


Figure IV.9: ^1H NMR of **IV.7** after reaction of **IV.4** with 5.0 equivalents of Et_3GeH in CD_2Cl_2

A similar reaction was attempted with Bu_3SnH but all attempts (even at low T°) resulted in a vigorous H_2 evolution and the formation of $\text{Bu}_3\text{Sn-SnBu}_3$. The observed trend of reaction for the activation of E-H bonds ($\text{Sn-H} \gg \text{Ge-H} > \text{Si-H}$) is in accordance with the strength of the

respective bonds and is in line with DFT calculations reported on the DmpS-Ru complex of Ohki and Tatsumi.^[23] Indeed, this comparative theoretical work shows that the E-H activation across the Ru-S motif follows the previously mentioned trend (Sn-H \gg Ge-H $>$ Si-H). The transfer of the R_3E^+ cation to terminal alkynes was also studied *in silico* and was found to be the rate-determining step in all cases. However, the transition states were found prohibitively high in energy for the R_3Ge^+ and R_3Si^+ cations. In line with these findings, only the dehydrogenative stannylation of alkynes was reported by Oestreich and no hydroelementation (Sn, Ge, Si) with the DmpS-Ru system has been reported yet.^[24]



Scheme IV.26: Catalytic dehydrogenative stannylation of terminal alkynes with the DmpS-Ru complex

With the product of cooperative Ge-H activation **IV.7** in hand the catalytic hydrogermylation of alkynes was attempted. When subjected to the symmetric hex-3-yne, the reaction was much faster compared to the previously described silyl version with 62% yield after 24 h at rt (vs 22h at 70°C for Si-H). In accordance with an easier Ge-H bond activation step compared to Si-H. However, the selectivity for both were close with 82% *syn* and 18% *anti* (vs 87% *syn* and 13% *anti* for Si-H) (Figure IV.8).

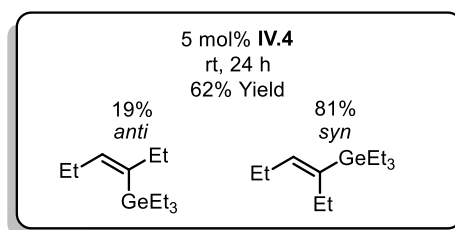
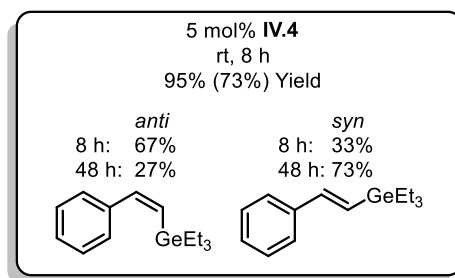


Figure IV.10: Hydrogermylation of symmetric hex-3-yne using **IV.4**

With terminal alkynes such as Ph-CC-H, 95% yield was observed after 8 h at rt with a fully β -selective reaction and a *syn/anti* ratio of 33/67 (Figure IV.11). However, an isomerization process occurred and after two days, a 73/27 ratio of *syn/anti* product was observed.

Figure IV.11: Hydrogermylation of phenylacetylene with **IV.4**

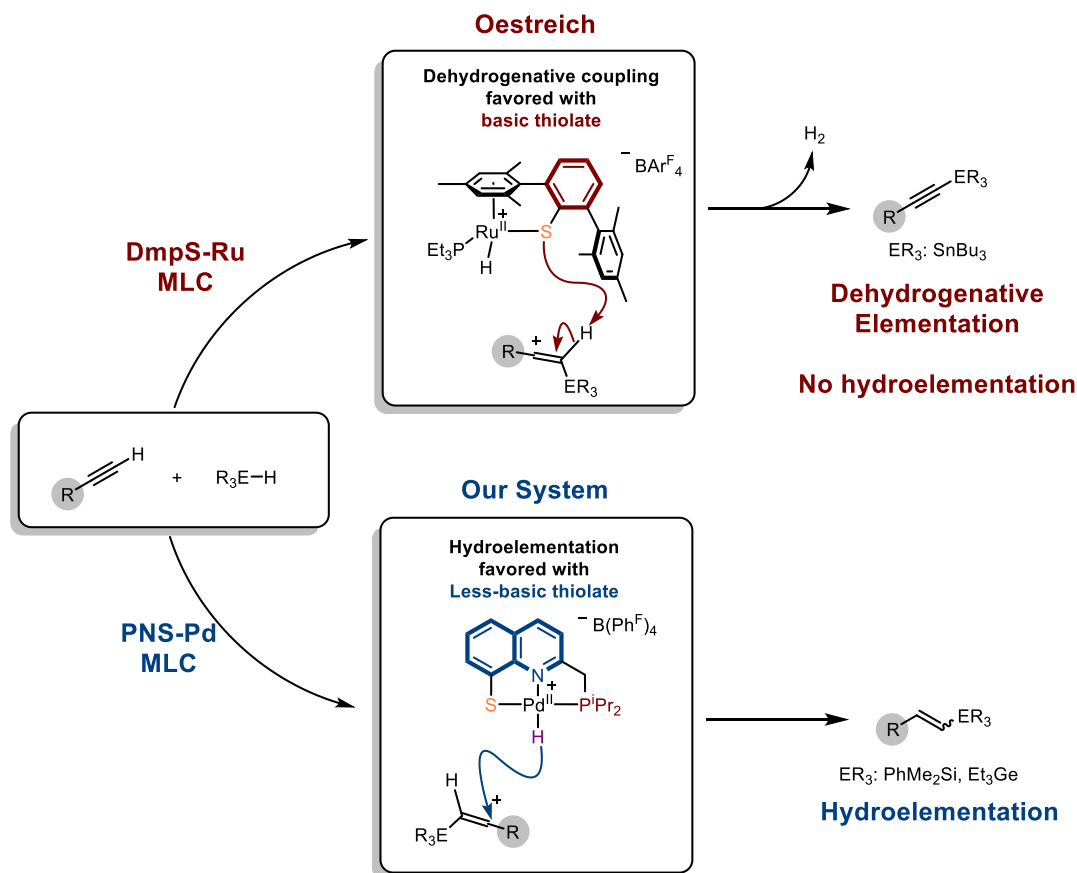
With these two examples, it appears that a mechanism of R_3Ge^+/H^- transfer is in play similarly to the Si analog. Hex-3-yne seems to follow a concerted pathway (with formation of the *syn* isomer as the major product) while phenylacetylene would favor a stepwise pathway, with the initial formation of the *anti* product as major one.

IV.7) Conclusion and perspectives

In this chapter, a new active complex was generated by halide abstraction from the PNS-Pd-Cl complex **III.5** forming a dicationic S-bridged dimeric species **IV.4**. The bifunctional character of the Pd-S motif was demonstrated with stoichiometric reactions such as with MeI and extended to more challenging E-H bond activation reactions (Si-H and Ge-H). This system was found amenable to the catalytic hydroelementation of alkynes. Even if hydrosilylation catalysts are abundant in type and number, the objectives of this work were not to simply add another system to the already vast literature, but rather to bring mechanistic diversity and a new entry point to vinylsilanes (and vinylgermanes). In our case, a mechanism involving E^+/H^- transfer was suggested by the experimental product distribution but the full mechanistic picture still needs to be clarified (DFT calculations, KIE experiments).

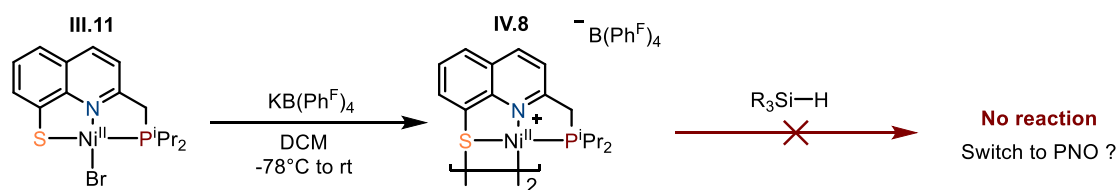
New transformations, with complementary results compared to other systems such as DmpS-Ru, were displayed by our PNS palladium complex. This contrast in reactivity can be rationalized by the difference in the ligand architecture. In the DmpS-Ru complex, a “simple” aromatic ring is tethered to the thiolate resulting a more pronounced basic character of the lone pairs at sulfur (Scheme IV.27). After deprotonation, the $DmpS^H-Ru^H$ is highly susceptible to H_2 elimination, and thus the system is prone to dehydrogenative couplings. In our case, the increased π -delocalization imported by the quinoline backbone probably reduces the basic

character of the lone pairs at sulfur to the point where hydroelementation is preferred compared to dehydrogenative coupling (Scheme IV.27).



Scheme IV.27: Comparison of the DmpS-Ru system applied to the dehydrogenative stannylation of alkynes by Oestreich and our PNS-Pd system for the catalytic hydroelementation

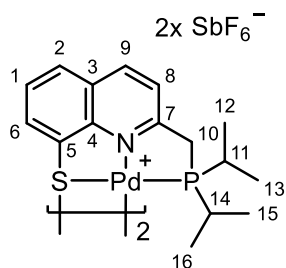
To go even one-step further, H-H and B-H bond activation would certainly merit to be explored with this ligand architecture. Extension to other metals such as Nickel is also under investigation. Initial results thanks to the internship of András Kotschy showed that a similar dicationic nickel complex could be generated but unfortunately, no reactivity in Si-H bond activation was observed at this stage (Scheme IV.28). In this case, making the switch back from the PNS architecture to the PNO might unlock the Si-H activation (by addition across the Ni-O bond).^[12]



Scheme IV.28: Generation of a cationic PNS-Ni complex and Si-H bond activation

IV.8) Experimental section

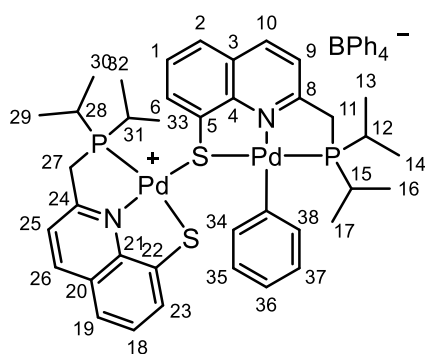
Synthesis of complexes:

Cationic SbF_6 complex - IV.1:

To a chilled suspension of $AgSbF_6$ (32 mg, 0.0931 mmol, 1.01 equiv) in 4 mL of DCM at $-78^\circ C$ was dropwise added a solution of **III.5** (40 mg, 0.0925 mmol, 1.0 equiv) in 2 mL of DCM and the resulting mixture was allowed to warm up to rt. After 1h at rt a lot of precipitate was formed, the suspension was filtered, and the solid was washed with copious amounts (around 15 mL) of DCM. The organic phases were combined and evaporated to yield the corresponding cationic complex **IV.1** as an orange solid (22 mg, 72%).

1H NMR (300 MHz, CD_2Cl_2): $\delta = 8.60$ (d, $J = 8.5$ Hz, 2H, H_9), 8.23 (dd, $J = 7.5, 1.0$ Hz, 2H, H_6), 8.17 – 8.10 (m, 2H, H_2), 7.84 – 7.78 (m, 4H, $H_{1,8}$), 4.34–4.17 (m, 2H, H_{a10}), 4.17– 3.99 (m, 2H, H_{b10}), 2.52 – 2.40 (m, 2H, $H_{11/14}$), 1.79 (dd, $J_{H-P} = 20.0, J_{H-H} = 7.1$ Hz, 6H $H_{12,13,15,16}$; masked dhept, 2H, $H_{11/14}$) 1.49 (dd, $J_{H-P} = 17.4, J_{H-H} = 7.0$ Hz, 6H, $H_{12,13,15,16}$), 0.82 (dd, $J_{H-P} = 16.2, J_{H-H} = 7.0$ Hz, 6H, $H_{12,13,15,16}$), 0.16 (dd, $J_{H-P} = 20.0, J_{H-H} = 7.1$ Hz 6H, $H_{12,13,15,16}$).

$^{31}P\{^1H\}$ NMR (121 MHz, CD_2Cl_2) $\delta = 76.8$ (s).

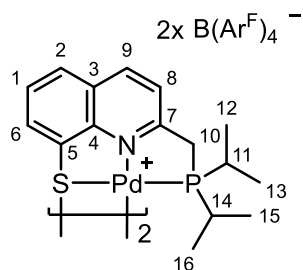
Partially cationic BPh_4 complex - IV.2':

To a chilled suspension of $NaBPh_4$ (79 mg, 0.231 mmol, 1.0 equiv) in 10 mL of DCM at $-78^\circ C$ was dropwise added a solution of **III.5** (100 mg, 0.231 mmol, 1.0 equiv) in 10 mL of DCM and the resulting mixture was allowed to warm up to rt. After 20 min the reaction was filtered, and the volatiles were removed *in vacuo*. The residue was dissolved in 3 mL of DCM and dropwise added to a stirred pentane solution (10 mL). The resulting precipitate was washed with pentane (2x3 mL) and dried *in vacuo* to yield **IV.2'** (109 mg, 79%). The structure of **IV.2'** was confirmed

by single crystal XRD.

1H NMR (300 MHz, CD_2Cl_2): $\delta = 8.43$ (d, $J = 8.5$ Hz, 1H, H_{26}), 8.25 (d, $J = 8.5$ Hz, 1H, H_{23}), 8.18 (d, $J = 7.3$ Hz, 1H, H_{19}), 8.00 – 7.81 (m, 5H), 7.75 – 7.35 (m, 20H), 7.20 – 6.83 (m, 7H), 3.88 (d, $J_{H-P} = 9.7$ Hz, 2H, H_{27}), 3.59 (d, $J_{H-P} = 10.6$ Hz, 2H, H_{11}), 2.42 – 2.23 (m, 2H, $H_{28,31}$), 2.22 – 1.98 (m, 2H $H_{12,15}$), 1.37 – 1.25 (m, 12H, H_{29-33}), 1.22 – 1.03 (m, 12H, $H_{13,14,16,17}$).

$^{31}P\{^1H\}$ NMR (121 MHz, CD_2Cl_2): $\delta = 54.8$ (s), 53.0 (s).

Cationic BAr^F_4 complex - IV.3:

To a stirred suspension at $-78\text{ }^\circ\text{C}$ of NaBAr^F_4 (410 mg, 0.46 mmol, 1.0 equiv) in DCM (15 mL) was added a solution of **III.5** (200 mg, 0.46 mmol, 1.0 equiv) in DCM (10 mL). The reaction was allowed to warm up to rt. After 1 h at rt, the mixture was filtered and the solvent was removed *in vacuo* to yield the cationic complex **IV.3** (544 mg, 94%).

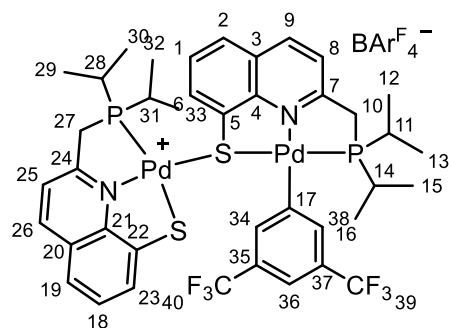
$^1\text{H NMR}$ (500 MHz, CD_2Cl_2): δ = 8.52 (dd, J = 8.6, 0.9 Hz, 2H, H_9), 8.20 (dd, J = 7.5, 1.2 Hz, 2H, H_6), 8.06 (dd, J = 8.2, 1.2 Hz, 2H, H_2), 7.86-7.82 (m, 2H, H_1), 7.81 (d, J = 8.6 Hz, 2H, H_8), 7.73-7.68 (m, 16H,

$\text{H}_{\text{orthoBAr}^F}$), 7.56-7.52 (m, 8H, $\text{H}_{\text{paraBAr}^F}$), 4.19 – 4.07 (m, 2H, $\text{H}_{\text{a}10}$), 3.87 – 3.74 (m, 1H, $\text{H}_{\text{b}10}$), 2.44 (dhept, $J_{\text{H-P}}$ = 8.9, $J_{\text{H-H}}$ = 7.0 Hz, 2H, $\text{H}_{11,14}$), 1.77 (dd, $J_{\text{H-P}}$ = 20.4, $J_{\text{H-H}}$ = 7.1 Hz, 3H, $\text{H}_{12,13,15,16}$); masked dhept, 2H, $\text{H}_{11,14}$), 1.46 (dd, $J_{\text{H-P}}$ = 17.3, $J_{\text{H-H}}$ = 7.0 Hz, 3H, $\text{H}_{12,13,15,16}$), 0.78 (dd, $J_{\text{H-P}}$ = 16.2, $J_{\text{H-H}}$ = 6.9 Hz, 3H, $\text{H}_{12,13,15,16}$), 0.05 (dd, $J_{\text{H-P}}$ = 19.6, $J_{\text{H-H}}$ = 7.2 Hz, 3H, $\text{H}_{12,13,15,16}$).

$^{13}\text{C}\{^1\text{H}\}$ NMR (126 MHz, CD_2Cl_2): δ = 164.1 (C_7), 162.2 (q, $J_{\text{C-B}}$ = 50.0 Hz, $\text{C}_{\text{quatB B(Ar}^F)_4}$), 153.1 (C_4), 143.4 (C_9), 140.4 (t, $J_{\text{C-P}}$ = 2.3 Hz, C_6), 135.2 (s, $\text{CH}_{\text{orthoBAr}^F}$), 131.0 (C_5), 130.9 (C_2), 130.9 (C_3), 129.9 (C_1), 129.3 (qq, $J_{\text{C-F}}$ = 31.6, 2.9 Hz, $\text{C}_{\text{metaBAr}^F}$), 125.0 (q, $J_{\text{C-F}}$ = 272.8 Hz, CF_3BAr^F), 121.9 (t, $J_{\text{C-P}}$ = 5.6 Hz, C_8), 117.9 (pseudo hept, $\text{CH}_{\text{paraBAr}^F}$), 38.32-37.88 (m, C_{10}), 26.34-25.80 (m, $\text{C}_{11,14}$), 25.26-24.79 (m, $\text{C}_{11,14}$), 19.2 (s, $\text{C}_{12,13,15,16}$), 18.0 (s, $\text{C}_{12,13,15,16}$), 17.1 (s, $\text{C}_{12,13,15,16}$), 17.0 (s, $\text{C}_{12,13,15,16}$).

$^{31}\text{P}\{^1\text{H}\}$ NMR (202 MHz, CD_2Cl_2): δ = 72.6 (s).

^{15}N NMR (51 MHz, CD_2Cl_2): δ = 231.3 (s).

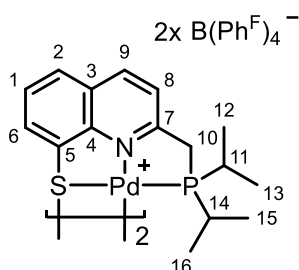
Cationic $B(\text{Ph}^F)_4$ complex - IV.3':

A J-young NMR tube was charged with **IV.3** (15 mg, 0.012 mmol, 1.0 equivalent) in 0.5 mL of CD_2Cl_2 and the tube was heated at $80\text{ }^\circ\text{C}$. After 16 h complete conversion was observed by ^1H and ^{31}P NMR. The structure of **IV.3'** was confirmed by XRD.

$^1\text{H NMR}$ (300 MHz, CD_2Cl_2): δ = 8.52 (d, J = 7.7 Hz, 1H, H_{26}), 8.25 – 8.07 (m, 2H, $\text{H}_{19,23}$), 8.01 – 7.94 (m, 4H, $\text{H}_{25,18,38,34}$), 7.84 – 7.66 (m, 13H, $\text{H}_{1,2,6,8,9, \text{H}_{\text{orthoBAr}^F}}$), 7.60 – 7.52 (m, 4H, $\text{H}_{36, \text{H}_{\text{paraBAr}^F}}$), 3.98 (d, J = 10.2 Hz, 2H, H_{27}),

3.69 (d, J = 10.7 Hz, 2H, H_{10}), 2.53 – 2.29 (m, 2H, $\text{H}_{28,21}$), 2.36 – 2.13 (m, 2H, $\text{H}_{11,14}$), 1.28 (dd, J = 16.1, 7.3 Hz, 12H, $\text{H}_{29,30,32,33}$), 1.21 – 1.04 (m, 12H, $\text{H}_{12,13,15,16}$).

^{31}P NMR (121 MHz, CD_2Cl_2): δ = 55.7 (s), 55.1 (s).

Cationic $B(\text{Ph}^F)_4$ complex - IV.4:

To a stirred suspension at $-78\text{ }^\circ\text{C}$ of $\text{KB}(\text{Ph}^F)_4$ (332 mg, 0.46 mmol, 1.0 equiv) in DCM (20 mL) was added a solution of **III.5** (200 mg, 0.46 mmol, 1.0 equiv) in DCM (10 mL). The reaction was allowed to warm up to rt. After 1 h at rt, the mixture was filtered and the solvent was removed *in vacuo* to yield the cationic complex **IV.4** as a red solid (440 mg, 89%).

$^1\text{H NMR}$ (500 MHz, CD_2Cl_2): $\delta = 8.60$ (d, $J = 8.5$ Hz, 2H, H_9), 8.23 (dd, $J = 7.5, 1.0$ Hz, 2H, H_6), 8.17 – 8.10 (m, 2H, H_2), 7.84 – 7.78 (m, 4H, $\text{H}_{1\text{H}8}$), 4.22 – 4.08 (m, 2H, $\text{H}_{\text{a}10}$), 3.92 – 3.79 (m, 2H, $\text{H}_{\text{b}10}$), 2.52 – 2.40 (m, 2H, $\text{H}_{11/14}$), 1.79 (dd, $J_{\text{H-P}} = 20.0$, $J_{\text{H-H}} = 7.1$ Hz, 6H, masked dhept, 2H, $\text{H}_{11/14}$) 1.49 (dd, $J_{\text{H-P}} = 17.4$, $J_{\text{H-H}} = 7.0$ Hz, 6H, $\text{H}_{12,13,15,16}$), 0.82 (dd, $J_{\text{H-P}} = 16.2$, $J_{\text{H-H}} = 7.0$ Hz, 6H, $\text{H}_{12,13,15,16}$), 0.00 (dd, $J_{\text{H-P}} = 20.0$, $J_{\text{H-H}} = 7.1$ Hz 6H, $\text{H}_{12,13,15,16}$).

$^{13}\text{C}\{^1\text{H}\}$ NMR (126 MHz, CD_2Cl_2): $\delta = 164.3$ (C_7), 153.1 (C_4), 148.1 (d, $J_{\text{C-F}} = 241$ Hz, C_{BPhF}), 143.3 (C_9), 140.4 (C_6), 138.18 (d, $J_{\text{C-F}} = 245$ Hz, C_{BPhF}), 138.18 (d, $J_{\text{C-F}} = 242$ Hz, C_{BPhF}), 131.0 (C_5), 130.9 (C_3), 130.9 (C_2), 129.8 (C_1), 121.9 (C_8), 38.2–38.0 (m, C_{10}), 26.2–26.0 (m, $\text{C}_{11,14}$), 25.1–25.0 (m, $\text{C}_{11,14}$), 19.2 ($\text{C}_{12,13,15,16}$), 18.0 ($\text{C}_{12,13,15,16}$), 17.0 ($\text{C}_{12,13,15,16}$), 16.8 ($\text{C}_{12,13,15,16}$).

$^{31}\text{P}\{^1\text{H}\}$ NMR (202 MHz, CD_2Cl_2): $\delta = 75.8$ (s).

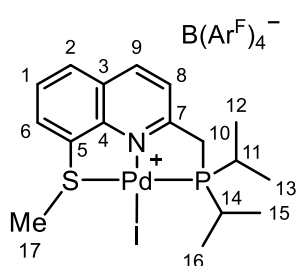
^{15}N NMR (51 MHz, CD_2Cl_2): $\delta = 231.4$ (s).

$^{11}\text{B}\{^1\text{H}\}$ NMR (160 MHz, CD_2Cl_2): $\delta = -16.7$ (s).

$^{19}\text{F}\{^1\text{H}\}$ NMR (471 MHz, CD_2Cl_2): $\delta = -132.8$ - -133.3 (m), -163.4 (t, $J = 20.4$ Hz), -167.1 - -167.5 (m).

HRMS (ESI+) m/z : calculated: 793.0272 ($\text{C}_{32}\text{H}_{41}\text{N}_2\text{P}_2\text{S}_2\text{Pd}_2$), found: 793.0276.

HRMS (ESI-) m/z : calculated: 678.9774 ($\text{C}_{24}\text{B}_1\text{F}_{20}$), found: 678.9771.

Cationic BAr^F₄ complex + MeI - IV.5:

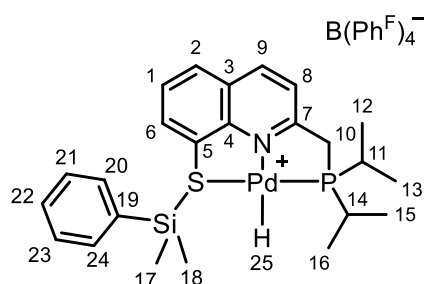
A J-young NMR tube was charged with [PNS-Pd-BAr^F]₂ (44 mg, 0.035 mmol, 1.0 equivalent) in 0.5 mL of CD₂Cl₂. A solution of MeI in CD₂Cl₂ was then added (0.1 mL, 5mg, 1.0 equivalent) and the reaction was heated at 80°C. After 16h 30% conversion was reached by ³¹P NMR analysis. Another fresh solution of MeI in CD₂Cl₂ was added (0.4 mL, 20 mg, 4.0 equivalents) and after 4h at 80°C, complete conversion was observed by ¹H and ³¹P NMR. The solvent and excess MeI is removed *in vacuo* to yield the corresponding cationic complex.

¹H NMR (500 MHz, CD₂Cl₂): δ = 8.55 (dd, *J* = 8.5, 1.2 Hz, 1H, H₉), 8.21 (dd, *J* = 7.5, 1.2 Hz, 1H, H₆), 8.06 (dd, *J* = 8.2, 1.2 Hz, 1H, H₂), 7.86-7.82 (m, 1H, H₁), 7.81 (d, *J* = 8.5 Hz, 1H, H₈), 7.74-7.71 (m, 8H, H_{ortho}BAr^F), 7.56-7.54 (m, 4H, H_{para}BAr^F), 4.04 (d, *J*_{H-P} = 10.8 Hz, 2H, H₁₀), 3.08 (d, *J* = 3.8 Hz, 3H, H₁₇), 2.61 (dhept, *J*_{H-P} = 9.9, *J*_{H-H} = 7.0 Hz, 2H, H₁₁₋₁₄), 1.50 (dd, *J*_{H-P} = 19.6, *J*_{H-H} = 7.1 Hz, 6H, H_{12,13,15,16}), 1.26 (dd, *J*_{H-P} = 17.6, *J*_{H-H} = 7.0 Hz, 6H, H_{12,13,15,16}).

¹³C{¹H} NMR (126 MHz, CD₂Cl₂): δ = 164.9 (d, *J*_{C-P} = 3.3 Hz, C₇), 162.2 (q, *J*_{C-B} = 50.0 Hz, C_{quat}B B(Ar^F)₄), 148.7 (C₄), 142.3 (C₉), 139.7 (d, *J*_{C-P} = 2.9 Hz, C₆), 135.2 (s, CH_{ortho}BAr^F), 134.1 (d, *J*_{C-P} = 2.8 Hz, C₅), 131.6 (C₂), 130.0 (C₁), 129.9 (C₃), 129.3 (qq, *J*_{C-F} = 31.6, 2.9 Hz, C_{meta}BAr^F), 125.0 (q, *J*_{C-F} = 272.8 Hz, CF₃BAr^F), 121.6 (d, *J*_{C-P} = 12.1 Hz, C₈), 117.9 (pseudo hept, CH_{para}BAr^F), 40.1 (d, *J*_{C-P} = 24.9 Hz, C₁₀), 27.5 (d, *J*_{C-P} = 27.2 Hz, C_{11,14}), 26.6 (d, *J*_{C-P} = 2.0 Hz, C₁₇), 19.3-19.2 (m, C_{12,13,15,16}), 17.9 (d, *J*_{C-P} = 2.5 Hz, C_{12,13,15,16}).

³¹P{¹H} NMR (202 MHz, CD₂Cl₂): δ = 83.0 (s).

¹⁵N NMR (51 MHz, CD₂Cl₂): δ = 240.1 (s).

Cationic complex of SiH activation IV.6:

A J-young NMR tube was charged with **IV.4** (20 mg, 0.018 mmol, 1.0 equivalent), PhMe₂SiH (14.2 μL, 0.093 mmol, 5.0 equivalent) and 1 mL of CD₂Cl₂ the tube was vigorously shaken, and the reaction was monitored by NMR. After 16h the product **IV.6** was seen as the only species by ³¹P NMR analysis and characterized spectroscopically in presence of excess PhMe₂SiH.

¹H NMR (500 MHz, CD₂Cl₂): δ = 8.43 (d, *J* = 8.5 Hz, 1H, H₉), 8.01 – 7.95 (m, 1H, H₂), 7.73 – 7.62 (m, 3H, H_{6,1,8}), 7.38 – 7.32 (m, 1H, H₂₂), 7.31 – 7.27 (m, 2H, H_{20,24}), 7.23 – 7.18 (m, 2H, H_{21,23}), 3.86 (d, *J*_{H-P} = 9.9 Hz, 2H, H₁₀), 2.46 – 2.27 (m, 2H, H_{14,11}), 1.31 (dd, *J*_{H-P} = 19.5, *J*_{H-H} = 7.0 Hz, 6H, H_{16,12}), 1.19 (dd, *J*_{H-P} = 17.2, *J*_{H-H} = 7.0 Hz, 6H, H_{15,13}), 0.83 (s, 6H, H_{17,18}) -12.74 (d, *J*_{H-P} = 6.5 Hz, 1H, H₂₅)

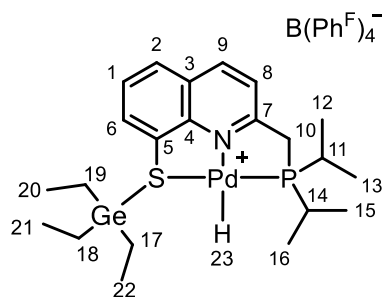
¹³C{¹H} NMR (126 MHz, CD₂Cl₂): δ = 161.6 (d, *J*_{C-P} = 3.9 Hz, C₇), 148.1 (d, *J*_{C-F} = 241 Hz, C_{BPhF}), 146.2 (d, *J*_{C-P} = 2.0 Hz, C₄) 140.5 (C₉), 138.2 (d, *J*_{C-F} = 245 Hz, C_{BPhF}), 138.63 (d, *J*_{C-P} = 2.4 Hz, C₆), 136.3 (d, *J*_{C-F} = 244 Hz, C_{BPhF}), 133.8 (C_{20,24}), 132.2 (C₁₉), 131.5 (C₂₂), 131.4 (C₅), 129.1 (C₂), 128.9 (C₃), 128.1 (C₁), 121.0 (d, *J*_{C-P} = 10.4 Hz, C₈), 38.47 (d, *J*_{C-P} = 23.1 Hz, C₁₀), 25.2 (d, *J*_{C-P} = 28.1 Hz, C_{11,14}), 19.2 (d, *J*_{C-P} = 4.0 Hz, C_{16,12}), 17.9 (C_{15,13}) -0.3 (C_{17,18}).

³¹P{¹H} NMR (202 MHz, CD₂Cl₂): δ = 76.4 (s).

²⁹Si NMR (99 MHz, CD₂Cl₂): δ = 23.0 (s).

¹¹B NMR (160 MHz, CD₂Cl₂): δ = -16.7 (s).

¹⁹F NMR (471 MHz, CD₂Cl₂): δ = -133.0 – -133.2 (m), -163.5 (t, *J* = 20.4 Hz), -167.2 – -167.6 (m).

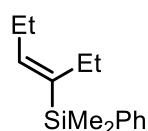
Cationic complex of GeH activation IV.7:

A J-young NMR tube was charged with **IV.4** (20 mg, 0.018 mmol, 1.0 equivalent), Et₃GeH (16.2 μL, 0.093 mmol, 5.0 equivalent) and 1 mL of CD₂Cl₂ the tube was vigorously shaken, and the reaction was monitored by NMR. After <5 min the product **IV.7** was seen as the only species by ³¹P NMR analysis and characterized spectroscopically in presence of excess Et₃GeH.

¹H NMR (500 MHz, CD₂Cl₂): δ = 8.50 (d, *J* = 8.5 Hz, 1H, H₉), 8.03 (d, *J* = 7.4 Hz, 1H, H₆), 8.00 (d, *J* = 8.2 Hz, 1H, H₂), 7.77 (d, *J* = 8.5 Hz, 1H, H₈), 7.75 – 7.68 (m, 1H, H₁), 3.99 (d, *J*_{H-P} = 9.8 Hz, 2H, H₁₀), 2.49 – 2.32 (m, 2H, H_{14,11}), 1.32 (dd, *J*_{H-P} = 19.5, *J*_{H-H} = 7.0 Hz, 6H, H_{12,14,15,16}), 1.26 – 1.17 (m, 12H, H_{12,14,15,16}; H₁₉₋₂₁), 1.11 – 1.02 (m, 9H, H₂₀₋₂₂), -12.62 (d, *J*_{H-P} = 4.9 Hz, 1H, H₂₃).

¹³C{¹H} NMR (126 MHz, CD₂Cl₂): δ = 162.4 (C₇), 148.5 (d, *J*_{C-F} = 239.0 Hz, C_{BPhF}), 147.0 (C₄), 141.1 (C₉), 138.4 (d, *J*_{C-P} = 2.7 Hz, C₆), 138.2 (d, *J*_{C-F} = 245 Hz, C_{BPhF}), 135.9 (d, *J*_{C-F} = 246 Hz, C_{BPhF}), 133.4 (d, *J*_{C-P} = 1.4 Hz, C₄) 129.5 (C₃), 129.4 (C₂), 129.1 (C₁), 121.2 (d, *J*_{C-P} = 10.5 Hz, C₈), 38.5 (d, *J*_{C-P} = 23.0 Hz, C₁₀), 25.16 (d, *J*_{C-P} = 28.0 Hz, C_{11,14}), 19.07 (d, *J*_{C-P} = 4.2 Hz, C_{16,12}), 17.8 (C_{15,13}), 10.4 (C₁₇₋₁₉), 9.7 (C₂₀₋₂₂)

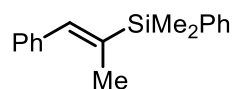
³¹P{¹H} NMR (121 MHz, CD₂Cl₂): δ = 74.8 (s).

(E)-hex-3-en-3-yl dimethyl(phenyl)silane - [80279-07-8]:

Using the general procedure with hex-3-yne (23 μL , 0.20 mmol, 1.0 equiv), PhMe_2SiH (37 μL , 0.24 mmol, 1.2 equiv), $[\text{PNS-Pd-B}(\text{Ph}^{\text{F}})_4]$ (5 mol%) and 1,2,4,5-tetramethylbenzene as internal standard (E)-hex-3-en-3-yl dimethyl(phenyl)silane was formed along with the *anti*-isomer with 84% yield as estimated by ^1H NMR analysis. Isolated as mixture by column chromatography (using 100% pentane - 25 mg - 58% combined yield). Attribution of the various products was based on literature data. For minor products, a detailed ^1H NMR analysis could not be provided, diagnostic signals however are listed below.

^1H NMR (300 MHz, CDCl_3): δ = 7.62 – 7.46 (m, 2H, H_{arom}), 7.43 – 7.29 (m, 3H, H_{arom}), 5.78 (t, J = 6.8 Hz, 1H, H_{vinyl}), 2.24 – 2.06 (m, 4H, $2\times\text{CH}_2$), 1.00 (t, J = 7.5, 3H, CH_3), 0.85 (t, J = 7.5, 3H, CH_3), 0.35 (s, 6H, SiCH_3). Spectroscopic data in accordance with the literature.^[26]

Anti-isomer: CH signal at 6.05 ppm (t, J = 7.6, 1H) in accordance with literature data.^[25]

(E)-dimethyl(phenyl)(1-phenylprop-1-en-2-yl)silane - [106621-01-6]:

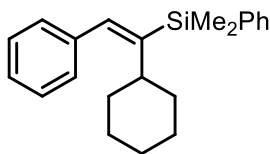
Using the general procedure with prop-1-yn-1-ylbenzene (25 μL , 0.20 mmol, 1.0 equiv), PhMe_2SiH (37 μL , 0.24 mmol, 1.2 equiv), $[\text{PNS-Pd-B}(\text{Ph}^{\text{F}})_4]$ (5 mol%) and 1,2,4,5-tetramethylbenzene as internal standard (E)-dimethyl(phenyl)(1-phenylprop-1-en-2-yl)silane was formed along with the β -*anti*, α -*syn* and α -*anti* isomer with 88% yield as estimated by ^1H NMR analysis. Isolated as mixture by column chromatography (using a gradient from 100:0 to 95:5 Pentane:EtOAc - 40 mg - 80% Combined yield). Attribution of the various products was based on literature data supported by NOESY NMR. For minor products, a detailed ^1H NMR analysis could not be provided, diagnostic signals however are listed below.

^1H NMR (300 MHz, CDCl_3): δ = 7.61 – 7.54 (m, 2H, H_{arom}), 7.40 – 7.29 (m, 8H, H_{arom}), 1.95 (d, J = 1.8 Hz, 3H, CH_3), 0.44 (s, 6H, $2\times\text{SiCH}_3$). Spectroscopic data in accordance with literature.^[27]

β -*anti*: CH_3 signal at 2.00 ppm (d, J = 1.7 Hz, 3H) in accordance with literature data.^[25]

α -*anti*: CH_3 signal at 1.76 ppm (d, J = 7.1 Hz, 3H)

α -*syn*: CH_3 signal at 1.58 ppm (d, J = 6.6 Hz, 3H) in accordance with literature data.^[27]

(Z)-(1-cyclohexyl-2-phenylvinyl)dimethyl(phenyl)silane:

Using the general procedure with (cyclohexylethynyl)benzene (37 mg, 0.20 mmol, 1.0 equiv), PhMe_2SiH (37 μL , 0.24 mmol, 1.2 equiv), $[\text{PNS-Pd-B}(\text{Ph}^{\text{F}})_4]$ (5 mol%) and 1,2,4,5-tetramethylbenzene as internal standard (E)-dimethyl(phenyl)(1-phenylprop-1-en-2-yl)silane was formed along with the β -*anti*, α -*syn* and α -*anti* isomer with 91% yield as estimated by ^1H NMR analysis. Isolated as mixture by column chromatography (using 100% petroleum ether - 38 mg - 60% Combined yield). Attribution of the various products was based on NOESY NMR. For minor products, a detailed ^1H NMR analysis could not be provided, diagnostic signals however are listed below.

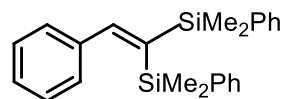
^1H NMR (300 MHz, CDCl_3): δ = 7.64 – 7.53 (m, 2H, H_{arom}), 7.38 – 7.15 (m, 8H, H_{arom}), 6.79 (s, 1H, H_{vinyl}), 2.82 (tt, J = 11.9, 3.5 Hz, 1H, CH_{Cy}), 1.74 – 0.87 (m, 10H, $\text{CH}_{2\text{Cy}}$), 0.51 (s, 6H, SiCH_3).

β -*anti*: SiCH_3 signal at 0.29 ppm (s, 6H)

α -*anti*: CH_{vinyl} signal at 6.00 ppm (d, J = 10.5 Hz, 1H).

α -*syn*: CH_{vinyl} signal at 5.82 ppm (d, J = 9.4 Hz, 1H).

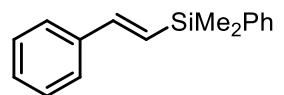
(2-phenylethene-1,1-diyl)bis(dimethyl(phenyl)silane) - [914810-30-3]:



Using the general procedure with dimethyl(phenyl)(phenylethynyl)silane (37 mg, 0.20 mmol, 1.0 equiv), PhMe₂SiH (37 μ L, 0.24 mmol, 1.2 equiv), [PNS-Pd-B(Ph^F)₄] (5 mol%) and 1,2,4,5-tetramethylbenzene as internal standard (2-phenylethene-1,1-diyl)bis(dimethyl(phenyl)silane) was formed with 58% yield as estimated by ¹H NMR analysis. Isolated by column chromatography (using 100% pentane - 38 mg - 51% Yield).

¹H NMR (300 MHz, CDCl₃): δ = 7.93 (s, 1H, H_{vinyl}), 7.58 – 7.49 (m, 4H, H_{arom}), 7.43 – 7.07 (m, 16H, H_{arom}), 0.40 (s, 6H, 2xSiCH₃), 0.05 (s, 6H, 2xSiCH₃). Spectroscopic data in accordance with literature.^[28]

(E)-dimethyl(phenyl)(styryl)silane - [64788-85-8]

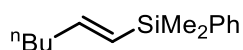


Using the general procedure with phenylacetylene (22 μ L, 0.20 mmol, 1.0 equiv), PhMe₂SiH (37 μ L, 0.24 mmol, 1.2 equiv), [PNS-Pd-B(Ph^F)₄] (5 mol%) and 1,2,4,5-tetramethylbenzene as internal standard (E)-dimethyl(phenyl)(styryl)silane was formed with 70% yield as estimated by ¹H NMR analysis.

¹H NMR (300 MHz, CD₂Cl₂): δ = 7.68 – 7.59 (m, 2H, H_{arom}), 7.55 – 7.27 (m, 13H, H_{arom}), 7.04 (d, J = 19.2 Hz, 1H, Ph-H_{vinyl}), 6.68 (d, J = 19.2 Hz, 1H, Si-H_{vinyl}), 0.51 (s, 6H, 2xSiCH₃). Spectroscopic data in accordance with literature.^[27]

The formation of the β -*syn* product was monitored with the CH_{vinyl} signal at 6.08 ppm (d, J = 15.1 Hz, 1H). In accordance with literature data.^[25]

(E)-hex-1-en-1-yldimethyl(phenyl)silane - [64545-10-4]



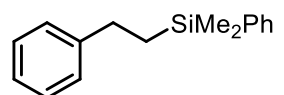
Using the general procedure with hex-1-yne (23 μ L, 0.20 mmol, 1.0 equiv), PhMe₂SiH (37 μ L, 0.24 mmol, 1.2 equiv), [PNS-Pd-B(Ph^F)₄] (5 mol%) and 1,2,4,5-tetramethylbenzene as internal standard (E)-hex-1-en-1-yldimethyl(phenyl)silane was formed along with the β -*anti* isomer and the product resulting from chain walking with 95% yield as estimated by ¹H NMR analysis (300 MHz, CD₂Cl₂).

β -*syn*: CH_{vinyl} signals at 6.19 ppm (dt, J = 18.5, 6.3 Hz, 1H) and 5.80 ppm (dt, J = 18.5, 1.5 Hz, 1H). In accordance with literature data.^[29]

β -*anti*: CH_{vinyl} signal at 6.48 ppm (dt, J = 14.0, 7.4 Hz, 1H) and 5.66 ppm (dt, J = 14.0, 1.3 Hz, 1H). In accordance with literature data.^[29]

Chain-walking: CH_{vinyl} signals at 5.48 – 5.28 (m, 1H). In accordance with literature data.^[29]

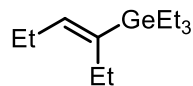
Dimethyl(phenethyl)(phenyl)silane - [62257-76-5]:



Using the general procedure with styrene (23 μ L, 0.20 mmol, 1.0 equiv), PhMe₂SiH (37 μ L, 0.24 mmol, 1.2 equiv), [PNS-Pd-B(Ph^F)₄] (5 mol%) and 1,2,4,5-tetramethylbenzene as internal standard dimethyl(phenethyl)(phenyl)silane was formed with 94% yield as estimated by ¹H NMR analysis. Isolated by column chromatography (using 100% pentane - 26 mg - 55% Yield).

$^1\text{H NMR}$ (300 MHz, CDCl_3): δ = 7.59 – 7.48 (m, 2H, H_{arom}), 7.45 – 7.36 (m, 5H, H_{arom}), 7.30 – 7.22 (m, 4H, H_{arom}), 7.20 – 7.12 (m, 3H, H_{arom}), 2.70 – 2.59 (m, 2H, Ph- CH_2), 1.19 – 1.08 (m, 2H, Si- CH_2), 0.30 (s, 6H, 2xSi CH_3). Spectroscopic data in accordance with literature.^[30]

(E)-triethyl(hex-3-en-3-yl)germane:



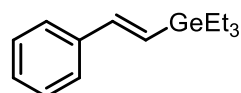
Using the general procedure with phenylacetylene (22 μL , 0.20 mmol, 1.0 equiv), Et_3GeH (39 μL , 0.24 mmol, 1.2 equiv), [PNS-Pd-B(Ph^F) $_4$] (5 mol%) and 1,2,4,5-tetramethylbenzene as internal standard (E)-triethyl(hex-3-en-3-yl)germane was formed along with the β -anti isomer with 62% yield as estimated by $^1\text{H NMR}$ analysis (300 MHz, CD_2Cl_2).

β -syn: 5.51 ppm (tt, J = 6.9, 1.0 Hz, 1H, H_{vinyl}), 2.20 – 2.07 ppm (m, 4H, 2x CH_2 - C_{vinyl}), 1.25 – 0.71 ppm (m, 21H, 5x CH_3 , 3x CH_2).

For the minor β -anti product a detailed $^1\text{H NMR}$ analysis could not be provided.

β -anti: CH_{vinyl} signal at 5.93 ppm (tt, J = 7.3, 1.4 Hz, 1H).

(E)-triethyl(styryl)germane - [19319-12-1]:



Using the general procedure with phenylacetylene (22 μL , 0.20 mmol, 1.0 equiv), Et_3GeH (39 μL , 0.24 mmol, 1.2 equiv), [PNS-Pd-B(Ph^F) $_4$] (5 mol%) and 1,2,4,5-tetramethylbenzene as internal standard (E)-triethyl(styryl)germane along with the β -anti isomer was formed with 95% yield as estimated by $^1\text{H NMR}$ analysis. Isolated as mixture by column chromatography (using 100% pentane - 39 mg - 73% Yield).

$^1\text{H NMR}$ (300 MHz, CDCl_3): δ = 7.46 – 7.40 (m, 2H, H_{arom}), 7.37 – 7.17 (m, 3H, H_{arom}), 6.83 (d, J = 19.0 Hz, 1H, Ph- H_{vinyl}), 6.61 (d, J = 19.0 Hz, 1H, Ge- H_{vinyl}), 1.08 (t, J = 7.8 Hz, 9H, 3x CH_3), 0.87 (q, J = 7.8 Hz, 6H, 3x CH_2). Spectroscopic data in accordance with literature.^[31]

For the minor β -anti product a detailed $^1\text{H NMR}$ analysis could not be provided.

CH_{vinyl} signals at 7.48 ppm (d, J = 14.1 Hz, 1H) and 5.93 ppm (d, J = 14.1 Hz, 1H). In accordance with literature data.^[32]

IV.9)References

- [1] L. Omann, C. D. F. Königs, H. F. T. Klare, M. Oestreich, *Acc. Chem. Res.* **2017**, *50*, 1258–1269.
- [2] Y. Ohki, Y. Takikawa, H. Sadohara, C. Kesenheimer, B. Engendahl, E. Kapatina, K. Tatsumi, *Chem. – Asian J.* **2008**, *3*, 1625–1635.
- [3] A. Lefranc, Z.-W. Qu, S. Grimme, M. Oestreich, *Chem. – Eur. J.* **2016**, *22*, 10009–10016.
- [4] H. F. T. Klare, M. Oestreich, J. Ito, H. Nishiyama, Y. Ohki, K. Tatsumi, *J. Am. Chem. Soc.* **2011**, *133*, 3312–3315.
- [5] T. Stahl, P. Hrobárik, C. D. F. Königs, Y. Ohki, K. Tatsumi, S. Kemper, M. Kaupp, H. F. T. Klare, M. Oestreich, *Chem. Sci.* **2015**, *6*, 4324–4334.
- [6] C. D. F. Königs, H. F. T. Klare, M. Oestreich, *Angew. Chem. Int. Ed.* **2013**, *52*, 10076–10079.
- [7] S. Wübbolt, M. Oestreich, *Angew. Chem. Int. Ed.* **2015**, *54*, 15876–15879.
- [8] C. D. F. Königs, H. F. T. Klare, Y. Ohki, K. Tatsumi, M. Oestreich, *Org. Lett.* **2012**, *14*, 2842–2845.
- [9] J. Hermeke, H. F. T. Klare, M. Oestreich, *Chem. – Eur. J.* **2014**, *20*, 9250–9254.
- [10] S. Bähr, A. Simonneau, E. Irran, M. Oestreich, *Organometallics* **2016**, *35*, 925–928.
- [11] T. Stahl, K. Müther, Y. Ohki, K. Tatsumi, M. Oestreich, *J. Am. Chem. Soc.* **2013**, *135*, 10978–10981.
- [12] J. Liu, J.-Y. Chen, M. Jia, B. Ming, J. Jia, R.-Z. Liao, C.-H. Tung, W. Wang, *ACS Catal.* **2019**, *9*, 3849–3857.
- [13] S.-F. Hou, J.-Y. Chen, M. Xue, M. Jia, X. Zhai, R.-Z. Liao, C.-H. Tung, W. Wang, *ACS Catal.* **2020**, *10*, 380–390.
- [14] A. Clerc, N. Saffon-Merceron, J. Monot, B. Martin Vaca, D. Bourissou, *Acta Crystallogr. Sect. E Crystallogr. Commun.* **2022**, *78*, 18–22.
- [15] A. J. Chalk, J. F. Harrod, *J. Am. Chem. Soc.* **1965**, *87*, 16–21.
- [16] W. J. Teo, C. Wang, Y. W. Tan, S. Ge, *Angew. Chem. Int. Ed.* **2017**, *56*, 4328–4332.
- [17] N. Hazari, J. E. Heimann, *Inorg. Chem.* **2017**, *56*, 13655–13678.
- [18] H.-W. Suh, T. J. Schmeier, N. Hazari, R. A. Kemp, M. K. Takase, *Organometallics* **2012**, *31*, 8225–8236.
- [19] N. Asao, T. Sudo, Y. Yamamoto, *J. Org. Chem.* **1996**, *61*, 7654–7655.
- [20] S. H. Yeon, J. S. Han, E. Hong, Y. Do, I. N. Jung, *J. Organomet. Chem.* **1995**, *499*, 159–165.
- [21] M. Pérez, L. J. Hounjet, C. B. Caputo, R. Dobrovetsky, D. W. Stephan, *J. Am. Chem. Soc.* **2013**, *135*, 18308–18310.
- [22] K. Jakobsson, T. Chu, G. I. Nikonov, *ACS Catal.* **2016**, *6*, 7350–7356.
- [23] Y. Li, M. Zhou, S. Park, L. Dang, *Inorg. Chem.* **2021**, *60*, 6228–6238.
- [24] F. Forster, V. M. Rendón López, M. Oestreich, *J. Am. Chem. Soc.* **2018**, *140*, 1259–1262.
- [25] H. Liang, Y.-X. Ji, R.-H. Wang, Z.-H. Zhang, B. Zhang, *Org. Lett.* **2019**, *21*, 2750–2754.
- [26] C. Xu, B. Huang, T. Yan, M. Cai, *Green Chem.* **2018**, *20*, 391–397.
- [27] J. C. Gee, B. A. Fuller, H.-M. Lockett, G. Sedghi, C. M. Robertson, K. V. Luzyanin, *Chem. Commun.* **2018**, *54*, 9450–9453.
- [28] P. Pawluc, G. Hreczycho, B. Marciniec, *J. Org. Chem.* **2006**, *71*, 8676–8679.
- [29] L. Busetto, M. C. Cassani, C. Femoni, M. Mancinelli, A. Mazzanti, R. Mazzoni, G. Solinas, *Organometallics* **2011**, *30*, 5258–5272.

- [30] D. V. Jawale, V. Geertsen, F. Miserque, P. Berthault, E. Gravel, E. Doris, *Green Chem.* **2021**, *23*, 815–820.
- [31] B. Marciniak, H. Ławicka, M. Majchrzak, M. Kubicki, I. Kownacki, *Chem. – Eur. J.* **2006**, *12*, 244–250.
- [32] T. Schwier, V. Gevorgyan, *Org. Lett.* **2005**, *7*, 5191–5194.

General conclusion and perspectives

The general context of this PhD is in the frame of catalysis and in particular the development of new catalytic tools. More precisely, the work was focused on metal-ligand cooperative catalysis, with the little explored group 10 metals, Pd in particular as targets.

An overview of the existing strategies and ligand design for MLC with group 10 metals is presented in the first chapter of this manuscript (Figure 12). The combination of an electron-rich site at the backbone with a Lewis-acidic transition metal is the most developed strategy and impressive results in terms of reactivity and selectivity have been reported with such systems. Another approach based on a tethered Lewis-acid in the ligand skeleton is also used in MLC as a functional group reservoir or as an assistant for oxidative addition. Finally, miscellaneous examples where the backbone acts as an acceptor of organic fragments are also presented. In most cases, the MLC has been illustrated in stoichiometric reactions but catalytic applications are rare. This summary highlights the interest of developing new architectures capable of MLC with Pd (and other group 10 metals).

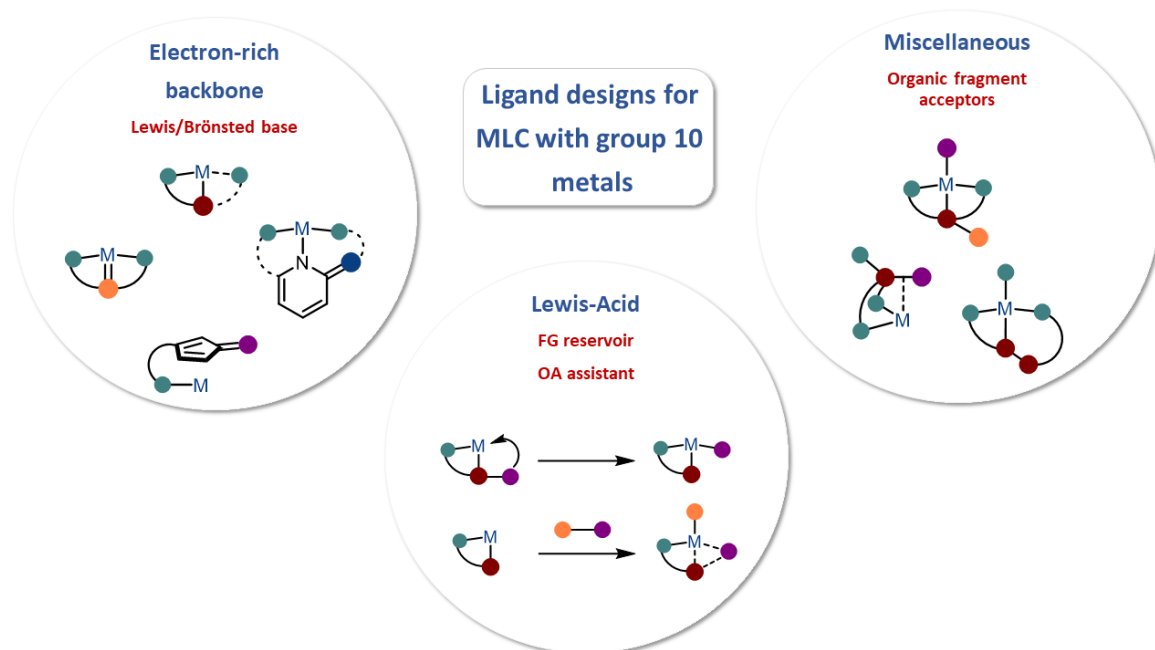


Figure 12: Ligand designs for MLC with group 10 transition metals classified in 3 categories, as seen in Chapter I

In this context, the first objective of this PhD work was to extend the catalytic applications of the [(SCS)-Pd] complex developed in the team. To this end, a multi-cooperative catalytic system combining MLC and an external LA was developed. Thanks to the simultaneous activation of a β -dicarbonyl function by the external LA and the non-innocent

electron-rich ligand, and of the $C\equiv C$ triple bond by the electrophilic metal center, the efficient formation of hetero and carbocycles with interesting selectivities was accomplished with this system (Figure 13). Cyclization could be promoted up to 7-membered rings with terminal alkynes. With internal alkynes, a complementary selectivity compared to the literature was displayed by our system, favoring the more sterically demanding Z-alkene. Finding a compatible partner for MLC and LA synergy is inherently challenging, due to the natural incompatibility between an electron-rich ligand backbone and a LA and this work represents as such, a rare example. To go even further, this is a unique opportunity to bring stereochemistry to this platform. Applying a chiral ligand at Mg (for example bisoxazolines) could be used for chiral induction, thanks to tight interaction between the Lewis-acid and the nucleophile in the ring forming step. This would represent an interesting perspective for this work, and Mg-chiral entities would be easy to screen. On the other hand, chiral modifications at the SCS-Pd complex would not be straightforward and the mechanism of π -activation and anti-addition to Pd would make chiral induction *a priori* less appropriate.

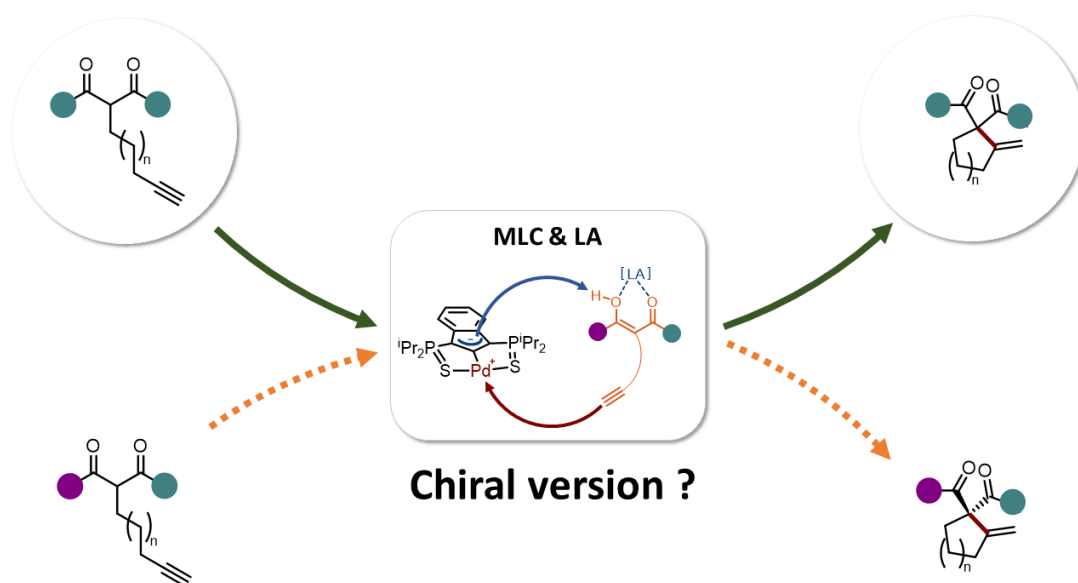


Figure 13: Carbocycle synthesis by combination of MLC with LA synergy with proposed mode of action of the two catalysts

The second objective of this work was to enlarge the diversity of ligands exhibiting MLC with Pd. Our design consists in a pincer ligand based on a quinoline skeleton bearing two coordinating side arms: a phosphine and a thiolate (PNS). Thanks to this design, two potential modes of cooperativity (aromatization/dearomatization & M-S type) could be available.

In the third chapter of this manuscript, dearomatized complexes of Pd and Ni bearing this new ligand were synthesized and the aromatization/dearomatization cooperativity was explored first through stoichiometric reactions. The activation of polar E-H bonds through MLC was demonstrated in both cases and a rare example of a Pd-H bearing an acidic proton within the non-innocent ligand was isolated and characterized. At this stage, no efficient catalytic reaction involving MLC has been evidenced, but understanding the evolution of this Pd-H complex and identifying ways to promote the cooperative H₂ release should help to achieve catalytic dehydrogenative couplings. In addition, divergent reactivity profiles between Ni and Pd were observed, which shall be explored further

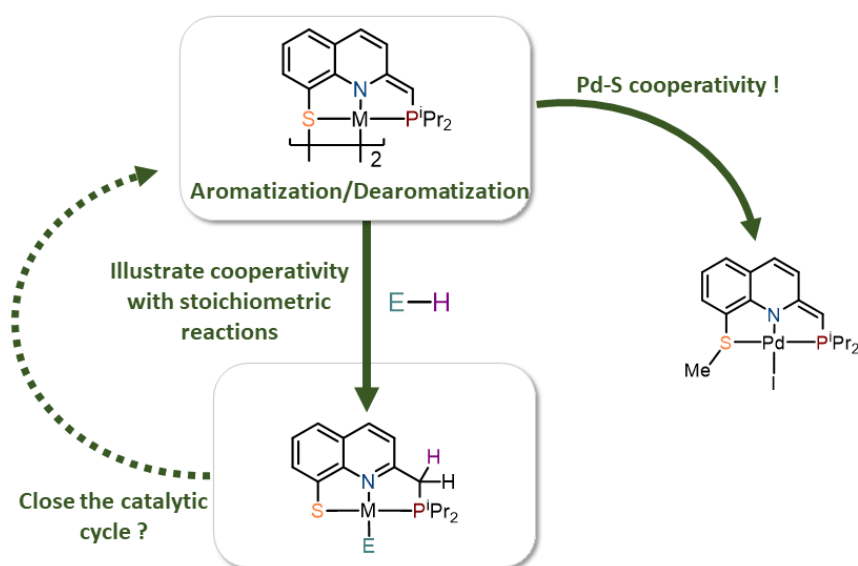


Figure 14: Overview of the results on the generation of the dearomatized complexes and illustration of the cooperativity

In the fourth chapter of this manuscript, the second mode of cooperativity based on the M-S bond was explored. Once again, stoichiometric reactions were first used to establish cooperative bond activation across the M-S bond. In this area, activation of Si-H and Ge-H bonds was achieved with Pd, and this system was found amenable to the catalytic hydrofunctionalization of alkynes. Notably, this reactivity contrasts with the one of the DmpS-Ru complex of Ohki and Oestreich, more prone to dehydrogenative couplings rather than hydroelementation. The product distribution and the substrate scope of the catalytic hydroelementation seem in accordance with a mechanism involving concomitant or stepwise transfer of a R₃Si⁺ group and a hydride to the alkyne rather than the usual Chalk-Harrod

mechanism. The full mechanistic picture has still to be clarified. To this end, kinetic studies, D-labeling experiments and DFT calculations would be of high-interest. Extending this cooperative reactivity to other types of substrates, including B-H bonds is also under study in the team. In terms of extension to other metals, although at this point no cooperative Ni-S bond activation was evidenced, here the ligand design to match the metal should again be considered and a switch to the PNO-architecture could unlock this cooperativity mode.

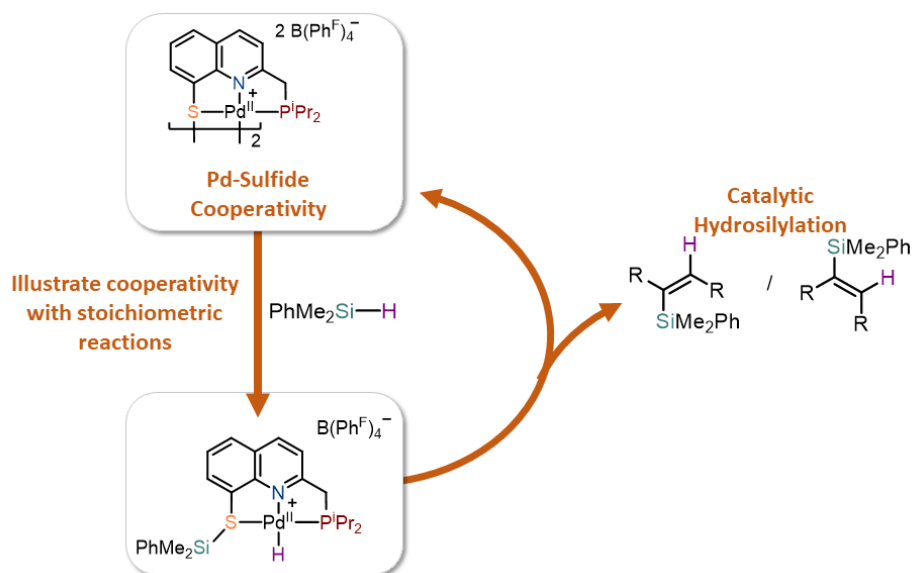


Figure 15: Pd-S cooperativity illustrated through stoichiometric Si-H activation and catalytic hydrosilylation

During this work, we were able to push forward the limits of MLC and use it in combination with an external LA in a multi-catalytic approach. We have also designed and synthesized a new non-innocent PNS platform applicable to multiple metals, with two modes of cooperativity illustrated through stoichiometric experiments. Regenerating a dearomatized species remains an elusive process at this point and work is currently underway to resolve this bottleneck. Future work in the catalytic hydroelementation reactions is also being conducted in the team.

We will also be interested in studying the extension of our PNS ligand design to other metals and the generality of the double MLC behavior (aromatization/dearomatization and M-S).

Combining the two modes of cooperativity in a tandem or one-pot catalytic process would also be highly attractive but very challenging. It would be the opportunity to combine the activation of E-H bonds of reverse polarity ($E^{\delta-}-H^{\delta+}/E^{\delta+}-H^{\delta-}$). First, we would need to

identify the conditions in which the two types of MLC occur and then try to find a common zone.

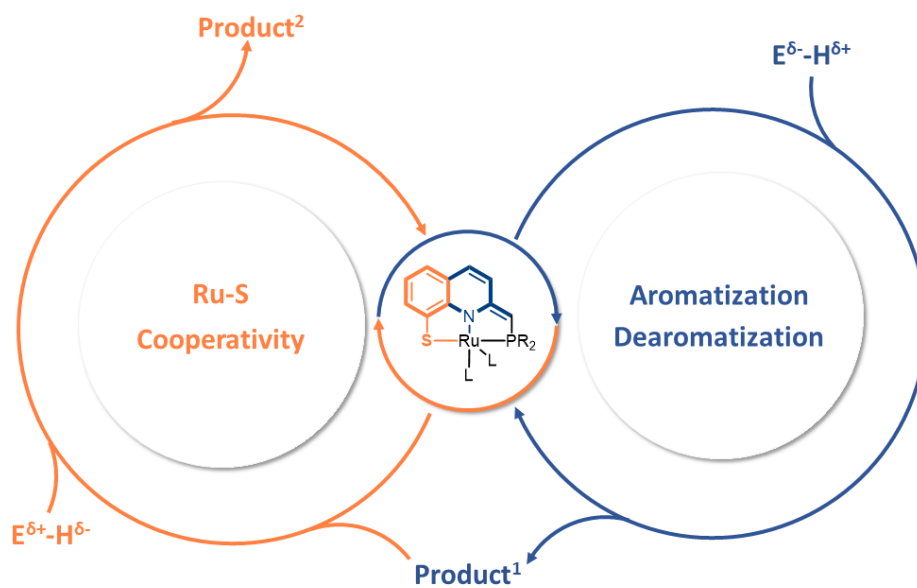
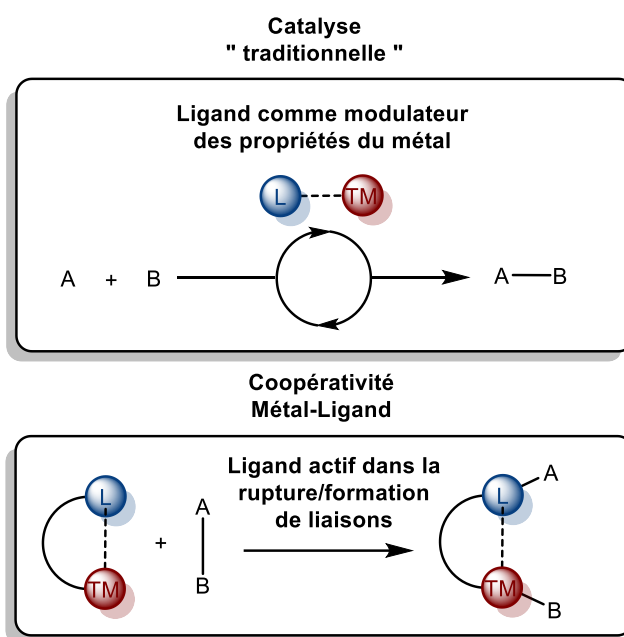


Figure 16: General representation of a tandem/one-pot approach involving the two modes of cooperativity

Résumé des travaux en Français

Dans le monde actuel, il est estimé que 85% des produits manufacturés impliquent un processus catalytique au cours de leur fabrication. On retrouve des catalyseurs dans pratiquement tous les domaines industriels : raffinage du pétrole, production d'engrais agricoles, produits pharmaceutiques, etc.... La recherche de nouvelles approches catalytiques et la conception de nouveaux catalyseurs est donc un enjeu majeur du monde moderne. Dans ce contexte, une approche originale et inspirée par la nature a été introduite récemment par les chimistes. En effet, dans la catalyse homogène par les métaux de transitions que l'on pourrait qualifier de « traditionnelle », un ligand est utilisé afin de stabiliser et moduler les propriétés stéréo-électroniques du métal et atteindre une activité catalytique intéressante. En catalyse coopérative, et plus particulièrement dans le cadre de la coopérativité métal-ligand, le ligand prend une part active à la création et/ou la rupture de liaison au cours du cycle catalytique.



Scheme 1: Comparaison de la catalyse homogène traditionnelle et de la coopérativité métal-ligand

Ce manuscrit de thèse s'inscrit dans ce contexte et porte sur l'étude des effets coopératifs en catalyse. Plus particulièrement, dans les complexes pinces des métaux du groupe 10, avec une attention plus poussée sur le palladium.

Le premier chapitre de cette thèse propose un résumé de l'état de l'art sur les complexes pinces des métaux du groupe 10 portant un ligand chimiquement non-innocent avec un double objectif :

Premièrement, présenter d'un point de vue global le contexte et l'importance de l'étude de la coopérativité métal-ligand avec les métaux du groupe 10.

Deuxièmement, étant un domaine peu couvert par les études bibliographiques, proposer une première base en vue de la publication d'une revue en 2022.

Ainsi, dans ce chapitre, la coopérativité entre le métal et le ligand est étudiée d'abord d'un point de vue de la situation électronique, puis par la réactivité stœchiométrique illustrant le caractère coopératif. Enfin, quand elle est décrite, l'activité catalytique est présentée. Les différentes contributions dans ce domaine ont ainsi été divisées en 3 grandes familles en fonction de la réactivité du site non-innocent sur le ligand (riche en électrons, acide de Lewis, et divers, Figure 1).

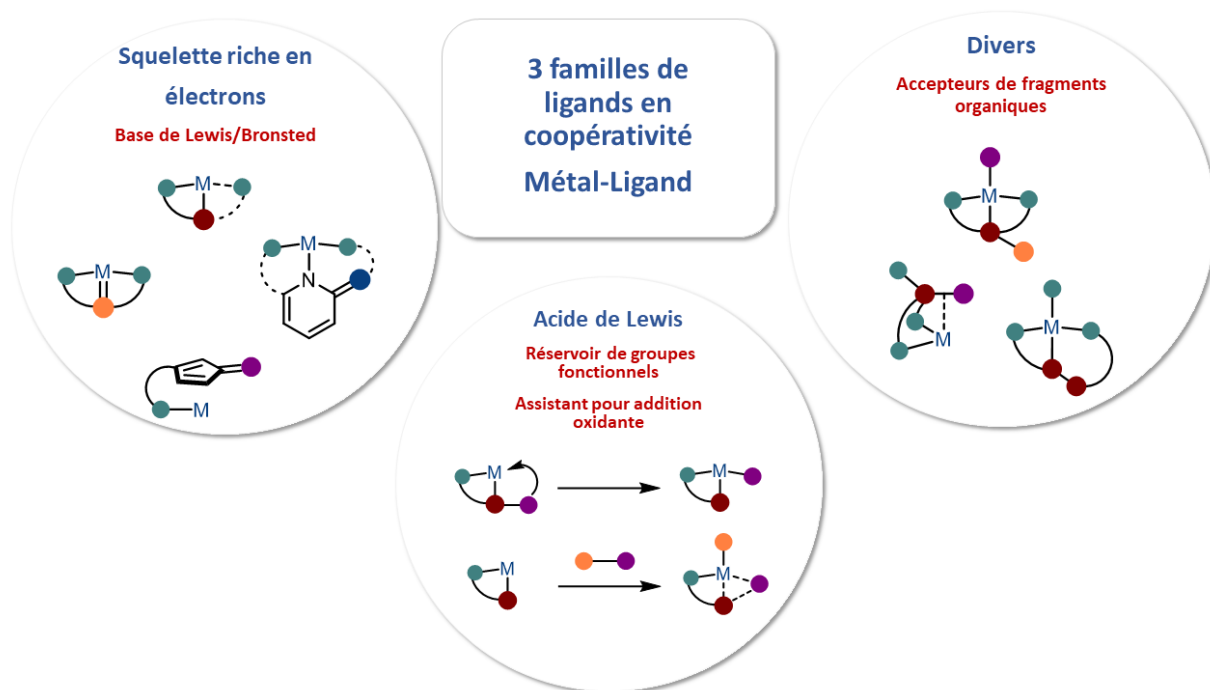


Figure 1: Vue générale des réactivités démontrées par les 3 grandes familles de ligand en coopérativité métal-ligand avec les métaux du groupe 10

De toutes ces approches, la plus développée consiste en la combinaison d'un site riche en électrons et d'un métal acide de Lewis. Dans l'ensemble, cette approche avec les métaux du groupe 10 a tout de même été peu appliquée en catalyse, surtout en comparaison avec les autres groupes. Il est donc d'autant plus intéressant de développer de nouveaux systèmes, capables de réaliser des transformations catalytiques.

Des travaux antérieurs de l'équipe LBPB du LHFA ont mis en évidence l'activité particulière dans des réactions de cycloisomérisation d'une famille de complexes bifonctionnels basée sur un squelette indenediide basique (au sens de Brønsted) et un centre métallique acide de Lewis (Pd/Pt). Des études mécanistiques poussées, ont aussi révélé l'impact de donneurs de liaisons hydrogène dans l'activité catalytique. Grâce à ce système, la cycloisomérisation catalytique d'acides et amides alcynoïques a permis d'accéder efficacement aux lactones et lactames correspondantes (création de liaisons C-O et C-N).

Le premier objectif de ces des travaux de thèse était d'étendre cette réactivité à la synthèse de carbocycles (création de liaisons C-C). La réaction de Conia-ène (une réaction de cycloisomérisation entre un dérivé carbonylé et une liaison triple $C\equiv C$) a donc été sélectionnée. En plus d'être un outil synthétique intéressant, différents obstacles et difficultés restent à adresser dans cette réaction. A titre d'exemple, les substrats de types dicéto sont classiquement plus faciles à cycliser que les diesters (Figure 2). Ceci s'explique par l'acidité du H-énolisable du dérivé carbonylé et de la prédominance de la forme énol, rendant plus ou moins facile la réaction.

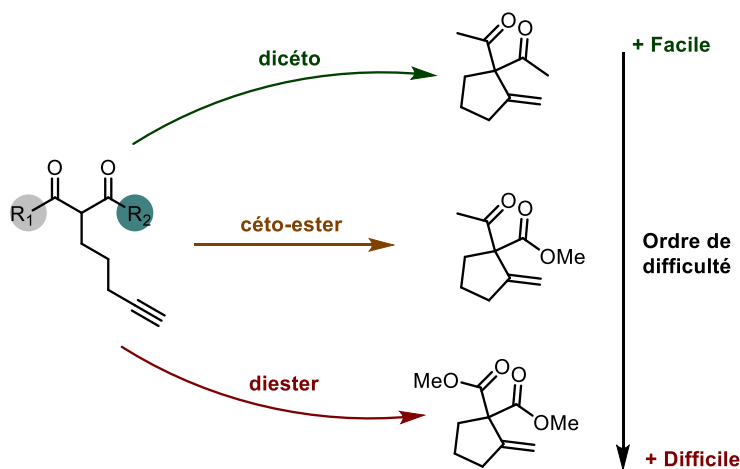
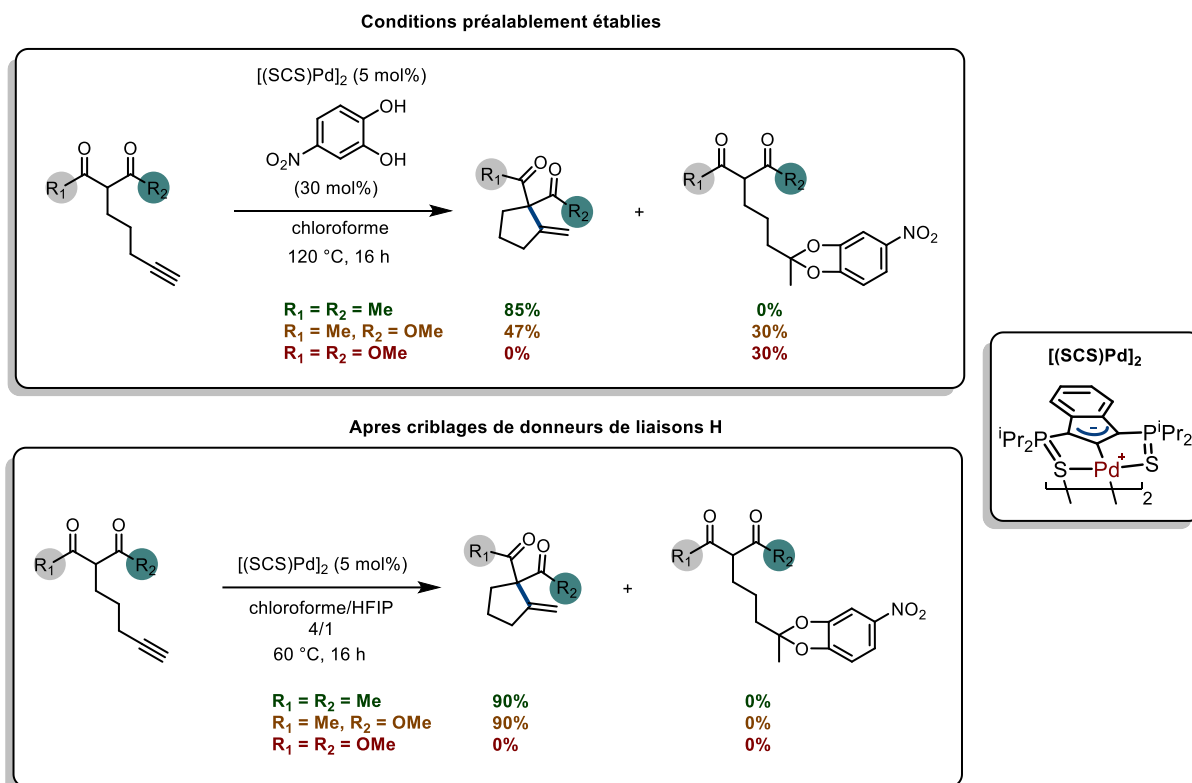


Figure 2: Ordre de difficulté de cyclisation de type Conia-ène des substrats dicéto, céto-esters et diesters

La transposition directe des conditions préalablement établies dans les cycloisomérisations des substrats a montré une activité catalytique pour les substrats dicéto et céto-ester dans des conditions relativement dures. En revanche, une réaction parasite d'addition du donneur de liaisons H sur la liaison triple $C\equiv C$ a lieu dans ces conditions (120 °C). Après un criblage d'additifs, l'hexafluoroisopropanol (HFIP) a été identifié comme bon donneur de liaison hydrogène pertinent dans cette réaction catalytique, mais faiblement nucléophile (*i.e.* pas de réaction d'addition de HFIP sur la liaison triple a été observée). Ainsi,

nous avons pu accéder aux motifs dicéto et céto-esters dans des conditions plus douces (60°C) mais les substrats de type diesters restent inaccessibles avec ce système (Scheme 2).



Scheme 2: Premier résultats en cycloisomérisation et identification de HFIP comme co-solvant approprié

Pour promouvoir la réactivité de ce type de substrats (diesters), nous avons envisagé l'activation du dérivé carbonylé par un acide de Lewis dur. En effet, la combinaison d'acides de Lewis durs et mous en réaction de Conia-ène a déjà été utilisée, en particulier avec les substrats dicéto et céto-esters. En revanche, la combinaison d'un système coopératif avec un acide de Lewis externe est une occurrence rare dans la littérature (Figure 3).

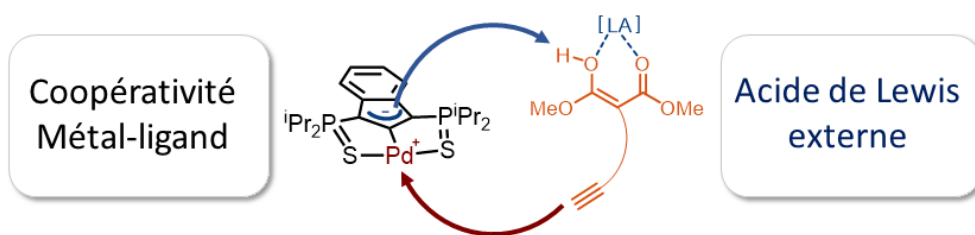


Figure 3: Combinaison de la coopérativité métal-ligand et d'un acide de Lewis externe pour la cycloisomérisation Conia-ène

Après un criblage d'acides de Lewis, nous avons identifié $\text{Mg}(\text{OTf})_2$ comme étant compatible et efficace, et nous permettant d'accéder à la cyclisation du motif diester. Avec ce nouveau système optimisé en main, nous avons étudié son étendue et son activité vis-à-vis de divers substrats.

Cyclisations 5-exo:

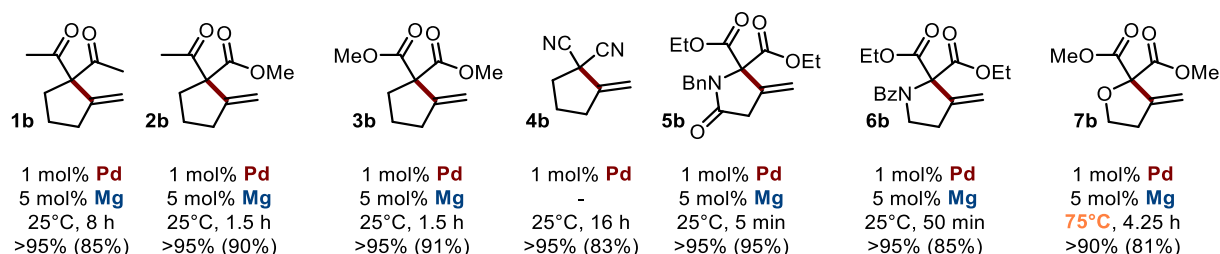


Figure 4: Produits de cyclisations 5-exo obtenus

Une première série de substrats (**1b** à **3b**, Figure 4) montre bien la capacité du système à cycliser les composés carbonylés avec différents degrés de difficulté. Dans le cas du malonitrile (**4b**, Figure 4), nous avons pu remarquer que l'addition de Mg n'influe pas sur la cinétique de la réaction (quantitative après 16h). Ce qui peut s'expliquer par la géométrie défavorable des groupements nitriles ne permettant pas la chélation du Mg.

Nous avons aussi étudié l'effet des substituants en α de la position énoisable avec l'addition de groupements électrodonneurs (O,N). Dans le cas de l'amide **5b** (Figure 4), nous avons observé la cyclisation quantitative en 5 min. Lorsque le dérivé benzoylé (**6b**, Figure 4) a été employé afin de ne plus avoir l'effet rigidifiant *endo*-cyclique de l'amide, nous avons observé la cyclisation en moins d'une heure. Le dérivé du furane (**7b**, Figure 4) a aussi pu être obtenu avec un très bon rendement de 90% après 4.25 h à 75 °C.

Avec l'intention de tester les limites de cette approche multi-coopérative, nous avons décidé de varier la taille des cycles.

Cyclisations >5-exo:

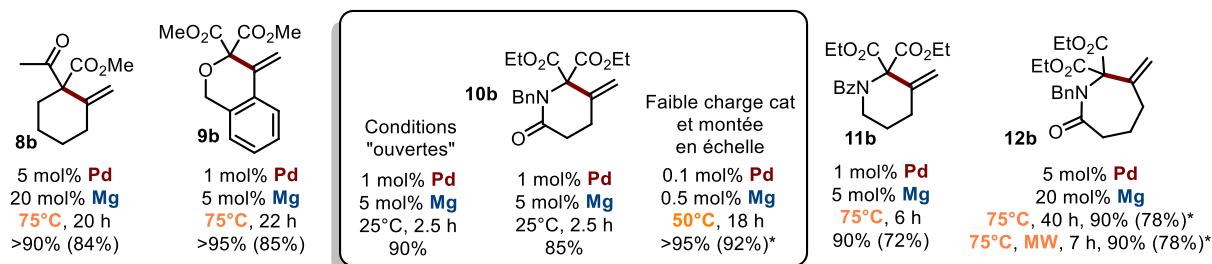


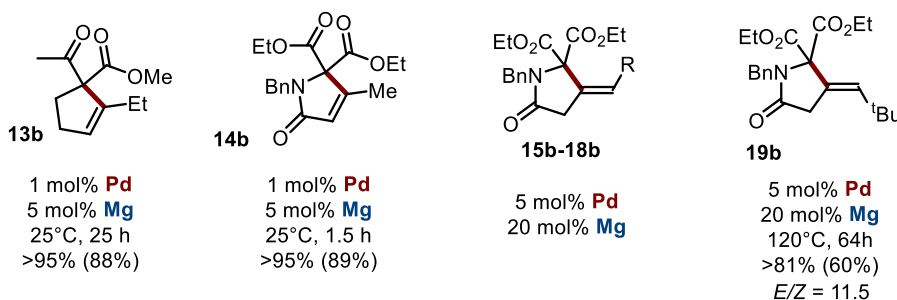
Figure 5: Produits de cyclisations >5-exo obtenus avec le système multi-coopératif

Nous avons premièrement testé la cyclisation à 6-chainons d'un précurseur céto-ester flexible. Nous avons obtenu le carbocycle **8b** (Figure 5) avec un bon rendement de 90 % après 20 h à 75 °C en utilisant 5% de complexe de palladium et 20% de sel de magnésium. Des hétérocycles β -diesters ont ensuite été étudiés, et **9b** (Figure 5) a pu être obtenu à plus de 95% de rendement après 22 h à 75°C avec une faible charge catalytique (1% Pd, 5% Mg). De manière intéressante, la δ -valerolactame **10b** (Figure 5) a été formée en seulement 2.5 h à 25°C. L'effet rigidifiant a été diminué comme dans le cas de **11b** (Figure 5) tout en gardant une activité catalytique intéressante (90% de rendement après 6 h à 75°C). Il a même été possible d'augmenter la taille de cycle jusqu'à 7-chainons (**12b**, Figure 5).

La robustesse du système a ensuite été évaluée en réalisant la réaction dans les conditions optimisées mais sans précautions particulières (réactifs non-séchés et de qualité technique, réaction exposée à l'air). Dans ce cas, le produit **10b** (Figure 5) a été obtenu dans des rendements similaires. De plus, la charge catalytique a pu être diminuée par un facteur 10 et le produit **10b** (Figure 5) a tout de même été formé dans de très hauts rendements (>95% après 18 h à 50 °C). Ces conditions ont pu être appliquée à l'échelle du gramme et 920 mg de produit **10b** (Figure 5) ont pu être préparées en utilisant seulement 1.4 mg de complexe de palladium et 4.5 mg de sel de magnésium. Ces résultats montrent bien la généralité et la robustesse du système, ainsi que sa capacité à former une variété de carbo et hétérocycles.

Pour aller encore plus loin, nous avons souhaité tester la cyclisation de substrats portant une fonction alcyne interne, peu développés dans la littérature.

Cyclisations d'alcynes internes:



R	T °C	Temps (h)	Rendement	Z/E
Me (15b)	25	3	85%	>50
Et (16b)	25	24	85%	>50
Cy (17b)	120	32	76% (52% Z)	7

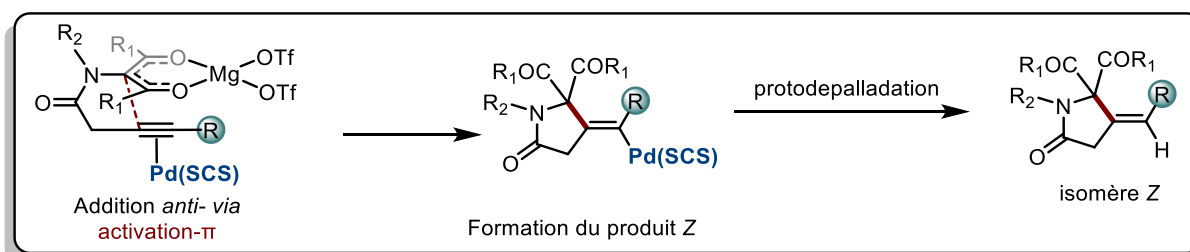
Ph (18b)	75	16	79% (65% Z)	10
-------------------	----	----	-------------	----

Figure 6: Cyclisations 5-endo et 5-exo d'alcynes internes

Etant classiquement beaucoup plus difficiles à cycliser que les alcynes terminaux, des problèmes de régio-sélectivité (*endo* / *exo*) peuvent apparaître. Vu la préférence de la cyclisation 5-*endo* comparé à la 4-*exo*, nous nous sommes tout d'abord intéressés à la formation des composés **13b** et **14b** (Figure 6). Dans les deux cas, la réaction a eu lieu dans des conditions douces avec d'excellents rendements et aucune trace de composés 4-*exo* n'ont pu être détectées par spectroscopie RMN.

Nous avons ensuite étudié la cyclisation 5-*exo* d'alcynes internes avec différents substituants (Me, Et, Cy, Ph, ^tBu) afin d'étudier l'impact de l'encombrement stérique et des effets électroniques sur la réaction. Dans le cas des alcynes les moins encombrés (Me, Et) la cyclisation a pu être réalisée à 25 °C en 3 et 24 h respectivement (**15b** et **16b**, Figure 6). Pour les plus encombrés (Cy, Ph, ^tBu) un chauffage à 75 ou 120 °C était requis pour promouvoir la réaction (**17b** à **19b**, Figure 6). Mais, quel que soit le substituant, la réaction est hautement sélective. Pour les produits **15b** à **18b** (Figure 6) la formation majoritaire (voir exclusive) de l'isomère le plus stériquement encombré (*Z*) est observée. Dans le cas de **19b** (Figure 6) en revanche, le produit *E* est formé majoritairement.

D'un point de vue mécanistique, ces résultats peuvent s'expliquer par le mode d'activation de la triple liaison par le palladium provoquant ainsi l'addition *anti* de l'énolate (Scheme 3). Dans le cas de groupements Me, Et, Cy et Ph, la protodépalladiation aurait ensuite lieu pour former l'isomère *Z*. En revanche, pour le produit fortement encombré ^tBu, une isomérisation de l'intermédiaire vinyl-Pd pourrait avoir lieu avant la protodépalladiation expliquant ainsi la formation majoritaire du produit *E* dans ce cas.



Scheme 3: Mode d'activation du palladium sur la triple liaison, induisant la sélectivité *Z* dans le cas d'alcynes internes

Ici, il a donc été montré que le complexe bifonctionnel (SCS)-Pd est un catalyseur efficace pour des réactions de cycloisomérisations de type Conia-ène lorsqu'il est utilisé en combinaison avec du $Mg(OTf)_2$ et du HFIP. Une large librairie de substrats a ainsi pu être cyclisée par formation de liaison C-C avec une importante régiosélectivité. Ce système multi-coopératif est aussi remarquablement actif dans la cyclisation d'alcynes internes et, de manière générale, une stéréo-sélectivité complémentaire vis-à-vis des systèmes reportés dans la littérature est observée.

Afin de continuer notre étude dans la coopérativité métal-ligand, nous nous sommes intéressés à la conception d'un nouveau ligand non-innocent avec deux objectifs principaux :

Premièrement, généraliser l'approche coopérative et introduire un nouveau ligand pertinent en coopérativité métal-ligand.

Deuxièmement, étendre à de nouvelles transformations cette coopérativité avec le palladium et l'appliquer à d'autres métaux (du groupe 10 et potentiellement d'autres métaux de transition). Dans cette optique, plusieurs critères importants ont été sélectionnés pour la conception du nouveau ligand (Scheme 4) :

i) Un ligand pince.

De manière générale, la modularité et la robustesse de ces ligands et des complexes dérivés en fait des candidats particulièrement adaptés aux applications de type coopérativité métal-ligand.

ii) Un ligand P- donneur.

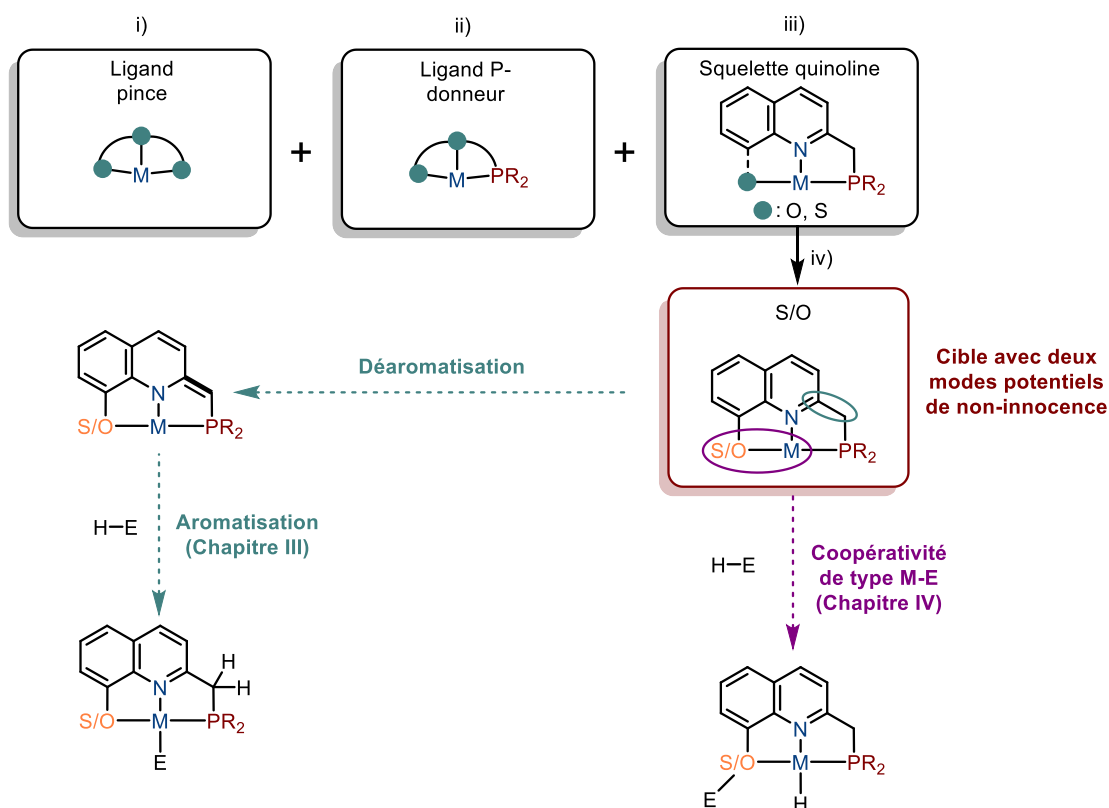
En effet, les interactions phosphore-métal sont classiquement robustes (en particulier phosphore-palladium) et l'aspect pratique d'avoir une sonde RMN directement liée au centre métallique est crucial dans notre approche.

iii) Un squelette quinoline avec espaceur CH_2 .

Cet espaceur avec ce motif quinoline permettrait d'accéder à des processus d'aromatisation/désaromatisation.

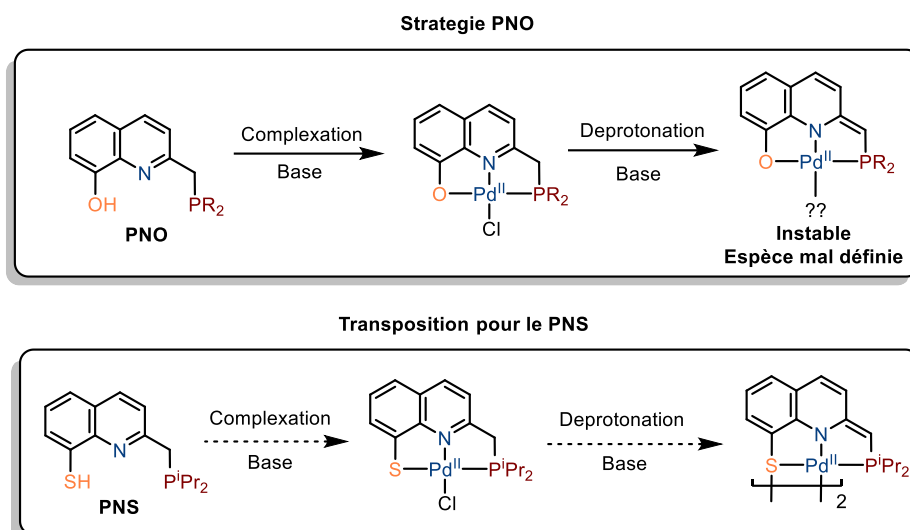
iv) Dans notre approche, nous avons aussi voulu favoriser au maximum la coordination pince en utilisant un groupement donneur O- ou S- comme troisième site de coordination du ligand.

Un des avantages de ce modèle réside aussi dans le mode de coopérativité potentiel basé sur l'interaction M-O/S.



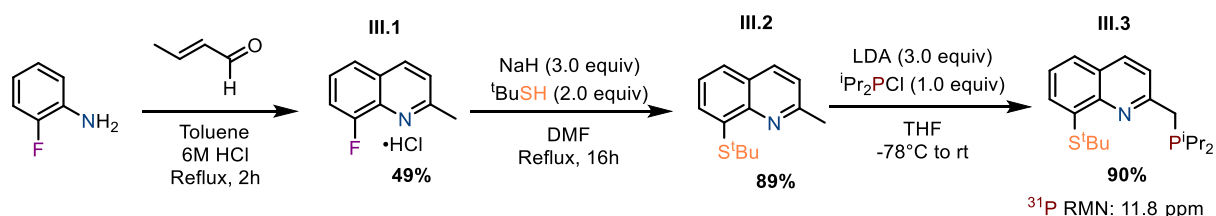
Scheme 4: Critères généraux pour le squelette du ligand avec deux modes de coopérativité potentiels

Dans un premier temps, la synthèse d'un complexe PNO- de palladium a été réalisée par Laurens Vedder au cours de son stage de Master. Les premiers tests de réactivité ont montré une stabilité du complexe modérée, ceci probablement dû à la labilité de la liaison Pd-O. Nous avons ainsi décidé de nous diriger vers une nouvelle plateforme avec une interaction Pd-Ligand plus forte ainsi qu'une capacité plus importante à former des dimères : Le PNS (Scheme 5).



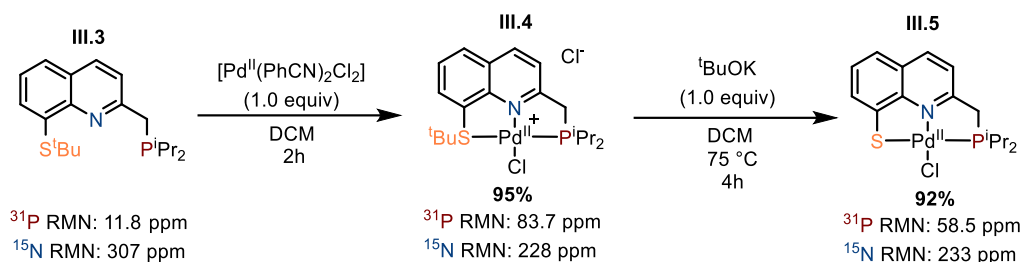
Scheme 5: Transposition de la synthèse développée pour le PNO avec la nouvelle architecture PNS et conséquences sur la formation d'une espèce binucléaire désaromatisée

L'équivalent soufré (le 2-méthylquinolinethiol) n'étant pas disponible commercialement, la synthèse du pro-ligand PNS a été reprise en amont. En partant de la 2-fluoroaniline, une réaction de Doebner-Miller nous a permis d'obtenir la 8-fluoro-2-méthylquinoline (Scheme 6). Cette dernière a pu être isolée sous sa forme chlorhydrate (**III.1**), permettant sa purification en quantité importante par recristallisation. La substitution du fluor par un groupement ^tBuS est ensuite réalisée (**III.2**) et le bras phosphoré est introduit par lithiation et addition de chlorophosphine (**III.3**).



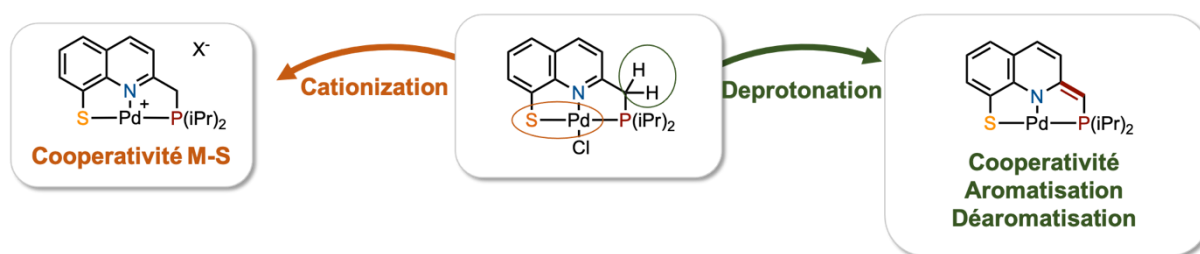
Scheme 6: Synthèse du ligand PNS en partant de la 2-fluoroaniline

En présence d'une source de Pd^{II} la rigidité du ligand ainsi que l'affinité du métal pour le soufre permettent sa complexation et ainsi la formation d'un complexe cationique possédant un chlorure en sphère externe (**III.4**). La déprotection du groupement ^tBu est ensuite réalisée en présence d'une base pour obtenir la plateforme ciblée (**III.5**).



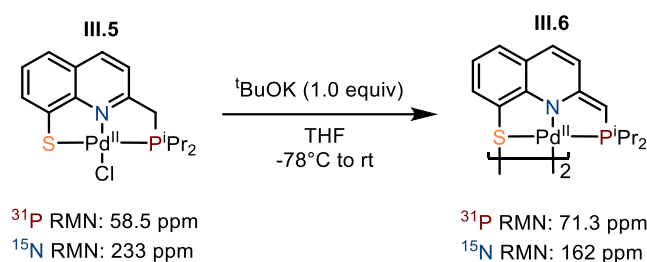
Scheme 7: Complexation du ligand PNS sur le palladium et formation de la plateforme III.5

Une fois la plateforme obtenue, l'objectif était donc de générer deux types d'espèces actives, avec deux modes de coopérativités différents (Scheme 8). L'un basé sur l'aromatisation/désaromatisation (chapitre III de ce manuscrit) et l'autre basé sur le caractère amphiphile du palladium et du soufre (chapitre IV).



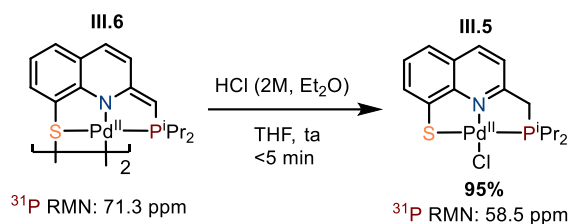
Scheme 8: Deux modes de coopérativité à partir d'une plateforme commune

En premier lieu, la désaromatisation/aromatisation a été étudiée. Ainsi, lorsque le complexe PNS-Pd-Cl III.5 est mis en présence d'une base on observe la déprotonation du bras CH₂, la désaromatisation du système π du complexe et la formation d'un dimère que nous avons pu caractériser par DRX.



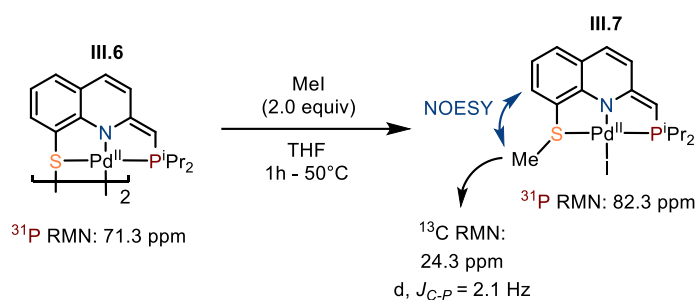
Scheme 9: Génération de l'espèce désaromatisée en présence d'une base

Une fois l'espèce active en main, notre premier objectif était de mettre en évidence le caractère non-innocent du ligand à travers des réactions stœchiométriques. Ainsi, le complexe a été mis en présence de HCl et la réaromatisation du squelette et la formation du complexe neutre III.5 a été observée avec un très bon rendement (Scheme 10).



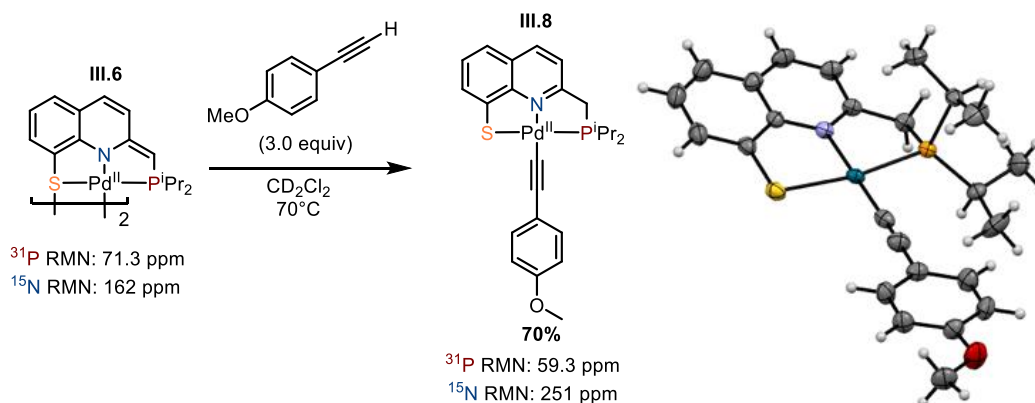
Scheme 10: Régénération du complexe neutre par traitement du complexe désaromatisé avec HCl

En revanche, lorsque le complexe est mis en présence d'un électrophile comme le iodométhane, une autre position sur le squelette réagit et on observe la méthylation du soufre avec la formation d'une liaison Pd-I (Scheme 11), mettant en avant la disponibilité des doublets non-liants du soufre.



Scheme 11: Réaction du complexe désaromatisé avec un électrophile

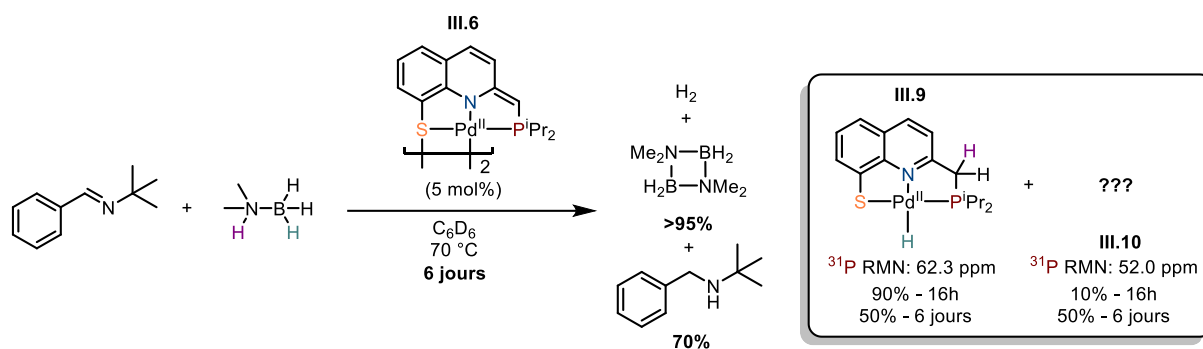
Après ces résultats prometteurs vis-à-vis de liaisons fortement activées, nous nous sommes tournés vers des liaisons plus difficiles comme les liaisons C-H d'alcynes. Dans ce cas, lorsque III.6 est mis en présence de *para*-méthoxyphénylacétylène, on observe la réaromatisation du squelette quinoline et la formation d'un complexe Pd-Alkynyl qui a pu être caractérisé par DRX (Scheme 12).



Scheme 12: Activation C-H par le complexe désaromatisé III.6

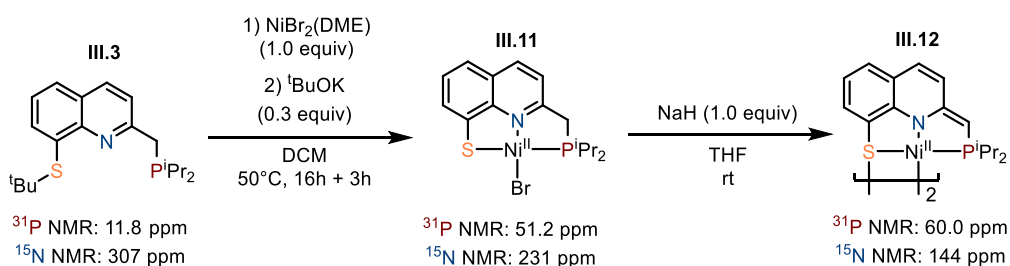
A la suite de ces résultats nous nous sommes intéressés à la réaction « classique » impliquant des processus coopératifs d'aromatisation/déaromatisation : la déshydrogénation d'alcools. Dans ce cas, le complexe III.6 n'a pas révélé d'activité catalytique. Nous avons

ensuite voulu tester la réactivité de ce complexe vis-à-vis d'une source polaire de H₂: la diméthylamine borane (Scheme 13). En présence de 5.0 équivalents de DMAB à 70 °C, la formation d'un complexe aromatisé Pd-H est observée et il a pu être caractérisé par DRX. Il s'agit ici, d'un complexe portant un hydrogène avec un caractère hydrure (lié au Pd) et un hydrogène acide lié à centre non-innocent sur le ligand. Ce type de complexes sont rare dans la littérature et avec des métaux du groupe 10 ils se comptent sur les doigts d'une main ! Le complexe Pd-H s'est aussi avéré instable et son évolution en une nouvelle espèce a été observée, mais malheureusement cette dernière n'a pas pu être identifiée à ce jour. La déshydrogénation catalytique de la diméthylamineborane a été étudiée avec **III.6** mais seule une faible activité a été observée.



Scheme 13: Réactivité du complexe III.9 avec la diméthylamineborane et déshydrogénation catalytique

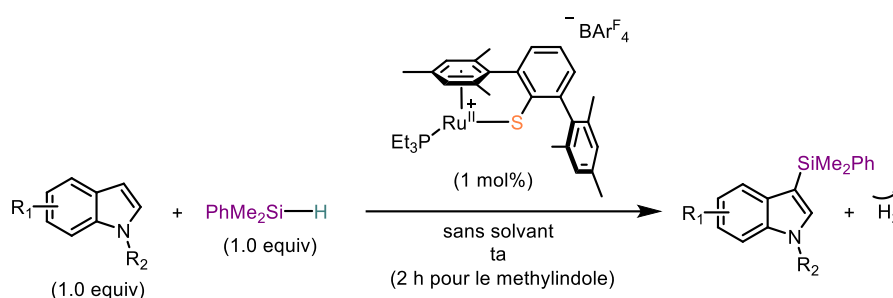
Un autre objectif de notre stratégie avec cette architecture de ligand était de l'étendre à d'autres métaux. Grâce à Andràs Kotschy, un étudiant de Master, le complexe PNS de nickel a pu être synthétisé en suivant un schéma réactionnel similaire à celui utilisé avec le palladium (Scheme 14). Des premiers tests de réactivité de ce complexe désaromatisé **III.12** ont ensuite été effectués et des divergences de réactivités comparées au complexe de palladium **III.6** ont été observées, ce qui fera l'objet d'études ultérieures dans le groupe.



Scheme 14: Synthèse du complexe de PNS de nickel

En parallèle de ces travaux, l'étude de la coopérativité du motif Pd-S a été réalisée. L'activation de liaisons E-H par un motif M-S a déjà été étudiée avec d'autres métaux que le palladium et c'est actuellement un domaine de recherche dynamique.

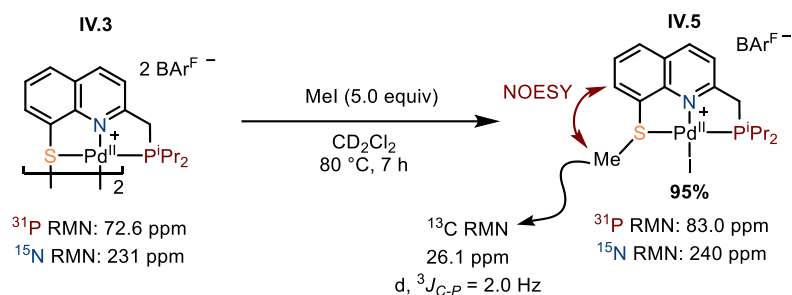
Comme exemple représentatif, nous pouvons citer le système DmpS-Ru de Ohki dont la réactivité a été développée en collaboration avec Oestreich. Ici le motif Ru-S agit comme une paire de Lewis. Le ruthénium étant acide de Lewis et les doublets non-liants du soufre base de Lewis. Ce système a été appliqué à la rupture hétérolytique de liaisons Si-H avec la formation d'une liaison S-Si et Ru-H. Ce système s'est avéré particulièrement pertinent dans des réactions de silylations déshydrogénantes (Scheme 15).



Scheme 15: Silylation déshydrogénante du méthylindole par le complexe DmpS-Ru

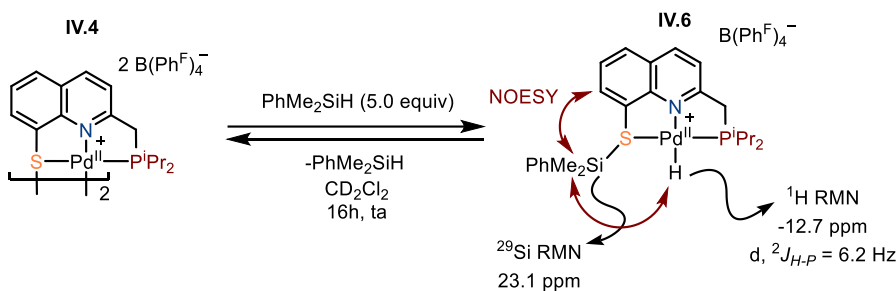
Pour étudier la capacité de notre système à montrer une coopérativité Pd-S nous avons souhaité tout d'abord générer une espèce active par cationisation, pour ensuite illustrer le mode de réactivité par des réactions stœchiométriques et l'appliquer à des transformations catalytiques.

La génération de l'espèce active avec $\text{KB}(\text{Ph}^{\text{F}})_4$ nous permet de former un dimère di-cationique robuste et soluble. Avec le complexe di-cationique en main, notre premier objectif était d'illustrer le caractère bifonctionnel du motif Pd-S à travers des réactions stœchiométriques. Dans un premier temps, le complexe **IV.3** a été mis en présence de iodométhane et nous avons pu observer la formation d'une liaison Me-S avec incorporation de l'iode sur le palladium, en accord avec un soufre base de Lewis et un centre métallique acide de Lewis (Scheme 16).



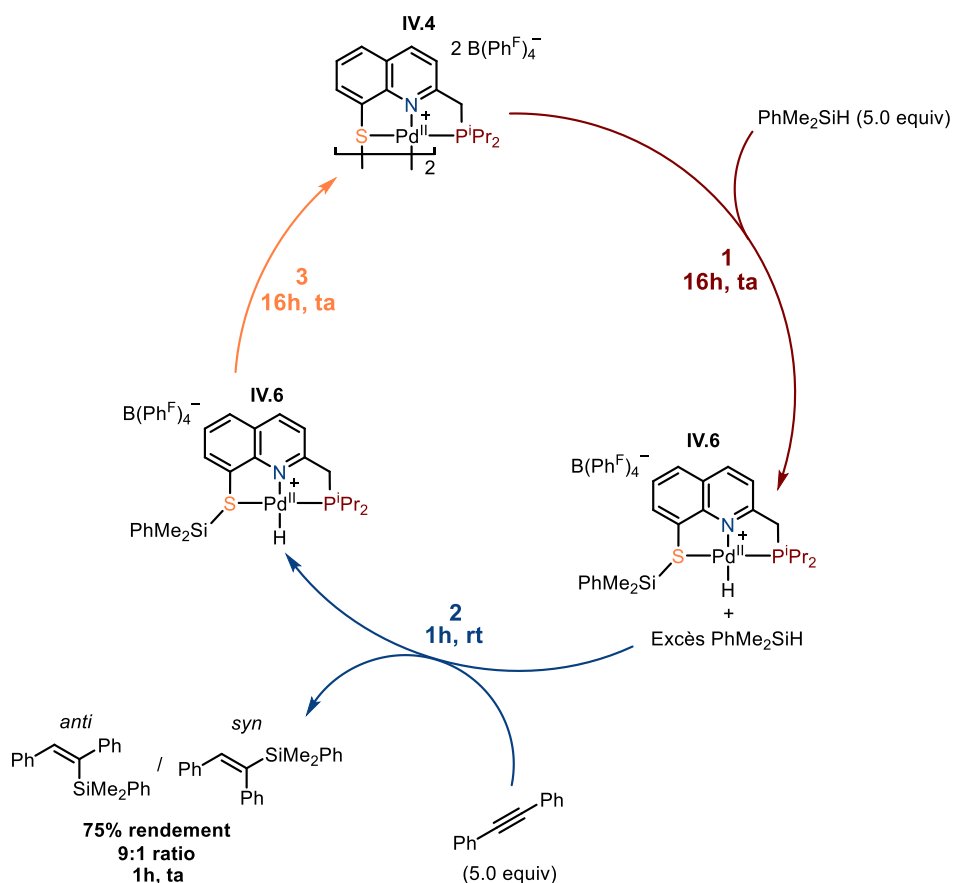
Scheme 16: Illustration du caractère bifonctionnel du motif Pd-S par réaction avec le iodométhane

Nous avons ensuite cherché à activer d'autres liaisons à plus grands enjeux. Lorsque le complexe est mis en présence de PhMe_2SiH , on observe une réactivité similaire avec une rupture hétérolytique de la liaison Si-H pour former le complexe cationique Pd-H avec incorporation du fragment silylé sur le soufre (Scheme 17 ; données spectroscopiques en accord avec la structure proposée). Ce complexe s'est avéré stable qu'en présence d'un excès de silane la régénération du dimère **IV.4** a lieu si ce dernier est supprimé.



Scheme 17: Rupture hétérolytique de la liaison Si-H par le motif Pd-S

Avec ce résultat en main, nous avons souhaité tester la capacité de ce système à transférer le motif Si-H. Dans un premier temps, le complexe d'activation Si-H a donc été généré (**1** - Scheme 18), ce dernier a ensuite été mis en présence de tolane (**2** - Scheme 18) et 75% de rendement d'hydrosilylation a été observé. D'un point de vue de la stéréosélectivité, un ratio 9/1 de produit *anti/syn* est formé au cours de la réaction. Après réaction, le dimère di-cationique **IV.4** est régénéré (**3** - Scheme 18)

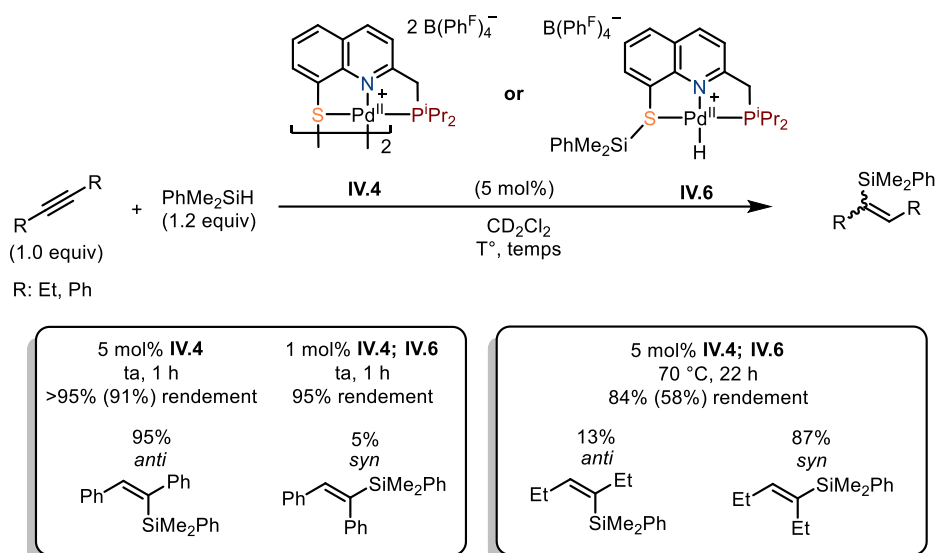


Scheme 18: Expériences de transferts Si-H "stœchiométriques"

Ici, la capacité du système à transférer une quantité supra-stœchiométrique de silane à un alcyne a été démontrée et de fait, son potentiel catalytique (ici à 20% mol). De plus, la formation de l'isomère *anti* comme produit majoritaire à la fin de la réaction suggère une réactivité rare d'hydrosilylation *anti*.

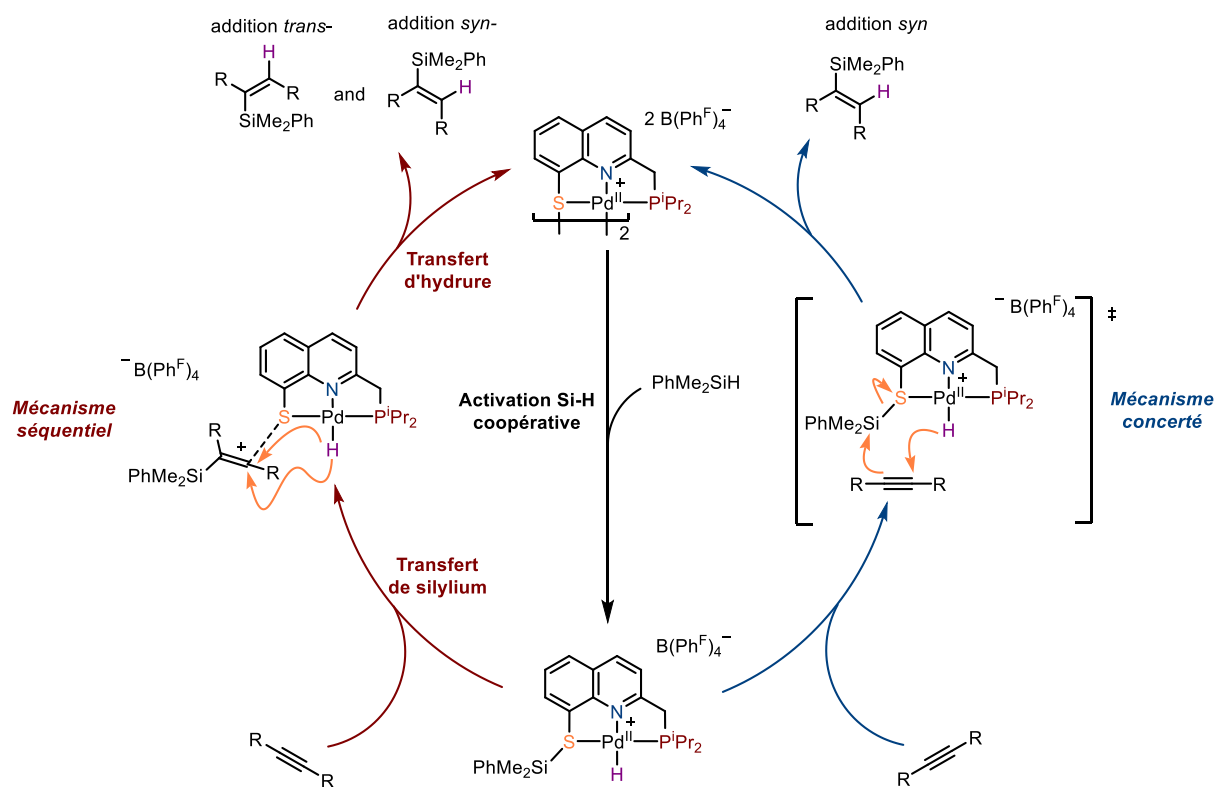
Dans la continuité directe des expériences stœchiométrique, l'hydrosilylation d'alcynes internes symétriques a été testée, en premier lieu avec 5% de charge catalytique (Scheme). Dans le cas du tolane (Ph-CC-Ph), l'hydrosilylation quantitative a été observée en moins d'une heure (97% *anti*/3% *syn*). La charge catalytique a ensuite été réduite à 1 mol% et dans ce cas, 95% de rendement est observé en 1 h avec 95% de produit d'hydrosilylation *anti*-et 5% de produit d'hydrosilylation *syn*.

Avec l'hex-3-yne, des conditions plus dures sont nécessaires et la distribution des produits est inversée. 84% de rendement est atteint après 22 h à 70°C, mais cette fois, 87% de produit *syn* et 13% de produit *anti* sont formés. Quand le complexe préformé IV.6 est utilisé, la réactivité et la distribution de produit est comparable avec une légère amélioration de l'activité, en particulier en début de réaction.



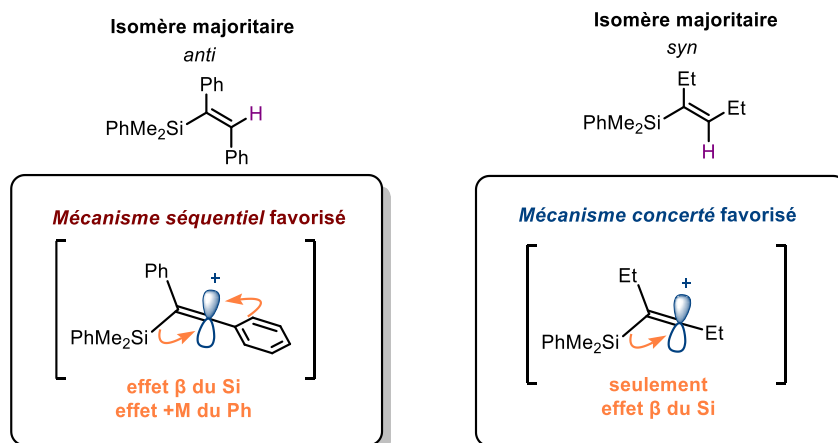
Scheme 19: Hydrosilylation catalytique d'alcynes internes symétriques

D'un point de vue mécanistique, comparé aux mécanismes classiques d'hydrosilylation (Chalk-Harrod), ici, deux mécanismes peuvent être proposés et peuvent ainsi expliquer la différence de sélectivité observé dans les deux cas (Scheme 20). Ces deux mécanismes démarrent par l'activation Si-H coopérative pour former **IV.6**. Ensuite dans le cas d'un mécanisme séquentiel, le transfert d'un cation silylium a lieu en premier pour générer un vinyl-cation stabilisé par le soufre. Ce dernier réagit dans un second temps avec le complexe palladium-hydrure pour générer le produit d'hydrosilylation *syn* ou *anti* (en fonction de la sélectivité du transfert d'hydrure). Dans le second mécanisme, le transfert de cation silylium et d'hydrure a lieu de manière concertée, résultant en la formation exclusive du produit d'hydrosilylation *syn*. En fonction des paramètres stériques et électroniques des alcynes utilisés, les deux mécanismes peuvent être opérationnels ou l'un pourrait être favorisé.



Scheme 20: Mécanismes alternatifs proposés comme opératifs dans le cas de l'hydrosilylation par le complexe cationique PNS-Pd

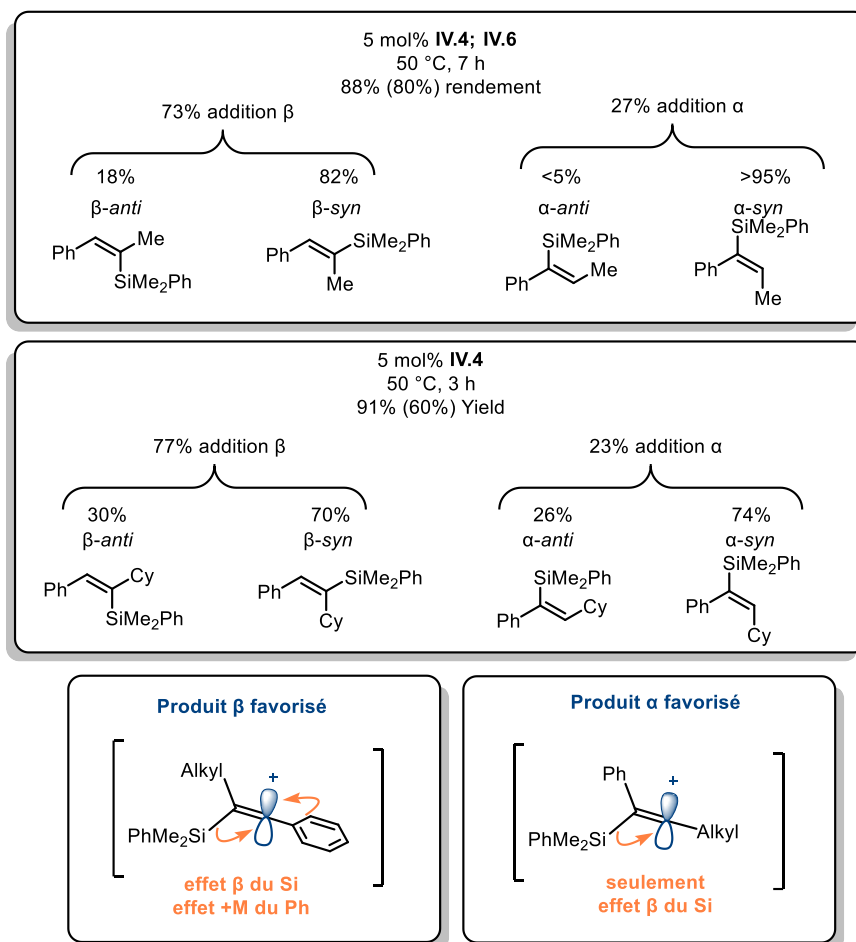
Dans le cas du toluène, la formation du produit *anti* comme isomère majoritaire peut s'expliquer par un mécanisme asynchrone, impliquant un carbocation vinylique. Dans ce cas, ce dernier serait stabilisé non seulement par l'effet β du silicium mais aussi par l'effet mésomère du groupement phényle (Scheme 21). Dans le cas de l'hex-3-yne en revanche, seulement l'effet β du silicium serait présent, ainsi le carbocation serait comparativement moins stable et un mécanisme concerté serait favorisé. Ce qui pourrait expliquer dans ce cas la formation du produit *syn* comme produit majoritaire.



Scheme 21: Formation d'un carbocation vinylique dans le cas du tolane et de l'hex-3-yne et illustrations des effets stabilisants dans les deux cas

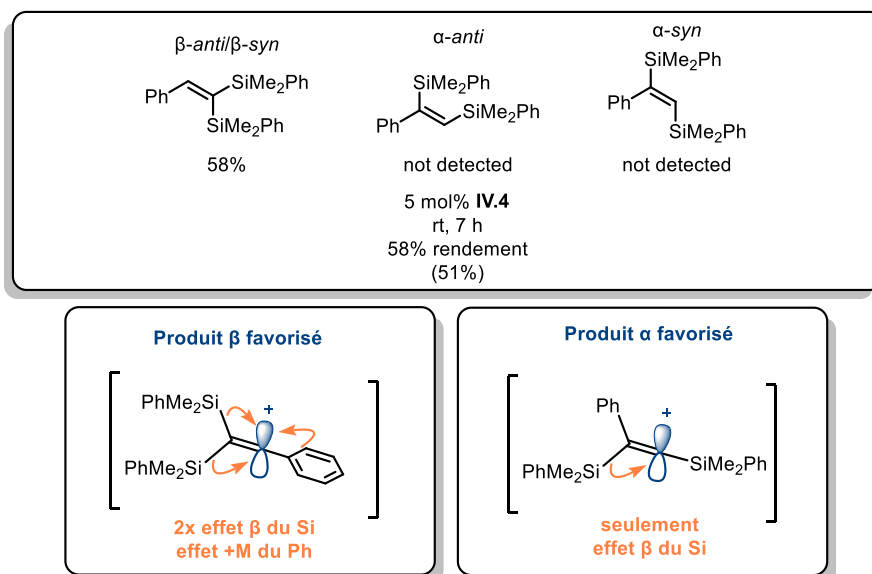
Avec ces éléments en tête, plusieurs substrats avec des effets électroniques et stériques différents ont pu être testés pour obtenir plus d'informations sur le cycle catalytique opérationnel et sur l'étendue de la transformation.

Des alcynes internes dissymétriques ont ensuite été testés comme Ph-CC-Me et Ph-CC-Cy. Dans les deux cas, la formation du produit d'hydrosilylation β a été observée. Cette observation est à nouveau en accord avec un mécanisme impliquant un transfert de Si⁺ / H⁻ (quelque que soit la synchronicité).



Scheme 22: Hydrosilylation catalytique d'alcynes dissymétriques Aryl-Alkyl

Pour continuer notre étude, un alcyne biaisé électroniquement a ensuite été utilisé pour étudier l'impact des effets électroniques sur la distribution de produits. L'hydrosilylation de Ph-CC-SiMe₂Ph a donc été réalisée et une sélectivité complète de l'addition du fragment R₃Si en β du phényle est observée (Scheme 23). Considérant les mécanismes proposés, cette distribution est à nouveau en accord les mécanismes proposés. Ainsi, un carbocation stabilisé par les deux effets β des deux R₃Si en plus de l'effet mésomère du phényle serait formé après transfert de R₃Si⁺ (Scheme 23). *A contrario*, l'addition en α du Si⁺ générerait un carbocation vinylique stabilisé uniquement par l'effet β du Si.



Scheme 2329: Hydrosilylation d'alcyne interne biaisé électroniquement et stabilisation des carbocations vinyliques correspondants

Des alcynes terminaux ont aussi été testés, et une réactivité similaire a été observée avec formation exclusive du produit de β -hydrosilylation. En revanche, d'autres phénomènes d'isomérisations ont lieu et sont en cours d'étude dans l'équipe.

Cette réaction a aussi pu être étendue à l'hydrosilylation du styrène, mais un alcène plus encombré (méthylcyclohexène) n'est pas réactif dans ces conditions.

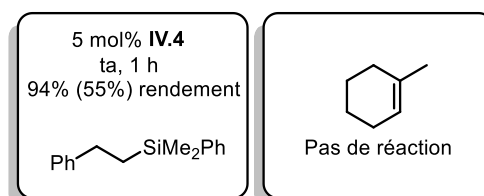
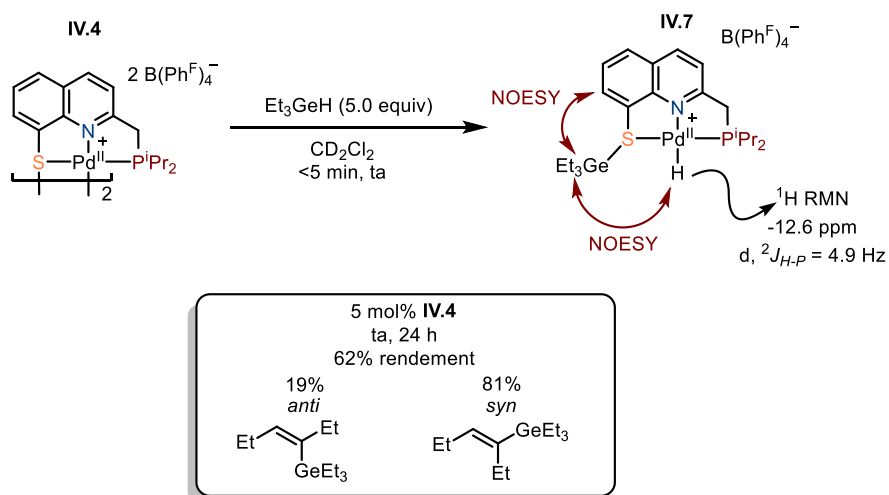


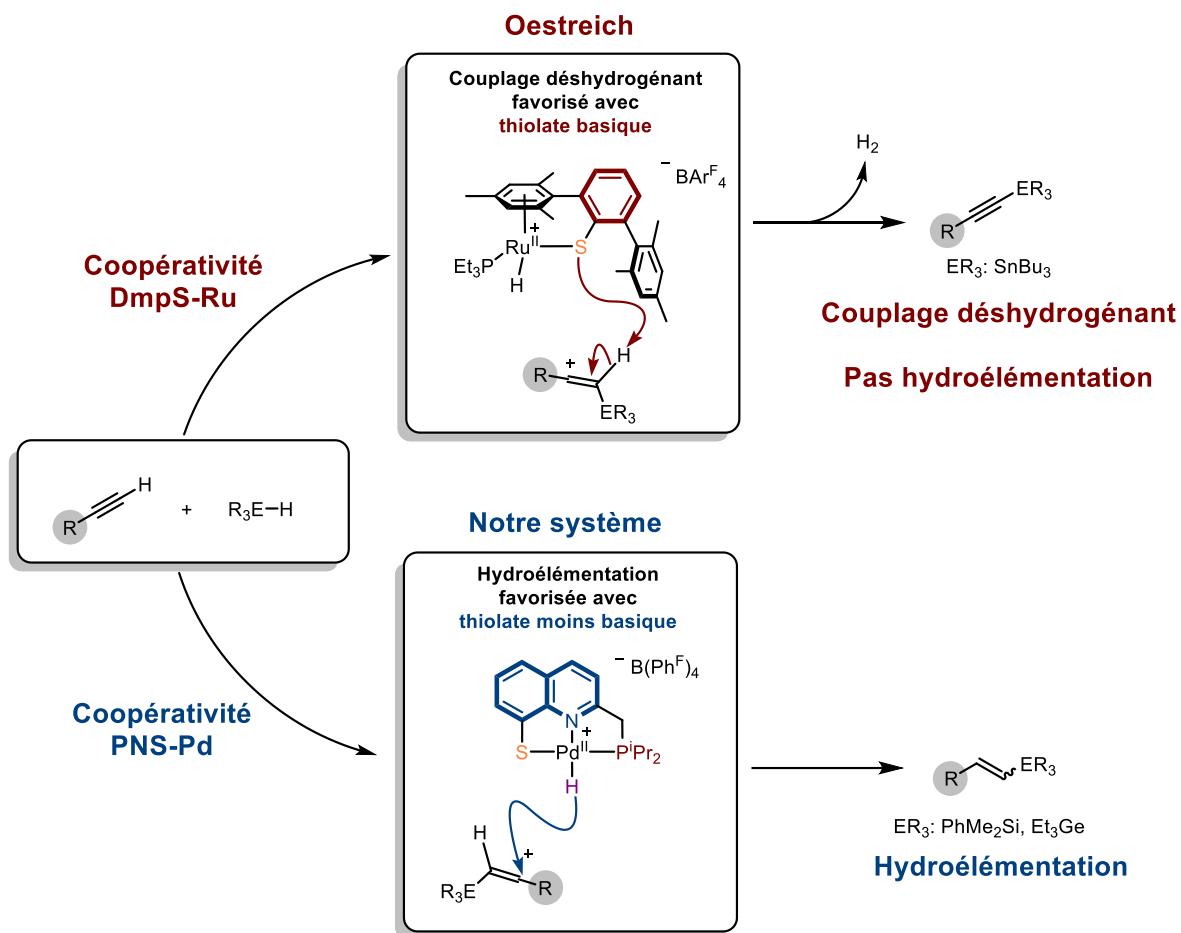
Figure 7: Hydrosilylation d'alcènes par **IV.4**

L'activation coopérative de liaisons a pu être étendue à la liaison Ge-H. A nouveau, l'activation de la liaison de manière coopérative a été mise en évidence de manière stœchiométrique, et la structure proposée du produit d'activation est supportée par une étude spectroscopique poussée. Ensuite, le transfert R_3Ge^+/H^- vers un alcyne interne a été appliqué de manière catalytique.



Scheme 24: Activation GeH coopérative et hydrogermylation catalytique

Dans cette partie, un nouveau complexe pince de palladium capable d'activer des liaisons de manière coopérative autour du motif Pd-S a été synthétisé. Il est d'autant plus intéressant qu'il s'agit du premier exemple bien défini de ce mode de coopérativité au palladium. Ce complexe est capable d'effectuer la rupture hétérolytique de liaisons Si-H et de réaliser l'hydrosilylation catalytique de substrats insaturés comme des alcynes ou le styrène. Dans ce cas, un mécanisme impliquant un transfert R_3Si^+/H^- est suggéré par la distribution de produits mais des expériences complémentaires sont en cours pour obtenir un mécanisme détaillé. Tout de même, une nouvelle transformation par rapport aux systèmes de la littérature avec ce mode de coopérativité (par exemple DmpS-Ru) est observée grâce à notre complexe et la nouvelle architecture de ligand. Une explication de cette différence de réactivité peut prendre son origine au caractère basique (au sens de Bronsted) plus prononcé du soufre and le complexe DmpS-Ru par rapport à notre système PNS-Pd. Ainsi, le couplage déshydrogénant est favorisé dans le cas du DmpS-Ru, alors que dans nôtre cas l'hydroélémentation est préférée (Scheme 25).



Scheme 25: Comparaison des deux systèmes DmpS-Ru et PNS-Pd proposant une explication pour la différence de réactivité des deux systèmes

De manière générale, ce travail de thèse montre le développement d'un nouveau système multi-coopératif combinant la coopérativité métal-ligand et un acide de Lewis externe. Ce système a été appliqué à la formation efficace de carbocycles et d'hétérocycles.

Un autre objectif de cette thèse était d'étendre la diversité des ligand capables d'agir de manière coopérative avec un métal. Ainsi, un nouveau ligand pince basé sur un squelette quinoline a été synthétisé (PNS). Sa coordination au palladium et au nickel a ensuite été étudiée et deux espèces actives (avec deux modes de coopérativité différents) ont été générées. Dans un premier temps, des réactions stœchiométriques ont permis de mettre en évidence ces deux modes de coopérativité. Une activité catalytique intéressante en hydroélémentation à travers un mécanisme original a ensuite été démontrée par le complexe de palladium. Des études complémentaires sont en cours dans l'équipe pour étudier plus en profondeur ce système.

Abstract

This PhD work relates to the study of cooperative effects in catalysis with group 10 metals pincer complexes, with a particular focus on palladium.

In the first chapter of this manuscript, an extensive bibliographic survey on group 10 metals pincer complexes bearing a chemically non-innocent ligand is presented. Common ground and differences between the presented systems are highlighted and discussed. They have been divided in 3 big families, depending on the reactivity exhibited by the ligand backbone (electron-rich, Lewis-acid, functional group reservoir).

The second chapter presents the development and application in catalysis of a new system based not only on MLC but its use in synergy with an external Lewis acid. Thanks to this new multi-cooperative system, the formation of carbocycles (and heterocycles) was efficiently promoted through a cycloisomerization reaction involving a C-C bond formation. A wide scope of substrates could be cyclized and a complementary stereoselectivity compared to that reported in the literature was displayed by our system.

The third chapter is focused on the design and the synthesis of a new non-innocent pincer ligand along with its coordination to palladium. A new dearomatized species could be generated and characterized. The non-innocent behavior of the dearomatized ligand was demonstrated through stoichiometric reactions. During this work, a rare example of a palladium-hydride complex bearing an acidic hydrogen center at a non-innocent ligand was isolated and characterized.

Thanks to our ligand design, a second cooperativity mode based on a palladium-sulfide interaction could be explored and is presented in the fourth chapter of this manuscript. The stoichiometric E-H bond activation ($E = \text{Si}, \text{Ge}$) with this complex results in the formation of a E-sulfide bond and a palladium hydride. This cooperativity was then applied to catalysis with the hydroelementation of alkynes. In this reactivity, our ligand design brings mechanistic diversity and a complementary reaction profile compared to known systems.

Keywords : Metal-ligand cooperativity, multi-cooperative, ligand design, pincer complexes catalysis

Résumé

Ce travail de thèse porte sur l'étude des effets coopératifs en catalyse avec des complexes pince des métaux du groupe 10, et en particulier le palladium.

Dans le premier chapitre de ce manuscrit, une étude bibliographique approfondie sur les complexes pince des métaux du groupe 10 comportant un ligand chimiquement non-innocent est présentée. Les points communs et les différences entre les différents systèmes sont discutés. Ils ont été divisés en 3 grandes familles, en fonction de la réactivité du site non-innocent sur le ligand (riche en électrons, acide de Lewis, réservoir de groupes fonctionnels).

Le second chapitre présente le développement et l'application en catalyse d'un nouveau système multi-catalytique basé non-seulement sur la coopérativité métal-ligand mais sur sa synergie avec un acide de Lewis externe. Grâce à ce nouveau système multi-coopératif, la formation de cycles carbonés (et d'hétérocycles) a été réalisée efficacement à travers une réaction de cycloisomérisation impliquant la création d'une liaison C-C. Une large librairie de substrats a pu être cyclisée et une stéréochimie complémentaire par rapport à la littérature a été montrée par notre système multi-coopératif.

Ensuite, le troisième chapitre porte sur le design et la synthèse d'un nouveau ligand pince non-innocent ainsi que sa coordination sur le palladium. Une nouvelle espèce désaromatisée a pu être générée et caractérisée. Le caractère non-innocent du ligand désaromatisée a été mis en évidence au travers de réactions stœchiométriques. Au cours de ces travaux, un rare exemple de complexes palladium-hydrure portant un atome d'hydrogène acide au sein d'un ligand non-innocent a été isolé et caractérisé.

Grâce à notre design de ligand, un second mode de coopérativité basé sur une liaison palladium-soufre a pu aussi être exploré, et il est présenté dans le quatrième chapitre de ce manuscrit. L'activation stœchiométrique de liaisons E-H (E = Si, Ge) par ce complexe se traduit par la formation d'une liaison E-soufre et palladium-hydrure. Cette coopérativité a pu être ensuite appliquée en catalyse à travers l'hydroélémentation d'alcynes. Dans cette réactivité, notre design de ligand apporte une diversité mécanistique et offre un profil réactionnel complémentaire par rapport aux systèmes déjà connus.

Mots clés : Coopérativité métal-ligand, multi-coopérativité, design de ligand, complexes pince, catalyse